Faculty of Science and Engineering
Department of Applied Geology

Utilisation of microvertebrates in biostratigraphy and chemostratigraphy

Brett Peter Ashworth Roelofs

This thesis is presented for the Degree of
Doctor of Philosophy
of
Curtin University

February 2016

Declaration

To the best of my knowledge and belief this thesis contains no material previously published by any other person except where due acknowledgment has been made.

This thesis contains no material which has been accepted for the award of any other degree or diploma in any university.

Brett Peter Ashworth Roelofs

09/02/16

Abstract

The exceptionally preserved Devonian reef complexes of the Canning Basin, Western Australia, provide an excellent opportunity for testing the utility of different chronostratigraphic methods. In order to construct a robust temporal framework for the reef system, an Australian Research Council Linkage Project (LP0883812) utilised an integrated approach involving sequence stratigraphy, magnetostratigraphy, chemostratigraphy and biostratigraphy. This thesis contributed the biostratigraphic component to this larger chronostratigraphic project, as well as investigated the novel application of marine microvertebrates in chemostratigraphy. Conodont biostratigraphy provided the finest temporal resolution of slope facies but was less successful in reefal platform facies due to a paucity of biostratigraphically useful conodonts. Microvertebrate taxa offered a potential solution for correlation of reefal platform and marginal environments as they occurred where other more traditional biostratigraphical taxa, such as palynomorphs, corals, brachiopods, ammonoids and conodonts, were absent or long ranging.

A rich microvertebrate fauna was recovered from measured sections of outcropping Frasnian slope and Famennian to Tournaisian ramp facies along the Lennard Shelf, northern Canning Basin. Thelodont (jawless fish) scales were recorded from both Late Devonian strata, with the Famennian aged scales (Late *marginifera* CZ) representing the youngest thelodont scales discovered to date. The recovery of Frasnian phoebodont shark teeth revealed previously undocumented morphological variation in *Phoebodus bifurcatus* and *Phoebodus latus*. In addition, revised phoebodont age ranges in the Canning Basin are now more comparable to those of the global phoebodont zonation. The discovery of a new species, *Diademodus*

dominicus sp. nov., provides the first evidence of this genus in Gondwana. A total of fourteen chondrichthyan species, twelve of which had not previously been documented in the Canning Basin, were identified from the Famennian-aged Bugle Gap Limestone and Virgin Hills Formation. In addition, a diverse shark fauna, including teeth from *Ageleodus* sp. *Thrinacodus ferox*, *Cladodus thomasi*, *Protacrodus aequalis* and *Protacrodus* sp., are described from early Tournaisian ramp facies of the Laurel Formation. The presence of *Thrinacodus ferox* and *Protacrodus aequalis*, in addition to the absence of *Thrinacodus biscuspidatus*, indicates an age range of *sulcata* to *duplicata* Conodont Zones for the lower Laurel Formation. Prior to this work, only a general Tournaisian Age, based on conodonts, could be attributed to this formation.

Microvertebrate fossils were analysed to determine if the preserved $\delta^{18}O$ signatures were viable proxies in palaeoclimatic reconstructions and chemostratigraphic correlation. Gas isotope ratio mass spectrometry, which involved testing homogenised tissues, indicated $\delta^{18}O_{microvertebrate}$ signatures were typically depleted by 2-4‰ when compared to conodont apatite, which is considered to record primary O-isotope ratios. Secondary ion mass spectrometry enabled targeted in-situ analyses of enamel, dentine and bone microvertebrate tissues. Hypermineralised microvertebrate tissues (enamel, acrodin, ganoine) were identified as consistently hosting $\delta^{18}O$ signatures comparable to associated conodont elements. In addition, results indicate that less mineralised tissues, such as dentine and bone, are more susceptible to alteration of the constituent phosphate and should be avoided in O-isotope analysis. The fidelity of O-isotopes in microvertebrate bioapatite indicates that these common, environmentally ubiquitous Phanerozoic microfossils have the potential to act as a

substitute for other oxygen-isotope media which may be facies-controlled or affected by diagenesis (e.g. bulk-rock or fossil carbonates).

The Famennian chondrichthyan biofacies model was found applicable to both Late Devonian and Early Carboniferous strata. Although the Early Carboniferous saw an increase in the diversity of sharks and the niche space they occupied, those sharks with a crushing dentitions showed continuous occupation of the shallow, near shore environments from the Late Devonian to the Early Carboniferous.

Late Devonian microvertebrate fossils, described herein, indicate a significant cosmopolitan fauna existed within the Canning Basin. Cosmopolitan phoebodont species, present along the northern margins of Gondwana and throughout Laurussia, were recorded in Frasnian sediments of the Lennard Shelf. In the Famennian, taxa such as *Thrinacodus tranquillus, Protacrodus serra, Deihim mansureae* and *Lissodus lusavorichi* indicate faunal relationships with northern Gondwana and to a lesser extent, the South China terrane. By the Carboniferous, the shallow water chondrichthyan faunas previously shared with the South China and the Indochina regions appear to have decreased, with only pelagic taxa in common. The data from the microvertebrates supports global reconstructions including northward separation of South China from Gondwana.

The results indicate microvertebrate fossils offer not only a powerful biostratigraphic tool but may also provide additional palaeoecological and palaeoenvironmental information in addition to a potential proxy for use in chemostratigraphy. The utilisation of microvertebrates in biostratigraphy and chemostratigraphy will enhance the successfulness of integrated chronostratigraphic approaches, particularly where correlation of restricted facies is involved.

Acknowledgments

The last four years has been the most interesting and challenging chapters in my life. I am very grateful for the experience and would like to thank all those, family friends and academics, who made getting through it possible. To anyone I have left out, I apologise and I'm sure I'll remember you after submission.

First and foremost, I would like extend a most sincere thank you to my supervisors Kate Trinajstic and Milo Barham. Kate, thank you for all the years of guidance. You have provided me with the opportunity to follow a dream I have had ever since I can remember. I truly appreciate all the time and generosity you have provided me. To Milo Barham, thank you for your endless patience and always making the time to assist me. I will always cherish what you have taught me. I consider myself truly fortunate to have had the two of you as my supervisors.

I would especially like to thank my family for their continued support over the decades (I promise to move out one day). And to my Nanna, thank you for your support, I'll try to find a 'real' job one day. This thesis is dedicated to you.

I am also very grateful to Ted Playton, John Maisey, John Long, Gavin Young, Michal Ginter, Kim Dennis-Bryan, Vachik Hairapetian, Sue Turner, Carole Burrow, Catherine Boisvert, Ken McNamara, Michael Joachimski, Laure Martin, John Cliff, Daniele Lutz, Arthur Mory, Roger Hocking, Peter Haines and Mikael Siversson for their helpful comments and assistance over the course of my PhD. Thanks to Elaine Miller at the Curtin University Electron Microscope Facility for having the patience to go through procedures every time I used the Evo. And of course, Annette Labroy; for the last ten years you have solved every issue I have come to you with.

I would like to acknowledge financial assistance provided to me from the Department of Applied Geology, Curtin University and the Commonwealth Government. I would also like to recognise the Australian Research Council (LP0883812), MERIWA, WAERA, CSIRO, Arc Energy, Chevron Australia Business Unit and Chevron Energy Technology Company. Thank you to Wundargoodie Aboriginal Safaris and the Geological Survey of Western Australia for providing field support and safety. An additional thank you to the Mimbi Community, Mt. Pierre Station, Fossil Downs access to the field areas.

A thank you to all my friends who were willing to help me one way or another (especially to those willing to listen to my endless complaints about life, aka PhD). Of course, a special thanks to Pat (after telling me for four years to include him), Stan and Maggie for reminding me of life outside of my PhD. A special thank you to Charlotte and Lucy, who had to put up with being in close proximity to me over the years. You both saved me on numerous occasions.

And lastly, but most certainly not least, a special thank you to Holly who was there for me when I really needed it. I wouldn't have been able to finish this without you.

Copyright Declaration

To the best of my knowledge and belief this thesis contains no material previously published by any other person except where due acknowledgment has been made.

This thesis contains no material which has been accepted for the award of any other degree or diploma in any university.

List of publications as Part of this Thesis

This thesis comprises a series of research papers that were either published or accepted for publication in scientific journals. Papers where I was not the primary author are included in this thesis as my contribution to these works would have formed independent publications or chapters. However, collaboration with other authors allowed for the compilation of more comprehensive works.

Trinajstic, K., **Roelofs, B**., Burrow, C., Long, J., and Turner, S. 2014. Devonian vertebrates from the Canning and Carnarvon Basins with an overview of Paleozoic vertebrates of Western Australia. Journal of the Royal Society of Western Australia 97, 133-151.

Roelofs, B., Playton, T., Barham, M., and Trinajstic, K. 2015. Upper Devonian microvertebrates from the Canning Basin, Western Australia. Acta Geologica Polonica 65, 69-101.

Hairapetian, V., **Roelofs, B.P.A**., Trinajstic, K.M., and Turner, S. 2015. Famennian survivor turiniid thelodonts of North and East Gondwana. Geological Society, London, Special Publications 423, 423-433.

Roelofs, B., Barham, M., Mory, A. and Trinajstic, K. 2016. Late Devonian and Early Carboniferous chondrichthyans from the Fairfield Group, Canning Basin, Western Australia. Palaeontologia Electronica 19, 1-28.

Roelofs, B., Barham, M., Cliff, J., Joachimski, M., Martin, L. and Trinajstic, K. Assessing the fidelity of marine vertebrate microfossil $\delta^{18}O$ signatures and their potential for palaeo-ecological and -climatic reconstructions. Palaeogeography, Palaeoclimatology, Palaeoecology.

Additional Publications Relevant to This Thesis but Not Forming Part of it

Work carried out over the course of my PhD, contributed the biostratigraphic framework used in the publications listed below and are included in the appendicies.

Hansma, J., Tohver E., Yan, M., Trinajstic, K., **Roelofs, B**., Peek, S., Slotznick, S.P., Kirschvink, J., Playton, P. Haines, P. and Hocking, R. 2014. Late Devonian carbonate magnetostratigraphy from the Oscar and Horse Spring Ranges, Lennard Shelf, Canning Basin, Western Australia. Earth and Planetary Science Letters 409, 232-242.

Hillbun, K., Katz, D., Playton, T., Trinajstic, K., Tohver, E., Ratcliff, K., Caulfield-Kerney, S., Wray, D., Haines, P., Hocking, R., **Roelofs, B**., Montgomery, P. and Ward. P. 2015. Upper Kellwasser excursion pre-dates the F-F boundary in the Upper Devonian Lennard Shelf carbonate system, Canning Basin, Western Australia. Palaeogeography, Palaeoclimatology, Palaeoecology 438, 180-190.

Playton, T.E., Tohver, E., Hillbun, K.,Hocking, R.M., Haines, P.W., Trinajstic, K., **Roelofs, B.,** Katz, D.A., Kirschvink, J., Grice, K., Montgomery, P., Hansma, J., Yan, M., Pisarevsky, S., Tulipani, S., Ratcliffe, R., Caulfield-Kerney, S. and Wray, D. 2016. Integrated Stratigraphic Correlation of Upper Devonian Platform-to-Basin Carbonate Sequences, Lennard Shelf, Canning Basin, Western Australia: Advances in Carbonate Margin-to-Slope Sequence Stratigraphy and Stacking Patterns. Society for Sedimentary Geology.

Conference Presentations

Roelofs, B., Trinajstic, K., Turner, S. 2013. The use of Conodont and Vertebrate Biostratigraphy in determining key boundaries in Late Devonian to Early Carboniferous Sections; Canning Basin, Western Australia, and the implications for correlation across North Gondwana. SDS - SCS -IGCP 596 - Institute Scientifique Meeting, Morocco.

Roelofs, B., Trinajstic, K., Turner, S., Hairapetian, V. and Hansma, J. 2013. Vertebrate diversity and faunal turnover from the Late Devonian to Early Carboniferous in the Canning Basin, Western Australia. Conference on Australian Vertebrate Evolution, Palaeontology and Systematics, Adelaide, Australia.

Roelofs, B., Trinajstic, K., Playton, T., Tohver, E., Haines, P., Hocking, R., Hansma. J., Hillbun, K., Grice, K., Yan, M., Ratcliffe, K., Pisarevesky, S. and Montgomery, P. 2013. Vertebrate biostratigraphy from the Devonian and Carboniferous in the Canning Basin, Western Australia. In: Keep M and Moss S J (eds) The Sedimentary Basins of Western Australia 4, Abstracts. Proceedings of the Petroleum Exploration Society of Australia Symposium, Perth, WA, 2013.

Roelofs, B., Trinajstic, K., Turner, S. and Hairapetian, V. 2014. Vertebrate diversity and biostratigraphy from the Late Devonian to Early Carboniferous in the Canning Basin, Western Australia. Royal Society of Western Australia symposium, Perth.

Roelofs, B., Trinajstic, K., Playton, T., Barham, M., Haines, P., Hocking, R., Grice, K. and Hillbun, K. 2014. Utilisation of Microvertebrates in Biostratigraphy and Chemostratigraphy for the Late Devonian and Early Carboniferous in the Canning Basin, Western Australia. 2014. American Association of Petroleum Geologists, Houston, Texas.

Roelofs, B., Barham, M., Cliff, J., Joachimski, M., Martin, L. and Trinajstic, K. 2015. Application of microvertebrate fossils in paleoclimate reconstructions and chemostratigraphy using biogenic apatite $\delta^{18}O$. 13th International Symposium on Early and Lower Vertebrates: Royal Society of Victoria, Melbourne, Australia.

Table of Contents

F-F Boundary in the Upper Devonian Lennard Shelf Carbonate System, Canning Basin, Western Australia

4. Integrated Stratigraphic Correlation of Upper Devonian Platform-to-Basin Carbonate Sequences, Lennard Shelf, Canning Basin, Western Australia: Advances in Carbonate Margin-to-Slope Sequence Stratigraphy and Stacking Patterns
5. Statements of Co-authors
6. Copyright clearances

List of Figures

List of Tables

1.0 Introduction

1.1 Background

Chronostratigraphy is the branch of geology that studies the rock record in relation to time and integrates event or sequence stratigraphy, magnetostratigraphy, biostratigraphy and chemostratigraphy to determine the temporal context of geological events. The main aim of these methods is to correlate temporally equivalent strata. A successful ARC Linkage Project "Chronostratigraphic framework for the Devonian Canning Basin - a multidisciplinary study of environmental change" (LP0883812) aimed to take an integrated approach to establish a high-resolution chronostratigraphic framework for the Middle to Upper Devonian Canning Basin reef systems, where extensive carbonate platforms provide one of the best exposed and least deformed examples of ancient reef systems in the world (Playford et al., 2009). Despite nearly 350 km of reef outcrop along the Lennard Shelf, exposure is discontinuous and correlation between different sections and facies has proved difficult (Playford, 1976; Playford et al., 2009, Playton et al., 2013). In order to improve chronostratigraphic resolution for the Canning Basin, the Linkage Project (LP0883812) aimed to utilise magnetostratigraphy (see Appendix 1) for the first time in the Lennard Shelf, refine sequence stratigraphy (Appendix 2) for the Devonian, establish enhanced chemostratigraphy (see Appendix 3) and develops microvertebrate biostratigraphy from the Late Devonian to the Early Carboniferous. Conodont biostratigraphy provides the correlative control for the sequence stratigraphic, magnetostratigraphic and chemostratigraphic methods in addition to providing the temporal ranges for microvertebrate taxa. The aim is to incorporate

data from Western Australia into global schemes and improve global chronostratigraphy for this time interval.

1.1.1 Microvertebrate Biostratigraphy

The main focus of this thesis is to determine the utility of microvertebrates from the Canning Basin, Western Australia in biostratigraphy and chemostratigraphy. Biostratigraphy is an effective tool for relative dating and chronostratigraphic correlation. Conodonts and ammonoids are well studied in the Palaeozoic and have proved useful in determining depositional ages in the Canning Reef slope and basinal facies (Glenister and Klapper, 1966, Druce, 1976; Becker, 2000; Becker et al., 1993; Klapper, 2007; summaries in Playford et al., 2009, appendix 1, 2). Nevertheless, conodont and ammonoid taxa have been of limited use in resolving time intervals from sub-surface samples and restricted backreef and lagoonal facies (Seddon, 1970; Nicoll and Druce, 1979; Becker et al., 1991).

Trinajstic and George (2009) recovered co-occurring conodonts and chondrichthyans at Horse Spring (Virgin Hills Formation) and noted the potential for chondrichthyans to be useful for dating more restricted depositional environments in Western Australia where conodonts were absent or long ranging. Chondrichthyan biozones have been determined for the Frasnian and Famennian based on the teeth of Phoebodont sharks (Ginter, 2000). However, a lack of data has meant that these microvertebrate biozones, with the exception of the Gneudna and Virgin Hills formations (Trinajstic and George, 2009), have not been applied in Western Australia. Microvertebrates however, have been utilised for both outcrop and subsurface correlation in Ordovician to Early Devonian strata (see Trinajstic et al.,

2014; Chapter 2 herein). The Frasnian macrovertebrate fauna of the Canning Basin is well described (see Long and Trinajstic, 2010 for a review), in comparison to vertebrate faunas from earlier and later Devonian strata (Long and Trinajstic, 2000; Trinajstic et al., 2014). Despite the use of microvertebrates such as thelodonts (Trinajstic and George, 2009; Hairapetian et al., 2015); acanthodians (Burrow et al., 2012) and placoderm scales (Trinajstic, 1999) for correlation of Frasnian strata across the northern margins of Gondwana, the significant endemic component of the Canning Basin macrofauna (Long and Trinajstic, 2010) limits their use to more regional correlation in north-western Australia.

In eastern Australia vertebrate biozonation for the Palaeozoic is more finely resolved, covering both marine and non-marine strata (Young, 1995; Young and Turner, 2000; Turner and Burrow, 2000). These zonations have culminated from extensive studies of both thelodont and acanthodian scales as well as the teeth and scales of chondrichthyes from over 20 Ages (e.g. Turner, 1986, 1991; Turner and Long, 1987; De Pomeroy, 1996; Turner and Young 1997; Young, 1997; Burrow et al., 1998; review in Burrow et al., 2010). These works have led to a better understanding of faunal distribution and biogeography and highlighted major faunal and temporal differences between eastern and north-western Australia. Current data suggest that the Western Australian fauna is more similar to that occurring along the northern Gondwanan margin than to that in eastern Australia and Antarctica (Burrow et al., 2010; Young et al., 2000; Trinajstic et al., 2014, Hairapetian et al., 2015). This premise; however, requires further investigation as it is possible that a lack of data from Western Australian sites has influenced the interpretation of these faunal relationships.

1.1.2 Faunal turnover in the Late Devonian and Early Carboniferous

The Givetian to end Famennian represented a period of continuous reef building in the Canning Basin (Playford and Lowry, 1966; Southgate et al., 1993, Wood, 2000). However, the nature of the reefs changed from metazoan-microbial dominated (Givetian-Frasnian) to microbial-dominated build-ups in the Famennian, following the Frasnian-Famennian (F-F) extinction event, recognized as one of the five greatest biotic crises of the Phanerozoic (Playford et al., 1984; Sepkoski et al., 1996; George, 1999; Wood, 2000; House, 2002; Stephens and Sumner, 2003). Although both the Late Devonian extinction events resulted in numerous species level extinctions in the marine biosphere, the taxa affected varied, with the Frasnian-Famennian event mostly affecting marine invertebrate species (McGhee, 1982; Copper, 1986; Sepkoski, 1996; Hallam, 1989), and the Late Famennian Hangenberg event, which coincided with the cessation of reef building in the Canning Basin (Playford et al., 2009), affecting primarily vertebrate groups (Walliser, 1996; Sallan and Coates, 2010; Blieck et al., 2010).

Both conodont (e.g. Klapper, 2007) and ammonoid (e.g. House, 1973; Becker, 2001; Becker and House, 2009) faunas show the same patterns of extinction in the Canning Basin as seen in Europe, North America and North Africa. More specifically, a decrease in species diversity is observed around the F-F boundary at Conodont Zone (CZ) 13a, followed by a recovery phase during CZ 13b and a further decrease in diversity at CZ 13c (Becker, 2000; McNamara and Feist, 2006; Klapper, 2007; Feist and McNamara, 2007, 2013; McNamara et al., 2009; Girard et al., 2010). These decreases in faunal diversity correspond to the lower and upper Kellwasser events. Sallan and Coates (2010) recognised key global changes in vertebrate faunas from the Late Devonian to Early Carboniferous. These included a decrease in the

diversity of agnathans and placoderms during the Famennian and final disappearance of the placoderms at the end Devonian. The chondrichthyians, sarcopterygians and tetrapod groups in contrast, saw increased radiation in the Carboniferous. Analysing these recognised events in the Canning Basin is difficult as only limited data is available on the vertebrate fauna that inhabited the Famennian to Tournaisian ramp facies and Famennian fore reef facies of the Canning Basin.

1.1.3 Recognising major geological boundaries

The major biotic crises that occurred around the Frasnian-Famennian boundary are often associated with the deposition of anoxic black shale facies (Hallam and Wignall, 1997; Bond et al., 2004; Becker and Kirchgasser, 2007). These same facies however, are not present in either outcrop or subsurface in the Canning Basin (Becker et al., 1991; George et al., 2014). It has been hypothesized that local tectonic activity may be responsible for the lack of these anoxic facies (Chow et al., 2004). Despite the lack of characteristic lithological changes, carbon isotope stratigraphy has identified excursions associated with the F-F boundary in the Canning Basin (Stephens and Sumner, 2003; George et al., 2014; Hillbun et al., 2015) that correspond to globally recognised $\delta^{13}C$ excursions. Correlative $\delta^{18}O$ global excursions are also recorded across the F-F boundary (e.g. Joachimski and Buggisch, 2002). More data are needed to determine if the $\delta^{18}O$ excursions are present across extinction boundaries in the Canning Basin as only minimal data exists surrounding these boundaries (Playford et al., 1989; Talent et al., 1993).

Due to its resistance to post-mortem modification, bioapatite has become a preferred medium for eliciting Palaeozoic O-isotope records (Joachimski et al., 2009; 2004). The oxygen isotope ratios of conodont fluorohydroxyapatite have been used

for palaeoenvironmental reconstructions and the identification of major shifts in sea water temperature and chemistry associated with key geological boundaries (e.g. Trotter et al., 2008; Sun et al., 2012). However, the general lack of conodont fossils in restricted facies of the Canning Basin limits their practical use in O-isotope analysis to slope and basinal facies. It has been suggested that microvertebrate remains may be used as a substitute for conodonts in chemostratigraphy (Žigaitė et al., 2009; 2010; Barham et al., 2012). Analyses of Palaeozoic marine vertebrate fossils however, have often yielded $\delta^{18}O$ values depleted in ^{18}O when compared to the $\delta^{18}O$ values of associated conodont elements (Joachimski et al., 2004). One of the contributing factors in this depletion may lie in the analytical technique employed. Teeth and scales from fossil gnathostomes are typically heterogeneous, comprising tissues that are mineralised to different degrees. Traditionally, heterogeneous tissues were homogenized prior to analysis as a single entity via gas isotope ratio mass spectrometry (GIRMS). The typical depletion in ^{18}O using this method, likely results from analysing incorporated dentine and/or bone which is more susceptibility of diagenetic alteration due to its less mineralised tissues. Tissue specific analysis, using secondary ion mass spectrometry (SIMS), on modern shark teeth has determined significant variation in $\delta^{18}O$ values between tissues (Žigaitė and Whitehouse, 2014). Crucially however, the data obtained from hypermineralised tissue revealed that enamel hosted $\delta^{18}O$ values are reflective of the water mass in which it precipitated. Using SIMS on Palaeozoic vertebrate elements to elicit O-isotope signatures has yet to be performed, but may prove useful as a chemostratigraphic tool across open, shallow, restricted and fresh- water facies. In addition, if primary O-isotopes signals can be identified in vertebrate fossils, this

technique has the ability to be applied on fossil vertebrate material as old as the Ordovician.

1.1.4 Objectives

1. Define a high-resolution microvertebrate chronology between platform and basin within the Canning Basin for late Givetian through Early Carboniferous strata, and correlate this to known global records for intercontinental correlation.

2. Utilise microvertebrate fossil groups to examine the extent of faunal overturn at key horizons during, and at the end of, the Late Devonian within a robust sedimentological-stratigraphic framework independently dated by conodonts.

3. Utilise geochemical signatures (notably oxygen isotopes) in conodonts and microvertebrate as independent indicators of environmental change and potential proxies for chemical stratigraphy; in order to approximate palaeo- sea-surface temperature and hydrology fluctuations that are not expressed in the sedimentological record of the Canning Basin.

1.2 Materials and methods

To avoid repetition in this thesis, details of the geological settings studied are presented as part of the published papers which comprise subsequent chapters and Appendices 1, 2 and 3. The following section presents a more detailed methodology than appropriate for submission in published papers.

1.2.1 Sample origin and stratigraphic techniques

Sections at Horse Spring, Casey Falls and South Oscar Range were initially measured and sampled by Ted Playton and Eric Tohver in 2008. In 2012 sampling for chemo- and magnetostratigraphic analysis as well as conodont fossils was undertaken by Ted Playton, Kelly Hillbun, Eric Tohver, Jerone Hansma and Kate Trinajstic and Roger Hocking. Subsequent remeasuring of the sections was undertaken in 2013 by Kate Trinajstic and myself, which including photographing and structural measurements of the sections, in additional to further bulk rock sampling (20 kg) for conodont and microvertebrate biostratigraphy. Half of each sample collected was curated at the Geological Survey of Western Australia as a reference. Samples used for the extraction of Givetian macro- and microvertebrate remains were collected in 2012 by Peter Haines and Kate Trinajstic from a site near Cadjebut Mine. Microvertebrate fossils from the Fairfield Group were sourced from unprocessed rocks collected in 2011 and 2013.

1.2.2 Extraction of microvertebrates

The extraction of microfossils from the rock matrix followed the methodology of Jeppsson et al. (1999). Carbonate rock samples weighing between five and 20 kg were each submerged in a 10% buffered acetic acid solution at Macquarie and Curtin universities. At 48 hour intervals rocks and microfossil residues were removed from acid and rinsed in water. Rocks and large fragments were returned to acid and the process repeated. If macrovertebrate remains were exposed following digestion, rocks were thoroughly rinsed in water and left to dry. Cyanoacrelate was then used to coat, support and protect the remains. Once dry the material was resubmerged in the acetic acid solution. Vertebrate remains used for isotopic analysis were not coated in any substance.

Residues resulting from disaggregation of the rock were either separated using a heavy liquid fractionation (Macquarie University) method or sieved (0.125 mm sieve; Curtin University) before being left to dry at room temperature (~24° Celsius). The residues were placed in picking trays and investigated under a Nikon stereomicroscope. A fine (No. 00), moistened paintbrush was used to isolate microvertebrate remains and transfer them to cavity slides.

For SEM imaging, specimens were mounted on adhesive carbon tape, which was fixed to 10 mm diameter aluminium stubs. Specimens photographed using a Zeiss Evo 40XVP SEM at the Centre for Materials Research at Curtin University were coated with 5 μm of platinum. Delicate specimens were left uncoated and imaged using a Hitachi TM-3030 desktop SEM at Applied Geology at Curtin University. Specimens were subject to variable pressures and accelerating voltages ranging from 5-15 kV. Larger fossil specimens were photographed using a Nikon D7100 with a Tokina 100 mm macro lense.

Microvertebrate remains described herein were placed within cavity slides and fixed to the base using methylcellulose. Larger specimens were stored in vials lined in tissue paper. Specimens were registered in the collections at the Western Australian Museum (WAM).

1.2.3 Description of microvertebrates and biostratigraphic control

Classification of vertebrate remains was based on either one or a combination of: comparison to type material; comparison to registered museum specimens; previously determined character states and published diagnosis (Turner, 1991; Goujet and Young, 1995; Lund and Grogan, 1997; Grogan et al., 2012). If precise taxonomic determination to species rank was not possible, open nomenclature to the

family and/or genus level was employed. Descriptive terminology for thelodont taxa followed that of Märss and Ritchie (1998), Märss et al., (2007) and Žigaitė and Goujet (2012), while those of Cappetta et al. (1993) and Ginter et al., (2010) were used in the description of chondrichthyan fossils.

Age constraints for Frasnian and Fmaennian microvertebrate fossils were provided by associated conodont elements. For the Frasnian, the 13-division Montagne Noir (MN) Conodont Zonation (CZ) (Klapper, 1989, 2007) modified by Girard et al., (2005) was followed. For the Famennian, the standard conodont Zonation (Zeigler and Sandberg, 1990) was employed. The conodont zonation of Nicoll and Druce (1979) was used for Carboniferous strata.

1.2.4 Gas Isotope Ratio Mass Spectrometry (GIRMS) analysis

Analyses of phosphatic micro remains and standards were carried out at the Stable Isotope Laboratory at Geozentrum Nordbayern, Friedrich-Alexander University of Erlangen-Nürnberg, under the supervision of Prof. Michael Joachimski.

The methodology was as follows:

1) Biogenic apatite samples comprising well preserved, clean microfossils weighing between 0.5 and 2.2 mg (exact weights of each sample were recorded on a 6 decimal Mettler Toledo AT20 scale) were picked and isolated in 2 ml plastic vials. Approximately 1 mg aliquots of the standards NBS120c and Tübingen apatite were prepared into 2 ml plastic vials in parallel with the unknowns.

2) 33 µl of 2M HNO_3 was added to each vial of phosphatic material (standards and unknowns) weighing between 0.5 and 1.5 mg. 66 µl of 2M HNO_3 was added to samples weighing in excess of 1.5 mg. Samples were left for 48 hours to dissolve. This process resulted in a clear solution over a minor organic residue situated at the base of the vial.

3) 2M KOH was added to the vials in equivalent volumes (33 µl or 66 µl) as the acid in step 2 to neutralise the solutions.

4) Equivalent volumes (33 µl or 66 µl) of 4% HF was added to the samples in order to precipitate liberated Ca^{2+} ions from the solution.

5) Vials were placed within a Heraeus multifuge and centrifuged for 10 minutes at 3000 rpm to separate the clear phosphate-bearing solution from the calcium fluoride precipitate and organic residues. The supernatant was subsequently pipetted into new vials. Washings, resulting from the addition of ~20 µl of distilled water into residual vials, were also pipetted into the fresh containers to optimise phosphate solution yields. The old vials containing the calcium fluoride and organic precipitate were then discarded.

6) 500 to 1000 µl of silver amine solution (0.34 g $AgNO_3$, 0.28 g NH_4NO_3, 1 ml 25% NH_3) was added to each of the sample vials. Initial addition of the silver amine solution caused the development of a yellow cloudiness. Sufficient silver amine solution must be added until the liquid becomes transparent.

7) The vials were placed within an oven at 60^o Celsius and left for between 8 and 24 hours until all the ammonia had evaporated and Ag_3PO_4 crystals formed, lining the vial.

8) Approximately 1.5 ml of distilled water was added to, and then pipetted out of, each of the vials in order to dissolve and remove chemical residues whilst leaving the insoluble Ag_3PO_4 crystals intact.

9) Step 8 was repeated three times in order to remove all remaining chemical residue. Each time the vials were filled with 1.5 ml of water, they were placed in an ultrasonic bath for 15 minutes.

10) After removal from the ultrasonic bath, the final distilled water washings were pipetted out leaving the Ag_3PO_4 crystals. The vials were then placed in an oven at 60^o for 24 hours until dry. Once dry the samples were left at room temperature before being weighed with a Mettler Toledo AT20 scale.

11) The dry Ag_3PO_4 crystals were removed from the vials into a clean mortar. Foreign contaminants were carefully removed under a microscope with a sterilised pin.

12) Using a clean pestle, the Ag_3PO_4 were ground and homogenised into a fine powder, followed by transferal of the sample into a new, labelled 2 ml plastic vial.

13) Between 0.10 and 0.40 mg of homogenised Ag_3PO_4 was measured into small 0.2 ml silver (Ag 99.99) foil caps. These were then folded to seal in the sample and expel any air. A total of three analyses were taken from each sample and placed within a gridded sample tray. The position of each sample was recorded on to a master sheet.

14) The folded silver caps were placed within the sample carousel of the TC-EA (high temperature reduction furnace) before being dropped one at a time into

the machine. At 1450 °C the silver phosphate is reduced and CO forms as the analyte gas (Vennemann et al., 2001). The CO is transferred in a helium stream through a gas chromatograph via a Conflo III interface to a ThermoFinnigan Delta Five Plus mass spectrometer and reported in ‰ relative to Vienna Standard Mean Ocean Water (Vienna Standard Mean Ocean Water). Accuracy and reproducibility of results were maintained via:

a) Comparing and averaging the results of triplicate analyses of each sample.

b) Running both international (NBS120c) and internal (Tübingen apatite and a synthesised Ag_3PO_4) standards at the beginning, middle and end of every day.

c) Standards of either NBS120c or Tübingen apatite prepared in the same batch as the other samples and tested as unknowns every fourth run.

d) Monitoring standard gas throughflow and backgrounds on the instrumentation.

15) Results were adjusted for variation, attributed to machine 'drift', by monitoring the values of tested isotopic standards.

1.2.5 Secondary Ion Mass Spectrometry (SIMS) analysis

Vertebrate fossils were placed within beakers containing 50 ml of distilled water and then transferred to a sonic bath for 1-3 minutes (with regular visual inspections to avoid damage) in order to remove any abiogenic grains or detritus. The fossils were then removed and left to dry for 48 hours. Microvertebrate remains, with single pieces of *Carcharhinus plumbeus* tooth fragments and Durango apatite

standard grains, were placed within a 10 mm diameter circle on double sided tape adhered to a glass plate. Large teeth were cut labio-lingually using a Dremel rotary tool then sanded with 1200 grit sandpaper prior to mounting on the tape along the cut surface. A 25 mm plastic tube, acting as the mould, was placed on the tape with the collection of adhered fossils centrally located. Struers EpoFix epoxy resin was carefully mixed according to manufacture instructions and sonicated in order to remove all bubbles. The mixture was then slowly poured into the slightly tilted mould and allowed to flood across the surface in order to reduce bubble formation. For mounts bearing larger fossil fragments, the moulds were also placed in a vacuum flask in order to assist resin impregnation. All mounts were filled to ~10 mm (to account for any leakage as well as loss of volume during curing) and left for a minimum of 48 hours to set.

Once cured the mount was removed from the mould and adhesive tape and cut to an initial thickness of 5 mm, removing the irregular meniscus of the mount. The face bearing fossils was initially ground used a 1200 grit sandpaper to remove any obvious signs of relief and expose the fossil tissue of interest. The mount was then fixed in a Struers Rotopol-35 polishing machine and polished with consecutively finer Largo polishing discs and corresponding Struers Diapro diamond suspensions (9 µm, 3 µm and 1 µm) until the scratches from the previous polishing were sufficiently reduced. The duration for each polishing stage reduced with successively fine cloths to prevent topographic relief. Struers DP-Lubricant was used with each polishing run to prevent scratching of the mount face. After each polishing session, the mounts were rinsed and then placed into a clean 50 ml beaker containing distilled water. Three minutes cleaning in an ultrasonic bath was used to remove any residual diamond paste. Mounts were then inspected under a stereomicroscope to

determine if further polishing was required. Once polishing was complete, the mounts were cleaned with detergent, distilled water and ethanol prior to being coated with 30 nm of gold.

Detailed procedure using the CAMECA IMS 1280 is provided in the materials and methods of Chapter 6.

1.4 Thesis Overview

Chapter 1 introduces the Canning Basin and its importance as a study area due to the preservation of Late Devonian reef complexes and Late Devonian to Early Carboniferous ramp deposits. The chapter introduces the various methods used to correlate different facies and the issues associated with these techniques. Microvertebrate fossils are introduced as a tool in biostratigraphic and chemostratigraphic based correlation.

Chapter 2 is a peer reviewed paper detailing the Palaeozoic vertebrate fossils of Western Australia spanning the Ordovician to the Permian. Contribution towards this paper included both a review on microvertebrate taxa from various ages and formations in the Lennard Shelf, as well as information on the use of microfossils in both regional and global correlation as well as providing data for biogeographic recontructions.

Chapter 3 provides additional data on a previously described Frasnian Phoebodont fauna from the Canning Basin. This includes refined age ranges for known taxa as well as the first documentation of other shark species from the Lennard Shelf. In addition, a new species of filter feeding shark is described. The Famennian shark fauna of the Canning Basin is described in detail for the first time in this chapter and includes species previously undescribed from the basin.

Chapter 4 focuses on the discovery of Famennian thelodont genera. This taxon had been previously thought extinct at the Frasnian-Famennian boundary. The presence of the youngest known thelodont remains in the Canning Basin offer the potential for a thelodont biostratigraphic scheme to extend into the latest Devonian. Faunal connections between the central Iran and north-western Australia are further explored. Contributions to this chapter included the sampling, figuring and writing up of the Australian material as well as contributions toward the figures of the Iranian based thelodont scales.

Chapter 5 provides an analysis of 18 shark species from the latest Devonian to Early Tournaisian. This chapter provides the first known Canning Basin occurrences of many cosmopolitan shark taxa. Faunal links with other areas of Gondwana are expanded on from previous chapters.

Further uses of microvertebrates in stratigraphic correlation are explored in Chapter 6. In order to employ microvertebrates as a basis for chemostratigraphic correlation, the identification of original O-isotope signatures is necessary. This chapter explores the O-isotope fidelity and ecological and palaeoenvironmental significances of signal from a range of taxa in addition to analysing the differences in O-isotopes between specific tissues. This chapter is included as a corrected version following recommendations by the examiners. The final version submitted to the journal of Palaeogeography, Palaeoclimatology, Palaeoecology is included as Appendix 1.

Chapter 7 summarises the major findings of this thesis, including: newly resolved biostratigraphic schemes using microvertebrates in the Canning Basin; the implications of the newly discovered shark species for palaeogeographical

reconstructions; and the potential for hypermineralised tissue in microvertebrates to be used in palaeoenvironmental reconstructions and chemostratigraphy.

1.5 References

Barham, M., Joachimski, M., Murray, J., Williams, D., 2012a. Diagenetic alteration of the structure and δ 18 O signature of Palaeozoic fish and conodont apatite: Potential use for corrected isotope signatures in palaeoenvironmental interpretation. Chemical Geology 298, 11-19.

Becker, R. 2000. Ammonoidea. In: Wright, A.J., Young, G.C., Talent, J.A. and Laurie, J.R. (Eds). Paleobiogeography of Australasian faunas and floras. Association of Australasian Paleontologists, Memoir 23, 177-180.

Becker, R. 2001. Palaeobiogeographic relationships and diversity of Upper Devonian ammonoids from Western Australia. Records of the Western Australian Museum Supplement 58, 385-401.

Becker, R. and House, M. 2009. Devonian ammonoid biostratigraphy of the Canning Basin. Geological Survey of Western Australia, Bulletin 145, 415-439.

Becker, R. and Kirchgasser, W. 2007. Devonian events and correlations.Geological Society of London, Special Pubiicaiton 278, 1-283.

Becker, R.T., House, M.R. and Kirchgasser, W.T. 1993. Devonian goniatite biostratigraphy and timing of facies movements in the Frasnian of the Canning Basin, Western Australia. Geological Society, London, Special Publications 70, 293-321.

Becker, R.T., House, M.R., Kirchgasser, W.T. and Playford, P.P. 1991. Sedimentary and faunal changes across the Frasnian/ Famennian boundary in the Canning Basin of Western Australia. Historical Biology 5, 183-196.

Blieck, A., Clement, G. and Streel, M. 2010. The biostratigraphical distribution of earliest tetrapods (Late Devonian) - a revised version with comments on biodiversification. In Vecoli, M., Clément, G. and Meyer Berthaud, B. (eds), The terrestrialization process: modelling complex interactions at the biosphere-geosphere interface. Geological Society of London, Special Publication 339, 129-138.

Bond, D., Wignall, P.B. and Racki, G. 2004. Extent and duration of marine anoxia during the Frasnian-Famennian (Late Devonian) mass extinction in Poland, Germany, Austria and France. Geological Magazine 141, 173-193.

Burrow, C.J., Long, J.A. and Turner, S. 1998. Lower Devonian microvertebrates from the Point Hibbs Formation, Tasmania. Alcheringa 22, 9-20.

Burrow, C.J., Trinajstic, K. and Long. J.A. 2012. First acanthodian from the Upper Devonian (Frasnian) Gogo Formation, Western Australia. Historical Biology 24, 349-357.

Burrow, C.J., Turner, S. and Young, G.C.2010. Middle Palaeozoic microvertebrate assemblages and biogeography of East Gondwana (Australasia, Antarctica). Palaeoworld 19, 37-54.

Cappetta, H., Duffin, C.J. and Zidek, J. 1993. Chondrichthyes. In: M.J. Benton (Eds). The Fossil Record 2: 593-609. Chapman and Hall, London.

Chow, N., George, A.D. and Trinajstic, K.M. 2004. Tectonic control on development of a Frasnian-Famennian (Late Devonian) palaeokarst surface, Canning Basin reef complexes, northwestern Australia. Australian Journal of Earth Sciences 51, 911 - 917

Copper, P. 1986. Frasnian/Famennian mass extinction and cold-water oceans. Geology 14, 835-839.

De Pomeroy, A.M. 1996. Biostratigraphy of Early and Middle Devonian microvertebrates from Broken River, north Queensland. Records of the Western Australian Museum 17, 417-437.

Druce, E.C. 1976. Conodont biostratigraphy of the Upper Devonian reef complexes of the Canning Basin, Western Australia. Bulletin 158. Bureau of Mineral Resources, Geology and Geophysics.

Feist, R. and McNamara, K.J. 2007. Biodiversity, distribution and patterns of extinction of the last odontopleuroid trilobites during the Devonian (Givetian, Frasnian). Geological Magazine 144, 777-796.

George, A.D. 1999. Deep-water stromatolites, Canning Basin, northwestern Australia. Palaios 14, 493-505.

George, A.D., Chow, N. and Trinajstic, K.M., 2014. Oxic facies and the Late Devonian mass extinction, Canning Basin, Australia. Geology 42, 327-330.

Ginter, M. 2000. Late Famennian pelagic shark assemblages. Acta Geologica Polonica 50, 369-386.

Ginter, M. and Ivanov, A. 1995. Middle ⁄ Late Devonian phoebodont-based ichthyolith zonation. Geobios, Memoire Special 19, 351-355.

Ginter, M., Duffin, C. and Hampe. O. 2010. Chondrichthyes (Paleozoic Elasmobranchii: teeth). In: Schultze H-P., (ed.) Handbook of Paleoichthyology, vol. 3D. Friedrich Pfeil Verlag, München.

Girard, C., Phuong, T.H., Savage, N. and Renaud, S. 2010. Temporal dynamics of the geographic differentiation of Late Devonian *Palmatolepis* assemblages in the Prototethys. Acta Palaeontologica Polonica 55, 675-687.

Girard, C., Klapper, G. and Feist, R. 2005. Subdivision of the terminal Frasnian *linguiformis* conodont Zone, revision of the correlative interval of the

Montagne Noire Zone 13, and discussion of the stratigraphically significant associated trilobites. In: Over, D.J., Morrow, J.R. and Wignall, P.B. (Eds). Understanding Late Devonian and Permian-Triassic biotic and climatic events: towards an integrated approach: Towards an Integrated Approach. Developments in Paleontology and Stratigraphy Series 20, 181-198. Elsevier, Amsterdam.

Glenister, B.F. and Klapper, G. 1966. Upper Devonian conodonts from the Canning Basin, Western Australia. Journal of Palaeontology 40, 777-842.

Goujet, D. and Young, G.C. 1995. Interrelationships of placoderms revisited. Geobios 28, 89-95

Grogan E.D., Lund, R. and Greenfest-Allen, E. 2012. The origin and relationship of early chondrichthyans. Biology of Sharks and Their Relatives. Second Edition, Carrier, J.C., Musick J.A. and Heithaus, M.R. (eds). CRC Press, Taylor & Francis group, Boca Raton.

Hairapetian, V., Roelofs, B.P.A., Trinajstic, K.M., and Turner, S. 2015. Famennian survivor turiniid thelodonts of North and East Gondwana. Geological Society, London, Special Publications 423, 423-433..

Hallam, A. and Wignall, P.B. 1997. Mass Extinctions and their Aftermath. Oxford University. Press, Oxford.

Hallam, A. 1989. The Case for Sea-Level Change as a Dominant Causal Factor in Mass Extinction of Marine Invertebrates, Philosophical Transactions of the Royal Society 325, 437-455

Hillbun, K., Playton, T.E., Tohver, E., Ratcliffe, K., Trinajstic, K., Roelofs, B., Caulfield-Kerney, S., Wray, D., Haines, P., Hocking, R., 2015. Upper Kellwasser carbon isotope excursion pre-dates the F-F boundary in the Upper

Devonian Lennard Shelf carbonate system, Canning Basin, Western Australia. Palaeogeography, Palaeoclimatology, Palaeoecology 438, 180-190.

House, M. 1973. An analysis of Devonian goniatite distributions. Palaeontology Special Papers 12, 305-317.

House, M.R. 2002. Strength, timing, setting and cause of mid-Palaeozoic extinctions. Palaeogeography. Palaeoclimatology. Palaeoecology 181, 5–25

Jeppsson, L., Anehus, R, and Fredhold, D. 1999. The Optimal Acetate Buffered Acetic Acid Technique for Extracting Phosphatic Fossils. Journal of Paleontology 73, 964-972.

Joachimski, M., Breisig, S., Buggisch, W., Talent, J., Mawson, R., Gereke, M., Morrow, J., Day, J. and Weddige, K. 2009. Devonian climate and reef evolution: insights from oxygen isotopes in apatite. Earth and Planetary Science Letters 284, 599-609.

Joachimski, M.M. and Buggisch, W. 2002. Conodont apatite δ18O signatures indicate climatic cooling as a trigger of the Late Devonian mass extinction. Geology 30, 711-714.

Joachimski, M.M., Van Geldern, R., Breisig, S., Buggisch, W., Day, J., 2004. Oxygen isotope evolution of biogenic calcite and apatite during the Middle and Late Devonian. International Journal of Earth Sciences 93, 542-553.

Klapper, G. 1989. The Montagne Noire Frasnian (Upper Devonian) conodont succession. In: McMillan, N.J., Embry, A.F. and Glass, D.J. (eds) Devonian of the World 3, 449-468. Canadian Society of Petroleum Geologists Memoir 14.

Klapper, G. 2007. Frasnian (Upper Devonian) conodont succession at Horse Spring and correlative sections, Canning Basin, Western Australia. Journal of Paleontology 81, 513-537.

Long, J.A. and Trinajstic, K. 2000. Devonian micro vertebrate faunas of Western Australia. Courier Forschungs-Institut Senckenberg 22, 471-485.

Long, J.A. and Trinajstic, K. 2010. The Late Devonian Gogo Formation Lägerstatte of Western Australia: exceptional early vertebrate preservation and diversity. Annual Review of Earth and Planetary Sciences 38, 255-279.

Lund, R. and Grogan, E.D. 1997. Relationships of the Chimaeriformes and the basal radiation of the Chondrichthyes. Reviews in Fish Biology and Fisheries 7, 65-123.

Märss, T. and Ritchie, A. 1998. Articulated thelodonts (Agnatha) of Scotland. Transactions of the Royal Society of Edinburgh: Earth Sciences 88, 143-195.

Märss, T., Turner, S. and Karatajute-Talimaa, V. N. 2007. Agnatha II - Thelodonti. Volume 1B. In: Schultze, H. P. (Eds). Handbook of Paleoichthyology.

McGhee, G.R. 1982. The Frasnian-Famennian extinction event: A preliminary analysis of Appalachian marine ecosystems. Geologic Society of America 182, 491-500.

McNamara, K.J. and Feist, R. 2006. New styginids from the Late Devonian of Western Australia - The last corynexochid trilobites. Journal of Paleontology 80, 981-92.

McNamara, K., Feist, R. and Ebach, M. 2009. Patterns of evolution and extinction in the last harpetid trilobites during the Late Devonian (Frasnian). Palaeontology 52, 11-33.

Nicoll, R.S. and Druce, E.C. 1979. Conodonts from the Fairfield Group, Canning Basin, Western Australia. Bureau of Mineral Resources Australia Bulletin 190, 1-134.

Playford, P.E. 1976. Devonian Reef Complexes of the Canning Basin, Western Australia. 25th International Geological Congress, Excursion Guide No. 38A, Sydney, Australia.

Playford, P.E. and Lowry D.C. 1966. Devonian reef complexes of the Canning Basin, Western Australia. Geological Survey of Western Australia Bulletin 118, 1-150.

Playford, P.E., Hurley, N.F. and Middleton, M.F. 1989. Reefal platform development, Devonian of the Canning Basin, Western Australia. Controls on carbonate platform and basin development. SEPM Special Publications 44, 187-202.

Playford, P.E, Hocking, R.M. and Cockbain, A.E. 2009. Devonian reef complexes of the Canning Basin, Western Australia. Geological Survey of Western Australia Bulletin 145.

Playford, P.E., McLaren, D.J., Orth, C.J., Gilmore, J.S. and Goodfellow, W.D. 1984. Iridium anomaly in the Upper Devonian of the Canning Basin, Western Australia. Science 226, 437-439.

Playton, T. E., Montgomery, P., Tohver, E., Hillbun, K., Katz, D., Haines, P., Trinajstic, K., Yan, M., Hansma, J., Pisarevsky, S., Kirschvink, J., Cawood, P., Grice, K., Tulipani, S., Ratcliffe, K., Wray, D., Caulfield-Kerney, S., Ward, P. and Playford, P.E. 2013. Development of a regional stratigraphic framework for Upper Devonian reef complexes using integrated chronostratigraphy: Lennard Shelf, Canning Basin, Western Australia. In:

Keep, M. and Moss, S. J. (Eds). The Sedimentary Basins of Western Australia IV. Proceedings of the Petroleum Exploration Society of Australia Symposium, Perth, Western Australia.

Sallan, L.C. and Coates, M.I. 2010. End-Devonian extinction and a bottleneck in the early evolution of modern jawed vertebrates. Proceedings of the National Academy of Sciences 107, 10131-10135.

Seddon, G. 1970: Frasnian conodonts from the Sadler Ridge - Bugle Gap area, Canning Basin, Western Australia. Geological Society of Australia 16, 723-753. Sydney.

Sepkoski, J.J. 1996. Patterns of Phanerozoic extinction: a perspective from global data bases. In: Walliser, O.H. (Ed.), Global Events and Event Stratigraphy in the Phanerozoic. Springer, Berlin.

Southgate, P.N., Kennard. J.M., Jackson, M.J., O'Brien, P.E. and Sexton, M.J. 1993. Reciprocal lowstand clastic and highstand carbonate sedimentation, subsurface Devonian reef complex, Canning Basin, Western Australia. In: Loucks, R.G. and Sarg, J.F. (Eds). Carbonate sequence stratigraphy, recent developments and applications. American Association of Petroleum Geologists, Memoir 57, 157-159.

Stephens, N.P. and Sumner, D.Y., 2003. Famennian microbial reef facies, Napier and Oscar Ranges, Canning Basin, western Australia. Sedimentology 50, 1283-1302.

Sun, Y., Joachimski, M.M., Wignall, P.B., Yan, C., Chen, Y., Jiang, H., Wang, L. and Lai, X., 2012. Lethally hot temperatures during the Early Triassic greenhouse. Science 338, 366-370.

Talent, J.A., Mawson, R., Andrew, A.S., Hamilton, P.J. and Whitford, D.J. 1993. Middle Palaeozoic extinction events: faunal and isotopic data. Palaeogeography, Palaeoclimatology, Palaeoecology 104, 139-152.

Trinajstic, K. 1999. New anatomical information on *Holonema* (Placodermi) based on material from the Frasnian Gogo Formation and the Givetian-Frasnian Gneudna Formation, Western Australia. Geodiversitas 21, 69-84.

Trinajstic, K. and George, A.D. 2009. Microvertebrate biostratigraphy of Upper Devonian (Frasnian) carbonate rocks in the Canning and Carnarvon basins of Western Australia. Palaeontology 52, 641.

Trinajstic, K., Roelofs, B., Burrow, C., Long, J., and Turner, S. 2014. Devonian vertebrates from the Canning and Carnarvon Basins with an overview of Paleozoic vertebrates of Western Australia. Journal of the Royal Society of Western Australia 97, 133-151.

Trotter, J.A., Williams, I.S., Barnes, C.R., Lécuyer, C. and Nicoll, R.S., 2008. Did cooling oceans trigger Ordovician biodiversification? Evidence from conodont thermometry. Science 321, 550-554.

Turner, S. 1986. Vertebrate fauna of the Silverband Formation, Grampians, western Victoria. Proceedings of the Royal Society of Victoria 98, 53-62.

Turner, S. 1991. Palaeozoic vertebrate microfossils in Australasia. In: Vickers-Rich, P., Monaghan, J.M., Baird, R.F. and Rich, T.H. (eds) Vertebrate palaeontology of Australasia, pp. 429-464. Pioneer Design Studio, Melbourne.

Turner, S., Burrow, C.J., 2000. Annotations to the Devonian Correlation Table, B705di000-B70ds00: Microvertebrate zonations of East Gondwana. In:

Weddige, K. (Ed.), Devon-Korrelationstabelle. Ergänzungen 2000. Senckenberg lethaea 80, 761-763.

Turner, S. and Long, J.A. 1987. Carboniferous palaeoniscoid fishes (Osteichthyes, Actinopterygii) from Queensland. Memoirs of the Queensland Museum 25, 193-200.

Turner, S. and Young, G.C. 1997. Devonian vertebrate response to eustatic sea level changes. pp. 117-127. In House, M.R. and Ziegler, W. (Eds) On Devonian sea-level fluctuations. 1994 IGCP 328:SDS DECWOL volume, Courier Forschungsinstitut Senckenberg vol. 199, 146 pages. Frankfurt.

Vennemann, T., Hegner, E., Cliff, G. and Benz, G. 2001. Isotopic composition of recent shark teeth as a proxy for environmental conditions. Geochimica et Cosmochimica Acta 65, 1583-1599.

Walliser, O.H. 1996. Global Events and Event Stratigraphy in the Phanerozoic - Results of the International Interdisciplinary Cooperation in the IGCPProject 216, Global Biological Events in Earth History. Springer, Berlin and Heidelberg.

Wood, R. 2000. Palaeoecology of a Late Devonian back reef, Canning Basin, Western Australia. Palaeontology 43, 671-703.

Young, G.C. 1995. Australian Phanerozoic timescales 4: Devonian. Record 1995/33. Australian Geological Survey Organisation.

Young, G.C. 1997. Ordovician microvertebrate remains from the Amadeus Basin, central Australia. Journal of Vertebrate Paleontology 17, 1-25.

Young, G.C. and Turner, S. 2000. Devonian microvertebrates and marine nonmarine correlation in East Gondwana: overview. In: Blieck, A. and Turner, S. (eds) Palaeozoic vertebrate biochronology and global marine/non-

marine correlation. Final report of IGCP 328 (1991-1996), pp. 453-470. Courier Forschungsinstitut Senckenberg 223.

Young, G.C., Moody, J. and Casas, J. 2000. New discoveries of vertebrates from South America, and implications for Gondwana-Euramerica contact. Comptes Rendus de l'Académie des Sciences, Paris 331, 755-761.

Žigaitė, Ž. and Goujet, D. 2012. New observations on the squamation patterns of articulatedspecimens of Loganellia scotica (Traquair, 1898) Vertebrata: Thelodonti) from the Lower Silurian of Scotland. Geodiversitas 24, 253-270.

Ziegler, W. and Sandberg, C.A. 1990. The Late Devonian standard conodont zonation. Courier Forshungsinstitut Senckenberg 121, 1-115.

Žigaitė, Ž. and Whitehouse, M., 2014. Stable oxygen isotopes of dental biomineral: differentiation at the intra-and inter-tissue level of modern shark teeth. GFF 136, 337-340.

Žigaitė, Ž., Joachimski, M. and Lehnert, O. 2009. Stable oxygen isotope stratigraphy using conodontbiogenic apatite from the Pridolof the Baltic Basin. In: Corriga, M. and Piras, S. (eds) Time and life in the Silurian: a multidisciplinary approach. Bollettino della Società Paleontologica Italiana 48, 356-360.

Žigaitė, Ž., Joachimski, M.M., Lehnert, O., Brazauskas, A. 2010. The 18O/16/O ratio in verterbate biogenic apatite as a proxy to Palaeozoic seawater temperatures. Palaeogeography, Palaeoclimatology, Palaeoecology 294, 242–247.

2.0 Devonian vertebrates from the Canning and Carnarvon Basin with an overview of Palaeozoic vertebrates of Western Australia

Trinajstic, K. [1], **Roelofs, B**. [2], Burrow, C. [3], Long, J. [4], and Turner, S.[5]

[4]Kate Trinajstic*. Department of Environment and Agriculture, Curtin University, GPO Box U1987, Perth, WA 6845, Australia. K.Trinajstic@curtin.edu.au

[2]Brett Roelofs. Department of Applied Geology, Curtin University, GPO Box U1987 Perth, WA 6845, Australia. brett.roelofs@postgrad.curtin.edu.au

[3]Carole Burrow. Queensland Museum, Ancient Environments, 122 Gerler Road, Hendra, Qld 4011, Australia. carole.burrow@gmail.com

[4]John Long. School of Biological Sciences, Flinders University, POB 2100, Adelaide, SA 5001, Australia. john.long@flinders.edu.au

[5]Sue Turner. Museum Victoria, PO Box 666, Melbourne, Vic 3001, Australia. paleodeadfish@yahoo.com

2.1 Abstract

A diverse vertebrate fauna, comprising both micro- and macrovertebrate remains, is known from the Palaeozoic of Western Australia. However, it is the Late Devonian fauna of the Gogo Formation that shows exceptional preservation and which is the best known. Advances in tomographic techniques, both micro-CT and synchrotron, have revealed new histological data providing information on bone growth, muscle attachments and the evolution of teeth. The fishes from the Gogo Formation have also revealed new information on the evolution of reproductive structures and live

birth in early vertebrates. Recent work on the Frasnian reefs that crop out along the Lennard Shelf and mineral drillcore through Palaeozoic sedimentary rocks have yielded scales of agnathan thelodonts, and the bones, teeth and scales of sharks, acanthodians and osteichthyans, all of which have increased our knowledge of Ordovician-Late Devonian microfaunas in the Canning Basin, contributing to our understanding of biostratigraphy and correlation within Australia and globally. Less work has been undertaken in the Carnarvon Basin, although like the Canning Basin this has concentrated on Late Devonian strata. More recently, work has commenced on describing Early Carboniferous faunas from the Canning, Carnarvon and Bonaparte Basins. All this work is providing information on faunal patterns and exchange of vertebrates through the Palaeozoic. However, the palaeogeographic evidence provided by the vertebrates is sometimes at odds with palaeogeographic reconstructions based on palaeomagnetic evidence and further investigation is required to resolve these differing interpretations.

2.2 Introduction

Palaeozoic fossil fishes of Western Australia, particularly those from the Gogo Formation Lagerstätten located in the Canning Basin, have been invaluable for investigating major evolutionary transitions due to the exceptional preservation and diversity of the fauna. The gnathostomes (jawed vertebrates) recovered from the Gogo Formation in the Kimberley region comprise members of all the major groups and demonstrate key evolutionary shifts from the development of jaws and teeth, the first expression of live-young bearing invertebrates, to the emergence of stem tetrapods. However, and unlike many other sites in the State, to date no jawless vertebrates have been recovered from this site. In contrast to the excellent

preservation found in the fossils of the Gogo Formation, those from the more southerly Carnarvon Basin are disarticulated but show high faunal diversity.

In Western Australia the fossil record of Palaeozoic fishes includes both microvertebrate and macrovertebrate remains (Long and Trinajstic, 2000, 2010; Burrow et al., 2010). The majority of the research conducted to date has been on the Devonian, especially Late Devonian marine faunas, with studies on Ordovician, Silurian, Carboniferous and Permian fossils less common. There are no reports of Cambrian vertebrate fossils from Western Australia, although rare, purported vertebrate fossils of this age are known from deposits in central Australia (Young et al., 1996). Studies on Western Australian Ordovician to Early Devonian taxa are restricted to microvertebrate faunas recovered from mineral drillcore. However, the extensive outcrops of Devonian reefs in the Canning Basin are rich in both macro- and microvertebrate faunas and numerous studies on both have been undertaken.

In the early 20th century predominantly morphological descriptions and taxonomic studies were undertaken. In the latter part of the 20th century research began to focus on biostratigraphy, particularly in the areas of marine-non-marine correlation under the UNESCO: IUGS IGCP328 Palaeozoic Microvertebrates project led by Alain Blieck, Susan Turner and Gavin Young (Blieck and Turner, 2000). Unlike many of the currently used invertebrate zone fossils including conodont elements, Palaeozoic fish often occur in transitional environments, with the same species inhabiting marine, nearshore and/or non-marine facies. Some marine units bearing microvertebrates are extremely well dated through tying the vertebrate faunas to standard conodont zonations (Trinajstic and George, 2009). In continental rocks microvertebrates are often the only age indicators preserved. Since 1980 there has been to recover microvertebrate remains from Gondwanan Palaeozoic rocks

from Australia and neighbouring countries (Long, 1990; Turner, 1982a, b, 1991, 1993, 1997; Young, 1986, 1987; Basden et al., 2000; Young and Turner, 2000; Burrow, 2002; Macadie, 2002; Burrow et al., 2010; Young et al., 2010). Morphological studies of macrovertebrates have recently taken the forefront again with the advent of new computerised tomographic techniques, allowing for the first time non-destructive histological 'sectioning' of dermal plates and in situ teeth and scales at high resolution. The fossils from the Gogo Formation have been significant in the utilisation of these new technologies in answering questions on the evolution and development of teeth (Rücklin et al., 2012) and scales (Qu et al., 2013a, b), muscle attachments to bone (Sanchez et al., 2012, 2013), soft tissue preservation (Trinajstic et al., 2013) and reproduction in vertebrate animals (Long et al., 2008, 2009; Ahlberg et al., 2009; Trinajstic and Johanson, 2014; Trinajstic et al., in press a). Knowledge of the diversity and stratigraphy of vertebrate faunas from the three Palaeozoic basins in Western Australia is variable, with some faunas, e.g. the Gogo fauna, having been more studied than others, e.g. the Moogooree Limestone and Utting Calcarenite faunas. However, recent research has given greater insights into the diversity, taxonomy, phylogeny and biogeographic relationships of the Western Australian faunas and indicates differences from the longer-studied faunas in central and eastern Australia.

2.3 Canning Basin

The Palaeozoic Canning Basin is characterised by deposition of fine-grained marine clastics and carbonates on extensive carbonate platforms and marine shelves (Cadman et al., 1993). Vertebrate fossils are known from Ordovician to Carboniferous sedimentary rocks. One of the most studied areas is the Upper

Devonian reef complexes, which are well exposed along the Lennard Shelf and form a belt ~350 km long and up to 50 km wide (Hocking et al., 2008). However, the units can be discontinuous at times, narrow and devoid of complete sections due to margin collapse, as is evident in the Napier Range (Shen et al., 2008). The Frasnian strata of Western Australia, especially those in the Canning Basin, have had more numerous studies undertaken on them than those in other areas and ages, yielding a variety of macro- and microvertebrate fossils (Long, 1993). The strata are divided into a number of formations representing different reef facies, some of which are laterally equivalent. For example, the contemporaneous Gogo, Saddler and Pillara formations represent basinal, slope and backreef facies, respectively (Playford et al., 2009).

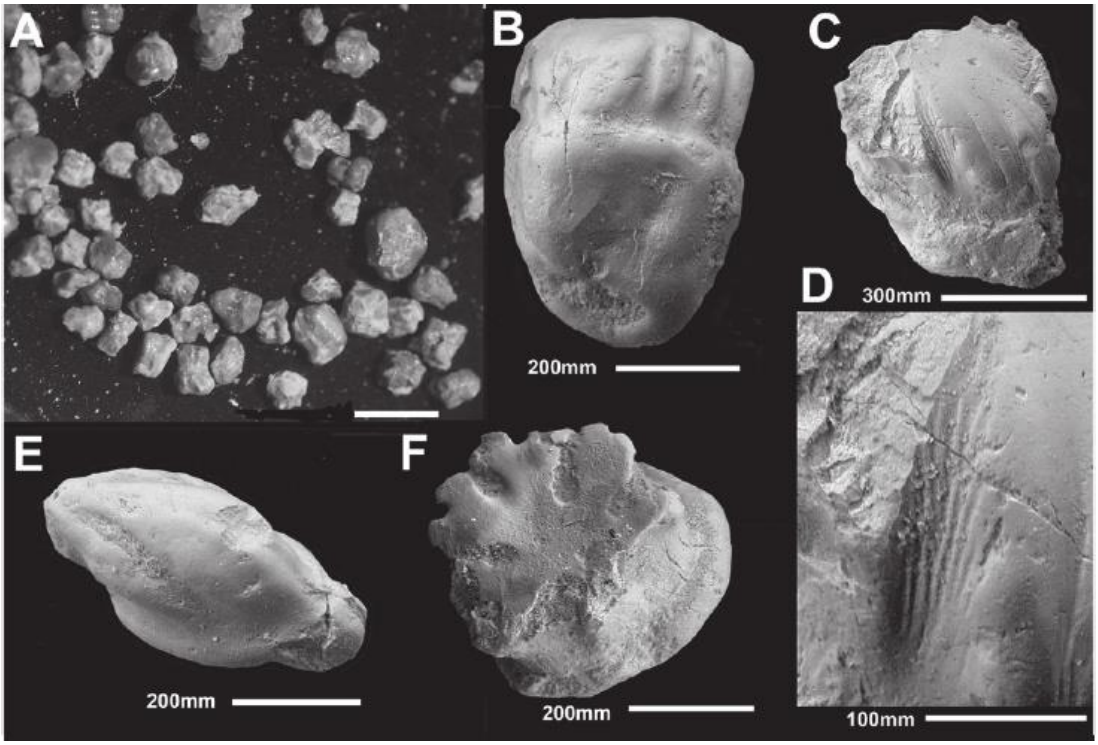

Figure 2.1. Thelodont scales from Wilson Cliffs 1, Kidston Sub-basin. (A) Isolated scales with grains of quartz attached. (B) Eroded head scale in lateral view. (C) Body scale in anterior view showing linear micro-ornament. (D) Detail of micro-ornament. (E) Body scale in lateral view. (F) Head scale in crown view.

The best known of these in respect to vertebrate fauna is the early Frasnian Gogo Formation, which represents the basinal facies of the reef complex (Long and Trinajstic, 2010). This fauna is represented exclusively by macroremains.

The Virgin Hills Formation extends from the lower Frasnian to the uppermost Famennian and represents both basinal and reef slope facies (Playford et al., 2009).Rare macrovertebrate remains, mostly of isolated placoderm plates, have been recovered from the Famennian part of the measured section whereas microvertebrates are common from the Frasnian and Famennian reef-slope facies (Trinajstic and Long, 2009; Hansma et al., 2015).

2.4 Vertebrate fossils of the Canning Basin

2.4.1 Ordovician

The first description of an Ordovician fish from the Canning Basin was based on fragmentary dermal armour in core recovered from Kidson 1 well, attributed to a new genus and species of arandaspid (jawless fish) *Ritchieichthys nibili* (Sansom et al., 2013). Prior to this discovery, reports of Ordovician vertebrate taxa from Australia, including remains from Early to mid-Ordovician, were restricted to marginal marine deposits in central and southeast Australia (Ritchie and Gilbert-Tomlinson, 1977; Young, 1991, 1997, 2009). Arandaspid fishes are also known from central South America (Bolivia) (Gagnier et al., 1996) and Oman in the Arabian Peninsula (Sansom et al., 2009) indicating a perigondwanan distribution, in a narrow, nearshore environment. This is part of the Gondwanan Evolutionary Assemblage of Blieck and Turner (2003) and Turner et al. (2004).

2.4.2 Silurian

Fossil vertebrates from the Silurian of Western Australia are represented solely by microfossils recovered from boreholes. These primarily comprise thelodont and

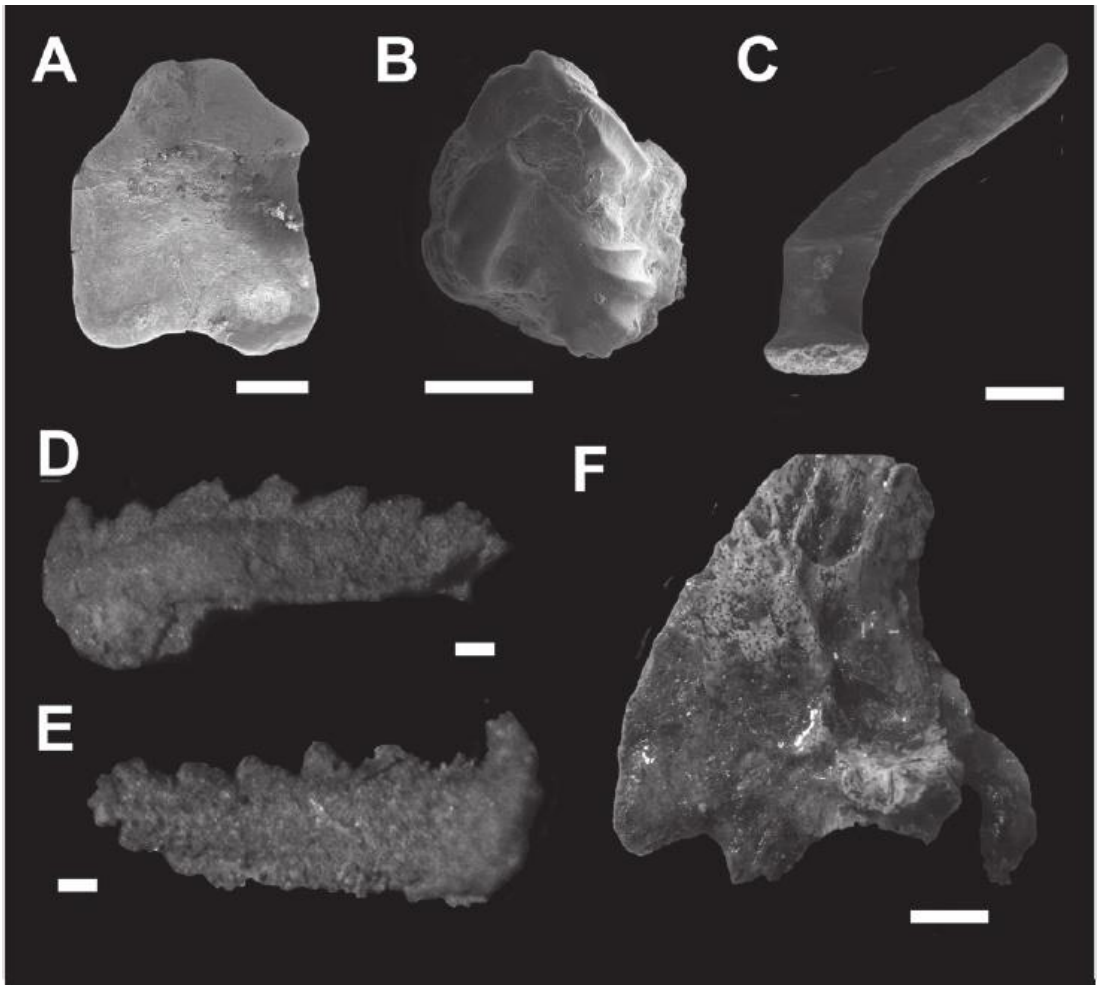

Figure 2.2. Givetian vertebrate remains from the Cadjebut Formation, Canning Basin. (A) Chondrichthyan tooth gen. et sp. indet. in labial view. (B) Chondrichthyan scale in crown view. (C) Placoderm neural spine. (D, E) Arthrodire infragnathal biting division; (D) left lateral view, (E) right lateral view. (F) Ptyctodont left preorbital plate in visceral view. Scale bar: 0.5 mm in A-C; 0.1 mm in D-E; 5 mm in F.

acanthodian micro-remains with rare scales attributed to actinopterygians. Upper Silurian horizons in Pendock 1A well yielded scales tentatively attributed either to the thelodont *Loganellia* sp. cf. *L. grossi* (V N Karatjute-Talimaa pers comm., 1994) or more probably cf. *Niurolepis* sp. (per. obs. ST) and acanthodian *Nostolepis* cf.

alta and ?stem actinopterygian *Andreolepis*. These taxa suggest correlation with Late Silurian (Ludlow) in Iran and northern Europe and suggest a relative closeness between northern Gondwana and Laurentia, rather than any massive oceanic barrier at this time. Upper Silurian horizons in Kempfield 1 yield scales similar in morphology to *Thelodus parvidens* from Avalonia and Laurentia, and in addition those from a possible Silurian level in Gingerah Hill 1 resemble other European *loganelliids* and *Niurolepis susanae* from Iran, although these have not yet been formally described (Burrow et al., 2010; Turner, 2014). There are no known later Ordovician to Early Silurian vertebrates anywhere in Australia probably because of the Hirnantian into Early Silurian glaciation (Turner et al., 2004).

2.4.3 Devonian

2.4.3.1 Emsian-Eifelian

Early Devonian (late Pragian?-Emsian) scales of the thelodont *Turinia australiensis* (Figure 2.1A-F) and unnamed acanthodians were described from the Wilson Cliffs 1 borehole (Gross, 1971) from the Tandalgoo Red Beds (now named Tandalgoo Formation), a unit underlying the well-known reef complexes of the southern Canning Basin. The recognition of thelodont scales led to the re-dating of the strata from Permian to Early Devonian, demonstrating the utility of microvertebrates in dating rocks in the absence of conodonts, or where conodonts are undiagnostic. The type material was redescribed and refigured by Turner (1995). The assemblage also includes placoderm dermal scales and bone fragments, an onychodont tooth and a single shallow-marine unidentified conodont element (personal observation, CJB, ST). Turner (1997) reviewed known records of *T. australiensis* in relation to conodont data across Australia.

2.4.3.2 Givetian

The Givetian Cadjebut Formation represents a restricted marine environment and to date only a small number of invertebrate fossils of low diversity have been reported. In 2010 isolated tooth plates were recovered by Peter Haines (GSWA) and identified (by KT) as those of a ptyctodont placoderm. Further collecting in 2011 yielded a single chondrichthyan tooth of indeterminate affinity (Figure 2.2A) and chondrichthyan scales (Figure 2.2B). Additional 3D-preserved placoderm material was also collected including vertebral elements (Figure 2.2C), dermal plates and tooth plates (Figure 2.2D, E) representing new genera and species of arthrodires, and dermal plates from the headshield of a ptyctodont (Figure 2.2F). Elsewhere in Australia, placoderm remains are common components in Lochkovian to Famennian strata throughout eastern Australia (Young, 1993; Parkes, 1995; Turner et al., 2000; Burrow, 2003), as well as in early Givetian strata in the MacDonnell Ranges of central Australia (Young et al., 1987; Young and Goujet, 2003; Young, 2005). Their rarity in Lower Devonian strata of Western Australia is possibly a result both of lack of outcrop as well as lack of exploration.

2.4.3.3 Frasnian

The first fishes were collected from the Gogo Formation in the 1940s by Curt Teichert who identified placoderm fossils, which he recognised as being similar in morphology to the European coccosteids (Long, 2006). It was not until Harry Toombs from the British Museum (Natural History) (BMNH) visited the University of Western Australia in 1955 and was given material to prepare using his new acetic acid technique that the full extent of this find was realised (Figure 2.3A1-3). The limestone concretions were found to contain fossils preserved in 3D with the original bones intact and undistorted (Figure 2.3B). Toombs returned and represented the

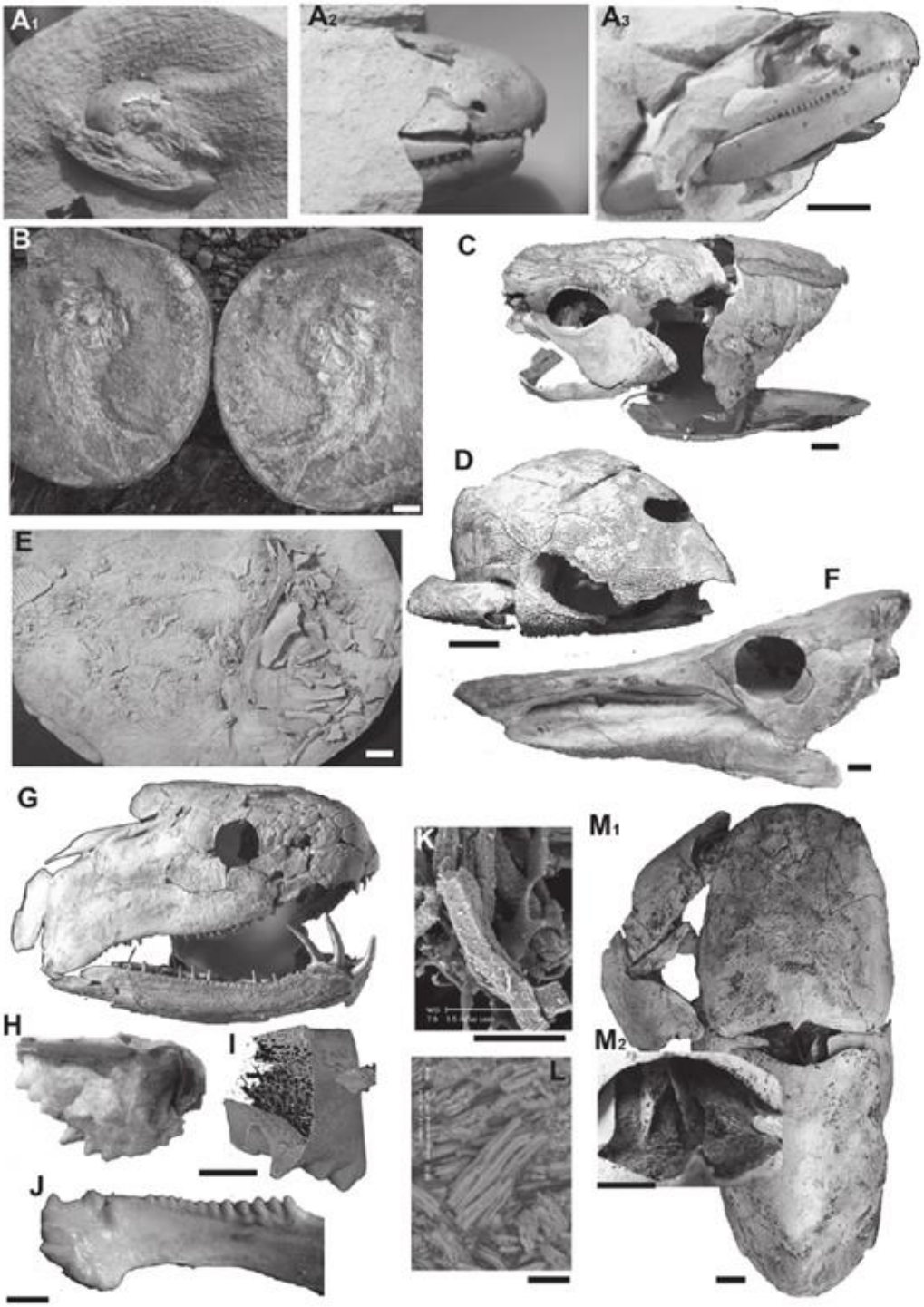

Figure 2.3. Vertebrate remains of the Gogo Formation, Canning Basin. (A1-3) *Gogonasus andrewsae* head at various stages of acetic acid preparation. (B) A split nodule in the field containing a palaeoniscoid in part and counterpart. (C)Arthrodire *Incisoscutum ritchiei* head and trunk shield in lateral view. (D) Head and trunk shield of *Bothriolepis* sp. (E) *Austroptyctodus gardineri* (counterpart) in lateral view. (F) Head of *Griphognathus whitei* in lateral view. (G) *Onychodus jandemarrai* in lateral view. (H) *Compagopiscis croucheri* upper tooth plate in ventral view. (I) CT scan of upper tooth plate of *Compagopiscis croucheri* showing histological detail; (J) lower tooth plate of *C. croucheri* in lateral view. (K) Mineralised muscle fibres from *Incisoscutum ritchiei*. (L) Mineralised biofilm surrounding muscle fibres in *Eastmanosteus calliaspis*. (M_1) *Eastmanosteus calliaspis* with nuchal gap musculature preserved; (M_2) detail of nuchal gap musculature. Scale bar: 1 cm in A-J, M; 50 μm in K, L. Images A-G from Long, 1995; J from Trinajstic, 2009.

BMNH in two major expeditions, which systematically collected fish and crustaceans from the Gogo Formation in 1963 and 1967, in collaboration with the Western Australian Museum and Hunterian Museum (Glasgow, Scotland). The Gogo Formation has to date yielded 45 species of fish (Long and Trinajstic, 2010), the majority being arthrodire placoderms (25%) (Figure 2.3C), with antiarchs (10%) (Figure 2.3D), and ptyctodonts (5%) (Figure 2.3E), recovered in lesser numbers. Of the osteichthyans, palaeoniscoids (Figures 2.3B, 5C, D) represent the next most abundant group (24%), followed by dipnoans (20%) (Figure 2.3F), and osteolepiforms (2%) (Figure 2.3G). More recently, a single acanthodian was described by Burrow et al. (2012). In addition two sharks and a coelacanth have been prepared but await full description. Long and Trinajstic (2010) gave a recent review of the faunal composition and so only a brief overview of discoveries post-2010 will be presented here.

With the advent of new technologies, including micro CT and synchrotron tomography, the first non-destructive examinations of histological structures of the fishes from the Gogo Formation have been undertaken (Long et al. 2008; Sanchez et al. 2013; Trinajstic et al. 2013). The ontogenetic history is largely conserved within the dermal bones preserved as lines of arrested growth (Sanchez et al. 2012, 2013). This characteristic has enabled changes in growth of the jaws to be ascertained and led to significant advances in our understanding of the development of teeth (Figure 2.3H-J) in some early jawed vertebrates (Smith and Johanson, 2003; Rücklin et al., 2012). The presence or absence of teeth in placoderms has been a controversial topic, particularly since the proposition by Smith and Johanson (2003) that teeth were secondarily developed in arthrodire placoderms from ‘toothless’ ancestors. Synchrotron scans of the jaws of an arthrodire (*Compagopiscis*) showed the pulp

canal within each tooth became infilled during growth (Rücklin et al., 2012). This discovery supports Smith and Johanson's (2003) hypothesis that the dental structures in arthrodires are true teeth, and teeth might have evolved at least twice in early vertebrate evolution. Studies on the antiarch *Bothriolepis* (Figure 2.3D) show tooth-like structures on biting surfaces that are consistent with the histology of the dermal armour, further indicating that teeth and jaws may not have evolved simultaneously (Rücklin et al., 2012), as antiarchs are considered to be basal phylogenetically to arthrodires (Zhu et al., 2013).

Reconstructing the soft anatomy of extinct animals has often been a pipe dream in palaeontology, and has until recently mostly relied on functional interpretation and the preservation of muscle scars on the skeleton. The interolateral plate (= clavicle) of placoderms was hypothesised to be the site of the coracobrachialis muscle (Johanson, 2003). Synchrotron studies of the interolateral plate from *Compagopiscis* a placoderm from Gogo revealed the presence of numerous embedded extrinsic fibres indicating muscle attachment points. The principal fibre alignments are anteroposterior in the anterior part of the attachment and anterodorsal in the more dorsal part indicating the presence of two muscles (Sanchez et al., 2012), where previously only one muscle had been predicted (Heintz, 1932; Miles, 1969; Johanson, 2003). Changes in the distribution of osteocyte lacunae within the bone indicated where deep enthesis (connective tissue between the tendon and the bone) of tendon-attached muscles formed, often leaving a muscle scar on the external bone, whereas more shallow muscle insertions left no muscle scars (Sanchez et al., 2012). These superficial muscle entheses had not previously been predicted on the basis of visual examination of the bone and so the number of muscles present in these extinct organisms has been underestimated

(Trinajstic et al., 2012). Thus not only can the synchrotron reveal the site of muscle attachment but also the type of attachment. This technique, pioneered on Gogo fish, has made the reconstruction of soft anatomy far more accurate than previously realised.

The exceptional preservation of fossils in the Gogo Formation is not restricted to the preservation of bone but includes mineralised muscles also preserved in 3D, in placoderms, chondrichthyans and palaeoniscoids. Initially only small amounts of muscle were recovered from under the dermal plates of the headshield (Figure 2.3K, L), which had collapsed onto themselves forming a closed micro-environment providing the condition conducive to soft-tissue preservation (Trinajstic et al., 2007). Low pH and rapid burial were important factors in the preservation of the muscle tissues but recent research on invertebrate taxa from the Gogo Formation has shown that the action of sulfur-reducing bacteria prior to burial was also significant in the mineralisation of soft tissues (Melendez et al., 2013). In some instances individual cells are replicated by a single crystal of apatite, exactly replicating the structure of muscle and nerve fibres (Trinajstic et al., 2007). The recognition that mineralised soft tissues were present in the fossils (vertebrate and invertebrate) from Gogo led to different preparation techniques, reduced concentrations of acid and virtual preparation through synchrotron scanning. Using these techniques nearly all the postcranial musculature within the arthrodire *Compagopiscis croucheri* and the nuchal gap muscles in *Incisoscutum ritchiei* and *Eastmanosteus calliaspis* (Figure 2.3M1 -M2) have been identified (Trinajstic et al., 2013). The significance of this discovery was that more muscles were found to be present in the neck than originally predicted from studies based on comparative morphology. Although the presence of paired head elevator and depressor muscles

was predicted based on functional consideration, the division of the head elevators into medial and lateral muscles had not (Trinajstic et al., 2013). In addition, the presence of the cucullaris muscle, a head depressor muscle presumed to be common to all jawed vertebrates, was confirmed for the first time. A second group of specialised muscles, which had never been predicted, was found to be present in the ventral body wall (Trinajstic et al., 2013). Although their function is yet to be determined, their position at the junction of the trunk armour and the tail suggests that they play a role in minimising shear during tail propulsion (Trinajstic et al., 2013).

Although sexual dimorphism had been recognised in ptyctodonts (Watson, 1934, 1938), it was not until the identification of claspers in the ptyctodontid *Ctenurella* (Ørvig 1960) that the possibility of internal fertilization in ptyctodonts was suggested (Patterson, 1965). In a review of the Scottish ptyctodont *Rhamphodopsis*, Miles (1967), noted it was impossible at that time to determine whether the mode of copulation in ptyctodonts resulted in oviparity or viviparity. This conundrum was finally solved when a single embryo (Figure 2.4A) was discovered in the ptyctodontid *Materpiscis attenboroughi*, which demonstrated beyond doubt the presence of internal fertilisation with live birth almost 200 million years earlier in the fossil record then previously known (Long et al., 2008; Trinajstic et al., 2012). One of the most crucial pieces of evidence in the determination of embryos in placoderms was the presence of the mineralised umbilical cord (Figure 2.4A) in *M. attenboroughi* (Long et al., 2008). Following this discovery, three embryos, previously identified as scales, were recorded from *Austroptyctodus gardineri* (Figure 2.4B) (Long et al., 2008). Male claspers had previously been identified by Miles and Young (1977) in *Austroptyctodus* (Figure 2.4C). Small

dermal plates had also been recovered from the abdominal area of an arthrodire *I. ritchiei* (Figure 2.4D, E), but the absence of any evidence for sexual dimorphism and the honeycomb nature of the bone, which was originally interpreted as being the result of digestion, meant that these plates were identified as prey items (Dennis and Miles, 1981). Comparison with the honeycomb nature of the embryonic plates in the ptyctodonts (Figure 2.4F) allowed the reinterpretation of the arthrodire plates as embryonic bones (Long et al., 2009). The presence of an articulation surface on the pelvic girdle of *Austrophyllolepis*, interpreted as for claspers (Long et al. 2009), suggested that sexual dimorphism also occurred in arthrodires. The final piece of the puzzle was revealed with the discovery of a male clasper (Figure 2.4G-I) in *I. ritchiei* (Ahlberg et al., 2009), which could be distinguished from the pelvic girdle (Figure 2.4G, I, J) and in *Holonema westolli* (Figure 2.5A, B) confirming sexual dimorphism with viviparity in ptyctodont and arthrodire placoderms (Trinajstic et al., in press a). Soft tissues have also been recovered in the first and only acanthodian, *Halimacanthodes ahlbergi* described from the Gogo Formation (Burrow et al., 2012). The body outline is preserved in the resin-embedded side of the nodule, and was therefore protected during acetic acid preparation. The specimen represents a juvenile, as there is no scale cover in the mid-body region of the fish and there are a low number of growth zones in the scales. These features have been recognised as indicating a juvenile stage from comparison with the ontogenetic series in *Lodeacanthus gaujicus* (Upeniece, 1996) from the Frasnian Lode Quarry, Latvia. The Gogo acanthodian shows a close affinity to *Howittacanthus kentoni* from the Frasnian lacustrine mudstones of Mt Howitt, Victoria (Long, 1986).

The palaeoniscoid actinopterygians or ray-finned fishes have been revised in recent years by Choo et al. (2009) and Choo (2011), who have extended the

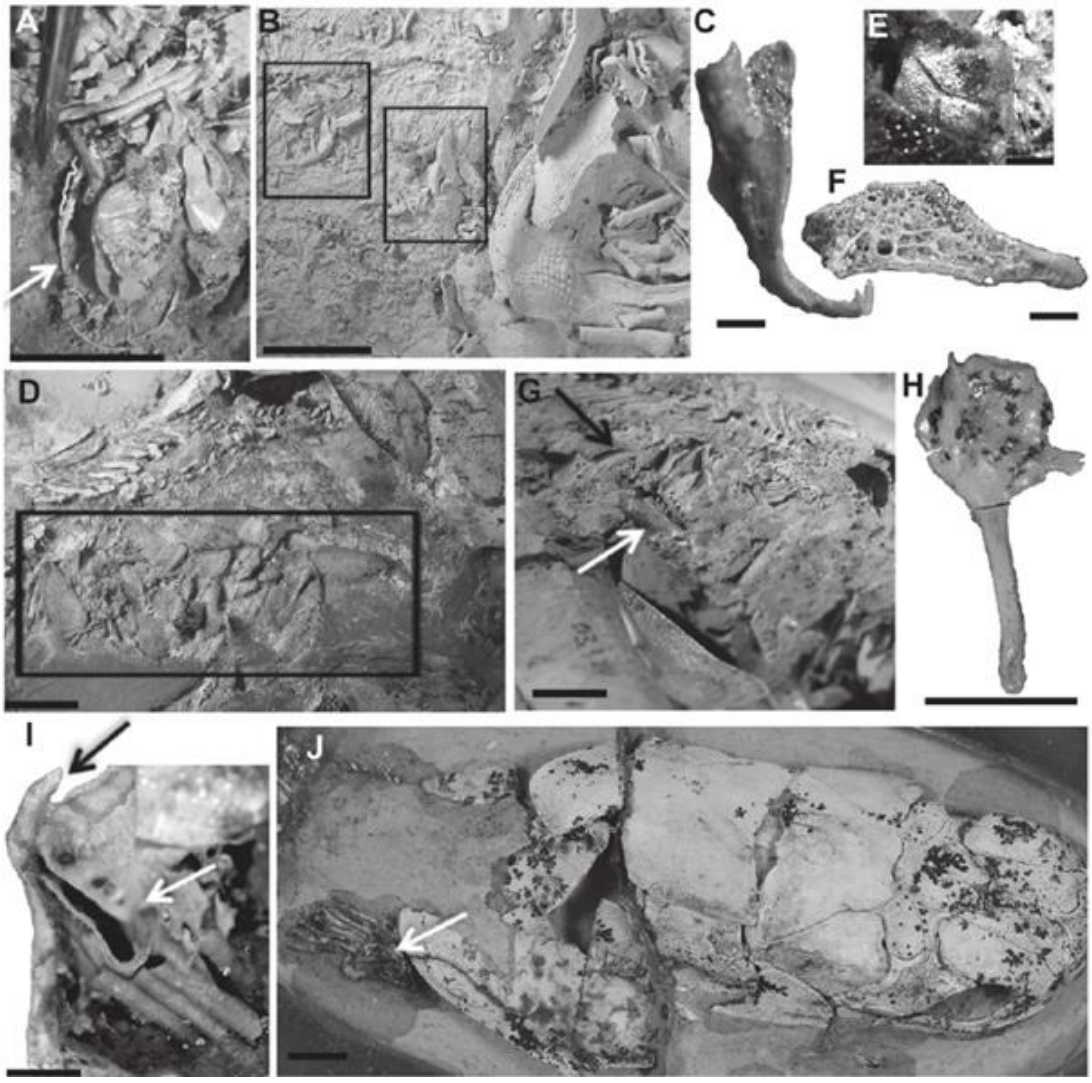

Figure 2.4. Reproductive structure in placoderms from the Gogo Formation. (A) *Materpiscis* embryo with detail of the mineralised umbilical cord indicated by a white arrow. (B) Austroptyctodus gardineri, internal view with 2 embryos within the rectangular outline. (C) Male clasper from Austroptyctodus gardineri. (D) Internal view of Incisoscutum ritchiei with embryonic bones within the rectangular outline. (E) Close up of embryonic plate from Incisoscutum ritchiei. (F) Embryonic plate from *Austroptyctodus gardineri*. (G) Internal view of *Incisoscutum ritchiei* showing male clasper (black arrow) and pelvic girdle (white arrow). (H) Detail of male clasper from *Incisoscutum ritchiei*; (I) close up of male clasper (black arrow) and pelvic girdle (white arrow) in *Incisoscutum ritchiei*. (J) Female specimen of *Compagopiscis croucheri* showing the pelvic girdle (white arrow). Scale bar: 1 cm in A, B, D, G, H, J; 1 mm in C, F; 2 mm in E; 5 mm in I.

actinopterygian faunal list of the site to five taxa, from the original two described by Gardiner (1984). The Gogo actinopterygians also show preserved soft tissues (Figure 2.5C) and, in rare cases, organs including the gut, gill area and liver (Trinajstic et al., in press b). The anatomical positions of these organs are comparable to those of extant actinopterygians. The path of the intestine is identified, as the cavity where

the intestine ran has been infilled with calcite cement. Although this sort of replacement precludes preservation of gut contents (Trinajstic et al., in press b), conodont animals recovered from within the abdominal cavity (Nicoll, 1977) and the branchial region (Figure 2.5D) of two specimens indicate that these fish were carnivores, consistent with the diet indicated by their dentition (Choo et al., 2009).

Most recent work on Gogo lungfishes includes description of new taxa of holodontid lungfishes including *Xeradipterus* (Clement and Long, 2010) plus a new species of rhinodipterid, *Rhinodipterus kimberleyensis* (Clement, 2012). Clement and Long (2010) also reported the first record of a marine lungfish showing air breathing adaptations based on a specimen of *Rhinodipterus* from the Gogo Formation with cranial rib articulations on its braincase.

The tetrapodomorph fish *Gogonasus andrewsae* (Long, 1985) is now known from several relatively complete specimens (Holland and Long, 2009) (Figure 2.3A). Holland (2013) has recently described the pectoral girdle and fin in detail. Large holes on top of the head are identified as spiracles in this genus and were suggested as accessory breathing structures by Long et al. (2006). Recent work on the physiology of the modern air-breathing fish *Polypterus* now confirms that spiracular breathing was common in basal osteichthyans and most likely explains why fish like *Gogonasus* have such large spiracles (Graham et al., 2014).

The other important aspect of the exceptional preservation from the Gogo Formation has been the ability to identify and compare isolated scales from the contemporaneous Gneudna Formation, Carnarvon Basin (see below) and the Virgin Hills Formation, Canning Basin. The variation in scale morphology present in palaeoniscoids is exhibited in key features including shape and ornamentation, enabling identification of the body area from which isolated scales originated.

Following Esin (1990), different squamation areas in the Gogo palaeonsicoids have been recognised, enabling two species, *Moythomasia durgaringa* and *Mimia toombsi* to be identified from the Gneudna Formation (Figure 2.5E, F) (Trinajstic, 1999c, 2000) and scales from *M. durgaringa* to be identified from the Virgin Hills Formation (Trinajstic and George, 2009) and Hull Range (Chow et al., 2013), Canning Basin, providing biostratigraphic constraints for these strata. In addition scales from the placoderm *Holonema westolli* Miles 1971 (Figure 2.5B) were also identified in the Gneudna Formation (Figure 2.5B1) based on the description of a complete tail recovered from the Gogo Formation (Trinajstic, 1999a).

As noted above, the Gogo Formation fishes are further contributing important information on reproduction in early jawed fishes, including viviparity as an early vertebrate reproductive strategy, multiple embryos and ontogenetic series, which enable questions of taxonomy, phylogeny and development to be addressed (Johanson and Trinajstic, 2014; Trinajstic et al., in press b).

2.4.3.4 Virgin Hills Formation: Frasnian

The microvertebrate fauna described from a measured section at Horse Spring in the Canning Basin is dominated by thelodont scales (Figure 2.5G, H) and phoebodont teeth (Figure 2.5I) with a smaller number of acanthodian and palaeoniscoid scales as well as protacrodont teeth also recovered (Turner, 1997; Trinajstic, 2000; Trinajstic and George, 2009). The discovery by Trinajstic (2000) represented the first record of the thelodont *Australolepis seddoni* (Figure 2.5G, H) co-occurring with conodonts and extended the known stratigraphic range to as young as the standard Montagne Noire conodont zone 10 (CZ10 MN) (Trinajstic and George, 2009). This thelodont is a useful index fossil that defines the early Frasnian in East Gondwana (Turner, 1997). The presence of *A. seddoni* scales in the Hull

Range has confirmed the Frasnian age of back-reef facies, which are difficult to date with conodonts and ammonoids (Chow et al., 2013). The biogeographic range of *A. seddoni* is now known to have extended westwards along the northern margin of Gondwana with new discoveries in Iran and possibly Poland (Turner et al., 2002; Hairapetian et al., 2015).

Numerous small acanthodian scales have also been recovered from the lower beds of the Horse Spring section and their generic morphology and lack of ornament led to them to be placed in open nomenclature (Trinajstic and George, 2009). Following the description of *Halimacanthodes ahlbergi* the scales from Horse Spring have now tentatively been referred to this taxon (Burrow et al., 2012). Smooth-crowned acanthodiform scales are common components in Frasnian strata (Burrow et al., 2010). Other taxa that co-occur in the Virgin Hills and Gogo formations are scales attributed to the palaeoniscoid *Moythomasia durgaringa* and tooth plates from the lungfish *Chirodopterus australis.*

Teeth of phoebodont sharks (Figure 2.5I) have also been recovered from the Horse Spring section (Trinajstic and George, 2009) and can be correlated with the standard phoebodont zonations elsewhere in Australia and worldwide (Young and Turner, 2000, Ginter et al., 2010). Although known to have a global (at least Palaeotethyan) range, phoebodont taxa had not been recorded in Western Australia until their recovery from conodont residues at Horse Spring (Trinajstic and George, 2009). Phoebodonts have proved useful for biostratigraphy in Givetian to Famennian strata (Ginter et al., 2010) and their range into the Famennian has recently been reported in Western Australia (Roelofs et al., 2013).

2.4.3.5 Napier Formation: Frasnian

Long (1988) recorded a large upper tooth plate (supragnathal) of a ptyctodontid placoderm identified as cf. *Campbellodus* sp. from the Napier Formation in the Canning Basin. In addition, a microvertebrate fauna including scales from thelodonts, acanthodians, chondrichthyans and actinopterygians, and teeth from at least three species of stethacanthid and cladodont sharks have been recovered from beds throughout the section at South Oscar Range.

2.4.3.6 Virgin Hills Formation: Famennian

A single large placoderm, *Westralichthys*, was recovered from the *crepida* conodont zone of the Virgin Hills Formation by Curt Teichert and this was subsequently prepared and described by Long (1987). In 2009, Peter Haines identified bone from a large placoderm in a measured section at Casey Falls, from close to where the original specimen was thought to have been recovered. The new specimen was excavated from the rock in 2011 and is currently undergoing preparation. The plates represent the trunk armour of a large dinichthyid and have been tentatively identified as belonging to *Westralichthys*, but they await formal description. Towards the top of the section there is a breccia where large isolated, but broken, placoderm plates are present. It has not been possible to identify these fragmentary remains but as they occur in a horizon above strata dated by conodonts as mid-Famennian, this confirms a Famennian age for the uppermost beds. Placoderms did not survive the end-Famennian extinction event, and therefore a younger Carboniferous age for the upper part of the section measured at Casey Falls is ruled out.

The measured section at the Casey Falls locality yielded few microvertebrates, mostly shark teeth, with a small number of acanthodian and palaeoniscoid scales. Preliminary work on the shark fauna confirms the presence of

phoebodonts, as elsewhere in Australia (Turner 1982b, 1993; Young and Turner 2000). The ramp facies, above the Casey Falls section, is dominated by a diverse shark assemblage, which includes teeth from protacrodontids, stethacanthids, lonchidiids and the phoebodont *Thrinacodus tranquillus*. Numerous palaeoniscoid scales and teeth and lower numbers acanthodian, scales are also present. Interestingly, thelodonts, phoebodonts and porolepiformes are yet to be recorded from the Gogo Formation, even though these taxa are known from the Frasnian and

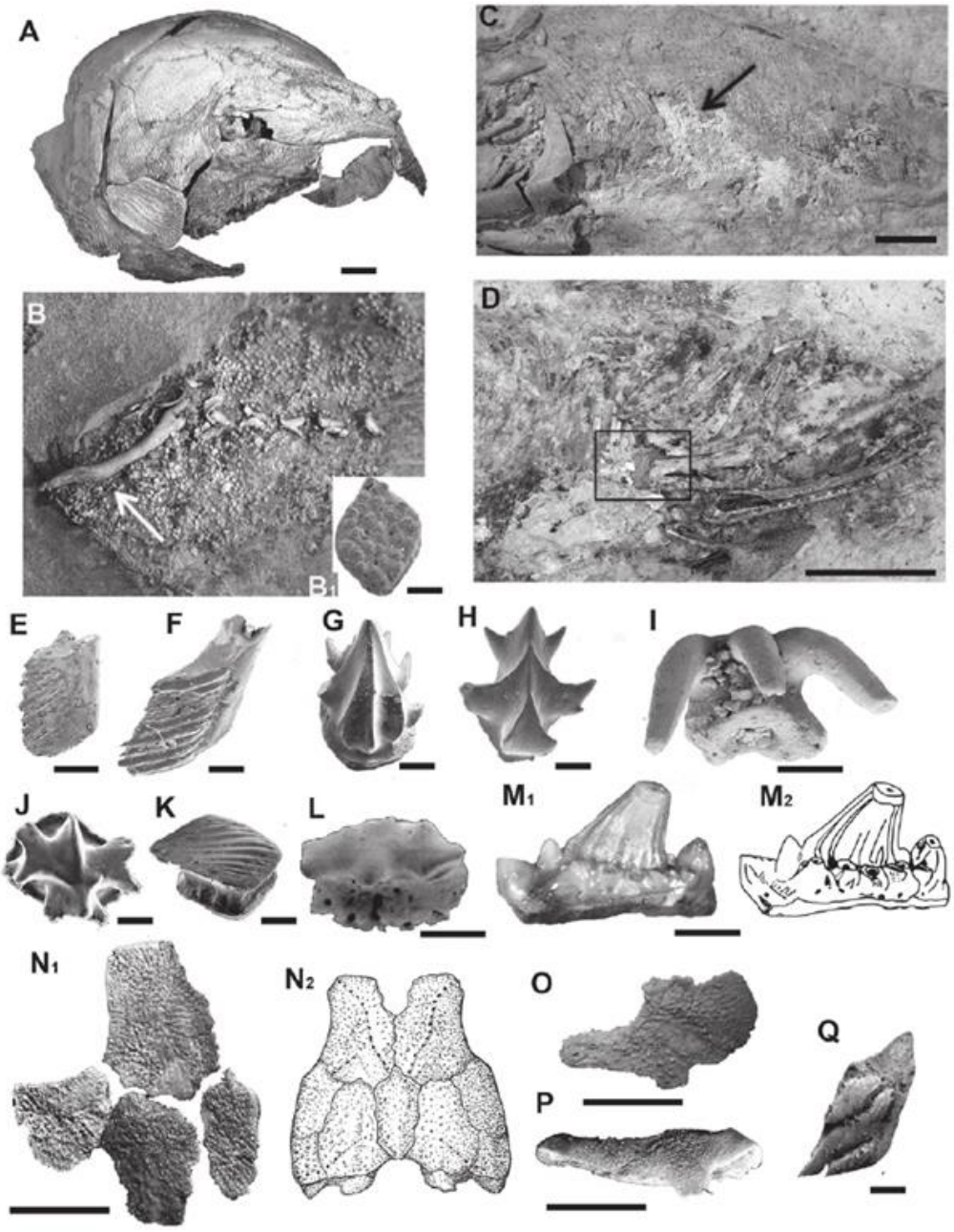

Figure 2.5. Vertebrate remains from the Gogo, Virgin Hills and Gneudna Formations. (A) Head shield of *Holonema westolli*. (B) Body scales and clasper (white arrow) Holonema westolli from the Gogo Formation; (B1) body scale of Holonema westolli from the Gneudna Formation. (C) *Moythomasia durgaringa* in lateral and internal view showing mineralised soft tissue (white arrow). (D) *Gogosardinia* with conodont (rectangular outline) in the branchial regions. (E) *Moythomasia durgaringa* type A scale and (F) type B scale from the Gneudna Formation. (G, H) Scales from *Australolepis seddoni* in crown view Virgin Hills Formation, Horse Spring, Canning Basin. (I) *Phoebodus bifurcatus* tooth in crown view Virgin Hills Formation, Horse Spring, Canning Basin. (J) Scale from *Australolepis seddoni* in crown view, Gneudna Formation, Carnarvon Basin. (K) Cheiracanthus sp. body scale in crown view. (L) *Phoebodus* sp. tooth in crown view, Gneudna Formation. (M1) *Emerikodus* tooth in lingual view from the Gneudna Formation; (M2) line drawing of *Emerikodus.* (N1) Head shield plates of *Kimbryanodus* from the Gneudna Formation; (N2) line drawing of reconstruction of the head shield of *Kimbryanodus*, (O) Marginal plate in lateral view of *Kimbryanodus* from the Gneudna Formation. (P) Lower tooth plate of *Kimbryanodus* from the Gneudna Formation. (Q) Palaeoniscoid scale Gogosardinia coatesi in crown view from the Gneudna Formation. Scale bar: 2 cm in A; 1 mm in B, F-M, Q; 2 mm in E; 1 cm in O, N; 5 mm in P.

Famennian Virgin Hills and Napier formations in the Canning Basin. This is probably a reflection of the preferred environments of these fish, with thelodonts typically in shallower marine, marginal marine to freshwater settings (Turner 1997). Phoebodont sharks, apart from one thrinacodont from the late Mississippian of the USA, are only known from isolated teeth but typically occur in marine rocks (Ginter and Turner 2010).

2.4.3.7 Napier Formation: Famennian

One of the earliest records of Famennian aged vertebrate material in the Canning Basin is from Barker Gorge, in the Napier Range. The fossil was collected by H P Woodward in 1906 and identified as: '…a large Devonian fish (new to science) allied to *Coccosteus'* by his father Henry Woodward, then Keeper of Geology at the British Museum (Glauert, 1910 p. 112). A Smith Woodward, who took over as Keeper from Henry Woodward (no relation) in 1901, agreed writing: 'The Western Australian Fossil looks remarkably like a piece of a large Devonian Coccostean, hitherto unknown in the Australian Region' (Glauert, 1910 p. 113). Etheridge (1918) described (but did not figure) similar material collected in 1916 by

H Basedow from ‘near Old Napier Downs homestead’ as the stromatoporoid *Stromatoporella kimberleyensis*. During a study of the stromatoporoids from the reef complexes, Cockbain (1976) re-examined the Woodward and Basedow material and concluded that it was not a stromatoporoid: additional testing including thin sectioning and X-ray diffraction analyses confirmed the original identification as arthrodire bone (R S Miles in Cockbain, 1976). The recovery of further vertebrate fossils from the area has been scant, with a single sharks tooth *Stethacanthus* cf. *thomasi* recovered from mineral drill core (NRD103) at Napier Range and a single tooth of *Thrinacodus ferox* recovered from Napier Range 1 well located east of Chedder Cliffs and dated as Late Famennian (Chow et al., 2004), based on the associated conodont fauna. Vertebrate remains have been recovered in outcrop from Chedder Cliffs however, with the exception of some incomplete placoderm dermal plates, most are so broken they are impossible to identify. Conodont samples from Barker River have yielded a single phoebodont tooth and some isolated ‘ctenacanthid’ type scales.

2.4.4 Carboniferous

There is a major environmental change towards the end of the Famennian with the cessation of reef building; the marine habitats of the Carboniferous period are dominated by carbonate ramps. The end Famennian is also marked by a major extinction event that affected vertebrates and marked the demise of the placoderms (although the number of families was already reduced after the Frasnian-Famennian extinction event) and a major radiation of sharks and actinopterygians, which is reflected in the shallow-water facies of the Laurel Formation in the Canning Basin. Palaeoniscoid remains (teeth, scales and radial bones) and acanthodian scales

dominate the fossiliferous units. Turner (1982a) identified *Thrinacodus ferox* from Oscar Hill and renamed earlier Lower Carboniferous shark material described by Thomas (1957). Edwards (1997) found teeth of a new *Thrinacodus* sp. from a trench dug across the Upper Devonian-Lower Carboniferous by Mawson et al. (1988) to obtain conodont data; Ginter and Sun (2007) named this taxon *Thrinacodus bicuspidatus* and its range is within the basal Tournaisian in China and Western Australia. Recent work (Roelofs et al., 2013) has also uncovered shark teeth, scales and spines from 21 different taxa including *Ageleodus* sp., *Thrinacodus ferox* (Figure 2.6A), *Stethacanthus* spp., Protacrodont spp., (Figure 2.6B, E), *Deihim mansureae*, *Cassisodus* sp., *Helodus* spp. (Figure 2.6C), *Lissodus* spp.), *Orodus* sp. (Figure 2.6D) and a ctenacanthid sp. (Figure 2.6F). A partial tooth from a large stethacanthid shark is also of note as it bears strong affinities to teeth in a fragmented but 3D preserved partial jaw and palate from a large specimen of *Stethacanthus* sp. from the Bonaparte Basin (Turner 1991; Turner in Jones et al., 2000; Turner et al., 1994; Burrow et al., 2010). This indicates the presence of large predatory sharks early in the Carboniferous across north Western Australia (Burrow et al., 2010).

Further work on the diverse shark fauna of the Viséan Utting Calcarenite, Weaber Group, of the Bonaparte Basin has brought to light at least 18 different taxa of eugeneodontid and other sharks as well as sarcopterygian and actinopterygian remains (Chambers, 2003; Burrow et al., 2010).

2.5 Carnarvon Basin

Fish fossils are mostly known only from Late Devonian sediments in the Carnarvon Basin. The early Frasnian Gneudna Formation is interpreted as being deposited along a shallow marine shelf (Hocking et al., 1987). Conformably

overlying and interfingering with the Gneudna Formation is the Munabia Sandstone where deposition was initially in a tidal environment grading up to a braided-fluvial system (Moors, 1981) with conodonts indicative of marine incursion in the upper part of the section (Nicoll, 1979; Hocking et al., 1987). The Frasnian-Famennian

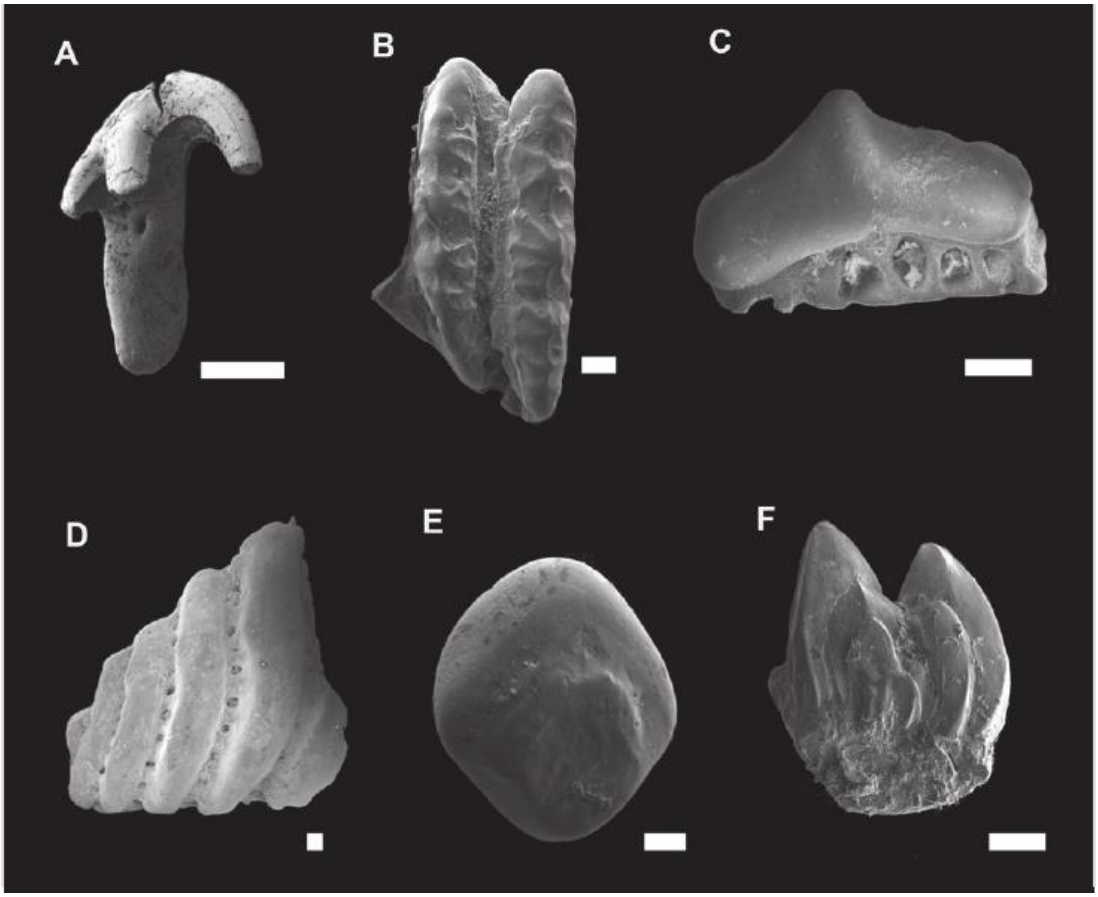

Figure 2.6. Carboniferous microremains from the Laurel Formation, Canning Basin. (A) *Thrinacodus ferox* tooth in crown view. (B) Partial *Protacrodus* sp. tooth whorl in crown view. (C) Lissodus sp. tooth in lingual view. (D) *Lissodus* sp. tooth whorl in crown view. (E) *Protacrodus* sp. scale in basal view. (J) Ctenacanthid scale in crown view. Scale bar: 0.4 mm.

boundary occurs within the Munabia Sandstone and the upper part of the section grades into the Famennian Willaraddie Formation, which is at least partly laterally equivalent (Gorter et al., 1998). During the latest Devonian and into the Tournaisian a shallow sea transgressed across the region, reflected by the deposition of the Moogooree Limestone (Hocking, 1990). The Permian Byro Group represents cold-water facies, predominantly comprising black shale deposited under anoxic

conditions in the outer offshore zone and a lighter coloured shale deposited under less-restricted conditions in the inner offshore zone (Hocking et al., 1987). The changes in bathymetry are thought to reflect tectonic events related to the breakup of Gondwana (Hocking et al., 1987).

2.6 Vertebrate fossils of the Carnarvon Basin

2.6.1 Devonian

2.6.1.1 Frasnian

The Gneudna Formation is laterally discontinuous, with most palaeontological studies (vertebrate and invertebrate) having been concentrated on the type section. The Gneudna type section was described as depauperate in fossil taxa (Dring, 1980), however, this statement is only accurate for the invertebrates: the fish fauna is now known to be one of the most diverse marine vertebrate assemblages of this age, with nearly 20 taxa present, the majority of which are represented as microfossils (Turner and Dring, 1981; Trinajstic, 1999a, b, c; Long and Trinajstic, 2000; Trinajstic, 2001a, b; Trinajstic and George, 2009).

George Seddon (1969) discovered the first vertebrate fossils in conodont residues and determined the remains as either teeth or scales belonging to fish species. Dring (1980) recovered additional fish remains and recorded the presence of placoderms, palaeoniscoids, acanthodians and lungfish; only the thelodonts were formally described following Turner's identification of some of Seddon and Dring's scales, formally described as *Australolepis seddoni* by Turner and Dring (1981). This was the first evidence of the thelodonts surviving the Givetian/Frasnian extinction event and into the Late Devonian and at the time represented the youngest occurrence of thelodonts in the world. Scales of *A. seddoni* (Figure 2.5J) have been

used by Turner (1997) to define the early-mid-Frasnian zone in East Gondwana. So far this species is confirmed from Frasnian deposits CZ 4-10 of the Gneudna and Virgin Hills formations, Western Australia (Trinajstic and George, 2009) and eastern Iran (Hairapetian et al. 2006).

Following these discoveries, a rich microvertebrate fauna was described that includes additional scales types from *Australolepis seddoni*, tail scales from the arthrodire *Holonema westolli* (Figure2. 5B1), body scales from the palaeoniscoids *Mimia gardineri* (Figure 2.5E) and *Moythomasia durgaringa* (Figure 2.5F), acanthodian scales recently identified as coming from *Homalacanthus ahlbergi* and *Cheiracanthus* sp. (Figure 2.5K), tooth plates from the lungfish *Chirodipterus australis*, porolepiform scales, phoebodont teeth (Figure 2.5L), and a new genus of shark *Emerikodus* (Figure 2.5M1, M2). At the time of these descriptions (Trinajstic, 2000) the vertebrate fauna was considered far more diverse than that recovered from the Gogo Formation because shark, acanthodian and coelacanths had not yet been discovered in it (Long and Trinajstic, 2010). As noted, thelodonts, phoebodonts and porolepiformes are yet to be recorded from the Gogo Formation although these taxa are known from the Frasnian and Famennian Virgin Hills and Napier Formations in the Canning Basin.

In addition to the microvertebrates a small number of macrovertebrates have also been found, with placoderm remains the most common. An anterior dorsolateral plate (WAM 91.4.35), part of the shoulder armour, attributed to the actinolepid placoderm *Groenlandaspis* sp. was identified by Long (1993). Groenlandaspids occur in the Early-Middle Devonian *Wuttagoonaspis* fauna in central New South Wales and the Toomba Range southern Queensland (Ritchie, 1973, 1975; Young, 1993; Young and Goujet, 2003), and right through the Middle and Late Devonian

successions throughout Australia. Although common in purported freshwater facies of this age and yet known to have a global occurrence, *Groenlandaspis* has not been reported from the Gogo Formation (Long and Trinajstic, 2010).

Other placoderm material comprises plates from the trunk armour and includes a right mesial lateral 2 plate, an anterior ventrolateral plate and an anterior dorsolateral plate of *Bothriolepis* and a head shield plate (nuchal plate) from the arthrodire *Holonema westolli*. The most complete placoderm remains are from the ptyctodont *Kimbryanodus* described by Trinajstic and Long (2009) (Figure 2.5N1, P). The holotype comprises the dermal plates that make up the shoulder girdle and represent the only articulated remains recovered. However, one bed, in the lower part of the section, contains a large number of isolated, but associated plates, including a complete set of dermal head (Figure 2.5 N1, N2) and trunk shield plates and some endochondral elements of the braincase (Trinajstic and Long, 2009). This ptyctodont is one of four species known from Western Australia, the other three occurring in the Gogo Formation. A phylogenetic analysis (Trinajstic and Long, 2009) places this taxon as closely related to Materpiscis and Austroptyctodus, both endemic to the Gogo Formation.

Long (1985) referred the lungfish, originally ascribed by Seddon (1969) to *Dipterus* cf. *digitatus*, to *Chirodipterus australis*. Many new specimens of isolated lungfish tooth plates have been found throughout the section and one partial dipnoan braincase from near the top of the section. Comparisons with the Gogo osteolepiform *Gogonasus andrewsae* (Long, 1985, name amended) show that the Gneudna specimens are significantly larger. Large sigmoid-shaped symphyseal teeth and a nearly complete dentary lined with large conical teeth suggest affinity with the genus *Onychodus*, in particular to *Onychodus jandemarrai* from Gogo Formation

(Andrews et al., 2006), although the Gneudna species is much larger with more robust teeth (Long and Trinajstic, 2000). Isolated rounded scales with regions of small upturned flat tubercles have been referred to an indeterminate porolepiform, with the scales somewhat similar to those of *Glyptolepis* sp. (Jarvik, 1980 figure 178).

The dipnoan genera *Chirodipterus* and *Adololopas*, as well as the placoderms *Bothriolepis* and *Holonema*, are found in the top of the section, which lies in the *falsiovalis* conodont zone and has been dated as lower Frasnian. *Holonema* is represented both in the Gneudna and the Gogo Formations by the species *H. westolli* (Trinajstic, 1999a). The palaeoniscoid species, including scales attributed to juvenile specimens, recorded from the Gneudna and Gogo Formations are *Moythomasia durgaringa* (Trinajstic, 1997, 1999a, b) and *Mimia toombsi* (Trinajstic, 1999c), both species occurring throughout the section. Choo et al. (2009) described three additional palaeoniscoid taxa from the Gogo Formation. One of these, *Gogosardina coatesi*, has scales with linear ornament, which indicates that the juvenile scales from the Gneudna Formation (Trinajstic, 1999b) were misidentified and thus need to be attributed to *Gogosardina coatesi* (Figure 2.5Q).

2.6.1.2 Frasnian-Famennian

A scant macrovertebrate fauna including remains of *Bothriolepis* sp., *Holonema* sp. and indeterminate scales of an osteolepiform sarcopterygian was collected from the lowermost outcrops of the Munabia Sandstone and described by Long (1991). These fossils constitute the only record of macrovertebrates from this horizon; however, collecting and processing by CJB in 2011 revealed a similar microvertebrate fauna to the underlying Gneudna Formation. Long (1991) attributed the fauna to a likely Frasnian age based on the similarities in shape and dermal

ornament of the Munabia *Holonema* anterior median ventral plate to the Gogo *Holonema westolli* plates.

2.6.1.3 Famennian

As with the Canning Basin, vertebrate fossils are rare in Famennian strata of the Carnarvon Basin. Within the Willaraddie Sandstone, John Long in 1995 first collected placoderm remains preserved as natural impressions including plates from *Bothriolepis* and a phyllolepid posterior ventrolateral plate. Recently in 2011, Eva Papp (ANU) collected additional phyllolepid plates but these are undiagnostic. Phyllolepids are widespread in the Givetian and younger rocks in Gondwana (around Australia, Antarctica, Turkey, Venezuela) but do not occur until the Late Devonian (Famennian) in the Northern Hemisphere (Europe, Russia, Greenland, North America) following the post-Givetian Laurentia-North Gondwana collision and thus a Gondwanan origin for the group was proposed by Young (2005).

2.6.1 Carboniferous

The Moogooree Limestone has yielded a rich microvertebrate fauna that has yet to be formally described, although there is a preliminary report (Trinajstic and George, 2009). Abundant actinopterygian (palaeoniscoid teeth, radial bones and scales) and acanthodian (scales) (Figure 2.7B) remains have been recovered. The chondrichthyan taxa show great diversity with representatives of the Phoebodontidae (*Thrinacodus ferox* Figure 2.7A, *Thrinacodus bicuspidatus* Figure 7C), Protacrodontidae (*Deihim mansureae* Figure 2.7D-E, Protacrodus sp.), Stethacanthidae (*Stethacanthus* sp. Figure 2.7F), Ctenacanthidae (scales) and Helodontidae (*Helodus* sp.) present. The diverse shark assemblage shows strong affinities with the Canning Basin shark fauna as well as with faunas from

Queensland (Turner, 1990; Burrow et al., 2010), South China (Wang and Turner, 1995; Ginter and Sun, 2007), Morocco (Derycke, 1992) and Iran (Hairapetian and Ginter, 2009).

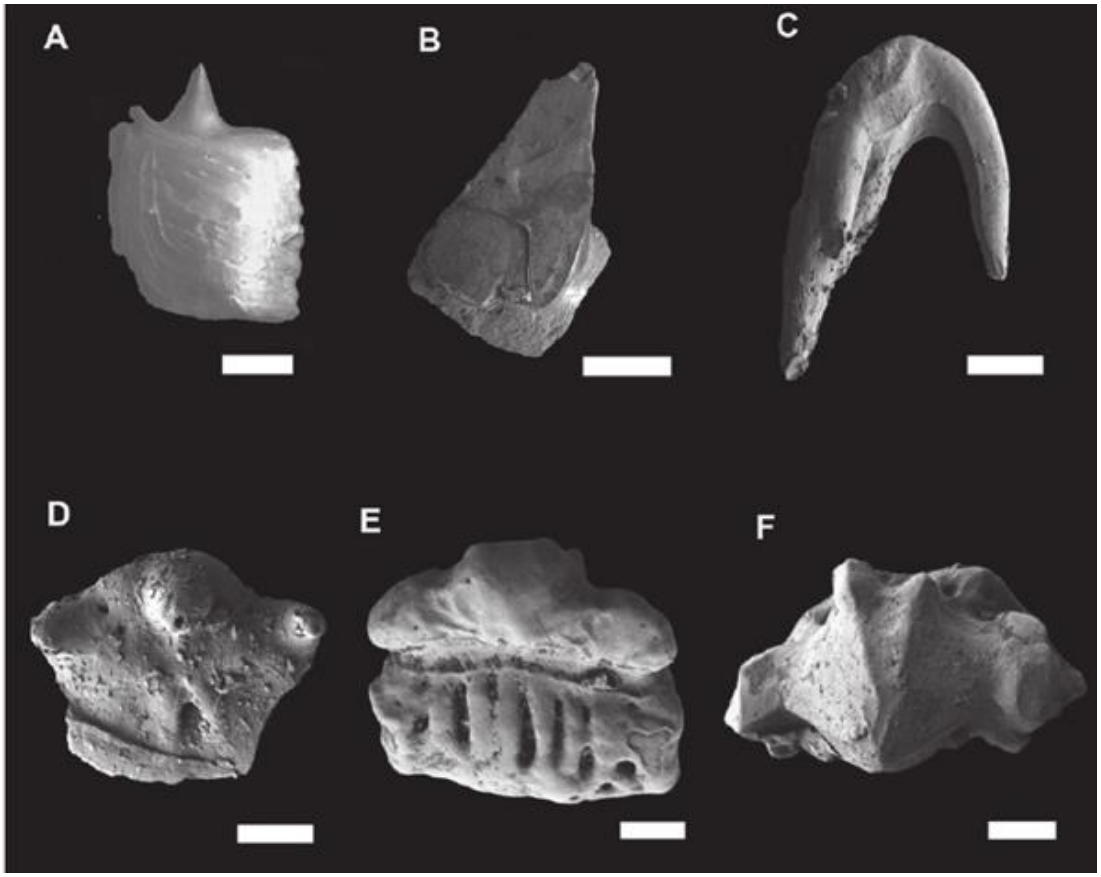

Figure 2.7. Carboniferous microremains from the Moogooree Formation, Carnarvon Basin. (A) Palaeoniscoid scale in crown view. (B) Acanthodian scale in crown view. (C) *Thrinacodus bicuspidatus* tooth in labial view. (D) Stethacanthid sp. tooth in crown view. (E) *Deihim mansureae* tooth in lingual view. (F) *Deihim mansureae* tooth in occlusal view. Scale bar: 0.4 mm.

2.6.2 Permian

In contrast to eastern Australia (Turner 1993), the Permian record of fossil fishes in Western Australia is sparse, with chondrichthyans the only taxon so far represented. The first shark tooth to be recognised from Permian strata in the Carnarvon Basin comprises 15 teeth arranged along a common spiral root and was designated as *Edestus davisii* by Woodward (1886). The specimen was collected in the valley of the Arthur River, although as the tooth whorl was not found in situ its

exact locality could not be determined. The discovery represented the first record of a novel group of chondrichthyans characterised by the presence of a continuous spiralled tooth whorl. The first description of this unique shark was of *Helicoprion bessonowi* from the Ural Mountains by Karpinsky (1899) and in his monograph he referred the tooth recovered by Woodward to his new genus *Helicoprion*. However, Eastman (1902) referred the Western Australian tooth whorl to the genus *Campyloprion*, which he had erected, and Hay (1909) referred the material to another genus *Lissoprion*. Controversy remained as to the exact taxonomic affinities of the Western Australian tooth whorl until in 1937 a second specimen comprising 5 teeth was recovered from the bed of the Minilya River near Wandagee Station, although, it too was not in situ. Two years later a third specimen was recovered in situ (Teichert. 1940) from the Wandagee Stage (Teichert, 1939) [now Wandagee Formation (Condon, 1967)] and this new material confirmed the interpretation of Karpinsky (1912) that Woodward's original Western Australian tooth whorl belonged to the genus *Helicoprion*, and all three specimens were referred to *Helicoprion davissi* by Teichert (1940).

Helicoprion has a worldwide distribution and its importance in biostratigraphy and correlation was documented early (David and Sussmilch, 1931). However, it is the unique morphology of the continuous spiralled tooth whorl and how it functioned that has intrigued scientists the most. Karpinsky (1899) variously reconstructed the spiral tooth whorl at the extreme anterior of the upper mouth, on the leading edge of the dorsal fin and even on the tail, although most recent reconstructions show the tooth whorl overhanging the lower jaw (Long, 1995). Computerised tomographic scans of the only *Helicoprion* specimen to preserve endoskeletal elements associated with the tooth whorl have revealed that it occupied

the complete mandibular arch (Tapinila et al., 2013). The largest teeth on the tooth whorl were positioned at the back of the mouth and the shark is interpreted to have eaten soft prey such as squid, using a saw-like motion to slice prey (Tapinila et al., 2013).

2.7 Biogeography

2.7.1 Ordovician

The distribution of arandaspids indicates interchange between Australia and South America via northern Gondwana with occurrences in Bolivia, Argentina and Oman as well as central and western Australia (Sansom et al., 2013), with all occurrences in a narrow environmental range in nearshore facies. The Larapinta seaway must have been open between the latter two regions, at least intermittently in the Middle to Late Ordovician to allow dispersal from the Amadeus to the Canning Basin (Blewett, 2012).

2.7.2 Silurian

The rare vertebrate faunas recovered from the Silurian of Western Australia show possible affinities with mid to Late Silurian assemblages from Iran, the Baltic and northern Eurasia, and possibly South China (Hairapetian et al., 2008; Burrow et al., 2010; Turner, 2014), all in deposits that are also from shallow marine to evaporitic environments. The faunas differ markedly from those of a similar age in southeastern Australia (Burrow et al., 2010). Porosiform poracanthodid remains are found in several of the eastern Australian deposits, but are so far lacking from Western Australia. The only described thelodont known from eastern Australia is a purported turiniid, *Turinia fuscina* (Turner, 1997). This form, however, is similar to

that described as *Niurolepis susanae* in Iran; for now it is best left as ?*Turinia fuscina* (Burrow et al., 2010). The new Western Australian thelodont(s) 147 resemble thelodontidid and loganelliid taxa found elsewhere in northern Gondwana and parts of Laurentia; there are possible links also with rare thelodont scales found in Indonesia (Turner et al., 1995; Hairapetian and Ginter, 2009).

2.7.3 Devonian

2.7.3.1 Emsian

The key taxon of the Wilson Cliffs borehole assemblage, *Turinia australiensis* (Figure 2.1A-D), has an interesting transcontinental distribution. In southeastern Australia, all occurrences of *Turinia australiensis sensu stricto*, both marine and non-marine, are of late Pragian to early Emsian age (Turner, 1997). Distribution of *T. australiensis* and closely related species extends westward from beds referred to the Cravens Peak Formation, western Queensland, from the Mulga Downs Group, Darling Basin, western New South Wales, and Mt Winter beds of the Pertnjara Group, Amadeus Basin, central Australia (Young et al., 1987; Turner, 1997), on to the type locality of Wilson Cliffs in the Canning Basin, and other boreholes in Western Australia (Burrow et al., 2010; Turner, 2014). These records indicate periodic shallow-water marine incursions of the predominantly non-marine basins of central Australia, following the alignment of the older ephemeral Larapinta seaway.

2.7.3.2 Frasnian

The common vertebrate fauna in the three Palaeozoic Basins of Western Australia supports tectonic data indicating a connection, via the North West Shelf, between the Carnarvon and Canning Basins (Stuckmeyer and Totterdell, 1992).

There are also greater faunal similarities between the marine faunas of Western Australia and those of northern and western Gondwana, consisting primarily of what are now South America, Africa, Iran and the Arabian Peninsula and Armorica than with the faunas of East Gondwana comprising eastern Australia, Antarctica and south-eastern parts of China, a pattern similar to that seen with certain invertebrates (Feist and McNamara, 2007, 2013; McNamara et al., 2009). This may reflect the fact that the vertebrate faunas of eastern Australia come from predominantly marginal/non-marine facies. However, an alternative hypothesis is that during the early Frasnian, eastern Australia was influenced by different ocean currents, which favoured migration to regions other than Western Australia. Klapper (1989) reported a similar pattern in the biogeographic relationship of conodonts, and concluded that migration of cosmopolitan species (both offshore and nearshore) was affected mainly by oceanic currents. A palaeogeographic map indicating the main palaeocurrents supports this view (Hairapetian et al., 2015), with the coast of Western Australia influenced by different currents than the shores of what is now eastern Australia.

2.7.3.3 Famennian-Carboniferous

The Famennian is characterised by a more cosmopolitan vertebrate fauna (Young et al., 2010, Hairapetian et al., in press). This is reflected primarily in the occurrence of chondrichthyan taxa common to the Canning, Carnarvon and Bonaparte basins in Western Australia.

2.8 Conclusions

In general, studies over recent decades have increased the known biodiversity of Palaeozoic vertebrate taxa from that part of Gondwana that is now Western Australia. Both new exploration and re-study of former drill cores and sites is

yielding much new data, which is proving valuable in biostratigraphical studies and understanding of how this part of Gondwana was positioned at that time.

The significance of the macro- and microvertebrate faunas of Western Australia is their remarkable preservation, predominantly 3D, and in the majority of cases showing the fine histological details of the original hard tissues, without recrystallisation or other diagenetic processes obscuring their structure. The exception is the vertebrates from the Famennian Willaraddie Sandstone, where they are preserved as impressions, although 3D latex casts can be made of these. This has allowed significant breakthroughs in understanding of vertebrate faunas in Western Australia. The Gogo Formation area is also now noted as a rich and important contribution to Australian and global geoheritage (Long, 2004, 2006; Turner, 2009); the astonishing detail of preservation is grounds enough for putting this area forward for World Heritage status.

The recognition of variation in morphology, both ontogenetic and regional variation on articulated macrovertebrate fossils from the Gogo Formation, has made the identification of isolated scales to generic and, in some cases, to species level possible at other sites in Western Australia and globally. This has increased the known range of some taxa and also enabled the greater use of microvertebrate taxa for correlation, and phylogenetic, biostratigraphic and biogeographic studies.

2.9 Acknowledgements

We would like to thank several people for providing access to collections under their care: Peter Haines/Heidi Johnson (Geological Survey of Western Australia, Perth), Martha Richter (Natural History Museum, London), Mikael Siversson (Western Australian Museum) and David Pickering (Museum Victoria).

Thanks to the reviewer Ken McNamara for helpful comments. This work is funded by Australian Research Council (ARC) QEII Fellowship to KT, ARC DP110101127 to KT, and JL, ARC DP 1092870 to KT, CB and JL.

2.10 References

Ahlberg, P., Trinajstic, K., Johanson, Z. and Long, J. 2009. Pelvic claspers confirm chondrichthyan-like internal fertilization in arthrodires. Nature 460, 888-889.

Andrews, M., Long. J., Ahlberg, P., Barwick, R. and Campbell, K. 2006. The structure of the sarcopterygian *Onychodus jandemarrai* n. sp. from Gogo, Western Australia: with a functional interpretation of the skeleton. Transactions of the Royal Society of Edinburgh Earth Sciences 96, 197-307.

Basden, A., Burrow, C.J., Hocking, R., Parkes, R. and Young, G.C. 2000. Siluro-Devonian microvertebrates from south-eastern Australia. In: Blieck., A. and Turner., S. (eds) Palaeozoic vertebrate biochronology and global marine/non-marine correlation. Final report of IGCP 328 (1991-1996), pp. 201-222. Courier Forschungsinstitut Senckenberg 223.

Blewett, R. 2012. Shaping a Nation: A geology of Australia. Geoscience Australia and ANU E Press, Canberra.

Blieck, A. and Turner, S. 2000. IGCP 328: Palaeozoic microvertebrates final scientific report - Introduction. In: Blieck A and Turner S (eds) Palaeozoic vertebrate biochronology and global marine/non-marine correlation. Final report of IGCP 328 (1991-1996), pp. 1- 67. Courier Forschungsinstitut Senckenberg 223.

Blieck, A. and Turner. 2003. Global Ordovician vertebrate biogeography. Palaeogeography, Palaeoclimatology, Palaeoecology 195, 37-54.

Burrow, C.J. 2002. Lower Devonian acanthodian faunas and biostratigraphy of south-eastern Australia. Memoirs of the Association of Australasian Palaeontologists 27, 75-137.

Burrow, C.J. 2003. Redescription of the gnathostome fauna from the mid-Palaeozoic Silverband Formation, the Grampians, Victoria. Alcheringa 27, 37-49.

Burrow, C.J., Trinajstic, K. and Long, J. 2012. First acanthodian from the Upper Devonian (Frasnian) Gogo Formation, Western Australia. Historical Biology 24, 349-357.

Burrow, C.J., Turner, S. and Young, G.C.2010. Middle Palaeozoic microvertebrate assemblages and biogeography of East Gondwana (Australasia, Antarctica). Palaeoworld 19, 37-54.

Cadman, S.J., Pain, L., Vuckovic, V. and Le Poidevin, R. 1993. Canning Basin, W.A. Bureau of Resource Sciences, Australian Petroleum Accumulations Report 9.

Chambers, B.L. 2003. Early Carboniferous vertebrate microfossils from the Bonaparte Basin, Northern Australia. MSc thesis (unpublished), James Cook University, Townsville (unpublished) [not 2002 as in Burrow et al., 2010].

Choo, B. 2011. Revision of the actinopterygian genus Mimipiscus (=Mimia) from the Upper Devonian Gogo Formation of Western Australia and the interrelationships of the early Actinopterygii. Earth and Environemntal Science Transactions of the Royal Society of Edinburgh 102, 71-104.

Choo, B., Long, A. and Trinajstic, K. 2009. A new genus and species of basal actinopterygian fish from the Upper Devonian Gogo Formation of Western Australia. Acta Zoologica 90, 194-194.

Chow, N., George, A.D. and Trinajstic, K.M. 2004. Tectonic control on development of a Frasnian-Famennian (Late Devonian) palaeokarst surface, Canning Basin reef complexes, northwestern Australia: Australian Journal of Earth Sciences, 51, 911–917.

Chow, N., George, A., Trinajstic, K. and Chen, Z.Q. 2013. Stratal architecture and platform evolution of an early Frasnian syntectonic carbonate platform, Canning Basin, Australia. Sedimentology 60, 1583-1620.

Clement, A 2012. A new species of long-snouted lungfish from the Late Devonian of Australia, and its functional and biogeographical implications. Palaeontology 55, 51-71.

Clement, A. and Long, J. 2010. *Xeradipterus hatcheri*, a new dipnoan from the late Devonian (Frasnian) Gogo Formation, Western Australia, and other new holodontid material. Journal of Vertebrate Paleontology 30, 681-695.

Cockbain, A.E. 1976. *Stromatoporella kimberleyensis* Etheridge Jr. 1918 is a piece of bone. Geological Survey of Western Australia Annual Report for 1975 133-135.

Condon, M.A. 1967. The geology of the Carnarvon Basin, Western Australia. Part 2: Permian stratigraphy. Bureau of Mineral Resources Bulletin 77.

David, T. and Sussmilch, C. 1931. Upper Palaeozoic glaciation of Australia: Geology Society of America Bulletin 42, 481-522.

Dennis, K. and Miels, R.S. 1981. A pachyosteomorph arthrodire from Gogo, Western Australia. Zoological Journal of the Linnean Society 73, 213-258.

Derycke, C. 1992. Microrestes de sélaciens et autres Vertebres du Dévonien supérieur du Maroc. Bulletin de Muséum national d'Histoire naturelle 14, 15-61.

Dring, R. 1980. Palaeobiology of the Gneudna Formation, Late Devonian (Frasnian), Carnarvon Basin, Western Australia. PhD thesis, University of Western Australia, Nedlands (unpublished).

Eastman, C.R. 1902. On Campyloprion, a new form of Edestus-like dentition. Geological Magazine (Decade IV) 9, 148-152.

Edwards, A.F. 1997. Ichthyolith remains from the Devonian Carboniferous Boundary of the Canning Basin, Western Australia. MSc thesis, Macquarie University, Sydney (unpublished).

Esin, D. 1990. The scale cover of *Amblypterina costata* (Eichwald) and the paleoniscid taxonomy based on isolated scales. Paleontological Journal 2, 90-98.

Etheridge, R.J.R. 1918. Observations on Carboniferous and other fossils. In: Basedow, H. Narrative of an expedition of exploration in northwestern Australia, pp. 250-262. Royal Geographical Society of Australasia, South Australian Branch, Transactions 18.

Feist, R. and McNamara, K.J. 2007. Biodiversity, distribution and patterns of extinction of the last odontopleuroid trilobites during the Devonian (Givetian, Frasnian). Geological Magazine 144, 777-796.

Feist, R., and McNamara, K.J. 2013. Patterns of evolution and extinction in proetid trilobites during the Late Devonian mass extinction event, Canning Basin, Western Australia. Palaeontology 56, 229-259.

Gagnier, P.Y., Blieck, A., Emig, C.C., Sempere, T., Vachard, D. and Vanguestaine, M. 1996. New paleontological and geological data on the Ordovician and Silurian of Bolivia. Journal of South American Earth Sciences 9, 329-347.

Gardiner, B. 1984. Relationships of the palaeoniscoid fishes, a review based on new specimens of Mimia and Moythomasia from the Upper Devonian of Western Australia. Bulletin of the British Museum of Natural History (Geology) 37, 173-428.

Gholamalian, H. and Kebriaei, M.R. 2008. Late Devonian conodonts from the Hojedk section, Kerman Province, Southeastern Iran. Rivista Italiana di Paleontologia e Stratigrafia, 114, 17-181.

Ginter, M., Duffin, C. and Hampe. O. 2010. Chondrichthyes (Paleozoic Elasmobranchii: teeth). In: Schultze H-P., (ed.) Handbook of Paleoichthyology, vol. 3D. Friedrich Pfeil Verlag, München.

Ginter, M. and Ivanov, A. 1992. Devonian phoebodont shark teeth. Acta Palaeontologica Polonica 37, 55-75.

Ginter, M. and Sun, Y. 2007. Chondrichthyan remains from the Lower Carboniferous of Muhua, southern China. Acta Palaeontologica Polonica 52, 705-727.

Ginter, M. and Turner, S. 2010. The Middle Palaeozoic selachian genus *Thrinacodus*. Journal of Vertebrate Paleontology 30, 1666- 1672.

Glauert, L. 1910. New fossils from Barker Gorge, Napier Range, Kimberley Geological Survey of Western Australia Bulletin 36, 111-114.

Gorter, J., Mory, A. and Nicoll, R. 1998. Sequence stratigraphy and hydrocarbon potential of the Middle to Upper Devonian (Givetian-Frasnian) sequences in the Carnarvon Basin, Western Australia. In Purcell, P.C. and Purcell, R.R. (eds) The sedimentary basins of Western Australia 2, pp. 450-510. Petroleum Exploration Society of Australia Symposium, Perth, WA, 1998 Proceedings.

Graham, J.B., Wegner, N.C., Miller, L.A., Jew. C.J., N-C., Berquist, R.M., Frank, L. and Long, J.A. 2014. Spiracular air breathing in polypterid fishes and its implications for aerial respiration in stem tetrapods. Nature Communications 5, doi:10.1038/ncomms4022.

Gross, W. 1971. Unterdevonische Thelodontier und Acanthodier Schuppen aus Westaustralien. Paläontologische Zeitschrift 45, 97-106.

Hairapetian, V., Blom, H. and Miller, G.C. 2008. Silurian thelodonts from the Niur Formation, central Iran. Acta Palaeontologica Polonica 53, 85-95.

Hairapetian, V. and Ginter, M. 2009. Pelagic chondrichthyan microremains from the Upper Devonian of the Kale Sardar section, eastern Iran. Acta Geologica Polonica 60, 357-371.

Hairapetian, V., Roelofs, B.P.A., Trinajstic, K.M., and Turner, S. 2015. Famennian survivor turiniid thelodonts of North and East Gondwana. Geological Society, London, Special Publications 423, 423-433.

Hairapetian, V., Valiukevičius, J. and Burrow, C.J. 2006. Acta Palaeontologica Polonica 51, 499-520.

Hansma, J., Tohver E., Yan, M., Trinajstic, K., Roelofs, B., Peek, S., Slotznick, S.P., Kirschvink, J., Playton, P. Haines, P. and Hocking, R. 2015. Late Devonian carbonate magnetostratigraphy from the Oscar and Horse Spring Ranges, Lennard Shelf, Canning Basin, Western Australia. Earth and Planetary Science Letters. 409, 232-242.

Hay, O. 1909. On the nature of *Edestus* and related genera, with descriptions of one new genus and three new species. Proceedings United States National Museum 37, 43-61.

Heintz, A. 1932. The structure of Dinichthys: a contribution to our knowledge of the Arthrodira. In: Gudger, E. (ed.) The Bashford Dean Memorial Volume: Archaic Fishes, pp. 115-224. American Museum of Natural History, New York.

Hocking, R.M. 1990. Carnarvon Basin. In: Geology and Mineral Resources of Western Australia, pp. 457-495. Geological Survey of Western Australia Memoir 3.

Hocking, R.M., Moors, H.T.. and Van De Graafe, J.E. 1987. Geology of the Carnarvon Basin, Western Australia. Geological Survey of Western Australia Bulletin 133.

Hocking, R.M., Playford, P.E., Haines, P.W. and Mory, A.J. 2008. Paleozoic geology of the Canning Basin - a field guide Geological Survey of Western Australia Record 2008/18.

Holland, T 2013. Pectoral girdle and fin anatomy of *Gogonasus andrewsae* Long 1985: implications for tetrapodomorph limb evolution. Journal of Morphology 274, 147-164.

Holland, T and Long, J.A. 2009. On the phylogenetic position of *Gogonasus andrewsae* Long, J.. 1985, within the Tetrapodamorpha. Acta Zoologica 90, 285-96

Jarvik, E. 1980. Basic structure and evolution of vertebrates. Academic Press, London.

Johanson, Z 2003. Placoderm branchial and hypobranchial muscles and origins in jawed vertebrates. Journal of Vertebrate Paleontology 23, 735-749.

Johanson, Z. and Trinajstic, K. 2014. Fossilized ontogenies: the contribution of placoderm ontogeny to our understanding of the evolution of early gnathostomes. Palaeontology DOI: 10.1111/pala.12093.

Jones, P., Metcalfe, I., Engel. B.A., Playford, G., Rigby, J. Roberts, J., Turner, S. and Webb, G.E. 2000. Carboniferous palaeobiogeography of Australasia. In: Wright, A.J., Young, G.C., Talent, J.A. and Laurie, J.R. (eds) Palaeobiogeography of Australasian faunas and floras, pp. 259-286. Memoir of the Association of Australasian Palaeontologists 23.

Karpinksy, A.P. 1899. On the edestid remains and its new genus *Helicoprion*. Zapiski Imperatorski Akademii Nauk 7, 1-67 (in Russian).

Karpinksy, A.P. 1912. On *Helicoprion* and other Edestidae. Proceedings of the Russian Mineralogical Society 49, 69-94 (in Russian).

Klapper, G. 1989. The Montagne Noire Frasnian (Upper Devonian) conodont succession. In: McMillan, N.J., Embry, A.F. and Glass, D.J. (eds) Devonian of the World, vol 3, pp. 449-468. Canadian Society of Petroleum Geologists Memoir 14.

Long, J.A. 1985. A new osteolepidid fish from the Upper Devonian Gogo Formation, Western Australia. Records of the Western Australian Museum 12, 361-377.

Long, J.A. 1986. A new Late Devonian acanthodian fish from Mt. Howitt, Victoria, Australia, with remarks on acanthodian biogeography. Proceedings of the Royal Society of Victoria 98, 1- 17.

Long, J.A. 1987. A new dinichthyid fish (Placodermi: Arthrodira) from the Upper Devonian of Western Australia, with a discussion of dinichthyid interrelationships. Records of the Western Australian Museum 13, 515-540.

Long, J.A. 1988. Late Devonian fishes from Gogo, Western Australia National Geographic Research 4, 436-449.

Long, J.A. 1990. Late Devonian chondrichthyans and other microvertebrate remains from northern Thailand. Journal of Vertebrate Paleontology 10, 59-71.

Long, J.A. 1991. The long history of Australian fossil fishes. In: Vickers-Rich, P., Monaghan, J.M., Baird, R.F. and Rich, T.H. (eds) Vertebrate palaeontology of Australasia, pp. 337-428. Pioneer Design Studio, Melbourne.

Long, J.A. 1993. Palaeozoic vertebrate biostratigraphy of SouthEast Asia and Japan. In: Long, J.A. (ed.) Palaeozoic vertebrate biostratigraphy and biogeography, pp. 277-289. Belhaven Press, London.

Long, J.A. 1995. The rise of fishes. The Johns Hopkins University Press, Baltimore.

Long, J.A. 2004. Gogo fish! The story of the Western Australian State Fossil emblem. Western Australian Museum, Perth.

Long, J.A. 2006. Swimming in Stone: The Amazing Gogo Fossils of the Kimberley. Fremantle Press, Perth.

Long, J.A. and Trinajstic, K. 2000. Devonian microvertebrate faunas of Western Australia. In: Blieck, A. and Turner, S. (eds) Palaeozoic vertebrate biochronology and global marine/non-marine correlation. Final report of IGCP 328 (1991-1996), pp. 471-486. Courier Forschungsinstitut Senckenberg 223.

Long, J.A. and Trinajstic, K. 2010. The Late Devonian Gogo Formation Lägerstatte of Western Australia: exceptional early vertebrate preservation and diversity. Annual Review of Earth and Planetary Sciences 38, 255-279.

Long, J.A., Trinajstic, K. and Johanson, Z. 2009. Devonian arthrodire embryos and the origin of internal fertilization in vertebrates. Nature 457, 1124-1127.

Long, J.A., Trinajstic, K., Young, G.C. Senden, T. 2008. Live birth in the Devonian period. Nature 453, 650-652.

Long, J.A., Young,, G.C., Holland, T., Senden, T. and Fitzgerald, E.M.G. 2006. An exceptional Devonian fish sheds light on tetrapod evolution. Nature 444, 199-202.

Macadie, C.I. 2002. Thelodont fish and conodonts from the Lower Devonian of Reefton, New Zealand. Alcheringa 26, 423-433.

Mawson, R., Talent, J.A., Bear, V.C., Benson, D.S., Brock, G.A, Farrell, J.R., Hyland, K.A., Pyemont, B.D, Sloan, T.R, Sorentino, L, Stewart, M.I., Trotter, J.A, Wilson, G.A. and Simpson, A. 1988. Conodont data in relation to resolution of Stage and zonal boundaries for the Devonian of Australia. In: McMillan, N.J., Embry, A.F. and Glass, D.J. (eds) Devonian of the World, vol 3, pp. 485-527. Canadian Society of Petroleum Geologists Memoir 14.

McNamara, K., Feist, R. and Ebach, M. 2009. Patterns of evolution and extinction in the last harpetid trilobites during the Late Devonian (Frasnian). Palaeontology 52, 11-33.

Melendez, I., Grice, K., Trinajstic, K., Ladjavardi, M., Greenwood, P. and Thompson, K. 2013. Biomarkers reveal the role of photic zone euxinia in exceptional fossil preservation: an organic geochemical perspective. Geology 41, 123-126.

Miles, R.S. 1967. Observations on the ptyctodont fish *Rhamphodopsis* Watson. Zoological Journal of the Linnean Society of London 47, 99-120.

Miles, R.S. 1969. Features of placoderm diversification and the evolution of the arthrodire feeding mechanism. Transactions of the Royal Society of Edinburgh 68, 123-170.

Miles, R.S. 1971. The Holonematidae (placoderm fishes): a review based on new specimens of *Holonema* from the Upper Devonian of Western Australia. Philosophical Transactions of the Royal Society B263, 101-234.

Miles, R.S. and Young, G.C. 1977. Placoderm interrelationships reconsidered in the light of new ptyctodontids from Gogo Western Australia. Linnean Society of London Symposium Series 4, 123-198.

Moors, H.T. 1981. An alluvial fan-fluvial plain depositional model for the Devonian Willaraddie Formation and Manubia sandstone of the Carnarvon Basin, W.A. Geological Survey of Western Australia Annual Report for 1980, 62-67.

Nicoll, R.S. 1977. Conodont apparatuses in an Upper Devonian palaeoniscoid fish from the Canning Basin, Western Australia. BMR Journal of Australian Geology and Geophysics 2, 217-278.

Nicoll, R. 1979. A Late Devonian age for the Munabia Sandstone, Carnarvon Basin, W.A. Bureau of Mineral Resource, Professional Oil Geology 79/034 (unpublished).

Ørvig, T. 1960. New finds of acanthodians, arthrodires, crossopterygians, ganoids and dipnoans in the upper Middle Devonian Calcareous Flags (Oberer Plattenkalk) of the bergisch-Paffrath Trough. (Part 1). Paläontologische Zeitschrift 34, 295-335.

Patterson, C. 1965. The phylogeny of the chimaeroids. Philosophical Transactions of the Royal Society B249, 101-219.

Parkes, R. 1995. Late Silurian-Early Devonian vertebrate microremains from Nevada and southeastern Australia: biochronology, biogeography and application of novel histological techniques. BSc (Hons) thesis, Macquarie University, North Ryde (unpublished).

Playford, P.E, Hocking, R.M. and Cockbain, A.E. 2009. Devonian reef complexes of the Canning Basin, Western Australia. Geological Survey of Western Australia Bulletin 145.

Qu. Q., Sanchez, S., Blom, H., Tafforeau, P. and Ahlberg, P. 2013a. Scales and tooth whorls of ancient fishes challenge distinction between external and oral 'teeth' PloS One 8 (8), e71890.

Qu, Q., Zhu, M. and Wang, W. 2013b. Scales and dermal skeletal histology of an early bony fish *Psarolepis romeri* and their bearing on the evolution of rhombic scales and hard tissues. PLoS ONE 8, e61485.

Ritchie, A. 1973. *Wuttagoonaspis* gen. nov., an unusual arthrodire from the Devonian of western New South Wales, Australia. Palaeontographica A 143, 58-72.

Ritchie, A. 1975. *Groenlandaspis* in Antarctica, Australia and Europe. Nature 254, 569-574.

Ritchie, A. and Gilbert-Tomlinson, J. 1977. First Ordovician vertebrates from the Southern Hemisphere Alcheringa 1, 351- 368.

Roelofs, B., Trinajstic, K., Playton, T.E., Tohver, E., Haines, P., Hocking, R., Barham, M., Hansma, J., Hillbun, K., Grice, K., Maodu, Y., Ratcliff, K., Pisarevsky, S. and Montgomery, P. 2013. Vertebrate biostratigraphy from the Devonian and Carboniferous in the Canning Basin, Western Australia. In: Keep, M. and Moss, S.J. (eds) The Sedimentary Basins of Western Australia 4, Abstracts. Proceedings of the Petroleum Exploration Society of Australia Symposium, Perth, WA, 2013.

Rucklin, M., Donoghue, P.C.J., Johanson, Z., Trinajstic, K., Marone, F. and Stampanoni, M 2012. Development of teeth and jaws in the earliest jawed vertebrates. Nature 491, 748-751.

Sanchez, S., Ahlberg, P.E., Trinajstic, K., Mirone, A. and Tafforeau, P. 2012. Three-dimensional synchrotron virtual paleohistology: a new insight into the world of fossil bone microstructures. Microscopy and Microanalysis 18, 1095-1105.

Sanchez, S., Dupret, V., Tafforeau, P., Trinajstic, K.M., Ryll, B., Gouttenoire, P.-J., Wretman, L., Zylberberg, G.L., Peyrin, F. and Ahlberg, P.E. 2013. 3D Microstructural architecture of muscle attachments in extant and fossil vertebrates revealed by Synchrotron Microtomography. PLoS ONE 8, e56992.

Sansom, I.J., Haines, P.W, Andreev, P. and Nicoll, R.S. 2013. A new pteraspidomorph from the Nibil Formation (Katian, Late Ordovician) of the Canning Basin, Western Australia. Journal of Vertebrate Paleontology 33, 764-769.

Sansom, I.J., Miller, G.C., Heward, A., Davies, N.S., Booth, G.A,, Fortey, R.A. and Paris, F. 2009. Ordovician fish from the Arabian peninsular. Palaeontology 52, 337-342.

Seddon, G. 1969. Conodont and fish remains from the Gneudna Formation, Carnarvon Basin, Western Australia. Journal of the Royal Society of Western Australia 52, 21-30.

Shen, J., Webb, G. and Jell, J. 2008. Platform margins, reef facies, and microbial carbonates; a comparison of Devonian reef complexes in the Canning Basin,

Western Australia, and the Guilin region, South China. Earth-Science Reviews 88, 33-59.

Smith, M. and Johanson, Z. 2003. Separate evolutionary origins of teeth from evidence in fossil jawed vertebrates. Science 299, 1235-1236.

Struckmeyer, H.I.M. and Totterdell, J.M. (Editors). 1992. Australia, Evolution of a Continent / BMR Palaeogeographic Group. Australian Government Publishing Service, Canberra.

Tapanila, L., Pruitt, J., Pradel, A., Wilga, C., Ramsay, J., Schlader, R. and Didier, D. 2013. Jaws for a spiral tooth whorl: CT images reveal novel adaptation and phylogeny in fossil *Helicoprion*. Biology Letters doi 10.1098/rsbl.2013.0057.

Teichert, C. 1939. Recent research work in the Permian of Western Australia. Australian Journal of Science 2, 5-7.

Teichert, C. 1940. *Helicoprion* in the Permian of Western Australia. Journal of Paleontology 14, 140-149.

Thomas G.A. 1957. Lower Carboniferous deposits in the Fitzroy Basin, Western Australia. Australian Journal of Science 19, 160-161.

Trinajstic, K.M. 1997. The biostratigraphic implications of isolated scales from Late Devonian palaeoniscoids. Abstract of paper presented at the Sixth Conference on Australasian Vertebrate Evolution Palaeontology and Systematics 7-11 July 1997: 60, Western Australian Museum, Perth.

Trinajstic, K. 1999a. New anatomical information on *Holonema* (Placodermi) based on material from the Frasnian Gogo Formation and the Givetian-Frasnian Gneudna Formation, Western Australia. Geodiversitas 21, 69-84.

Trinajstic, K. 1999b Scales of palaeoniscoid fishes (Osteichthyes: Actinopterygii) from the Late Devonian of Western Australia Records of the Western Australian Museum Supplement 57, 93- 106.

Trinajstic, K. 1999c. Scale morphology of the Late Devonian palaeoniscoid *Moythomasia durgaringa* Gardiner and Bartram, 1977. Alcheringa 23, 9-19.

Trinajstic, K. 2000. Conodonts, thelodonts and phoebodonts— together at last Geological Society of Australia Abstracts 61, 121.

Trinajstic, K. 2001a. A description of additional variation seen in the scale morphology of the Frasnian thelodont *Australolepis seddoni* Turner and Dring, 1981. Records of the Western Australian Museum Supplement 20, 237-246.

Trinajstic, K. 2001b. Acanthodian microremains from the Frasnian Gneudna Formation, Western Australia. Records of the Western Australian Museum Supplement 20, 187-198.

Trinajstic, K. Boisvert, C., Long, J. Maksimenko, A. and Johanson, Z. in press a. Pelvic and reproductive structures in placoderms (stem gnathostomes). Biological Reviews.

Trinajstic, K. and George, A.D. 2009. Microvertebrate biostratigraphy of Upper Devonian (Frasnian) carbonate rocks in the Canning and Carnarvon basins of Western Australia. Palaeontology 52, 641.

Trinajstic, K., Grice, K., Downes, P., Botticher., M., Melendez, I., Dellwig, O, Burrow, C. and Verral;, M. in press b. Mineralized muscles and organs in a 380 million year old actinopterygian fish from the Gogo Formation, Western Australia. PLoS ONE.

Trinajstic, K. and Johanson, Z. 2014. Fossilized ontogenies: the contribution of placoderm ontogeny to our understanding of the evolution of early gnathostomes Palaeontology 57, 505- 516.

Trinajstic, K. and Long J.A. 2009. A new genus and species of ptyctodont (Placodermi) from the Late Devonian Gneudna Formation, Western Australia, and an analysis of ptyctodont phylogeny. Geological Magazine 146, 743-760.

Trinajstic, K., Long, J., Johanson, Z., Young, G. and Senden, T. 2012. New morphological information on the ptyctodontid fishes (Placodermi, Ptyctodontida) from Western Australia. Journal of Vertebrate Paleontology 32, 757-780.

Trinajstic, K., Marshall, C., Long, J.A. and Bifield, K. 2007. Exceptional preservation of nerve and muscle tissues in Late Devonian placoderm fish and their evolutionary implications. Biology Letters 3, 197-200.

Trinajstic, K., Sanchez, S., Dupret, V., Tafforeau, P., Long, J., Young, G., Senden, T., Boisvert, C., Power, N. and Ahlberg, 2013. Fossil musculature of the most primitive jawed vertebrates. Science 341, 160-164.

Turner, S. 1982a. Thelodonts and correlation. In: Rich P.V. and Thompson E.M. (eds) The Fossil Vertebrate Record of Australasia, pp. 128-132. Monash University Offset Printing Unit, Clayton.

Turner, S. 1982b. Middle Palaeozoic elasmobranch remains from Australia. Journal of Vertebrate Paleontology 2, 117-131.

Turner, S. 1990. Early Carboniferous shark remains from the Rockhampton District, Queensland. Memoirs of the Queensland Museum 28, 65-73. 151

Turner, S. 1991. Palaeozoic vertebrate microfossils in Australasia. In: Vickers-Rich, P., Monaghan, J.M., Baird, R.F. and Rich, T.H. (eds) Vertebrate palaeontology of Australasia, pp. 429-464. Pioneer Design Studio, Melbourne.

Turner, S. 1993. Palaeozoic microvertebrate biostratigraphy of Eastern Gondwana. In: Long J.A. (ed.) Palaeozoic vertebrate biostratigraphy and biogeography, pp. 174-207. Belhaven Press, London.

Turner, S. 1995. Devonian thelodont scales (Agnatha, Thelodonti) from Queensland. Memoirs of the Queensland Museum 38, 677- 685.

Turner, S. 1997. Sequence of Devonian thelodont scale assemblages in East Gondwana. In: Klapper, G., Murphy, M.A. and Talent, J.A. (eds) Paleozoic sequence stratigraphy, biostratigraphy, and biogeography: studies in honor of J. Granville ("Jess") Johnson, pp. 295-315.Geological Society of America Special Publication 321.

Turner, S. 2009. Fossil Lagerstätten in Australia: discovery and politics. In: Pemberton G (ed.) INHIGEO 34 Fossils and Fuels, Abstracts, pp. 73-74. University of Calgary, August 10-14 2009.

Turner, S. 2014. Report on Silurian and Devonian microvertebrates from Western Australian boreholes. Report to Geological Survey of Western Australia (unpublished).

Turner, S., Basden, A. and Burrow, C.J. 2000. Devonian vertebrates of Queensland. In: Blieck, A. and Turner, S. (eds) Palaeozoic vertebrate biochronology and global marine/non-marine correlation. Final report of IGCP 328 (1991-1996), pp. 487-522.Courier Forschungsinstitut Senckenberg 223.

Turner, S., Blieck, A.R.M and Nowlan, G.S. 2004. Cambrian- Ordovician vertebrates. In: Webby, B.D., Droser, M., Feist, R. and Percival, I. (eds) IGCP410. The Great Ordovician Biodiversity Event, pp. 327-335. Columbia University Press, New York.

Turner, S. Burrow, C.J., Gholamalian, H. and Yazdi, M. 2002. Late Devonian (early Frasnian) microvertebrates and conodonts from the Chahriseh area near Esfahan, Iran. Memoirs of the Association of Australasian Palaeontologists 27, 149-159.

Turner, S. and Dring, R.S. 1981. Late Devonian thelodonts (Agnatha) from the Gneudna Formation, Carnarvon Basin, Western Australia. Alcheringa 5, 39-48.

Turner, S., with contributions from Jones, R., Leu, M., Long, J.A., Palmier, V. and Stewart, I. 1994. IGCP 328: Carboniferous shark remains of Australia. In: Mawson, R. and Talent, J.A. (eds) APC- 94 (papers from the First Australian Palaeontological Convention, Macquarie University, 7-9 February 1994, Abstracts, p. 58.

Turner, S., Trinajstic, K., Hairapetian, V., Janvier, P. and Macadie, I. 2004. Thelodonts from western Gondwana. In: Richter, M. and Smith, M.M. (eds) 10th International Symposium on early vertebrates/lower vertebrates. Gramada, Brazil, 24-28 May 2004. Programme and Abstracts, pp. 45-46. UFRGS and Sociedade Brasiliera de Paleontologia.

Turner, S., Vergoossen, J.M.J. and Young, G.C. 1995. Fish microfossils from Irian Jaya. Memoirs of the Australasian Association of Palaeontologists 18, 165-178.

Upeniece, I. 1996. *Lodeacanthus gaugicus* n.g. et sp. (Acanthodii: Mesacanthidae) from the Late Devonian of Latvia. Modern Geology 20, 383-398.

Wang, S. and Turner, S. 1995. A reappraisal of Upper Devonian- Lower Carboniferous vertebrate microfossils in South China. Professional Papers of Stratigraphy and Palaeontology 26, 59-70.

Watson, D.M.S. 1934. The interpretation of arthrodires, Proceedings of the Zoological Society of London 3, 437-464.

Watson, D.M.S. 1938. On *Rhamphodopsis*, a ptyctodont from the Middle Old Red sandstone of Scotland. Transactions of the Royal Society of Edinburgh 59, 397-410.

Woodward, H. 1886. On a remarkable ichthyodorulite from the Carboniferous series, Gascoyne, Western Australia. Geological Magazine 3, 1–7.

Young, G.C. 1986. The relationships of placoderm fishes. Zoological Journal of the Linnean Society of London 88, 1-56.

Young, G.C. 1987. Devonian fish remains from Billiluna, eastern Canning Basin, Western Australia. BMR Journal of Australian Geology and Geophysics 10, 179-192.

Young, G.C. 1991. The first armoured agnathan vertebrates from the Devonian of Australia. In: Chang, M-M., Liu, Y-H. and Zhang, G-R. (eds) Early vertebrates and related problems of evolutionary biology, pp. 67-85. Science Press, Beijing.

Young, G.C. 1993. Middle Palaeozoic macrovertebrate biostratigraphy of Eastern Gondwana. In: Long J A (ed.) Palaeozoic vertebrate biostratigraphy and biogeography, pp. 208- 251. Belhaven Press, London.

Young, G.C. 1997. Ordovician microvertebrate remains from the Amadeus Basin, central Australia. Journal of Vertebrate Paleontology 17, 1-25.

Young, G.C. 2005. An articulated phyllolepid fish (Placodermi) from the Devonian of central Australia: implications for nonmarine connections with the Old Red Sandstone continent. Geological Magazine 142, 173-186.

Young, G.C. 2009. New arthrodires (Family Williamsaspididae) from Wee Jasper, New South Wales (Early Devonian), with comments on placoderm morphology and palaeoecology. Acta Zoologica 90, 69-82

Young, G.C., Burrow, C.J., Long, J.A., Turner, S. and Choo, B. 2010. Devonian macrovertebrate assemblages and biogeography of East Gondwana (Australasia, Antarctica). Palaeoworld 19, 55- 74.

Young, G.C. and Goujet, 2003. Devonian fish remains from the Dulcie Sandstone and Cravens Peak Beds, Georgina Basin, central Australia. Records of the Western Australian Museum Supplement 65,1-85.

Young, G.C., Karatajute-Talimaa, V. and Smith, M.M. 1996. A possible Late Cambrian vertebrate from Australia. Nature 383, 810-812.

Young, G.C. and Turner, S.. 2000. Devonian microvertebrates and marine nonmarine correlation in East Gondwana: overview. In: Blieck, A. and Turner, S. (eds) Palaeozoic vertebrate biochronology and global marine/non-marine correlation. Final report of IGCP 328 (1991-1996), pp. 453-470. Courier Forschungsinstitut Senckenberg 223.

Young, G.C., Turner, S., Owen, M., Nicoll, R.S., Laurie, J.R. and Gorter, J.D. 1987. A new Devonian fish fauna, and revision of post Ordovician stratigraphy in the Ross River Syncline, Amadeus Basin, central Australia. BMR Journal of Australian Geology and Geophysics 10, 233-242.

Zhu, M., Yu, X.B., Ahlberg, P.E., Choo, B., Lu, J., Qiao, T., Zhao, W., JIA, L., Blom, H. and Zhu, Y.A. 2013. Silurian placoderm with osteichthyan-like marginal jaw bones. Nature 502, 188-193.

3.0 Upper Devonian microvertebrates from the Canning Basin, Western Australia

Brett Roelofs[1], Ted Playton[2] Milo Barham[3], and Kate Trinajstic[4]

[1]Brett Roelofs. Department of Applied Geology, Curtin University, GPO Box U1987 Perth, WA 6845, Australia. brett.roelofs@postgrad.curtin.edu.au

[2]Ted Playton. Chevron Energy Technology Company, Houston, Texas, USA. E-mail: tedplay@tengizchevroil.com

[3]Milo Barham. Department of Applied Geology, Curtin University, GPO Box U1987 Perth, WA 6845, Australia. milo.barham@curtin.edu.au

[4]Kate Trinajstic*. Department of Environment and Agriculture, Curtin University, GPO Box U1987, Perth, WA 6845, Australia. K.Trinajstic@curtin.edu.au

3.1 Abstract

A diverse microvertebrate fauna is described from the Virgin Hills and Napier formations, Bugle Gap Limestone Canning Basin, Western Australia. Measured sections at Horse Spring and Casey Falls (Virgin Hills Formation) and South Oscar Range (Napier Formation) comprise proximal to distal slope carbonates ranging in age from the Late Devonian Frasnian to middle Famennian. A total of 18 chondrichthyan taxa are identified based on teeth, including the first record of *Thrinacodus tranquillus*, *Cladoides wildungensis*, *Protacrodus serra* and *Lissodus lusavorichi* from the Canning Basin. A new species, *Diademodus dominicus* sp. nov. is also described and provides the first record of this genus outside of Laurussia. In addition, the upper range of *Australolepis seddoni* has been extended to Late Devonian conodont Zone 11, making it the youngest known occurrence for this

species. The Virgin Hills and Napier formations microvertebrate faunas show close affinities to faunas recovered from other areas of Gondwana, including eastern Australia, Iran, Morocco and South China, which is consistent with known conodont and trilobite faunas of the same age.

3.2 Introduction

The Canning Basin, Western Australia (Figure 3.1) is well known for the preservation of Devonian reef complexes as well as both invertebrate and vertebrate fossils (Playford et al., 2009; Klapper, 2007; Becker et al., 1993), many of which have proved important in studies of biostratigraphy and correlation. Conodont and ammonoid faunas have both been extensively used in biostratigraphy over the past century with conodont zonations established for the Frasnian (Glenister and Klapper, 1966; Klapper, 2007; Nicoll and Playford, 1993; Metzger, 1994) as well as ammonoid zonations for the Frasnian and Famennian (Peterson, 1975; Becker et al., 1993; Becker, 2000) recognised in the Canning Basin. These fossils have proven useful in determining ages of slope and basin strata enabling successful correlation across physically disconnected localities (Glenister and Klapper, 1966; Becker et al., 1993; Becker, 2000). However, correlation between slope and platform facies within the Canning Basin remains problematic as many conodont and ammonoid faunas are absent or undiagnostic in shallow water environments. In contrast, microvertebrates have proven useful in correlating such environments (Turner, 1997; Hairapetian et al., 2000; Trinajstic and George, 2009). To date, globally correlative microvertebrate zonations are best resolved for the Silurian and early to middle Devonian (Turner, 1993; Young, 1995; Burrow and Simpson, 1995; Valiukevicius, 1995; Burrow, 1996, 1997; Turner, 1997; Burrow and Turner, 1998, 2000; Basden et al., 2000;

Valiukevicius and Kruchek, 2000). Furthermore, a Late Devonian zonation scheme based on phoebodont sharks has been established from the Frasnian to the end Famennian (Ginter and Ivanov, 1995a; Ginter, 2000; Jones and Turner, 2000; Young and Turner, 2000). Where known, the Devonian shark fauna of Western Australia (Trinajstic and George, 2009; Trinajstic et al., 2014) has been correlated to the Frasnian phoebodont zonation of Ginter and Ivanov (1995a). However, to date little work has been published on Famennian shark taxa from Western Australia. Thelodont zonation has also recently been extended into the Famennian (Hairapetian et al., 2015), although the known taxa are currently restricted to Iran and north-western Australia because other thelodonts appear to have become extinct at the end of the Givetian in other areas of the world (Turner, 1997; Trinajstic, 2001; Märss et al., 2007).

Detailed taxonomic studies on vertebrate faunas of Frasnian-age strata have been undertaken in the Carnarvon (Turner and Dring, 1981; Long, 1991; Trinajstic and George, 2009) and Canning basins of Western Australia (Long and Trinajstic, 2000; Trinajstic and George, 2009; Long and Trinajstic, 2010) with a greatest number of studies in Western Australia been done on the Frasnian macrovertebrate faunas of the Gogo Formation (see Trinajstic et al., 2014 for a review). Biostratigraphic studies into vertebrate faunas, from both the Canning and Carnarvon basins however, are less common.

The utility of Western Australian microvertebrates to date strata has been, in part, due to the ability to identify isolated scales through comparison with the exceptionally preserved fauna from the Frasnian Gogo Formation. This has been most successful with placoderms (Trinajstic, 1999a), acanthodians (Burrow et al.,

2010) and palaeoniscoids (Trinajstic, 1999b). However, a single articulated shark (Long and Trinajstic, 2010), which is not comparable with any of the isolated teeth

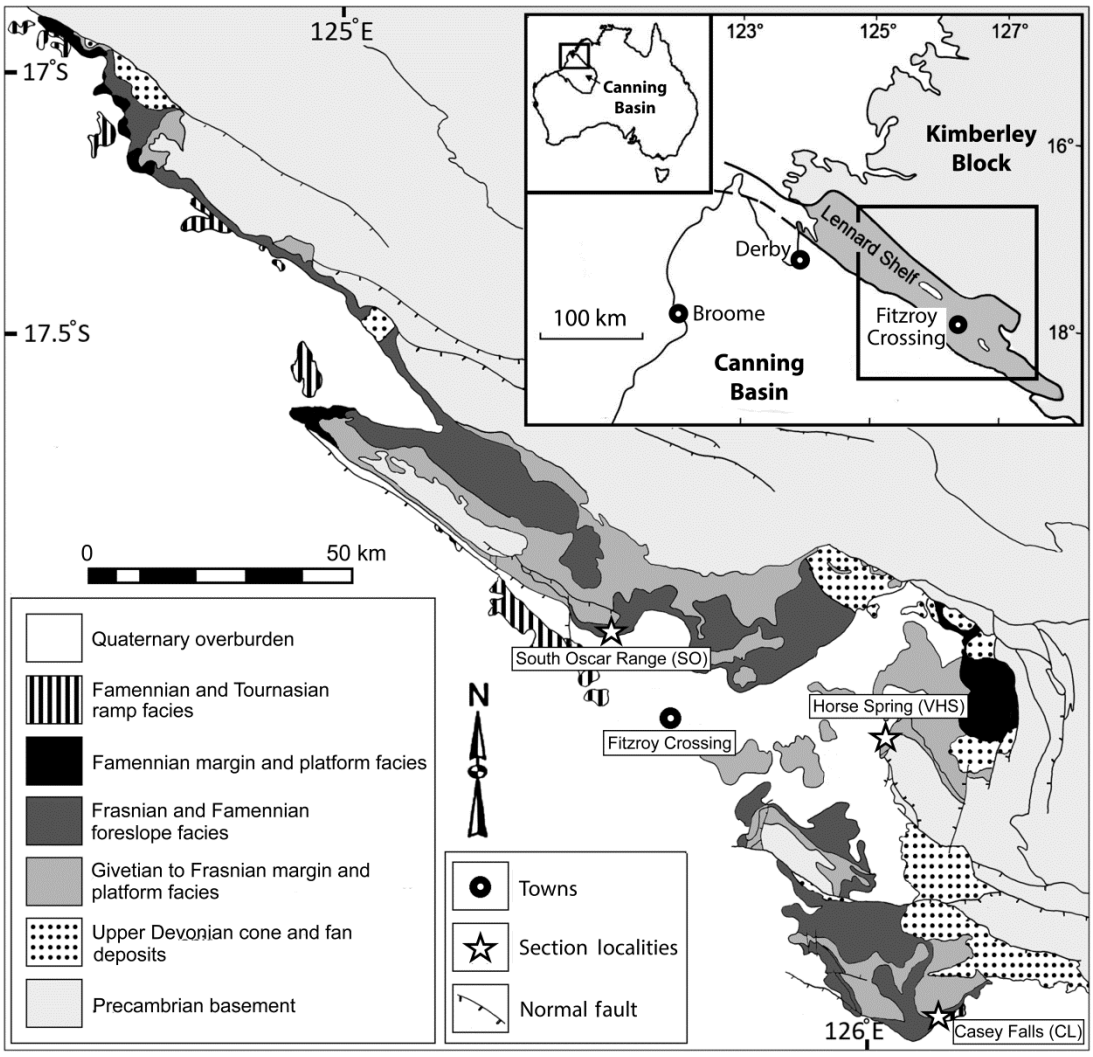

Figure 3.1. Simplified geological map of the Devonian Reef complexes of the Lennard Shelf, northern Canning Basin, showing the South Oscar Range, Horse Spring and Casey Falls measured sections and main facies types (modified after Playford et al., 2009).

recovered so far, has been reported from the Gogo Formation. A second, incomplete specimen comprising Meckle's cartilage, a shoulder girdle and associated teeth has highlighted the high degree of heterodonty present in Frasnian sharks and the recognition of this variation is important when diagnosing species from isolated teeth. Previous microvertebrate studies in the Canning and Carnarvon basins have revealed the presence of the youngest-recorded thelodont scales, first in early

Frasnian strata of the Carnarvon Basin (Turner and Dring, 1981) and later, younger scales in the middle Frasnian (Trinajstic and George, 2009) and middle Famennian of the Canning Basin (Hairapetian et al., 2015).

In contrast to Frasnian vertebrate faunas, Famennian macrovertebrates from Western Australia are rare (Trinajstic et al., 2014), with bothriolepid and phyllolepid placoderms reported from the Willaraddie Sandstone in the Carnarvon Basin (Long and Trinajstic 2000) and coccosteid and dinichthyid placoderms described from the Napier and Virgin Hills formations in the Canning Basin (Long, 1987; Trinajstic et al., 2014). Microvertebrate taxa from the Famennian in Canning Basin are even more understudied than those of the Frasnian with only a few reports of dipnoan, acanthodian and chondrichthyan remains from the Gumhole Formation and lower parts of the Yellow Drum Formations (Young, 1987; Turner, 1993; Edwards, 1997; Burrow et al., 2010; Trinajstic et al., 2014). Although rare, thelodont scales as well as the teeth of *Stethacanthus* cf. *thomasi* and *Thrinacodus ferox* Turner, 1982, and a possible late Famennian otolith have been reported from the Middle to Late Famennian in the Napier Formation (Turner, 1993; Trinajstic et al., 2014; Hairapetian et al., 2015). Even with a small number of Famennian microvertebrate fossils, the presence of *Thrinacodus ferox* and Famennian thelodonts, indicates a faunal connection with other areas in north Gondwana.

This work readdresses a previous lack of study through the description of a microvertebrate fauna recovered from measured sections (Figure 3.2; Table 3.1) that encompass distal slope to platform top facies and crop out along the Lennard Shelf in the Canning Basin of Western Australia. The discontinuous nature of the reef complexes has meant the use of microvertebrates adds a significant control to how the Lennard Shelf carbonate system is correlated and reconstructed. Microvertebrates

recovered from sampled strata are compared with the known age ranges reported from other sites globally as well as those species previously described from north-western Australia. In addition to providing the first comprehensive study into Late Famennian chondrichthyans within the Canning Basin, this work also determines faunal links between the Canning Basin and other areas along the margins of northern Gondwana and southern Laurussia.

3.3 Materials and methods

Carbonate rock samples (~20 kg each) were processed in a 10 % buffered acetic acid solution at Macquarie and Curtin universities (following the methodology of Jeppsson et al., 1999), with resulting residues further separated by either heavy liquid fractionation (Macquarie University) or sieving (0.125 mm sieve; Curtin University) before being picked under a Nikon stereomicroscope. Both conodont and microvertebrate remains were well preserved with the conodont elements indicating a Conodont Alteration Index (CAI) of 1. For SEM photography, specimens were mounted on adhesive carbon tape fixed to 10 mm diameter aluminium stubs and coated with 5 µm of platinum. Specimens were imaged using a Zeiss Evo 40XVP SEM at the Centre for Materials Research at Curtin University as well as a Hitachi TM-3030 desktop SEM at Applied Geology at Curtin University with accelerating voltages ranging from 5-15 kV and under variable pressure.

The 13-fold Montagne Noir (MN) conodont Zonation (Klapper, 1989, 2007) modified by Girard et al. (2005) was used to determine the age ranges of the associated Frasnian microvertebrates recovered in this study, as it provides greater resolution than that of Zeigler and Sandberg (1990). The standard conodont Zonation (Zeigler and Sandberg, 1990) is used in the Famennian.

Microvertebrate specimens are housed at the Western Australian Museum (WAM).

3.4 Geological Setting

Throughout the Devonian, the Canning Basin (Figure 3.1) occupied an equatorial position, approximately 12-14º south of the equator, along the northern margins of Gondwana (Scotese and McKerrow, 1990). Development of the basin was initiated during the Ordovician. Following a period of uplift and erosion in the early Devonian, extension during the middle Devonian to Early Carboniferous led to rapid subsidence of the NW trending Fitzroy Trough along the northern margin of the Canning Basin (Drummond et al., 1991). The margin successions include the late Givetian to late Famennian reef complexes, which are well exposed along the inner Lennard Shelf, and include numerous well-preserved fossilised fringing reefs and atolls (Playford, 1980). Difficulty in correlating Frasnian and Famennian sections within the Lennard Shelf is partly due to a complex underlying topography on which the reef was established, as well as depositional heterogeneity (Playford et al., 2009). Tectonic activity during the period of reef building (Chow et al., 2013) and deformation following post-depositional exhumation have also added to a fragmentary Frasnian and Famennian record across the basin (Playford et al., 2009).

3.4.1 Studied sections

3.4.1.1 Casey Falls

A section was measured at Casey Falls (18°44 0" S, 126°05'8" E; Figures 3.1 and 3.2) approximately 80 km south east of Fitzroy Crossing (Figure 3.1). The measured section represents 420 m of toe-of-slope to upper slope carbonate

sediments of the Virgin Hills Formation and overlying Bugle Gap Limestone, respectively. The lower 100 m of the section mainly comprises resedimented silty skeletal to non-skeletal wackestone/packstones derived from platform, margin and slope environments. The upper 320 m consists mostly of stromatactoid microbial boundstones and microbially stabilised packstones and grainstones (Playton et al., 2013). Minor platform derived skeletal-peloidal packstones and grainstones occur in the upper 40 m of the section. The Frasnian strata within the section are limited to the first 2 m of the section and range from Conodont Zones (CZ) 13a to 13b, with zone 13c not resolvable. The Frasnian-Famennian boundary is located between 2.2 and 7.9 m above the section base, however finer biostratigraphic resolution was impossible at this level due to a paucity of conodonts. Overlying Famennian sediments, from 7.9 m, yield conodont zones from Late *triangularis* to Late *marginifera* CZ. Additional samples were taken from poorly outcropping beds approximately 580 m north (samples 1984-95 and 1984-96) and 600 m (samples 1984-97 and 1984-98) north-north-east from the top of the measured section at Casey Falls with conodonts indicating a Late *marginifera* age. These samples represent the shallow water carbonate derived material of the Bugle Gap Limestone.

3.4.1.2 South Oscar Range

The section measured at the southern end of South Oscar Range (17°54'53" S, 125°17'56" E, Figures 3.1 and 3.2) spans 585 m of the Napier Formation and represents an the seaward side of an offshore island and fringing reef complexes (Playford et al., 2009). The preserved sequence comprises transported slope facies dominated by platform derived packstones and grainstones/rudstones with commonly occurring peloids, coated grains and skeletal fragments. Debris deposits consisting of allochthonous blocks and megabreccias of reefal margin material can

occur locally and are concentrated in particular parts of the section, reflecting brittle failure of the early-lithified bound margin. Bioclasts are abundant throughout the entire section and dominated by branching and laminar stromatoporoids (in the Frasnian; George, 1999; Stephens and Sumner, 2003), crinoids, corals and

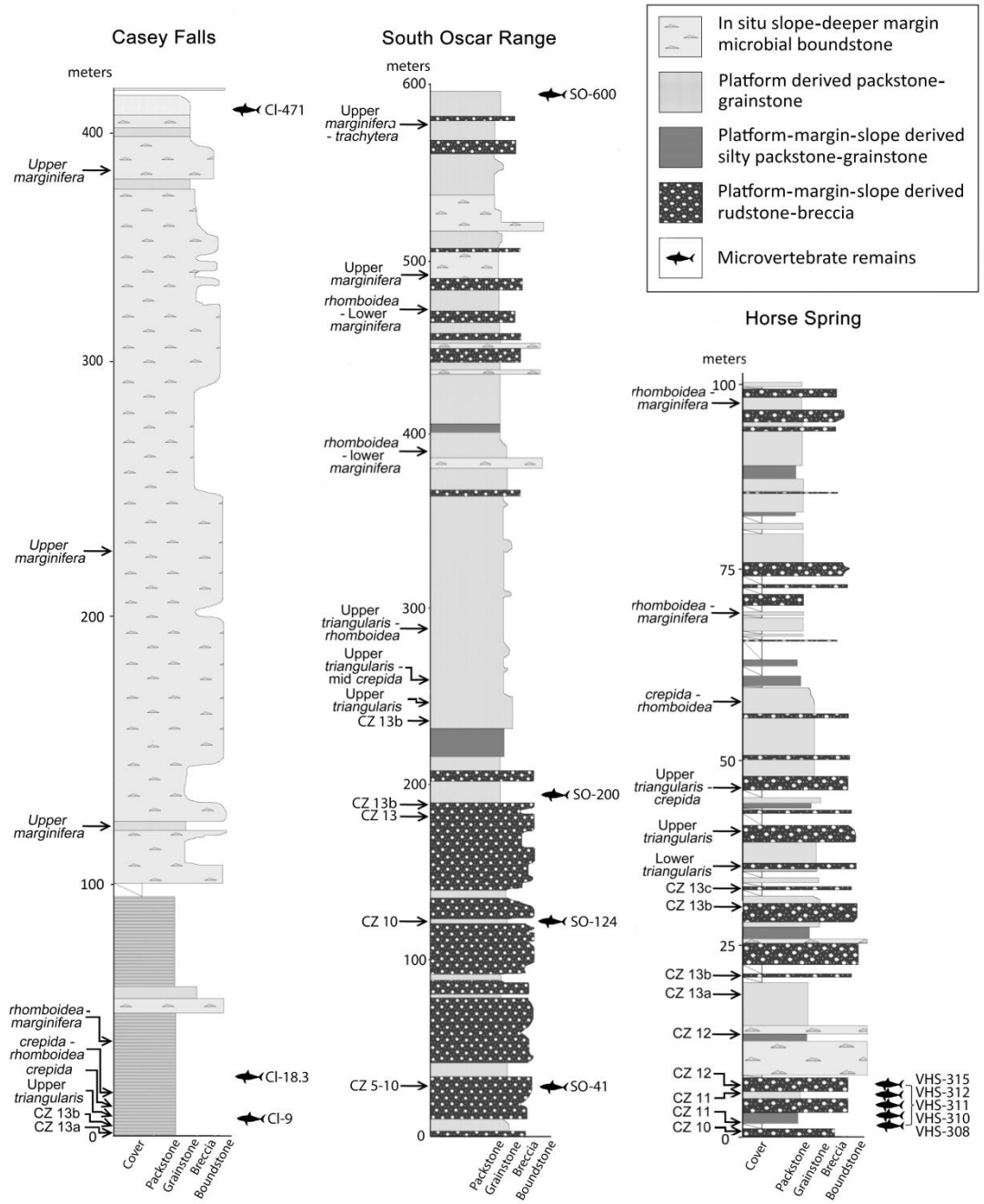

Figure 3.2. Simplified stratigraphic columns of the sections at Horse Spring, Casey Falls and South Oscar Range, showing main facies types and locations of recovered microvertebrate remains (modified after Playton et al., 2013).

brachiopods. The Frasnian beds range from MN 6 to 13b CZ and in addition to conodonts, yielded chondrichthyan teeth and scales as well as acanthodian scales. The Frasnian-Famennian boundary was located between 228.7 and 233 m above the section base. The Famennian portion of the section ranges from Upper *triangularis* to *marginfera* CZ with only the uppermost bed containing microvertebrate remains including acanthodian and palaeoniscoid scales as well as the youngest thelodont scales currently known (Hairapetian et al., 2015).

3.4.1.3 Horse Spring

The section measured at Horse Spring (GSWA reference section WCB 364) is located approximately 42 km east of Fitzroy Crossing, at the northern extremity of the Hull and Horse Spring Ranges (18°41'11" S, 126°05'12"; Figures 3.1 and 3.2). The section represents a lower slope succession dominated by platform derived skeletal to non-skeletal packstones and grainstones, slope derived rudstones, and margin-derived megabreccias. Stromatolitic and stromatactoid boundstones are minor and found in Frasnian beds, representing periods of deep-water in situ encrustation. The section at Horse Spring has been previously dated using conodonts (Klapper, 1989; 2007) and goniatites (Becker et al., 1993), with the Frasnian-Famennian boundary located between 34.6 and 36.6 m above the section base. A diverse Frasnian microvertebrate fauna has also been recorded by Trinajstic and George (2009) with scales of the thelodont *Australolepis seddoni* Turner and Dring, 1981 recorded as occurring with conodont elements and phoebodont teeth for the first time, thus allowing the age of *A. seddoni* to be constrained to MN 4-10 CZ. The phoebodont teeth were also correlated to the known phoebodont based zonation of Ginter and Ivanov (1995a).

Table 3.1. Distribution and abundances of microvertebrate remains from sections measured at Horse Spring, South Oscar and Casey Falls, Canning Basin, Western Australia. Abbreviations: Fr = Frasnian.

Localities	Casey Falls (CL)							South Oscar (SO)	Horse Spring (VHS)				
Age	Fr	Famennian						Fr	Fr				
Samples / Taxa	CL-9	CL127.5	CL-471	1984-94	1984-96	1984-97	1984-98	SO-200	VHS-308	VHS-310	VHS-311	VHS-312	VHS-315
Australolepis seddoni													1
Phoebodus bifurcatus									2	1		1	2
Phoebodus fastigatus										1	4	8	1
Phoebodus cf. *fastigatus*											1	2	
Phoebodus latus										4	3	1	
Phoebodus sp. 1												1	
Diademodus dominicus										2			
Thrinacodus tranquillus		1	3			7	2						
Stethacanthus sp. 1			1				1						
Cladoides cf. *wildungensis*	1												1
Ctenacanthiform gen. et sp. indet 1								1					
Ctenacanthiform gen. et sp. indet 2						1		1					
Protacrodus serra				1		1							
Deihim mansureae			1		1	2	4						
Deihim cf. *mansureae*							2						
Deihim sp. 1			1										
Protacrodontidae gen. et sp. indet. 1				1									
?Protacrodontidae fam. gen. sp. indet.							1						
Lissodus lusavorichi							2						
Total	1	1	6	2	1	11	12	2	2	8	8	13	5

3.5 Systematic Palaeontology

Class Thelodonti Jaekel, 1911

Order Thelodontiformes Kiaer, 1932

Family Turiniidae Obruchev, 1964

Genus *Australolepis* Turner and Dring, 1981

Type species. *Australolepis seddoni* Turner and Dring, 1981

Australolepis seddoni (Turner and Dring, 1981)

(Figure 3.3A)

1969. Fish tooth type b; Seddon, p 30, fig. 2a-b.

1981. *Australolepis seddoni* sp. nov.; Turner and Dring, 43, figs. 3A-P, 4A-K.

1981. Nikoliviid gen. et sp. indet. Turner and Dring: 46, fig. 6A-C.

1993. *Australolepis seddoni* Turner and Dring, 1981; Turner 1993, p. 183, fig. 8.3.

1997. *Australolepis seddoni* Turner and Dring, 1981; Turner 1997, p. 309, fig. 8.

2000. *Australolepis seddoni* Turner and Dring, 1981; Long and Trinajstic, p. 472, fig. 1.

2000. *Australolepis seddoni* Turner and Dring, 1981; Yazdi and Turner, p. 225, fig. 2.1.

2001. *Australolepis seddoni* Turner and Dring, 1981; Trinajstic, p. 239, fig. 2A-L, fig. 4.

2002. *Australolepis seddoni* Turner and Dring, 1981; Turner et al., p. 151, fig. 8.

2009. *Australolepis seddoni* Turner and Dring, 1981; Trinajstic and George, p. 647-648, p. l1, figs 1-8.

2013. *Australolepis seddoni* Turner and Dring, 1981; Chow et al., pl. 1C.

2014. *Australolepis seddoni* Turner and Dring, 1981; Hairapetian et al., in press.

Material. One broken scale from the Virgin Hills Formation, Horse Spring, sample VHS-315.

Description. A damaged scale, less than 1 mm in length, with part of the base and neck not preserved. Unornamented, conically shaped crown possessing six primary ribs radiating from the apex, with the two anterior ribs bifurcating towards the crown base (Figure 3.3A). The posterior of the scale is complete and preserves a shallow neck separating the crown from the elliptical base that has a well-developed pulp canal surrounded by tubercular swellings.

Remarks. Scales attributed to *A. seddoni* are found along the northern margins of Gondwana (Yazdi and Turner, 2000; Turner et al., 2002; Märss et al., 2007; Hairapetian et al., 2006; Trinajstic and George, 2009) and their presence in mainly shallow-water facies indicate that they inhabited a near-shore, marine to marginal marine environment (Burrow, 1997; Turner, 1999; Märss et al., 2007). Within the Canning Basin, the majority of scales (46) have been recovered from the Virgin Hills Formation at Horse Spring (Trinajstic and George, 2009; this work). This locality represents a distal slope environment formed in depths in excess of 200 m (Playford et al., 2009). This is in contrast to the high numbers (730) recovered from the shallow marine environment of the contemporaneous, Gneudna Formation, Carnarvon Basin, Western Australia (Turner and Dring, 1981; Trinajstic, 2001) and suggests that the scales were transported downslope, to deeper water prior to fossilization. This transport and likely consequential abrasion might have contributed to the lack of fine ornament, diagnostic for the taxon. However, as the co-occurring phoebodont teeth preserve the delicate lateral carinae and striations on the cusps, this explanation no longer seems likely for all scales. Another possibility for the absence of ornament is intraspecific variation, with both ornamented and non-ornamented scales present in shallow water facies at Hull Range (Chow et al., 2013).

Distribution and stratigraphic range. Associated conodont elements extend the upper-known age range of *A. seddoni* in the Canning Basin from MN 10 CZ to MN 11 CZ. As the upper age of the Gneudna Formation type section is constrained by the remains of *A. seddoni*, the youngest age for the Gneudna may now be extended to MN 11 CZ. Outside Australia scales of *A. seddoni* have been reported in the Shishtu Formation, Shotori Range, eastern Iran and Chahriseh section, Esfahan, Central Iran from *falsiovalis* to *rhenana* CZ (= MN 1-10 CZ) (Yazdi and Turner, 2000; Turner et al., 2002; Hairapetian et al., 2006).

Class Chondrichthyes Huxley, 1880

Subclass Elasmobranchii Bonaparte, 1838

Order Phoebodontiformes Ginter, Hairapetian and Klug, 2002

Family Phoebodontidae Williams, 1985

Genus *Phoebodus* St. John and Worthen, 1875

Type species. *Phoebodus sophiae* St. John and Worthen, 1875

Phoebodus bifurcatus Ginter and Ivanov, 1992

(Figure 3.3B-E)

1991. *Phoebodus* sp.; Ginter 1991: p. 74, pl. 8, figs. 1-2.

1992. *Phoebodus bifurcatus* sp. nov.: Ginter and Ivanov, p. 65-66, figs 4A-F, 5D-H, 6A.

1995a. *Phoebodus bifurcatus* Ginter and Ivanov, 1992; Ginter and Ivanov, pl. 1, figs. 5-6.

1995. *Phoebodus bifurcatus* Ginter and Ivanov, 1992; Ginter, p. 61, fig. 1F-G.

1995. *Phoebodus bifurcatus* Ginter and Ivanov, 1992; Turner and Youngquist, p. 390-391, fig. 1.

1995. *Phoebodus bifurcatus* Ginter and Ivanov, 1992; Wang and Turner, p. 65, pl. 7, fig. 7.

2009. *Phoebodus bifurcatus* Ginter and Ivanov, 1992; Trinajstic and George, p. 648, fig. 9.

2010. *Phoebodus bifurcatus* Ginter and Ivanov, 1992; Hairapetian and Ginter, p. 360-361, fig. 2B-C.

Material. Six teeth from the Virgin Hills Formation, Horse Spring, samples VHS-308, VHS-310, VHS-311, VHS-315.

Description. Teeth with three lingually inclined cusps bearing a thin, lateral carinae extending from the bases of the cusps to the apices and lacking a distinct neck between the base and crown (Figure 3.3B-E). The cusps are generally of nearly equal size however the size of the central cusp is significantly reduced in one specimen (WAM 14.8.2, Figure 3.3D). The base is characterised by a labially directed semicircular arch which defines the lingual border and varies between specimens from strongly (Figure 3.3C) to weakly bifurcated (Figure 3.3E). A distinct button is lacking on most specimens, although a rounded thickening, close to the lingual rim is sometimes present (Figure 3.3E). A large foramina is located in the centre of the lingual arch and in some specimens there are smaller adjacent canal openings.

Remarks. The teeth typical of *Phoebodus bifurcatus* Ginter and Ivanov, 1992 are characterised by having five ornamented cusps and a bifurcating base with a distinct button surrounded by foramina (Ginter and Ivanov, 1992). However, tricuspid forms, lacking intermediate cusplets, are known from the Confusion Range, Utah, USA and were attributed to juveniles (Turner and Youngquist, 1995). Within the Canning

Basin only tricuspid forms of *Ph. bifurcatus* have been identified but were previously attributed to juvenile sharks based on deeply bifurcated bases, an indistinct button and lack of ornament on the cusps (Trinajstic and George, 2009, pl. 1, Fig. 9). The teeth attributed to juvenile individuals have been found in association with adult forms in the South Urals, Holy Cross Mountains and central Iran (Ginter and Ivanov, 1992; Hairapetian and Ginter, 2010) whereas in the Confusion Range, Utah, USA and the Canning Basin only juvenile teeth have been reported. Here we question the assignment of these tricuspid teeth to juvenile sharks as the size of some deeply bifurcated, tricuspid teeth (Figure 3.3C-D, measuring up to 1.2mm from furthest point on the lingual margin of the base to the labial edge), recovered from Horse Spring, are of comparable or larger size than other teeth attributed to adult forms previously reported (Ginter and Ivanov, 1992, fig. 4B-F)). It is also unlikely that these larger teeth are symphyseal due to the asymmetry of the base and crown on one specimen (WAM 14.7.4, Figure 3.3C). This would leave the possibility that the Canning Basin teeth, and potentially other smaller tricuspid teeth, represent sexual dimorphism (e.g. Peyer 1968; Bass et al., 1973; Pfeil, 1983; Straube et al., 2008), a sub species of *Ph. bifurcatus*, intraspecific variation or even a separate, closely related species.

Distribution and stratigraphic range. In the Canning Basin, Australia *Ph. bifurcatus* has only been recorded from MN 11 CZ; within the Holy Cross Mountains, Poland, South Urals, Russia, southern China and Utah, USA *Ph. bifurcatus* ranges from MN 11-12 CZ; in Kale Sardar, eastern Iran the range extends from the *rhenana*-lower *linguiformis* Zones (MN 11-13b CZ).

Phoebodus fastigatus Ginter and Ivanov, 1992

(Figure 3.3F-H)

1973. *Phoebodus floweri* Wells, 1944; Gross, p. 131. pl. 35, fig. 7a-b.

1990. *Phoebodus limpidus* sp. nov.; Ginter, p. 75-76, pl. 4, fig. 6a-b.

1992. *Phoebodus fastigatus* sp. nov.: Ginter and Ivanov, p. 66-67, fig. 3A-B, G.

1993. *Phoebodus* sp.: Liszkowski and Racki, fig. 3F, H, K.

1995. *Phoebodus fastigatus* Ginter and Ivanov, 1992; Ginter, p. 59, fig. 1C-D.

1995. *Phoebodus* aff. *fastigatus* Ginter and Ivanov, 1992; Wang and Turner, p. 65, pl. 7, fig. 6.

1997. *Phoebodus* cf. *Ph. fastigatus* Ginter and Ivanov, 1992; Turner, p. 112-113, figs 4, 11, 12.

1998. *Phoebodus fastigatus* Ginter and Ivanov, 1992; Kaufmann, pl. 13, figs. 1-4.

2000. *Phoebodus fastigatus* Ginter and Ivanov, 1992; Ginter and Ivanov, p. 327, pl. 1, fig. E.

2003. *Phoebodus fastigatus* Ginter and Ivanov, 1992; Aboussalam, pl. 27, figs 13-16.

2004. *Phoebodus fastigatus* Ginter and Ivanov, 1992; Ginter, fig. 2H-J.

2004. *Phoebodus fastigatus* Ginter and Ivanov, 1992; Hampe et al., p. 494-495, fig. 5.

2007. *Phoebodus fastigatus* Ginter and Ivanov, 1992; Liao et al., p. 173. fig. 3A-M.

2008. *Phoebodus fastigatus* Ginter and Ivanov, 1992; Ginter et al., p. 170, text fig. 2E-H.

2009. *Phoebodus fastigatus* Ginter and Ivanov, 1992; Trinajstic and George, p. 649-650, fig. 11-16.

Material. Fourteen teeth from Virgin Hills Formation, Horse Spring, samples VHS-310, VHS-311, VHS-312 and VHS-315.

Description. Teeth with three main cusps. The medial cusp is approximately a third of the length of the lateral cusps and one half to one third the size at the base of the lateral cusps (Figure 3.3F-H). When present the accessory cusps are reduced in size, approximately half the size of the central cusp. The lateral cusps are long and slender with some specimens bearing slight torsion (Figure 3.3F). The central and lateral cusps are all rounded in cross section (Figure 3.3G), however, the labial faces of the cusps vary between teeth from smooth (Figure 3.3H) to ornamented with faint to strongly developed striations (Figure 3.3F). The base is rectangular to trapezoidal in outline, extending further mesio-distally than labio-lingually and bearing a straight to slightly convex thin lingual edge. The lingual face of the base is perforated by numerous small foramina with a round to slightly ovoid centrally located button (Figure 3.3F).

Remarks. The teeth are attributed to *Phoebodus fastigatus* Ginter and Ivanov, 1992 based on the thin elongate lingual base with a straight lingual margin and centrally located ovoid button (Ginter and Ivanov 1992). The tooth crowns vary from the diagnostic thin elongate recurved lateral cusps (Figure 3.3F-G) to shorter more robust cusps with less distal divergence (Figure 3.3H). A smooth labial cusp face is described as a diagnostic feature of *Ph. fastigatus* (Ginter and Ivanov, 1992, 2000) and one of the features distinguishing it from *Ph. bifurcatus*. This feature is not present in all teeth from the Canning Basin with faint to coarse cristae observed here and on teeth previously described by Trinajstic and George (2009, pl 1, fig. 11-16). As there is no correlation between tooth size and the presence of or lack of ornament, these differences are attributed to intraspecific variation rather than ontogeny.

Distribution and stratigraphic range. This species ranges from MN 6-11 CZ in the Canning Basin, Western Australia. Worldwide the range is greater, from the Givetian to Frasnian *rhenana* CZ in the USA, Morocco, Mauritania, Spain, Poland, China, Russia and eastern Australia.

Phoebodus cf. *fastigatus* (Ginter and Ivanov 1992)

(Figure 3.3I-J)

Material. Three teeth from the Virgin Hills Formation, Horse Spring, sample VHS-312.

Description. Three small teeth, measuring less than 0.5 mm mesio-distally across the base, with damage to both the cusps and bases (Figure 3.3I-J). Crowns with three to five lingually inclined cusps, comprising a main central cusp, two lateral cusps and, when present, smaller intermediate cusplets (Figure 3.3J). The lateral cusps, when preserved, are slightly larger in size than the medial cusp and in one specimen show torsion towards the apex of one lateral cusp (Figure 3.3I). When present, the intermediate cusps are small and fused to the base of the mesial margin of the lateral cusps. Prominent striations are present on the labial faces of the cusps, whereas the lingual faces are smooth. The base forms a roughly rectangular to trapezoid outline and is perforated by numerous small foramina. A rounded oval button is often difficult to determine on most specimens, however a faint outline can be seen, positioned centrally on one specimen (Figure 3.3I).

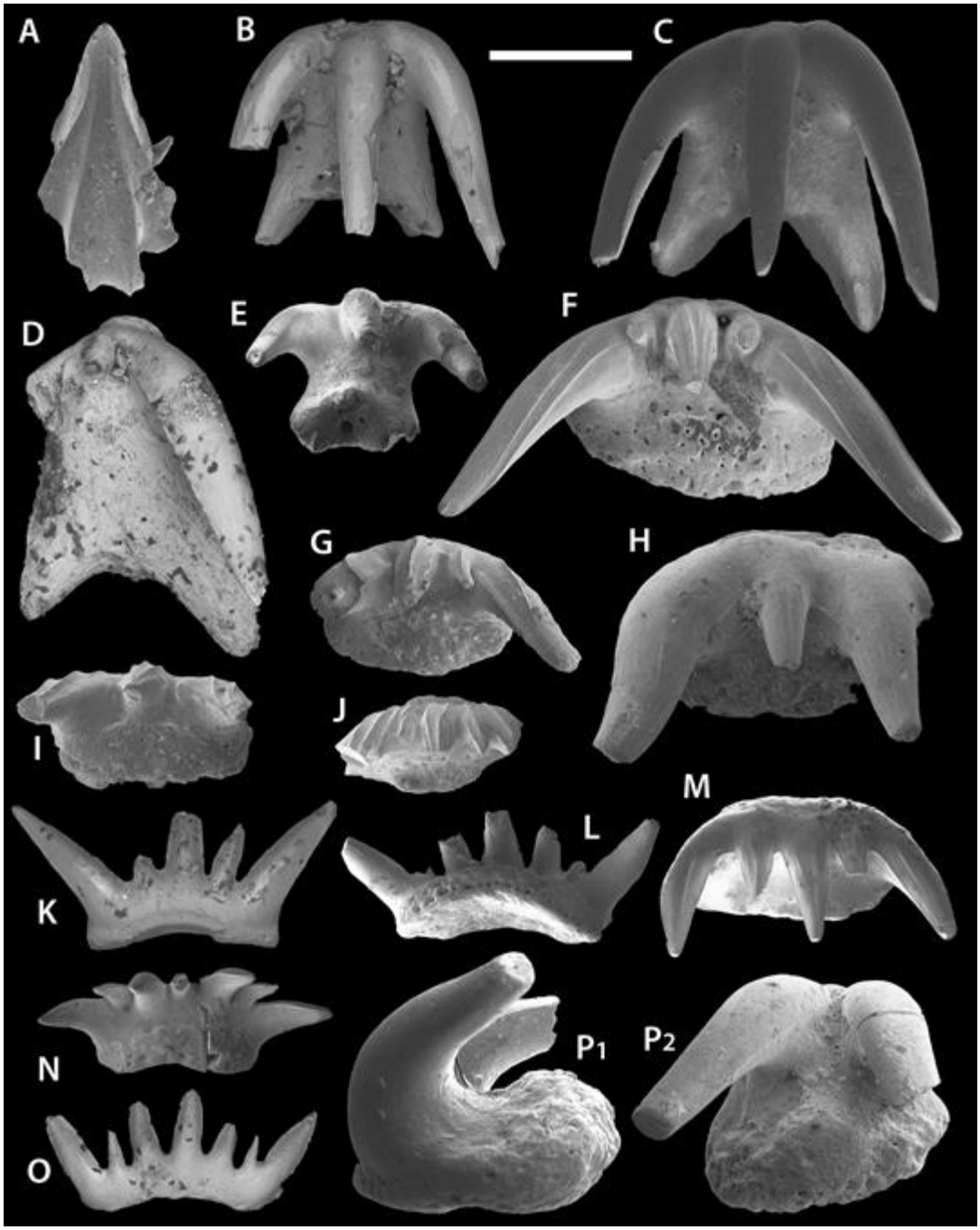

Figure 3.3. Late Frasnian phoebodonts from the Virgin Hills Formation, Horse Spring, Canning Basin, Western Australia. A - *Australolepis seddoni* scale, WAM 14.7.3, sample VHS-315, in crown view; B-E, *Phoebodus bifurcatus* teeth in occlusal view. B - WAM 14.8.1, sample VHS-315; C - WAM 14.7.4, sample VHS-310; D - WAM 14.8.2, sample VHS-315; E - WAM 14.7.5, sample VHS-310. F-H, *Phoebodus fastigatus* teeth in occlusal view. F - WAM 14.7.9, sample VHS-311; G - WAM 14.7.11, sample VHS-312; H - WAM 14.7.10. I-J, *Phoebodus* cf. *fastigatus* in occlusal view. I - WAM 14.8.5, sample VHS-311; J - WAM 14.7.12, sample VHS 310. K-O, *Phoebodus latus*. K - WAM 14.8.3, sample VHS-312, in labial view; L - WAM 14.7.7, sample 311, in occlusal view; M - WAM 14.7.8, sample 312, in lingual view; N - WAM 14.9.13, sample VHS-312, in occlusal view; O - WAM 14.8.4, sample 311, in labial view; P, *Phoebodus* sp. 1 WAM 14.7.6, in lateral and occlusal views. Scale bar 0.5 mm.

Remarks. The teeth described here are too poorly preserved for a definitive diagnosis, however they share similarities to the teeth attributed to the ornamented forms of Ph. fastigatus in this work. When preserved, the lingual margin of the base in Ph. cf. fastigatus is thin; a diagnostic feature of Ph. fastigatus (Ginter and Ivanov 1992), however, the cusps of Ph. cf. fastigatus are ornamented with strong striations, ovoid in cross section and lack a distinct rounded button. The bases are not well enough preserved for an outline to be determined. Despite poor preservation, in one specimen the base appears lingually narrow (Text-fig. 3I). The teeth described here are consistently smaller than other teeth attributed to Ph. fastigatus and this may be evidence of ontogenetic variation. Furthermore the teeth commonly lack a distinct button, a feature attributed to juvenile forms in both Phoebodus gothicus Ginter, 1990 and Phoebodus bifurcatus (Ginter and Ivanov 1992). One tooth (WAM 14.7.10, Text-fig. 3G) may represent an intermediate form between teeth designated Ph. fastigatus and the smaller teeth of Ph. cf. fastigatus as it possesses an elongate lateral cusp and more prominent ovoid button similar to Ph. fastigatus, but exhibits the coarse cristae and smaller size of Ph. cf. fastigatus. Therefore an ontogenetic series is supported by the presence of this transitional form.

Distribution and stratigraphic range. This species ranges from MN 6-11 CZ in the Canning Basin, Western Australia. Worldwide the range is greater, from the Givetian to Frasnian *rhenana* CZ in the USA, Morocco, Mauritania, Spain, Poland, China, Russia and eastern Australia.

Phoebodus latus Ginter and Ivanov, 1995a

(Figure 3.3K-O)

1992. *Phoebodus* sp. A Ginter and Ivanov 1992, p. 70, fig. 7A-1.

1993. *Phoebodus* sp. Liszkowski and Racki, p. fig. 5L-M.

1995a. *Phoebodus latus* sp. nov.; Ginter and Ivanov, p. 355, pl. 1, figs 3-4.

1995b. *Phoebodus latus* Ginter and Ivanov, 1995b; Ginter and Ivanov, p. 19, fig. 1.

1995. *Phoebodus latus* Ginter and Ivanov, 1995b; Ginter, fig. 1E.

2009.*Phoebodus latus* Ginter and Ivanov, 1995b; Trinajstic and George, pl. 1, fig. 18-19.

2011. *Phoebodus latus* Ginter and Ivanov, 1995b; Ivanov and Lucas, fig. 2A-B.

Material. Eight teeth from the Virgin Hills Formation, Horse Spring, samples VHS-310 VHS-311 and VHS-312.

Description. The teeth here attributed to *Phoebodus latus* Ginter and Ivanov, 1995a are highly variable with three different morphotypes identified here. The first morphotype (Figure 3.3K-L) comprises five to seven smooth and almost straight conically shaped cusps with well-developed lateral carinas. The cusps diverge from the centre of the crown, which is defined by a central cusp with a base approximately 25% smaller than the base of the two lateral cusps (Figure 3.3K-L). A pair of intermediate cusplets, slightly smaller than the medial cusp, are present on all specimens. One specimen (WAM 14.7.7, Figure 3.3L) exhibits a second pair of small broken cusplets fused at the base of the lateral cusps. The base is roughly trapezoidal in outline, thickened along the lingual edge and slightly arched. A faint outline of an ovoid button is preserved.

A single, well preserved tooth represents the second morphotype (Figure 3.3M). The crown comprises three main cusps of almost equal size with a pair of intermediate cusplets approximately a third of the length of the lateral cusps. The cusps are ovoid in cross section and all lingually directed, with the medial and lateral

cusps extending beyond the lingual margin of the base (Figure 3.3M). The cusps exhibit a well-defined lateral carina as well as striations on the labial faces. The lingual faces of the cusps are smooth .The base forms a roughly rectangular outline with the very faint outline of a centrally located ovoid button.

Morphotype three (Figure 3.3N-O) is characterised by three main cusps and two pairs of intermediate cusplets, all of which are smooth with well-developed lateral carinas and a slight lingual inclination. The size of the central cusp ranges from small (Figure 3.3O), with the basal width approximately half of the size of the first intermediate cusplets, to significantly larger (Figure 3.3N), almost the same size as the lateral cusps. The second pair are approximately half the size of the intermediate cusplets. The base is arched and slightly bifurcated (Figure 3.3N) along the lingual rim which is also perforated by a horizontal row of foramina. The mesio-distally elongate button is positioned toward the edge of the lingual rim of the base (Figure 3.3N).

Remarks. The crown morphology of *Phoebodus latus* Ginter and Ivanov, 1995a is highly variable with the presence of intermediate cusplets greater than other known species attributed to *Phoebodus* (Ginter 2008). The third morphotype (Figure 3.3N-O) resembles other *Ph. latus* teeth recovered from the South Urals, Russia and the Holy Cross Mountains, Poland (Ginter and Ivanov 1992, fig. 7A). The tooth also bears strong resemblance to another tooth from Horse Spring, previously described by Trinajstic and George (2009, pl 1. fig. 18-19). The first and third morphotypes identified here lack the ornament on the labial faces of the cusps (Figure 3.3K, O) seen in other examples of *Ph. latus* (Ginter and Ivanov, 1995a). The crown of the second morphotype more closely resembles other teeth from *Ph. latus* (Figure 3.3M) with the presence of three almost equally sized main cusps ornamented with ridges

on the labial faces. However the base does not show the diagnostically distinct ovoid button positioned close to the lingual rim (Figure 3.3M). There appears to be a great deal of diversity attributed to *Ph. latus* that would suggest a high degree of heterodonty. Until more specimens are found, it is difficult to determine whether the teeth attributed to *Ph. latus* in the Canning Basin are products of heterodonty or if they represent intraspecific variation.

Distribution and stratigraphic range. Within the Canning Basin, the range of this species is confined to MN 9-11 CZ. In other regions, the species is longer ranging, from the *falsiovalis* to *linguiformis* conodont Zones (MN 1-13b) in Poland, the Middle and South Urals, and Timan of Russia.

Phoebodus sp. 1

(Figure 3.3P)

Material. One tooth from the Virgin Hills Formation, Horse Spring, sample VHS-312.

Description. A robust tooth comprising two lingually inclined, almost equally sized laterally diverging cusps, which are rounded in cross section and bear a single faint lateral carina on the inner face (Figure 3.3P_{1-2}). There is no evidence of a third cusp forming. The base is asymmetric and perforated by numerous pores concentrated along the basal rim (3P_2). The base is thickest along the lingual rim, forming a rounded bulbous edge. A well-defined circular button is located centrally on the base and reaches almost to the lingual edge. A rounded, striated labiobasal thickening extends from the base (Figure 3.3P_1).

Remarks. The thin, smooth cusps, which are rounded in cross section, and the centrally located spherical button are similar to the morphological features that

diagnose *Ph. fastigatus* (Ginter and Ivanov 1992 fig. 3A-B). In addition, the tooth shares a similar cusp morphology to teeth from the same horizon, attributed to *Ph. fastigatus* (Figure 3H). However, the bicuspid crown, asymmetric outline of the base and thickened lingual rim makes an accurate diagnosis problematic. It is suggested that these differences are pathological, and that the tooth is most likely from *Ph. fastigatus.* However, as less than 1% of chondrichthyan teeth, both fossil and extant (Becker et al., 2000) are known to exhibit pathology, the diagnosis of *Ph. fastigatus* cannot be confirmed and until further teeth are recovered this tooth is placed in open nomenclature.

Genus *Thrinacodus* St. John and Worthen, 1875

Type species. *Thrinacodus nanus* St. John and Worthen, 1975

Thrinacodus tranquillus Ginter, 2000

(Figure 3.4A-C)

2000. *Thrinacodus tranquillus* sp. nov.; Ginter, p. 374-377, figs 2a-C, 3a-F, 4a-C, 5h-k.

2000. *Thrinacodus* cf. *ferox* (Turner); Long and Hairapetian, p. 214-216, fig. 4n.

2002. *Thrinacodus tranquillus* Ginter, 2000; Ginter et al., p. 186-188, text-fig. 9F-h, pl. 2, fig. h, pl. 3, fig. h, pl. 11, figs h-I.

2008. *Thrinacodus tranquillus* Ginter, 2000; Derycke et al., p. 988, text-fig. 4(1-2).

2009. *Thrinacodus tranquillus* Ginter, 2000; Hairapetian and Ginter, p. 191, text-fig 9c-d.

2010. *Thrinacodus tranquillus* Ginter, 2000; Ginter et al., p. 41, fig. 33A.

2010. *Thrinacodus tranquillus* Ginter, 2000; Ginter and Turner, p. 1668, fig. 2C.

Material. Four teeth from the Virgin Hills Formation, Casey Falls, samples CF-127.5 and CF-471; ten teeth from the Bugle Gap Limestone, Casey Falls, samples 1984-97 and 1984-98.

Description. A total of three morphotypes are attributed to *Thrinacodus tranquillus* in this work. The first morphotype (Text-fig 4A), is the most common and features a symmetrical crown with three sub-equal cusps, often with one dominant lateral cusp. When preserved, the lingually extended base is positioned asymmetrically in relation to the crown. A centrally located canal is present on the occlusal face of the base, which also shows slight torsion towards the distal end.

The second morphotype (?symphyseal teeth *sensu* Ginter 2000; symphyseal tooth Ginter pers comm.), represented by a single tooth (Figure 3.4B), comprises a symmetrical crown with three thin, straight, equally sized and lingually directed cusps, each with lateral carinae and faint striations on the labial face. The base is thin, extends lingually further than the cusp apices and bears a small nutritive canal approximately half way down the occlusal face of the base. There is no obvious sign of torsion towards the end of the base.

The third morphotype is represented by a single asymmetric tooth (WAM 14.7.29, Figure 3.4C) that is characterised by a crown consisting of three unequal cusps. The straight, lingually directed central cusp is preserved with lateral carinae and faint striations on the labial face. The thin base extends further lingually than the apex of the central cusp and is curved distally in relation to the crown. The posterior end of the base is contorted toward a vertical orientation with a small nutritive canal located approximately half way down the occlusal face.

Remarks. These teeth largely conform to the diagnosis of *Thrinacodus tranquillus* Ginter, 2000, and the differences between the tooth forms are attributed to

heterodonty. Previous work (Ginter, 2000; Ginter et al. 2002; Duncan 2003; Ginter and Turner, 2010) has suggested the presence of two tooth types; the first with a flattened base positioned asymmetrically in relation to the crown and a smaller almost completely symmetrical form (Duncan, 2003). The first morphotype (Figure 3.4A) is the most common tooth form attributed to *Th. tranquillus* and has been reported from various locations across northern Gondwana (Ginter and Turner 2010). The second, smaller morphotype (Figure 3.4B), which has had its assignment to *Th. tranquillus* recently questioned (Ginter and Turner, 2010), is less common and with few examples recorded from the Montagne Noire (Ginter, 2000). Based on reconstructions of tooth placement within thrinacodont jaws (Turner,1982; Ginter et al. 2002; Duncan 2003), the supposed symmetrical symphyseal teeth only comprise a small proportion of teeth thus likely lower yields of these teeth are to be expected.

A third morphotype (Figure 3.3.4C) has been attributed to *Th. tranquillus* with similar teeth previously recorded from Montagne Noire and Oum El Jerane and Tizi Nersas, Morocco, conversely these specimens were designated *Thrinacodus* cf. *ferox* (Ginter ,2000, fig. 2; Ginter et al., 2002, fig. 9A-E). It was suggested by Ginter et al., (2002) that the teeth of *Th.* cf. *ferox* may represent the lateral most teeth of *Th. tranquillus*, which was supported by the presence of intermediate forms between the typical teeth of *Th. tranquillus* and *Th.* cf. *ferox*. A similar variety of tooth forms is present in the Canning Basin, however the teeth are recovered from Late *marginifera* CZ dated deposits making their attribution to the *Th. ferox* unlikely as it is regarded as a late Famennian to late Tournaisian species (Ginter and Turner, 2010).

Distribution and stratigraphic range. In the Canning Basin this species is recorded from the Late *marginifera* CZ. A similar age *rhomboidea* or Late *marginifera* CZ is recorded for Chahriseh, Iran (Long and Hairapetian, 2000; Ginter et al., 2002;

Hairapetian and Ginter, 2009) and also a *marginifera* CZ for Hunan, China (Lelièvre and Derycke, 1998). In Oum El Jerane and Tizi Nersas, Morocco this species ranges from *rhomboidea* or Late *marginifera* CZ to Middle to Late *expansa* (Ginter et al., 2002; Derycke et al., 2008). Younger known occurrences have been recorded from the Late *trachytera* CZ, Holy Cross Mountains, Poland, Lower to upper *expansa* CZ, Thuringia, Germany and *expansa* CZ in Montagne Noire. Within the South Urals the range of this species is recorded from the Late *expansa* to Early *praesulcata* CZ (Ivanov, 1996).

Genus *Diademodus* Harris, 1951

Type species. *Diademodus hydei* Harris, 1951

Diademodus dominicus sp. nov.

(Figure 3.4D-E)

Etymology. In honour of Mr Dominicus 'Tim' Mueller, M.Sc., who guided the careers of many aspiring geoscientists.

Holotype. Specimen WAM 14.7.1 from the Virgin Hills Formation, Horse Spring, Canning Basin, Western Australia; sample VHS-310; Frasnian, MN 11 CZ; Figure 3.4D.

Material. Two teeth from the Virgin Hills Formation, Horse Spring, sample VHS-310.

Diagnosis. Teeth with a multicuspid phoebodont type crown comprising three cusps and three to four pairs of intermediate cusplets (Figure 3.4D). The cusps are thin and ovoid in cross section, becoming circular towards the cusp apex and bearing prominent lateral carinae. A slight lingual inclination is present on all cusps with the

larger lateral cusps recurving occlusally. The base is highly arched, trapezoid in outline and becoming narrower labially (Figure 3.4E$_2$). The labial margin is rounded and perforated by a row of foramina. A mesio-distally elongate hump occupies the majority of the baso-labial shelf with the labial margin abutting the base of the cusps. There is a slight decrease in height of the shelf towards the lingual margin.

Description. Distinctive teeth with symmetrical crowns that fan out mesio-distally and comprise three mains cusps and three to four pairs of lateral cusps (Figure 3.4D-E). The medial cusps are broken in both specimens, however the bases are approximately half the width of the lateral cusps. A pair of small, first lateral cusplets are independent of the medial cusp but are fused at the base with the second lateral cusplets which are slightly smaller in size than the lateral cusps. In one holotype (WAM 14.7.1, Figure 3.4E) a small fourth cusplet is present and erupts from the base of the lateral cusp. The preserved cusps appear ovoid in cross section (elongate labio-lingually), at the base and exhibit smooth lingual and labial faces with well-developed lateral carinae. No discernible crown-base interface is present on the labial faces of the teeth. The base is highly arched (Figure 3.4E$_1$), approximately twice as long mesio-distally as it is labio-lingually (Figure 3.4E$_2$). A roughly trapezoid to almost rectangular shape of the base can be determined, with rounded lingual corners. A row of foramina is present running along the lingual rim. An ovoid button is positioned centrally on the base extending between the third lateral cusplets and gradually dissipates towards the lingual margin of the base. The labial face of the button preserves the openings to a row of canals and terminates abruptly, close to the base of the crown.

Remarks. The teeth of the type specimen *Diademodus hydei* Harris, 1951 are partially obscured in matrix thus similarities to the genus are based on the visible

labial tooth face of *Diademodus hydei* as well as comparison to the other member of this genus, *Diademodus utahensis* Ginter, 2008. The teeth of *Diademodus* all share the typical phoebodont tooth crown but can be differentiated on the number of intermediate cusplets (Ginter 2008). The cusp arrangement and variation in cusplet size present in *D. dominicus* sp. nov (Figure 3.4E) is similar to *D. utahensis* (Ginter 2008, fig. 1B) and differs from the original description of *D. hydei* which was figured having two prominent central cusps and intermediate cusplets of almost equal size (Harris, 1951, fig. 3b), however, reinterpreted by Ginter (2008) as possessing a single prominent central cusp. The teeth of *D. dominicus* sp. nov are further distinguished as some cusplets are fused at the base with the adjacent cusp or cusplets, a feature not apparent in *D. hydei* or *D. utahensis*. The lingual face of teeth from *D. dominucus* sp. nov. most closely resemble those of *D. hydei* as these teeth lack both the mesio-distal extension of the base beyond the crown as well as the presence of a baso-labial shelf, features both present in *D. utahensis*. The tooth is distinguished from both *D. hydei* and *D. utahensis* by a shorter mesio-distal length of the base which is also significantly arched. The basal outline of *D. dominicus* sp. nov. narrows lingually and is substantially different from that of *D. utahensis* which forms a trapezoid shape becoming wider lingually and slightly compressed centrally on the lingual margin. The orolingual hump of *D. dominicus* is also far more prominent than that of *D. utahensis*. We believe these differences are significant enough for the establishment of the species *Diademodus dominicus* sp. nov.

Despite the low number of teeth recovered from *D. utahensis* and the obscured nature of teeth from *D. hydei*, heterodonty within each species is so far limited to variation in the number of intermediate cusplets, reported in *D. utahensis* (Ginter 2008) and *D. domincus* sp. nov.. Ginter (2008) suggests that anterior teeth of

D. utahensis may be narrower and speculates they would be similar in form to teeth attributed to *Ph. fastigatus* (in Ginter 2008, fig. 3B). This would appear more likely than the teeth of *D. dominicus* sp. nov. representing anterior *D. utahensis* teeth as the base and cusp morphology is far more similar between *D. utahensis* and the *Ph. fastigatus* tooth examples.

Order Symmoriida Zangerl, 1981

Family Stethacanthidae Lund, 1974

Genus *Stethacanthus* Newberry, 1889

Type species. *Physonemus altonensis* St. John and Worthen, 1875.

Stethacanthus sp. 1

(Figure 3.4F-G)

Material. One tooth from the Virgin Hills Formation, Casey Falls, sample CL-471; one tooth from the Bugle Gap Limestone, Casey Falls, sample 1984-97.

Description. Small teeth, less than 1 mm mesio-distally and consisting of a slender prominent central cusp and two smaller, slightly diverging lateral cusps approximately one third of the size of the medial cusp (Figure 3.4F-G_1). A pair of small intermediate cusplets is present with one specimen possessing a second pair of cusplets on the distal side of the lateral cusps (Figure 3.4F_{1-2}). Thin vertical striations extend from the base to tip on the lateral and intermediate cusps on the well preserved cusps. The base forms a distinct triangular outline (Figure 3.4G_2), extending beyond the crown mesio-distally with rounded edges and a low profile. The apex of the lingual projection on the base is slightly thickened and possesses multiple foramina along the lingual rim.

Remarks. The teeth described here possess characters found in other stethacanthid tooth types including upright, unconnected cusps ornamented in sub-parallel cristae and a base lacking a labial depression. The triangular shaped lingual extension of the base (Figure 3.4G_2) is a common feature of Moroccan stethacanthid teeth (Ginter et al., 2002, pl. 10C) and also seen in other Famennian teeth from the Montagne Noire (Ginter, 2000, fig 7C) and Dalmeh, Iran (Long and Hairapetian, 2000, fig 4l). The teeth from the Canning Basin also appear to exhibit a thickening around the lingual

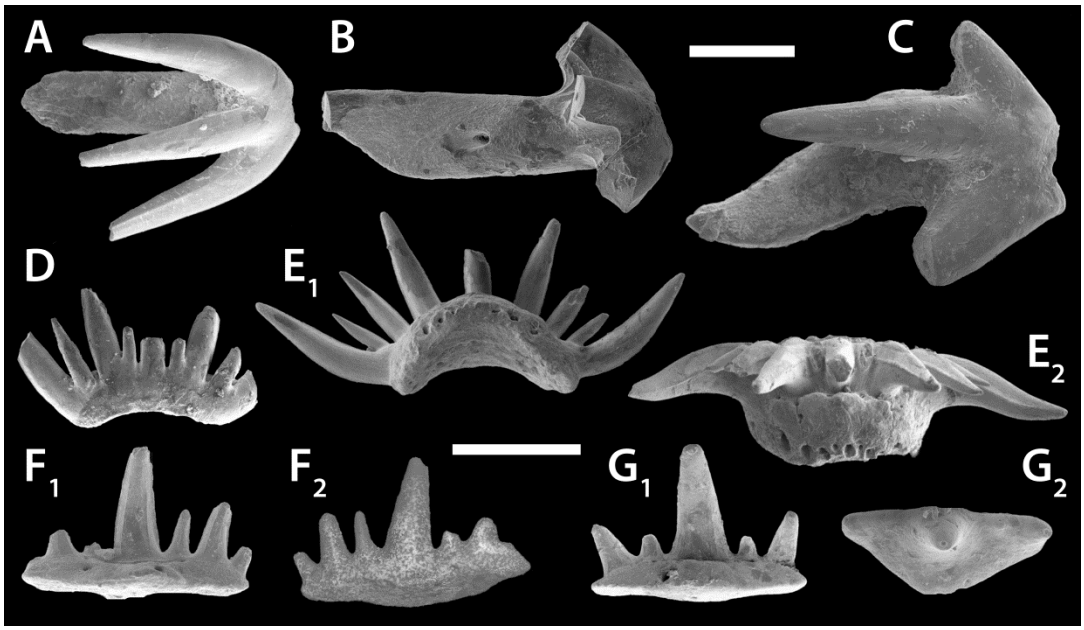

Figure 3.4. Shark teeth from the middle Famennian at Casey Falls (A-C, F-G) and Upper Frasnian at Horse Spring (D-E). A-C, *Thrinacodus tranquillus* in occlusal view. A - WAM 14.7.15, sample 1984-97; B - WAM 14.7.16, sample 1984-97; C - WAM 14.7.29, sample 1984-98. D-E, *Diademodus dominicus* sp. nov. teeth, sample VHS-310. D - WAM 14.7.2, in lingual view; E - WAM 14.7.1, holotype, in lingual and occlusal views; F-G - *Stethacanthus* sp. 1. F - WAM 14.7.26, sample Cl-471, in lingual and labial views; G - WAM 14.7.27, sample 1984-98 in lingual and occlusal views. A-E, scale bar = 0.5 mm; F-G, scale bar = 0.5 mm.

apex of the base, which is similar to a tooth from Dalmeh, Iran (Long and Hairapetian 2000, fig. 4e) but lack a well-formed labial boss. One tooth variant (WAM 14.7. 26, Figure 3.4F) exhibits a sixth cusp, a feature not usually found in Famennian stethacanthid teeth from Morocco and Iran (Ginter et al., 2002). Further

specimens are required to determine if this tooth represents a non-typical variant of *Stethacanthus* sp. 1 or if there is a degree of heterodonty within this species.

Order Ctenacanthiformes Glikman, 1964

Family Ctenacanthidae Dean, 1909

Genus *Cladoides* Maisey, 2001

Cladodoides wildungensis Jaekel, 1921

(Figure 3.5A)

1921. *Cladodoides wildungensis* sp. nov.: Jaekel, 1921.

1991. *Stethacanthus* sp.; Ginter, p. 75, pl. 8: 4, pl. 9: 2, 3.

1992. *Cladodus* cf. *C. thomasi* Turner; Ivanov et al., p. 89, pl. 36: 3, 4.

1992. *Stethacanthus thomasii* Turner [sic]; Derycke, p. 39-40, fig. 14, pl. 2: 10, 11.

1995b. *Stethacanthus* cf. *thomasi* Turner; Ginter, fig. 2A.

1996. "symmoriid with button partially divided"; Ginter and Ivanov, fig. 4C.

1996. "stethacanthid?"; Ginter and Ivanov, fig. 5C, D.

2000. *Stethacanthus* cf. *thomasi* (Turner); Ginter and Ivanov, pl. 1: J.

2002. *Stethacanthus resistens* sp. nov.; Ginter et al., figs 2, 3, 4C-I, 5C.

2010. *Cladodoides wildungensis* Jaekel; Ginter et al., fig. 66A-J.

Material. Two teeth from the Virgin Hills Formation, Horse Spring, sample VHS-310; Casey Falls, sample Cl-9.

Description. Symmetrical teeth with five lingually inclined and strongly diverging cusps. The central cusp is large, almost twice the width at the base of the lateral cusps (Figure $3.5A_1$). The intermediate cusps are significantly smaller, approximately half the height of the lateral cusps. Both the lingual and labial faces of

the cusps are ornamented with sub parallel ridges. The base is ovoid in outline, slightly arched and elongated mesio-distally, extending beyond the crown. A small baso-labial projection is preserved on one tooth (Figure 3.5A $_{2\text{-}3}$), between the distal edges of the medial cusp. Due to abrasion, only the remnants of a mesio-distally elongate button are preserved on both teeth. One tooth (Figure 3.5A$_1$) preserves an outline of a button, extending the distance between the two intermediate cusps, as well as a series of grooves, presumably once pore canals running labio-lingually.

Remarks. Ginter et al. (2010) recognises two morphotypes of *Cladodoides wildungensis* Jaekel (1921). The first morphotype, characterised by its larger size and long, slender medial cusp; and the second smaller morphotype, to which the Canning Basin teeth are here assigned, that are less than two mm across the length of the base with diverging cusps ornamented in coarse sub-parallel cristae. The teeth described here are markedly similar to the holotype of *C. wildungensis* (figured in Ginter et al., 2010, fig. 66l) as well as resembling teeth from Poland (Ginter *et al*. 2002, fig. 2C-F) designated *Stethacanthus resistens.* Ginter et al., (2010) suggests that it is possible that some, if not all teeth previously attributed to *Stethacanthus resistens* belong to the *C. wildungensis*. If so, at appears *C. wildungensis* is considerably cosmopolitan in nature.

Distribution and stratigraphic range. This species ranges from MN 11 CZ- lower *crepida* in the Canning Basin, Western Australia. Due to a degree of synonymy with *S. cf. thomasi* a definitive range is difficult to ascertain, however a range from the Upper Frasnian - middle Famennian is likely in Poland, Moravia, Germany, Morocco and Russia.

Ctenacanthiform gen. et sp. indet 1

(Figure 3.5B)

Material. One tooth from the Napier Formation, South Oscar Range, sample SO-200.

Description. This highly symmetrical tooth is well preserved, by comparison to other teeth in the sample, and possesses five slender, lingually inclined cusps that fan out mesio-distally (Figure 3.5B$_{1-2}$). A large prominent central cusp is flanked by two smaller intermediate cusps. The lateral cusps are approximately two thirds the length of the medial cusp and diverge at approximately 45 degrees to the medial cusp. In labial view, the cusps appear more triangular and connected at the bases (Figure 3.5B$_3$). All cusps are ovoid in cross section and ornamented on both the lingual and labial faces with strong vertical striations. The base is trapezoid in shape extending further lingually than labially and broadest along the lingual margin (Figure 3.5B$_2$). The base is thickest in a trapezoid area between the labial edge of the lingual button and lateral cusps. A thin baso-labial projection is present with a row of foramina. A well developed, ovoid shaped button is positioned close to the lingual border and perforated by a row of four large foramina (Figure 3.5B$_1$).

Remarks. The tooth shares commonalities between many cladodont-like teeth outlined by Duffin and Ginter (2006). The connection of the tooth cusps by an enameloid or orthodentine layer (Figure 3.5B$_3$) excludes this tooth from belonging to the symmoriids and stethacanthids (*sensu* Duffin and Ginter, 2006). The tooth lacks a baso-labial depression as seen in *Cladodus* and *Ctenacanthus* and is thereby more similar to *Cladoides* which may also lack this feature. The baso-labial shelf is straight which is characteristic of *Cladoides* but is far more developed in Ctenacanthiforme gen. et. sp. indet 1 and this projection may obscure the presence of any baso-labial depression. The tooth is differentiated from other Ctenacanthiformes

based on the strongly rounded or biconvex central cusp and lateral cusps, which are almost two thirds the size of the central cusps. The tooth is referred to the Ctenacanthiformes, perhaps temporally, based on the orthodentine or enameloid connective tissue present between the cusps and similarities with the genus *Cladoides*.

Ctenacanthiform gen. et sp. indet 2

(Figure 3.5C)

Material. One tooth from the Virgin Hills Formation, Casey Falls, sample 1984-97; one tooth from the Napier Formation, South Oscar Range, sample SO-200.

Description. Heavily abraded teeth with a large medial cusp flanked by four smaller triangular shaped cusps consisting of a pair of small lateral cusps and a pair of intermediate cusplets approximately half the size of the lateral cusps (Figure 3.5C_{1-2}). The medial cusp is inclined slightly and convex along the lingual edge in cross section. Where the outer enameloid is preserved on the central cusp, faint vertical striations can be observed. The intermediate and lateral cusps do not show any ornamentation with the lateral cusps diverging at a 45 degree angle. A distinct rim is preserved on the labial face of the teeth and marks the crown base interface (Figure 3.5C_{1-2}). The base extends lingually almost three times the width of the crown and forms a large dome shape that extends beyond the crown mesio-distally (Figure 3.5A_2). A very faint ovoid button, approximately twice as long as it is wide, is preserved on one specimen and positioned closer to the lingual margin than the crown (Text- fig. 3.5A_2). A series of foramina perforate the lingual face of the base with a single large nutritive canal positioned centrally along the lingual margin. The

labial face of the base in both specimens is highly abraded (Figure 3.5A_3), however remnants of a thickened baso-labial shelf and slight depression are present.

Remarks. These teeth have been attributed to the Ctenacanthiformes based on features shared with other members of this group. The prominent central cusp and diminished lateral and intermediate cusps are similar to *Cladodus conicus* Agassiz, 1843 although the base on the tooth from the Canning Basin specimens is much thicker and the striations preserved on the cusps are coarser. The central cusp is flattened along the labial face and exhibits a convex lingual face, and in this respect closely resembles *Cladodus*. The significant abrasion to the labial faces of the teeth does not allow further taxonomic refinement. The teeth do feature a unique rim running across the crown base interface that is not typically seen in other cladodont type teeth.

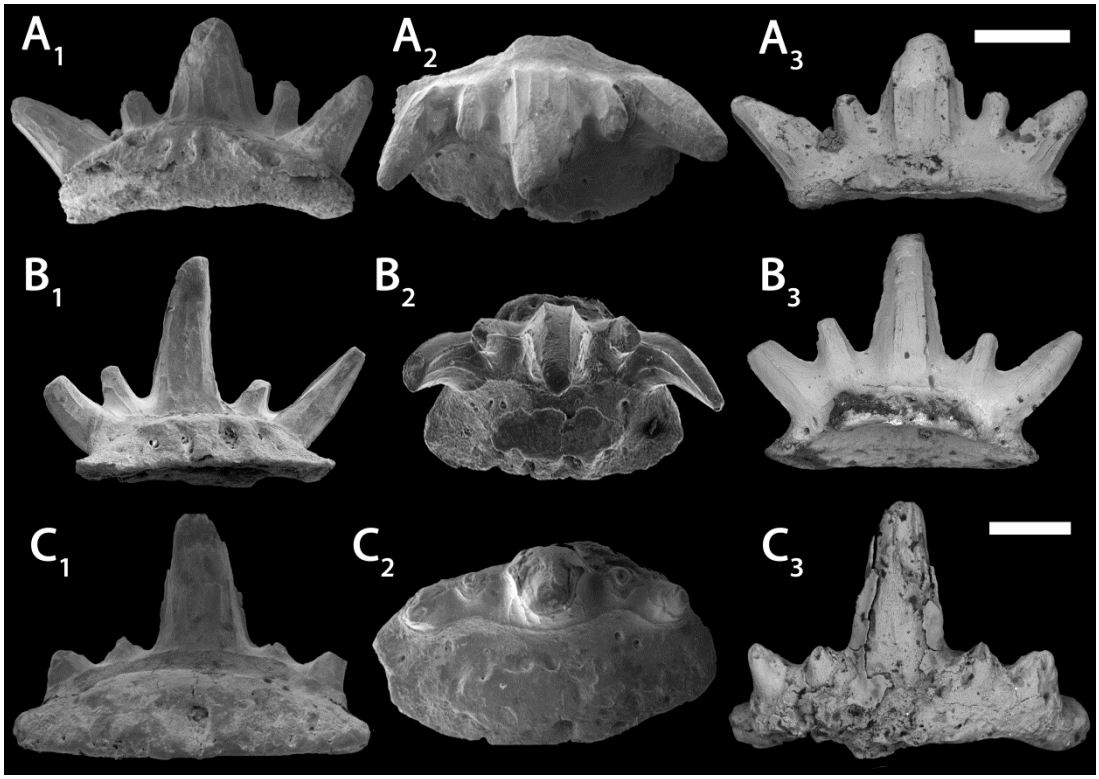

Figure 3.5. Ctenacanthiform teeth from the Famennian at Casey Falls (A) and South Oscar Range (B-C). A, *Cladoides wildungensis*, WAM 14.7.14, sample CL-9, in lingual, occlusal and labial views. B, Ctenacanthiform gen. et. sp. indet 1, WAM 14.7.19, sample SO-200, in lingual, occlusal and labial views; C, Ctenacanthiform gen. et. sp. indet 2, WAM 14.7.20, sample SO-200, lingual, occlusal and labial views. A-B, scale bar = 0.5 mm; C, scale bar 1 mm.

Distribution and stratigraphic range. Frasnian conodont Zone 13b to Late *marginifera* conodont Zone in the Canning Basin, Western Australia.

Cohort Euselachii Hay, 1902

Order indet.

Family *Protacrodontidae* Zangerl, 1981

Genus *Protacrodus* Jaekel, 1925

Type species. *Protacrodus vetustus* Jaekel, 1925

Protacrodus serra Ginter, Hairapetian and Klug, 2002

(Figure 3.6A-B)

1990. "*Cladodus*" sp.; Ginter, p. 77, pl. 4, fig. 9.

2000 .*Protacrodus* cf. *vetustus* Jaekel; Ginter, p. 378-379, fig. 8.

2002. *Protacrodus serra*, sp. nov.; Ginter, Hairapetian and Klug, p. 195, figure 11; pl. 2, figs. L-N; pl. 11, figs. A-C.

2007. *Protacrodus serra* Ginter, Hairapetian and Klug, 2002; Gillis and Donoghue, p. 40, fig. d-e.

2007. *Protacrodus* cf. *serra* Ginter, Hairapetian and Klug, 2002; Ginter and Sun, p. 711, 4C.

2010. *Protacrodus serra* Ginter, Hairapetian and Klug, 2002; Ginter et al., p. 87, fig. 80A-C.

2011. *Protacrodus serra* Ginter, Hairapetian and Klug, 2002; Ginter et al., p. 168, fig. 10I-J.

Material. Two teeth from the Bugle Gap Limestone, Casey Falls, samples 1983-94; 1984-97.

Description. The teeth described here can be assigned to morphotype one of *Protacrodus serra* (Ginter et al., 2002, fig. 11 C-E) and comprise asymmetrical crowns with three cusps directed distally to one side (Figure 3.6A). The medial cusp is large, over twice the size of the lateral cusps with a narrow labio-lingual profile. Both the lingual and labial faces of the cusps are ornamented in strong cristae. In one specimen (WAM 14.7.23, Figure 3.6B), a row of small pointed cusplets is present along the crown base interface on the labial face. The base is narrow lingually, with a slightly extended and straight lingual rim (Figure 3.6B) that is perforated by a large canal located centrally. The labial face of the base does not protrude and is perforated by a row of small foramina (Figure 3.6A_2).

Remarks. Evaluating variation present in the teeth of different shark taxa is difficult as odontological studies remain incomplete (Straube et al., 2008). The presence of labial cusplets (Figure 3.6B) on *P. serra* may be evidence of intraspecific variation or the presence of sexually based heterodonty which is seen in the dentition of some fossil (Parmley and Cicimurri, 2003) and extant shark species (Raschi et al., 1982). The same labial cusplets are apparent in other teeth attributed to *P. serra* from Iran (Ginter et al., 2002, pl. 2L-M; Ginter et al., 2011, text-fig 10I-J), which rules out regional influences for variation. Cusplets also appear on teeth independent of size (Figure 3.6A-B) and morphotype (Ginter et al., 2002, pl. 2L-M) which makes ontogenetic variation unlikely.

Distribution and stratigraphic range. This species has an older occurrence in the Canning Basin, Western Australia (Lower *crepida* to Upper *marginifera* Zone) as compared to other areas of the world where it occurs in the Early *expansa* Zone in Dalmeh, Iran, Late *expansa* Zone, Tizi and Oum El Jerane, Morocco and probable *expansa* Zone Khor Virap, Armenia. In China this species has been recorded from

the middle Tournaisian. Another protacrodont species, *D. masureae* (Burrow et al., 2010) is known to range from the Late Devonian into the Carboniferous.

Genus *Deihim* Ginter, Hairapetian and Klug, 2002

Type species. *Deihim mansureae* Ginter, Hairapetian and Klug, 2002

Deihim mansureae Ginter, Hairapetian and Klug, 2002

(Figure 3.6C-D)

2000. *?Protacrodus* sp. Long and Hairapetian, p. 217-218, fig. 4O.

2000. *Protacrodus* sp. *cf. "P. aequalis" sensu* Ginter and Turner; Yazdi and Turner, p. 226, figs 3.4-7, 4.4.

2002. *Deihim mansureae* gen. et sp. nov.; Ginter, Hairapetian and Klug, p. 191-193, figure 10; pl. 1, fig. r; pl. 2, fig. k; pl. 4, figs F-G, J-M; pl. 5, figs A-M.

2005. Polycrodontidae *insertae sedis* Derycke-Khatir, p. 76, pl. VII, figs 7-10.

2005. *Bobbodus* sp. Derycke-Khatir, p. 95-96, pl. XII, figs 1-2.

2009. *Deihim mansureae* Ginter, Hairapetian and Klug, 2002; Hairapetian and Ginter, p. 176, 179, fig. 2D, 4H.

2010. *Deihim mansureae* Ginter, Hairapetian and Klug, 2002; Hairapetian and Ginter, p. 362, fig. 3A.

2010. *Deihim mansureae* Ginter, Hairapetian and Klug, 2002; Ginter et al., p. 88, fig. 81A-J.

2011. *Deihim mansureae* Ginter, Hairapetian and Klug, 2002; Ginter et al., p. 166, 169, 8A-E, 11C.

2011. *Deihim mansureae* Ginter, Hairapetian and Klug; Ivanov and Lucas, p. 60, fig. 8.

2013. *Deihim mansureae* Ginter, Hairapetian and Klug; Habibi et al., p. 30, fig. 4.

Material. One tooth from the Virgin Hills Formation, Casey Falls, sample CL-471 and seven teeth from the Bugle Gap Limestone, samples 1984-96, 1984-97, 1984-98.

Description. Four morphotypes were originally assigned to the species *Deihim mansureae* Ginter et al. (2002), of which, two are represented here (Figure 3.6C-D). A single tooth attributed to morphotype one (Figure 3.6D_{1-2}) appears to possess a significantly worn central and lateral cusps with only the base of the crown preserved. The base of a large main central cusp can be distinguished, flanked by two smaller highly fused lateral cusps. Cristae is present on the base of the lateral cusps on the lingual face. The labial face of the crown possesses three large, robust cusplets (Figure 3.6D_2), immediately above the base. The crown-base interface on the lingual face is highly arched and defined by a shallow groove. The base is narrower, mesio-distally, than the crown and extends lingually with a series of deep canals.

Two teeth (Figure 3.6C_{1-2}), assigned to morphotype four were recovered and are characterised by an elongate central cusp and two well-spaced diverging lateral cusps approximately a third of the size of the medial cusp. Sub-parallel cristae are present on both the labial and lingual faces of each cusp. Four cusplets are present above the crown-base interface on the labial face. The base is roughly ovoid in outline (Figure 3.6C_2) and does not extend beyond the crown mesio-distally. The lingual face of the base forms an arch, protruding lingually and is perforated by a few foramina.

Remarks. The teeth described here conform to the diagnosis of *D. mansureae* with the presence of a prominent central cusp and lateral cusps that bear strong cristae, on a convex crown-base interface. A row of labial cusplets are also present above the

crown base interface is also characteristic of this species. The teeth assigned to morphotype four resemble those of Ginter et al. (2010, pl. 5 D-F) with the presence of a slender central cusp with two lateral cusps, approximately half the size of the central cusp and diverging at 45 degree angles. These teeth also appear less perforated by foramina on the lingual face of the base and lack the fusing of the central and lateral cusps that is seen in the other morphotypes of this species.

Distribution and stratigraphic range. *D. mansureae* ranges from the Late *marginifera* CZ to possibly the Tournaisian in the Canning Basin. An older occurrence of this species is known from the *rhenana* (MN 11 CZ) in Kale Sardar area of Iran (Hairapetian and Ginter 2010). In the Famennian of Iran and Armenia *D. mansureae* ranges into the Upper *crepida* conodont Zone. Teeth attributed to this species have also been found in the Sly Gap Formation, New Mexico, USA (Ivanov and Lucas 2011), however no concise age range beyond the Late Devonian and Early Carboniferous can be ascertained.

Deihim cf. *mansureae*

(Figure 3.6E)

Material. Two teeth from the Bugle Gap Limestone, Casey Falls, sample 1984-98.

Description. Teeth with prominent central cusps and two smaller lateral cusps approximately one third the size of the medial cusp, diverging at approximate 45 degree angles (Figure 3.6E$_1$). Each cusp is rounded with sub parallel striations on both the labial and lingual faces. A row of seven rounded cusplets, ornamented in strong cristae are present on the base of the crown along the labial face (Figure 3.6E$_2$). The base is ovoid in outline, extending lingually and possessing a single

small pore located centrally on the lingual rim. On the labial face the base is thin and forms an undulated contact with the crown.

Remarks. These teeth are similar to the morphotype 1 of *Deihim mansureae* as they comprise a crown with a large central cusp with two strongly diverging lateral cusps, all ornamented in a strong cristae as well as a row of lingual cusplets along the labial face of the tooth. The cusplets present on the teeth described here are unusual but

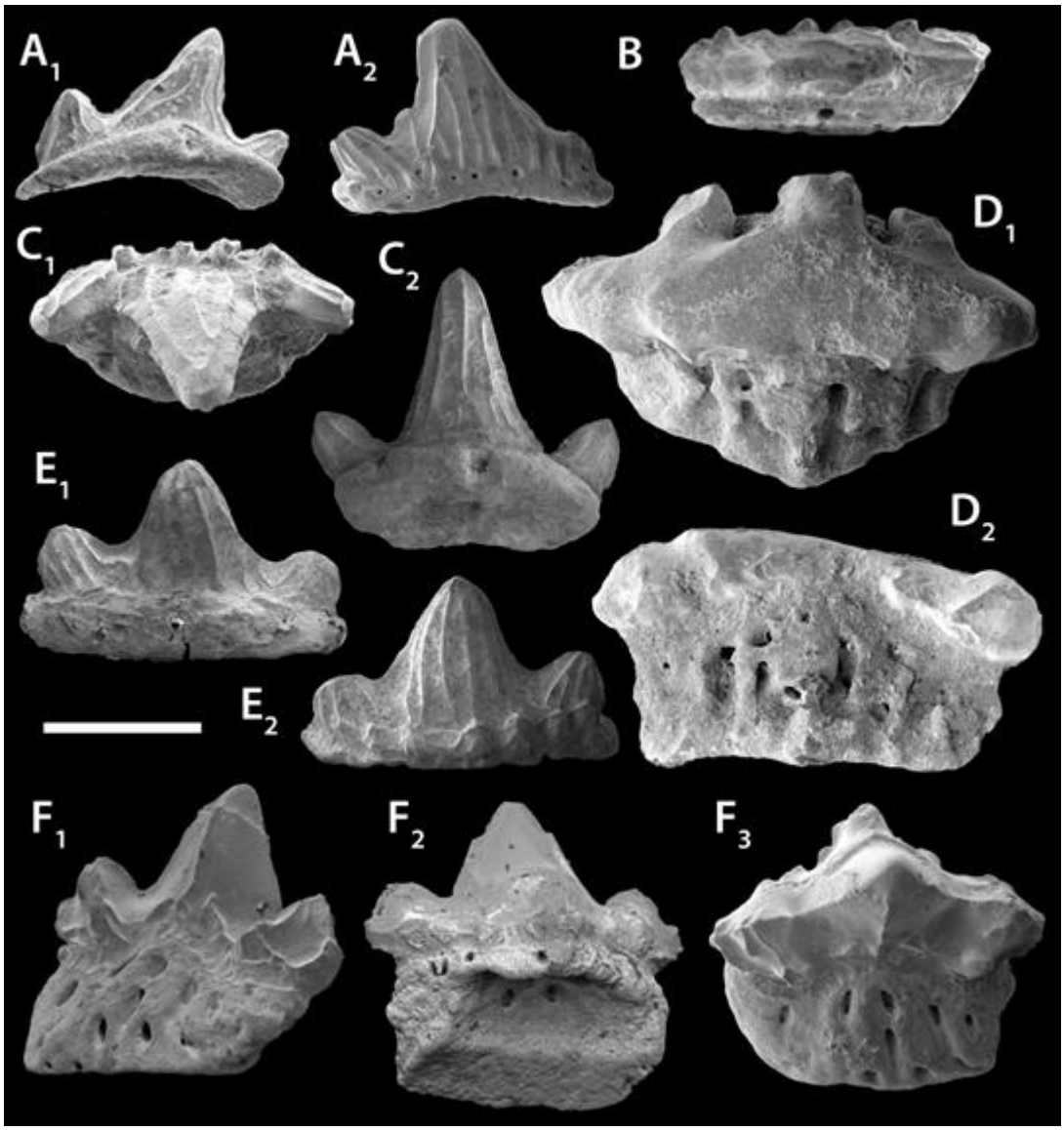

Figure 3.6. Protacrodont teeth from Casey Falls. A-B, *Protacrodus serra*. A - WAM 14.7.21, sample 1984-97, in lingual and labial views; B - WAM 14.7.23, sample CL-471, in occlusal view; C-D - *Deihim mansureae*. C - WAM 14.7.25, sample 1984-98, in lingual and occlusal views; D - WAM 14.7.28, sample 1984-97, in lingual and occlusal views; E, *Deihim* cf. *mansureae*, WAM 14.7.24, sample 1984-98, in lingual and labial views; F, *Deihim* sp. 1, WAM 14.7.17, sample CL-471, in lingual, baso-labial and occlusal views Scale bar 0.5 mm.

bear a strong resemblance to the cusplets on a tooth from *D. mansureae* in central Iran (Hairapetian and Ginter 2009, figs. $5H_{2-3}$). Despite the similarities with *D. mansureae*, the tooth lacks both the arched lingual groove associated with the crown base interface as well as the series of deep pore canals on the lingual face diagnostic of this species (Ginter et al. 2002).These features are also lacking on a tooth attributed to *Protacrodus* cf. *vetustus* from the Montagne Noire (Ginter 2000, fig. 8C). The Montagne Noire tooth shares the similar sub-parallel cristae to the teeth from the Canning Basin, however it lacks labial cusplets.

Deihim sp.1

Figure 3.6F

Material. One tooth from Bugle Gap Limestone, Casey Falls, sample CL-471.

Description. A well preserved, almost symmetrical tooth with a prominent central cusp and two pairs of highly fused lateral cusplets (Figure $3.6F_1$). Cusps are ornamented on the lingual face in strong cristae along the base of the cusps with a single ridge running up the centre of the central cusp. A crown-base interface is prominent, marked by a groove on both the lingual and labial faces of the tooth (Figure $3.6F_1$). A triangular labial peg is positioned at the base of the central cusp with accompanying smaller projections on either side (Figure $3.6F_{2-3}$). The base is approximately the same height as the central cusp with a straight lingual edge and rounded distal margins. A series of foramina are present on the lingual face of the base in almost two rows, one slightly below the crown base interface and another close to the lingual rim (Figure $3.6F_1$). A large articulation socket is present on the baso-labial face of the base (Figure $3.6F_2$).

Remarks. The tooth described here comprises a large central cusp with diverging cusps ornamented in strong cristae which are diagnostic of the genus *Deihim* (Ginter et al., 2002). Further similarities include the presence of a crown base interface separating a lingually extended base perforated by a series of canals. Despite the similarities, *Deihim* sp. 1 comprises a central cusp which is more prominent than that found on morphotype 1 of *D. mansureae* and it also lacks the characteristic labial cusplets. Instead the tooth from the Canning Basin bears small tubercle-like projections above the crown base interface on the extended labial face of the crown. The general morphology of *Deihim* sp. 1 also bears a slight resemblance to *Protacrodus orientalis* Li, 1988 with the high central cusp, fused laterals and a labial projection of the central cusp (Li, 1988, pl. 1, fig. 2), however the size difference in the cusps excludes this tooth from *P. orientalis* (Ginter et al., 2002). There is also a very strong resemblance to another tooth attributed to *P. orientalis* from the Menggongao Formation, South China (Lelièvre and Derycke, 1998, fig. 7B) which is narrower mesio-distally with the same cusp morphology and deep base. Recently, the inclusion of *P. orientalis* as a species of *Protacrodus* has been questioned (Ginter et al., 2010). It is possible *P. orientalis* belongs to the genus *Deihim* and the tooth from the Canning Basin represents a less abraded form of this species.

Protacrodontidae gen. sp. indet. 1

(Figure 3.7A)

Material. One tooth from the Bugle Gap Limestone, Casey Falls, sample 1984-94.

D**escription.** Highly elongate and slightly arched tooth comprising a prominent pyramidal central cusp accompanied by four to five fused lateral cusps approximately a quarter of the size of the central cusp (Figure 3.7A$_1$). Both the labial

and lingual faces of the cusps are ornamented in coarse wavy cristae directed towards the cusp apices. Approximately 80% of the lingual face of the base is broken, however the preserved section is the same height as the lateral cusps and extends both lingually and further mesio-distally than the crown on one side (Figure 3.7A_2). A small number of foramina are present on the lingual face of the base. The labial margin of the base is thin and perforated by small foramina and lacks a distinct crown base interface (Figure 3.7A_2).

Remarks. The tooth is placed under Protacrodontidae based on the coarse cristae and lack of articulation devices also found in other Devonian Protacrodonts as well as its occurrence within the middle Devonian. The tooth is also similar to a partial tooth of a ?Protacrodontid (Ginter and Sun 2007, fig. 4E) from Muhua, southern China in that it shares the highly elongate shape, with extensively fused lateral cusps flanking a prominent central cusp and a well-developed cristae. However, the tooth described here lacks the festoon-like sculpture on the lower aspect of the crown present on the Chinese tooth (Ginter and Sun 2007).

?Protacrodontidae fam. gen. sp. indet.

(Figure 3.7B)

Material. One tooth from the Bugle Gap Limestone, Casey Falls, sample CL-471.

Description. A mesio-distally elongate tooth with a crown consisting of highly fused cusps that are almost indistinguishable. Strong cristae are present on the labial and lingual faces as well as the occlusal surface (Figure 3.7B_{1-3}). The labial face of the crown is higher and slopes lingually. The distal margins of the crown taper inward to the crown-base interface, whereas the labial and lingual faces are almost straight. The base is roughly rectangular in outline with a slightly thickened, protruding

lingual margin. A row of pore canals are present along the lingual face of the base (Figure 3.7B_2), where as possible remnants of canals are present on the labial face (Figure 3.7B_3).

Remarks. Teeth with coarse cristae, a reduced base lacking both a lingual extension and articulation devices are common among Devonian protacrodonts. The crown of the tooth described here, retains more highly fused cusps than other protacrodont teeth and in this respect it more closely resembles an orodont. The reduced base and lack of distinct margin between the crown and base along the labial margin appear similar to the lingual face of the teeth attributed to *P. serra* and *P. aequalis* Ivanov 1996. The samples taken above the section measured at Casey Falls are dominated by protacrodontid-type teeth (*Protacrodus serra*, *Deihim mansureae*, *D.* cf. *mansureae*, *Deihim* sp. 1, Protacrodontidae gen. et sp. indet.; Table 3.1), which could suggest it belongs to the family Protacrodontidae and is highly modified, possibly representing a lateral crushing tooth.

Order Hybodontiformes Cappetta, Duffin and Zidek, 1993

Superfamily Hybodontoidea Owen, 1846

Family Lonchidiidae Herman, 1977

Genus *Lissodus* Brough, 1935

Type species. *Hybodus africanus* Bloom, 1909.

Lissodus lusavorichi Ginter, Hairapetian and Grigoryan, 2011

(Figure 3.7C)

2011 *Lissodus lusavorichi* sp. nov.: Ginter, Hairapetian and Grigoryan: 160, fig. 10E-F.

Material. Two teeth from the Virgin Hills Formation, Casey Falls, sample 1983-94.

Description. The tooth crown is broadly triangular with a well-developed occlusal crest (Figure 3.7C_1). The crown extends laterally beyond the base terminating in triangular shoulders. The crown base interface is slightly arched on the lingual face and prominent on the labial face (Figure 3.7C_2). A well-developed labial peg is present and accompanied by small cusplets or tubercle like projections. The base is *typically* euselachian, projecting lingually with a rounded margin. A series of deep, elongated canals perforate the lingual face of the base (Figure 3.7C_1).

Remarks. The teeth from Casey Falls are attributed to *Lissodus lusavorichi* Ginter et al. 2011, as they possess the same smooth broad triangular crown, well developed occlusal crest and horizontal longitudinal crown shoulders as well as the tubercles associated with the labial peg. The presence of this species represents the oldest record of the family Lonchiididae in the Canning Basin.

Distribution and stratigraphic range. The species has been previously described from the *expansa* zone in Dalmeh, Iran and probable *expansa* zone, Khor Virap

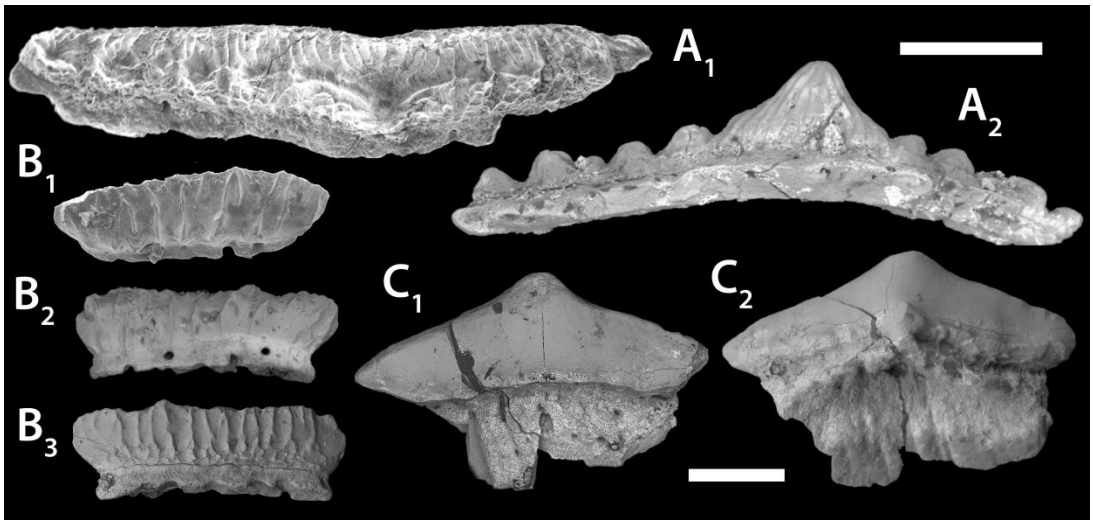

Figure 3.7. Shark teeth from the Casey Falls. A, Protacrodontidae gen. et. sp. indet 1, WAM 14.7.22, sample 1984-94, in occlusal and labial views; B, ?Protacrodontidae gen. et sp. indet WAM 14.7.31, 1984-98,.in occlusal, lingual and labial views; C, *Lissodus lusavorichi*, WAM 14.7.30, sample 1984-98, in labial and lingual views. A, scale bar 0.5 mm; B-C, scale bar 0.5 mm.

Armenia. Its presence in the Upper *marginifera* conodont Zone in the Canning Basin, refines the lower age range of this species.

3.6 Discussion

3.6.1 Biostratigraphy

Thelodonts have been successfully used in biostratigraphy since the 1960's (Gross, 1967) with current global zonation schemes (in Gradstein et al., 2012) developed for the Silurian (Turner, 1973; Bassett et al., 1982; Märss et al., 1995; Blom, 1999; Talimaa, 2000) and Devonian (Turner, 1995a, 1999; Blom and Goujet 2002; Hairapetian et al., in press). Subsequent to the Givetian-Frasnian boundary, thelodonts are restricted to the margins of northern Gondwana (Turner, 1997; Trinajstic 2001; Märss et al., 2007) and there is a marked reduction in diversity with the Turinidae Family represented by the species *Australolepis seddoni* (Seddon, 1969; Turner and Dring, 1981; Trinajstic and George, 2009), *Turinia hutkensis* (Blieck and Goujet, 1978; Hairapetian et al., 2006) and a new genus and species of turiniid (Hairapetian et al., in press). Of these, *A. seddoni* has been particularly useful in defining shallow water Frasnian strata in northern Gondwana (Turner et al., 2002). The species is known from the *falsiovalis* to *rhenana* conodont Zones (MN 1-10 CZ) in Iran and provided a lower Frasnian age constraint for the Chariseh section (Turner et al., 2002). Within Australia this species is now recognised as ranging from MN 6-11 CZ and has been previously used to constrain a Frasnian age for the base of the Gneudna Formation type section in the Carnarvon Basin (Turner and Dring, 1981; Trinajstic and George, 2009). Within the Canning Basin *A. seddoni* has been used to confirm a Frasnian age for the Hull platform (Chow et al. 2013). Although the

increased range of *A. seddoni*, decreases the ability to obtain more finely resolved ages for strata, its confinement to the Frasnian still makes this species an important zone fossil.

The phoebodont taxa recovered in this study conform to previously established age ranges obtained for these species in the Canning Basin (Trinajstic and George, 2009) with the exception of *Phoebodus latus* where the range has been extended from MN 10 CZ to MN 11 CZ. This newly extended range of *Ph. latus* in the Canning Basin brings it closer in line with the known upper age range for this species (MN 13 CZ) in the Southern Urals and South Timan in Russia as well as the Holy Cross Mountains in Poland (Ginter and Ivanov 1995b; Ivanov 1999; Ivanov and Lucas 2011). The extension of the known age ranges for *A. seddoni* and *Ph. latus* in the Canning Basin indicates further refinement of the age ranges for other Phoebodont taxa such as *Ph. bifurcatus* and *Ph. fastigatus* is likely with further collecting. Work so far undertaken describing the phoebodont fauna from the Canning Basin (Trinajstic and George 2009), has proven their utility in biostratigraphy as well as increasing the geographic distribution in which these species can be used.

A disappearance in phoebodont fauna is seen in the section at Horse Spring from MN 11 CZ and occurs too early to be attributed to the global Kellwasser Events. Despite the distinct anoxic black limestones and shales associated with the Kellwasser horizons not being recognised in the Canning Basin (Becker et al., 1993), perturbations are recorded in the faunas. Reductions in the species diversity and abundances are recorded within conodonts (Klapper, 2007), ammonoids (Becker et al., 1993) and trilobites (Feist and McNamara, 2013) in the Canning Basin which are also seen in the rest of the world. The absence of microvertebrates at Horse Spring

above MN CZ 11 was previously noted by Trinajstic and George (2009) who suggested post depositional dolomitisation as the main factor contributing to the lack of microvertebrates. However, this does not seem to be the cause as microvertebrates are often recovered from dolomitised beds. In addition, conodonts were found in the dolomitised beds from 13-19 m (Figure 3.2) in the section at Horse Spring where microvertebrate fossils were lacking. A global non-occurrence of the *Phoebodus bifurcatus* group from the *linguiformis* Zone (MN 13b CZ) in the Frasnian to the Famennian late *crepida* conodont Zone has been identified in the Northern Hemisphere (Ginter and Ivanov, 1995b; Ginter et al., 2002). Ginter et al. (2002) suggests the disappearance mainly resulted from global cooling (Copper, 1998) rather than fluctuations in sea level or anoxia. Given the much earlier disappearance of phoebodonts in the section at Horse Spring, and no evidence of major temperature excursions in sea surface temperatures during the MN 11 CZ (Joachimski et al., 2004), it is not likely temperature fluctuations are the reason for the disappearance of a phoebodont non-occurrence at Horse Spring.

Another notable global change recorded towards the end of the Frasnian is the *semichatovae* Transgression (Sandberg et al., 1997). This event occurs at the base of the MN 11 Zone and coincides with the absence of phoebodont taxa in the Canning Basin. Despite reported localised tectonic overprinting (Southgate et al., 1993; George and Chow, 2002; Chow et al., 2013), evidence of a longer-term 2nd order transgressive event is observable in these sections. The effect of these localised and global events may be highly influential in the faunal changes and extinctions seen in the basin (George and Chow, 2002). The phoebodont group has been previously noted as niche sensitive (Ginter and Turner, 1999), which may explain their apparent confinement to specific sites in the Canning Basin. Following any

ecological disturbance within the Horse Spring area, a migration of phoebodont taxa may have occurred. In this scenario, the disappearance in MN 11 CZ would reflect a movement of these sharks rather than the extinction seen in other areas of the world, such as Poland at the *linguiformis* CZ (13b) (Ginter et al., 2002). It is important to note that a re-emergence of the phoebodont group in the Famennian is present along both the North and Eastern margins of Gondwana as well as Laurussia (Ginter and Turner, 1999; Ginter and Ivanov, 2000; Ginter et al., 2002). Interestingly, this re-emergence is not reflected in the studied sections here and could indicate the factor or factors influencing the non-occurrence of phoebodonts in the Canning Basin were potentially long lasting and perhaps localised. A collecting bias can also not be ignored as there have only been limited studies in the Canning Basin focusing on Frasnian microvertebrate faunas.

The current phoebodont based zonation established for the Famennian (Ginter and Ivanov, 1995b; Gradstein et al., 2012) has not yet been correlated in the Canning Basin and this is partly due to the study of Famennian vertebrates being in its infancy. The sections described also do not encompass the open shelf environment where this scheme is most applicable (Ginter et al., 2002) and may account for the lack of *Phoebodus* teeth in the Famennian dated intervals. Despite a lack of *Phoebodus* species in the Bugle Gap Limestone, the recovered shark species exhibit comparable ages for the same species found in other areas of the world. Of these, *Thrinacodus tranquillus* has been recorded as occurring from the Middle to Late Devonian in Laurussia and North Gondwana (Ginter and Turner, 2010). The presence of this species in the Canning Basin makes it one of the oldest global occurrences (Upper *marginfera* CZ) with similar ages recorded in Morocco, South China and Iran (Lelièvre and Derycke, 1998; Hairapetian and Long, 2000; Ginter et

al., 2002). The oldest report of the protacrodont *Deihim mansureae* is from the Late Frasnian, *rhenana* (MN 11 CZ) in Kale Sardar area of Iran (Hairapetian and Ginter, 2010). This species is far more widespread in the Famennian, extending from the east of Laurussia (Ivanov and Lucas, 2011) to the north-west of Gondwana. An Upper *crepida* conodont Zone is recorded as the upper range of *D. mansureae* in both Iran and Armenia. In the Canning Basin, Australia the range extends further, from Upper *marginifera* CZ, into the lower Tournaisian (Burrow et al., 2010). Two other shallow water shark species, *Protacrodus serra* and *Lissodus lusavorichi,* been recorded from the *expansa* CZ of the Khor Virap region in Armenia and Dalmeh in Iran (Ginter et al., 2011). The presence of both *P. serra* and *L. lusavorichi* in the Canning Basin extends the lower age range of these species from the *expansa* conodont Zone to Upper *marginifera*. Like *D. mansureae*, an increased Famennian distribution of *Th. tranquillus*, *L. lusavorichi* and *P. serra* in Northern Gondwana is established. The presence of small, shallow water genera such as *Deihim*, *Lissodus* and *Protacrodus* across the margins of North Gondwana, would support the presence of a continuous shallow platform and reef environmental (Golonka, 2007) suitable for faunal exchange.

3.6.2 Biogeography and chondrichthyan assemblages

Chondrichthyan biofacies present in the depauperate Famennian intervals of the Virgin Hills and Napier formations are often difficult to determine. These intervals often comprise largely shallow water and slope derived material. This results in the microvertebrate remains often not representing an original environment of habitation. In contrast to the described sections, samples taken from the shallow fore-reef deposits of the Bugle Gap Limestone (Guppy et al., 1958; Playford and

Lowry, 1966; Playford et al., 2009) preserve a more original chondrichthyan biofacies. A diverse shark genera including *Thrinacodus*, *Stethacanthus*, *Protacrodus*, *Deihim* and *Lissodus* were present in these shallow water facies. Despite the low numbers of teeth recovered from the Bugle Gap Limestone, the proportionally higher number of protacrodont and hybodont type sharks (62% of the overall number of teeth) as well as the absence of *Phoebodus* and *Jalodus*, is indicative of a shallow water *Protacrodus* biofacies (Ginter, 2000, 2001). Similar assemblages have also been recorded in Famennian strata from both Dalmeh and Chahriseh, Iran (Ginter et al., 2002; Hairapetian and Ginter, 2010).

An increase in cosmopolitanism is seen in many Late Devonian marine groups, including brachiopods (Copper, 1998), ammonoids (House, 1973), trilobites (McNamara and Feist, 2006), crustaceans (Rode and Lieberman, 2005), conodonts Girard et al., 2010) and fish (Ginter and Turner, 1999; Burrow et al., 2010). This faunal exchange between areas was likely driven by the closure of the Rheic Ocean (Nance et al., 2012; Domeier and Torsvik, 2014) during the Late Devonian, culminating in an increased proximity of Laurussia and Gondwana (Young, 2003; Burrow et al., 2010; Young et al., 2010). This period also saw the rifting of the Palaeotethys resulting in a separation of the north China, Indochina, Tarim and South China blocks from Gondwana (Metcalfe, 1984, 2011). Connections between South China and north-west Australia were maintained in the Late Devonian by the occurrence of an extensive, shallow water shelf (Golonka, 2007; Metcalfe, 2011; Golonka and Gaweda, 2012). Previous work on Late Devonian conodonts (Burrett et al., 1990; Girard et al., 2010) and fish (Long, 1993) support a close relationship between the two areas. In addition, Trinajstic and George (2009) had previously shown close affinities, in regards to the temporal ranges, of the Frasnian

phoebodonts *Ph. fastigatus* and *Ph. bifurcatus* in the Canning Basin and South China. The presence of a likely shallow water taxon, *Deihim* sp.1 (Figure 3.6G$_{1-3}$) in both the Canning Basin and Menggongao Formation of South China (Lelièvre and Derycke, 1998, figure 7B), would support the presence of a shallow water platform between the two areas into the middle part of the Famennian. Determining the extent of faunal exchange further into the Famennian or even Carboniferous is difficult to determine as studies into shark faunas of these ages are limited for the north west of Australia. However *Th. ferox* has been reported in the late Famennian in both South China and Australia (Long and Burrett, 1989). The similarities between the tooth identified here as Protacrodontidae sp. 1 (Figure 3.7A$_{1-2}$) found in a middle Famennian of the Virgin Hills Formation and a tooth from the middle Tournaisian in Muhua, South China (Ginter and Sun, 2007, fig. E$_{1-2}$) provides further support for a close connection between China and Australia (Metcalfe, 2001) however, further data from microvertebrates are required.

Clear links between the shark taxa in the north-west of Australia and other parts of Laurussia, South China and Northern areas of Gondwana are demonstrated here. Despite the similarities, there is also a degree of endemism amongst some of the shark species present in the Canning Basin. This is not unusual as endemism in some conodont (Klapper, 1995, 2007) and many placoderm (Long, 2006) species has also been noted. Of the Frasnian taxa *Diademodus dominicus* sp. nov. had not been previously recorded outside of Laurussia. The presence of this species along the eastern margins of North Gondwana would also suggest a greater distribution of this genus than previously recognised. Of the other phoebodontids, *Phoebodus* tooth forms found in the Horse Spring section often possess unusual features. These include the tricuspid form of *Ph. bifurcatus* which appear relatively common in the

Canning Basin but rare in other areas of the world. The teeth of *Ph. fastigatus* also differ from the diagnostic smooth cusps, often possessing cusps with heavy ornament on the labial face. In addition to the Frasnian taxa, there are two types of ctenacanthiform and a species of *Stethacanthus* that have not been found anywhere else. Despite an increased cosmopolitanism in Devonian shark faunas, a considerable endemic component is present in the Canning Basin. The mechanisms for this are difficult to determine and may be the result of lack of sampling, although unique palaeoenvironmental conditions or environmental niches might have existed in this part of East Gondwana (north-western Australia) at this time.

3.7 Conclusions

A largely undescribed chondrichthyan fauna ranging in age from MN 11 CZ in the late Frasnian to the late *marginifera* Zone in the middle Famennian was recorded from the Virgin Hills Formation, and the Bugle Gap Limestone, and Napier Formation in the Canning Basin. The section at Horse Springs reveals a similar diversity of phoebodonts to that previously described by Trinajstic and George (2009). A new species of diademodont, *Diademodus dominicus* sp. nov., a genus which until now had only previously been described from Laurussia was recovered from the phoebodont-rich beds. This species, in addition to variation in *Phoebodus fastigatus*, as well as newly described cladodont and stethacanthid teeth, reveals a potentially endemic Frasnian component to the Canning Basin.

The Famennian Bugle Gap limestone and uppermost beds of the section at Casey Falls reveals a diverse shark fauna that had not been previously described from the Canning Basin. Many of these, including *Th. tranquillus*, *C. wildungensis*, *P. serra*, *D. mansureae* and *L. lusavorichi*, represent ages similar to or the same as

those previously described for these species. The presence of this shark fauna in the Canning Basin also allows for a more comprehensive understanding of species distribution in the Famennian. A number of genera including *Phoebodus* and *Protacrodus* occur in both eastern Australia and Western Australia (Turner and Young, 2000), however, these new reports on chondrichthyans from the Canning Basin indicate stronger faunal links between the Canning Basin and other areas of Gondwana such as Iran and Morocco as well as Poland and the United States of America in Laurussia. In addition, faunal similarities between South China and the Canning Basin are present, with some shark species indicating potential faunal exchange extending into the Late Famennian and possible Early Carboniferous.

3.8 Acknowledgements

We would like to thank Michal Ginter, Vachik Hairapetian, and Sue Turner for their helpful comments and assistance in the preparation of this work. Thank you to Arthur Mory, Roger Hocking and Peter Haines from the Geological survey of Western Australia for their assistance in fieldwork. The authors acknowledge the use of equipment, scientific and technical assistance of the Curtin University Electron Microscope Facility, which has been partially funded by the University, State and Commonwealth Governments. A thank you to Mikael Siversson from the Western Australian Museum for the use of the facilities. We would also like to acknowledge Australian Research Council, MRIWA, WAERA, CSIRO, Arc Energy, Chevron Australia Business Unit, Chevron Energy Technology Company, University of Greenwich, National Science Foundation and Chemostrat Inc. Field support and safety provided by Wundargoodie Aboriginal Safaris and the Geological Survey of Western Australia. Thank you to Mimbi Community, Mt. Pierre Station, Fossil

Downs, for field area access. BR also acknowledges an Australian Postgraduate Award.

3.9 References

Aboussalam, Z.S. 2003. Das "Taghanic-Event" im höheren Mittlel-Devon von West-Europa und Marokko. Münstersche Forschungen zur Geologie und Paläontologie 97, 1-330.

Agassiz, J.L.R. 1833-44. Recherches sur les poissons fossils, 5 vols. 1420 pp. with supplements. Petitpierre, Neuchâtel et Soleure.

Basden, A., Burrow, C.J., Hocking, M., Parkes, R. and Young, G.C. 2000. Siluro-Devonian microvertebrates from south-eastern Australia. In: Blieck, A., Turner, S. (Eds). Palaeozoic Vertebrate Biochronology and Global Marine/Non-Marine Correlation. Final Report of IGCP 328 (1991-1996). Courier Forschungsinstitut Senckenberg 223, 201-222.

Bass, A.J., D'Aubrey, J.D. and Kistnasamy, N. 1973. Sharks of the east coast of Southern. Africa. I. The genus *Carcharinus* (Carcharhinidae). Investigational Report Oceanographic Research Institute 33, 1-168.

Bassett, M.G., Lawson, J.D. and White, D.E. 1982. The Downton Series as the fourth series of the Silurian System. Lethaia 15, 1-24.

Becker, M.A., Chamberlain, J.A. and Stoffer, P.W. 2000. Pathological tooth deformities in modern and late Cretaceous chondrichthyans: A consequence of feeding related injury. Lethaia 36, 1-16.

Becker, R.T. 2000. Ammonoidea. In: Wright, A.J., Young, G.C., Talent, J.A. and Laurie, J.R. (Eds). Paleobiogeography of Australasian faunas and floras. Association of Australasian Paleontologists, Memoir 23, 177-180.

Becker, R.T., House, M.R. and Kirchgasser, W.T. 1993. Devonian goniatite biostratigraphy and timing of facies movements in the Frasnian of the Canning Basin, Western Australia. Geological Society, London, Special Publications 70, 293-321.

Blieck, A. and Goujet, D. 1978. **A** propos de nouveau matériel de thelodontes (vertébrés agnathes) d'Iran et de Thaïlande: aperçu sur la répartition géographique et stratigraphique des agnathes des regions gondwaniennes au Paléozoïque moyen, Annales de la Societe Géologique du Nord, 97, 363-373.

Blom, H. 1999. *Loganellia* (Thelodonti, Agnatha) from the Lower Silurian of North Greenland. Acta Geologica Polonica 49, 97-104.

Blom, H. and Goujet, D. 2002. Thelodont scales from the Lower Devonian Red Bay Group, Spitsbergen. Palaeontology 45, 795-820.

Bonaparte, C.L.J.L. 1838. Selachorum *tabula analytica*. Nuovi Annali delle Scienze Naturali 1, 195-214.

Brough, J. 1935. On the structure and relationships of the hybodont sharks. Memoirs and Proceedings of the Manchester Literary and Philosophical Society 79, 35-49.

Burrett, C.F., Long, J. A. and Stait, B. 1990. Early-Middle Palaeozoic biogeography of Asian Terranes derived from Gondwana. Memoirs of the Geological Society of London 12, 163-174.

Burrow, C. 1996. Taphonomy of acanthodians from the Devonian Bunga Beds (Late Givetian/Early Frasnian) of New South Wales. Boucot Festschrift. Historical Biology 11, 213-228.

Burrow, C.J. 1997. Microvertebrate assemblages from the Lower Devonian (*pesavis*/*sulcatus* zones) of central New South Wales, Australia. Modern Geology 21, 43-77.

Burrow, C.J. and Simpson, A.G. 1995. A new ischnacanthid acanthodian from the Late Silurian (Ludlow, *ploeckensis* zone) Jack Formation, north Queensland. Memoirs of the Queensland Museum 38, 383-395.

Burrow, C.J. and Turner, S. 1998. Devonian placoderm scales from Australia. Journal of Vertebrate Paleontology 18, 677-695.

Burrow, C.J. and Turner, S. 2000. Silurian vertebrates from Australia. In: Blieck, A., Turner, S. (Eds). Palaeozoic Vertebrate Biochronology and Global Marine/Non-Marine Correlation. Final Report of IGCP 328 (1991-1996). Courier Forschungsinstitut Senckenberg 223, 169-174.

Burrow, C.J., Turner, S. and Young, G.C. 2010. Middle Palaeozoic microvertebrate assemblages and biogeography of East Gondwana (Australasia, Antarctica). Palaeoworld 19, 37-54.

Cappetta, H., Duffin, C.J. and Zidek, J. 1993. Chondrichthyes. In: M.J. Benton (Eds). The Fossil Record 2: 593-609. Chapman and Hall, London.

Chow, N., George, A.D., Trinajstic, K.M. and Chen, Z. 2013. Stratal architecture and platform evolution of an early Frasnian syn-tectonic carbonate platform, Canning Basin, Australia. Sedimentology 38, 1-38.

Copper, P. 1998. Evaluating the Frasnian-Famennian mass extinction: Comparing brachiopod faunas. Acta Palaeontologica Polonica 43, 137-154.

Dean, B. 1909. Studies on fossil fishes (sharks, chimaeroids and arthrodires). American Museum of Natural History Memoir 9, 211-287.

Derycke, C. 1992. Microrestes de sélaciens et autres Vertebres du Dévonien

supérieur du Maroc. Bulletin de Muséum national d'Histoire naturelle 14, 15-61.

Derycke, C,, Spalletta, C,. Perri., M.C. and Corradini, C. 2008. Famennian chondrichthyan microremains from Morocco and Sardinia. Journal of Palaeontology 82, 984-995.

Derycke-Khatir, C., 2005. Microrestes de Vertébrés du Paléozoïque supérieur de la Manche au Rhin. Société géologique du Nord 33, 261.

Domeier, M. and Torsvik, T.H. 2014. Plate tectonics in the late Paleozoic. Geoscience Frontiers 5, 303-350.

Drummond, B.J., Sexton, M.J., Barton, T.J. and Shaw, R.D. 1991. The nature of faulting along the margins of the Fitzroy Trough, Canning Basin and implications for the tectonic development of the trough. Exploration Geophysics 22, 111-116.

Duffin, C.J. and Ginter, M. 2006. Comments on the selachian genus *Cladodus* Agassiz 1843. Journal of Vertebrate Paleontology 26, 253-266.

Duncan, M. 2003. Early Carboniferous chondrichthyan *Thrinacodus* from Ireland, and a reconstruction of jaw apparatus. Acta Palaeontologica Polonica 48, 113-122.

Edwards, A.F. 1997. Ichthyolith remains from the Devonian-Carboniferous Boundary of the Canning Basin, Western Australia. M.Sc, Thesis (unpublished). School of Earth Sciences, Macquarie University, Sydney.

Feist, R., and McNamara, K.J. 2013. Patterns of evolution and extinction in proetid trilobites during the late Devonian mass extinction event, Canning Basin, Western Australia. Palaeontology 56, 229-259.

George, A.D. 1999. Deep-water stromatolites, Canning Basin, northwestern Australia. Palaios 14, 493-505.

George, A.D. and Chow, N. 2002. The depositional record of the Frasnian/Famennian boundary interval in a fore-reef succession, Canning Basin, Western Australia. Palaeogeography, Palaeoclimatology, Palaeoecology 181, 347-374.

Ginter, M. 1990. Late Famennian shark teeth from the Holy Cross Mts, Central Poland. Acta Geologica Polonica 40, 69-81.

Ginter, M. 1991. Ichthyoliths and fish−fauna. In: J. Hladil, Z. Krejci, J. Kalvoda, M. Ginter, A. Galle, and P. Berousek. Carbonate ramp environment and biostratigraphy of Kellwasser time−interval (Lesni Lom, Moravia, Czechoslovakia), 75-77. Bulletin de la Société belge de Géologie 100, 57-119.

Ginter, M. 1995. Ichthyoliths and Late Devonian events in Poland and Germany. In: S. Turner (Ed.), Ichthyolith Issues, Special Publication 1, 23-30.

Ginter, M. 2000. Late Famennian pelagic shark assemblages. Acta Geologica Polonica 50, 369-386.

Ginter, M. 2001. Chondrichthyan biofacies in the Late Famennian of Utah and Nevada. Journal of Vertebrate Paleontology 21, 714-729.

Ginter, M. 2002. Chondrichthyan fauna of the Frasnian-Famennian boundary beds in Poland. Acta Palaeontologica Polonica 47, 329-338.

Ginter M. 2004. Devonian sharks and the origin of Xenacanthiformes. In: Arratia G., Wilson M.V.H. and Cloutier R. (Eds). Recent Advances in the Origin and Early Radiation of Vertebrates, 473-486. Verlag Friedrich Pfeil, München.

Ginter, M. 2008. Devonian filter feeding sharks. Acta Geologica Polonica 58, 147-153.

Ginter, M. and Ivanov, A. 1992. Devonian phoebodont shark teeth. Acta Palaeontologica Polonica 37, 55-75.

Ginter, M. and Ivanov, A. 1995a. Middle ⁄ Late Devonian phoebodont-based ichthyolith zonation. Geobios, Memoire Special 19, 351-355.

Ginter, M. and Ivanov, A. 1995b. New Late Devonian species of *Phoebodus*. In: Turner, S. (Ed.), Ichthyolith Issues Special Publication 1, 19-22.

Ginter, M. and Ivanov, A. 1996. Relationships of *Phoebodus*. Modern Geology 20, 263-274.

Ginter, M. and Ivanov, A. 2000. Stratigraphic distribution of chondrichthyans in the Devonian on the East European Platform margin. In: Blieck, A., Turner, S. (Eds). Palaeozoic Vertebrate Biochronology and Global Marine/Non-Marine Correlation. Final Report of IGCP 328 (1991-1996). Courier Forschungsinstitut Senckenberg 223, 325-339.

Ginter, M. and Sun, Y. 2007. Chondrichthyan remains from the Lower Carboniferous of Muhua, southern China. Acta Palaeontologica Polonica 52, 705-727.

Ginter, M. and Turner, S. 1999. The early Famennian recovery of phoebodont sharks. Acta Geologica Polonica 49, 105-117.

Ginter, M. and Turner, S. 2010. The Middle Paleozoic selachian genus *Thrinacodus*. Journal of Vertebrate Paleontology 30, 1666-1672.

Ginter, M., Hairapetian, V. and Grigoryan, A. 2011. Chondrichthyan microfossils from the Famennian and Tournaisian of Armenia. Acta Geologica Polonica 61, 153-173.

Ginter, M., Hairapetian, V. and Klug, C. 2002. Famennian chondrichthyans from the shelves of North Gondwana. Acta Geologica Polonica 52, 169-215.

Ginter, M., Hampe, O. and Duffin, C. J. 2010. Chondrichthyes. Paleozoic Elasmobranchii: Teeth. In: H.-P. Schultze (Ed.), Handbook of Paleoichthyology 3D, pp. 1-168. Verlag Dr. Friedrich Pfeil, München.

Ginter, M., Liao, J.C. and Valenzuela-Rios, J.I. 2008. New data on chondrichthyan microremains from the Givetian of the Renanue section in the Aragonian Pyrenees (Spain). Acta Geologica Polonica 58, 165-172.

Girard, C., Klapper, G. and Feist, R. 2005. Subdivision of the terminal Frasnian *linguiformis* conodont Zone, revision of the correlative interval of the Montagne Noire Zone 13, and discussion of the stratigraphically significant associated trilobites. In: Over, D.J., Morrow, J.R. and Wignall, P.B. (Eds). Understanding Late Devonian and Permian-Triassic biotic and climatic events: towards an integrated approach: Towards an Integrated Approach. Developments in Paleontology and Stratigraphy Series 20, 181-198. Elsevier, Amsterdam.

Girard, C., Phuong, T.H., Savage, N. and Renaud, S. 2010. Temporal dynamics of the geographic differentiation of Late Devonian *Palmatolepis* assemblages in the Prototethys. Acta Palaeontologica Polonica 55, 675-687.

Glenister, B.F. and Klapper, G. 1966. Upper Devonian conodonts from the Canning Basin, Western Australia. Journal of Palaeontology 40, 777-842.

Glikman, L.S. 1964. Subclass Elasmobranchii. Sharks. In: Obručev, D.V. (Ed.), Osnovy paleontologii. Besčelustnye, ryby: 196-237. Nauka, Moskva.

Golonka, J. 2007. Phanerozoic Paleoenvironment and Paleolithofacies Maps. Late Paleozoic. Geologia 33, 145-209.

Golonka, J. and Gaweda, A. 2012. Plate tectonic evolution of the southern margin of Laurussia in the Paleozoic. In: Sharkov, E. (Ed.), Tectonics recent advances. InTech: 261-282.

Gradstein, F.M., Ogg, J.G., Schmitz, M. and Ogg, G. (Eds). 2012. The geological timescale 2012. Elsevier, Oxford.

Gross, W. 1967. Über Thelodontiers Schuppen. Palaeontographica Abteilung A 127, 1-67.

Gross, W. 1973. Kleinschuppen, Flossenstacheln und Zähne von Fischen aus europäischen und nordamerikanischen Bonebeds des Devons. Palaeontographica A 142, 51-155.

Guppy, D.J., Lindner, A.W., Rattigan, J.H. and Casey, J.N. 1958. The geology of the Fitzroy Basin, Western Australia: Australia. Bureau of Mineral Resources Bulletin 36, 1-116.

Habibi, T., Yazdi, M., Zarepoor, S. and Shirazi, M.P. 2013. Late Devonian fish micro-remains from Central Iran. Geopersia 3, 25-34.

Hairapetian, V. and Ginter, M. 2009. Famennian chondrichthyan remains from the Chahriseh section, central Iran. Acta Geologica Polonica 59, 173-200.

Hairapetian, V. and Ginter, M. 2010. Pelagic chondrichthyan microremains from the Upper Devonian of the Kale Sardar section, eastern Iran. Acta Geologica Polonica 60, 357-371.

Hairapetian, V., Yazdi, M. and Long, J.A. 2000. Devonian vertebrate biostratigraphy of central Iran. Records of the Western Australian Museum, Supplement 58, 241-247.

Hairapetian, V., Roelofs, B., Trinajstic, K. and Turner, S. 2016. Famennian survivor turiniid thelodonts of North and East Gondwana. In: Koenigshoef, P. and Becker, T. (Eds). Geological Society Special Publication.

Hairapetian, V., Valiukevičius, J. and Burrow, C. 2006. Early Frasnian acanthodians from Central Iran. Acta Palaeontologica Polonica 51, 499-520.

Hampe, O., Aboussalam, Z.S. and Becker, R.T. 2004. *Omalodus* teeth (Elasmobranchii: Omalodontida) from the northern Gondwana margin (middle Givetian: ansatus conodont Zone, Morocco). In: G. Arratia, M.V.H. Wilson et al., (Eds). Recent advances in the origin and early radiation of vertebrates, 473-486. Friedrich Pfeil, München.

Harris, J.E. 1951. *Diademodus hydei*, a new fossil shark from the Cleveland Shale. Proceedings of the Zoological Society of Londo, 120, 683-697.

Hay, O.P. 1902. Bibliography and catalogue of the fossil Vertebrata of North America. Bulletin, United States Geological Survey 179, 1-868.

Herman, J. 1977. Les sélaciens des terrains néocrétacés et paléocènes de Belgique et des contrées limitrophes: Eléments d'une biostratigraphie intercontinentale. Mémoirs pour servir à l'éxplication des Cartes géologiques et minières de la Belgique 15, 1-450.

House, M. 1973. An analysis of Devonian goniatite distributions. Palaeontology Special Papers 12, 305-317.

Huxley, T.H. 1880. On the application of the laws of evolution to the arrangement of the Vertebrata, and more particularly of the Mammalia. Proceedings of the Zoological Society, London 43, 649-662.

Ivanov, A. 1992. Vertebrate fauna at the Frasnian/Famennian boundary of the South Urals. The International Symposium on Devonian System and Its Economic Oil and Mineral Resources, 9-12.09.92, Guilin, China. Abstract.

Ivanov, A. 1996. The Early Carboniferous chondrichthyans of the South Urals, Russia. In: Strogen, P., Somerville, I.D. and Jones, G.L. (Eds). Recent Advances in Lower Carboniferous Geology. Geological Society, Special Publication 107, 417-425.

Ivanov, A. 1999. Late Devonian - Early Permian chondricthyans of the Russian Arctic. Acta Geologica Polonica 49, 267-285.

Ivanov, A.O. and Lucas, S.G. 2011. Paleozoic Sly Gap Formation of southern New Mexico, USA. New Mexico Museum of Natural History and Science Bulletin 53, 52-70.

Ivanov, A., Vûškova, L.], and Esin, D. 1992. Ichthyofauna. In: V. Krasnov and M. Ržonsnickaâ (Eds). Tipovye razrezy pogranič nyh otloženij srednego i verhnego devona, franskogo ifamenskogo ârusov okrain Kuzneckogo bassejna. Materialy V vyezdnojsessii komisii MSK po devonskoj sisteme, Kuzbass 16-29 iûlâ 1991 g., 89-91.

Jaekel, O. 1911. Die Wirbeltiere. Eine Übersicht über die fossilen und lebenden Formen. Borntraeger, Berlin.

Jaekel, O. 1921. Die Stellung der Paläontologie zur einigen Problemen der Biologie und Phylogenie. Schadelprobleme. Paläontologische Zeitschrift 3, 213-239.

Jaekel, O. 1925. Das Mundskelett der Wirbeltiere. Gegenbaurs Morphologishes Jahrbuch 55, 402-409.

Jeppsson, L., Anehus, R, and Fredhold, D. 1999. The Optimal Acetate Buffered Acetic Acid Technique for Extracting Phosphatic Fossils. Journal of Paleontology 73, 964-972.

Jones, R.K. and Turner, S. 2000. Late Devonian fauna from the Columbine Sandstone (Coffee Hill Member), Gap Creek, central New South Wales. In: Blieck, A. and Turner, S. (Eds). Palaeozoic Vertebrate Biochronology and Global Marine/Non-marine Correlation (final report IGCP 328, 1991-1996). Courier Forschungsinstitut Senckenberg 223, 523-542.

Kaufmann, B. 1998. Facies, stratigraphy and diagenesis of Middle Devonian reef and mud mounds in the Mader (eastern Anti-Atlas, Morocco). Acta Geologica Polonica 48, 43-106.

Kiaer, J. 1932. New coelolepids from the Upper Silurian on Oesel (Esthonia). Eesti Loodusteaduse Arhiiv, Seeria 1 10, 167-176.

Klapper, G. 1989. The Montagne Noire Frasnian (Upper Devonian) conodont succession. In: McMillan, N.J, Embry, A. F. and Glass, D.J. (Eds). Devonian of the World, Canadian Society of Petroleum Geologists Memoir 14, 449-468.

Klapper, G. 1995. Preliminary analysis of Frasnian, Late Devonian conodont biogeography. Historical Biology 10, 103-117.

Klapper, G. 2007. Frasnian (Upper Devonian) conodont succession at Horse Spring and correlative sections, Canning Basin, Western Australia. Journal of Paleontology 81, 513-537.

Joachimski, M.M., van Geldern, R., Breisig, S., Buggisch, W. and Day, J. 2004. Oxygen isotope evolution of biogenic calcite and apatite during the Middle and Late Devonian. International Journal of Earth Sciences 93, 542-553.

Lelièvre, H. and Derycke, C. 1998. Microremains of vertebrates near the Devonian-Carboniferous boundary of Southern China (Hunan province) and their biostratigraphical significance. Revue de Micropaléontologie 41, 297-320.

Li, G.Q. 1988. A new species of Protacrodus from northern Jiangsu. Vertebrata Palasiatica 26, 101-106.

Liao, J.C., Ginter, M. and Valenzuela-Rios, J.I. 2007. Chondrichthyan microremains from the Givetian of the Aragonian Pyrenees (Spain). Bulletin de la Société Géologique de France 178, 171-178.

Liszkowski, J. and Racki, G. 1993. Ichthyoliths and deepening events in the Devonian carbonate platform of the Holy Cross Mountains. Acta Palaeontologica Polonica 37, 407-426.

Long, J.A. 1987. A new dinichthyid fish (Placodermi; Arthrodira) from the Upper Devonian of Western Australia, with a discussion of dinichthyid interrelationships. Records of the Western Australian Museum 13, 515-540.

Long, J.A. 1991. Devonian fish remains from the Munabia Sandstone, Carnarvon Basin, Western Australia. Records of the Western Australian Museum 15, 503-515.

Long, J.A. (Ed.), 1993. Palaeozoic Vertebrate Biostratigraphy and Biogeography. Belhaven Press, London.

Long, J. 2006. Swimming in Stone - the Amazing Gogo Fossils of the Kimberley. Fremantle Arts Centre Press, Fremantle.

Long, J.A. and Burrett, C.F. 1989. Fish from the Upper Devonian of the Shan-Thai Terrane indicate proximity to East Gondwana and South China Terranes. Geology 17, 811-813.

Long, J.A. and Hairapetian, V. 2000. Famennian microvertebrates from the Dalmeh area, central Iran. Records of the Western Australian Museum, Supplement 58, 211-221.

Long, J.A. and Trinajstic, K. 2000. An overview of the Devonian microvertebrate faunas of Western Australia, 471-486. In: Blieck, A. and Turner, S. (Eds). Palaeozoic vertebrate biochronology and global marine/non-marine correlation - Final report of the IGCP 328 (1991-1996). Courier Forshungsinstitut Senckenberg 223, 1-575.

Long, J.A. and Trinajstic, K. 2010. The Late Devonian Gogo Formation Lagerstatte of Western Australia: Exceptional Early Vertebrate Preservation and Diversity. Annual Review of Earth and Plantary Sciences 38, 255-279.

Lund, R. 1974. *Stethacanthus altonensis* (Elasmobranchi) from the Bear Gulch Limestone of Montana. Annals of the Carnegie Museum 45, 43-56.

Maisey, J.G. 2001. A primitive chondrichthyan braincase from the Middle Devonian of Bolivia. In: Ahlberg, P. (Ed.), Major events in Early Vertebrate Evolution, 263-288. Paleontology, Phylogeny and Development, London.

Märss, T., Fredholm, D., Talimaa, V., Turner, S., Jeppsson, L. and Nowlan, G. 1995. Silurian Vertebrate Biozonal Scheme. In: Lelievre, H., Wenz, S., Blieck, A. and Cloutier, R. (Eds). Premiers Vertèbrès et Vertèbrès Inferieurs. Geobios 19, 368-372.

Märss, T., Turner, S. and Karatajūtė-Talimaa, V.N. 2007. Agnatha II: Thelodonti. In: Shultze, H.P. (Ed.), Handbook of Paleoichthyology Volume 1B, 1-143. Verlag Dr. Friedrich Pfeil, München.

McNamara, K.J. and Feist, R. 2006. New styginids from the Late Devonian of Western Australia - The last corynexochid trilobites. Journal of Paleontology 80, 981-92.

Metcalfe, I. 1984. Stratigraphy, palaeontology and palaeogeography of the Carboniferous of Southeast Asia. Memoires de La Société Géologiqu de France 147, 107-118.

Metcalfe, I. 2001. Palaeozoic and Mesozoic tectonic evolution and biogeography of SE Asia-Australasia. In: Metcalfe, I., Smith, J.M.B., Morwood, M., Davidson, I. (Eds). Faunal and Floral Migrations and Evolution in SE Asia-Australasia. A.A, Balkema, Lisse.

Metcalfe, I. 2011. Palaeozoic-Mesozoic history of South Asia. In: Hall, R., Cottam, M. and Wilson, M.E.J. (Eds). The SE Asian Gateway: History and Tectonics of the Australia-Asia Collision. Geological Society, London, Special Publication 355, 7-35.

Metzger, R.A. 1994. Multielement reconstructions of *Palmatolepis* and *Polygnathus* (Upper Devonian, Famennian) from the Canning Basin, Australia and Bactrian Mountain, Nevada. Journal of Paleontology 68, 617-647.

Nance, R.D., Gutiérrez-Alonso, G., Keppie, J.D., Linnemann, U., Murphy, J.B., Quesada, C., Strachan, R.A. and Woodcock, N. 2012. A brief history of the Rheic Ocean. Geoscience Frontiers 3, 125-135.

Newberry, J.S. 1889. The Paleozoic fishes of North America. U.S. Geological Survey, Monograph 16, 1-340.

Nicoll, R.S. and Playford, P.E. 1993. Upper Devonian iridium anomalies, conodont zonation and the Frasnian-Famennian boundary in the Canning Basin,

Western Australia. Palaeogeography, Palaeoclimatology, Palaeoecology 104, 105-113

Obruchev, D.V. 1964. Agnatha and fish. In: Orlov, Y.U. (Ed.). Fundamentals of Palaeontology 11, 1-522, Nauka, Moscow.

Owen, R. 1846. Lectures on the comparative anatomy and physiology of the vertebrate animals, delivered at the Royal College of Surgeons of England in 1844 and 1846. Part 1: Fishes, 1-308. Longman, Brown, Green, and Longmans, London.

Parmley, D. and D. J. Cicimurri. 2003. Late Eocene sharks of the Hardie Mine local fauna of Wilkinson County, Georgia. Georgia Journal of Science 61, 153-179.

Peterson, M.S. 1975. Upper Devonian (Famennian) ammonoids from the Canning Basin, Western Australia. Paleontological Society 8, 1-55.

Peyer, B. 1968. Comparative Odontology. University of Chicago Press, Chicago.

Pfeil, F.H. 1983. Zahnmorphologische Untersuchungen an rezenten und fossilen Haien der Ordnungen Chlamydoselachiformes und Echinorhiniformes. Palaeoichthyologica 1, 1-315.

Playford, P.E. 1980. Devonian 'Great Barrier Reef' of the Canning Basin, Western Australia. American Association of Petroleum Geologists 6, 814-840.

Playford, P.E. and Lowry D.C. 1966. Devonian reef complexes of the Canning Basin, Western Australia. Geological Survey of Western Australia Bulletin 118, 1-150.

Playford, P.E., Hocking, R.M. and Cockbain. A.E. 2009. Devonian reef complexes of the Canning Basin. Geological Survey of Western Australia Bulletin 145, 1-444.

Playton, T. E., Montgomery, P., Tohver, E., Hillbun, K., Katz, D., Haines, P., Trinajstic, K., Yan, M., Hansma, J., Pisarevsky, S., Kirschvink, J., Cawood, P., Grice, K., Tulipani, S., Ratcliffe, K., Wray, D., Caulfield-Kerney, S., Ward, P. and Playford, P.E. 2013. Development of a regional stratigraphic framework for Upper Devonian reef complexes using integrated chronostratigraphy: Lennard Shelf, Canning Basin, Western Australia. In: Keep, M. and Moss, S. J. (Eds). The Sedimentary Basins of Western Australia IV. Proceedings of the Petroleum Exploration Society of Australia Symposium, Perth, Western Australia.

Raschi, W., Musick, J.A. and Compagno, L.J.V. 1982. *Hypoprion bigelowi*, a synonym of *Carcharhinus signatus* (Pisces: Carcharhinidae), with a description of ontogenetic heterodonty in this species and notes on its natural history. Copeia, 102-109.

Rode, A.L. and Lieberman, B.S. 2005. Integrating evolution and biogeography: A case study involving Devonian crustaceans. Journal of Paleontology 79, 267-276.

Sandberg, C.A., Morrow, J.R. and Warme, J.E. 1997. Late Devonian Alamo impact event, global Kellwasser events, and major eustatic events, eastern Great Basin, Nevada and Utah. Brigham Young University, Geology Studies 42, 129-160.

Scotese, C.R. and McKerrow, W.S. 1990. Revised World maps and introduction. In: McKerrow, W.S. and Scotese, C.R. (Eds). Palaeozoic Palaeogeography and Biogeography. Geological Society, London, Memoir 12, 1-21.

Seddon, G. 1969. Conodont and fish remains from the Gneudna Formation, Carnarvon Basin, Western Australia. Journal of the Royal Society of Western Australia 52, 21-30.

Southgate, P.N., Kennard. J.M., Jackson, M.J., O'Brien, P.E. and Sexton, M.J. 1993. Reciprocal lowstand clastic and highstand carbonate sedimentation, subsurface Devonian reef complex, Canning Basin, Western Australia. In: Loucks, R.G. and Sarg, J.F. (Eds). Carbonate sequence stratigraphy, recent developments and applications. American Association of Petroleum Geologists, Memoir 57, 157-159.

St. John, O. and Worthen, A.H. 1875. Part II. Palaeontology of Illinois, Section I: Description of Fossil Fishes. Geological Survey of Illinois 6, 247-488.

Stephens, N.P and Sumner, D.Y. 2003. Famennian microbial reef facies, Napier and Oscar Ranges, Canning Basin, Western Australia. Sedimentology 50, 1283-1302.

Straube, N., Schliewen, U. and Kriwet, J. 2008. Dental structure of the Giant lantern shark *Etmopterus baxteri* (Chondrichthyes: Squaliformes) and its taxonomic implications. Environmental Biology of Fishes 82, 133-141.

Talimaa, V. 2000. Significance of thelodonts (Agnatha) in correlation of Upper Ordovician to Lower Devonian of the northern part of Eurasia. In: Blieck, A. and Turner, S. (Eds). Palaeozoic Vertebrate Biochronology and Global Marine/Non-marine Correlation (final report IGCP 328, 1991-1996). Courier Forschungsinstitut Senckenberg 223, 69-80.

Trinajstic, K. and George, A.D. 2009. Microvertebrate biostratigraphy of Upper Devonian (Frasnian) carbonate rocks in Canning and Carnarvon Basins of Western Australia. Palaeontology 52, 641-659.

Trinajstic, K. 1999a. New anatomical information on Holonema (Placodermi) based on material from the Frasnian Gogo Formation and the Givetian-Frasnian Gneudna Formation, Western Australia. Geodiversitas 21, 69-84.

Trinajstic, K. 1999b. Scale morphology of the Late Devonian palaeoniscoid *Moythomasia durgaringa* Gardiner and Bartram, 1977. Alcheringa 23, 9-19.

Trinajstic, K. 2001. A description of additional variation seen in the scale morphology of the Frasnian thelodont *Australolepis seddoni* Turner and Dring, 1981. Records of the Western Australian Museum 20, 237-246.

Trinajstic, K., Roelofs, B., Burrow, C.J., Long, J.A. and Turner, S. 2014. Devonian vertebrates from the Canning and Carnarvon Basins with an overview of Paleozoic vertebrates of Western Australia. Journal of the Royal Society of Western Australia 97, 133-151.

Turner, S. 1973. Siluro-Devonian thelodonts from the Welsh Borderland. Journal of the Geological Society of London 129, 557-584.

Turner, S. 1982. Middle Palaeozoic elasmobranch remains from Australia. Journal of Vertebrate Paleontology 2, 117-131.

Turner, S. 1993. Palaeozoic microvertebrates from eastern Gondwana. In: Long, J.A. (Ed.). Palaeozoic Vertebrate Biostratigraphy and Biogeography, 174-207. Belhaven Press, London.

Turner, S. 1995. Devonian thelodont scales (Agnatha, Thelodonti) from Queensland. Memoirs of the Queensland Museum 38, 677-685.

Turner, S. 1997. Sequence of Devonian thelodont scale assemblages in East Gondwana. In: Paleozoic Sequence Stratigraphy, Biostratigraphy, and Biogeography: Studies in Honor of Dr J. Granville ("Jess") Johnson: Boulder,

Colorado, Klapper, G, Murphy, M.A. and Talent, J.A. (Eds). Geological Society of America, Special Paper 321, 295-315.

Turner, S. 1999. Early Silurian to Early Devonian thelodont assemblages and their possible ecological significance. In: Boucot, A.J. and Lawson, J. (Eds). Palaeocommunities: a case study from the Silurian and Lower Devonian. International Geological Correlation Programme 53, Project Ecostratigraphy, Final Report, 42-78. Cambridge University Press, Cambridge.

Turner, S. and Dring, R.S. 1981. Late Devonian thelodonts (Agnatha) from the Gneudna Formation, Carnarvon Basin, Western Australia. Alcheringa 5, 39-48.

Turner, S and Youngquist, W. 1995. Late Devonian phoebodont (Chondrichthyes) from the Confusion Range, Utah, USA. Geobios Mémoire Spécial 19, 389-392.

Turner, S., Burrow, C. J., Gholomalian, H. and Yazdi, M. 2002. Late Devonian (early Frasnian) microvertbrates and conodonts from the Chahriseh area near Esfahan, Iran. Association of Australasian Palaeontologists Memoir 27, 149-159.

Valiukevičius, J. 1995. Acanthodians from marine and non-marine Early and Middle Devonian deposits. In: Lelievre, H., Wenz, S., Blieck, A. and Cloutier, R. (Eds). Premiers Vertébrés et Vertébrés inférieurs (Ville Congress International, Paris, 4-9 Sept. 1995). Geobios, Mémoire Spécial 19, 393-397.

Valiukevičius, J. and Krucheck, S. 2000. Acanthodian biostratigraphy and interregional correlations of the Devonian of the Baltic States, Belarus, Ukraine and Russia. In: Blieck, A. and Turner, S. (Eds). Palaeozoic

Vertebrate Biochronology and Global Marine/Non-marine Correlation (Final Report of IGCP 328, 1991-1996). Courier Forschungsinstitut Senckenberg 223, 271-289.

Wang, S.T. and Turner, S. 1995. A reappraisal of Upper Devonian-Lower Carboniferous vertebrate microfossils in South China. Professional Papers of Stratigraphy and Palaeontology 26, 59-70.

Wells, J.W. 1944. Fish remains from the Middle Devonian bone beds of the Cincinnati Arch Region. Palaeontographica Americana 3, 5-62.

Williams, M.E. 1985. The "Cladodont level" sharks of the Pennsylvanian black shales of central North America. Palaeontolographica Abteilunf A 190, 83-158.

Yazdi, M. and Turner, S. 2000. Late Devonian and Carboniferous vertebrates from the Shishtu and Sardar Formations of the central Shotori Range, Iran. Records of the Western Australian Museum Supplement 58, 223-240.

Young, G.C. 1987. Devonian fish remains from Billiluna, eastern Canning Basin, Western Australia. BMR Journal of Australian Geology and Geophysics 10, 179-192.

Young, G.C. 1995. Devonian. Australian Phanerozoic Timescales. Biostratigraphic charts and explanatory notes. Second Series. AGSO Record 1995/33, 1-47.

Young. G.C. 2003. North Gondwana mid-Palaeozoic connections with Euramerica and Asia: Devonian vertebrate evidence. Courier Forschungsinstitut Senckenberg 242, 169-185.

Young, G.C. and Turner, S. 2000. Devonian microvertebrates and marine-nonmarine correlation in East Gondwana: overview. In: Blieck, A. and Turner, S. (Eds). Palaeozoic Vertebrate Biochronology and Global Marine/Non-marine

Correlation (final report IGCP 328, 1991-1996). Courier Forschungsinstitut Senckenberg 223, 453-470.

Young, G.C., Burrow, C.J., Long, J.A., Turner, S. and Choo, B. 2010. Devonian macrovertebrate assemblages and biogeography of East Gondwana *(*Australasia, Antarctica*)*. Palaeoworld 19, 55-74.

Zangerl, R. 1981. Paleozoic Elasmobranchii. In: Schultze, H.P. (Ed.). Handbook of Paleoichthyology 3A, 1-115. Gustav-Fischer, Stuttgart, New York.

Ziegler, W. and Sandberg, C.A. 1990. The Late Devonian standard conodont zonation. Courier Forshungsinstitut Senckenberg 121, 1-115.

4.0 Famennian Survivor Turiniid Thelodonts of North and East Gondwana

Hairapetian, V.[1], **Roelofs, B**.[2], Trinajstic, K. [3], Turner, S.[4]

[1]Vachik Hairapetian. Department of Geology, Islamic Azad University, Khorasgan branch, PO Box 81595-158, Esfahan, Iran. E-mail: vachik@khuisf.ac.ir

[2]Brett Roelofs. Department of Applied Geology, Curtin University, GPO Box U1987 Perth, WA 6845, Australia. brett.roelofs@postgrad.curtin.edu.au

[3]Kate Trinajstic*. Department of Environment and Agriculture, Curtin University, GPO Box U1987, Perth, WA 6845, Australia. K.Trinajstic@curtin.edu.au

[5]Sue Turner. Museum Victoria, PO Box 666, Melbourne, Vic 3001, Australia. paleodeadfish@yahoo.com

4.1 Abstract

Microvertebrate samples from the Upper Devonian Hojedk section, southeastern Iran, and the Napier Formation, northwestern Australia, have yielded scales of agnathan thelodonts, dated as early/mid-Famennian (*crepida-marginifera*/*trachytera* conodont zones). These scales are referred to *Arianalepis megacostata*, a new genus and species, and *Arianalepis* sp. indet., a second indeterminate species of this new turiniid genus. Further recorded scales of *Australolepis seddoni* from the Napier Formation confirm the age range for this taxon as extending into the late Frasnian. The new remains post-date the previously youngest thelodonts from Iran and Western Australia and provide the first evidence of thelodonts surviving the Frasnian-Famennian extinction events.

4.2 Introduction

Thelodonts (jawless fishes) have a long history in the fossil record, appearing at least by the Late Ordovician (Turner et al., 2004) and becoming extinct at some point before the end of the Devonian along with most other agnathans, with the exception being the extant cyclostomes (Märss et al., 2007). Despite the relative lack of taxa based on articulated remains compared to scales (c. 25: c. 140), the latter have proved useful in biostratigraphic correlation for many decades, particularly between shallow-marine and non-marine sequences (e.g. Turner, 1993, 1997; papers in Blieck and Turner, 2000). Although articulated taxa are fewer (Märss et al., 2007), most are known from Silurian deposits and none are known from the Southern Hemisphere or in post-Emsian or younger sediments. The youngest known occurrences of thelodont taxa were previously reported from Western Australia and Iran as isolated scales in Frasnian strata (Turner and Dring, 1981; Trinajstic, 2000, 2001; Turner et al., 2002; Trinajstic and George, 2009) until the discovery in the early 2000s of the first Famennian thelodont scales from Iran (Hairapetian and Turner, 2003; Turner and Hairapetian, 2005; Hairapetian, 2008). Here we report in detail the first Famennian thelodonts that co-occur with conodont elements and jawed vertebrate assemblages in the Hojedk section in the north of Kerman, southeastern Iran (Figure 4.1), and also the recent discovery of thelodont scales from a mid-Famennian sequence in the South Oscar Range, Canning Basin, northwestern Australia (Figure 4.2). The Iranian scales are placed within a new turiinid genus *Arianalepis* gen. nov., which represents the youngest known thelodont remains; the Australian material is more sparse and so its assignment is less certain. These new discoveries furthermore support the closeness of faunal relationships in the mid-Palaeozoic of northern Gondwana, especially between Iran and Australia. In

addition, the finds offer an opportunity to further establish and extend biostratigraphic schemes utilizing thelodont taxa in the Devonian (Turner, 1997; Long and Trinajstic, 2000; Young and Turner, 2000).

4.3 Geographical and geological setting

4.3.1 Iran

The Hojedk section (c. 4 km west of Haruz village and c. 48 km north of Kerman; 30843′N, 5780′E; Figure 4.1) is measured on the southeastern flank of Kuh-e-Kanseh Mountain, Kerman Province, central Iran. The stratigraphy of the Hojedk Devonian strata has recently been studied in detail by Wendt et al. (2005), Gholamalian and Kebriaei (2008) and Gholamalian et al. (2013). The underlying Lower (?) Devonian/Eifelian Padeha Formation commences with a breccia unit followed by sandstones and dolomites. There is a disconformity at the top of the Padeha Formation, where a sandstone unit is overlain by a dolomitic horizon of the Bahram Formation containing small gastropods, large plates of the placoderm Holonema and plant remains; the unit has been dated as late Givetian based on conodonts (see Gholamalian and Kebriaei 2008). The limestones in the uppermost Bahram Formation are overlain with an apparent major temporal unconformity by dolomites of the Permian Jamal Formation. Conodont samples collected from the limestone beds in the upper part of the section, however, revealed an early Famennian age, from the Lower *Palmatolepis crepida* Zone (see Gholamalian and Kebriaei, 2008, fig. 1, table 1, pp. 183-184).

The new thelodont material came from Sample R4, a red sandy limestone bed in the uppermost part of the section, just below the level of the Devonian/Permian

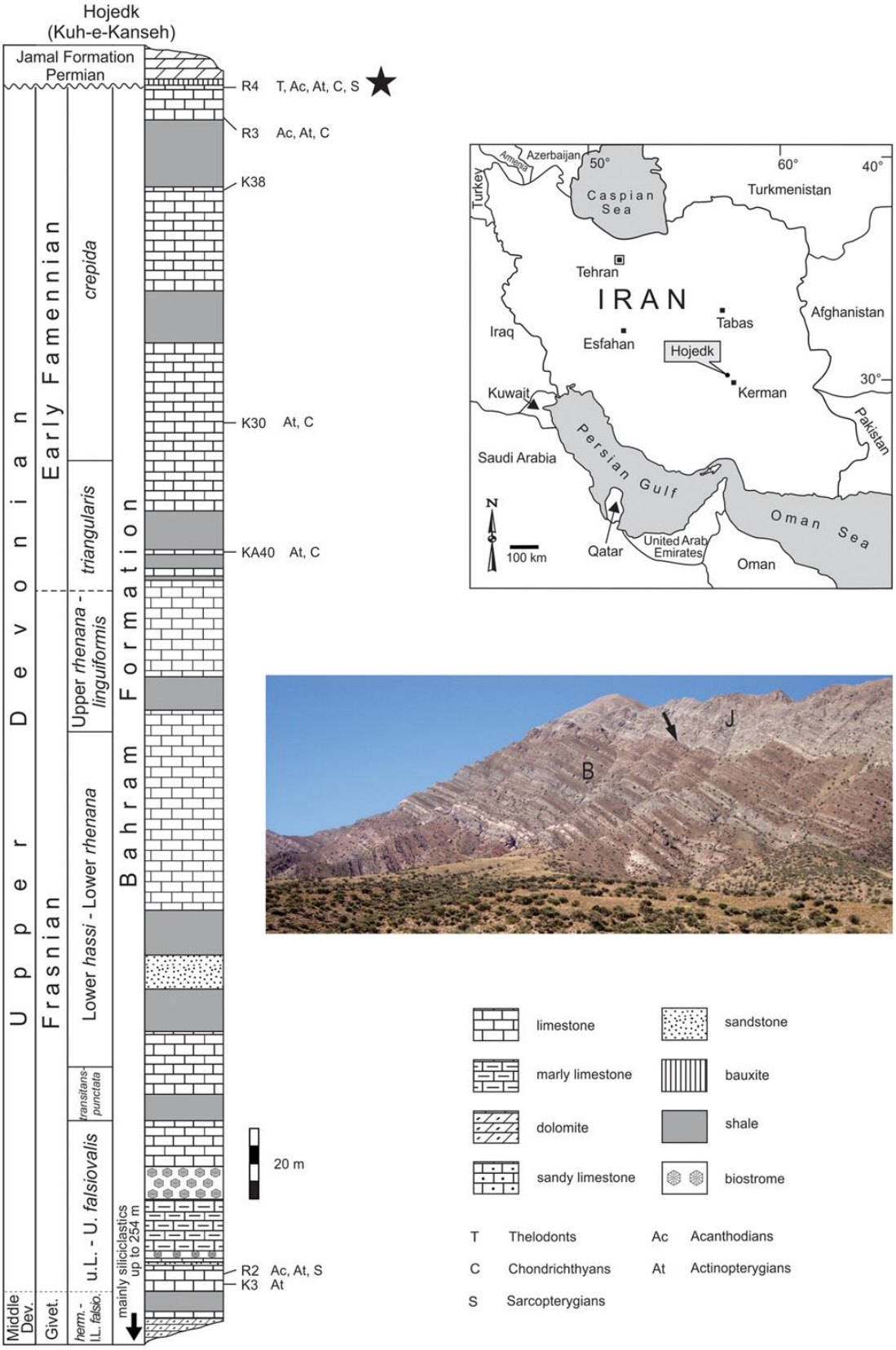

Figure 4.1. Stratigraphy and location of the studied Iranian sequence. Simplified stratigraphic column of the Hojedk section in central Iran showing the main facies and fish-bearing horizons; the asterisk marks the bed with thelodont scales. Map of Iran showing the location of the section. Photograph of the Hojedk section showing the Bahram Formation (B) and the Permian Jamal dolomites (J). The distinct level of the unconformity is indicated by the arrow.

unconformity (Figure 4.1) (Hairapetian and Turner 2003; Turner and Hairapetian 2005; Hairapetian 2008). The bed is now dated as early Famennian based on conodonts and fish remains. Associated with the thelodont scales are conodont elements indicative of a shallow-water fauna, including *Icriodus alternatus* cf. *helmsi* Sandberg and Dreesen, 1984, *Icriodus cornutus* Sannemann, 1955, *Pelekysgnathus inclinatus* Thomas, 1949, *Polygnathus semicostatus* Branson and Mehl, 1934 and the *Polygnathus communis* group Branson and Mehl, 1934, dating of which spans the Middle-Upper *Palmatolepis crepida* Zone (Hairapetian, 2008). The new thelodont taxon is associated with stratigraphical index chondrichthyan species from the Hojedk section (Figure 4.1); the assemblage comprises several chondrichthyan and actinopterygian taxa, with shark teeth of phoebodonts *Phoebodus gothicus gothicus* Ginter, 1990, *Phoebodus turnerae* Ginter and Ivanov, 1992 and *Phoebodus aff. Turnerae* Ginter and Ivanov, 1992, the protacrodonts *Protacrodus* sp. and *Deihim mansureae* Ginter, Hairapetian and Klug, 2002, the cladodontomorphs *Ctenacanthus* sp. and Elasmobranchii gen. et sp. indet., as well as sarcopterygian and actinopterygian scales, all supporting an early Famennian age (Ginter et al., 2002; Hairapetian, 2008, fig. 4).

4.3.2 Australia

A section through the proximal slope facies of the Napier Formation was measured at South Oscar Range (17855′S, 125817′E; Figure 4.2) (Playton et al., 2013), located along the southwestern edge of the Lennard Shelf in the Kimberley Region of NW Western Australia (Playford et al., 2009). The Napier Formation unconformably overlies Proterozoic basement and in outcrop ranges from early Frasnian to late Famennian. The lithology of the measured section is predominantly

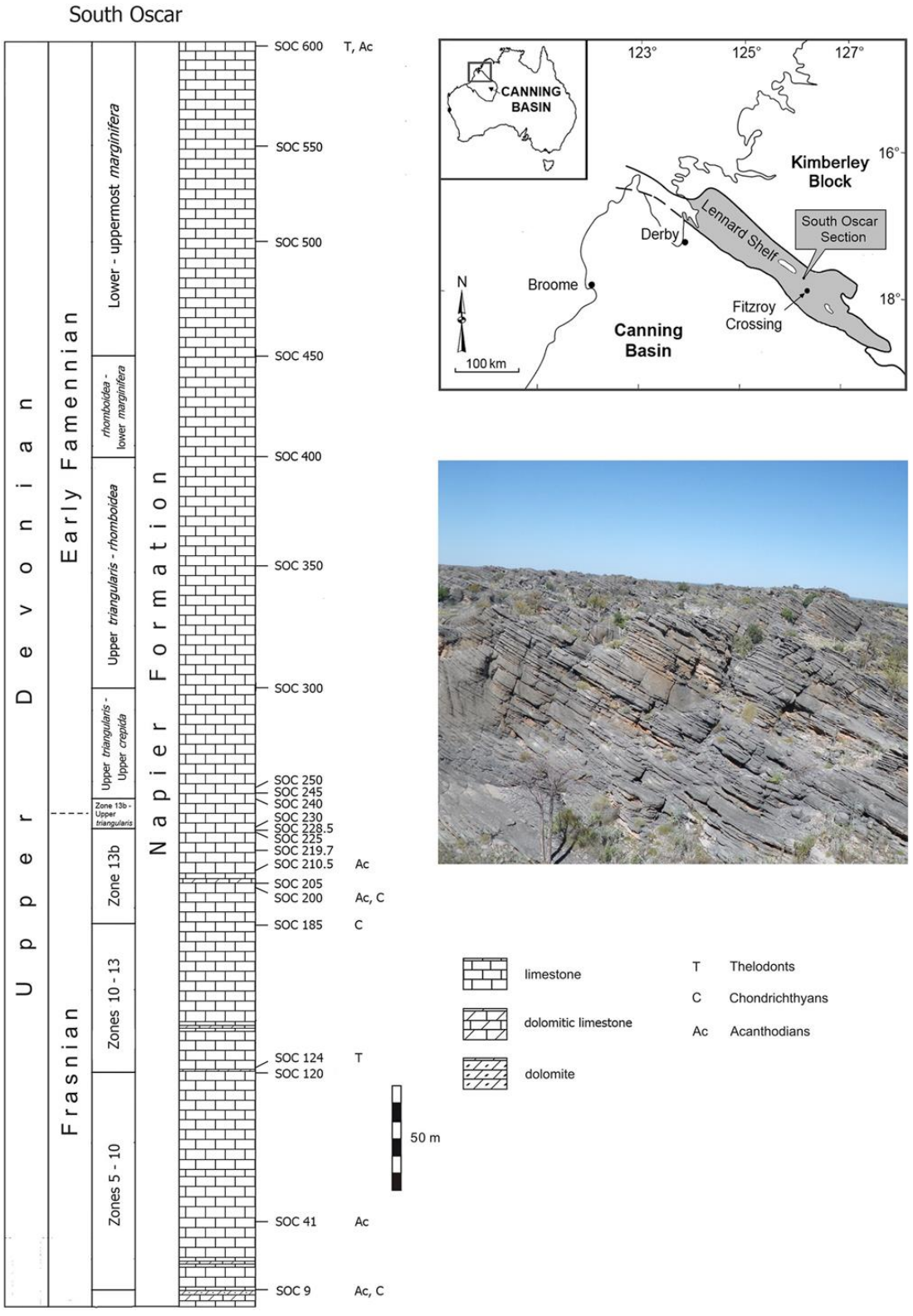

Figure 4.2. Stratigraphy and location of the studied Australian sequence with simplified stratigraphic column of the South Oscar Range (SOC) section in the Canning Basin, Western Australia, showing the main facies and fish-bearing horizons (after Playton et al., 2013). Map of the Lennard shelf showing the location of the studied section, with inset map of Australia showing the location of the Canning Basin. Photograph of the South Oscar Range section in the Napier Formation.

limestone with the basal part of the section comprising marginal and slope-derived mega breccias with minor dolomitic microbial boundstones, rudstones and breccias. The upper interval of the South Oscar Range section from approximately 185 m consists mainly of platform-derived skeletal packstone-grainstone facies as well as in situ stromatactoid boundstones and skeletal-peloid-coated packstones to grainstones. Overlying the mixed slope facies of the Napier Formation are the siliciclastic shelf deposits of the uppermost Devonian to Lower Carboniferous Fairfield Group (Playford and Lowry 1966). The Frasnian-Famennian boundary is placed within the upper part of the section, between 223.8 and 233.2 m, with its location based on conodont data (Hansma et al., 2015) in addition to the last occurrence of Frasnian stromatoporoids (Hurley, 1986; Playford et al., 1989).

The new thelodont material comes from Sample South Oscar Range (SOC) 600 in the uppermost bed of the section and co-occurs with acanthodian and palaeoniscoid scales. This horizon has been dated as ranging from the Upper *Palmatolepis marginifera* to *Palmatolepis trachytera* conodont zones, which is supported by the overlap of *Palmatolepis gracilis gracilis* Branson and Mehl, 1934, and *Palmatolepis minuta minuta* Branson and Mehl, 1934 in Sample SOC 600. A lower *Palmatolepis rhomboidea* age is not supported because *Scaphignathus velifer* Helms, 1959 is not known below the Upper *Palmatolepis marginifera* conodont Zone within the Canning Basin and this taxon has been recovered below from Sample SOC 500 (Figure 4.2). The Frasnian conodont succession at South Oscar Range is conformable with the Montagne Noire (MN) conodont zonation (Klapper 1989).

Additional thelodont scales identified here as *Australolepis seddoni* Turner and Dring, 1981 (Figures 4.3 and 4.4) have been found in the lower part of the

section (SOC 124), dated as Frasnian MN Zone 10. Immediately above this horizon (MN 13b), there are shark teeth of *Stethacanthus* sp. as well as palaeoniscoid and acanthodian scales. The Frasnian part of the section has a diverse palmatolepid conodont fauna indicative of open-marine conditions (Sandberg and Ziegler 1979).

4.4 Materials and methods

A buffered solution of 10% acetic acid was employed to extract the Iranian Sample R4 residue and specimens were then picked using a sieve of 0.177 mm mesh. Sixteen thelodont scales (Figure 4.5-7) have been found, most of which are broken and reddish brown in colour (Figure 4.7). The scales are densely covered with adhering sedimentary quartz grains, which are not easy to remove with a needle (Figure 4.7).

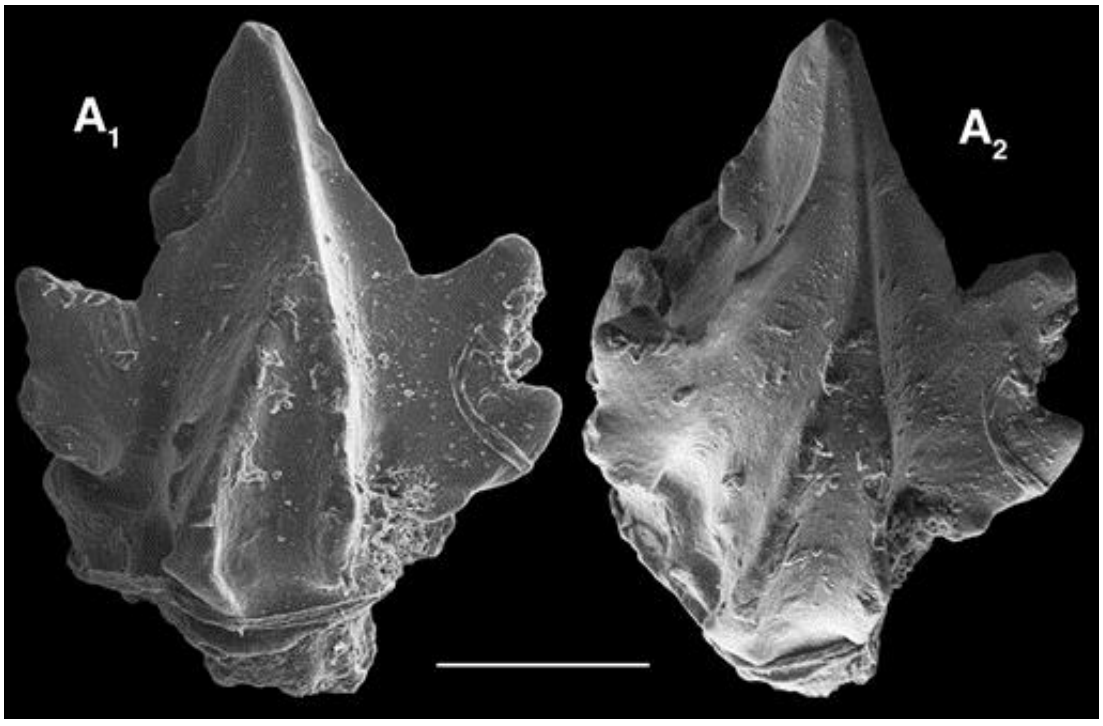

Figure 4.3. Scale of *Australolepis seddoni* WAM 13.10.2 from Sample SOC 124, South Oscar Range section, Canning Basin, Western Australia. A1, crown view; A2, dorsolateral view. Scale bar 0.2 mm.

Scanning electron micrographs were prepared in Esfahan with a Leica 360 scanning electron microscope and in the Institute of Palaeobiology, Polish Academy of Sciences (Warsaw, Poland) using a Philips XL 20. The Iranian specimens are deposited in the Department of Geology, Azad University, Esfahan (AEU).

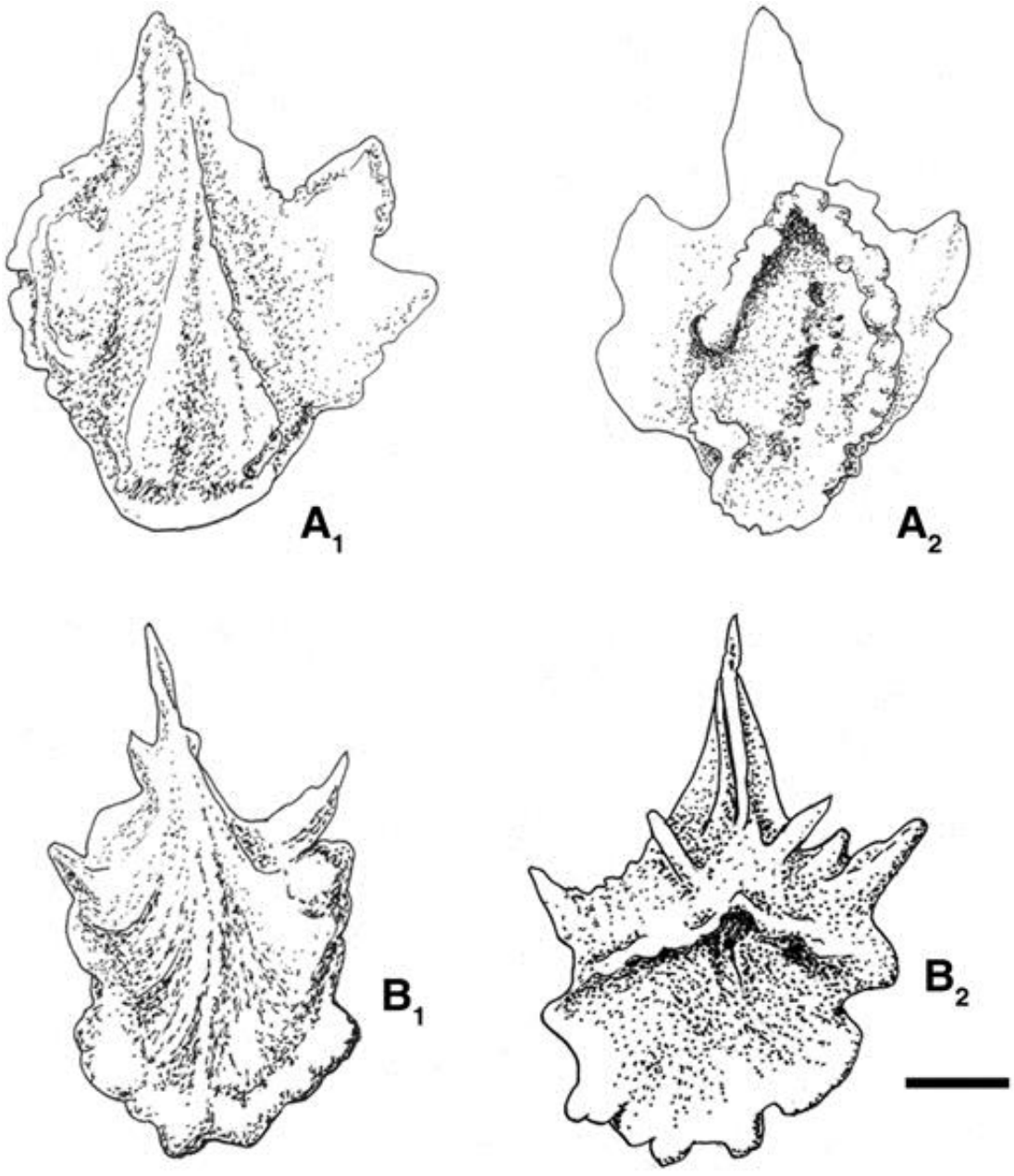

Figure 4.4. Drawings of scales of *Australolepis seddoni* WAM 13.10.2 (A); WAM 13.10.3 (B) from Sample SOC 124, South Oscar Range section, Canning Basin, Western Australia. A1, crown view; A2, ventral view; B1, crown view; B2, ventral view. Scale bar 0.2 mm. Bulk rock samples (20 kg) were taken within the measured South Oscar. Range section

Acid digestion of the carbonates in 10% acetic acid and heavy-liquid separation of the residue was undertaken at Macquarie University and the fractionated residues returned for picking. One of two scales recovered from SOC 124 was photographed using a Zeiss EVO 40XVP and both scales were drawn while magnified using a binocular microscope. One scale from SOC 600 was photographed using a Leica XX2V 7S stereomicroscope camera version 3.4.1 at the Western Australian Museum and drawn under a binocular microscope. Owing to the paucity and poor preservation of the SOC 600 scale, scanning electron microscope or histological work was not possible. Specimens are deposited in the Western Australian Museum (WAM). The 13-fold Frasnian conodont zonation, first proposed for the MN succession (Klapper ,1989) and subsequently modified to a 15-fold zonation (Girard et al., 2005), was used to describe the stratigraphic ranges of the conodont and vertebrate taxa recovered from the Canning Basin sections. The standard conodont zonation of Ziegler and Sandberg (1990) were used for both sections to describe Famennian age ranges and for the Frasnian in the Iranian sections, because the ranges of MN zonal markers have not yet been replicated for Iran.

4.5 Systematic Palaeontology

Thelodonti Jaekel, 1911

Order Thelodontiformes Kiaer in Kiaer and Heintz, 1932

Family Turiniidae Obruchev, 1964

Australolepis seddoni Turner and Dring, 1981

(Figures 4.3 and 4.4)

Material: WAM 13.10.2; one scale.

Locality and geology. South Oscar Range, Canning Basin, Western Australia (17855′ S, 125817′ E). Bed SOC 124, CZ 10, reef, margin and slopederived skeletal limestone: Upper Devonian Napier Formation.

Stratigraphic range. Australia: Napier Formation, South Oscar Range, Canning Basin: MN Zone 10, MN Zones 6-10, Virgin Hills Formation, Horse Spring, Canning Basin; earliest Frasnian to MN Zone 10 in the Gneudna Formation type section, Carnarvon Basin, Western Australia (Turner and Dring, 1981; Trinajstic, 2000, 2001; Turner et al., 2002; Trinajstic and George, 2009). In Iran the range extends from the early Frasnian *Mesotaxis falsiovalis* Zone, MN Zones 1-3, to, in the Chahriseh section, *Palmatolepis hassi* Zone, MN Zone 10 (Hairapetian et al., 2000; Yazdi and Turner, 2000).

Description. The scales measure less than 1 mm in length with an elliptical base and triangular crown, terminating in a sharp apex. The anterior face of the tripartite crown has two bifurcating ribs that fuse to form a single rib that extends to the crown apex (Figures 4.3 and 4.4, drawing A1). The anterior ribs are ornamented with small tubercles (Figure 4.4, drawing A1). A well-developed, ridged lateral lappet is present at the medial region of the scale (Figures 4.3 and 4.4, drawings A1, B1). The lateral extent of the lappet curves posteriorally and bifurcates to form two anteriorward-pointing projections (Figure 4.4, drawing B1).The posterior lappets are reduced compared with the medial lappets and lack the terminal projections. The mesial face adjoins the central ridge. A shallow neck separates the crown from a narrow base, which does not possess an anterior spur. The base exhibits the lobate thickenings typical in scales of this species (Figure 4.4, drawings A2, B2). An elongate pulp canal is visible on the underside of the scale.

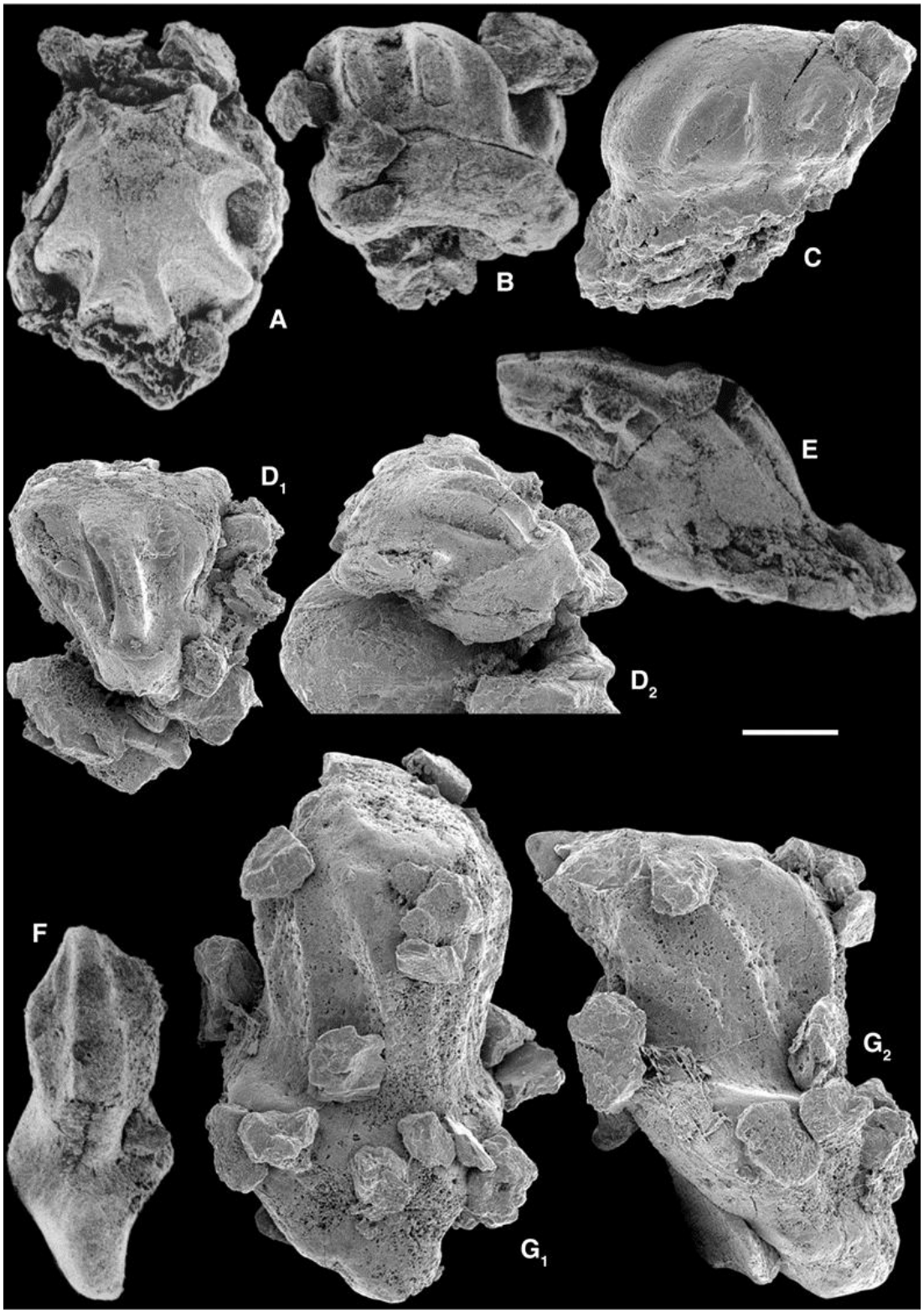

Figure 4.5. Scanning electron micrographs of early Famennian thelodont scales of *Arianalepis megacostata* gen. et sp. nov. from sample R4, Hojedk, Kerman Province, Iran. A, B, head scales; C, cephalopectoral scale; and D-G, trunk scale. A, AEU 720 in crown view; B, AEU 721 in lateral crown view; C, AEU 722 in lateral view; D, AEU 723 in antero-crown (D1) and lateral (D2) view; B, AEU 724 in lateral view; F, AEU 725 in crown view; G, AEU 726, holotype in antero-crown (G1) and lateral (G2) view. Scale bar 0.2 mm.

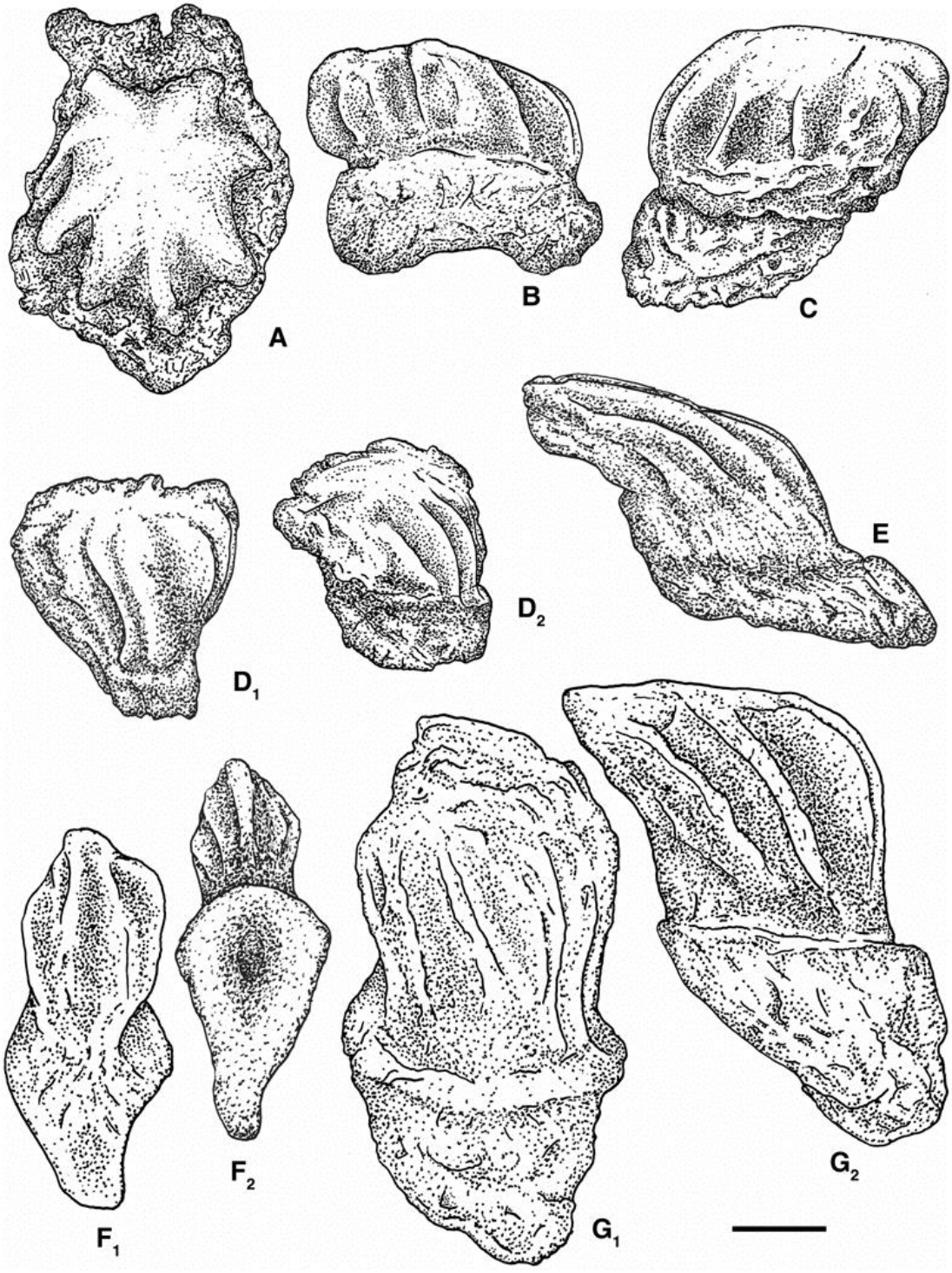

Figure 4.6. Drawings of scales of *Arianalepis megacostata* gen. et sp. nov. from sample R4, Hojedk, Kerman Province, Iran. A, AEU 720 in crown view; B, AEU 721 in lateral crown view; C, AEU 722 in lateral view; D, AEU 723 in antero-crown (D1) and lateral (D2) view; E, AEU 724 in lateral view; F, AEU 725 in crown view (F1) and ventral (F2) view; G, AEU 726, holotype in antero-crown (G1) and lateral (G2) view. Scale bar 0.2 mm.

Histology. As only two single scales were recovered no thin sections were made. However, the large pulp cavities are typical of turiniid histology (Märss et al.,

2007).

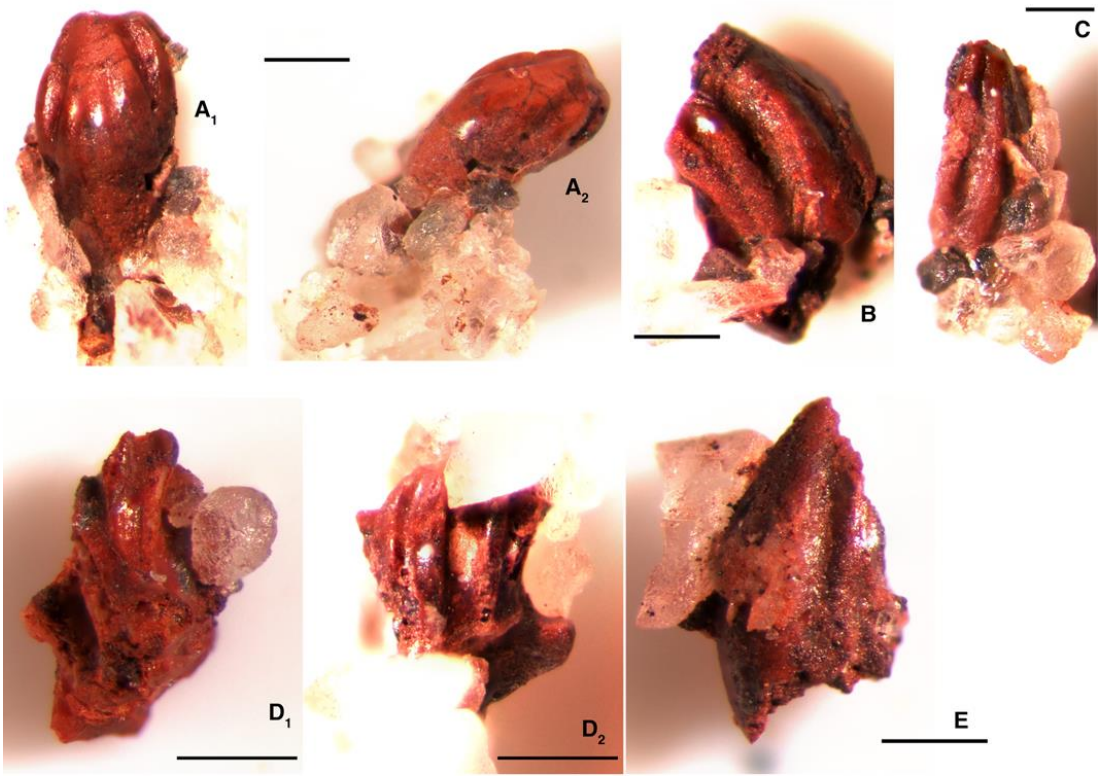

Figure 4.7. Photographs of early Famennian thelodont scales from sample R4, Hojedk, Kerman Province, Iran, to show colour and taphonomic nature of the adhering quartz grains. (A) AEU 782 in crown (A1) and lateral-crown views (A2); (B) AEU 783 in lateral crown view; (C) AEU 783, in basal view; (D) AEU 784 in antero-crown (D1) and lateral-crown (D2) view; (E) AEU 785 in crown view. Scale bars, 0.2 mm.

Taphonomic analyses. The scale is pristine. The crowns are uniformly light brownish in colour with a white base, typical of thelodont scales, where the two hard tissues - dentine in the crown and neck, and aspidin in the base (see e.g. Märss et al., 2007) - are often present, with very different colours related to the varying mineralization effects based on the porosity of the tissue. No diagenetic alteration is detectable and associated conodont remains have a conodont alteration index (CAI) of 0.5.

Remarks. These scales conform to the original diagnosis of *A. seddoni* (Turner and Dring, 1981) and are attributed to this taxon. Their small size, gracile construction, bifurcating crown ribs and smooth shallow neck, with a base wider than the crown,

are all consistent with the type diagnosis. Small tubercles are present on the crown ribs, which are also seen in scales from Horse Spring (Turner, 1997; Trinajstic and George, 2009). Following currently accepted concepts of squamation patterns (Märss et al., 2007), the scales originate from the cephalopectoral region of the body.

The scale conforms to those from the known uppermost range of *A. seddoni* (MN Zone 10) within Australia based on well-constrained conodont remains (Trinajstic and George, 2009).

Genus Arianalepis gen. nov.

Etymology. From 'Ariana', an old name for the country of origin of the first Famennian thelodonts; and Greek: lepis, a scale.

Diagnosis. As for type and only species. Stratigraphic range. Early Famennian, *crepida* Zone.Type and only species. *Arianalepis megacostata* sp. nov.

Remarks. The Iranian and Western Australia thelodont scales are the youngest to be recorded to date; those from Iran were reported earlier and considered tentatively to be within the family Turiniidae, which is the only clade found thus far in post-Lochkovian Gondwana (Hairapetian and Turner, 2003; Märss et al., 2007). Hairapetian and Turner (2003) and then Märss et al. (2007) retained them as an undetermined turiniid taxon. However, as there are significant morphological differences from earlier turiniid taxa and considering their much younger age, the new scales are referred here to a new genus (see further discussion below).

Arianalepis megacostata gen. et sp. nov.

(Figure 4.5-7)

2003 new turiniid Hairapetian and Turner: 26-27.

2005 new turiniid Turner and Hairapetian: 24.

2007 Turiniidae gen. et sp. indet. Marss et al.,: 110.

Type specimens. Holotype: AEU 726, trunk scale (Figures 4.5, micrographs G1, G2 and 6, drawings G1, G2); paratypes: 15 scales (Figure 4.7A-E), AEU 720-725, 782-790.

Type locality and stratigraphy. Section c. 4 km W of Haruz village; 30843′N, 5780′E, SE Kuh-e-Kanseh Mt, Hojedk, c. 48 km N of Kerman, central Iran. Sample R4, red sandy limestone bed, Bahram Formation, Late Devonian, early Famennian, *crepida* Zone.

Stratigraphic range. c*repida* Zone, early Famennian.

Etymology. From Latin mega ‘large’ and costata,‘ribs’ for the ribbed nature of the crowns.

Diagnosis. Turiniid with robust medium-sized scales with a few simple coarse ribs on crowns. Base is horizontally extended with anterior basal extensions.

Description. The scales all show a robust structure and measure less than 1 mm in length. The head scales are rounded as in most thelodonts with robust crowns having a few, up to eight, strong ribs. There are eight ribs radiating from a high, rounded central apex to a shallow neck; wide troughs separate the ribs (Figures 4.5, micrographs A, B and 6, drawings A, B). Cephalopectoral scales are poorly preserved but can be seen to be more elliptical (Figure 4.5, micrograph C and 6, drawing C). The crowns exhibit simple coarse ribbing and well developed bases.

Trunk scale crowns (Figures 4.5, micrographs D2-G2 and 6, drawings D1, D2, G1, G2) are characterized by simple coarse ribbing and a protruded, prominent median area, which can be flat and horizontally placed as in the holotype scale shown in Figure 4.5, micrograph G1, G2. One scale (Figure 4.5, micrograph F)

shows a smooth, wide median and two lateral areas at a lower level. Another scale shown in side view (Figure 4.5, micrograph E) exhibits the high crown with ribs down to the shallow neck and the horizontally placed base with the scale axis at around 458. Some indication of split ribs is seen in other scales (Figure 4.7). The anterior base is developed into a single, thick basal root or spur, which extends in a lateral plane (Figure 4.5, micrograph F). The holotype scale (Figures 4.5, micrographs G1, G2 and 6, drawings G1, G2) exhibits a relatively deeper base with an incomplete anterior anchoring root directed vertically downwards.

Unlike many turiniid taxa, especially in Gondwana (e.g. Turner 1997), there is no sign of microornament on the crown surface of any scales but this is probably a factor of the removal of the external shiny layer of dentine (see taphonomic remarks below).

Histology. Owing to the relatively few scales and poorly preserved material, direct histological studies were not possible. However, all exhibit the typical single rounded pulp opening in the base found in thelodontidid scales as is usual in turiniids (cf. Märss et al., 2007); a quite large pulp cavity is seen in Figure 4.5, micrograph B, and remnants of the pulp canal in Figure 4.5, micrograph C. Based on comparison the crowns are formed of typical thelodont orthodentine and the base of aspidin. As noted above, the outer layer of dentine (vasodentine called 'enameloid' by some workers) is not as shiny as normal and the dentine tubules of the crown are exposed clearly in some scales (Figure 4.5, micrographs G1, G2). The pulp cavity is relatively large and the scales are neither in their first dentine crown 'cap' stage nor senescent with large overgrown bases with closed pulp openings.

Taphonomic remarks. There are two possibilities that could explain why some of the Iranian thelodont scales are densely covered with adhering sedimentary quartz

grains (e.g. Figures 4.5, micrographs G1, G2 and 7A-E). This could imply reworking and mean that the thelodont scales are older than the other remains, that is, not Famennian, and the presence in some scales of crown ribs divided into two might support this, as there is a similarity to the older Iranian turiniid Turinia hutkensis Blieck and Goujet, 1978. However, comparing the state of preservation of the thelodont scales with the other fish microfossils, they are identical in preservation and with the same deep red colour taken from the surrounding rock/grains. The conodont elements were also checked for evidence of reworking but all are light grey in colour, indicating an identical and low CAI, so that reworking does not seem to be a possibility.

Therefore, this leaves the alternative option that the fossils are diagenetically affected and therefore we need to look at post-depositional environmental conditions to account for these changes. The most likely explanation is that the phenomenon is a consequence of water chemistry after the scales were shed or lost from the dead animal; there is no sign of algal or fungal boring as seen in certain marginal environments (e.g. Märss et al., 2007). Other Gondwana samples of turiniid scales show similar adhering grains, such as those from central Australia and New Zealand, but these scales also show more extreme diagenetic effects such as silicification or loss of tissue structure (Turner, 1997; Macadie, 2002).

?*Arianalepis* sp. indet.

(Figures 4.8 and 4.9)

Material.WAM 13.10.1; one cephalopectoral scale.

Locality and stratigraphy. The South Oscar Range section (17855′S, 125817′E) lies 42 km NW of Fitzroy Crossing, South Oscar Range, Canning Basin, Western

Australia. Sample SOC 600, white crinoidal packstone, Napier Formation, Late Devonian, Middle Famennian, *marginifera*/*trachytera* conodont zones.

Stratigraphic range. Middle Famennian, *marginifera*/*trachytera* conodont zones.

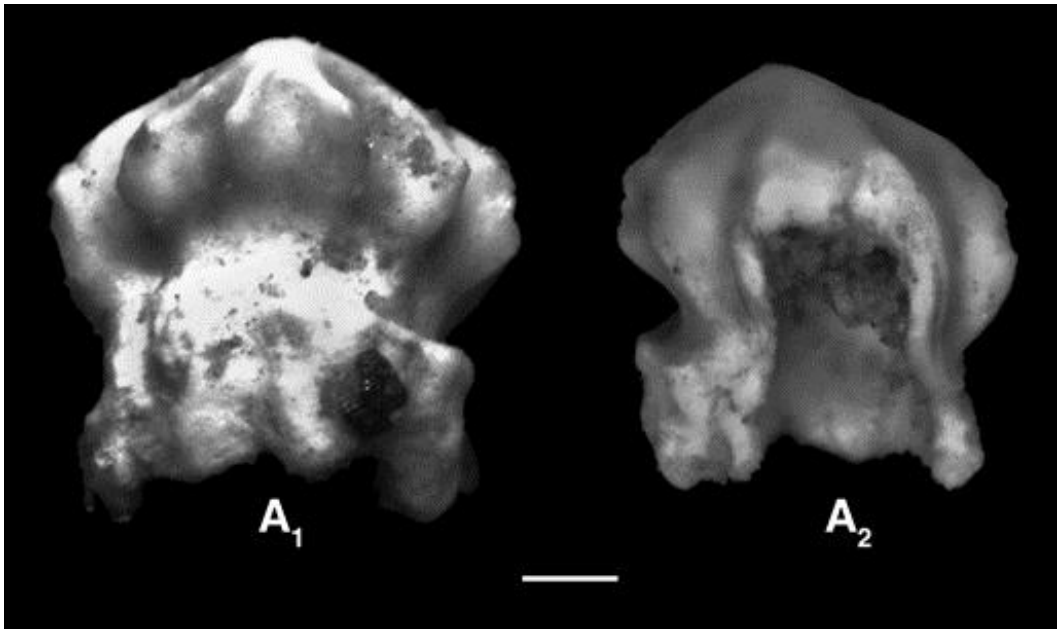

Figure 4.8. Transmission microphotographs of scales of ?*Arianalepis* sp. indet. WAM 13.10.1 from sample SOC 600. A1 and A2 in lateral view. Scale bar 0.2 mm.

Description. The one almost complete specimen is a young, medium-sized (0.8 mm) robust scale with a small break anteriorly across the crown, neck and base (Figures 4.8A2 and 4.9, drawing A1-3). The total range of the number of ribs cannot be determined; however, 12 broad crown ribs are reconstructed based on the spacing of the ten preserved ones. The ribs radiate from a dome-shaped apex with a centrally raised point directed posteriorly (Figures 4.8A1 and 4.9, drawing A4). Two of the medial anterior ribs bifurcate halfway between the crown apex and neck-crown interface. Deep troughs separate the ribs, which diminish at a deep, narrow neck (Figure 4.8A1 and 4.9, drawing A4). A series of small crenulations occurs on the terminal dorsal edge of each rib (Figure 4.9, drawing A2).

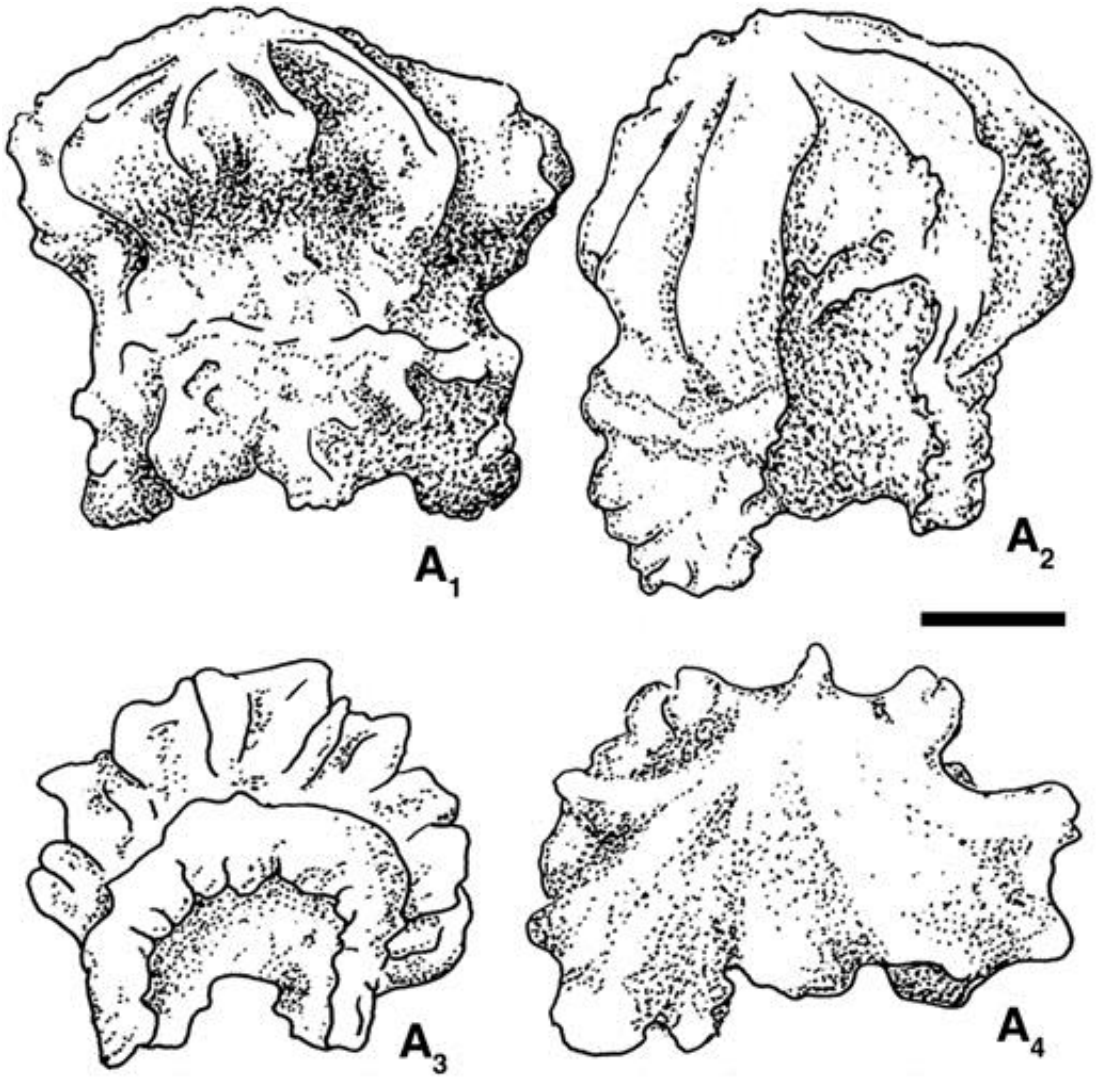

Figure 4.9. Drawings of scale of ?*Arianalepis* sp. indet. WAM 13.10.1 from SOC 600. A1 and A2, lateral view; A3, basal view; A4, crown view. Scale bar, 0.2 mm.

Histology. Histology was not possible as only a single scale was recovered. However, the complete scale exhibits the typical large pulp cavity of a morphogenetically young turiniid scale where dentine has not yet grown centripetally to form a narrow pulp opening on the base.

Taphonomic analyses. The colour of the scale is uniformly white with no evidence of biogenic alteration. Numerous, well-preserved acanthodian scales are also present within Sample SOC 600, suggesting a deeper-marine environment where thelodonts are relatively scarce (cf. Märss et al., 2007). The associated conodont elements are

pristine with a CAI of 0.5. There is no evidence to suggest reworking in this sample as the conodont assemblage conforms to the other assemblages immediately below Sample SOC 600.

Remarks. The scale from SOC 600 is referred tentatively to the new genus *Arianalepis* with indeterminate species, on the basis of similar morphology of a crown with few coarse ribs. Not being a body scale, however, specimen WAM 13.10.1 generally resembles all turiniid head scales and probably lacks diagnostic features. The head scale from SOC 600 has a higher number of radiating ribs: 12 compared with 8, and also seems to be more robust than the specimens from Hojedk. This might be because of normal variation, the different age of the scales, or dependent on the age of the individual animal (Märss et al., 2007).

Microcrenulation of scale crowns also seems to be phylogenetically significant in the Turiniidae; however, the relatively poor preservation of the Iranian scales means that micro-ornament is not preserved and, because most turiniid taxa do exhibit some ornament on the ribs, the crenulations in the Australian scale may just be due to variation within individual scales or within species.

For now we tentatively place the Australian scales within the genus *Arianalepis* gen. nov. based on the single scale.

4.6 Comparison and discussion

The scales of *Arianalepis megacostata* gen. et sp.nov. from Hojedk are superficially more simple than other turiniid species from the Devonian of Gondwana and, interestingly, are most like those of the late Silurian *Turinia fuscina* Turner, 1986 of southern Australia, and mid-Late Devonian taxa, such as *T. hutkensis* Blieck and Goujet, 1978. The single complete scale from South Oscar

Range shows some resemblance to the scales of *Jesslepis johnsoni* Turner, 1995 in being relatively robust, having bifurcating and deeply dissecting ribs, and a large pulp cavity. The complete scale from South Oscar Range can be distinguished based on the greater number of ribs, which do preserve microcrenulations.

The scales from Hojedk and South Oscar Range are distinguishable from any known species. Most interesting is that these youngest thelodont scales have large robust crowns and bases unlike the slightly older taxa known from Iran and Western Australia, especially *Australolepis seddoni*, which has delicate ribbing and sculpture on the crowns. Other older Devonian taxa from the same region are *Turinia antarctica* Turner and Young, 1992 and J. johnsoni from the Givetian of eastern Australia and Antarctica (Turner 1995, 1997).

T. hutkensis of Iran is most similar to scales from Thailand and Antarctica (see Turner and Young, 1992; Turner, 1997). Some of the *Turinia* cf. *hutkensis* scales from the Chahriseh locality resemble Turinia pagoda Wang, Dong and Turner, 1986 and *Turinia* spp. from the western Yunnan Province and *A. seddoni* in their out-turned ridges. Scales that share features with *T. hutkensis*, such as the tight crown double-ribbing, have also been found in the central Australian basins and were earlier thought to be related to the older *Turinia australiensis* (Turner, 1997: see Table 4.1). Could *Australolepis* be the result of paedomorphic evolution from T. hutkensis or *T. pagoda*? Heterochrony in the morphogenesis would leave all the scales with wide-open pulp cavities throughout life and shallow bases with only small anterior prongs, and with a base capable of only thickening sporadically, resulting in the lobate papillae that are typical of *A. seddoni* bases (cf. Figure 4.9, drawing A2).

Table 4.1. Turiniid taxa from the Middle (Givetian) and Upper (Frasnian and Famennian) Devonian of Gondwana. Abbreviations: CEIM, central-east Iran microcontinent; NT, Northern Territory; QLD, Queensland; SA, South Australia; SS, Sanadaj Sirjan; WA, Western Australia.

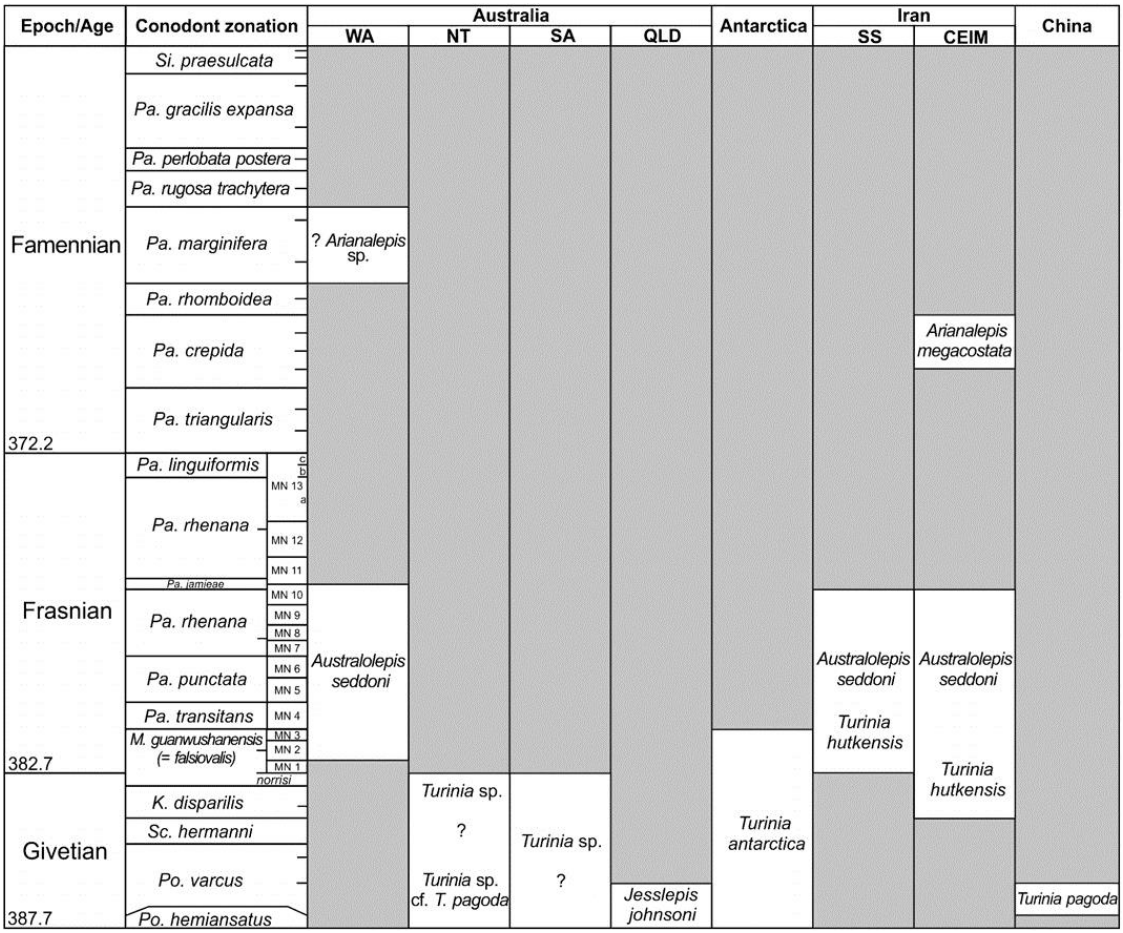

Turinia hutkensis and *T. antarctica* both share the fine ultrastructual lines on the crown, seen in earlier *T. australiensis* (see e.g. Turner, 1997; Marss et al., 2007) but these are not apparent in *A. seddoni* (Figure 4.4A1-2) or *A. megacostata* gen. et sp. nov. (Figure 4.7, photographs A1, D2) although the latter does have the double ribbing seen in some scales of *T. hutkensis.*

Historically, studies on Laurasian/Laurentian thelodonts have been more numerous than those on Gondwana (Märss et al., 2007). This disparity began to be addressed especially during IGCP work from the 1980s onwards, when several new thelodont taxa and increased stratigraphic ranges were reported from Gondwanan faunas (e.g. Blieck et al., 1980; Turner et al., 1981, 2000; Turner, 1986; Wang et al.,

1986; Turner and Young, 1992; Young and Turner, 2000; Trinajstic, 2001; Hairapetian, 2008; Trinajstic and George, 2009, table 1). Most notable was the discovery that thelodont taxa survived the Givetian-Frasnian boundary event (Turner and Dring, 1981). Turiniid remains recovered from the Aztec siltstone in Antarctica (Turner and Young ,1992) have shown a potential age range from the middle Givetian to the early Frasnian based on faunal associations with *Antarctilamna* (Young, 1993). However, the presence of the spore *Geminospora lemurata* Balme, 1960 has dated this unit as Givetian (Young 1988; Young and Turner 2000). Thelodont remains were first found in the Middle Devonian of Iran in the 1970s and other taxa in Australia, Thailand and China in conodont-dated strata (e.g. *J. johnsoni* in Queensland) (Turner and Janvier ,1979; Blieck et al., 1980; Hamdi and Janvier, 1981; Turner, 1997).

The first early Frasnian thelodont scales, *A. seddoni*, were recorded from the Gneudna Formation, Carnarvon Basin, of Western Australia (Turner and Dring, 1981). Spore assemblages (Balme, 1988) gave a possible Givetian to Frasnian age for the lower part of the section; however, microvertebrate assemblages suggested a Frasnian age for the whole section (Trinajstic, 2001). In the last decade thelodont scales identified as *T. hutkensis* and *A. seddoni* were reported from the early-middle Frasnian of Iran (e.g. Yazdi and Turner, 2000; Turner et al., 2002) and poorly preserved scales possibly from *A. seddoni* were recovered from slightly younger Frasnian strata in the Canning Basin of Western Australia (Turner, 1997, 1999). Until recently, this was the youngest record of any thelodont taxon (Turner, 1997). Ranges for thelodonts have been further refined in Western Australia based on the co-occurrence of thelodonts and phoebodonts in conodont-dated sequences at Horse Springs, with the age range of *A. seddoni* extended into the upper Frasnian

(Trinajstic and George, 2009). Younger thelodont scales were recovered from younger early Famennian strata in the Canning Basin of Western Australia; however, as the preservation was poor these were not formally identified (Turner, 1997, 1999). Subsequent studies by Hairapetian and Turner (2003) and Hairapetian (2008) reported the first Famennian scales in Iran.

4.6.1 Palaeobiogeography

The continuance of thelodont taxa into the Famennian may suggest a displacement post the Givetian-Frasnian extinction and the foundation of a refuge in Northern Gondwana (Kauffman and Harries, 1996; Harries et al., 1996). As the Frasnian and Famennian turiniid fish are found in shallow to very shallow water, 'challenging' environments, for example, marginal, lagoonal and hyper-saline, were they then pre-adapted or opportunistic survivors and thus these new taxa are evidence of a survival lineage? There is no sign yet of any thelodont in the immediate earliest Famennian 'bloom' of recovery, but with evidence now in two disparate parts along the Palaeotethyan southern shore we consider *Arianalepis* gen. nov. as a Lazarus taxon. Few agnathan fishes survived the massive Late Devonian extinctions and until recently only two thelodont taxa, *T. hutkensis* from the early-middle Frasnian of Iran (Turner et al., 2002) and *A. seddoni* from the early-late Frasnian (MN zones 6-10) of Western Australia and Iran (Yazdi and Turner, 2000; Trinajstic, 2001; Turner et al., 2002; Trinajstic and George, 2009; Burrow et al., 2010) were known. However, now at least one thelodont genus with one or more species appears to have weathered the Frasnian-Famennian extinction and appears to represent a surviving Lazarus taxon (Kauffman and Harries, 1996). *Australolepis seddoni* is now known from the Gneudna and Virgin Hills formations of Western

Australia and the Shotori Range and Chahriseh sections in Iran (Turner, 1997; Yazdi and Turner, 2000; Turner et al., 2002; Trinajstic and George, 2009). To date, scales have been recovered from different facies including distal and medial slope and back reef in the Canning Basin (Chow et al., 2013), as well as shallow carbonate ramp in Iran and the Carnarvon Basin (Hocking et al., 1987; Wendt et al., 2002; Trinajstic and George, 2009). A few possible *Australolepis* scales are recorded from the Late Devonian of Holy Cross Mountains (M. Ginter and S. Turner, pers. obs. 1990). The presence of thelodonts in sediments from Hull Range, Western Australia, has confirmed an early Frasnian age for these strata (Chow et al., 2013), where previously the date could only be constrained to the late Givetian-early Frasnian. This demonstrates again the utility of microvertebrates in general and thelodont scales in particular to help date strata where conodonts and other open-marine taxa are absent. The first appearance has been linked to conodonts by Long and Trinajstic (2000). The younger Frasnian *Australolepis* scales from the Horse Spring section (GK 364), Canning Basin, Western Australia, were also identified as *A. seddoni* (Trinajstic and George, 2009). Scales from *A. seddoni* are therefore being reported from a number of sections throughout northern and East Gondwana and are proving useful for correlating early to late Frasnian sections.

Most thelodonts had died out in the Early to early Mid-Devonian and after this the only taxa are known outside of the Laurentian continental terranes (Turner, 1997; Turner et al., 2004). Later Middle and Late Devonian thelodonts are known in East and northern Gondwana as far ‘south’ as Antarctica, that is, possibly up to 50-608S in Gondwana (Turner, 1997; Märss et al., 2007). From the records now available, it seems that the turiniids were most widespread in Gondwana in the Early

to Mid-Devonian, with restriction in range by late Frasnian times to Iran and Western Australia.

The fact that at least a small population of thelodonts seems to have survived the Frasnian-Famennian Kellwasser extinction events and lived well into the Famennian is most surprising. We can only speculate on the factors that protected these turiniids from that dramatic time in vertebrate evolution (e.g. Hart, 1996). However, it is clear that the area was home to several thelodont taxa from the late Silurian (Hamedi et al., 1997; Turner, 1997; Hairapetian et al., 2008) onwards and their ability to adapt to high-latitude climatic zones must have been in their favour. Chen et al., (2002) have attributed a major transgression and eutrophic fluctuations that led to severe algal blooms especially in low-latitude continental shelves to related anoxic events. Now it is certain that least one thelodont taxon and possibly more did weather the Frasnian-Famennian extinction events with recovery and survival of the turiniids.

Blieck and Goujet (1978) and Turner (in Turner and Tarling, 1982; Turner, 1997) considered the relationship of Iranian thelodonts to others in Asian localities. We have seen above further evidence of the Gondwanan distribution of turiniid thelodonts and showed the links between Iran and Western Australia in the Mid- to early Late Devonian, supporting a Palaeotethyan dispersal route in shallow water between Gondwana and Euramerica (Laurentia) in the Mid-Late Devonian along the northern Gondwana shoreline. Other vertebrate taxa show a similar biogeographical pattern: Ginter et al. (2002) discussed the Famennian Acanthodian populations of the Palaeotethys; the youngest known ischnacanthiform *Grenfellacanthus zerinae* Long,

Burrow and Ritchie, 2004 exhibits a similar pattern with a possible second species of *Grenfellacanthus* occurring in the early Famennian of Chahriseh, Iran (Long et al., 2004; C. Burrow, pers. comm. August 2013).

Lebedev and Zakharenko (2010) put forward a new hypothesis of vertebrate provinces for the Givetian, one of which is the Phyllolepid-Thelodont Province; several taxa of phyllolepid placoderms being endemic and earlier in East and northern Gondwana, whereas turiniid thelodonts occur there later. However, they seem to have been unaware that thelodonts did exist in western Gondwana in the Early Devonian (Turner et al., 2004) and also that thelodonts occur in the Broken River, North Queensland/China realm in the Mid-Devonian (Turner, 1997).

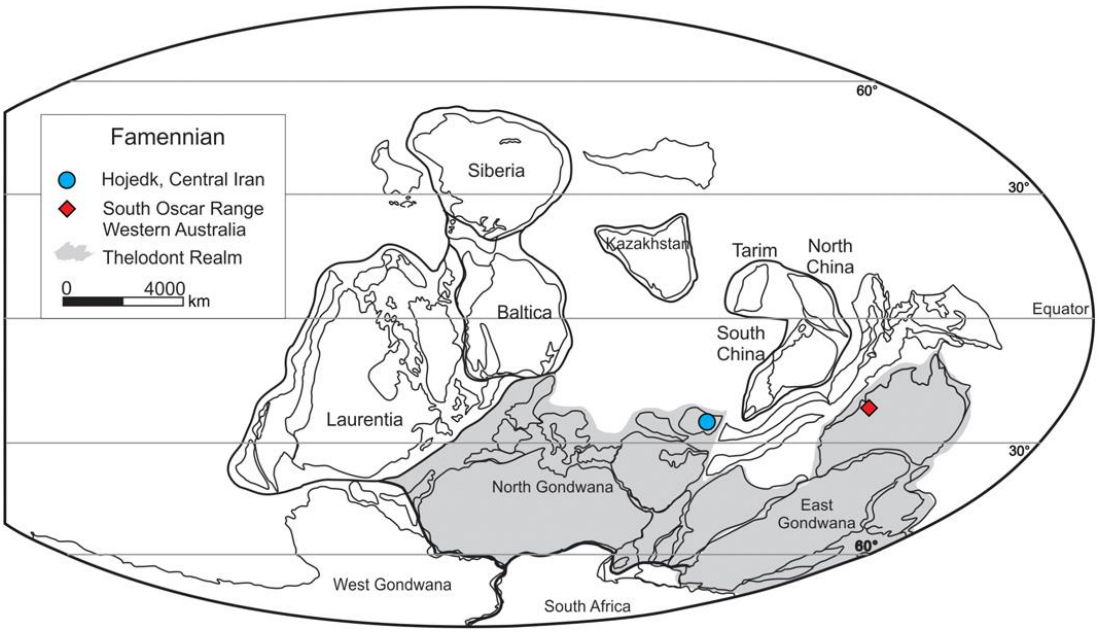

Figure 4.10. Palaeogeographical map showing the position of the Famennian thelodont localities in southeastern Iran and Western Australia during the Late Devonian (Famennian). Base map after Golonka (2007) and Lebedev and Zakharenko (2010), with modifications.

Although they put northern Gondwana further south, the south of central Iran including Hojedk is positioned in the subtropics.

A different opinion on the palaeoposition of central Iran was presented on a recent map by Torsvik and Cocks (2013, fig. 10), which they considered at c. 408S.

This southern latitude still might be feasible as thelodonts are thought to have been able to live in relatively high latitudes (see Turner, 1997).

4.7 Conclusions

The new genus and species of turiniid thelodont, *Arianalepis megacostata* gen. et sp. nov., found in the Upper Devonian (early Famennian) Bahram Formation of the Hojedk section of Iran, and a further uncertain species referred tentatively here to the same genus from the Upper Devonian (middle Famennian) Napier Formation of Western Australia, are younger than the previously youngest known thelodonts from Iran and Western Australia. These are the first thelodont scales known from the early-middle Famennian in both countries and worldwide, and their presence provides new data for biostratigraphic correlation between Iran and Australia. The conodont successions at South Oscar Range and in the Hojedk section constrain the dating.

Most agnathan fishes did not survive the Frasnian-Famennian event and so the presence of a survivor 'Lazarus' thelodont taxon is surprising. *Arianalepis megacostata* gen. et sp. nov. in northern Gondwana (central Iran) and the turiniid ?*Arianalepis* sp. indet. in East Gondwana (Western Australia) provide evidence of the only thelodont lineage surviving the Frasnian-Famennian extinction. These records extend the evolutionary history of the Thelodonti by some 2-6 Ma beyond the Kellwasser events into the crepida (Kerman) to Upper *marginifera*/*trachytera* (South Oscar Range) zones.

We emphasize here that it is now necessary to seek more diligently for further examples in the Famennian of the broad northern and eastern Gondwana area, especially in the carbonates of Western Australia.

4.8 Acknowledgements

VH thanks Prof Michal Ginter (Univ. Warsaw) for support and use of facilities in Warsaw. We thank Curtin University WA-OIGC/Applied Chemistry for use of facilities and acknowledge the use of equipment and scientific and technical assistance of the Curtin University Electron Microscope Facility, which has been partially funded by Curtin University, WA State, and Commonwealth Governments. Dr Mikael Siversson from the Western Australian Museum is thanked for photographic assistance and the use of facilities. KT and BR would like to further acknowledge funding from an Australian Research Council Grant (LP0883812), MERIWA, WA ERA, CSIRO, Buru, Chevron Australia Business Unit, Chevron Energy Technology Company, University of Greenwich, National Science Foundation and Chemostrat Inc. Field support and safety were provided by Wundargoodie Aboriginal Safaris and the Geological Survey of Western Australia. Thank you to the Mimbi Aboriginal Community, Mt Pierre Station and Fossil Downs, for field area access. BR acknowledges an Australian Postgraduate Award. This is a contribution to IGCP 596: Climate and biodiversity patterns in the Mid-Paleozoic '(Early Devonian to Late Carboniferous)'.

4.9 References

Balme, B. E. 1988. Miospores from the Late Devonian (Early Frasnian) strata, Carnarvon Basin, Western Australia. Palaeontographica 209, 109-166.

Blieck, A. and Goujet, D. 1978. A propos de nouveau mate´riel de The´lodontes (Ve´rte´bre´s, Agnathes) d'Iran et de Thaı¨lande: aperc¸u sur la re´partition ge´ographique et stratigraphique des Agnathes des're´gions

gondwaniennes'au Pale´ozoı¨que moyen. Annales de la Socie´te´ge´ologique du Nord 97, 363-372.

Blieck, A. and Turner, S. 2000 (Eds). Palaeozoic Vertebrate Biochronology and Global Marine/Nonmarine Correlation. Final report of IGCP 328 (1991-1996). Courier Forschungsinstitut Senckenberg 223.

Blieck, A., Golshani, F., Goujet, D., Hamdi, A., Janvier, P., Mark-Kurik, E. and Martin, M. 1980. A new vertebrate locality in the Eifelian of the Khush-Yeilagh Formation, Eastern Alborz, Iran. Palaeovertebrata, Montpelier 9, 133-154.

Branson, E. B. and Mehl, M. G. 1934. Conodonts from the Bushberg Sandstone and equivalent formations of Missouri. University of Missouri Studies 8, 265-300.

Burrow, C. J., Turner, S. and Young, G. C. 2010. Middle Palaeozoic microvertebrate assemblages and biogeography of East Gondwana (Australasia, Antarctica). Palaeoworld 19, 37-54.

Chen, D., Tucker, M. E., Shen, Y., Yans, J. and Preat, A. 2002. Carbon isotope excursions and sea level change: implications for the Frasnian-Famennian biotic crisis. Journal of the Geological Society, London 159, 623-626, http://doi.org/10.1144/0016- 764902-027.

Chow, N., George, A. D., Trinajstic, K. M.andChen, Z. 2013. Stratal architecture and platform evolution of an early Frasnian syn-tectonic carbonate platform, Canning Basin, Australia. Sedimentology, 60, 1583-1620.

Gholamalian, H. and Kebriaei, M. R. 2008. Late Devonian conodonts from the Hojedk section, Kerman Province, South-eastern Iran. Rivista Italiana di Paleontologia e Stratigrafia 114, 17-181.

Gholamalian, H., Hairapetian, V., Barfehei, N., Mangelian, S. and Faridi, P. 2013. Givetian-Frasnian boundary conodonts from Kerman province, Central Iran. Rivista Italiana di Paleontologia e Stratigrafia 119, 133-146.

Ginter, M. 1990. Late Famennian shark teeth from the Holy Cross Mountains, Central Poland. Acta Geologica Polonica 40, 69-81.

Ginter, M. and Ivanov, A. 1992. Devonian phoebodont shark teeth. Acta Palaeontologica Polonica 37, 55-75.

Ginter, M., Hairapetian, V. and Klug, C. 2002. Famennian chondrichthyans from the shelves of North Gondwana. Acta Geologica Polonica 52, 169-215.

Girard, C., Klapper, G. and Feist, R. 2005. Subdivision of the terminal Frasnian *linguiformis* conodont Zone, revision of the correlative interval of the Montagne Noire Zone 13, and discussion of the stratigraphically significant associated trilobites. In: Over, D. J., Morrow, J. R. and Wignall, P. B. (Eds).Understanding Late Devonian and Permian-Triassic Biotic and Climatic Events: Towards an Integrated Approach. Developments in Paleontology and Stratigraphy Series 20, 181-198.

Golonka, J. 2007. Phanerozoic paleoenvironment and paleolithofacies maps. Late Palaeozoic. Geologia 33, 145-209.

Hairapetian, V. 2008. Late Devonian-Early Carboniferous fish micro-remains from central Iran. PhD thesis, University of Esfahan.

Hairapetian, V. and Turner, S. 2003. Upper Devonian fish microremains from eastern and southeastern Iran. In: Schultze, H.-P., Luksevics, E. and Unwin, D. (Eds). UNESCO-IUGS IGCP 491: The Gross Symposium 2: Advances In Palaeoichthyology, Riga, Latvia, September 8-14, 2003, Abstracts, 26-27.

Hairapetian, V., Yadzi, M. and Long, J. A. 2000. Devonian vertebrate biostratigraphy of central Iran. Records of the Western Australian Museum 58 (suppl.), 241-247.

Hairapetian, V., Blom, H.andMiller, C. G. 2008. Silurian thelodonts from the Niur Formation, central Iran. Acta Palaeontologica Polonica 53, 85-95.

Hamdi, B. and Janvier, P. 1981. Some conodonts and fish remains from Lower Devonian (lower part of the Khoshyeylaq Formation) north east Shahrud, Iran. Geological Survey of Iran Reports 49, 195-212.

Hamedi, M. A., Wright, A. J. et al. 1997. Cambrian to Silurian of east-central Iran: new biostratigraphic and biogeographic data. Neues Jahrbuch für Geologie und Palaöntologie, Monatshefte 7, 412-424.

Hansma, J., Tohver E., Yan, M., Trinajstic, K., Roelofs, B., Peek, S., Slotznick, S.P., Kirschvink, J., Playton, P. Haines, P. and Hocking, R. 2014. Late Devonian carbonate magnetostratigraphy from the Oscar and Horse Spring Ranges, Lennard Shelf, Canning Basin, Western Australia. Earth and Planetary Science Letters 409, 232-242.

Harries, P. J., Kauffman, E. G. and Hansen, T. A. 1996. Models for biotic survival following mass extinction. In: Hart, M. B. (ed.) Biotic Recovery from Mass Extinction Events. Geological Society, London, Special Publications 102, 41-60, http://doi.org/10.1144/ GSL.SP.1996.001.01.03

Hart, M. B. (ed.) 1996. Biotic Recovery from Mass Extinction Events. Geological Society, London, Special Publications 102, http://sp.lyellcollection.org/content/102/1.toc

Helms, J. 1959. Conodonten aus dem Saalfelder Oberdevon (Thuringen). Geologie 8, 634-677.

Hocking, R. M., Moors, H. T. and Van De Graaf, W. J. E. 1987. Geology of the Carnarvon Basin, Western Australia. Western Australia Geological Survey Bulletin 133, 1-289.

Hurley, N. F. 1986. Geology of the Oscar Range Devonian Reef Complex, Canning Basin, Western Australia. PhD thesis, University of Michigan.

Jaekel, O. 1911. Die Wirbeltiere. Eine Übersicht über die fossilen und lebende Formen. Gebrüder Borntraeger, Berlin.

Kauffman, E. G.and Harries, P. J. 1996. The importance of crisis progenitors in recovery from mass extinction. In: Hart, M. B. (Eds). Biotic Recovery from Mass

Extinction Events. Geological Society, London, Special Publications 102, 15-39, http://doi.org/10.1144/ GSL.SP.1996.001.01.02

Kiaer, J. and Heintz, A. 1932. New coelolepids from Upper Silurian on Oesel (Esthonia). Eesti Loodusteaduse Archiiv 10, 1-8.

Klapper, G. 1989. The Montagne Noire Frasnian (Upper Devonian) conodont succession. In: McMillan, N. J., Embry, A. F. and Glass, D. J. (Eds). Devonian of the World. Memoir of the Canadian Society of Petroleum Geologists 14, 449-205.

Lebedev, O. A. and Zakharenko, G. V. 2010. Global vertebrate-based palaeozoogeographical subdivision for the Givetian-Famennian (Middle-Late Devonian): endemism-cosmopolitanism spectrum as an indicator of interprovincial faunal exchanges. Palaeoworld 19, 186-205.

Long, J. A. and Trinajstic, K. M. 2000. An overview of the Devonian microvertebrate faunas of Western Australia. Courier Forschungsinstitut Senckenberg 223, 471-485.

Long, J. A., Burrow, C. J. and Ritchie, A. 2004. A new Late Devonian acanthodian fish from the Hunter Formation new Grenfell, New South Wales. Alcheringa 28, 147-156.

Macadie, C. I. 2002. Thelodont fish and conodonts from the Early Devonian of Reefton, New Zealand. Alcheringa 26, 423-433.

Märss, T., Turner, S. and Karatajute-Talimaa, V. N. 2007. Agnatha II - Thelodonti. Volume 1B. In: Schultze, H. P. (Eds). Handbook of Paleoichthyology.

Verlag Dr Friedrich Pfeil, Munich, 143. Obruchev, D. V. 1964. Osnovy Paleontologi. v. 11. Ryby i Byescheliustnikh. Fundamentals of Palaeontology Fishes and Agnatha. Nauka, Moscow [In Russian].

Playford, P. E. and Lowry, D. C. 1966. Devonian reef complexes of the Canning Basin, Western Australia. Geological Survey of Western Australia Bulletin 118, 1-150.

Playford, P. E., Hurley, N. F. and Middleton, M. F. 1989. Reefal platform development, Devonian of the Canning Basin, Western Australia. In: Crevello, P., Wilson, J. I., Sarg, J. F. and Read, J. F. (Eds). Controls on Carbonate Platform and Basin Development. SEPM Special Publication 44, 187-202.

Playford, P. E., Hocking, R. M. and Cockbain, A. E. 2009. Devonian reef complexes of the Canning Basin, Western Australia. Geological Survey of Western Australia Bulletin 145, 444.

Playton, T., Montgomery, P., Tohver, E., Hillbun, K., Katz, D., Haines, P., Trinajstic, K., Yan, M., Hansma, J. and Pisarevsky, S. 2013. Development of a regional stratigraphic framework for Upper Devonian reef complexes using integrated chronostratigraphy: Lennard Shelf, Canning Basin, Western

Australia, The Sedimentary Basins of Western Australia IV. Proceedings of the Petroleum Exploration Society of Australia Symposium, Perth, Western Australia.

Sandberg, C. A. and Dreesen, R. 1984. Late Devonian icriodontid biofacies models and alternate shallow water conodont zonation. In: Clark, D. L. (Eds). Conodont Biofacies and Provincialism. Geological Society of America, Special Papers 196, 143-178.

Sandberg, C. A. and Ziegler, W. 1979. Taxonomy and biofacies of important conodonts of Late Devonian *styriacus*-Zone, United States and Germany. Geologica et Palaeontologica 13, 173-212.

Sannemann, D. 1955. Oberdevonische Conodonten (to IIa). Senckenbergiana Lethaea 36, 123-156.

Thomas, L. A. 1949. Devonian-Mississippian formations of southeast Iowa. Geological Society of America Bulletin 60, 403-438.

Torsvik, T. H. and Cocks, L. R. M. 2013. Gondwana from top to base in space and time. Gondwana Research 24, 999-1030.

Trinajstic, K. 2000. Conodonts, thelodonts and phoebodonts together at last. Geological Society of Australia, Abstract 61, 121.

Trinajstic, K. 2001. A description of additional variation seen in the scale morphology of the Frasnian thelodont *Australolepis seddoni* Turner and Dring, 1981. Records of the Western Australian Museum 20, 237-246.

Trinajstic, K. and George, A. D. 2009. Microvertebrate biostratigraphy of Upper Devonian (Frasnian) carbonate rocks in Canning and Carnarvon Basins of Western Australia. Palaeontology 52, 641-659.

Turner, S. 1986. Vertebrate fauna of the Silverband Formation, Grampians, western Victoria. Proceedings of the Royal Society of Victoria 98, 53-62.

Turner, S. 1993. Palaeozoic microvertebrates from eastern Gondwana. In: Long, J. A. (Eds). Palaeozoic Vertebrate Biostratigraphy and Biogeography. Belhaven Press, London, 174-207.

Turner, S. 1995. Devonian thelodont scales (Agnatha, Thelodonti) from Queensland. Memoirs of the Queensland Museum 38, 677-685.

Turner, S. 1997. Sequence of Devonian thelodont scale assemblages in East Gondwana. In: Klapper, G., Murphy, M. A. and Talent, J. A. (Eds). Paleozoic Sequence Stratigraphy, Biostratigraphy, and Biogeography: Studies in Honor of Dr J. Granville ("Jess") Johnson. Geological Society of America, Special Papers 321, 295-315.

Turner, S. 1999. Early Silurian to Early Devonian thelodont assemblages and their possible ecological significance. In: Boucot, A. J. and Lawson, J. (Eds). Palaeocommunities: A Case Study From the Silurian and Lower Devonian. Cambridge University Press, Cambridge, 42-78.

Turner, S. and Dring, R. S. 1981. Late Devonian thelodonts (Agnatha) from the Gneudna Formation, Carnarvon Basin, Western Australia. Alcheringa 5, 39-48.

Turner, S. and Hairapetian, V. 2005. Thelodonts from Gondwana. In: Hairapetian, V. and Ginter, M. (Eds). IGCP 491 Armenia Field Conference, Devonian Vertebrates of the Continental Margins, May 24-28. Ichthyolith Issues, Special Publication 8, 1-24.

Turner, S. and Janvier, P. 1979. Middle Devonian Thelodonti (Agnatha) from the Khush-Yeilagh Formation, North-East Iran. Geobios 12, 889-892.

Turner, S. and Tarling, D. 1982. Thelodont and other agnathan distributions as tests of Lower Palaeozoic continental reconstructions. Palaeogeography, Palaeoclimatology, Palaeoecology 39, 295-311.

Turner, S. and Young, G. C. 1992. Thelodont scales from the Middle-Late Devonian Aztec siltstone, southern Victoria Land Antarctica. Antarctic Science 4, 89-105.

Turner, S., Jones, P. J. and Draper, J. J. 1981. Early Devonian thelodonts (Agnatha) from the Toko Syncline, western Queensland, and a review of other Australian discoveries. BMR Journal of Australian Geology and Geophysics 6, 51-69.

Turner, S., Basden, A. and Burrow, C. J. 2000. Devonian vertebrates of Queensland. In: Blieck, A. and Turner, S. (Eds). IGCP: 328, Final Report. Courier Forschungsinstitut Senckenberg 223, 487-521.

Turner, S., Burrow, C. J., Gholamalian, H. and Yazdi, M. 2002. Late Devonian (early Frasnian) microvertebrates and conodonts from the Chahriseh area near Esfahan, Iran. Memoirs of the Association of Australasian Palaeontologists 27, 149-159.

Turner, S., Trinajstic, K., Hairapetian, V., Janvier, P. and Macadie, I. 2004. Thelodonts from western Gondwana. In: Richter, M. and Smith, M. M. (Eds).10th Early/Lower Vertebrates. IGCP 491 Symposium, Gramado, Brazil, 45-46.

Wang, S. T., Dong, Z. and Turner, S. 1986. Middle Devonian Turinidae (Thelodont, Agnatha) from western Yunnan, China. Alcheringa 10, 315-325.

Wendt, J., Kaufmann, B., Belka, Z., Farsan, N. and Karimi Bavandpour, A. 2002. Devonian/Lower Carboniferous stratigraphy, facies patterns and

palaeogeography of Iran. Part I, southeastern Iran. Acta Geologica Polonica 52, 129-168.

Wendt, J., Kaufmann, B., Belka, Z., Farsan, N. and Karimi Bavandpour, A. 2005. Devonian/Lower Carboniferous stratigraphy, facies patterns and palaeogeography of Iran. Part II, northern and central Iran. Acta Geologica Polonica 55, 31-97.

Yazdi, M. and Turner, S. 2000. Late Devonian and Carboniferous vertebrates from the Shishtu and Sardar Formations of the central Shotori Range, Iran. Records of the Western Australian Museum 58 (suppl.), 223-240.

Young, G. C. 1988. Antiarchs (Placoderm fishes) from the Devonian Aztec Siltstone, southern Victoria Land, Antarctica. Palaeontographica 202, 1-125.

Young, G. C. 1993. The teeth of the Devonian shark *Antarctilamna*, and its relationships. In: K.S.W. Campbell Symposium (A.N.U., Canberra, A.C.T., 8-10 February, 1993) Abstracts. Association of Australasian Palaeontologists, Canberra, 28.

Young, G. C. and Turner, S. 2000. Devonian microvertebrates and marine-nonmarine orrelation in East Gondwana: overview. Courier Forschungsinstitut Senckenberg 223, 453-470.

Ziegler,W. and Sandberg, C. A. 1990. The Late Devonian standard conodont zonation. Courier Forschungsinstitut Senckenberg 121, 1-115.

5.0 Late Devonian and Early Carboniferous chondrichthyans from the Fairfield Group, Canning Basin, Western Australia

Brett Roelofs[1], Milo Barham[2], Arthur J. Mory[3], and Kate Trinajstic[4]

[1]Brett Roelofs. Department of Applied Geology, Curtin University, GPO Box U1987 Perth, WA 6845, Australia. brett.roelofs@postgrad.curtin.edu.au

[2]Milo Barham. Department of Applied Geology, Curtin University, GPO Box U1987 Perth, WA 6845, Australia. milo.barham@curtin.edu.au

[3]Arthur J. Mory. Geological Survey of Western Australia, Mineral House, 100 Plain Street, East Perth, WA 6004, Australia. arthur.mory@dmp.wa.gov.au

[4]Kate Trinajstic*. Department of Environment and Agriculture, Curtin University, GPO Box U1987, Perth, WA 6845, Australia. K.Trinajstic@curtin.edu.au

5.1 Abstract

Teeth from 18 shark taxa are described from Upper Devonian to Lower Carboniferous strata of the Lennard Shelf, Canning Basin, Western Australia. Spot samples from shoal facies in the upper Famennian Gumhole Formation and shallow water carbonate platform facies in the Tournaisian Laurel Formation yielded a chondrichthyan fauna including several known species, in particular *Thrinacodus ferox, Cladodus thomasi, Protacrodus aequalis* and *Deihim mansureae*. In addition, protacrodont teeth were recovered that resemble formally described, yet unnamed, teeth from Tournaisian deposits in North Gondwanan terranes. The close faunal relationships previously seen for Late Devonian chondrichthyan taxa in the Canning Basin and the margins of northern Gondwana are shown here to continue into the

Carboniferous. However, a reduction in species overlap for Tournaisian shallow water microvertebrate faunas between the Canning Basin and South China is evident, which supports previous studies documenting a separation of faunal and terrestrial plant communities between these regions by this time. The chondrichthyan fauna described herein is dominated by crushing type teeth similar to the shallow water chondrichthyan biofacies established for the Famennian and suggests some of these biofacies also extended into the Early Carboniferous.

5.2 Introduction

The Late Devonian saw an increase in the cosmopolitanism of many vertebrate taxa across parts of North and East Gondwana, and extending into South China and south-east Asia (Young et al., 2010). A shallow seaway along the northern margins of Gondwana is thought to have, at least in part, facilitated large scale faunal exchanges during this period (Lebedev and Zakharenko, 2010). At that time, the Canning Basin was located on the north-west corner of the East Gondwanan margin, which was contiguous with the North Gondwanan margin, with South China and south-east Asian landmasses further north (Golonka, 2007; Metcalfe, 2011). The Canning Basin was thus situated at the junction of major terranes and is therefore an ideal study area to evaluate Late Devonian faunal exchanges between these landmasses. Common faunal components between the Canning Basin and areas in South China and south-east Asia are known for several vertebrate groups from the Late Devonian, including placoderms (Young, 1984; Young et al., 2010) and chondrichthyans (Trinajstic and George, 2009; Roelofs et al., 2015). In addition, the jawless thelodonts are known from the uppermost Devonian in Iran (Hairapetian et al., 2015) North Gondwana and north-western

Australia (Trinajstic, 2001; Hairapetian et al., 2015). Of these groups, only the sharks survived the Devonian-Carboniferous extinctions (Janvier, 1996). Whether the same chondrichthyan taxa persisted into the Carboniferous in intermediate regions between the Canning Basin and areas surrounding South China and the northern margin of Gondwana, is difficult to resolve. This is partly due to a significant faunal overturn in the Early Carboniferous with subsequent radiations of many groups including osteichthyes, chondrichthyes and tetrapods (Janvier, 1996; Sallan and Coates, 2010). In addition, Early Carboniferous tectonic movements, such as the northwards migration of the South China block, led to increased separation between this terrane and East Gondwana (Scotese and McKerrow, 1990).

Recent studies on Carboniferous shark faunas of Western Australia have been limited. Earlier works (Thomas, 1957, 1959) described a rich shark assemblage from the Lower Carboniferous Laurel Formation that included both "cladodont" and "bradyodont" teeth (for a review see Trinajstic et al., 2014). In addition, Turner (1982) described a species of ctenacanthiform, *Cladodus thomasi* Turner, 1982, and attributed associated teeth to the genus *Helodus*. Edwards (1997) detailed further chondrichthyan genera from a trench across the Devonian-Carboniferous boundary, approximately 45 km north-west of Fitzroy Crossing (Figure 5.1). Despite the paucity of published material, some similarity of the shark fauna between north-western and eastern Australia was recognised by Turner (1982). Here we aim to show the extent of the faunal links between the Canning Basin and the margins of Palaeo-Tethys along North and East Gondwana and southern Laurussia.

In addition to providing information on faunal ties, the rich chondrichthyan assemblage (Table 5.1), comprising 16 taxa from the Laurel Formation, allows a detailed analysis of a shark fauna from Tournaisian shallow water facies. The

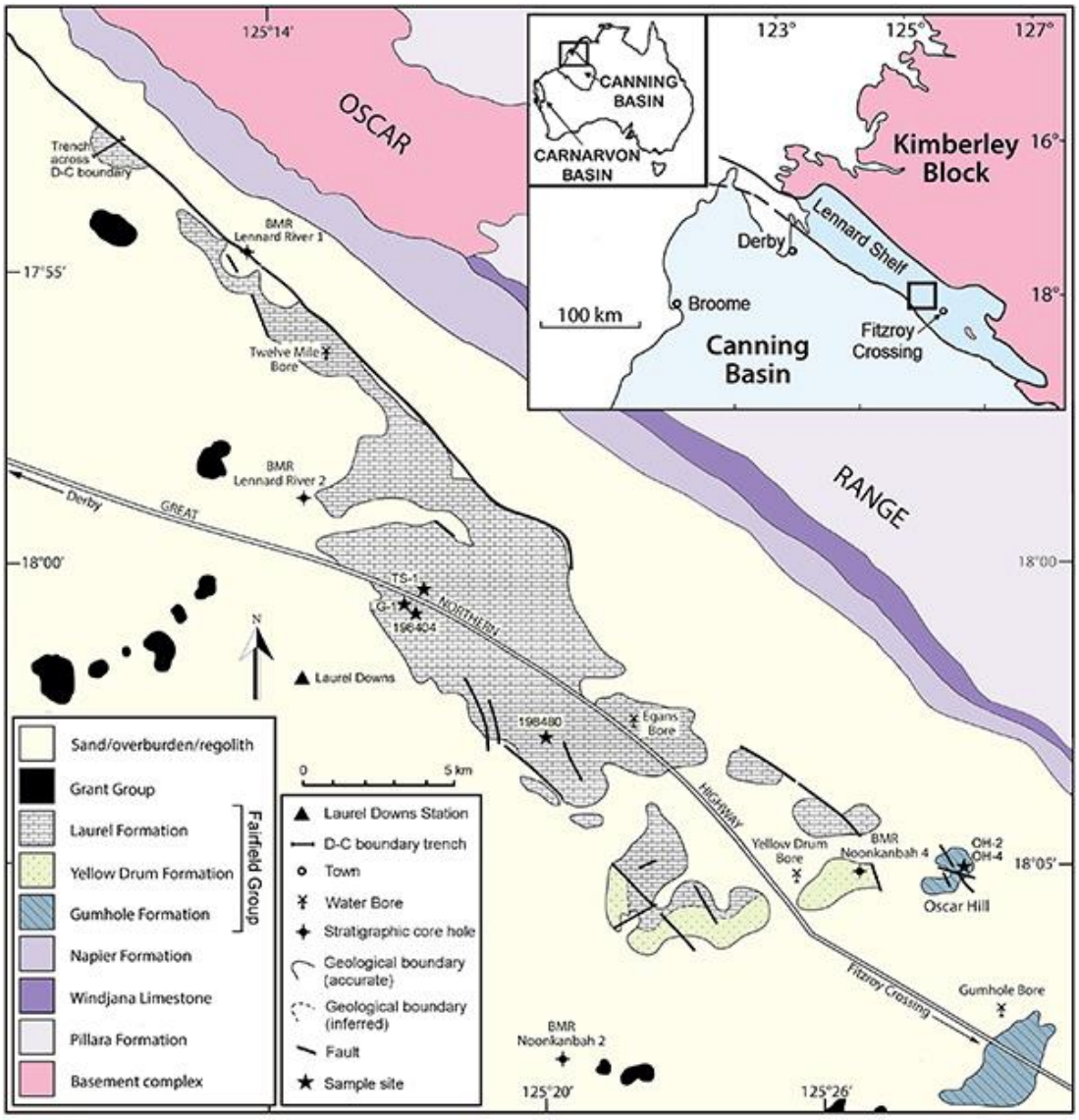

Figure 5.1. Simplified geological map of the Upper Devonian and Lower Carboniferous Fairfield Group outcrop, Lennard Shelf, northern Canning Basin, showing sampled sites at Oscar Hill and Laurel Downs (after Druce and Radke, 1979).

association between chondrichthyan taxa and the environments they inhabited has been analysed by Ginter (2000, 2001), who established three shark biofacies based on the percentages of shark teeth in Famennian pan-tropical regions. This biofacies model has been applied to a shallow water Famennian shark assemblage from the Canning Basin (Roelofs et al., 2015). Here we test if the Famennian shark biofacies model is applicable for the Carboniferous. This is in light of the Late Devonian mass extinction that caused significant niche reorganisations in which the placoderms, the

dominant faunal component of the Devonian (Young, 2010) and the last of the thelodonts, which had survived into the Famennian only in Western Australia and Iran (Hairapetian et al., 2015), became extinct.

5.3 Geological setting

Extensive carbonate platforms with associated slope and basin facies developed along the northern margin of the Canning Basin, northern Western Australia from the late Givetian to late Famennian (Playford et al., 2009). Outcrops of these deposits extend along the Lennard Shelf for approximately 350 km and are amongst the world's best preserved examples of a Devonian reef complex (Hocking et al., 2008; Playford et al., 2009). Near the end of the Famennian an abrupt regression along the northern margin of the basin led to exposure, erosion and minor karstification of the reef platform prior to a change to ramp facies including carbonate, mudstone and sandstone, of the Fairfield Group (Druce and Radke, 1979; Southgate et al., 1993) (Figure 5.2). Along the southern, basin-ward margin of the Lennard Shelf and throughout much of the Fitzroy Trough, deposition of mostly fine-grained siliciclastic facies with minor carbonate appears to have been continuous into the Tournaisian. These southern basin-ward facies are only known from the subsurface and are largely attributed to the Upper Famennian Luluigui and Clanmeyer formations (Willmott, 1962). However, this part of the succession needs revision (Jones, 1987) given the somewhat arbitrary formation designations for petroleum wells in Druce and Radke (1979).

The oldest stratigraphic unit of the Fairfield Group, the Gumhole Formation, consists mostly of bioclastic and oolitic sandy limestone with interbedded carbonate, siltstone and shale. The formation is best exposed at Oscar Hill, approximately 19

km west-northwest of Fitzroy Crossing (Druce and Radke, 1979). Within the Horseshoe Range and Red Bluffs, the Gumhole Formation overlies a birdseye limestone likely to be the uppermost facies of the Nullara Limestone, whereas Druce and Radke (1979) and Edgell (2004) claim the Gumhole Formation overlies the Luluigui Formation in the Napier and Oscar Ranges. The overlying Yellow Drum Formation (Figure 5.2) consists of a series of massive calcareous sandstone and carbonate beds, with minor mudstone, breccia and evaporitic facies.

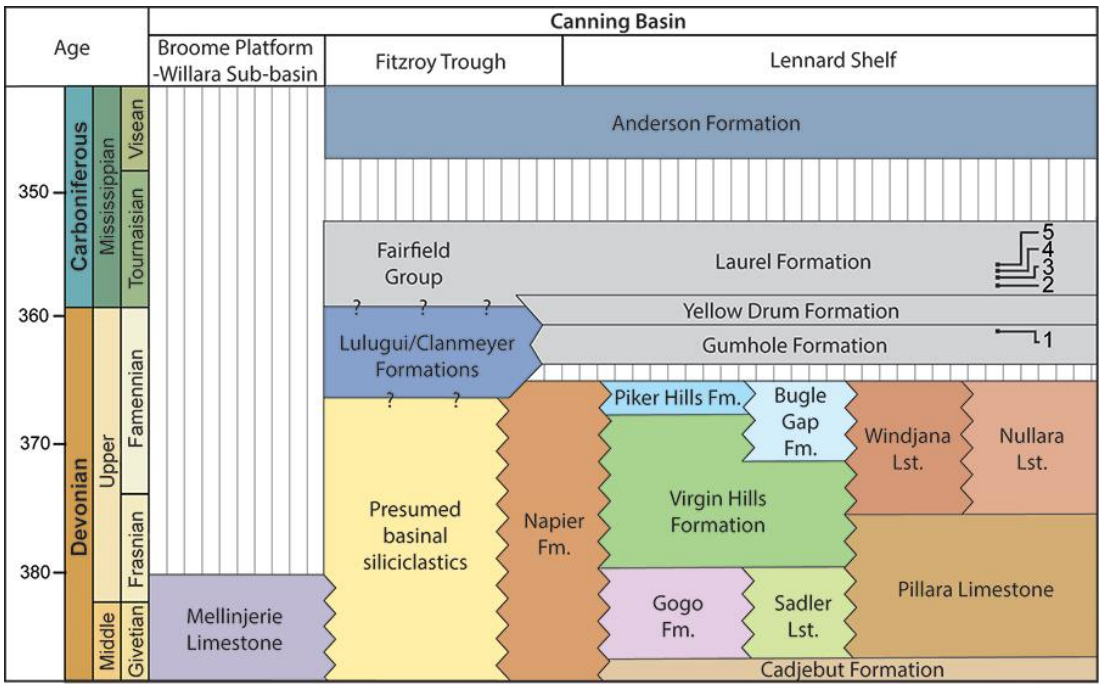

Figure 5.2. Stratigraphy and correlation of Upper Devonian and Lower Carboniferous units of the Lennard Shelf (after Playford et al., 2009; Smith et al., 2013). Approximate temporal positions of the sampled localities: **1**, OH4; **2**, 198480; **3**, 198404; **4**, LG-1; and **5**, TS-1. Abbreviations: Fm, Formation; and Lst, Limestone.

The Devonian-Carboniferous boundary has been located in a trench 1 km northwest of Linesman Creek (Figure 5.1), excavated by researchers from Macquarie University, Sydney, Australia. In this section the boundary was placed at 7.5 m above the base of the Yellow Drum Sandstone based on the first appearance of the conodont *Siphonodella sulcata* Huddle, 1934. Unfortunately little data from the

trench has been published apart from brief mentions by Andrew et al., (1994) and Burrow et al., (2010), the latter incorrectly indicating a location near Oscar Hill. The boundary also appears to lie within the Yellow Drum Formation in many petroleum wells, including near the base of BMR Noonkanbah 4 (Figure 5.1) based on palynomorphs (Playford, 1976) and conodonts (Nicoll and Druce, 1979); however, the position of the boundary in these sections is approximate at best.

A transgressive interval in the Early Carboniferous following deposition of the Yellow Drum Formation led to the development of lagoonal and shallow ramp facies of the Laurel Formation, the uppermost unit of the Fairfield Group (Figure 5.2). The formation is poorly exposed in a 2-10 km wide belt southwest of the Napier and Oscar Ranges, with somewhat better exposures in the vicinity of Twelve Mile Bore. The Laurel Formation is characterised by a series of interbedded fossiliferous calcarenite, siltstone, sandstone and minor dolomitic beds, and contains a diverse fauna including bryozoans and corals (Thomas, 1959), foraminifera (Edgell, 2004), ostracods (Jones, 1959, 1974), rare ammonoids (Glenister and Klapper, 1966) and fish (Thomas, 1957, 1959; Turner, 1982; Long, 1989; Burrow et al., 2010). Studies of the brachiopod (Veevers, 1959; Thomas, 1971) and conodont (Glenister and Klapper, 1966; Nicoll and Druce, 1979) faunas indicate a general Tournaisian age, later revised to early to mid-Tournaisian by Jones (1995).

5.4 Materials and methods

The examined teeth were extracted from 5 kg rock samples collected in 2012 from carbonate beds exposed at Oscar Hill and on Laurel Downs Station, Canning Basin, Western Australia (Figure 5,1). Samples were dissolved in buffered acetic acid following the methodology of Jeppsson et al. (1999). Residues were

Table 5.1. Distribution and abundance of Devonian and Carboniferous chondrichthyan teeth from the Lennard Shelf, Canning Basin, Western Australia.

Localities	Oscar Hill (Famennian)		Laurel Downs (Tournaisian)			
Taxa / Sample	OH-2	OH-4	LG-1	198404	198480	TS-1
Ageleodus sp.	-	-	-	1	-	3
Phoebodus cf. *turnerae*	-	1	-	-	-	-
Thrinacodus ferox	-	-	5	8	12	9
Stethacanthus? sp.	-	-	-	2	-	-
Cladodus thomasi	-	-	-	4	1	8
Cladodoides cf. *wildungensis*	-	-	-	3	1	2
Cladodontomorphi indet. sp.	-	-	-	-	1	-
Ctenacanthiform gen. et sp. indet 1	-	-	-	3	1	4
Ctenacanthiform gen. et sp. indet 2	-	-	-	-	-	1
Protacrodus aequalis	-	-	-	-	-	1
Protacrodus sp. 1	-	-	-	-	-	1
Deihim mansureae	1	-	-	12	2	6
Dalmehodus cf. *turnerae*	-	-	7	11	-	2
Protacrodontidae gen. et sp. indet	-	1	-	-	-	-
Lissodus sp.	-	-	-	-	-	1
Hybodontoidea gen. et sp. indet.	-	-	-	-	-	1
Euselachii gen. et sp. indet	-	-	-	6	2	9
Holocephali gen. et sp. indet.	-	-	-	7	-	9
Total	1	2	12	57	20	57
	3		146			

washed and sieved (mesh size of 0.250 mm) before being picked under a Nikon stereomicroscope.

Teeth used for imaging under a scanning electron microscope (SEM) were adhered to carbon tabs on 10 mm aluminium stubs. The mounted fossils were then coated with 10 µm platinum and imaged using a Zeiss Evo 40XVP SEM at the Centre for Materials Research at Curtin University. A Hitachi TM-3030 desktop SEM at the Department of Applied Geology (Curtin University) was also used for imaging fragile teeth. Imaging was undertaken using accelerating voltages ranging from 5 to 15 kV under variable pressure.

The standard conodont zonation of Ziegler and Sandberg (1990) cannot be readily applied to the Famennian shallow water facies in the Canning Basin due to

the dominance of polygnathids and paucity of palmatolepids (Klapper, 2007; Mory and Hocking, 2011). However, it is possible to indirectly correlate the succession at Oscar Hill to the standard conodont zones (CZ) using ammonoids (Becker and House, 2009). Similarly, the Carboniferous conodont zonation of Nicoll and Druce (1979) is dominated by shallow-water conodont genera, the ranges of which are strongly tied to local facies, and so do not provide a direct correlation to the standard zonation. According to Jones (1995), the conodont faunas from the Laurel Formation do not extend above the range of *Siphonodella* (Tn 1-2) in spite of the paucity of that genus.

All microvertebrate specimens are housed in the Western Australian Museum (WAM).

5.4.1 Sample Localities

5.4.1.1 Oscar Hill

Two samples (OH2, OH4) were taken in 2012 from large cross stratified, sandy oolitic grainstone beds at the base of Oscar Hill (Figure 5.1, 18° 04' 07" S, 125° 26' 41" E), approximately 15 km north west of Fitzroy Crossing. That section consists mainly of ooidal and bioclastic sandstone deposited within a shoal environment (Druce and Radke, 1979). Previous work at Oscar Hill documented a diverse fauna including ostracods (Jones and Thomas, 1959), brachiopods (Veevers, 1959), goniatites (Teichert, 1949), corals (Hill, 1954) and bryozoans (Ross, 1961). Numerous crinoid, bivalves, and gastropod fossils have also been identified (Druce and Radke 1979) but are yet to be described. Conodont faunas (Nicoll and Druce, 1979; West Canning Basin [WCB] section 002) place the section within the Devonian *Icriodus platys* Assemblage Zone (A.Z.), equivalent to the

praesulcata conodont zone of Ziegler and Sandberg (1990). A range of vertebrate material has been reported from the Oscar Hill area including arthrodire plates (Druce and Radke, 1979) and dipnoan remains (Young, 1987). Shark teeth have been previously found in the area (Edwards, 1997 unpublished thesis; Burrow et al., 2010) with some beds yielding abundant orodont teeth.

5.4.1.1 Laurel Downs

Exposure of the Lower Carboniferous Laurel Formation on Laurel Downs station (Figure 5.1) is poor and largely confined to thin shallowly dipping limestone beds. Muddy intervals are weathered and covered by black soil. Determining detailed stratigraphic relationships between sections is hindered by poor exposure and numerous faults. Spot samples from thickly bedded, fossiliferous silty boundstone contain intact bryozoans, brachiopods and tabulate corals (Sample 198404, Figure 5.1, locality 18° 01' S, 125° 18' E). Samples TS-1 (Figure 5.1, 18° 01' S, 125° 17' E), 198480 (Figure 5.1, 18° 02' S, 125° 20' E) and LG-1 (Figure 5.1, 18° 01' S, 125° 19' E) were extracted from a series of sandy bioclastic grainstone beds containing a rich ichthyolith fauna as well as minor, disarticulated brachiopod valves and crinoid ossicles. Conodonts from sample 198404 include *Bispathodus aculeatus plumulus* Rhodes, Austin, and Druce, 1969 and *Clydagnathus cavusformis* Rhodes, Austin, and Druce, 1969, indicating an Early Carboniferous age.

5.5 Systematic Palaeontology

Class CHONDRICHTHYES Huxley, 1880

Family INCERTAE SEDIS sedis

Genus AGELEODUS Owen, 1867

Type Species. *Ctenopychius pectinatus* Agassiz, 1838

Ageleodus sp.

Figure 5.3.1-4

Material. Four incomplete teeth: one tooth from sample 198404, and three teeth from TS-1, Laurel Formation, Laurel Downs, Tournaisian.

Description. Labio-lingually compressed crown that is slightly arched along the occlusal margin (Figure 5.3.1-3). The crown comprises a single row of four to five unornamented triangular cusps, decreasing in size distally (Figure 5.5.3.1). Most teeth bear cusp apices with a slight lingual inclination that are typically worn flat or slightly rounded (Figure 5.3.2-3). One specimen, WAM 15.6.33, (Figure 5.3.4) preserves three pointed triangular cusps with little wear. Shallow, vertical grooves originating at the juncture of the cusps are present on the top half of both crown faces. On one tooth (WAM 15.6.34, Figure 5.3.2), the crown is labio-lingually convex between the base of the cusps and the crown base interface. The lateral sides of the crown are rounded and taper mesially to a shallow depression along the crown-base interface (Figure 5.3.1-3). The labio-lingually flattened base is short and bears small foramina and longitudinal furrows.

Remarks. Due to the high level of heterodonty previously recorded for *Ageleodus pectinatus* Agassiz, 1838 and the absence of multiple complete teeth from the samples, species determination is not possible. The teeth do share similarities with

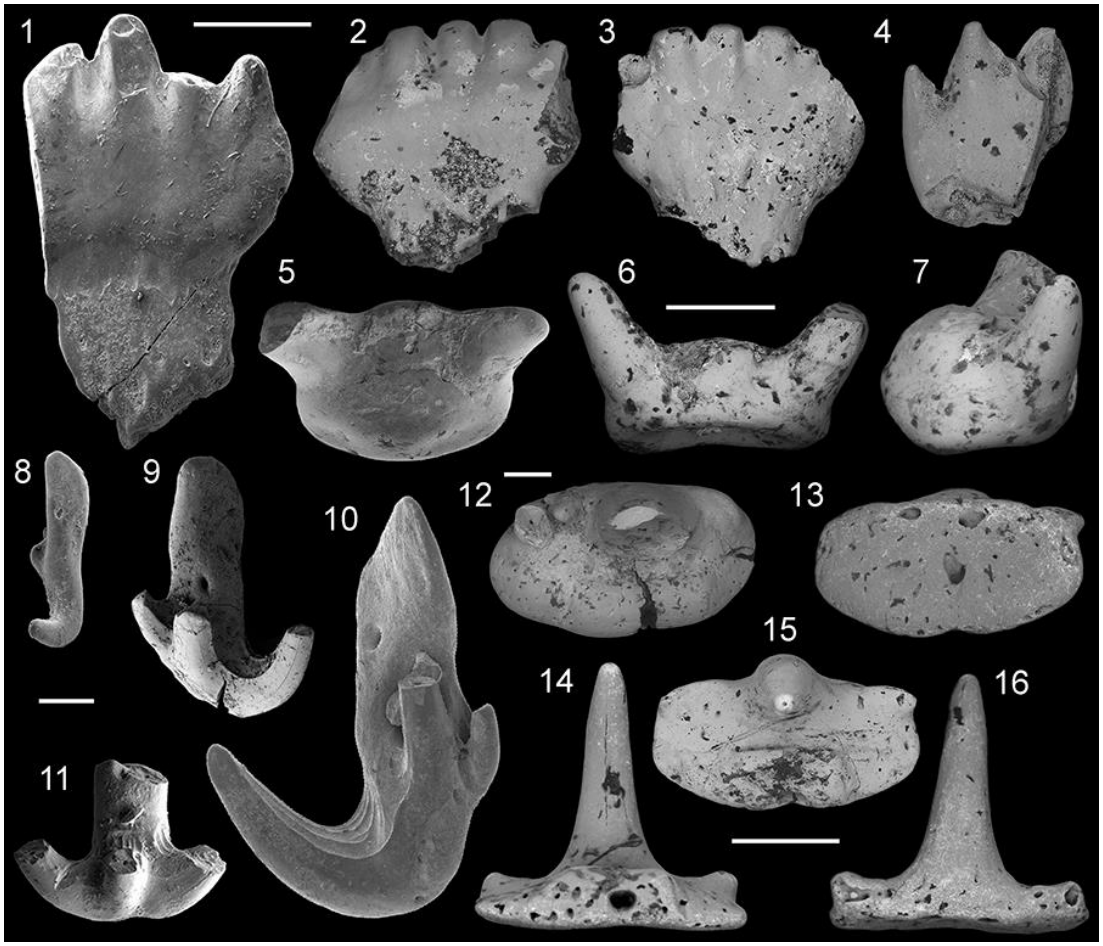

Figure 5.3. Late Devonian and Early Carboniferous shark teeth from the Lennard Shelf, Canning Basin, Western Australia. **1-4**,*Ageleodus* sp., WAM 15.6.23, sample 198404, in lingual view (**1**), WAM 15.6.34, sample TS-1, in labial (**2**) and lingual (**3**) views, and WAM 15.6.33, sample TS-1, in lingual view (**4**); **5-7**, *Phoebodus* cf. *turnerae*, WAM 15.6.28, sample OH-4, in occlusal (**5**), labial (**6**) and lateral (**7**) views; **8-11**, *Thrinacodus ferox* , WAM 15.6.32, sample LG-1, in occlusal view (**8**), WAM 15.6.8, sample 198404, in occlusal view (**9**), WAM 15.6.11, sample 198404, in lateral view (**10**), and WAM 15.6.9, sample 198404, in occlusal view (**11**); **12-16**, *Stethacanthus* ? sp., WAM 15.6.6, sample 198404, in occlusal view (**12**), and WAM 15.6.7, sample 198404, in basal (**13**), lingual (**14**), occlusal (**15**) and labial (**16**) views. Scale bar length: **1-4**, 1 mm; **5-7**, 0.5 mm; **8-11**, 0.25 mm; **12**, 0.5 mm;**13-16**, 0.5 mm.

other known *Ageleodus* species. One partial tooth crown (WAM 15.6.33, Figure 5.3.4) possesses the pointed triangular cusps typical of the Late Devonian *Ageleodus pectinatus* Downs and Daeschler, 2001 and the *Ageleodus* teeth described by

Lebedev (1996, figure 13). The rounded apicies on one tooth (WAM 15.6.23, Figure 5.3.1) are similar to *Ageleodus altus* Garvey and Turner, 2006 from the Carboniferous of Victoria, Australia. As cusp morphology appears to diagnose different species of *Ageleodus*, it is possible more than one species inhabited the Canning Basin at this time. However, given the large amount of variation in the small sample size, it is more likely physical wear has contributed to the cusp shape than species specific morphology.

Subclass ELASMOBRANCHII Bonaparte, 1838

Order PHOEBODONTIFORMES Ginter, Hairapetian and Klug, 2002

Family PHOEBODONTIDAE Williams, 1985

Genus PHOEBODUS St. John and Worthen, 1875

Type Species. *Phoebodus sophiae* St. John and Worthen, 1875

Phoebodus cf. turnerae

Figure 5.3.5-7

Material. One tooth from sample OH-4, Gumhole Formation, Oscar Hill, Famennian.

Description. Tooth within complete crown, comprising a single medial cusp flanked by two mesio-distally diverging lateral cusps (Figure 5.3.5-6). The central cusp is broken with a faint sub ovoid basal outline (Figure 5.3.5). The lateral cusps are rounded along the lingual margins and flattened on the labial face. Faint vertical striations are preserved on the baso-labial face of one cusp (Figure 5.3.6). The base is sub-rectangular in outline with well-rounded margins (Figure 5.3.7). A large lenticular button, with a single medially located canal, is positioned centrally on the

lingual face of the base and extends between the mesial margins of the lateral cusps (Figure 5.3.5). The labial face of the base is thickened and borders a well-developed concave under-surface.

Remarks. This tooth resembles *Phoebodus turnerae* Ginter and Ivanov, 1992 in having a rounded, lingually extended base and hemispherical button perforated by a large canal along its lingual face. The thin, sub-parallel cristae diagnostic of this species are not clearly recognisable on this tooth; however, faint ornament is present on the baso-labial face of the broken lateral cusp (Figure 5.3.6). The rounded nature of the tooth and low relief of the button may be due to abrasion consistent with the high energy shoal facies from which this tooth was recovered. The current upper age range for *Ph. turnerae* is from the lower (*crepida* CZ) to middle (*marginifera* CZ) Famennian (Ginter et al., 2010) whereas the Oscar Hill area is dated as latest Famennian (Nicoll and Druce, 1979), and suggests either the tooth does not belong to *Ph. turnerae,* or the range of *Ph. turnerae* extends into the late Famennian in the Canning Basin. Further phoebodont teeth need to be recovered, along with more precise age constraints, before the taxonomy of this tooth can be resolved.

Genus THRINACODUS St. John and Worthen, 1875

Type Species. *Thrinacodus nanus* St. John and Worthen, 1875

Thrinacodus ferox (Turner, 1982)

Figure 5.3.8-11

v. 1982 *Harpago ferox* sp. nov.; Turner, pp. 119, 121-122, figs. 2-4.

v. 1985 *Harpagodens ferox* Turner; Wang and Turner, pp. 226-227, pl. 2, figs. 11-12.

v. 1989 *Harpagodens ferox* Turner; Wang, pp. 105-106, pl. 28, figs. 6-7, pl. 29, fig. 2a, b, pl. 30, figs. 1-4.

v. 1991 *Thrinacodus* (*Harpagodens*) *ferox* Turner; Turner, fig. 6, pl. 2, fig. G.

v. 1992 cf. *Thrinacodus ferox* Turner; Kietzke and Lucas, p. 18, fig. 2D-H.

v. 1993 *Thrinacodus ferox* Turner; Turner, fig. 8.7F.

v. 1996 *Thrinacodus ferox* Turner; Ginter and Ivanov, p. 267, figs. 1, 2C-D.

v. 1999 *Thrinacodus ferox* Turner; Ginter, p. 34, pl. 3, figs. 1-3, 5-7.

v. 1999 *Thrinacodus* sp. Ivanov, p. 273, pl. 4, figs. 2-4.

v. 2001 *Thrinacodus ferox* Turner; Ginter, p. 719, figs. 3C-E, 4A-C.

v. 2003 *Thrinacodus incurvus* Duncan, pp. 119-120, figs. 5-6.

v. 2010 *Thrinacodus ferox* Turner; Ginter and Turner, p. 1669, fig. 3A-H.

v. 2010 *Thrinacodus ferox* Turner; Ginter, Hampe and Duffin, p. 41, fig. 33B-F.

v. 2011 *Thrinacodus ferox* Turner; Habibi and Ginter, pl.1, fig. A-B.

v. 2011 *Thrinacodus ferox* Turner; Ivanov and Lucas, p. 55, fig. 3A-L.

v. 2012 *Thrinacodus ferox* Turner; Behan, Walken and Cuny, p. 1249, fig. 3A-M.

Material. Eight teeth from sample 198404, 12 from TS-1, and nine teeth from sample LG-1, Laurel Formation, Laurel Downs, Tournaisian.

Description. Tricuspidate teeth with symmetrical (Figure 5.3.11) to highly asymmetrical forms (Figure 5.3.10). All cusps are strongly inclined lingually, circular in cross section and typically bear faint striations on both lingual and labial faces. The symmetrical tooth form (WAM 15.6.9, Figure 5.3.10-11) is incomplete but comprises a crown and three cusps with equally sized basal circumferences. Asymmetrical teeth comprise one enlarged lateral cusp, a second medial cusp approximately one-third to two-thirds its size and the third smaller lateral cusp varying from a quarter of the size of the central cusp to equal in proportion. The

tooth base is elongate lingually and when preserved, shows a greater than 45 degrees of torsion towards the distal end of the base. A large canal is present on the occlusal face of the base (Figure 5.5.3.8-11) with a few smaller foramina on both the lingual and labial faces of the base (Figure 5.5.3.10).

Remarks. We consider both the symmetric and asymmetric teeth to be from the one species due to the gradation from symmetric to asymmetric forms recovered from the sample. The presence of just one symmetrical tooth (Figure 5.3.11) supports Turner's (1982, figure 5) reconstruction of the *Thinacodus ferox* Turner, 1982 jaw placing the symmetrical forms in a symphyseal position of the jaw and the asymmetric teeth in more lateral positions. The teeth with lower degrees of symmetry (Figure 5.3.9) were not figured in the original description (Turner, 1982) but appear similar in form to end member teeth figured in a reconstruction of *Thrinacodus incurvus* Newberry and Worthen, 1866 by Duncan (2003).

Among the teeth attributed to *Th. ferox*, are six significantly smaller teeth. These teeth typically have a well-formed base; however, the cusps are shorter than in larger specimens and bear well-rounded apices (Figure 5.3.8). It is possible the teeth belong to juvenile specimens and the susceptibility to wear contributed to the well-rounded cusps.

Distribution and stratigraphic range. In Australia Th. ferox is recorded from the latest Famennian in Queensland (Turner, 1982) and Tournaisian in both the Canning and Carnarvon basins of Western Australia (Trinajstic et al., 2014) and New South Wales (Turner, 1982). Globally, Th. ferox is known from the Famennian in southern China (Wang, 1993), Germany (Ginter, 1999), Morocco (Derycke, 1992; Derycke et al., 2008) and Utah, USA (Ginter, 2001). Teeth have also been recorded around the Devonian-Carboniferous boundary in New Mexico, USA (Kietzke and

Lucas, 1992). Thrinacodus ferox is known from the Mississippian in the South Urals and Moscow syncline Russia (Ivanov, 1996), Belgium (Delsate et al., 2003), Ireland (Duncan, 2003).

Superorder CLADODONTOMORPHI Ginter, Hampe and Duffin, 2010

Order SYMMORIFORMES Zangerl, 1981

Family STETHACANTHIDAE Lund, 1974

Genus STETHACANTHUS Newberry, 1889

Stethacanthus ? sp.

Figure 5.3.12-16

Material. Two teeth from sample TS-1, Laurel Formation, Laurel Downs, Tournaisian.

Description. The description is primarily based on the most intact specimen (WAM 15.6.7, Figure 5.3.12-16) in which the tooth crown includes three (Figure 5.3.14-16) to four cusps (Figure 5.3.12). The tooth possesses a distinct and highly elongate medial cusp with a basal width occupying approximately one-third of the mesio-distal length crown (Figure 5.3.14-16). Two small, rounded lateral cusps are directed approximately 45 degrees from the centre of the tooth. The larger specimen (WAM 15.6.6, Figure 5.3.12) bears a single smaller, laterally-divergent cusplet between the medial and lateral cusp. The cusps are relatively smooth apart from very faint vertical ridges on specimen WAM 15.6.7 (Figure 5.3.16). In the smaller specimen (WAM 15.6.7) the base extends lingually beyond the crown and is roughly rectangular in outline (Figure 5.3.15). The lingual margin is rounded with a small central indentation. The lateral margins of the base extend furthest at the corner of the lingual margin. In the larger specimen the base is asymmetrical, having a roughly

ovoid outline (Figure 5.3.12). A distinct crown-base interface is lacking on the labial face of the tooth (Figure 5.3.16) with only a slight thickening along the baso-labial margin. An ovoid button, approximately the same width as the base of the central cusp (Figure 5.3.14), is located close to the lingual margin of the tooth base. A large canal opening is positioned in the centre of the button (Figure 5.3.14) with the opposing end on the underside of a very shallow concave base (Figure 5.3.13).

Remarks. Stethacanthid affinities are suggested by the elongate and thin, biconvex central cusp, the lack of a baso-labial depression (with slight labial projection under the main cusp) and a large foraminal opening on the lingual face of the orolingual button (Duffin and Ginter, 2006). Furthermore, the larger tooth, which bears a single intermediate cusplet, suggests some of the teeth belonging to this species may be pentacuspid.

Order CTENACANTHIFORMES Glikman, 1964

Family CTENACANTHIDAE Dean, 1909

Genus CLADODUS Agassiz, 1843

Cladodus thomasi Turner, 1982

Figure 5.4.1-7

v. 1959 “Cladodont”; Thomas, p. 36, fig. 4a.

v. 1982 *Cladodus thomasi* sp. nov.; Turner, pp. 125, 127, figs. 6C, 7J.

Material. Four teeth from sample 198404, two teeth from sample 198480, eight teeth from TS-1, Laurel Formation, Laurel Downs, Tournaisian.

Revised diagnosis. Teeth with nine cusps; a large central cusp, a pair of large lateral cusps and three smaller pairs of intermediate cusplets (Figure 5.5.4.1-4). The central

cusp is the largest followed by the outer cusps, which diverge in a slight distal direction. The first and third lateral cusps are small, approximately a quarter to one-

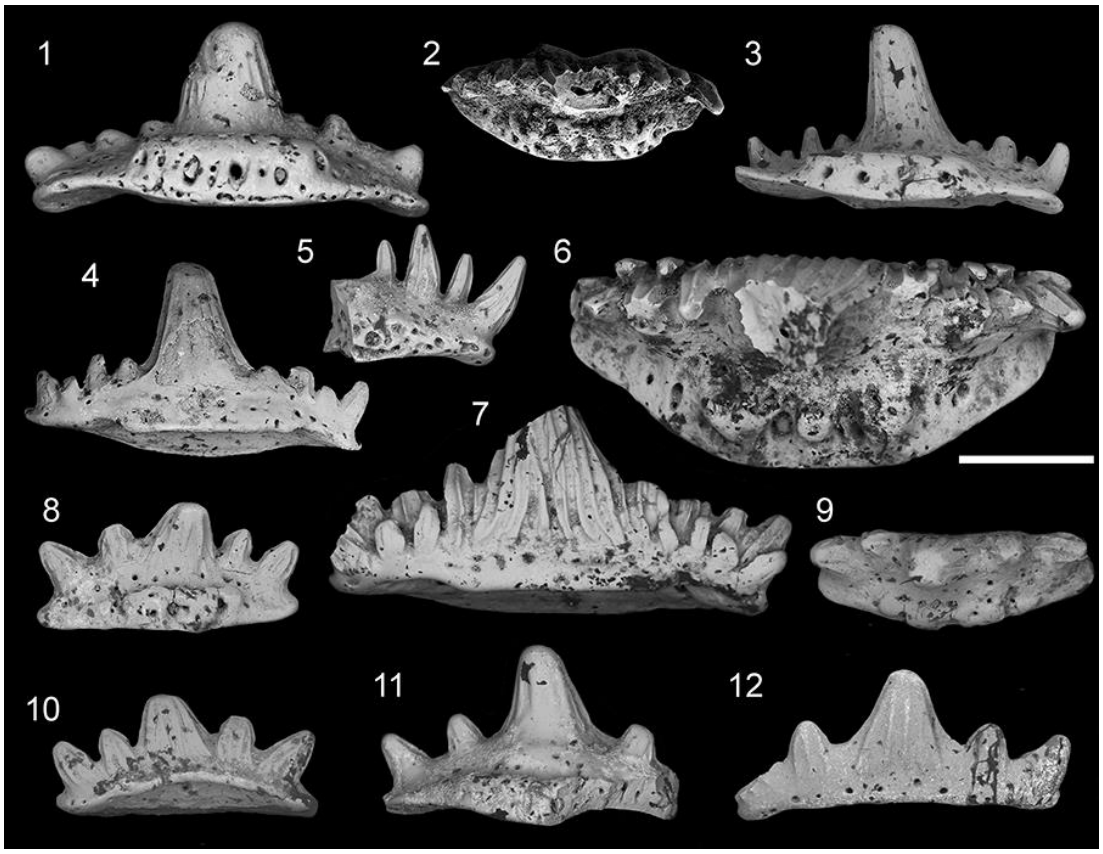

Figure 5.4. Ctenacanthiform teeth from the Lower Carboniferous Laurel Formation, Laurel Downs, Lennard Shelf, Canning Basin, Western Australia. **1 - 7,** *Cladodus thomasi*, WAM 15.6.50, sample 198404, in lingual view (**1**), WAM 15.6.25, sample 198404, in occlusal view (**2**), WAM 15.6.12, sample 198404, in lingual (**3**) and labial views (**4**), WAM 15.6.19, sample 198404, partial platform and crown in lingual view (**5**), and WAM 15.6.13, sample TS-1, in occlusal (**6**) and labial (**7**) views; **8 - 12**, *Cladodoides*cf. *wildungensis*, WAM 15.6.15, sample 198404, in lingual (**8**), occlusal (**9**) and labial (**10**) views, WAM 15.6.16, sample 198404, in labial (**11**) and lingual (**12**) views. Scale bar length: **1 - 7**, 1 mm; **8 - 10**, 0.25 mm; **11 - 12**, 0.5 mm.

third the size of the lateral cusps (Figure 5.4.5). The second pair of intermediate cusplets are almost equal in size to the outer lateral cusps. Converging ridges are present on the base of the main cusp (Figure 5.4.7) whereas the lateral cusps all bear strong, non-bifurcating ridges (Figure 5.4.6-7). The central cusp bears a slight depression along the baso-labial face and is rounded along the lingual face. A secondary row of small labial cusplets is present on the crown base of larger teeth (Figure 5.4.6-7). The basal outline is lozenge shaped in smaller teeth (Figure 5.4.2)

becoming trapezoid in larger specimens (Figure 5.4.6). An elongate oro-lingual button bearing four canal openings abuts the lingual margin. Small foramina accompany the pore canals on the lingual and the occlusal surface of the oro-lingual button. A row of small foramina also occur within an arched groove on the labial surface immediately below the crown-base interface (Figures 5.4.4, 5.4.7). A baso-labial shelf extends between the first set of lateral cusplets and is slightly thickened at the distal edges (Figures 5.4.4, 5.4.7). A shallow depression is present on the labial underside of the base, which also bears multiple canal openings. The lingual portion of the base is flattened under the oro-lingual button but may be flared occlusally along the distal edges of the lingual margin (Figures 5.4.1, 5.4.3).

Description. Teeth range in size from 2.2 mm to 90 mm in length, mesio-distally. The crown includes a prominent triangular central cusp, which is flattened to depressed along the labial margin and convex along the lingual face (Figure 5.4.6). A pair of lateral cusps and three pairs of intermediate cusplets flank both sides of the medial cusp. The outermost cusps are the largest and approximately one quarter larger than the second lateral cusplets. The first and third pairs of intermediate cusplets are of smaller size, ranging from a quarter to half the size of the lateral cusps (Figures 5.4.3, 5.4.5). Prominent, non-bifurcating ridges are present on both the labial and lingual faces of each lateral cusp. Larger specimens (Figure 5.4.6-7) show a small row of cusplets along the baso-labial face of the crown. Small teeth show a more lenticular outline to the base (Figure 5.4.2). A roughly trapezoid basal outline with rounded edges (Figure 5.4.6) is present in larger specimens. An elongate ovoid button, extending between the inner margins of the second pair of lateral cusps, is positioned close to the lingual rim and is perforated by four canal openings on the lingual face. A small baso-labial shelf, between the first lateral cusps, borders

an often weakly developed baso-labial depression below the central cusp (Figure 5.4.4).

Remarks. The original diagnosis of *Cladodus thomasi* Turner, 1982 was based on a small tooth from the Upper Bundock Formation, Queensland (Holotype UQG F73007) as well as a tooth partially obscured by matrix (Thomas, 1959, figure 4a) collected from the Laurel Formation in the vicinity of Twelve Mile Bore (Figure 5.1). The teeth recovered here, also collected from the Laurel Formation, conform to the original diagnosis for this species in addition to providing further diagnostic characters which allow for these teeth to be reassigned to the genus *Cladodus*. The central cusp morphology of *C. thomasi*, with its flattened labial face and convex lingual surface (Figure 5.4.6), is quite different to the biconvex cusp-type in *Stethacanthus*. *Cladodus thomasi* is further differentiated from *Stethacanthus* by multiple intermediate cusps. The baso-labial shelf and elongate oro-lingual ridge, typical of the genus *Cladodus*, are also found in *C. thomasi*.

The new specimens of *C. thomasi* from the Canning Basin have highlighted previously undescribed variation in tooth morphology. Differences are typically seen in the basal outline with smaller teeth possessing a more lozenge shaped outline that becomes more trapezoid in form as the size of the tooth increases. Further variation is present in some of the larger teeth (Figure 5.4.6-7) which bear a second small row of labial cusplets. These accessory cusplet rows are also found in other Carboniferous ctenacanthiform teeth such as *Tamiobatis vetustus* Eastman, 1897 (Williams, 1998, figure 5A-B) and *Saivodus striatus* Agassiz, 1843 (Ginter et al., 2010, figure 72A-B).

Several Famennian cladodont teeth, possessing a single intermediate cusplet, were previously attributed to "*Stethacanthus" thomasi* (Derycke, 1992, plate 2:10-

11; Hampe, 2000, plate 2:1-4). Given the morphological variation and large number of teeth, it is clear the teeth of *C. thomasi* possess three sets of intermediate cusplets, independent of the tooth size. This suggests the teeth figured in Derycke (1992) and Hampe (2000) are unlikely those of *C. thomasi* but instead belong to another ctenacanthiform shark. The tooth (MCD 177) formally figured by Derycke (1992, figure 14, plate 2: 10, 11) was synonymised firstly with *Stethacanthus resistens* Ginter, 2002 and then with *Cladodoides wildungensis* by Ginter et al., (2010), who also suggested many of the teeth formally attributed to "*Stethacanthus thomasi*" belong to *C. wildungensis*.

Cladodus thomasi was considered as a junior synonym of *Stethacanthus obtusus* Trautschold, 1874 by Lebedev (1996); however, Hampe (2000) noted *S.obtusus* had a greater number of cusps than *C. thomasi* in addition to more foramina along the edge of a less distinguished button and therefore the species determination of *S. thomasi* was retained. The holotype of *C. thomasi* (Turner, 1982, figure 6C) is an asymmetric tooth possessing eight cusps. The newly recovered teeth of *C. thomasi* indicate the possession of nine cusps is common for these teeth, similar to *S. obtusus*. The lingual button appears more developed in *C. thomasi*, as noted by Hampe (2000) and typically possesses four large foramina on the lingual face. In comparison, *S. obtusus* is described as possessing two to six large foramina. The larger forms of *C. thomasi*, comparable in size to *S. obtusus* figured by Lebedev (1996), possess a distinct secondary row of cusplets along the labial face of the tooth, a feature lacking in the 40 specimens of *S. obtusus*. Further distinguishing *C. thomasi* from the Canning Basin is the shape of the base, which takes on a more trapezoid form in larger specimens compared to the lozenge shape seen in *S. obtusus*. The baso-labial shelf is also more elongate in *S. obtusus*, than *C.*

thomasi, extending to the medial cusplets. In *C. thomasi* the baso-labial shelf only extends between the distal margins of the first pair of intermediate cusplets. We believe these differences are sufficient for *C. thomasi* to be retained as a distinct species.

We note there are similarities between the teeth, designated here as *C. thomasi* and *Tamiobatis* sp. (Ginter and Sun, 2007) from Muhua, south China, including the presence of three pairs of intermediate lateral cusplets, that alternate in height, as well as a basal outline, which extends lingually furthest in front of the lingual button. However, the teeth from the Canning Basin are distinct in that they lack a small lateral cusplet often present in the teeth from Muhua and have a far more angular basal outline. The teeth of *Tamiobatis* sp. (Ginter and Sun, 2007) also lack the row of accessory labial cusplets despite being of comparable size to the teeth of *C. thomasi*. Another member of the genus, *Tamiobatis vetustus* Eastman, 1897 (Williams, 1998), is known for the presence of labial cusplets, however they are present behind the main cusp, a feature not found in the teeth of *C. thomasi* (Figure 5.4.7). Although there are some features of the genus *Tamiobatis*, which are present in the teeth of *C. thomasi*, the greater number of morphological differences precludes these teeth from being assigned to *Tamiobatis.*

Distribution and stratigraphic range. Given the revised diagnosis, *C. thomasi* is restricted to the Lower Carboniferous of Australia. Teeth have been recovered from the Lower Carboniferous upper Bundock Formation, North Queensland and from the Tournaisian Laurel Formation, Canning Basin, Western Australia.

Cladodoides cf. *wildungensis*

Figure 5.4.8-12

Material. Three teeth from sample 198404, one tooth from sample 198480, two teeth from sample TS-1, Laurel Formation, Laurel Downs, Tournaisian.

Description. The pentacuspid crown comprises a large triangular central cusp with a pair of distally diverging lateral cusps and small (approximately two thirds the size of the lateral cusps) intermediate cusplets (Figure 5.4.8-12). Cusp faces are ornamented in coarse, predominantly parallel ridges converging toward the cusp apex (Figures 5.4.8, 5.4.12). The labial face of the central cusp is flattened with a slight baso-labial depression. The base is lenticular in outline (Figure 5.4.9) and extends furthest in front of the central cusp. The crown-base interface is marked by a low arch along the labial face (Figure 5.4.8). The lateral end of the base extends beyond the crown in most specimens; however, this is significantly less extended in one specimen (Figure 5.4.12). A row of small pores is present along the crown base interface on the labial side. An ovoid button extends between the distal margins of the intermediate cusplets and is positioned centrally along the occlusal edge of the baso-lingual rim. The baso-labial thickening lies between the intermediate cusps and does not protrude far lingually (Figures 5.4.10, 5.4.12).

Remarks. The teeth bear a resemblance to the teeth originally described as *Stethacanthus resistens* by Ginter (2002) and later synonymised with *Cladodoides wildungensis* Jaekel, 1921 (Ginter et al., 2010). The teeth from the Canning Basin share the pentacuspid crown and strong divergence of the lateral cusps seen in the smaller tooth forms of *C. wildungensis* (Ginter et al., 2010, figure 66F). The basal features are also comparable, with an elongated lenticular base extending beyond the crown foot as well as possessing the mesio-distally elongated lingual button. Despite these similarities, the cusps on the Canning Basin teeth appear shorter and more robust than those seen in teeth attributed to *C. wildungensis*, including the holotype

(Ginter et al., 2010, figure 66). Similar teeth with shorter cusps are evident in a tooth from the Famennian of north-western Iran (Hampe, 2000, plate 2.1-4). Whether these Carboniferous forms belong to *C. wildungensis* is difficult to determine given the limited number of teeth recovered.

Cladodontomorphi indet. sp.

Figure 5.5.1-5

Material. One tooth from sample 198404, Laurel Formation, Laurel Downs, Tournaisian.

Description. Asymmetrical tooth comprising five cusps with a large laterally inclined medial cusp and a pair of diverging lateral cusps approximately twice the size of the intermediate cusplets (Figure 5.5.1). There are fine ridges on the cusp faces with bifurcating ridges on the basal margins of the lateral cusps (Figure 5.5.1-3). The labial face of the crown is concave at the base with a row of small pores along the base-crown limit. The lingual extension of the base is short and almost trapezoid in outline, extending furthest between the mesial margins of the lateral cusps (Figure 5.5.4-5). There is a slight lateral extension of the base where it forms a laterally directed point (Figure 5.5.4). The lingual torus hosts a highly elongate ridge, which along the lingual face. The oro-lingual ridge is thickened at its termination point on one distal end and gradually reduces its size at the other (Figure 5.5) The baso-labial shelf is thickest between the accessory cusps, becoming less distinct at one distal margin as opposed to thickening at the other end (Figure 5.3-4). The underside of the tooth bears a shallow depression under the lingual torus that deepens below the main cusp (Figure 5.5.4).

Remarks. This tooth bears a few features associated with the genus *Cladodus*. These

include a central cusp, which is short and triangular in form, as well as an elongate

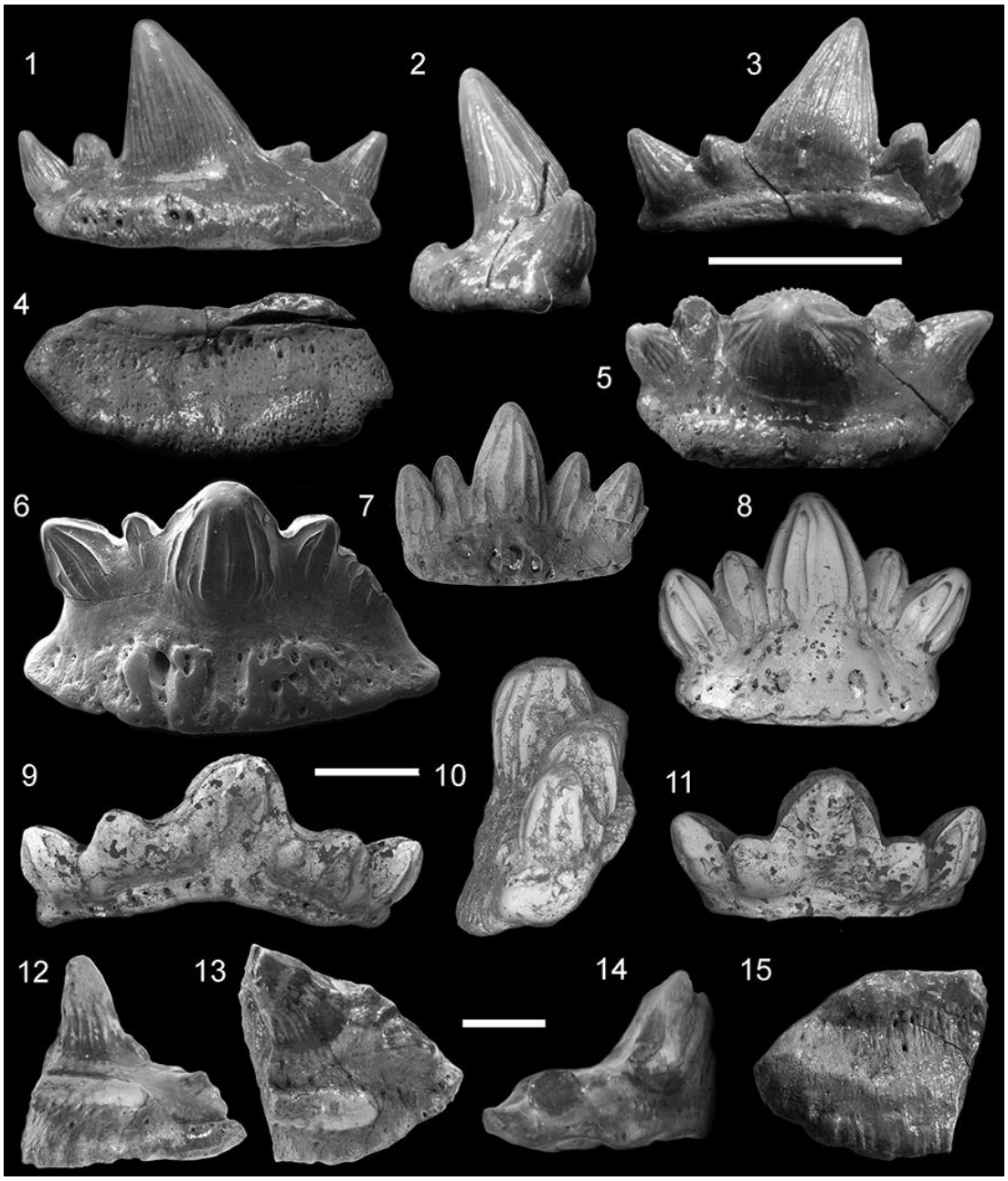

Figure 5.5. Ctenacanthiform teeth from the Lower Carboniferous Laurel Formation, Laurel Downs, Lennard Shelf, Canning Basin, Western Australia. **1 - 5,** Cladodontomorphi indet. sp., WAM 15.6.5, sample 198404, in lingual (**1**), lateral (**2**), labial (**3**), basal (**4**) and occlusal (**5**) views; **6 - 11,** Ctenacanthiform gen. et sp. indet. 1, WAM 15.6.24, sample 198404, in lingual view (**6**), WAM 15.6.36, sample TS-1, in lingual view (**7**), WAM 15.6.35, sample TS-1, in lingual view (**8**), WAM 15.6.37, sample TS-1, in labial (**9**) and lateral (**10**) views, and WAM 15.6.35, sample TS-1, in labial view (**11**); **12 - 15,** Ctenacanthiform gen. et sp. indet 2, WAM 15.6.3.8, in lingual (**12**), occlusal (**13**), labial (**14**) and basal (**15**) views. Scale bar length: **1-5**, 10 mm; **6-11**, 0.5 mm; **12-15**, 5 mm.

baso-labial shelf and long oro-lingual ridge. The tooth resembles *Cladodus marginatus*Agassiz, 1843 (figured in Duffin and Ginter, 2006, figure 3A-G) with its

broad, robust based central cusp directed distally to one side. In addition, the central cusp is biconvex apart from the baso-labial portion where a shallow depression develops. In contrast to *C. marginatus*, the tooth here bears much finer ridges that cover the entirety of each cusp. In *C. marginatus* the ridges terminate approximately halfway up the cusp from the crown-base interface, with the majority of the upper central cusp surface remaining smooth.

Ctenacanthiform gen. et sp. indet. 1

Figure 5.5.6-11

Material. Three teeth from sample 198404, one tooth from sample 198480, four teeth from sample TS-1, Laurel Formation, Laurel Downs, Tournaisian.

Description. The tooth crown comprises a bulbous central cusp flanked by a pair of intermediate cusplets and a pair of lateral cusps diverging distally from the crown centre (Figure 5.5.6-8). The intermediate cusplets erupt from a more labial position on the crown (Figure 5.5.9-11) and are strongly fused mesially and distally with the neighbouring cusps. Both cusp faces bear ridges, rarely bifurcating at the base. The base forms a lenticular outline, extending lingually and, in some specimens, mesio-distally beyond the crown base (Figure 5.5.6). The lingual face of the base forms a steep angle between the lingual margin and the crown-base interface. In some specimens the basal height along the lingual face exceeds that of the crown. An oro-lingual ridge is often poorly developed; however, a series of canals can be found on some specimens, running from the lingual edge of the oro-lingual ridge to almost the crown base interface (Figure 5.5.6). A row of foramina along an elongate baso-labial shelf extend between the far lateral cusps (Figure 5.5.9).

Remarks. The tooth crowns are quite distinct in comparison to other cladodont type teeth in that the cusps are highly fused, up to two-thirds of the intermediate cusps with the lateral and central cusps (Figures 5.5.9, 5.5.11). Low profiled and similarly fused teeth belonging to *Tamiobatis vetustus* Eastman, 1897 were recovered from the Cleveland Shale of Ohio, USA (Williams, 1998, figure 5E-F). Williams (1998) suggested these teeth represent the posterior teeth of the shark thereby indicating an unusual degree of heterodonty in this group of sharks. Whether this explains the unusually compact nature of the teeth described here is unclear. The differences in mesio-distal elongation, suggests these teeth occupy a range of positions in the jaw rather than just representing the posterior teeth of one species. The small sample size makes it difficult to correlate any impacts of ontogeny on tooth form. However, a comparison between the smallest tooth (Figure 5.5.7) and the largest tooth (Figure 5.5.6), suggests the highly compacted nature of the cusps is not a feature of either juvenile or adult teeth but is a unique character for this species.

Ctenacanthiform fam. gen. et sp. indet. 2

Figure 5.5.12-15

Material. 1 partial tooth from sample TS-1, Laurel Formation, Laurel Downs, Tournaisian.

Description. Only a small distal portion of the central cusp and part of the lingual torus are preserved (Figure 5.5.12-15). The remnant of a large central cusp as well as the basal outline of a lateral cusp and intermediate cusplet can be detected. The baso-lingual face of the lateral cusp is approximately twice the size of the basal outline of the intermediate cusplet (Figure 5.5.13). Approximately one-third of the distal side of the central cusp is preserved. The basal part of the central cusp shows a slight

convexity of the lingual face, whereas the labial face is flattened. In unabraded areas, the lingual faces of both the central and lateral cusps bear thin vertical striae (Figure 5.5.12-13). The distal limit of a baso-labial depression can be seen on the central cusp (Figure 5.5.14). A row of faint foramina runs along the crown-base interface on the labial side of the tooth. The base extends lingually with the preserved part of the crenulated lingual rim showing a gentle curvature (Figure 5.5.15). Part of a well-defined, elongate oro-lingual button is positioned midway between the crown base and the lingual margin and extends from the broken face of the tooth to the base of the intermediate cusp. A thickened but incomplete baso-labial shelf lies between the broken edge of the distal margin of the central cusp and the mesial margin of the lateral cusp.

Remarks. The small fragment of the tooth does not preserve many of the diagnostic features in their entirety and makes any in depth comparisons difficult. The preserved end of the baso-labial shelf extends to the basal part of the lateral cusp and appears slightly thickened. The preserved section of the oro-lingual ridge is straight and extends to the inner edge of the lateral cusp base. These features indicate affinities to the Ctenacanthiforms. The oro-lingual button on many *Cladodus terrelli* Newberry, 1889 teeth is similar in shape and positioned centrally on the lingual torus, extending between the inner margins of the lateral cusps. The thin nature of the baso-lingual margin and vertical ridges are similar to those on the teeth of *Cladodus terrelli*.

Cohort EUSELACHII Hay, 1902

Superfamily PROTACRODONTOIDEA Zangerl, 1981

Family PROTACRODONTIDAE Cappetta, Duffin and Zidek, 1993

Genus PROTACRODUS Jaekel, 1925

Type Species. *Protacrodus vestustus* Jaekel, 1921

Protacrodus aequalis Ivanov, 1996

Figure 5.6.1

v. 1982 *Protacrodus* sp. 'C'; Turner, pp. 125-126, fig. 7.

v. 1994 *Protacrodus* sp. C; Ivanov and Lukševičs, pp. 25-26, fig. i, j.

v. 1996 *Protacrodus aequalis* sp. nov.; Ivanov, p. 423, fig. 6A-G.

v. 1999 *Protacrodus aequalis* Ivanov; Ginter and Turner, p. 113, fig. 7A-C.

v. 2000 *Protacrodus aequalis* Ivanov; Ginter and Ivanov, p. 339, pl. 2I.

v. 2005 *Protacrodus* sp. 3; Derycke-Khatir, pp. 64-65, pl. VIII, fig. 8.

v. *2010 Protacrodus aequalis* Ivanov; Ginter, Hampe and Duffin, p. 87, fig. 80D, E.

v. 2011 *Protacrodus aequalis* Ivanov; Ivanov and Lucas, p. 58, fig. 6A-L.

Material. One tooth from sample TS-1, Laurel Formation, Laurel Downs, Tournaisian.

Description. Tooth with a tricuspid crown, comprising a central cusp and two lateral cusps diverging at 45 degrees from the base (Figure 5.6.1). The cusps are compressed labio-lingually, and short and wide in lingual view. The central cusp is slightly larger than the lateral cusps, which are fused at the base to the central cusp. The cusps are all ornamented with strong cristae, which converge at the cusp apices (Figure 5.6.1). The base is bulbous with a rounded lingual extension covered by small pores. A row of small foramina occur above a slightly arched crown-base interface on the labial side.

Remarks. The symmetrical nature of the tooth is unusual in comparison to the majority of teeth attributed to this species. Typically, the crown of *P. aequalis* comprises cusps that are inclined to a distal side. A similar symmetrical tooth, is figured in Ivanov (1996, figure 6F) but shows a pair of lateral cusps with less distal divergence than the tooth from the Canning Basin. The symmetrical nature of this tooth suggests placement within symphyseal region of the mandible and possibly explains the low numbers recovered.

Distribution and stratigraphic range. Recorded from the early Famennian in Arctic Canada (Ginter and Turner, 1999), middle Famennian of Latvia (Ivanov and Lukševičs, 1994) and the late Famennian in New Mexico, USA (Ivanov and Lucas, 2011). Within the South Urals, Russia, this species is known from the latest Famennian to early Tournaisian (*sulcata* CZ; Ivanov, 1996). In Australia, *P.aequalis* is known from the Famennian in Queensland (Turner, 1982) and the Tournaisian in the Canning Basin, Western Australia. This species has also been recorded from the Tournaisian in Belgium (Derycke-Khatir, 2005).

Protacrodus sp. 1

Figure 5.6.2-4

v. 2011 *Protacrodus* sp.; Habibi and Ginter, p. 39, pl. 2b-e.

Material. One tooth from sample TS-1, Laurel Formation, Laurel Downs, Tournaisian.

Description. Crown is thin labio-lingually with five cusps; a large triangular central cusp and two pairs of lateral cusps diminishing in size distally (Figure 5.6.2). The central cusp is three times the size of the first lateral cusps and makes up approximately half the size of the crown (Figure 5.6.2, 5.6.4). The second pair of

lateral cusps is approximately half the size of the first pair and diverge at approximately 45 degrees from the centre of the crown. Coarse cristae are present on both faces of the crown. On the labial face, the cristae thicken around the crown base

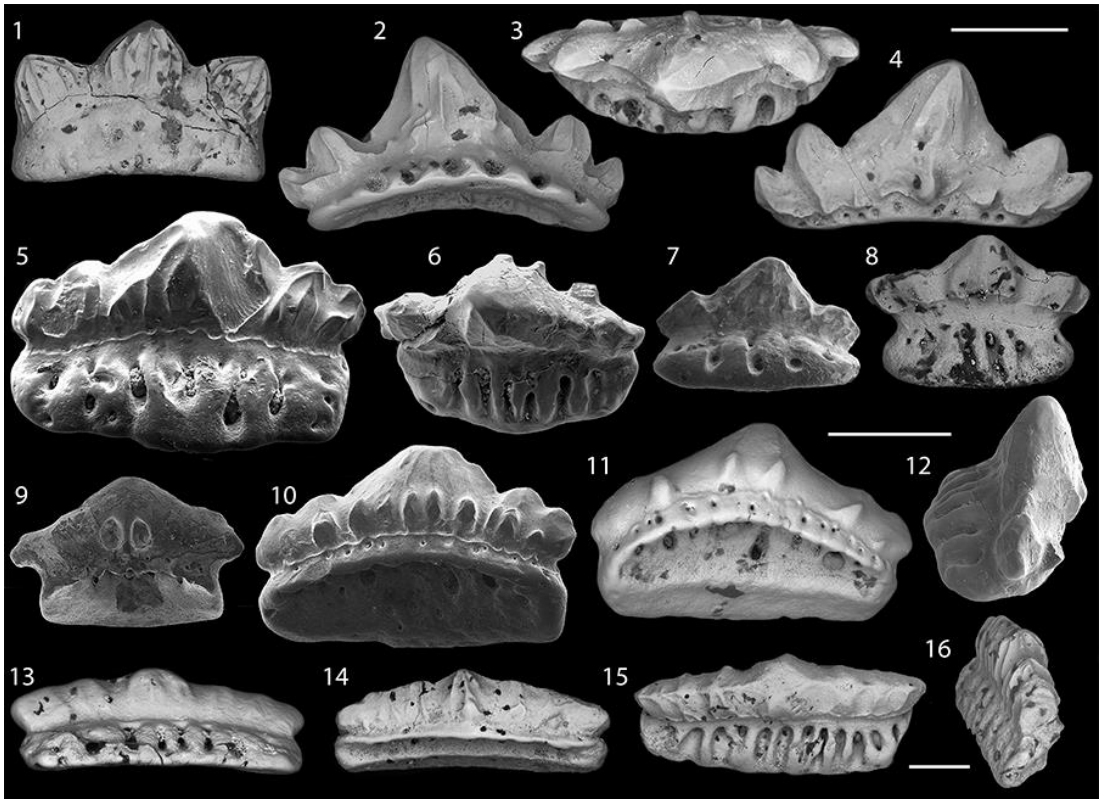

Figure 5.6. Protacrodont teeth from Lower Carboniferous Laurel Formation, Laurel Downs, Lennard Shelf, Canning Basin, Western Australia. **1,** *Protacrodus aequalis*, WAM 15.6.43, sample TS-1, in lingual view (**1**); **2 - 4,** *Protacrodus* sp. 1, WAM 15.6.45, sample TS-1, in lingual (**2**), occlusal (**3**) and labial (**4**) views; **5 - 12,** *Deihim mansureae*, WAM 15.6.17, in lingual view (**5**), WAM 15.6.18, sample 198408, in occlusal view (**6**), WAM 15.6.46, sample TS-1, in lingual view (**7**), WAM 15.6.48, sample TS-1, in lingual view (**8**), WAM 15.6.19, sample 198404, in labio-basal view (**9 10**), WAM 15.6.49, sample TS-1, in labio-basal view (**11**), and WAM 15.6.18, sample 198404, in lateral view (**12**); **13-16,** *Dalmehodus* cf. *turnerae*, WAM 15.6.30, sample LG-1, in lingual (**13**) and labial (**14**) views, WAM 15.6.44, sample TS-1, in occlusal (**15**) and lateral (**16**) views. Scale bar length: **1 - 45-12**, 1 mm; **13 16**, 0.25 mm.

interface to the extent they resemble small cusplets (Figure 5.6.3-4). In outline, the base is straight along the labial face with a gently curved lingual margin (Figure 5.6.3). The lingual face of the base is perforated by a row of large canals that decrease in size toward the distal margins. The labial face of the base is thin and gently arched with a single row of small pores (Figure 5.6.4).

Remarks. The tooth superficially resembles *Deihim mansureae* Ginter, Hairapetian and Klug, 2002 but differs in that the central cusp in Protacrodus sp. is more pronounced with the lateral cusps not as highly fused as they are in *D. mansureae*. In addition, the tooth described here bears a shorter lingual extension of the base and lacks the characteristic cusplets. The crown and basal morphologies bear a very strong resemblance to Protacrodus sp. teeth figured in Habibi and Ginter (2011, plate 2, figure b-e). The basal canals in the specimen from the Canning Basin are focused into a single row. The cristae around the crown-base interface on the labial side are also far coarser. These differences, however, do not appear significant enough to separate these species and so we determine this tooth belongs to the same species as Protacrodus sp. from the Central Alborz Mountains, Iran (Habibi and Ginter, 2011).

Genus DEIHIM Ginter, Hairapetian and Klug, 2002

Deihim mansureae Ginter, Hairapetian and Klug, 2002

Figure 5.6.5-12

v. 2000 *?Protacrodus* sp. ; Long and Hairapetian, pp. 217-218, fig. 4O.

v. 2000 *Protacrodus* sp. *cf. "P. aequalis" sensu* Ginter and Turner; Yazdi and Turner, p. 226, figs. 3.4-7, 4.4.

v. 2002 *Deihim mansureae* gen. et sp. nov.; Ginter, Hairapetian and Klug, pp. 191-193, Figure 10; pl. 1, fig. r; pl. 2, fig. k; pl. 4, figs. f-g, j-m; pl. 5, figs a-m.

v. 2005 *Polyacrodontidae incertae sedis*; Derycke-Khatir, p. 76, pl. VII, figs. 7-10.

v. 2005 *Bobbodus* sp.; Derycke-Khatir, pp. 95-96, pl. XII, figs. 1-2.

v. 2009 *Deihim mansureae* Ginter, Hairapetian and Klug; Hairapetian and Ginter, pp. 176- 179, figs. 2D, 4H.

v. 2010 *Deihim mansureae* Ginter, Hairapetian and Klug; Hairapetian and Ginter, p. 362, fig. 3A.

v. 2010 *Deihim mansureae* Ginter, Hairapetian and Klug; Ginter, Hampe and Duffin, p. 88, fig. 81A-J.

v. 2011 *Deihim mansureae* Ginter, Hairapetian and Klug; Ginter, Hairapetian and Grigoryan, pp. 166-169, figs. 8A-E, 11C.

v. 2011 *Deihim mansureae* Ginter, Hairapetian and Klug; Ivanov and Lucas, p. 60, fig. 8.

v. 2013 *Deihim mansureae* Ginter , Hairapetian and Klug; Habibi, Yazdi, Zarepoor and Shirazi, p. 30, fig. 4.

v. 2015 *Deihim mansureae* Ginter, Hairapetian and Klug; Roelofs, Playton, Barham and Trinajstic, p. 88, text-fig. 6.

Material. One tooth from sample OH-4, Gumhole Formation, Oscar Hill, Famennian; 12 teeth from sample 198404, two teeth from samples 198480, six teeth from sample TS-1, Laurel Formation, Laurel Downs, Tournaisian.

Description. Two different tooth morphotypes can be distinguished. The first tooth type is pentacuspid, comprising a large medial cusp approximately twice as high as the two pairs of highly fused lateral cusps (Figure 5.6.5-6). The crown is ornamented on both faces with coarse cristae. Four to nine cusplets are present on the labial side (Figure 5.6.10-12). A shallow groove marks the crown-base interface on the lingual face of the tooth. The base extends lingually, furthest at the centre of the lingual margin (Figure 5.6.6). A few large canals perforate the occlusal-lingual face of the base from the lingual margin to the crown base. A row of small pores are present along the labial face of the base, immediately below the crown (Figure 5.6.10-11).

The second tooth type is smaller, possessing a large triangular central cusp with one to two pairs of smaller, laterally diverging cusps (Figure 5.6.7-9). Cristae are most prominent on the lingual face of the crown. The labial face of the crown typically bears four cusplets with one tooth (WAM 15.6.19, Figure 5.6.9) possessing a single pair of prominent ovoid labial cusplets. A row of small pores within a shallow trough, mark the crown-base interface on the labial face. The crown-base interface forms a low arch. The base is semi-circular in outline extending distally and lingually beyond the crown base (Figure 5.6.7-8).

Remarks. The teeth bear the diagnostic characters of *D. mansureae*, including the large central cusp, diverging lateral cusps and a row of cusplets along the labial face of the crown. However, these teeth differ from the original morphotypes outlined by Ginter et al. (2002) in regards to cusp number and the variation in size between the central and lateral cusps. The first tooth type recovered from the Canning Basin consists of crowns resembling those of Morphotype 1 (*sensu* Ginter et al., 2002); however, the mesio-distally extended base and low profile of the central cusp is more similar to Morphotoype 2. Examples of Morphotype 3 are lacking from the teeth collected here. The few Morphotype 4 teeth that were recovered (Figure 5.6.7-8) comprise a central cusp that is significantly lower in profile than other examples of this morphotype figured in Ginter et al. (2002, plate 5D-F). The teeth from the Canning Basin do not fully conform to any of the morphotypes originally described (Ginter et al., 2002) and suggests these teeth may belong to a different species than the older Famennian forms found in Iran.

Genus DALMEHODUS Long and Hairapetian, 2000

Dalmehodus cf. *turnerae*

Figure 5.6.13-16

Material. Seven teeth from sample LG-1, 11 teeth from sample 198404 and two teeth from TS-1, Laurel Formation, Laurel Downs, Tournaisian.

Description. Mesio-distally elongated teeth with slightly arched crowns comprising a low central cusp and between two and four almost completely fused lateral cusps that decrease in size distally (Figure 5.6.13-14). The central cusp varies from equal in size to slightly larger than the first pair of lateral cusps. Cusps are ornamented with faint to strong cristae (Figures 5.6.14, 5.6.16). The base is roughly rectangular, extending lingually, and barely developed beyond the crown distally (Figure 5.6.15-16). A row of large furrows are present along the lingual face of the base and extend from the lingual margin of the base to the crown base interface. The labial face of the base is small with a few small pores. The underside of the base is concave below the crown and flattened on the underside of the baso-lingual extension.

Remarks. The teeth resemble those previously attributed to *Dalmehodus turnerae* Long and Hairapetian, 2000, in they possess a low, mesio-distally elongate crown covered in coarse cristae and a lingually short base with a row of rather large foramina. A key feature distinguishing teeth of *D. turnerae* from other protacrodonts is the lack of a discernible size difference between the central and lateral cusps. Typically, the teeth from the Canning Basin bear a central cusp slightly larger than the lateral cusps. Teeth with highly fused cusps figured in Ginter et al. (2011, text-figure 10H) and those in Hairapetian and Ginter (2009, text-figure 4B) most closely resemble the teeth from the Canning Basin and these were attributed to *D.turnerae*. Despite the large number of teeth from the Tournaisian deposits, the variation in

morphology is limited. Teeth resembling the holotype (Long and Hairapetian, 2000, figure 6f) and other specimens (Hairapetian and Ginter, 2009, text-figure 9A-B) with less fusing of the cusps have not been found in samples from the Canning Basin. It may be that the teeth found here, as well as similar forms in Iran (Hairapetian and Ginter, 2009) and Armenia (Ginter et al., 2011), represent different protacrodont species.

Protacrodontidae gen. et sp. indet.

Figure 5.7.1-2

Material. A partial tooth from sample OH-4, Gumhole Formation, Oscar Hill, Famennian.

Description. The preserved part of the crown comprises a large triangular cusp and four smaller lateral cusps (Figure 5.7.1-2) all ornamented with strong linear cristae. The first and second lateral cusps are almost equal in size with the third and fourth cusps diminishing in size distally. On the lingual side of the crown a row of four small rounded cusplets occur between the central and second lateral cusp (Figure 5.7.1). There is a row of larger, more irregularly shaped cusplets on the entire preserved labial side of the crown (Figure 5.7.2). A distinct crown-base interface is lacking on the labial side of the tooth. The base is mesio-distally shorter than the crown but extends lingually and is perforated by small pores.

Order HYBODONTIFORMES Cappetta, Duffin and Zidek, 1993

Superfamily HYBODONTOIDEA Owen, 1846

Family LONCHIDIIDAE Herman, 1977

Genus LISSODUS Brough, 1935

Type Species. *Lissodus africanus* Broom, 1909

Lissodus sp.

Figure 5.7.3-5

Material. One tooth from sample TS-1, Laurel Formation, Laurel Downs, Tournaisian.

Description. Asymmetrical tooth with an arched crown consisting of a high central cusp and a single, almost completely fused lateral cusp (Figure 5.7.3). A broad, rounded labial peg extends labially from the centre of the crown base (Figure 5.7.4). The crown is completely smooth, lacking any form of ornament. The base is labio-lingually narrow and extends lingually and distally beyond the crown base on one side. The crown overhangs a concave trough along the labial side of the base. The base has a row of large canal openings present on the lingual face with corresponding openings on the labial side (Figure 5.7.5).

Remarks. This tooth possesses characters typical of the genus *Lissodus*, including a single central cusp, labial peg and lingually extended base, perforated by large vascular canals. In comparison to other Early Carboniferous *Lissodus* teeth figured in Duncan (2004), the crown is much higher, forming a more pointed apex. The basal features are also distinct, with a row of very large canals on the lingual face of the base and large canal openings along the baso-labial side. The aforementioned features also distinguish the tooth from other Early Carboniferous *Lissodus* teeth listed in Fischer (2008). A reconstruction of the dentition of *Lissodus nodosus* Seilacher, 1943 (Duffin, 1985) and an interpretative reconstruction of *Lissodus* sp. by Duncan (2004) indicate a degree of variation among the tooth morphotypes. It is possible that the unusual features of the tooth described here may be a product of its position in the jaw.

The labial overhang of the main cusp and large canal openings on the base, present in the tooth here, are similar to the teeth of another Hybodont shark, *Cassissodus margaritae* Ginter and Sun, 2007 from Muhua, South China. The tooth however lacks a main diagnostic character of the genus *Cassisodus*, which is the presence of lingual and labial cusplets present on both faces of the crown. The

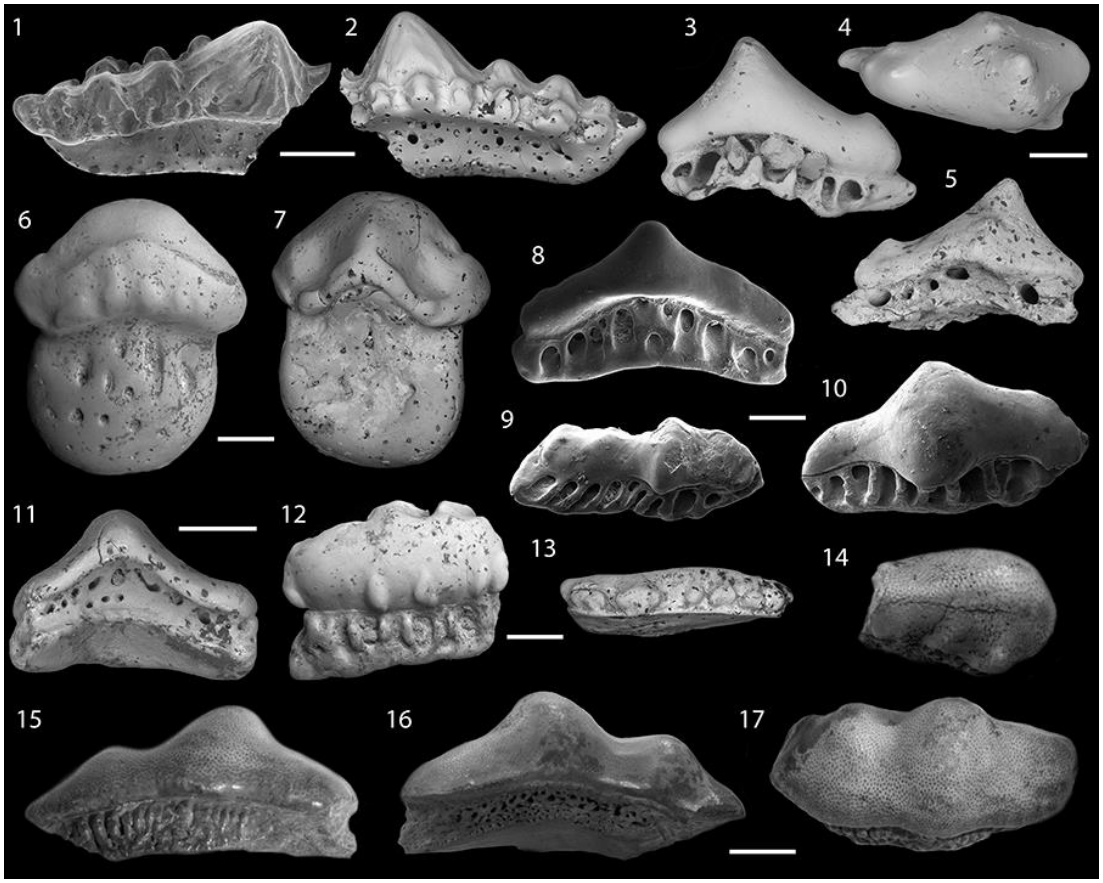

Figure 5.7. Shark teeth from the Upper Devonian Gumhole Formation, Oscar Hill and Lower Carboniferous Laurel Formation, Laurel Downs, Lennard Shelf, Canning Basin, Western Australia. **1 - 2,** Protacrodontidae gen. et sp. indet., WAM 15.6.29, sample OH-4, in lingual (**1**) and labial (**2**) views; **3-5,** *Lissodus* sp., WAM 15.6.42, sample TS-1, in lingual (**3**), occlusal (**4**) and labial (**5**) views; **6 - 7,** Hybodontoidea gen. et sp. indet., WAM 15.6.41, sample TS-1, in lingual (**6**) and labial (**7**) views; **8 - 11,** Euselachii gen. et sp. indet.1, WAM 15.6.21, sample 198404, in lingual view (**8**), WAM 15.6.20, sample 198404, in occlusal view (**9**), WAM 15.6.27, sample 198404, in occluso-lingual view (**10**), and WAM 15.6.39, sample TS-1 in labial view (**11**); **12 - 13,** Euselachii gen. et sp. indet. 2, WAM 15.6.40, sample TS-1, in occluso-lingual view (**12**) and WAM 15.6.22, sample TS-1, in labial view (**13**); **14 -17,** Holocephali gen. et sp. indet. 1, WAM 15.6.4, sample 198404, in occlusal view (**14**), and WAM 15.6.3, sample 198404, in lingual (**15**), labial (**16**) and occlusal (**17**) views. Scale bar length: **1-2**, 0.5 mm; **3 - 5**, 0.4 mm; **6 - 7**, 0.75 mm; **8 - 10**, 0.3 mm; **11**, 1 mm; **12 - 13**, 0.6 mm; **14 - 17** , 5 mm.

possibility of wear or abrasion contributing to the lack of cusplets is unlikely as the crown retains a shiny enameloid surface.

Hybodontoidea gen. et sp. indet.

Figure 5.7.6-7

Material. One tooth from sample TS-1, Laurel Formation, Laurel Downs, Tournaisian.

Description. A well-preserved tooth with a large vertical bulbous crown that overhangs the lingual and distal faces of the base. The lower half of the crown, on the lingual face, is raised and bears a row of low profiled ovoid cusplets running mesio-distally (Figure 5.7.6). A pair of large pits is present on the distal sides of the distinct labial peg (Figure 5.7.7). The crown base interface on the labial side is highly arched with a thickened margin. The lingual margin of the base is semicircular and approximately one and a half times as deep as the crown height. The lingual face is slightly convex and perforated by three horizontally aligned rows of pores (Figure 5.7.6). Small pores are present in and around the concave labial side of the base.

Remarks. This tooth is unusual with the elongate base directed under the crown. The labial peg and fused crown is similar to some Hybodonts such as *Lissodus*. However, the base lacks the large vascular foramina typical of that genus. In overall morphology, the tooth bears a resemblance with a hybodont tooth figured in Ginter and Sun (2007, figure 6A1-3) with the large labial peg, pyramidal crown and deep base orientated directly under the crown.

Euselachii gen. et sp. indet. 1

Figure 7.8-11

Material. Six teeth from 198404, two teeth from 198480, nine teeth from TS-1, Laurel Formation, Laurel Downs, Tournaisian.

Description. Tooth crowns with two morphologies but both with a similar euselachian basal form. The crown and base are separated by a small but distinct lingual groove on the lingual face of the tooth. The base extends lingually and ranges from symmetrical (Figure 5.7.8) to asymmetrical in outline (Figure 5.7.9). A row of large canals extend from baso-lingual margin to the crown base. On the labial face of the tooth, the margin between the crown and base is often marked by a significant concavity (Figure 5.7.11). A large pore network covers the concave underside of the crown whereas the underside of the baso-lingual extension is smooth.

Crown Morphotype 1 is symmetrical in form (Figure 5.7.8) with a high, prominent medial point and steeply tapering margins. The crown is smooth with only faint, rounded cusp type projections along the occlusal surface of some teeth (Figure 5.7.8). The crown margins are rounded and do not overhang the base.

Crown Morphotype 2 is asymmetrical with a large bulbous central cusp overhanging the lingual margin (Figure 5.7.10), and two to three smaller lateral cusps. Tooth crowns with three cusps, possess a slightly flattened and distally tapering lateral cusp on one side (Figure 5.7.10-11). The opposite lateral cusp forms a small dome, approximately half the size of the central cusp, and in some specimens overhangs the labial face of the crown. In one specimen (WAM 15.6.20, Figure 5.7.9), the tooth comprises four cusps; a central cusp with a single flattened lateral cusp on one side and two smaller rounded cusps, decreasing in size distally, on the

other. The cusps all possess a slight distally directed orientation with the largest cusp overhanging both the lingual and labial margins.

Remarks. Both morphotypes are here considered to represent a single taxon based on the high degree of heterodonty amongst other sharks with clutching-crushing dentitions (e.g., *Heterodontus*). Some of the teeth (Figure 5.7.10-11) superficially resemble the teeth attributed to Holocephali gen. et sp. indet. with their low profile bulbous cusps and lingually extending base perforated by a series of elongate canals. The crowns of the Holocephali gen. et sp. indet. teeth, however, differ from Euselachii gen. et sp. indet. 1 due to the small pores covering the crown and a central cusp that overhangs the labial face of the crown-base interface rather than overhanging the lingual margin.

Euselachii gen. et sp. indet. 2

Figure 5.7.12-13

Material. Seven teeth from sample 198404, nine partial teeth from sample TS-1, Laurel Formation, Laurel Downs, Tournaisian.

Description. Asymmetrical teeth that are highly flattened along the occlusal surface. The crown is almost rectangular in outline with a low convex occlusal surface (Figure 5.7.12-13). The surface of the tooth is covered by small rounded areas of discolouration, which are sometimes associated with small pits that do not appear to project into the dentine layer. There are two rows of cusplets: large irregularly shaped cusplets along the labial face (Figure 5.7.13) and smaller rounded cusplets along the lingual face (Figure 5.7.12). The occlusal facing base extends lingually and is perforated by a series of elongate canals. The baso-labial side of the crown is thin and lacks a clear crown-base interface.

Remarks. These teeth possess a range of characters including the wide canal openings similar to Euselachii gen. et sp. indet. 1; as well as different cusplet types on the labial and lingual faces of the crown that appear similar to Protacrodontidae gen. et. sp. The mesio-distal elongation of the teeth in conjunction with lingual and labial cusplets is diagnostic of lateral teeth attributed to the genus *Cassisodus.* In addition, the crown positions on the teeth of *Cassisodus margaritae* and Euselachii gen. et sp. indet. 2 are more labial, creating a slightly labio-lingual elongation. However, the crown of *Cassisodus* is far more pronounced with accessory labial and lingual cusplets of equal size. Due to the rarity of these teeth and the asymmetrical form, it is possible these teeth are part of a more complex dentition of another species.

Subclass EUCHONDROCEPHALI Lund and Grogan, 1997

Superorder HOLOCEPHALI Bonaparte, 1831

Holocephali gen. et sp. indet.

Figure 5.7.14-17

Material. 12 teeth from 198404, two teeth from 198480, seven teeth from TS-1, Laurel Formation, Laurel Downs, Tournaisian.

Description. Large teeth up to 21 mm across the crown, mesio-distally. The crown is asymmetrical and covered in a series of minute pores (Figure 5.7.14-15). The centre of the crown is elevated, forming a large bulbous projection with a rounded, labially directed apex that overhangs the base on the labial margin (Figure 5.7.16-17). On one side of the main projection is a smaller one, approximately half the size and also directed labially. The other distal end of the crown is flattened with no discernible elevation. A row of well-developed cusplets is present on the baso-labial

side of one incomplete tooth crown (WAM 15.6.14, Figure 5.7.14). The boundary between the crown and base on the lingual side of the tooth is marked by a shallow groove. The base has a short lingual extension with some teeth preserving thin distal margins extending beyond the crown. A row of tightly packed canals, extending from the lingual margin to the crown base, occupy the lingual face of the base (Figure 5.7.15). The labial face of the base is thin and borders a shallow trough perforated by small pores. The underside of the baso-linguinal extension and majority of the crown is gently convex and smooth, devoid of foramina.

Remarks. Teeth conforming to this morphology were first documented in the Canning Basin by Thomas (1957, 1959) who published photographs of "Bradyodont" teeth from the Laurel Formation. These teeth were later redescribed by Turner (1982) who tentatively attributed them to the genus *Helodus*. The teeth described here and the ones previously recovered from the Laurel Formation, both share crowns perforated by tiny pores as well as a base with small, elongate canals. In addition, the labial side of the base in these teeth are also highly vascularised. The teeth described here likely represent the same species previously recovered from the Laurel Formation with differences in crown and base shape that can be attributed to the high degree of heterodonty found in "bradyodont" sharks.

There are few features present in these isolated teeth that can be used to confidently identify them to a species level. Similar teeth have been recovered in Muhua, China, and attributed to *Helodus conicus* Newberry and Worthen, 1866, however no descriptive comparison to the original teeth of this species was given (Ginter and Sun, 2007). The mesio-distally elongate teeth from the Canning Basin share a general morphology including a high midpoint to the crown with a surface covered in small pores. In contrast, the presence of a more developed bulbous

projection on one side of the crown centre, tightly packed pore canals on the lingual face of the base as well as a wider labio-lingual morphology distinguishes these teeth from those of Muhua. Characters such as tubular dentine and a bulbous crown are typical of teeth assigned to the genus *Helodus*, however these are not genera specific. As the similarities do not appear significant enough to be included under the same genera, we have left the teeth in open nomenclature.

5.6 Discussion

5.6.1 Faunal provinces and biogeography

A chondrichthyan biofacies model, based on shark teeth, was proposed by Ginter (2000) for upper Famennian assemblages with a pan tropical distribution across south-east Laurussia and north-west Gondwana. Here we compare the shark fauna from the Carboniferous Laurel Formation with the biofacies model to ascertain if it also applies to Carboniferous faunas, especially in light of the end-Famennian vertebrate extinctions and environmental perturbations. The Famennian shark biofacies model consists of three distinct biofacies based on water depth and the percentages of shark teeth recovered (Ginter, 2000, 2001). These include: a *Jalodus* biofacies, containing more than 25% *Jalodus*, interpreted to indicate an open, deep water environment; a *Phoebodus* biofacies with more than 25% *Thrinacodus tranquillus* and *Phoebodus*, representing a shallower slope to shelf environment; and, a *Protacrodus* biofacies with more than 25% protacrodont and orodont teeth, indicating an even shallower marine environment. Previous work on the Late Devonian shark fauna from the Canning Basin has found similarities between the *Jalodus* biofacies type and the Frasnian shark fauna from the upper to distal slope facies of the Virgin Hills Formation, which largely comprises *Phoebodus* species

(Trinajstic and George, 2009; Roelofs et al., 2015). A *Protacrodus* biofacies has also been identified in a fossil rich shallow water middle Famennian Bugle Gap limestone, which mainly comprises protacrodonts and the phoebodont *Th. tranquillus* (Roelofs et al., 2015). However, it was not possible to apply the biofacies model to the latest Famennian Gumhole Formation in this work due to the low numbers of teeth recovered from the cross stratified ooidal grainstones, a facies type that has been previously recognised as not conducive to preserving vertebrate fossils (Boessenecker et al., 2014).

In contrast the lithofacies of the Laurel Formation comprise well bedded limestones with vertebrate remains recovered mostly from crinoidal grainstones, which are more favourable to the preservation and accumulation of vertebrate fossils (Druce and Radke, 1979). The shark fauna of the Laurel Formation is diverse, consisting of at least 16 species, and is dominated by three main tooth types: crushing or grinding (51%); phoebodont (represented by *Thrinacodus ferox*, 24%); and cladodont (22%).*Ageleodus* teeth comprise a small fraction of all teeth recovered (3%) and have been previously found in shallow water facies (Downs and Daeschler, 2001; Anderson, 2009). The high percentage of crushing or grinding teeth is comparable to the shallow water *Protacrodus* biofacies (*sensu* Ginter, 2000, 2001) in Famennian sections in Utah and Nevada, USA, and the Tafilalt Platform in Morocco (Ginter, 2001) and demonstrates that the *Prorocrodus* biofacies may be applied to the shallow water environments within the lower Carboniferous. The presence of this biofacies in the Canning Basin indicates comparable taxa, such as *Protacrodonts and Helodonts*, continued to inhabit equivalent, globally distributed, shallow water environments in the Early Carboniferous. Habibi and Ginter (2011) also noted the occurrence of the *Protacrodus* biofacies in Tournaisian shallow shelf facies at

Shahmirzad, central Iran. However, the proportions of Protacrodontidae teeth (= 25%), as well as Holocephali (= 12%) and the morphologically similar Euselachii gen. et sp. indet. 1 teeth (= 12%), are much higher in the Canning Basin than at Shahmirzad. This distinction may be influenced by localised environmental differences. The Laurel Formation contains a series of very shallow water carbonate facies, similar to those in the Tournaisian at Muhua, China (Ginter and Sun, 2007) and a similar high percentage of crushing Holocephalan type teeth. Drawing conclusions from these two assemblages is difficult; however, it is possible that high numbers of Holocephalan teeth may indicate an even shallow water biofacies. There is also the possibility the high numbers of Euselachii gen. et sp. indet. 1 and Holocephalan teeth are a response to changes in the shell durability of prey species. Kosnik et al. (2011) found a decrease in the shell reinforcement (*sensu* Kosnik et al., 2011) of brachiopods from the Carboniferous, which may have allowed the exploitation of such prey species by shark taxa with crushing and grinding dentitions

Several morphologically distinct teeth were collected from both the Upper Devonian Gumhole Formation (Protacrodontidae gen. et sp. indet.) and Lower Carboniferous Laurel Formation (*Stethacanthus*? sp., Ctenacanthiform sp., Hybontoidea sp.). These unique teeth may represent part of a radiation in shark faunas during the Early Carboniferous following the Hangenberg Event (Sallan and Coates, 2010). The notion of an endemic shark fauna is not unusual, as some Late Devonian shark species are known only from the Canning Basin (Trinajstic and George, 2009; Trinajstic et al., 2014; Roelofs et al., 2015). In addition, several known species, including some Frasnian phoebodonts, show unusual degrees of morphological variation in north-west Australia (Trinajstic and George, 2009; Roelofs et al., 2015). It is possible such unusual variations within species may be

directly correlated to the depositional environment. For example, the sampling of Famennian and Tournaisian facies that are representative of a shallow water environment in the Carnarvon and Canning basins (Trinajstic et al., 2014; Roelofs et al., 2015; this work) likely explains the absence of the cosmopolitan genus *Jalodus*, which is typically associated with deeper water pelagic facies across Laurussia and North Gondwana. Further studies on contemporaneous shallow marine platforms in North and East Gondwana are required to determine if some of the species from the Canning Basin represent localised endemism or are constrained by ecological and/or environmental factors.

5.6.2 Faunal assemblage and biofacies controls

Cosmopolitanism in Palaeozoic shark faunas has been recorded as early as the Givetian (Lebedev and Zakharenko, 2010; Potvin-Leduc et al., 2015), with the distributions of many taxa increasing towards the end of the Devonian (Lebedev and Zakharenko, 2010). The Canning Basin contains several elements of these Devonian cosmopolitan shark faunas, including representatives from the phoebodont, cladodont and protacrodont groups, from both the Frasnian (Trinajstic and George, 2009; Trinajstic et al., 2014) and Famennian (Roelofs et al., 2015) (Figure 5.8). The presence of *Thrinacodus ferox* and *Protacrodus aequalis* in this work demonstrates this cosmopolitan component continues from the Late Devonian into the Carboniferous (Figure 5.8.2). Shark taxa with more geographically restricted distributions, such as *Deihim mansureae* and *Protacrodus* sp., are found in the Canning Basin (Figure 5.6.2-4) and Iran (Habibi and Ginter 2011, plate 2B) and indicate close faunal ties between the Canning Basin and other regions to the west in the Late Devonian (Figure 5.8.1). Further evidence for a faunal exchange along the

northern Gondwana shelf is provided by the presence of *Thrinacodus ferox* (see Trinajstic et al., 2014) and *Cladodoides* cf. *wildungensis* (Figure 5.4.9-12), which closely resemble a tooth identified as *Stethacanthus thomasi* from north-western Iran (Hampe, 2000). Faunal links with East Gondwana are demonstrated by teeth

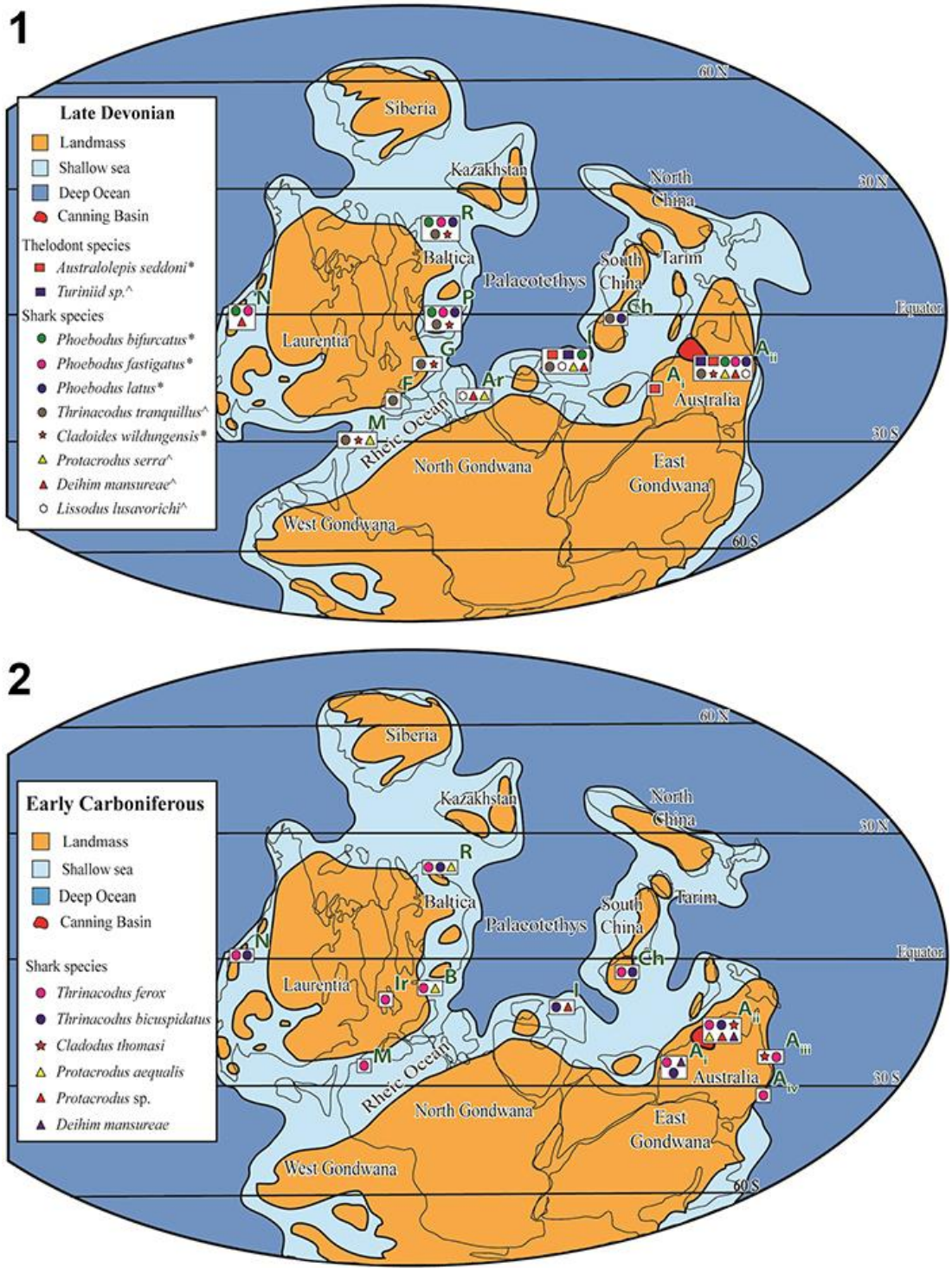

Figure 5.8. Maps depicting common taxa between the Canning Basin and other areas in Gondwana and Laurentia for the Late Devonian (**1**, Frasnian and Famennian chondrichthyans - * indicating Frasnian age, ^ indicating Famennian age) and Early Carboniferous (**2**, Tournaisian to Visean) (base map modified from Scotese and McKerrow, 1990; Golonka et al., 1994; Metcalfe, 2011). Abbreviations: **A**, Khor Virap and Erytch, Armenia; **A** $_{i}$, Carnarvon Basin, Australia; **A** $_{ii}$, Canning Basin, Australia; **A** $_{iii}$, Burdekin Star, Australia; **A** $_{iv}$, Broken River, Australia; **B**, Belgium; **Ch**, Hunan, South China; **F**, Montagne Noire, France; **G**, Thuringia, Germany; **I** , Chahriseh, Dalmeh, Hojedk, Hutk, and Kale-Sardar, Iran; **Ir** , Kilbride, Ireland: **M**, Tafilalt, Morocco; **N**, Nevada, Utah, and New Mexico, North America; **P**, Holy Cross Mountains, Poland; and **R**, South Urals, Russia. Sources of information: Armenia (Ginter et al., 2011), Australia (Turner and Dring, 1981; Turner, 1982; Trinajstic, 2001; Trinajstic and George, 2009; Roelofs et al., 2015), Royseux, Belgium (Derycke-Khatir et al., 2005), China (Wang and Turner, 1985; Ginter and Sun 2007), France (Derycke-Khatir et al., 2005), Germany (Ginter, 1999), Iran (Long and Hairapetian, 2000; Ginter et al., 2002; Hairapetian and Ginter, 2010), Ireland (Duncan, 2003), Morocco (Ginter et al., 2002; Derycke et al., 2008), North America (Ginter, 2001; Ivanov and Lucas, 2011), Poland (Ginter, 1990, 1995; Ginter and Ivanov, 2000), Russia (Ginter, 1994; Ginter and Ivanov, 1992, 2000; Ivanov, 1996), and South China (Lelièvre and Derycke, 1998).

determined as *Cladodus thomasi* which, given the revised diagnosis, have only been recorded from the Canning Basin and Rockhampton in Queensland (Turner, 1982). Shark species such as *Deihim mansureae* (also recovered from the Moogooree Limestone (Trinajstic et al., 2014), *Protacrodus* sp. 1 and *Cladodus thomasi*, from different parts of Gondwana suggests the Canning Basin lay at a junction between biogeographic regions to the east and west.

Late Devonian chondrichthyan taxa including *Phoebodus bifurcatus* Ginter and Ivanov, 1992 , *Phoebodus fastigatus* Ginter and Ivanov, 1992 , *Thrinacodus tranquillus* Ginter, 2000 and *Protacrodus serra* Ginter et al., 2002 co-occurred within South China and the Canning Basin (Figure 5.8.1; Trinajstic and George, 2009; Trinajstic et al., 2014; Roelofs et al., 2015). By the Early Carboniferous the shallow water faunal link appears to have been reduced, however, the pelagic component represented by taxa such as *Thrinacodusbicuspidatus* (see Edwards, 1997; Trinajstic et al., 2014) and *Thrinacodus ferox* continues between western Australia and South China (Ginter and Sun, 2007). It appears the pelagic sharks species were not as affected by the separation of the Gondwanan and South China

landmasses, whereas by the Tournaisian, there was little overlap between the shallow water chondrichthyan species. This is not unexpected, as previous studies (Metcalfe, 1988, 1998) noted the lack of plant and faunal similarities between Lower Carboniferous Gondwanan sections in South China and Australia. The reduced faunal overlap in shallow water chondrichthyan species appears to support a geographic separation between Gondwana and South China because of the northward migration of the South China terrane (Figure 5.8; Scotese and McKerrow, 1990; Golonka et al., 1994; Metcalfe, 1994); however, as noted above, it is difficult to determine isolated teeth of the crushing morphotype to a species level and therefore more species may await recognition.

5.7 Conclusions

The reported chondrichthyan fauna from the Tournaisian of the Lennard Shelf, Canning Basin, is diverse with 16 species identified from shallow marine platform facies. The position of the Canning Basin in the Early Carboniferous, adjacent to northern and eastern Gondwana, allows the investigation of faunal migration and exchange along this ancient continental margin during the recovery phase in the aftermath of significant Late Devonian mass extinctions. The similarities in shark fauna from the Late Devonian between the Canning Basin and North Gondwana are found here to continue into the Carboniferous. In contrast to the Famennian, the north western Australian Tournaisian shark fauna only shows pelagic species similarities with the South China faunas. Despite a limited number of species in common with South China, there is a high degree of similarity in tooth forms within faunas from the shallow water platform at Muhua and the facies analysed in this study. This study also supports the application of the microvertebrate biofacies

scheme, established by Ginter (2000) in late Famennian strata, to the Early Carboniferous, at least in shallow water depositional environments.

5.8 Acknowledgments

We thank A. Ivanov, Department of Palaeontology, St. Petersburg University and S. Turner from the Queensland Museum for their assistance in the preparation of this work and J. Maisey from the Natural History Museum in New York for his useful comments and access to the collections. We would also like to acknowledge the constructive comments and suggestions from two anonymous reviewers. The authors acknowledge the use of equipment, scientific and technical assistance of the Curtin University Electron Microscope Facility, which has been partially funded by the University, State and Commonwealth Governments. In addition, we thank the owners of Brooking Springs and Laurel Downs stations for allowing access to outcrops. BR recognises the receipt of an Australian Postgraduate Award. This research was funded under Australian Research Council grant DP 110101127. AJM publishes with the permission of the Director, Geological Survey of Western Australia.

5.9 References

Agassiz, J.L.R. 1833-1844. Recherches sur les Poissons Fossiles. Petitpierre, Neuchâtel. (In French)

Anderson, L.I. 2009. First non-calcified dasycladalean alga from the Carboniferous. Neues Jahrbuch für Geologie und Paläontologie-Abhandlungen 251, 119-128.

Andrew, A., Hamilton, P., Mawson, R., Talent, J., and Whitford, D. 1994. Isotopic correlation tools in the mid-Palaeozoic and their relation to extinction events. Australian Petroleum Exploration Association Journal 34, 268-277.

Becker, R. and House, M. 2009. Devonian ammonoid biostratigraphy of the Canning Basin. Geological Survey of Western Australia, Bulletin 145, 415-439.

Behan, C., Walken, G., and Cuny, G. 2012. A Carboniferous chondrichthyan assemblage from residues within a Triassic karst system at Cromhall Quarry, Gloucestershire, England. Palaeontology 55, 1245-1263.

Boessenecker, R.W., Perry, F.A., and Schmitt, J.G. 2014. Comparative taphonomy, taphofacies, and bonebeds of the Mio-Pliocene Purisima Formation, central California: Strong physical control on marine vertebrate preservation in shallow marine settings. PLoS ONE, 9:e91419.

Bonaparte, C.L.J.L. 1831. Saggio di una distribuzione metodica degli animali vertebrati. Giornale Arcadico di Scienze 49, 1-77. (In Italian)

Bonaparte, C.L.J.L. 1832-1838. Selachorum tabula analytica. Nuovi Annali delle Scienze Naturali 1, 195-214. (In Latin)

Broom, R. 1909. The fossil fishes of the upper Karroo beds of South Africa. Annals of the South African Museum 7, 251-269.

Brough, J. 1935. On the structure and relationships of the hybodont sharks. Memoirs and Proceedings of the Manchester Literary and Philosophical Society 79, 35-50.

Burrow, C.J., Turner, S., and Young, G.C. 2010. Middle Palaeozoic microvertebrate assemblages and biogeography of East Gondwana (Australasia, Antarctica). Palaeoworld 19, 37-54.

Cappetta, H., Duffin, C., and Zidek, J. 1993. Chondrichthyes, p. 593-609. In Benton, M.J. (ed.), The Fossil Record 2. Chapman and Hall, London.

Dean, B. 1909. Studies on fossil fishes (sharks, chimaeroids and arthrodires). American Museum of Natural History Memoir 9, 211-287.

Delsate, D., Smet, F., and Wille, E. 2003. New ichthyoliths from the Lower Carboniferous of Belgium. Ferrantia 36, 29-38.

Derycke, C. 1992. Microrestes de Selaciens et autres Vertébres du Dévonien superieur de Maroc. Bulletin du Muséum National d'Histoire Naturelle. Paris 4e series 14, 15-61. (In French)

Derycke-Khatir, C. 2005. Microrestes de vertébrés du Paléozöique supérieur de la Manche au Rhin. Société Géologique du Nord Publication 33, 1-261. (In French)

Derycke, C., Spalletta, C., Perri, M.C., and Corradini, C. 2008. Famennian chondrichthyan microremains from Morocco and Sardinia. Journal Information 82, 984-995.

Downs, J.P. and Daeschler, E.B. 2001. Variation within a large sample of Ageleodus pectinatus teeth (Chondrichthyes) from the Late Devonian of Pennsylvania, USA. Journal of Vertebrate Paleontology 21, 811-814.

Druce, E.C. and Radke, B. 1979. The geology of the Fairfield Group, Canning Basin, Western Australia, 200. Australian Government Public Service, Canberra, Australia.

Duffin, C.J. 1985. Revision of the hybodont selachian genus Lissodus Brough (1935). Palaeontographica Abteilung A 188, 105-152.

Duffin, C.J. and Ginter, M. 2006. Comments on the selachian genus *Cladodus* Agassiz, 1843. Journal of Vertebrate Paleontology 26, 253-266.

Duncan, M. 2003. Early Carboniferous chondrichthyan *Thrinacodus* from Ireland, and a reconstruction of jaw apparatus. Acta Palaeontologica Polonica 48, 113-122.

Duncan, M. 2004. Chondrichthyan genus *Lissodus* from the Lower Carboniferous of Ireland. Acta Palaeontologica Polonica 49, 417-428.

Eastman, C.R. 1897. *Tamiobatis vetustus*; a new form of fossil skate. *American* Journal of Science 20, 85-90.

Edgell, H.S. 2004. Upper Devonian and Lower Carboniferous Foraminifera from the Canning Basin, Western Australia. Micropaleontology 50, 1-26.

Edwards, A.F. 1997. Ichthyolith remains from the Devonian-Carboniferous Boundary of the Canning Basin, Western Australia. Unpublished MSc thesis, School of Earth Sciences, Macquarie University, Sydney, Australia.

Fischer, J. 2008. Brief synopsis of the hybodont form taxon *Lissodus* Brough, 1935, with remarks on the environment and associated fauna. Freiberger Forschungshefte C 528, 1-23.

Garvey, J.M. and Turner, S. 2006. Vertebrate microremains from the presumed earliest Carboniferous of the Mansfield Basin, Victoria. Alcheringa 30, 43-62.

Ginter, M. 1990. Late Famennian shark teeth from the Holy Cross Mountains, Central Poland. Acta Geologica Polonica 40, 69-81.

Ginter, M. 1994. Ichtiolity dewońskie z Polski i Uralu oraz ich znaczenie stratygraficzne. Unpublished Ph.D. thesis, Warsaw University, Warsaw, Poland. (In Polish)

Ginter, M. 1999. Famennian-Tournaisian chondrichthyan microremains from the eastern Thuringian Slate Mountains. Abhandlungen und Berichte für Naturkunde 21, 25-47.

Ginter, M. 2000. Late Famennian pelagic shark assemblages. Acta Geologica Polonica 50, 369-386.

Ginter, M. 2001. Chondrichthyan biofacies in the Late Famennian of Utah and Nevada. Journal of Vertebrate Paleontology 21,714-729.

Ginter, M. 2002. Chondrichthyan fauna of the Frasnian-Famennian boundary beds in Poland. Acta Palaeontologica Polonica 47, 329-338.

Ginter, M., Hairapetian, V., and Grigoryan, A. 2011. Chondrichthyan microfossils from the Famennian and Tournaisian of Armenia. Acta Geologica Polonica 61, 153-173.

Ginter, M., Hairapetian, V., and Klug, C. 2002. Famennian chondrichthyans from the shelves of North Gondwana. Acta Geologica Polonica 52, 169-215.

Ginter, M., Hampe, O., and Duffin, C.J. 2010. Paleozoic Elasmobranchii: Teeth, pp. 1-168. In Shultze, H.P. (ed.), Handbook of Paleoichthyology, volume 3D. Verlag Dr. Friedrich Pfeil, München, Germany.

Ginter, M. and Ivanov, A. 1992. Devonian phoebodont shark teeth. Acta Palaeontologica Polonica 37, 55-75.

Ginter, M. and Ivanov, A. 1996. Relationships of Phoebodus. Modern Geology 20, 263-274.

Ginter, M. and Ivanov, A. 2000. Stratigraphic distribution of chondrichthyans in the Devonian on the East European Platform margin. Courier-Forshungsinstitut Senckenberg 325-340.

Ginter, M. and Sun, Y. 2007. Chondrichthyan remains from the Lower Carboniferous of Muhua, southern China. Acta Palaeontologica Polonica 52, 705.

Ginter, M. and Turner, S. 1999. The early Famennian recovery of phoebodont sharks. Acta Geologica Polonica 49, 105-117.

Ginter, M. and Turner, S. 2010. The middle Paleozoic Selachian genus Thrinacodus. Journal of Vertebrate Paleontology 30, 1666-1672.

Glenister, B.F. and Klapper, G. 1966. Upper Devonian conodonts from the Canning Basin, Western Australia. Journal of Paleontology 40, 777-842.

Glikman, L. 1964. Class Chondrichthyes, Subclass Elasmobranchii. Osnovy Paleontologii 11, 195-236.

Golonka, J. 2007. Phanerozoic paleoenvironment and paleolithofacies maps: late Palezoic. Geologia/Akademia Górniczo-Hutnicza im. Stanisława Staszica w Krakowie 33, 145-209.

Golonka, J., Ross, M., and Scotese, C. 1994. Phanerozoic paleogeographic and paleoclimatic modeling maps. Canadian Society of Petroleum Geologists, 17:1-47.

Habibi, T. and Ginter, M. 2011. Early Carboniferous chondrichthyans from the Mobarak Formation, Central Alborz Mountains, Iran. Acta Geologica Polonica 61, 27-34.

Habibi, T., Yazdi, M., Zarepoor, S., and Parvanehnejad Shirazi, M. 2013. Late Devonian fish micro-remains from Central Iran.Geopersia 3, 25-34.

Hairapetian, V. and Ginter, M. 2009. Famennian chondrichthyan remains from the Chahriseh section, central Iran. Acta Geologica Polonica 59, 173-200.

Hairapetian, V. and Ginter, M. 2010. Pelagic chondrichthyan microremains from the Upper Devonian of the Kale Sardar section, eastern Iran. Acta Geologica Polonica 60, 357-371.

Hairapetian, V., Roelofs, B.P., Trinajstic, K.M., and Turner, S. 2015. Famennian survivor turiniid thelodonts of North and East Gondwana. Geological Society, London, Special Publications 423, 423-433.

Hampe, O. 2000. Occurrence of *Phoebodus gothicus* (Chondrichthyes: Elasmobranchii) in the middle Famennian of northwestern Iran (Province East Azerbaijan). Acta Geologica Polonica 50, 355-367.

Hay, O.P. 1902. Bibliography and catalogue of the fossil Vertebrata of North America. Bulletin, United States Geological Survey 179, 1-868.

Herman, J. 1977 (date of imprint 1975). Les Sélaciens de Terrains Néocrétacés et Paléocènes de Belgique et des Contreés Limitrophes Elements d'une Biostratigraphie Intercontinental. Mémoires pour servir à l'explication des Cartes géologiques et minières de la Belgique, 15. Service Geologique de Belgique, Brussels. (In French).

Hill, D. 1954. Coral faunas from the Silurian of New South Wales and the Devonian of Western Australia. Bureau of Mineral Resources Geology and Geophysics 23, 1-51.

Hocking, R.M., Playford, P.E., Haines, P.W., and Mory, A.J. 2008. Paleozoic Geology of the Canning Basin - A Field Guide.Geological Survey of Western Australia, Perth, Australia.

Huddle, J.W. 1934. Conodonts from the New Albany Shale of Indiana. Bulletins of American Paleontology 21, 1-136.

Huxley, T.H. 1880. On the application of the laws of evolution to the arrangement of the Vertebrata, and more particularly of the Mammalia. Proceedings of the Zoological Society, London 43, 649-662.

Ivanov, A. 1996. The Early Carboniferous chondrichthyans of the South Urals, Russia. Geological Society, London, Special Publications 107, 417-425.

Ivanov, A. 1999. Late Devonian-Early Permian chondrichthyans of the Russian Arctic. Acta Geologica Polonica 49, 267-285.

Ivanov, A.O. and Lucas, S.G. 2011. Paleozoic Sly Gap Formation of southern New Mexico, USA. NewMexico Museum of Natural History and Science Bulletin 53, 52-70.

Ivanov, A.O. and Lukševičs, E. 1994. Famennian chondrichthyans from the Main and Central Devonian Fields. Daba un muzejs 5, 24-29.

Jaekel, O. 1921. Die Stellung der Paläontologie zur einigen Problemen der Biologie und Phylogenie. Schadelprobleme. Paläontologische Zeitschrift 3, 213-239. (In German)

Jaekel, O. 1925. Das Mundskelett der Wirbeltiere. Gegenbaurs Morphologishes Jahrbuch 55, 402-409. (In German)

Janvier, P. 1996. Early Vertebrates, 33. Clarendon Press, Oxford.

Jeppsson, L., Anehus, R., and Fredhold, D. 1999. The optimal acetate buffered acetic acid technique for extracting phosphatic fossils. Journal of Paleontology 73, 964-972.

Jones, P. 1959. Preliminary report on Ostracoda from Bore BMR No. 2, Laurel Downs, Fitzroy Basin, Western Australia. Bureau of Mineral Resources, Australian Geology and Geophysics 38, 17-52.

Jones, P.J, 1974. Australian Devonian and Carboniferous (Emsian Visean) ostracod faunas: a review, p. 1-19. In Bouckaert, J. and Streel, M. (eds.), International Symposium on Belgian Micropaleontological Limits from Emsian to Visean, Namur, 1974. Geological Survey of Belgium, Brussels, Belgium.

Jones, P. 1987. *Rhytiobeyrichia*, a new beyrichiacean ostracod from the late Devonian of Western Australia. Bureau of Mineral Resources, Australian Geology and Geophysics 10, 287-300.

Jones, P. 1995. Timescales 5, Carboniferous. Australian Phanerozoic timescales, biostratigraphic charts and explanatory notes. Australian Geological Survey Organisation Record 1995/34, Canberra, Australia.

Jones, P. and Thomas, G.A. 1959. Preliminary report on probable Lower Carboniferous fossils from Station Creek area, Fitzroy Basin, (Westralian Oil Limited, Permite 106H). Record 1959/094, Bureau of Mineral Resources, Geology and Geophysics, Canberra, Australia.

Kietzke, K. and Lucas, S. 1992. Ichthyoliths from the Devonian-Carboniferous Boundary in the Sacramento Mountains, South Central New Mexico, USA. Ichthyolith issues 8,17-21.

Klapper, G. 2007. Frasnian (Upper Devonian) conodont succession at Horse Spring and correlative sections, Canning Basin, Western Australia. Journal of Paleontology 81, 513-537.

Kosnik, M.A., Alroy, J., Behrensmeyer, A.K., Fürsich, F.T., Gastaldo, R.A., Kidwell, S.M., Kowalewski, M., Plotnick, R.E., Rogers, R.R., and Wagner,

P.J. 2011. Changes in shell durability of common marine taxa through the Phanerozoic: evidence for biological rather than taphonomic drivers. Paleobiology 37, 303-331.

Lebedev, O. 1996. Fish assemblages in the Tournaisian-Viséan environments of the East European Platform. Geological Society, London, Special Publications 107, 387-415.

Lebedev, O. and Zakharenko, G. 2010. Global vertebrate-based palaeozoogeographical subdivision for the Givetian-Famennian (Middle-Late Devonian): Endemism-cosmopolitanism spectrum as an indicator of interprovincial faunal exchanges. Palaeoworld 19, 186-205.

Lelièvre, H. and Derycke, C. 1998. Microremains of vertebrate near the Devonian-Carboniferous boundary of southern China (Hunan province) and their biostratigraphical significance. Revue de Micropaléontologie 41, 297-320.

Long, J.A. 1989. A new rhizodontiform fish from the Early Carboniferous of Victoria, Australia, with remarks on the phylogenetic position of the group. Journal of Vertebrate Paleontology 9, 1-17.

Long, J.A. and Hairapetian, V. 2000. Famennian microvertebrates from the Dalmeh area, central Iran. Records of the Western Australian Museum, Supplement 58, 211-221.

Lund, R. 1974. *Stethacanthus altonensis* (Elasmobranchii) from the Bear Gulch Limestone of Montana. Annals of the Carnegie Museum 45, 43-56.

Lund, R. and Grogan, E.D. 1997. Relationships of the Chimaeriformes and the basal radiation of the Chondrichthyes. Reviews in Fish Biology and Fisheries 7, 65-123.

Metcalfe, I. 1988. Origin and assembly of south-east Asian continental terranes. Geological Society, London, Special Publications 37, 101-118.

Metcalfe, I. 1994. Gondwanaland origin, dispersion, and accretion of East and Southeast Asian continental terranes. Journal of South American Earth Sciences 7, 333-347.

Metcalfe, I. 1998. Palaeozoic and Mesozoic geological evolution of the SE Asian region: multidisciplinary constraints and implications for biogeography, pp. 25-41. In Hall, R. and Holloway, J.D. (eds.), Biogeography and Geological Evolution of SE Asia. Backhuys Publishers, Amsterdam, Netherlands.

Metcalfe, I. 2011. Palaeozoic-Mesozoic history of SE Asia. Geological Society, London, Special Publications 355, 7-35.

Mory, A.J. and Hocking, R.M. 2011. Permian, Carboniferous and Upper Devonian Geology of the Northern Canning Basin, Western Australia: A Field Guide. Geological Survey of Western Australia, Perth, Australia.

Newberry, J.S. 1889. The Paleozoic fishes of North America. U.S. Geological Survey, Monograph 16, 1-340.

Newberry, J.S. and Worthen, A.H. 1866. Descriptions of new species of vertebrates, mainly from the Sub-Carboniferous Limestone and Coal Measures of Illinois. Geological Survey of Illinois 2, 9-134.

Nicoll, R.S. and Druce, E.C. 1979. Conodonts from the Fairfield Group, Canning Basin, Western Australia. Bureau of Mineral Resources Australia Bulletin 190, 1-134.

Owen, R. 1846. Lectures on the Comparative Anatomy and Physiology of the Vertebrate Animals: Delivered at the Royal College of Surgeons of England in 1844 and 1846,1. Longman, Brown, Green, and Longmans.

Owen, R. 1867. On the mandible and mandibular teeth of cochliodonts. Geological Magazine, 4:59-63.

Playford, P.E. 1976. Devonian Reef Complexes of the Canning Basin, Western Australia. 25th International Geological Congress, Excursion Guide No. 38A, Sydney, Australia.

Playford, P.E., Hocking, R.M., and Cockbain, A.E. 2009. Devonian reef complexes of the Canning Basin, WA. Bulletin of the Geological Survey of Western Australia 145, 1-444.

Potvin-Leduc, D., Cloutier, R., Landing, E., Hernick, L.V., and Mannolini, F. 2015. Givetian (Middle Devonian) sharks from Cairo, New York (USA): Evidence of early cosmopolitanism. Acta Palaeontologica Polonica 60, 183-200.

Rhodes, F.H.T., Austin, R.L., and Druce, E.C. 1969. British Avonian (Carboniferous) conodont faunas and their value in local and intercontinental correlation. Bulletin of the British Museum (Natural History), Geology Supplement 5, 1-313.

Roelofs, B., Playton, T., Barham, M., and Trinajstic, K. 2015. Upper Devonian microvertebrates from the Canning Basin, Western Australia. Acta Geologica Polonica 65, 69-101.

Ross, J.P. 1961. Ordovician, Silurian and Devonian Bryozoa of Australia. Bureau of Mineral Resources Australia, Bulletin 50, 1-172.

Sallan, L.C. and Coates, M.I. 2010. End-Devonian extinction and a bottleneck in the early evolution of modern jawed vertebrates. Proceedings of the National Academy of Sciences 107, 10131-10135.

Scotese, C.R. and McKerrow, W.S. 1990. Revised world maps and introduction. Geological Society, London, Memoirs 12, 1-21.

Seilacher, A. 1943. Elasmobranchier-Reste aus dem oberen Muschelkalk und dem Keuper Württembergs. Neues Jahrbuch für Mineralogie, Geologie und Paläontologie, Monatshefte B 1943, 256-292. (In German)

Smith, T.E., Kelman, A.P., Nicoll, R.S., Laurie, J.R. and Le Poidevin, S.R. 2013. Geoscience Australia's Basin Biozonation and Stratigraphy Chart Series. Basin Biozonation and Stratigraphy Chart Series. Geoscience Australia, Canberra.

Southgate, P.N., Kennard. J.M., Jackson, M.J., O'Brien, P.E., and Sexton, M.J. 1993. Reciprocal lowstand clastic and highstand carbonate sedimentation, subsurface Devonian reef complex, Canning Basin, Western Australia, p. 157-159. In Loucks, R.G. and Sarg, J.F. (eds.), Carbonate Sequence Stratigraphy, Recent Developments and Applications. American Association of Petroleum Geologists Memoir 57. Tulsa, Oklahoma, USA.

St. John, O. and Worthen, A. 1875. Descriptions of fossil fishes. Geological Survey of Illinois 6, 245-488.

Teichert, C. 1949. Stratigraphy and palaeontology of Devonian portion of Kimberley Division, Western Australia. Australian Bureau of Mineral Resources, Geology and Geophysics 2, 1-50.

Thomas, G.A. 1957. Lower Carboniferous deposits in the Fitzroy Basin, Western Australia. The Australian Journal of Science 19, 160-161.

Thomas, G.A. 1959. The Lower Carboniferous Laurel Formation of the Fitzroy Basin. Bureau of Mineral Resources, Report 38, 31-36.

Thomas, G.A. 1971. Carboniferous and early Permian brachiopods from Western and Northern Australia. Bureau of Mineral Resources, Geology and Geophysics Australia, Bulletin 56, 1-276.

Trautschold, H. 1874. Die Kalkbrüche von Mjatschkowa. Eine Monographie des oberen Bergkalks. Erste Hälfte.Nouveaux mémoires de la Société impériale des naturalistes de Moscou 13, 277-326. (In German)

Trinajstic, K. 2001. A description of additional variation seen in the scale morphology of the Frasnian thelodont Australolepis seddoni Turner and Dring, 1981. Records of the Western Australian Museum 20, 237-246.

Trinajstic, K. and George, A.D. 2009. Microvertebrate biostratigraphy of Upper Devonian (Frasnian) carbonate rocks in the Canning and Carnarvon basins of Western Australia. Palaeontology 52, 641-659.

Trinajstic, K., Roelofs, B., Burrow, C., Long, J., and Turner, S. 2014. Devonian vertebrates from the Canning and Carnarvon Basins with an overview of Paleozoic vertebrates of Western Australia. Journal of the Royal Society of Western Australia 97, 133-151.

Turner, S. 1982. Middle Palaeozoic elasmobranch remains from Australia. Journal of Vertebrate Paleontology 2, 117-131.

Turner, S. 1991. Palaeozoic Vertebrate Microfossils in Australasia, p. 429-464. In Vickers-Rich, P., Monaghan, J.M., Baird, R.F., and Rich, T.H. (eds.), Vertebrate Palaeontology of Australasia. Monash University Publications Committee, Melbourne.

Turner, S. 1993. Early Carboniferous microvertebrates from the Narrien Range, central Queensland. Memoirs of the Association of Australasian Palaeontologists 15, 289-304.

Turner, S. and Dring, R.S. 1981. Late Devonian thelodonts (Agnatha) from the Gneudna Formation, Carnarvon Basin, Western Australia. Alcheringa 5, 39-48.

Veevers, J.J. 1959. Devonian brachiopods from the Fitzroy Basin, Western Australia. Bulletin of theBureau of Mineral Resources, Geology and Geophysics 45, 1-220.

Wang, S. 1989. Biostratigraphy of vertebrate microfossils, p. 36-38, 103-108. In Ji Q. (ed.), The Daspoushang Section--An Excellent Section for Devonian-Carboniferous Boundary Stratotype in China. Science Press, Beijing.

Wang, S. 1993. Vertebrate biostratigraphy of the Middle Palaeozoic of China, p. 252-276. In Long, J.A. (ed.), Palaeozoic Vertebrate Biostratigraphy and Biogeography. Belhaven Press, London.

Wang, S. and Turner, S. 1985. A re-appraisal of Upper Devonian-Lower Carboniferous verrtebrate microfossils in South China.Professional Papers of Stratigraphy and Palaeontology 26, 59-70.

Williams, M.E. 1985. The «cladodont level» sharks of the Pennsylvanian black shales of central North America.Palaeontographica Abteilung A, 83-158.

Williams, M.E. 1998. A new specimen of Tamiobatis vetustus (Chondrichthyes, Ctenacanthoidea) from the late Devonian Cleveland Shale of Ohio. Journal of Vertebrate Paleontology 18, 251-260.

Willmott, S. 1962. Geological report on Frome Rocks No2 Well. Bureau of Mineral Resources, Australia, Petroleum Search Subsidy Acts Publication 8, 15-20.

Yazdi, M. and Turner, S. 2000. Late Devonian and Carboniferous vertebrates from the Shishtu and Sardar formations of the Shotori Range, Iran. Records of the Western Australian Museum, Supplement 58, 223-240.

Young, G. 1984. Comments on the phylogeny and biogeography of antiarchs (Devonian placoderm fishes), and the use of fossils in

biogeography. Proceedings of the Linnean Society of New South Wales 107, 443-473.

Young, G. 1987. Devonian fish remains from Billiluna, eastern Canning Basin, Western Australia. BMR Journal of Australian Geology and Geophysics 10, 179-192.

Young, G.C. 2010. Placoderms (armored fish): dominant vertebrates of the Devonian Period. Annual Review of Earth and Planetary Sciences 38, 523-550.

Young, G.C., Burrow, C.J., Long, J.A., Turner, S., and Choo, B. 2010. Devonian macrovertebrate assemblages and biogeography of East Gondwana (Australasia, Antarctica). Palaeoworld 19, 55-74.

Zangerl, S. 1981. Paleozoic Elasmobranchii, p. 1-115. In Shultze, H.P. (ed.), Handbook of Paleoichthyology, volume 3A. Gustav Fischer Verlag, Stuttgart, Germany.

Ziegler, W. and Sandberg, C.A. 1990. The Late Devonian standard conodont zonation. Courier Forshungsinstitut Senckenberg 121, 1-115.

6.0 Assessing the fidelity of marine vertebrate microfossil $\delta^{18}O$ signatures and their potential for palaeoclimatic reconstructions

Brett Roelofs[1], Milo Barham[2], John Cliff[3], Michael Joachimski[4], Laure Martin[5] and Kate Trinajstic[6]

[1]Brett Roelofs. Department of Applied Geology, Curtin University, GPO Box U1987 Perth, WA 6845, Australia. brett.roelofs@postgrad.curtin.edu.au

[2]Milo Barham. Department of Applied Geology, Curtin University, GPO Box U1987 Perth, WA 6845, Australia. milo.barham@curtin.edu.au

[3] John Cliff. Environmental Molecular Science Laboratory, Pacific Northwest National Laboratory, P.O. Box 999 Richland, WA 99352. john.cliff@pnnl.gov

[4]Michael Joachimski. GeoZentrum Nordbayern, University of Erlangen-Nuremberg, Schlossgarten 5, 91054 Erlangen, Germany. michael.joachimski@fau.de

[5]Laure Martin. Centre for Microscopy Characterisation and Analysis, The University of Western Australia, Perth, WA 6009, Australia. laure.martin@uwa.edu.au

[6]Kate Trinajstic*. Department of Environment and Agriculture, Curtin University, GPO Box U1987, Perth, WA 6845, Australia. K.Trinajstic@curtin.edu.au

6.1 Abstract

Conodont biogenic apatite has become a preferred analytical target for oxygen isotope studies investigating ocean temperature and palaeoclimate changes in the Palaeozoic. Despite the growing application in geochemical based palaeoenvironmental reconstructions, the paucity or absence of conodont fossils in certain facies necessitates greater flexibility in selection of robust oxygen bearing

compounds for analysis. Microvertebrates offer a potential substitute for conodonts from the middle Palaeozoic. Microvertebrate bioapatite is particularly advantageous given a fossil record extending to the present with representatives across freshwater to fully marine environments, thus widening the scope of oxygen isotope studies on bioapatite. However, significant tissue heterogeneity within vertebrates and differential susceptibility of these tissues to diagenetic alteration have been raised as potential problems affecting the reliability of the oxygen isotope ratios as palaeoclimatic proxies. Well preserved microvertebrate and co-occurring conodont fossils from the Late Devonian and Early Carboniferous of the Lennard Shelf, Canning Basin, Western Australia, were analysed using bulk (gas isotope ratio mass spectrometry) and in-situ (secondary ion mass spectrometry) methodologies, with the latter technique allowing investigation of specific tissues within vertebrate elements. The $\delta^{18}O_{conodont}$ results may be interpreted in terms of palaeolatitudinally and environmentally sensible palaeotemperatures and provide a baseline standard for comparison against $\delta^{18}O_{microvertebrate}$ values. Despite an absence of obvious diagenetic influences, GIRMS of microvertebrate denticles yielded $\delta^{18}O$ values depleted in ^{18}O by 2-4 ‰ relative to co-occurring conodonts. SIMS analysis of hypermineralised tissues in both scales and teeth produced $\delta^{18}O$ values comparable with those of associated conodonts. The susceptibility of porous phosphatic fossil tissues to microbial activity, fluid interaction and introduction of mineral precipitates post-formation is demonstrated in microvertebrate dentine, which showed significant heterogeneity and consistent depletion in ^{18}O. The hypermineralised tissues present in both teeth and scales appear resistant to many diagenetic processes and indicate potential for palaeoclimatic reconstructions and palaeoecological investigations.

6.2 Introduction

6.2.1 O-isotope record

The Palaeozoic marine oxygen isotope record is punctuated by a series of excursions and perturbations reflecting climatic events that are often associated with significant biological reorganisations (e.g. Brand, 1989; Gruszcyński et al., 1989; Caplan and Bustin, 1999; Veizer et al., 1999; Jeppsson et al., 2002; Joachimski and Buggisch, 2002; Kaiser et al., 2006; Trotter, 2008; Schobben et al., 2015). Fluctuations in the oxygen isotope record have been elicited from analysis of marine organisms with the ability to precipitate mineralised tissues in isotopic equilibrium with the ambient water. The shells of Palaeozoic low-Mg calcite brachiopod taxa have been commonly used (Popp et al., 1986; Veizer et al., 1986, 1997; Brand, 1989, 2004; Carpenter et al., 1991; Hays and Grossman, 1991; Wadleigh et al., 1992; Azmy et al., 1996; Mii et al. 1997, 1999; Van Geldern et al., 2006; Korte et al., 2008) due to the relative resistance of low-Mg calcite to post-mortem modification, as well as their relative abundance and ease of sampling. However, screening methods for the identification of recrystallised calcite, which may cause resetting of oxygen isotope values, is imperfect (e.g. Wenzel et al., 2000). In addition, O-isotope heterogeneity has been identified in a number of brachiopod shells, indicating fractionation is occurring during the formation of these hard tissues (e.g. Auclair et al., 2003; Yamamoto et al., 2011; Rollion-Bard et al., 2016). The typically sessile ecology of brachiopods also means that each analysis must be independently considered in the context of the specific temperature and chemistry of the water depth it inhabited. Consequently, this limits the comparison of oxygen isotope signatures to brachiopod taxa occupying similar ecological niches (Popp et al., 1986; James et al., 1997).

Bioapatite offers a more reliable oxygen bearing alternative to brachiopod calcite due to the stability of the P-O bond in PO_4^{3-} (e.g., Grimes et al., 2003; Joachimski et al., 2004). The mineralised (composition $Ca_5Na_{0.13}(PO_4)_{3.01}(CO_3)_{0.16}F_{0.73}(H2O)_{0.85}$, Pietzner et al., 1986) feeding elements of conodonts (Lindström, 1974; Dzik, 1991; Goudemand et al., 2011) have become increasingly used in oxygen isotope studies. The elements comprise relatively homogenous and densely crystalline outer hyaline tissue with an inner 'white matter' made of finely crystalline apatite (Lindström, 1964; Pietzner et al., 1968; Barnes et al. 1973; Trotter et al., 2007; Jones et al., 2012). Analysis of the hypermineralised tissues indicates conodont elements offer greater consistency in $\delta^{18}O$ values in comparison to those obtained from brachiopod calcite (e.g. Wallace and Elrick, 2014). Consistent oxygen isotope signatures have been observed between conodont genera belonging to different biofacies in the Late Devonian (Joachimski et al., 2009), supporting a shared near sea-surface habitat and free swimming lifestyle, as suggested from their biology (e.g. Gabbott et al., 1995). Correlateable oxygen isotope ratios further indicate conodont elements reflect sea surface temperatures and can be utilised in wider geographical comparisons (Joachimski and Buggisch, 2002).

The biostratigraphic utility and widespread distribution and abundance of conodont elements in many marine deposits has facilitated the development of a temporally resolved isotope record spanning many significant faunal reorganisations associated with climatic perturbations from the Ordovician (Trotter et al., 2008) to the Triassic (Chen et al., 2016; Joachimski et al., 2009; Rigo et al., 2012; Sun et al., 2012; Trotter et al., 2015). However, conodont fossils are not ubiquitous in all facies, limiting their potential as a sea surface temperature proxy in many regions. Even where present, a paucity of conodont elements can preclude preferred single genera

sample analysis and fine resolution sampling due to minimum sample mass requirements in standard analytical methodologies. As a consequence of these limitations, other common, diagenetically stable oxygen-bearing compounds must be identified to expand accurate palaeoenvironmental interpretations across different temporal intervals and depositional settings.

6.2.2 Microvertebrate histology and application in Palaeozoic O-isotope studies

Marine microvertebrate fossils (typically less than 5 mm in size) most commonly comprise teeth, scales and fin spines. Unlike brachiopods and conodonts, vertebrate hard tissues are highly heterogeneous, consisting of three broad types; bone, dentine and enamel. These tissues are differentiated by the levels of mineralisation and organic matter content. Bone comprises a 50 - 70% mineralised component with 20 - 40% organic matter and 5 - 10% water (Clarke, 2005). Dentine is approximately 70% mineralised with 20 - 24% protein and 6 - 10% water, whereas enamel is highly mineralized (96%) with only 1% protein and approximately 3% water, which is present on or between the hydroxyapatite crystals (Stack, 1955, Pasteris et al., 2008; Goldberg et al., 2012; Hand and Frank, 2014). The low organic carbon, and high mineral content (>80 wt.%, Li, 2013) of hypermineralised tissues (enamel, enameloid, ganoine and acrodin) found in vertebrate teeth and scales results in a compound more resistant to physical and chemical alteration, compared to that of dentine and bone.

Chondrichthyans comprise two classes of the elasmobranchs (sharks skates and rays) and the holocephalans. The teeth of sharks consist of an outer layer of enamel and an inner core of dentine that surrounds a pulp canal. The basal tissue

typically comprises trabecular dentine (osteodentine), which superficially resembles bone in its structure (Smith and Tchernov, 1992). Holocephalan teeth are more variable in morphology and the holocephalan teeth analysed here possess a highly crystalline dentine type material (< 100 μm in thickness) that covers the outer layer of the tooth crown as well as bordering the pore canals that penetrate the dentine. The term 'enameloid' is here adopted to describe this hypermineralised tissue. The body of sharks are covered in denticles, which are characterised by a pulp cavity surrounded by dentine and a thin outer layer of enamel or a hypermineralised dentine (enameloid, Hamlett, 1999; Sire 2010). The basal body of the denticle, which was embedded in the skin during life, comprises acellular bone (Reif, 1978).

Acanthodians are an extinct group of vertebrates whose phylogenetic affinities are currently unresolved (Zaccone et al., 2016), variously considered either as basal sharks (Davis et al., 2012; Brazeau and de Winter, 2013) or osteichthyans (Miles, 1973; Teaford et al., 2007) or a mixture of each (Brazeau, 2008). The scales of acanthodians generally comprise an acellular or cellular bone base and dentine crown (Janvier, 1996; Karatajãt-Talimaa, 1998; Valiukevičius and Burrow, 2005). It should be noted that tissues interpreted as enamel (Richter et al., 1999) and ganoine (Richter and Smith, 1995) have also been reported in this group, reflecting significant diversity within this taxa.

From the mid Devonian (Givetian) Actinopterygians (ray finned fish) host two hypermineralised tissues, ganoine and acrodin, which are unique to this group. Ganoine, with its epidermal origin, is a hard shiny layer has been considered homologous with enamel and covers the dentine of scales (Janvier, 1996; Qu et al., 2015). Acrodin is a hardened dentine present as a cap on the teeth of most post Eifelian palaeoniscoid actinopterygians (Shultze, 2015). A thin layer of collar

enamel is also present covering the tooth shaft dentine of palaeoniscoid fish (Reif, 1982).

Oxygen isotopes of vertebrate bioapatite tissues has been successfully used to determine palaeoenvironmental conditions from the Palaeozoic (Fischer et al., 2013) and Mesozoic using GIRMS (Lécuyer et al., 1993; Pucéat et al., 2003; Billon-Bruyat et al., 2005; Fischer et al., 2012). Applying GIRMS to Palaeozoic vertebrate fossils, however, has been somewhat problematic, producing inconsistent results. Analysis of Late Devonian actinopterygian teeth (Joachimski and Buggisch, 2002) initially suggested that original oxygen isotope ratios were preserved in the tooth apatite. Other works however, have revealed that Palaeozoic vertebrate teeth and dermal denticles are typically depleted in ^{18}O (relative to conodont elements) between 2.4 and 2.9‰ (Barham et al., 2012a; Žigaite et al., 2010). This has led to the suggestion that microvertebrate elements are highly susceptible to diagenetic affects and thus not preserving original isotopic signatures. However, given that secondary alteration may be screened and subsequently avoided, the potential still exists for these fossils to serve as a palaeoclimatic archive.

6.2.3 Objectives

We studied a range of microvertebrate elements using GIRMS to determine the degree to which ecology, as well as diagenesis, influence the oxygen isotope ratios in different microvertebrate remains. Secondary ion mass spectrometry (SIMS) analysis was applied to test whether all microvertebrate tissues are equally prone or resistant to alteration of their O-isotopic ratios. In order to establish the validity of microvertebrate $\delta^{18}O$ signatures and their potential use as palaeoclimatic indicators, the oxygen isotope ratios of microvertebrates are compared with those of co-

occurring conodonts as well as coeval conodonts from latitudinally equivalent areas. Both GIRMS and SIMS analyses were undertaken on Frasnian (Devonian) conodont samples as well as multiple Famennian (Late Devonian) and Tournaisian (Eearly Carboniferous) microvertebrate remains to i) document any potential discrepancies between the two methods and; to ii) identify potential causes of disruption of primary oxygen isotope signatures in different vertebrate tissues.

6.3 Materials and methods

6.3.1 Sample collection, processing and imaging

Late Devonian microvertebrate fossils are common in the distal slope facies of the Virgin Hills Formation (late Frasnian – middle Famennian; Figure 6.1; Playford et al., 2009; Trinajstic and George, 2009; Trinajstic et al., 2014; Roelofs et al., 2015) and in the conodont-poor facies of the Fairfield Group (Late Devonian - Early Carboniferous) (Roelofs et al., 2016; Thomas 1957, 1959). Twenty kilogram samples were collected from Horse Spring (18°11′41″ S, 126°01′69″ E), Oscar Hill (18°04'07" S, 125°26'41" E) and Laurel Downs (18°01'37" S, 125°18'43" E) (Figure 6.1) and processed using a buffered 10% acetic acid solution (following the methodology of Jeppsson et al., 1999). The rock samples were disaggregated as whole rocks with rinsing occurring every 24-48 hours, depending on the degree of disaggregation. This process was repeated, with fresh 10% buffered acetic acid, until the rocks had been sufficiently broken down for picking. Residues were rinsed and sieved (0.125 mm sieve) to further separate microfossils before picking the >0.125 mm fraction under a Nikon stereomicroscope. Detailed examination of microfossils was performed using a Hitachi TM-3030 desktop Scanning Electron Microscope (SEM) at Curtin University with accelerating voltages ranging from 5-15 kV and

variable pressures. Eight larger holocephalan teeth (>10 mm mesio-distally) were recovered directly from the disaggregated rock residues. A single tooth (MTM1-H9) was exposed from the rock sample along its labial face and extracted prior to processing. Additional imaging of analysed specimens was performed using a Leica stereomicroscope camera at the Western Australian Museum.

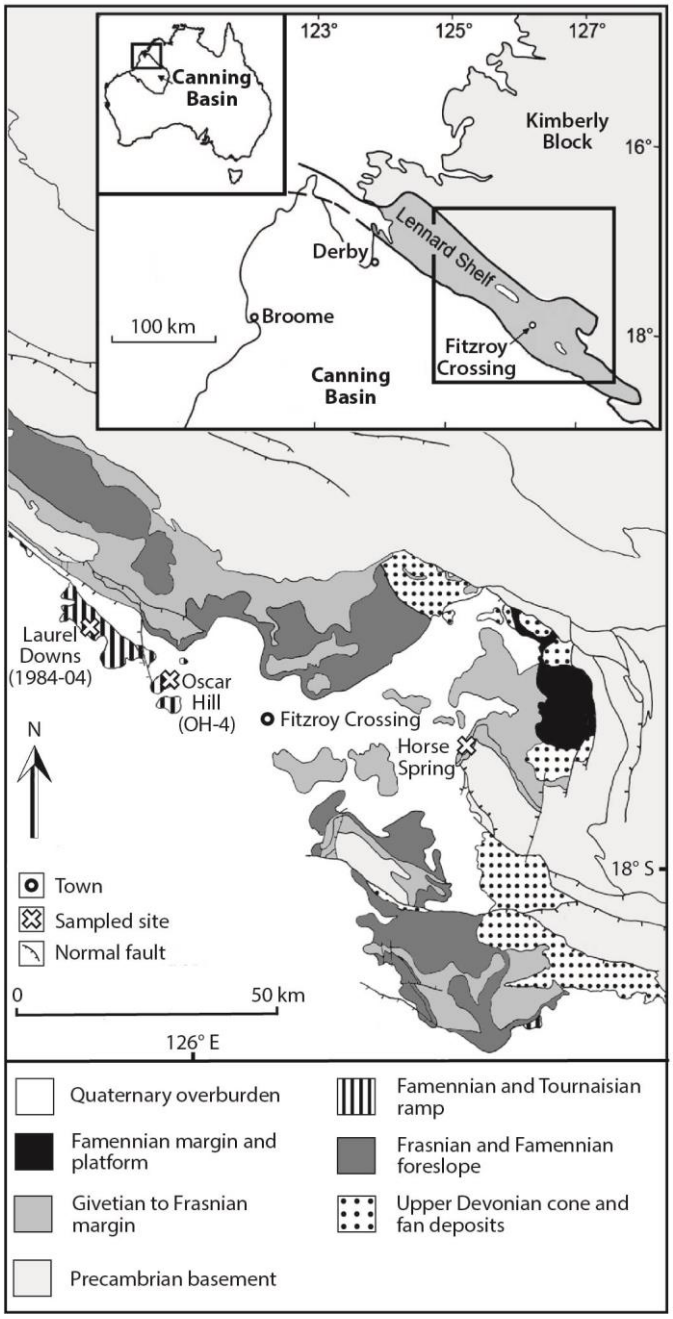

Figure 6.1. General regional geology and sampled sites from the Lennard Shelf, Canning Basin, Western Australia (modified from Playford et al., 2009).

Horse Spring samples yielded 200 conodont elements corresponding to Conodont Zone (CZ) 11 (Frasnian; Klapper, 1989). Conodont yields from Oscar Hill samples taken for this study yielded mainly undiagnostic elements with a single long ranging Famennian conodont *Spathognathodus aciedentatus* recovered. Previous sampling by Nicoll and Druce (1979) indicated a latest Famennian age (*praesulcata* Conodont Zone) for outcrop at Oscar Hill. Carboniferous rock samples (Table 2) were collected from a bioclastic limestone bed of the Laurel Formation (sample number 1984-04), exposed approximately 35 km north-west of the town of Fitzroy Crossing (Figure 1). A Tournaisian age is supported by the presence of the conodont taxa *Clydagnathus cavusformis* and *Bispathodus aculeatus*, and is consistent with previous age determinations (Druce and Radke, 1979; Nicoll and Druce, 1979). A refinement of early Tournaisian is indicated by the overlap of shark species *Thrinacodus ferox*, *Protacrodus aequalis* and *Protacrodus* sp. 1 (Roelofs et al., 2016).

6.3.2 Analytical methodology

The GIRMS method has conventionally been used to accurately determine the $\delta^{18}O$ values of pooled apatite fossils through the analysis of chemically purified Ag_3PO_4. To obtain ~1 mg of fossil material required for replicate analyses, samples comprising multiple microvertebrate elements, or single elements comprising multiple tissue types, are often required. The incorporation of different fossil tissues within analyses reduces data confidence as tissue geochemistry is differentially affected by biological processes including organism physiology, microbial activity as well as physical influences such as diagenesis (e.g. Rigo and Joachimski, 2010). The use of secondary ion mass spectrometry (SIMS) has been shown to be a useful alternative to GIRMS as it facilitates in-situ analysis of specific tissues within

individual microfossils (Vetter et al., 2011), although it is indiscriminate in its analysis of oxygen sites in the material (does not only analyse the stable phosphate). Application of this technique to modern shark teeth (Žigaite and Whitehouse, 2014) has shown preservation of original oxygen isotope signatures in hypermineralised tissues as well as heterogeneity and depletion of ^{18}O within the more permiable dentine. Although primary isotopic values can be elicited using a SIMS method (Wheeley, 2012; Trotter et al., 2015), the effects of tissue heterogeneity on $\delta^{18}O$ signatures within individual microvertebrate fossil elements is less understood.

6.3.2.1 GIRMS oxygen isotope analyses

Stable oxygen isotope ratios were determined on conodont and microvertebrate material at the Stable Isotope Laboratory at the University of Erlangen-Nürnberg, Germany, following a modified version of the procedure developed by O'Neil et al. (1994) and described in Joachimski et al. (2009). Conodont, microvertebrate, extant shark and Durango apatite samples (0.7 - 2.0 mg) were chemically converted to trisilverphosphate (Ag_3PO_4) and the oxygen isotope ratios of ~0.2 mg sample aliquots were analysed as CO produced in a high Temperature Conversion Elemental Analyser (TC−EA) attached on-line to a ThermoFinnigan Delta Five Plus mass spectrometer. Oxygen isotope composition is reported in δ notation in ‰ relative to Vienna Standard Mean Ocean Water (V-SMOW) (Table 6.1). Samples were measured in triplicate, with limited Ag_3PO_4 precipitate from samples OH4-C and 1984-C only allowing duplicate and single analyses respectively. Replicate analyses of the international standard NBS 120c and internal laboratory standards were performed for every seven unknowns as well as at the start, middle and end of each day to monitor accuracy and reproducibility.

Reproducibility was typically ±0.2‰ (1σ) with analyses calibrated for an average NBS120c $\delta^{18}O$ value of 21.7‰ V-SMOW (Pucéat et al., 2010).

6.3.2.2 SIMS oxygen isotope analyses

Conodont and microvertebrate fossils, with single pieces of *Carcharhinus plumbeus* tooth fragments and fragments of a Durango apatite crystal were mounted on double sided tape attached to standard glass plates. Large holocephalan teeth were cut labio-lingually using a Dremel rotary tool and ground flat with 1200 grit sandpaper prior to mounting on the tape along the smooth surface. Struers EpoFix epoxy resin was used to form standard one-inch round mounts and then polished to expose the desired tissues using successively finer polishing cloths to a 1 μm finish. The mounts were then carefully cleaned with detergent, distilled water and isopropanol in an ultrasonic bath and coated with gold (30 nm in thickness) prior to SIMS analyses.

Oxygen isotope ratios were determined using a Cameca IMS 1280 multi-collector ion microprobe located at the Centre for Microscopy, Characterisation and Analysis (CMCA), University of Western Australia (UWA) in March and November 2014. Analyses were performed with a ca. 2.5 nA Cs^+ beam with a total impact energy of 20 keV rastered on a ca. 20 x 20 μm area on the sample surface. Instrument parameters included a magnification of 130 × between the sample and field aperture (FA), 400 μm contrast aperture (CA), 4000 μm FA, 110 μm entrance slit, 400 μm exit slits, and a 40 eV band pass for the energy slit with a 5 eV gap toward the high energy side. Secondary O^- ions were accelerated to 10 keV and analysed with a mass resolving power of approximately 2200 using dual Faraday Cup detectors. A normal-incidence electron gun was used to provide charge compensation and NMR regulation was employed for magnetic field control.

Ten seconds of pre-sputtering was followed by automatic centering of the secondary beam in the FA and CA. Each analysis consisted of 20 four-second cycles, which gave an average internal precision of ±0.2 ‰ (1σ). Analytical sessions were monitored for drift and precision using at least two bracketing standards (Durango apatite; 9.9 ± 0.3 ‰, (1σ, n = 9); attained via GIRMS of three samples analysed in triplicate from the same crystal) for every six sample analyses. Instrumental mass fractionation (IMF) was corrected using Durango apatite following the procedure described in Kita et al. (2009). The spot-to-spot reproducibility (external precision) was typically ±0.3-0.4 ‰ (1σ) on Durango apatite during all of the analytical sessions, except two sessions at ±0.2 ‰ (sample HT2) and ±0.5 ‰ (sample MVM2). Uncertainty on each spot was calculated by propagating the errors on instrumental mass fractionation determination and internal error on each sample data point. The resulting uncertainty was typically between ±0.3 and ±0.6 ‰ (1σ). Raw $^{18}O/^{16}O$ ratios and corrected $\delta^{18}O$ (reported relative to V-SMOW) are presented in Table 6.2.

6.4 Results

6.4.1 Fossil preservation

Visual inspection (both macro- and microscopic) confirmed conodont elements were well preserved, showing no evidence of coarsening crystallites, pitting, overgrowths or other visible signs of diagenetic modification (Figure 6.2; Nöth, 1998). Microvertebrate elements are show smooth lustrous surfaces present on the cusps of teeth and dermal denticle crowns. In cross section, the dentine of all teeth was light grey to white in colour with the exception of sample MTM1-H9, which showed a dark grey discolouration around one margin that correlates to the previously exposed labial surface of the tooth. Reddish coloured staining is present

within the basal tissue in sample MTM1-H1, along with calcite cement in some of the pore canals that extend from the cusp surface to the basal tissue.

6.4.2 GIRMS $\delta^{18}O$ analysis of microvertebrate elements

The $\delta^{18}O$ values of Famennian microvertebrates ranged from 16.2-17.1 ‰ (V-SMOW) with a mean of 16.7 ‰ (Table 6.1). The $\delta^{18}O$ values obtained from the Tournaisian microvertebrate samples are more variable than Famennian values, ranging from15.7 to 19.1 ‰. The largest disparity in $\delta^{18}O$ was measured in the outer

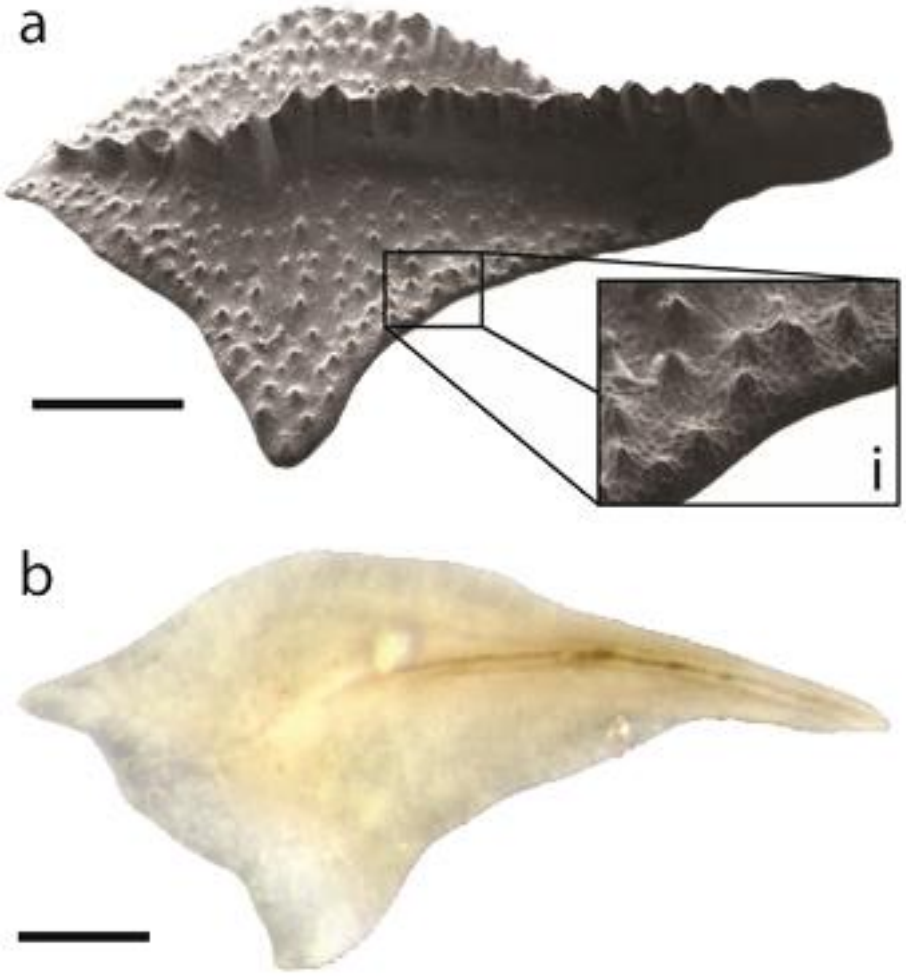

Figure 6.2. Frasnian *Palmatolepis* P-elements. (a) Back-scattered electron microscope image in aboral view with x4 magnified inset (i) highlighting the well-preserved ornamentation. (b) Stereo microscope image of a polished *Palmatolepis* sp. element showing the well preserved internal microstructures and low Colour Alteration Index (CAI). Scale bars = 250 µm.

cusp tissue of Tournaisian holocephalan teeth (16.0 to 19.1 ‰, mean of 17.8 ‰; Figure 6.3). Similar average $\delta^{18}O$ values were obtained from ctenacanthid (16.0 ‰) and protacrodont (17.1 ‰) scales from the Famennian. Inter-taxa variation of <1.2 ‰ was found for Tournaisian acanthodian (17.0 ‰), lungfish (16.5 ‰), ctenacanthiform (16.9 ‰), protacrodont (16.1 and 17.2 ‰) and palaeoniscoid scales (19.0 ‰). Significant intraspecific disparity in $\delta^{18}O$ values within Tournaisian microvertebrates scales was seen between protacrodont scales recording values of 16.1 and 17.2 ‰. The lowest $\delta^{18}O$ values were recorded in Tournaisian

Table 6.1. Late Famennian and early Tournaisian microvertebrate fossils and standards analysed using gas isotope ratio mass spectrometry (GIRMS). Abbreviations: Fr – Frasian; Fm – Famennian ; Tn – Tournaisian; mg – milligram (fossil weight); n – replicate analyses.

Sample no.	**Formation (Fm.)**	**Age**	**Sample**	**Taxa**	**(mg)**	**n.**	**$\delta^{18}O$**	**1σ**
VHS-312	Virgin Hills Fm.	Fr	*Ancyrodella*	Conodont	0.88	3	19.0	0.2
OH-4 A	Gumhole Fm.	Fm	Palatal teeth	Palaeoniscoid	0.99	3	17.0	0.1
OH-4 B	Gumhole Fm.	Fm	Scale	Protacrodont	2.04	3	17.1	0.2
OH-4 C	Gumhole Fm.	Fm	Scale	Ctenacanthid	0.60	2	16.0	0.6
OH-4 D	Gumhole Fm.	Fm	Tooth cusp	*Helodus*	0.89	3	17.2	0.3
SS1	Gumhole Fm.	Fm	Spine	Shark	-	3	16.3	0.1
1984-04 A	Laurel Fm.	Tn	Scale	Ctenacanthid	1.25	3	16.9	0.1
1984-04 B	Laurel Fm.	Tn	Palatal teeth	Palaeoniscoid	0.82	3	18.0	0.2
1984-04 C	Laurel Fm.	Tn	Radial bone	Palaeoniscoid	0.70	1	15.9	0.1
1984-04 D	Laurel Fm.	Tn	Teeth	Palaeoniscoid	0.85	3	15.7	0.5
1984-04 E	Laurel Fm.	Tn	Scale	Palaeoniscoid	1.51	3	17.3	0.6
1984-04 F	Laurel Fm.	Tn	Tooth cusp	Holocephalan	1.63	3	17.3	0.2
1984-04 M	Laurel Fm.	Tn	Tooth cusp	Holocephalan	0.87	3	17.7	0.1
1984-04 G	Laurel Fm.	Tn	Scales	Acanthodian	0.77	3	17	0.4
1984-04 H	Laurel Fm.	Tn	Palatal teeth	Palaeoniscoid	1.42	3	18.1	0.4
1984-04 J	Laurel Fm.	Tn	Scale	Lungfish	1.44	3	16.5	0.2
1984-04 K	Laurel Fm.	Tn	Scale	Protacrodont	1.13	3	16.1	0.3
1984-04 L	Laurel Fm.	Tn	Scale	Protacrodont	0.96	3	17.3	0.5
MT1-H1	Laurel Fm.	Tn	Tooth cusp	Holocephalan	-	3	19.1	0.1
MT2-H4	Laurel Fm.	Tn	Tooth cusp	Holocephalan	-	3	16	0.2
MT2-H5	Laurel Fm.	Tn	Tooth cusp	Holocephalan	-	3	18.8	0.2
MT2-H8	Laurel Fm.	Tn	Tooth cusp	Holocephalan	-	3	18.8	0.1
MT2-H9	Laurel Fm.	Tn	Tooth cusp	Holocephalan	-	3	17.4	0.3
MT4-LPS	Laurel Fm.	Tn	Scale	Lungfish	-	3	15.1	0.0

palaeoniscoids, which recorded $\delta^{18}O$ values of 15.7 (radial bone) and 15.9‰ (tooth) (Figure 6.3). However, $\delta^{18}O$ values of associated palatal teeth were consistently higher at 18.0 ‰ (sample 1984-B) and 18.1 ‰ (sample1984-H).

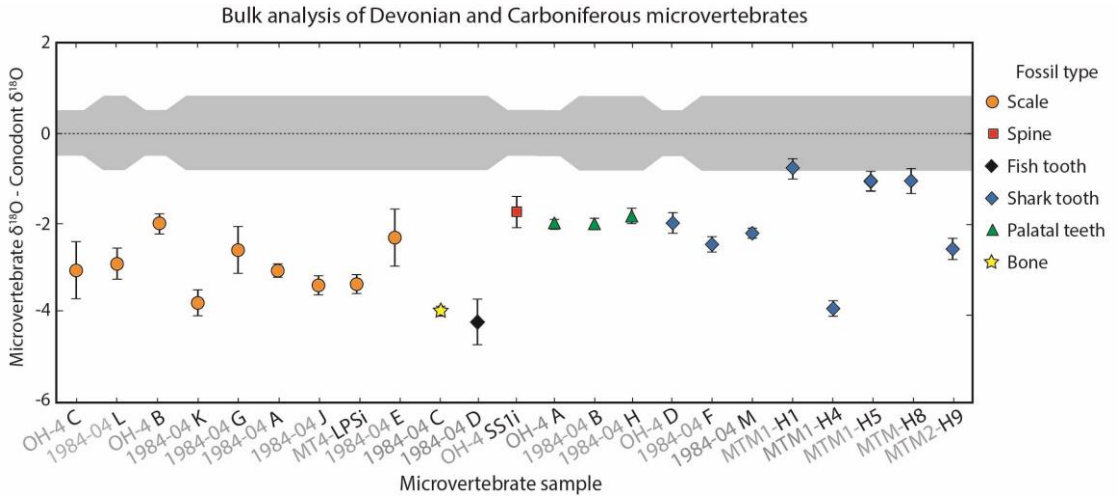

Figure 6.3. Gas Isotope Ratio Mass Spectrometry (GIRMS) analysis of microvertebrate elements from the late Famennian (i) and early Tournaisian (ii). Data points give average value of replicate analyses, vertical bars represent 1 std.dev. Coeval conodont values obtained from SIMS (late Famennian = 20.3 ±0.8 ‰ and; early Tournaisian = 19.6 ±0.5 ‰) were generally higher than microvertebrate values analysed by GIRMS.

6.4.3 SIMS $\delta^{18}O$ analyses

In-situ oxygen isotope analyses were performed on three late Famennian and two early Tournaisian conodont elements (Table 6.2). Conodont $\delta^{18}O$ values from individual spot analyses on three late Famennian S-elements range from 18.7 to 20.8 ‰, with an average value of 19.6 ‰ (Figure 6.4). Two to five individual spots were analysed on the blades of the S-elements with a deviation between spots on each element ranging from 0 to 1.0 ‰ (Table 6.2). Two P_1 elements (*sensu* Purnell et al., 2000) of the early Tournaisian conodont *Clydagnathus cavusformis* produced average $\delta^{18}O$ values of 19.9 ‰ (0.4 ‰, n = 4) and 20.9 ‰ (0.9 ‰, n = 5).

Clusters of three to five spots (within an area of <1 mm^2), were focused on enameloid, dentine and basal tissues of four holocephalan teeth. Occasionally, one or

more analytical spots missed the tissue targeted and average values were determined from remaining spot analyses. Average $\delta^{18}O$ values of spots (n = 5) targeting

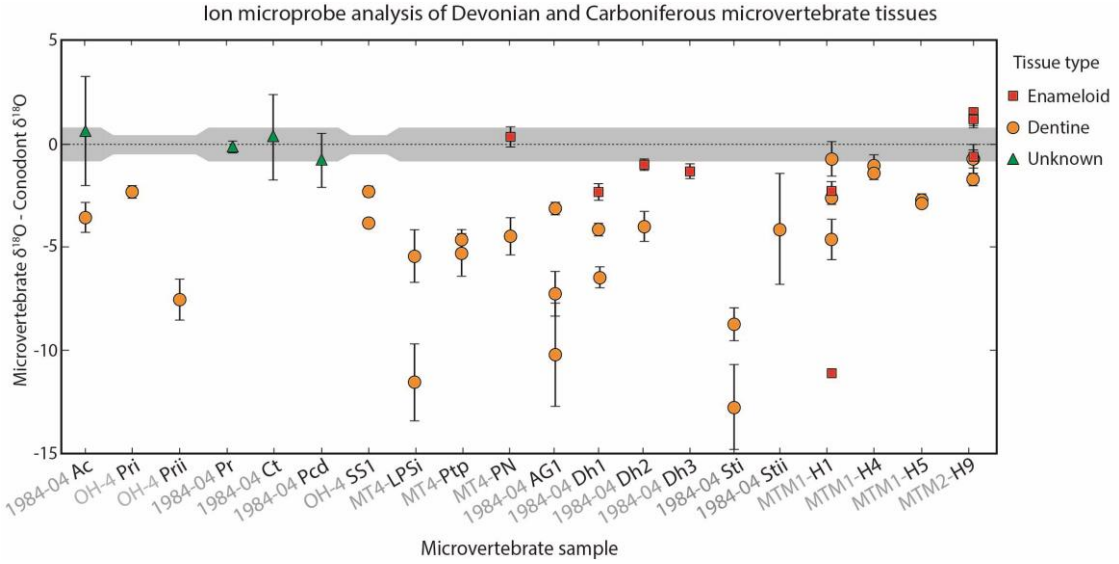

Figure 6.4. Secondary Ion Mass Spectrometry (SIMS) $\delta^{18}O$ analysis of microvertebrate elements from the late Famennian (i) and early Tournaisian (ii). Data points are the averages of spot clusters with 1 std.dev. given by the vertical error bars. Average microvertebrate $\delta^{18}O$ values are plotted as difference relative to $\delta^{18}O$ of conodonts from the same sample. Conodont $\delta^{18}O$ values were obtained from secondary ion mass spectrometry (SIMS) ($\delta^{18}O_{conodont}$ values for: the late Famennian = 20.3 ±0.8 ‰ and; early Tournaisian = 19.6 ±0.5 ‰).

enameloid tissues in tooth MTM1-H1 produced average values for spot clusters of 9.2 ‰ ±0.9 and 18.0 ‰ ±0.2 (Figure 6.5a). The same enameloid tissue in sample MTM1-H9 was analysed, with individual clusters comprising two to three spots from four areas of the tooth (Figure 6.5b) producing average $\delta^{18}O$ values between 21.4 ±0.7 and 21.8 ‰ ±0.1. Dentine was analysed in all four holocephalan teeth with an average $\delta^{18}O$ value of 17.9 ±1.4 ‰ (1σ, n = 35). No consistent differences in $\delta^{18}O$ are present between upper dentine, close to the occlusal surface of the tooth, and lower dentine tissues, located toward the basal body (Figure 6.5). The enamel of three protacrodont teeth was tested using clusters of three to four spots and exhibited average $\delta^{18}O$ values of 17.9 ±0.4, 18.8 ±0.2 and 19.3 ‰ ±0.3 (Figures 6.4, 6.6b). The dentine tissues in one tooth (1984-Dh1) showed a progressive depletion in ^{18}O from near the cusp apex (16.2 ‰) to less mineralised dentine in the basal tissues

Table 6.2. $\delta^{18}O$ values of Durango apatite and late Famennian to early Tournaisian microfossils analysed using SIMS. i and ii notation indicate different individual fossils. Abbreviations: Fr – Frasian; Fm – Famennian ; Tn – Tournaisian; Fm. – Formation; n = number of replicate analysis.

Sample no.	Formation	Age	Sample	Taxa	Tissue	n	$\delta^{18}O$	1σ
VHS-312a	Virgin Hills Fm.	Fr	P-element	*Palmatolepis*	Hyaline	4	18.6	0.3
VHS-312b	Virgin Hills Fm.	Fr	P-element	*Ancyrodella*	Hyaline	4	18.7	0.3
CS2	Gumhole Fm.	Fm	S-element	Conodont	Hyaline	5	19.4	0.5
Si-OH4i	Gumhole Fm.	Fm	S-element	Conodont	Hyaline	2	19.6	1
Si-OH4ii	Gumhole Fm.	Fm	S-element	Conodont	Hyaline	2	18.3	0
OH4-SS1	Gumhole Fm.	Fm	Shark Spine	Unknown	Dentine	4	16.0	0.4
OH4-SS1	Gumhole Fm.	Fm	Shark Spine	Unknown	Dentine	3	18.0	0.3
OH4-Pri	Gumhole Fm.	Fm	Scale	Protacrodont	Unknown	2	17.4	0.1
OH4-Prii	Gumhole Fm.	Fm	Scale	Protacrodont	Unknown	2	12.3	1
CCA1	Laurel Fm.	Tn	P-element	*Clydagnathus*	Hyaline	5	20.4	.9
CCA2	Laurel Fm.	Tn	P-element	Conodont		4	19.4	0.4
1984-04 Ac	Laurel Fm.	Tn	Scale	Acanthodian	Unknown	2	20.1	1.6
1984-04 Ac	Laurel Fm.	Tn	Scale	Acanthodian	Dentine	1	16.2	0
1984-04 Pr	Laurel Fm.	Tn	Scale	Protacrodont	Unknown	3	19.6	0.3
1984-04 Ct	Laurel Fm.	Tn	Scale	Ctenacanthid	Unknown	2	20.1	2.1
1984-04 Pcd	Laurel Fm.	Tn	Scale	Palaeoniscoid	Unknown	2	19.0	1.3
MT4-LPSi	Laurel Fm.	Tn	Scale	Lungfish	Unknown	3	8.3	1.9
MT4-LPSi	Laurel Fm.	Tn	Scale	Lungfish	Unknown	5	14.4	1.3
MT4 Ptp	Laurel Fm.	Tn	Palatal teeth	Palaeoniscoid	Cusp	4	15.2	0.5
MT4 Ptp	Laurel Fm.	Tn	Palatal teeth	Palaeoniscoid	Dentine	4	14.4	1.1
Mt-4 PN	Laurel Fm.	Tn	Tooth	Palaeoniscoid	Acrodin	4	20.2	0.5
Mt-4 PN	Laurel Fm.	Tn	Tooth	Palaeoniscoid	Dentine	3	15.4	0.9
1984-04 AG1	Laurel Fm.	Tn	Tooth	*Ageleodus* sp.	Dentine	3	16.7	0.1
1984-04 AG1	Laurel Fm.	Tn	Tooth	*Ageleodus* sp.	Dentine	5	12.6	1.1
1984-04 AG1	Laurel Fm.	Tn	Tooth	*Ageleodus* sp.	Dentine	2	9.6	2.5
1984-04 Dh1	Laurel Fm.	Tn	Tooth	Protacrodont	Enameloid	3	17.4	0.4
1984-04 Dh1	Laurel Fm.	Tn	Tooth	Protacrodont	Dentine	3	15.7	0.2
1984-04 Dh1	Laurel Fm.	Tn	Tooth	Protacrodont	Dentine	3	13.3	0.5
1984-04 Dh2	Laurel Fm.	Tn	Tooth	Protacrodont	Enameloid	4	18.7	0.2
1984-04 Dh2	Laurel Fm.	Tn	Tooth	Protacrodont	Dentine	4	15.9	0.7
1984-04 Dh3	Laurel Fm.	Tn	Tooth	Protacrodont	Enameloid	3	18.4	0.3
1984-04 Sti	Laurel Fm.	Tn	Tooth	Cladodont	Dentine	4	7.0	2.1
1984-04 Sti	Laurel Fm.	Tn	Tooth	Cladodont	Dentine	4	11.0	0.8
1984-04 Stii	Laurel Fm.	Tn	Tooth	Cladodont	Dentine	4	15.6	2.7
MTM1 H1	Laurel Fm.	Tn	Tooth	Holocephalan	Enameloid	5	17.5	0.5
MTM1 H1	Laurel Fm.	Tn	Tooth	Holocephalan	Enameloid	5	8.7	0.9
MTM1 H1	Laurel Fm.	Tn	Tooth	Holocephalan	Dentine	5	19.0	0.2
MTM1 H1	Laurel Fm.	Tn	Tooth	Holocephalan	Dentine	5	15.1	0.8
MTM1 H1	Laurel Fm.	Tn	Tooth	Holocephalan	Dentine	5	17.1	0.1
MTM1 H4	Laurel Fm.	Tn	Tooth	Holocephalan	Dentine	4	18.2	0.1
MTM1 H4	Laurel Fm.	Tn	Tooth	Holocephalan	Dentine	4	18.7	0.4
MTM1 H5	Laurel Fm.	Tn	Tooth	Holocephalan	Dentine	4	16.8	0.2
MTM1 H5	Laurel Fm.	Tn	Tooth	Holocephalan	Dentine	4	16.9	0.3
MTM1 H9	Laurel Fm.	Tn	Tooth	Holocephalan	Enameloid	3	20.9	0.3
MTM1 H9	Laurel Fm.	Tn	Tooth	Holocephalan	Enameloid	2	21.3	0.1
MTM1 H9	Laurel Fm.	Tn	Tooth	Holocephalan	Enameloid	1	20.9	0
MTM1 H9	Laurel Fm.	Tn	Tooth	Holocephalan	Dentine	3	19.0	0.7
MTM1 H9	Laurel Fm.	Tn	Tooth	Holocephalan	Dentine	3	16.7	0.4

(13.8 ‰) (Figure 6.4). A similar decrease in $\delta^{18}O$ is seen over 10 individual spots in an *Ageleodus* shark tooth (AG1, Figure 6.6c), which presented a general trend in $\delta^{18}O$ from 17.3 ‰ in the cusp dentine, to 8.3 ‰ in the basal tissue. Three sets of analyses were performed on the dentine tissue of three cladodont cusps, which showed average $\delta^{18}O$ values between 7.5 and 11.5 ‰.

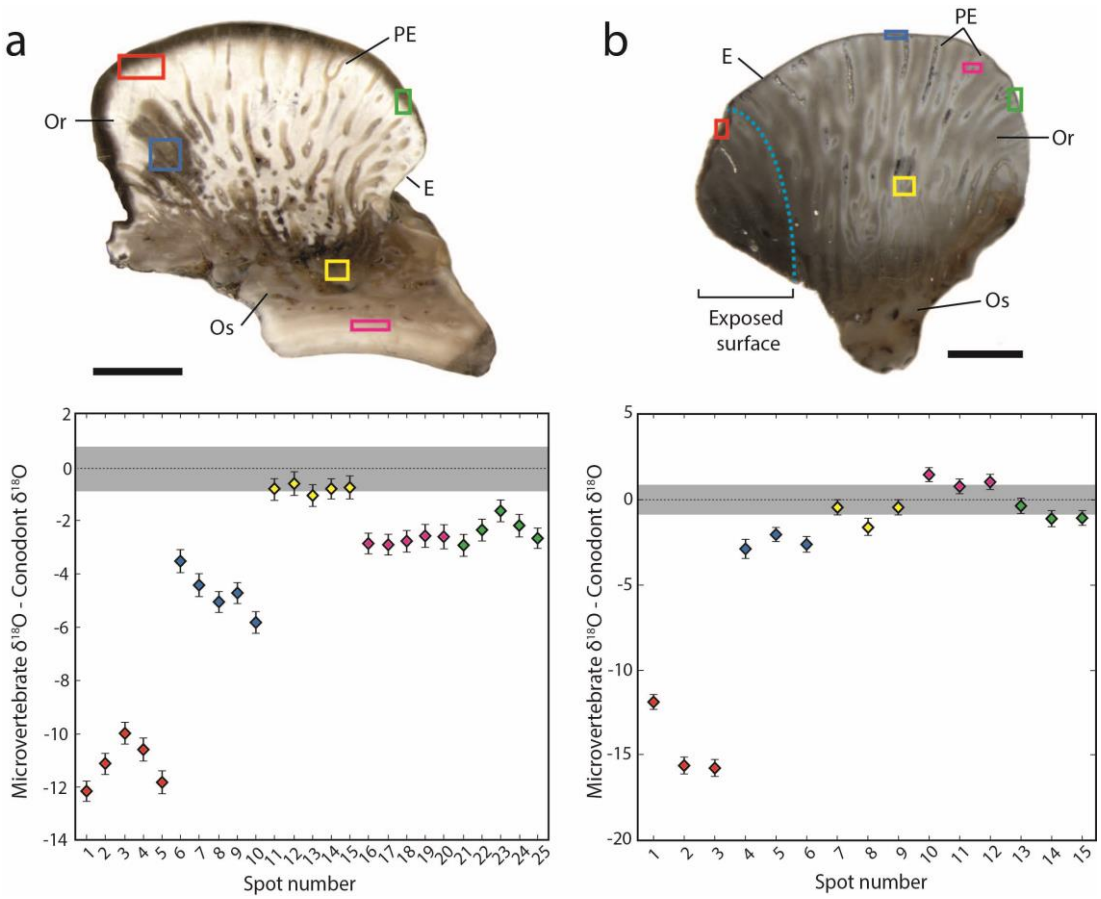

Figure 6.5. $\delta^{18}O$ of tissue types from two early Tournaisian Holocephalan teeth compared to average $\delta^{18}O$ of coeval conodonts (20.3 ±0.8 ‰). (a) Tooth (MTM1 H1) showing analysis of enameloid, dentine and osteodentine tissues; (b) Analysis of a tooth (MTM1 H9) showing variation in $\delta^{18}O$ values associated with exposure of the labial surface (indicated in blue). Scale bar = 2.5 mm. Coloured boxes correspond to spot clusters depicted in the graphs a, b. Grey area represents 1 std.dev. of average $\delta^{18}O$ of associated conodonts analysed by SIMS. Abbreviations: E – Enameloid; Or – Orthodentine; Os – Osteodentine; PE – Pore Enameloid..

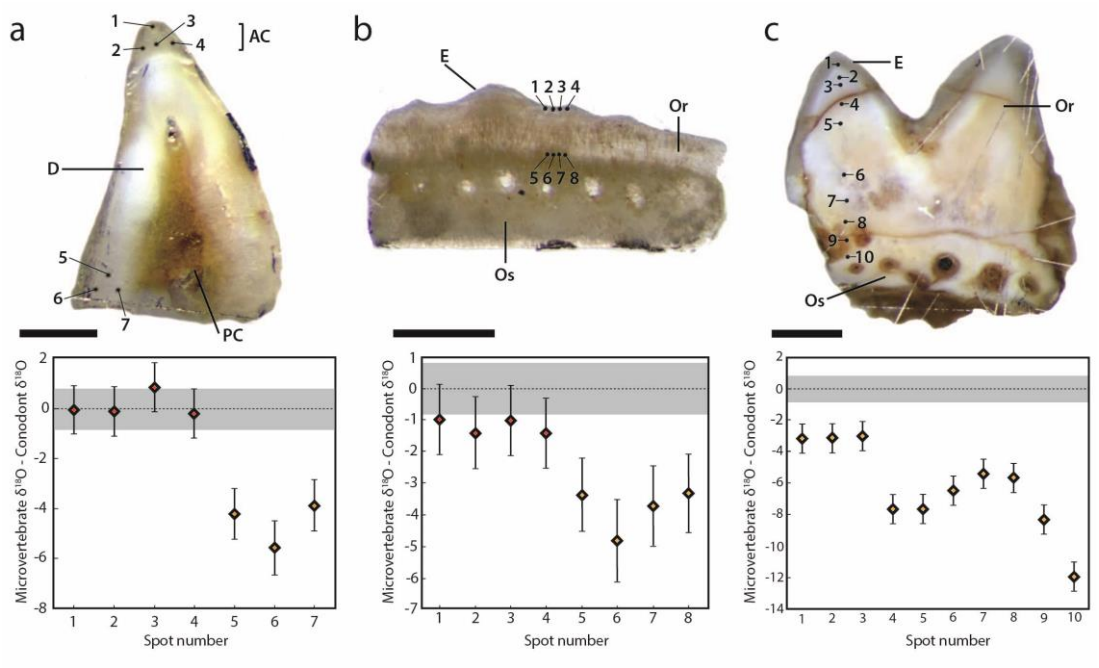

Figure 6.6. Systematic $\delta^{18}O$ variation in microvertebrate tissues. Location of ion-probe spots indicated on stereo-microscope images of polished analytical surface. All values plotted relative to coeval conodont $\delta^{18}O$ value of 20.3 ±0.8 ‰. Variation of $\delta^{18}O$ values in tissue types from early Tournaisian microvertebrate elements (a) Palaeoniscoid fish tooth with acrodin cap and dentine tissue analysed; (b) Analysis of enameloid and dentine tissues from Protacrodont tooth, referred to as *Dalmehodus* cf. *turnerae* (Roelofs et al., 2016); (c) Tooth of the shark *Ageleodus* showing a transect of spot analyses from the cusp apex to the base. Scale bar = 250 μm. Grey areas in graphs represent 1 std. dev. (±0.8 ‰) of $\delta^{18}O$ analyses of co-occurring conodonts. Abbreviations: E – Enamel; AC – Acrodin Cap; D – Dentine; Or – Orthodentine; Os – Osteodentine.

Two sets of $\delta^{18}O$ values were recorded from different areas on a Famennian shark spine, a series of three spots near the margin of the spine (average 16.5 ‰ ±0.3) and three spots located centrally (18.5 ‰ ±0.4). An average $\delta^{18}O$ value of 20.3 ‰ was recorded for scale crown surface tissues across different taxa from the Tournaisian samples. A difference of up to 2.1 ‰ was observed between spots on individual tissues. Dentine tissues from a Famennian protacrodont scale (12.8 ‰ ±1.0, n = 2) as well as a Tournaisian lungfish (8.8 ‰ ±1.9, n = 3 and 14.9 ‰ ±1.3, n = 5) and an acanthodian scale (16.7 ‰ ±1.3) recorded $\delta^{18}O$ values consistently lower than the dentine close to crown surfaces of the scales.

6.5 Discussion

6.5.1 Comparison of GIRMS and SIMS $\delta^{18}O$ analyses

Traditional GIRMS targets the PO_4^{3-} group and eliminates analysis of any less stable oxygen compounds (carbonate, organics, water). However, this method masks potential differences in the O-isotopic signal of fossilised phosphatic tissues when microvertebrate bioapatite is homogenised to obtain minimum sample masses (~0.3 - 1 mg). The porosity present in fossil dentine, which is the bulk component of fossil teeth and dermal denticles, is highly susceptible to physical and chemical alteration. This susceptibility results, in part, from greater surface area increasing potential isotopic exchange between bioapatite and circulating fluids associated with diagenesis, as well as the potential for microbe mediated phosphate precipitation and alteration.

The use of SIMS, as an alternative method for obtaining targeted $\delta^{18}O$ data from microvertebrate and conodont fossils, is advantageous where fossil yields are below the mass required by GIRMS methods and when samples comprise different tissues. However, SIMS indiscriminately analyses any oxygen bearing compounds in the apatite structure. The presence of the CO_3^{2-} anion in bioapatite (either primary or as a secondary cement) can be particularly problematic as it is more susceptible to diagenetic alteration than PO_4^{2-}, with the C-O bond comparably weaker than the P-O bond (e.g. Iacumin et al., 1996).

Recent work by Wheeley et al. (2012) has suggested $\delta^{18}O_{conodont}$ values obtained from SIMS are comparable with those of GIRMS for Ordovician to Silurian conodonts. However, subsequent work by Trotter et al. (2015) has suggested a ~1 ‰ difference between GIRMS and SIMS analyses. Published data are currently considered insufficient to fully assess the presence and/or reasons for any

discrepancies. Here fragments from a single crystal of Durango apatite were utilised to calibrate SIMS analyses. GIRMS analysis gave an average $\delta^{18}O$ value of 9.9 ‰ (± 0.3 ‰, 1σ) from triplicate analysis of three individual fragments of the same crystal, within error of the published value of 9.8 ‰ reported by Rigo et al., (2012). GIRMS analysis of the conodont genera *Ancyrodella* (19.0 ‰) indicated a <0.2 ‰ difference when compared to the $\delta^{18}O$ values obtained from SIMS of both *Ancyrodella* (19.2 ‰) and *Palmatolepis* (19.1 ‰) P_1 conodont elements from the same sample. The $\delta^{18}O_{conodont}$ values resolved from the two methods indicate valid comparisons can be made between SIMS and GIRMS analysis.

6.5.2 Canning Basin $\delta^{18}O_{conodont}$ values in a global context

The presence of open marine conditions in the Canning Basin, in the late Devonian and early Carboniferous, is important if $\delta^{18}O_{conodont}$ values are to be used as a globally representative baseline to assess the validity and palaeoenvironmental relevance of $\delta^{18}O_{microvertebrate}$ values. The significant faunal cosmopolitanism found in ammonoid (Becker 2000), conodont (Nicoll and Druce, 1979; Klapper, 2006) and microvertebrate taxa (Turner, 1982; Trinajstic and George, 2009; Hairapetian et al., 2015; Roelofs et al., 2015, 2016; Trinajstic et al., 2015) in the Late Devonian and early Carboniferous suggests that pathways existed for significant faunal exchange. Furthermore, the recovery, from the Lennard Shelf, of globally correlative carbon isotope signatures associated with the Kellwasser Event (Stephens and Sumner, 2003; Playton et al., 2013; George et al., 2014; Hillbun et al., 2015), and presence of a significant regression (Talent et al., 1993) and negative $\delta^{13}C$ excursion (Andrew et al., 1994) related to the Hangenberg Event, are all suggestive of a local marine system coupled to global oceanic conditions. Despite these indicators of an open

marine system, the $\delta^{18}O_{conodont}$ values from Frasnian conodont Zone 11 (*jamieae* CZ) in the Canning Basin (19.1-19.5 ‰) are almost 2 ‰ higher than the average pan tropical values reported in Joachimski et al. (2004). The difference between the Canning Basin CZ 11 values and other sites may be due to local variations in temperature and salinity and demonstrate the importance of natural global variations in water composition, particularly when constructing composite isotope curves. In contrast to the Frasnian sample, a paucity of conodont elements from the Famennian and Tournaisian makes it difficult for well constrained ages and, therefore, direct comparison of Canning Basin $\delta^{18}O_{conodont}$ with coeval global values. The Oscar Hill locality, from which the Devonian samples were taken, suggested deposition occurred during the latest Famennian based on conodont elements (*praesulcata* CZ, Nicoll and Druce, 1979). An average $\delta^{18}O$ value of 19.6 ‰ is comparable to values from other latitudinally similar sites from the *praesulcata* CZ from the Cantabrian Mountains, Spain (~19.4 ‰) and Montagne Noire, France (~17.6-19.5 ‰) (Buggisch et al., 2008; values published by Buggisch et al. (2008) were corrected by -0.7 ‰ to account for a difference in $\delta^{18}O$ of standard NBS120c). A Tournaisian age for the Carboniferous sample can be inferred from the presence of the conodont *Clydagnathus cavusformis* (Nicoll and Druce, 1979) with a refinement of early Tournaisian likely based off microvertebrate remains (Roelofs et al., 2016). The average $\delta^{18}O$ value for *C. cavusformis* P_1-elements tested was 20.3 ‰. This is similar to the $\delta^{18}O_{conodonts}$ from a *sulcata* CZ interval (~19.7 - 20.5 ‰, values were corrected by -0.7 ‰ to account for a difference in d18O of standard NBS120c) from Cantabrian Mountains, Spain (Buggisch et al., 2008). The results indicate that conodonts from the Frasnian to the Tournaisian in the Canning Basin are preserving isotopic signatures similar to conodonts from other pan tropical sites.

6.5.3 $\delta^{18}O$ variation in microvertebrate tissues

The enameloid and dentine of four holocephalan teeth, all attributed to the same species, showed significant differences in $\delta^{18}O$ values as a result of histology, and therefore, mineral composition and susceptibility to diagenesis. The dense enameloid tissue present in holocephalan teeth is similar in hardness to that of enamel (Ishiyama et al., 2012) and comprises the outer layer of the crown as well as pore linings penetrating the crown (Figure 6.5). The $\delta^{18}O$ values obtained (via SIMS) adjacent to pore canals produced more consistent results (mean value of 21.5 ‰) than the outer mineralised layer of the crown, where $\delta^{18}O$ averages of spot clusters varied between 9.2 and 19.4 ‰. The enameloid tissue found along the outer surface of tooth MTM1-H1 (Figure 6.5a) is considerably depleted in ^{18}O along a surface that had previously been exposed in the outcrop. Other teeth also showed lower $\delta^{18}O$ values along the edge of the crown. These values may be an analytical artefact due to topography induced through the differential polishing of the tooth and resin, or may result from diagenetic alteration, as the more discoloured areas in the tooth commonly show lower $\delta^{18}O$ values (Figure 6.5b). Recent work has indicated that apparently well preserved (i.e. lustrous) hypermineralised fossil tissues (e.g. Žigaitė et al., 2015) may not necessarily be indicative of pristine geochemistry. The presence of variable 'staining' in the teeth may reflect diagenetic mineralisation or alteration and may explain the significantly lower $\delta^{18}O$ values in peripheral hypermineralised tissues.

In general, the pore enameloid appears to more reliably preserve the original oxygen isotope ratios in comparison to the outer enameloid tissues (Figure 6.5), which are more readily exposed to post-mortem (or post-shedding) and burial processes. Dentine tissue, was analysed in two areas of the holocephalan teeth, the

first close to the cusp surface (mean value of 17.3 ‰) and the second lower, towards the basal body (17.7 ‰). Differences in dentine $\delta^{18}O$ values are not consistent between these areas and instead appear dependant on the individual tooth analysed (Table 6.2). In general, dentine yielded more variable and lower $\delta^{18}O$ values in comparison to enameloid (Figure 6.4). However, the dentine in one holocephalan tooth (MTM1-H1, Figure 5a) produced an average $\delta^{18}O$ value of 19.7 ‰ (five individual spots, Table 6.2), which is comparable to average $\delta^{18}O_{conodont}$ from the same sample 20.3 ‰. The high $\delta^{18}O$ value may indicate that parts of the basal tissue, even though primarily consisting of porous dentine, may be capable of preserving the original isotopic signatures under appropriate conditions.

The general structure of acrodin present in the tooth tip of many palaeonisciform fish is similar to the woven structure of enamel in elasmobranchs (Ripa et al., 1972; Ørvig, 1978a; Reif, 1985; Sasagawa et al., 2012) and thereby prospective in terms of resistance to diagenetic modification or disruption of isotopic signatures. The $\delta^{18}O$ values obtained from four spot analyses of the acrodin tip of a tooth (Mt-4 PN) support this histological robustness with a $\delta^{18}O$ value (20.7 ‰) and a standard deviation ($1\sigma = \pm 0.5$ ‰) comparable with associated conodonts (Figure 6a, Table 6.2). The average $\delta^{18}O$ value for the palaeoniscoid tooth dentine is depleted in ^{18}O (15.9 ‰) and similar to values from dentine in associated microvertebrate taxa.

SIMS analyses were conducted on a range of scales belonging to acanthodians, chondrichthyan and palaeoniscoids. Scales attributed to each of these groups hosted average $\delta^{18}O$ values within 1 ‰ of coeval conodont values (Figure 6.4), which indicate that some scale tissues are preserving primary isotopic signatures. However, identifying the tissues that host these signatures is difficult as

the spot size from the SIMS beam is larger than some of the targeted tissues. This causes a degree of ambiguity in the $\delta^{18}O$ results due to the unquantifiable influence of surrounding tissues. The presence of ganoine, a tissue homologous with enamel (Qu, et al., 2013), may explain the relatively high average $\delta^{18}O$ value of 19.5 ±1.3 ‰. Reconciling the average $\delta^{18}O$ value of 20.9 ±1.6 ‰ for the acanthodian scale (1984-04 Ac, Figure 6.4) analysed is difficult, as scales of this taxa typically lack hypermineralised tissues and instead comprise an acellular bone base and a dentine layer covering the crown (Sire et al., 2009). Hypermineralised tissues such as ganoine have been reported in Palaeozoic acanthodians (e.g. Richter and Smith, 1995), which highlights the need for individual scales to be analysed rather than relying on the generalised histology of particular taxa. Overall, the results obtained from scales indicate that multiple taxa have the potential to be used to elicit apparently original isotopic data and interpret ancient environmental conditions.

6.5.4 Comparison of GIRMS and SIMS $\delta^{18}O$ analyses of microvertebrates

As dentine tissues constitute the bulk of the microvertebrate fossils tested here, it is expected that results from GIRMS would be comparable to SIMS analyses of dentine from the same sample if the greater part of the signal detected by SIMS was from phosphate. This hypothesis is supported by $\delta^{18}O$ values of the shark spine (OH-4 SS1), lungfish scale (MT3-LPS) and some holocephalan teeth (MTM1-H4, MTM1-H5, MTM1-H9) analysed (Figure 6.7). Higher $\delta^{18}O$ values from the GIRMS method found in the lungfish scale (MT4-LPS) and two holocephalan teeth (MTM1-H1, MTM1-H5) are likely due to the influence of robust signals from

hypermineralised tissue analysed in conjunction with the dentine tissues when using GIRMS.

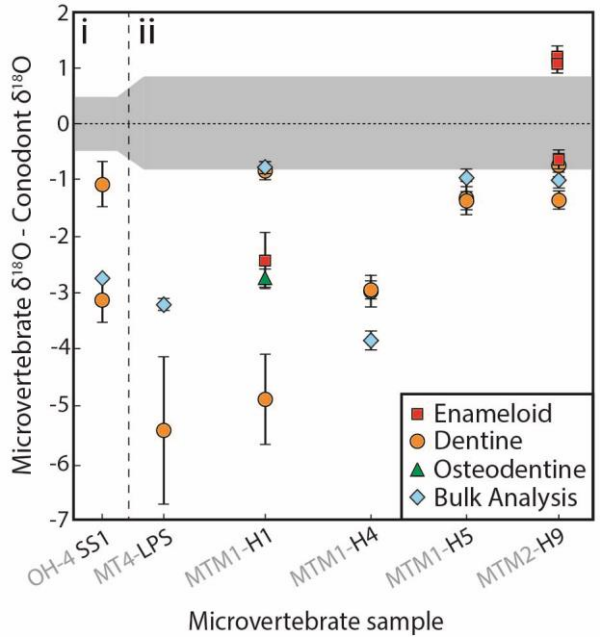

Figure 6.7. Comparison of GIRMS and tissue specific targeting via SIMS analysis on individual fossil elements from the (i) Famennian (average conodont $\delta^{18}O$ value of 19.6 ±0.5‰) and (ii) Tournaisian (average conodont $\delta^{18}O$ value of 20.3 ±0.8‰). Grey area in the graph represents the 1 std.dev. of $\delta^{18}O$ analyses of co-occurring conodonts.

6.5.5 Diagenetic influences

Microvertebrate fossils analysed using GIRMS are commonly depleted in ^{18}O when compared to coeval conodont elements (Žigaitė et al., 2010; Barham et al., 2012a, b; Fischer et al., 2013). Since it has been demonstrated that modern fish precipitate bioapatite in isotopic equilibrium with ambient water (Kolodny et al., 1983; Vennemann et al., 2001; Puceat et al., 2010), and the palaeoecology of many of the taxa are thought to overlap with those of coeval conodonts, the lower $\delta^{18}O$ values are interpreted to have occurred as a consequence of diagenetic changes in the less mineralised tissues. The 2.4 and 2.5‰ offsets found for Famennian and Tournaisian specimens examined herein (Figure 3), respectively, are close to those reported between Silurian conodonts and fish scales (2.5 ‰; Žigaitė et al., 2010).

The low colour alteration index (CAI) of the Silurian conodonts (<1.5 ‰; Žigaitė et al., 2010) indicate thermally immature sediments, similar to what is found in the Canning Basin, and may explain the similarity of the discrepancy in $\delta^{18}O$ values. Moreover, Barham et al. (2012a) reported a more significant depletion in ^{18}O from Mississippian, Carboniferous ichthyoliths from Ireland that were associated with conodonts with CAI of >5, and indicated that the lower $\delta^{18}O$ values were influenced, but not necessarily controlled, by increasing diagenesis and thermal alteration. It is difficult to extrapolate the results of thermal alteration from conodonts to microvertebrates given the significant taxonomic differences between these groups. However, significant degrees of homology have been identified between the hypermineralised tissues of vertebrates and conodont hyaline tissue (Donoghue, 1998; Donoghue et al., 2000; Nemliher and Kallaste, 2012). Therefore, it is not unreasonable to expect the preserved phosphate in both conodont and vertebrate hard tissues would be affected in a similar fashion to thermal maturation processes. Given the similar magnitude of conodont-microvertebrate $\delta^{18}O$ offset in thermally mature and immature regions, it can be concluded that there is no direct correlation between thermal maturation and depletion of $\delta^{18}O_{microvertebrate}$ tissues. This raises the possibility that the lower $\delta^{18}O$ values may be influenced by the susceptibility of less mineralised fossil tissues to chemical processes. These processes may include the recrystallization of existing minerals as well as precipitation of O-bearing phases, both with theoretically different O-isotope compositions, during early diagenesis or at shallow burial and low thermal maturation. Both apatite and calcite have been found to infill pore spaces after degradation of organic compounds such as collagen (Trueman and Palmer, 2003).

SIMS $\delta^{18}O$ analysis of modern shark teeth (Žigaitė and Whitehouse, 2014) identified variation in mean $\delta^{18}O$ values of 1.2 ‰ within the dentine tissue. Mean variation between the parallel bundled enameloid (21.2. – 23.1 ‰) and dentine tissue (20.6 - 21.8 ‰) was also recorded. Žigaitė and Whitehouse (2014) noted the use of H_2O_2 in the pre-treatment cleaning process may have contributed to variation in the ^{18}O values. However, it was concluded that organic matter, which is typically ^{18}O depleted, was the likely cause of this variation. The fossil shark teeth tested here also showed significant discrepancies, as well as depletion in ^{18}O (Figures 4, 5b, 6). However, such variation in the fossil specimens analysed here, cannot be attributed to original organic material as this would have degraded to the point where it would be undetectable, although decay products could have influenced the isotope ratios. Interestingly, analysis of teeth taken from freshly caught sharks (Vennemann et al., 2001) recorded comparable values between the dentine and enamel tissues using GIRMS. The isolation of PO_4 eliminates the influence of ^{18}O depleted organic matter, which may have resulted in $\delta^{18}O$ variation, seen by Žigaitė and Whitehouse (2014), between the dentine and enamel. Work by Zazzo et al. (2003), however showed fractionation of phosphate within bone can occur within a few days post-mortem under oxic conditions, with the presence of microbial enzyme activity significantly increasing the rate of oxygen isotope exchange. In contrast, enamel was found to be significantly resistant to changes in the original oxygen isotope ratios (Zazzo et al., 2003). The susceptibility for isotopic alteration under microbially-mediated conditions, for tissues with originally higher organic matter content, could explain the lower oxygen isotope values of the dentine of the shed teeth analysed by Žigaitė and Whitehouse (2014). The Devonian and Carboniferous microvertebrate elements analysed here were obtained from limestones formed in well oxygenated shallow

water marine settings (Druce and Radke, 1979). Given the lack of thermal maturity or any evidence for fluid alteration of the sequences studied, microbially-induced alteration within incompletely mineralised tissues in the microvertebrate fossils ex-vivo and/or during early diagenesis (eogenesis) must be considered a plausible mechanism for lower $\delta^{18}O$-values.

Evidence of recent weathering processes is present in one of the holocephalan teeth (MTM1-H9, Figure 5b). This tooth had a portion of the occluso-labial face of the crown protruding from a rock. It is difficult to constrain the length of time the tooth was exposed, however it is likely that it was affected by a range of weathering processes including frequent scrub fires and interaction with meteoric fluids. The effect of exposure was evident with the outer enameloid layer of the tooth producing values progressively depleted in ^{18}O toward the exposed surface. The low $\delta^{18}O$ values (average 5.2 - 5.9 ‰) at the exposed face correspond to significant degradation of the enameloid and dentine. However, the affected area was small and the dentine within the tooth (19.5 ‰) was found to be comparable to the outer enameloid surface on the non-exposed face (21.4 ‰, Figure 6b). This suggests relative localisation of alteration and overall robustness of the tissue to short-term abiotic processes.

6.5.6 Palaeoecological influences

Understanding the biology of ancient sharks and fish as well as the environment in which they inhabited must be considered as a factor in variation present in tissues, particularly hypermineralised tissues, where primary values are thought to be original. Glaciation, resulting in the preferential locking of ^{16}O in terrestrial ice-sheets, was present during the late Famennian and early Tournaisian

(Kaiser et al., 2006). Evidence suggests these glacial conditions were not as extensive as the modern climate state (Isaacson et al., 2008), hence a $\delta^{18}O_{seawater}$ offset of -0.5 ‰ (V-SMOW) is inferred to account for greater ^{16}O concentrations in the oceans, rather than being preferentially bound in ice-sheets. Assuming these glacial conditions and subsequent offset to $\delta^{18}O_{seawater}$, average $\delta^{18}O$ values (17.8, 18.9 and 19.2 ‰) from protacrodont tooth enamel (uncorrected for diagenetic alteration due to hypermineralised condition) indicate temperatures of between 34 and 42° C (Lécuyer et al., 2013). Such sea-surface temperatures are considerably high in comparison to the coeval conodont temperatures calculated (25 and 29° C) and, if truly pristine, may reflect a freshwater influence, which is relatively enriched in ^{16}O. Palaeozoic shark taxa are known to have inhabited freshwater environments on both a permanent (e.g. Xenacanths, Ginter et al., 2010) and temporary basis (e.g. *Lissodus*, Fischer et al., 2013). It is difficult to assess whether meteoric waters influenced the relative depletion of ^{18}O in the *Ageleodus* sp. tooth (Figure 5c) as spot analyses were not able to effectively target the enamel tissue that could preserve original values (Figure 6.6c). Teeth from the *Ageleodus* genus have been recovered from freshwater facies (Downs and Daeschler, 2009). The potential for members of this genus to exist in differing habitats could suggest the ability for at least some members to migrate between marine and meteoric waters, thereby affecting $\delta^{18}O$ values. Using similar explanations for the slightly lower $\delta^{18}O$ values in the protacrodont enamel (Figure 6b) is more problematic as members of this group have not been recorded in freshwater facies. However, this cannot preclude a fresh or brackish water influence in a specific protacrodont species. The extant shark genera *Carcharhinus* comprises almost entirely marine species, however it also includes the

species *Carcharhinus leucas* (bull shark), which is known to inhabit freshwater environments for extended periods of time (Copeia, 1971).

Significant ecological differences within extant shark genera are reflected in the O-isotope ratios of the mineralised tissues (Vennemann et al., 2001). The potential migration of ancient sharks through different hydrological settings (fresh-brackish-marine), or movement between extreme latitudes or water depths must also be taken into account when analysing the isotopes of these fossils. Analysis of Late Permian shark teeth by Fischer et al. (2013) showed a clear imprint of meteoric waters on the oxygen isotope signatures in multiple shark taxa. The extent to which other extinct shark species occupied fresh to brackish waters is not well understood. Significant migratory behaviour is observed in extant taxa such as *Odontaspis ferox* (Fergusson et al., 2008), which has been found at depths of 850 m as well as very shallow coastal waters. In addition, members of the species *Carcharodon carcharias* (great white shark) have been frequently observed migrating long distances, in some cases over 20,000 km in less than a year (Bonfil et al., 2005). These behaviours need to be considered in extinct shark taxa as well. Potential migratory issues of extinct species are compounded in groups such as the Ctenicanthiforms where tooth development is slower than that observed in modern sharks (Williams, 2001; Botella et al., 2009). Analysis of species with fast tooth replacement rates may mitigate some migratory factors as teeth are more likely to preserve local conditions. Tooth formation can be as quick as 9-12 days within some extant selachians (Moss, 1967), however determining similar tooth replacement in Palaeozoic species is difficult.

6.5.7 Chemostratigraphic capabilities of microvertebrates

The O-isotope values recorded in conodont elements have been used successfully in chemostratigraphic correlation (e.g Barrick et al., 2007). Correlative stratigraphic curves from $\delta^{18}O_{conodont}$ rely on the ability of these fossils to retain assumed original $\delta^{18}O$ values. Isotopic curves based on $\delta^{18}O$ from microvertebrate GIRMS analysis (e.g. Barham et al., 2012a; Žigaitė et al., 2010) have shown the ability to identify major fluctuations. However, as the difference in $\delta^{18}O_{conodont}$ and the $\delta^{18}O$ values of whole microvertebrate fossils using GIRMS are not consistent between sites, comparison is limited to within localised areas. SIMS however has shown the ability to elicit comparable $\delta^{18}O_{microvertebrate}$ and $\delta^{18}O_{conodont}$. This raises the potential for microvertebrates to be used in a similar fashion to conodonts, allowing for wider scale chemostratigraphic correlation.

6.6 Conclusions

The hypermineralised bioapatite present in microvertebrate teeth and scales provides a proxy capable of reconstructing marine oxygen isotope records from the middle Palaeozoic to the modern day. The densely crystalline tissues that form enamel, enameloid and acrodin suggest these tissues have the greatest potential of preserving primary oxygen isotope signatures. Results presented herein from a broad range of taxa (scales of acanthodians as well as the scales and teeth of chondrichthyans and actinopterygians) indicate eliciting palaeoenvironmental data from other vertebrate groups is likely.

The utilisation of SIMS, which permits tissue specific analysis, suggests dentine tissue is more susceptible to alteration due to a higher porosity inherited from an originally high organic component. The low CAI of conodont fossils analysed here suggests diagenetic influences such as thermal maturation may not be

a major factor in the lower $\delta^{18}O$ values obtained from microvertebrate remains. Instead this work suggests ex vivo microbial activity may be a more likely factor in the alteration of the original oxygen isotope ratios.

Going forward, it is clear that the targeting of hypermineralised tissues in the enamel and enameloid of microvertebrate teeth and scales offer an alternative tool for reconstructing palaeoenvironments. In addition, the presence of original isotopic signatures provides a basis for applications in chemical stratigraphy. Using microvertebrates as proxies for chemostratigraphy will be particularly useful where conodonts are rare or absent. SIMS analysis of targeted hypermineralised microvertebrate tissues may be able to resolve original O-isotope values, and therefore can be used in a similar fashion to, and correlated with, $\delta^{18}O_{conodont}$. However, minimising potential $\delta^{18}O$ variation as a consequence of species dependant factors such as migratory habits remains critical. Ideally analyses should include multiple species and comparisons to co-occurring or co-eval conodonts from other areas.

6.7 Acknowledgements

Thanks you to Daniele Lutz from the GeoZentrum Nordbayern, University of Erlangen-Nürnberg, Germany for aiding in the preparation of the fossil material for analysis. BR would like to thank the anonymous reviewers of his dissertation for their helpful comments. The authors acknowledge the use of equipment, scientific and technical assistance of the Curtin University Electron Microscope Facility, which has been partially funded by the University, State and Commonwealth Governments. In addition the authors would also like to acknowledge the facilities, and the scientific and technical assistance of the Australian Microscopy &

Microanalysis Research Facility at the Centre for Microscopy, Characterisation & Analysis, The University of Western Australia, a facility funded by the University, State and Commonwealth Governments. The authors are also indebted to Catherine Boisvert, Alison Edmunds and the Melbourne Aquarium for providing access to water samples and naturally shed shark teeth, collected during routine cleaning, for use as a matrix matched internal SIMS standard. Further appreciation goes to Bradley McDonald for access to Durango apatite. to the authors also acknowledge support from MRIWA, WA ERA, CSIRO, Chevron Australia Business Unit, Chevron Energy Technology Company, National Science Foundation and the Geological Survey of Western Australia. We would also like to thank the owners of Brooking Springs and Laurel Downs stations for allowing access to outcrops. BR recognises the receipt of an Australian Postgraduate Award as well as a Curtin Completion Scholarship. This research was funded under Australian Research Council grant DP 110101127.

7.0 References

Andrew, A., Hamilton, P., Mawson, R., Talent, J. and Whitford, D. 1994. Isotopic correlation tools in the mid-Palaeozoic and their relation to extinction events. Australian Petroleum Exploration Association Journal 34, 268-268.

Auclair, A., Joachimski, M.M. and Lécuyer, C. 2003. Deciphering kinetic, metabolic and environmental controls on stable isotope fractionations between seawater and the shell of *Terebratalia transversa* (Brachiopoda), Chemical Geology 202, 59-78.

Azmy, K., Veizer, J., Bassett, M.G. and Copper, P. 1998. Oxygen and carbon isotopic composition of Silurian brachiopods: implications for coeval seawater and glaciations. Geological Society of America Bulletin 110, 1499-1512.

Barham, M., Joachimski, M., Murray, J. and Williams, D. 2012a. Diagenetic alteration of the structure and δ 18 O signature of Palaeozoic fish and conodont apatite: Potential use for corrected isotope signatures in palaeoenvironmental interpretation. Chemical Geology 298, 11-19.

Barham, M., Murray, J., Joachimski, M. and Williams, D. 2012b. The onset of the Permo-Carboniferous glaciation: reconciling global stratigraphic evidence with biogenic apatite $\delta^{18}O$ records in the late Visean. Journal of the Geological Society 169, 119-122.

Barrick, J.E., Klapper, G., Kleffner, M.A. and Karlsson, H.R. 2011. Conodont biostratigraphy and stable isotope chemostratigraphy of the lower Henryhouse Formation (Gorstian-early Ludfordian, Ludlow, Silurian), southern Oklahoma, USA. Paleontographica Americana 62, 41-56.

Becker, R. and House, M. 2009. Devonian ammonoid biostratigraphy of the Canning Basin. Geological Survey of Western Australia, Bulletin 145, 415-439.

Billon-Bruyat, J.-P., Lécuyer, C., Martineau, F. and Mazin, J.-M. 2005. Oxygen isotope compositions of Late Jurassic vertebrate remains from lithographic limestones of western Europe: implications for the ecology of fish, turtles, and crocodilians. Palaeogeography, Palaeoclimatology, Palaeoecology 216, 359-375.

Bonfil, R., Meÿer, M., Scholl, M.C., Johnson, R., O'Brien, S., Oosthuizen, H., Swanson, S., Kotze, D. and Paterson, M. 2005. Transoceanic migration,

spatial dynamics, and population linkages of white sharks. Science 310,100-103.

Brand, U. 1989. Biogeochemistry of Late Paleozoic North American brachiopods and secular variation of seawater composition. Biogeochemistry 7, 159-193.

Brand, U. 2004. Carbon, oxygen and strontium isotopes in Paleozoic carbonate components: an evaluation of original seawater-chemistry proxies. Chemical Geology 204, 23-44.

Brazeau, M,D. 2009. The braincase and jaws of a Devonian 'acanthodian' and modern gnathostome origins. Nature 457, 305-308

Brazeau, M.D, de Winter, V. 2015, The hyoid arch and braincase anatomy of Acanthodes support chondrichthyan affinity of 'acanthodians'. Proceedings of the Royal Society B: Biological Sciences 282, 20152210.

Buggisch, W., Joachimski, M.M., Sevastopulo, G. and Morrow, J.R. 2008. Mississippian $\delta^{13}C$ carb and conodont apatite $\delta^{18}O$ records—their relation to the Late Palaeozoic Glaciation. Palaeogeography, Palaeoclimatology, Palaeoecology 268, 273-292.

Caplan, M.L. and Bustin, R.M. 1999. Devonian–Carboniferous Hangenberg mass extinction event, widespread organic-rich mudrock and anoxia: causes and consequences. Palaeogeography, Palaeoclimatology, Palaeoecology 148, 187-207.

Caputo, M.V. and Crowell, J.C. 1985. Migration of glacial centers across Gondwana during Paleozoic Era. Geological Society of America Bulletin 96, 1020-1036.

Carpenter, S.J., Lohmann, K.C., Holden, P., Walter, L.M., Huston, T.J. and Halliday, A.N. 1991. $\delta^{18}O$ values, $^{87}Sr^{86}Sr$ and Sr/Mg ratios of Late Devonian abiotic

marine calcite: Implications for the composition of ancient seawater. Geochimica et Cosmochimica Acta 55, 1991-2010.

Chen, B., Joachimski, M.M., Wang, X.-D. Shen, S., Qi, Y., Qie, W. 2016. Ice volume and paleoclimate history of the Late Paleozoic ice age from conodont apatite oxygen isotopes from Naqing (Guizhou, China). Palaeogeography, Palaeoecology, Palaeoclimatology 448, 151-161.

Davis, S.P., Finarelli, J.A. and Coates, M.I. 2012, *Acanthodes* and shark-like conditions in the last common ancestor of modern gnathostomes. Nature 486, 247–250.

Donoghue, P.C.J. 1998. Growth and patterning in the conodont skeleton. Philosophical Transactions of the Royal Society of London 353, 633-666.

Donoghue, P.C.J., Forey, P.L. and Aldridge, R.J. 2000. Conodont affinity and chordate phylogeny. Biological Reviews 75, 191-251.

Downs, J.P. and Daeschler, E.B. 2001. Variation within a large sample of *Ageleodus pectinatus* teeth (Chondrichthyes) from the Late Devonian of Pennsylvania, USA. Journal of Vertebrate Paleontology 21, 811-814.

Dzik, J. 1991. Evolution of the oral apparatuses in the conodont chordates. Acta Palaeontologica Polonica 36, 265-323.

Fischer, J., Schneider, J.W., Voigt, S., Joachimski, M.M., Tichomirowa, M., Tütken, T., Götze, J. and Berner, U. 2013. Oxygen and strontium isotopes from fossil shark teeth: Environmental and ecological implications for Late Palaeozoic European basins. Chemical Geology 342, 44-62.

Fischer, J., Voight, S., Franz, M., Schneider, J.W., Joachimski, M.M., Tichomirowa, M., Götze, J. and Furrer, H. 2012. Palaeoenvironments of the late Triassic

Rhaetian Sea: implications from oxygen and strontium isotopes of hybodont shark teeth. Palaeogeography Palaeoclimatology Palaeoecology 353, 60–72.

Gabbott, S. E., Aledridge, R.J. and Theron, J.N. 1995. A giant conodont with preserved muscle tissue from the Upper Ordovician of South Africa. Nature 374, 800-803.

George, A.D., Chow, N. and Trinajstic, K.M. 2014. Oxic facies and the Late Devonian mass extinction, Canning Basin, Australia. Geology 42, 327-330.

Ginter, M., Hampe, O. and Duffin, C.J. 2010. Paleozoic Elasmobranchii: Teeth. Pfeil.

Goldberg, M., Kulkarni, A.B., Young, M. and Boskey, A. 2011. Dentin: Structure, Composition and Mineralization: The role of dentin ECM in dentin formation and mineralization. Frontiers in bioscience (Elite edition) 3, 711.

Goudemand, N., Orchard, M.J., Urdy, S., Bucher, H. and Tafforeau, P. 2011. Synchrotron-aided reconstruction of the conodont feeding apparatus and implications for the mouth of the first vertebrates. Proceedings of the National Academy of Sciences 108, 8720-8724.

Grimes, S.T., Mattey, D.P., Hooker, J.J., and Collinson, M.E. 2003. Paleogene paleoclimate reconstruction using oxygen isotopes from land and freshwater organisms: the use of multiple paleoproxies. Geochimica et Cosmochimica Acta, 67, 4033-4047.

Gruszczyński, M., Hałas, S., Hoffman, A. and Małkowski, K. 1989. A brachiopod calcite record of the oceanic carbon and oxygen isotope shifts at the Permian/Triassic transition. Nature 337, 64-68.

Hairapetian, V., Roelofs, B.P., Trinajstic, K.M. and Turner, S. 2015. Famennian survivor turiniid thelodonts of North and East Gondwana. Geological Society, London, Special Publications 423.

Hamlett, W.C. 1999. Sharks, skates, and rays: the biology of elasmobranch fishes. JHU Press.

Hand, A.R. and Frank, M.E. 2014. Fundamentals of Oral Histology and Physiology. John Wiley & Sons.

Hays, P.D. and Grossman, E.L. 1991. Oxygen isotopes in meteoric calcite cements as indicators of continental paleoclimate. Geology 19, 441-444.

Hillbun, K., Playton, T.E., Tohver, E., Ratcliffe, K., Trinajstic, K., Roelofs, B., Caulfield-Kerney, S., Wray, D., Haines, P. and Hocking, R. 2015. Upper Kellwasser carbon isotope excursion pre-dates the F–F boundary in the Upper Devonian Lennard Shelf carbonate system, Canning Basin, Western Australia. Palaeogeography, Palaeoclimatology, Palaeoecology 438, 180-190.

Iacumin, P., Bocherens, H., Mariotti, A. and Longinelli, A. 1996. Oxygen isotope analyses of co-existing carbonate and phosphate in biogenic apatite: a way to monitor diagenetic alteration of bone phosphate? Earth and Planetary Science Letters 142, 1-6.

James, N.P., Bone, Y. and Kyser, T.K. 1997. Brachiopod $\delta^{18}O$ values do reflect ambient oceanography: Lacepede Shelf, southern Australia. Geology 25, 551-554.

Janvier, P. 1996. Early vertebrates. Clarendon Press Oxford.

Jeppsson, L., Anehus, R. and Fredholm, D. 1999. The optimal acetate buffered acetic acid technique for extracting phosphatic fossils. Journal of Paleontology, 964-972.

Joachimski, M., Breisig, S., Buggisch, W., Talent, J., Mawson, R., Gereke, M., Morrow, J., Day, J. and Weddige, K. 2009. Devonian climate and reef evolution: insights from oxygen isotopes in apatite. Earth and Planetary Science Letters 284, 599-609.

Joachimski, M.M. and Buggisch, W. 2002. Conodont apatite $\delta^{18}O$ signatures indicate climatic cooling as a trigger of the Late Devonian mass extinction. Geology 30, 711-714.

Joachimski, M.M., Van Geldern, R., Breisig, S., Buggisch, W. and Day, J. 2004. Oxygen isotope evolution of biogenic calcite and apatite during the Middle and Late Devonian. International Journal of Earth Sciences 93, 542-553.

Jones, D., Evans, A.R., Siu, K.K., Rayfield, E.J. and Donoghue, P.C. 2012. The sharpest tools in the box? Quantitative analysis of conodont element functional morphology. Proceedings of the Royal Society of London B: Biological Sciences 279, 2849-2854.

Kaiser, S.I., Steuber, T. and Becker, R.T. 2008. Environmental change during the Late Famennian and Early Tournaisian (Late Devonian–Early Carboniferous): implications from stable isotopes and conodont biofacies in southern Europe. Geological Journal 43, 241-260.

Kaiser, S.I., Steuber, T., Becker, R.T. and Joachimski, M.M. 2006. Geochemical evidence for major environmental change at the Devonian–Carboniferous boundary in the Carnic Alps and the Rhenish Massif. Palaeogeography, Palaeoclimatology, Palaeoecology 240, 146-160.

Karatajute-Talimaa, V. 1998. Determination methods for the exoskeletal remains of early vertebrates. Fossil Record 1, 21-51.

Kita, N.T., Ushikubo, T., Fu, B. and Valley, J.W. 2009. High precision SIMS oxygen isotope analysis and the effect of sample topography. Chemical Geology 264, 43-57.

Klapper, G. 1988. The Montagne Noire Frasnian (Upper Devonian) conodont succession. Journal of Paleontology 81, 513-537.

Klapper, G. 2007. Frasnian (Upper Devonian) conodont succession at Horse Spring and correlative sections, Canning Basin, Western Australia. Journal of Palaeontology 81, 513-527.

Kolodny, Y., Luz, B. and Navon, O. 1983. Oxygen isotope variations in phosphate of biogenic apatites, I. Fish bone apatite—rechecking the rules of the game. Earth and Planetary Science Letters 64, 398-404.

Korte, C., Jones, P.J., Brand, U., Mertmann, D. and Veizer, J. 2008. Oxygen isotope values from high-latitudes: clues for Permian sea-surface temperature gradients and Late Palaeozoic deglaciation. Palaeogeography, Palaeoclimatology, Palaeoecology 269, 1-16.

LaPorte, D., Holmden, C., Patterson, W., Prokopiuk, T. and Eglington, B. 2009. Oxygen isotope analysis of phosphate: improved precision using TC/EA CF-IRMS. Journal of mass spectrometry 44, 879-890.

Lécuyer, C. and Allemand, P. 1999. Modelling of the oxygen isotope evolution of seawater: implications for the climate interpretation of the $\delta^{18}O$ of marine sediments. Geochimica et Cosmochimica Acta 63, 351-361.

Lécuyer, C., Amiot, R., Touzeau, A., and Trotter, J. 2013. Calibration of the phosphate $\delta^{18}O$ thermometer with carbonate–water oxygen isotope fractionation equations. Chemical Geology 347, 217-226.

Lecuyer, C., Fourel, F., Martineau, F., Amiot, R., Bernard, A., Daux, V., Escarguel, G. and Morrison, J. 2007. High-precision determination of $^{18}O/^{16}O$ ratios of silver phosphate by EA-pyrolysis-IRMS continuous flow technique. Journal of Mass Spectrometry 42, 36-41.

Lécuyer, C., Grandjean, P., O'Neil, J.R., Cappetta, H. and Martineau, F. 1993. Thermal excursions in the ocean at the Cretaceous—Tertiary boundary (northern Morocco): $\delta^{18}O$ record of phosphatic fish debris. Palaeogeography, Palaeoclimatology, Palaeoecology 105, 235-243.

Lécuyer, C., Picard, S., Garcia, J.-P., Sheppard, S.M.F., Grandjean, P., Dromart, G., 2003.Thermal evolution of Tethyan surface waters during the Middle-Late Jurassic: evidence from d18O values of marine fish teeth. Paleoceanography 18, 1076-1091.

Lindström, M. 1964. Conodonts. Elsevier Publishing Company, Amsterdam.

Lindström, M., Racheboeuf, P. and Henry, J. 1974. Ordovician conodonts from the Postolonnec Formation (Crozon Peninsula, Massif Armoricain) and their stratigraphic significance. Geologica et Palaeontologica 8, 15-28.

Mii, H., Grossman, E.L. and Yancey, T.E. 1997. Stable carbon and oxygen isotope shifts in Permian seas of West Spitsbergen-Global change or diagenetic artifact? Geology 25, 227-230.

Mii, H., Grossman, E.L. and Yancey, T.E. 1999. Carboniferous isotope stratigraphies of North America: Implications for Carboniferous paleoceanography and Mississippian glaciation. Geological Society of America Bulletin 111, 960-973.

Nicoll, R.S. and Druce, E.C. 1979. Conodonts from the Fairfield Group, Canning Basin, Western Australia. Australian Government Publishing Service.

Nemliher, J. and Kallaste, T. 2012. Conodont bioapatite resembles vertebrate enamel by XRD properties. Estonian Journal of Earth Sciences 61, 191.

Nöth, S. 1998. Conodont color (CAI) versus microcrystalline and textural changes in Upper Triassic conodonts from Northwest Germany. Facies 38, 165-173.

O'Neil, J.R., Roe, L.J., Reinhard, E. and Blake, R. 1994. A rapid and precise method of oxygen isotope analysis of biogenic phosphate. Israel Journal of Earth Sciences 43, 203-212.

Ørvig, T. 1978a. Microstructure and growth of the dermal skeleton in fossil actinopterygian fishes: *Boreosomus*, *Plegmolepis* and *Gyrolepis*. Zoologica Scripta 7, 125-144.

Ørvig, T. 1978b. Microstructure and Growth of the Dermal Skeleton in Fossil Actinopterygian Fishes: *Nephrotus* and *Colobodus*, with Remarks on the Dentition in Other Forms1. Zoologica scripta 7, 297-326.

Ørvig, T. 1980. Histologic studies of ostracoderms, placoderms and fossil elasmobranchs. Zoologica Scripta 9, 219-239.

Pasteris, J.D., Wopenka, B. and Valsami-Jones, E. 2008. Bone and tooth mineralization: Why apatite? Elements 4, 97-104.

Pietzner, H., Vahl, J., Werner, H. and Ziegler, W. 1968. Zur chemischen zusammensetzung und mikromorphologie der conodonten. Palaeontographica Abteilung A 128, 115-152.

Playford, P.E., Hocking, R.M., and Cockbain, A.E. 2009. Devonian reef complexes of the Canning Basin, WA. Bulletin of the Geological Survey of Western Australia 145, 1-444.

Playton, T., Montgomery, P., Tohver, E., Hillbun, K., Katz, D., Haines, P., Trinajstic, K., Yan, M., Hansma, J. and Pisarevsky, S. 2013. Development of

a regional stratigraphic framework for Upper Devonian reef complexes using integrated chronostratigraphy: Lennard Shelf, Canning Basin, Western Australia, The Sedimentary Basins of Western Australia IV. Proceedings of the Petroleum Exploration Society of Australia Symposium, Perth, Western Australia.

Popp, B.N., Anderson, T.F. and Sandberg, P.A. 1986. Brachiopods as indicators of original isotopic compositions in some Paleozoic limestones. Geological Society of America Bulletin 97, 1262-1269.

Pucéat, E., Joachimski, M.M., Bouilloux, A., Monna, F., Bonin, A., Motreuil, S., Morinière, P., Hénard, S., Mourin, J. and Dera, G. 2010. Revised phosphate–water fractionation equation reassessing paleotemperatures derived from biogenic apatite. Earth and Planetary Science Letters 298, 135-142.

Pucéat, E., Lécuyer, C., Sheppard, S.M., Dromart, G., Reboulet, S. and Grandjean, P. 2003. Thermal evolution of Cretaceous Tethyan marine waters inferred from oxygen isotope composition of fish tooth enamels. Paleoceanography 18, 1-13.

Purnell, M.A., Donoghue, P.C. and Aldridge, R.J. 2000. Orientation and anatomical notation in conodonts. Journal Information 74, 113-122.

Qu, Q., Zhu, M. and Wang, W. 2013. Scales and dermal skeletal histology of an early bony fish Psarolepis romeri and their bearing on the evolution of rhombic scales and hard tissues. PloS one 8, doi: e61485.

Reif, W. E. 1982. Evolution of dermal skeleton and dentition in vertebrates. Springer.

Reif, W. E. 1985. Squamation and ecology of sharks. Senckenbergische Naturforschende Gesellschaft.

Reif, W. 1978. A note on the distinction between acellular bone and atubular dentine in fossil shark teeth. Neues Jahrbuch für Geologie und Paläontologie, Monatshefte 1978, 447-448.

Richter, M. and Smith, M. 1995. A microstructural study of the ganoine tissue of selected lower vertebrates. Zoological Journal of the Linnean Society 114, 173-212.

Richter, M., Neis, P.A. and Smith, M.M. 1999. Acanthodian and actinopterygian fish remains from the Itaituba Formation, Late Carboniferous of the Amazon Basin, Brazil, with a note on acanthodian ganoin. Neues Jahrbuch für Geologie und Paläontologie, Monatshefte 1999, 728–744.

Rigo, M., Trotter, J. A., Preto, N., & Williams, I. S. 2012. Oxygen isotopic evidence for Late Triassic monsoonal upwelling in the northwestern Tethys, Geology, 40, 515-518.

Ripa, L., Gwinnett, A., Guzman, C. and Legler, D. 1972. Microstructural and microradiographic qualities of lemon shark enameloid. Archives of oral biology 17, 118-165.

Roelofs, B., Barham, M., Mory, A. and Trinajstic, K. 2016. Late Devonian and Early Carboniferous chondrichthyans from the Fairfield Group, Canning Basin, Western Australia. Palaeontologia Electronica 19, 1-28.

Roelofs, B., Playton, T., Barham, M. and Trinajstic, K. 2015. Upper Devonian microvertebrates from the Canning Basin, Western Australia. Acta Geologica Polonica 65, 69-101.

Rollion-Bard, C., Saulnier, S., Vigier, N., Schumacher, A., Chaussidon, M. and Lécuyer, C. 2016. Variability in magnesium, carbon and oxygen isotope

compositions of brachiopod shells: Implications for paleoceanographic studies. Chemical Geology 423, 49-60.

Sasagawa, I., Yokosuka, H., Ishiyama, M., Mikami, M., Shimokawa, H. and Uchida, T. 2012. Fine structural and immunohistochemical detection of collar enamel in the teeth of Polypterus senegalus, an actinopterygian fish. Cell and tissue research 347, 369-381.

Schobben, M., Stebbins, A., Ghaderi, A., Strauss, H., Korn, D. and Korte, C. 2015. Flourishing ocean drives the end-Permian marine mass extinction. Proceedings of the National Academy of Sciences 112, 10298-10303.

Scholle, P.A. and Ulmer-Scholle, D.S. 2003. A Color Guide to the Petrography of Carbonate Rocks: Grains, Textures, Porosity, Diagenesis, American Association of Petroleum Geologists Memoir 77.

Schultze, H.P. 2015. Scales, Enamel, Cosmine, Ganoine, and Early Osteichthyans. Comptes Rendus Palevol. In press.

Sire, J.-Y., and Akimenko, M.-A. 2004. Scale development in fish: a review, with description of sonic hedgehog (shh) expression in the zebrafish (*Danio rerio*). International journal of developmental biology 48, 233-248.

Smith, P. and Tchernov, E. 1992. Structure, Function, and Evolution of Teeth. Freund Publishing House Ltd.

Stack, M.V. 1955. The chemical nature of the organic matrix of bone, dentin, and enamel. Annals of the New York Academy of Sciences 60, 585-595.

Stephens, N.P. and Sumner, D.Y. 2003. Famennian microbial reef facies, Napier and Oscar Ranges, Canning Basin, western Australia. Sedimentology 50, 1283-1302.

Sun, Y., Joachimski, M.M., Wignall, P.B., Yan, C., Chen, Y., Jiang, H., Wang, L. and Lai, X. 2012. Lethally hot temperatures during the Early Triassic greenhouse. Science 338, 366-370.

Talent, J.A., Mawson, R., Andrew, A.S., Hamilton, P.J. and Whitford, D.J. 1993. Middle Palaeozoic extinction events: faunal and isotopic data. Palaeogeography, Palaeoclimatology, Palaeoecology 104, 139-152.

Teaford, M. F., Smith, M. M. and Ferguson, M. W. J. 2000. Development, Function and Evolution of Teeth Cambridge University Press.

Thomas, G. 1957. Lower Carboniferous deposits in the Fitzroy Basin, Western Australia. Aust. J. Sci 19, 160-161.

Thomas, G. 1959. The Lower Carboniferous Laurel Formation of the Fitzroy Basin. Bureau of Mineral Resources Australia Report 38, 21-36.

Thorson, T.B. 1971. Movement of bull sharks, *Carcharhinus leucas*, between Caribbean Sea and Lake Nicaragua demonstrated by tagging. Copeia, 336-338.

Trinajstic, K., Roelofs, B., Burrow, C., Long, J. and Turner, S. 2014. Devonian vertebrates from the Canning and Carnarvon Basins with an overview of Paleozoic vertebrates of Western Australia. Journal of the Royal Society of Western Australia 97, 133-151.

Trotter, J.A., Williams, I.S., Barnes, C.R., Lécuyer, C. and Nicoll, R.S. 2008. Did cooling oceans trigger Ordovician biodiversification? Evidence from conodont thermometry. Science 321, 550-554.

Trotter, J.A., Williams, I.S., Nicora, A., Mazza, M. and Rigo, M. 2015. Long-term cycles of Triassic climate change: a new $\delta^{18}O$ record from conodont apatite. Earth and Planetary Science Letters 415, 165-174.

Trueman, C., Benton, M.J. and Palmer, M. 2003. Geochemical taphonomy of shallow marine vertebrate assemblages. Palaeogeography, Palaeoclimatology, Palaeoecology 197, 151-169.

Turner, S. 1982. Middle Palaeozoic elasmobranch remains from Australia. Journal of Vertebrate Paleontology 2, 117-131.

Valiukevicus, J. and Burrow, C.J. 2005. Diversity of tissues in acanthodians with *Nostolepis*-type histological structure. Acta Palaeontologica Polonica 50, 635-649.

Van Geldern, R., Joachimski, M., Day, J., Jansen, U., Alvarez, F., Yolkin, E. and Ma, X.-P. 2006. Carbon, oxygen and strontium isotope records of Devonian brachiopod shell calcite. Palaeogeography, Palaeoclimatology, Palaeoecology 240, 47-67.

Veizer, J., Ala, D., Azmy, K., Bruckschen, P., Buhl, D., Bruhn, F., Carden, G.A., Diener, A., Ebneth, S. and Godderis, Y. 1999. $^{87}Sr/^{86}Sr$, $\delta^{13}C$ and $\delta^{18}O$ evolution of Phanerozoic seawater. Chemical geology 161, 59-88.

Veizer, J., Fritz, P. and Jones, B. 1986. Geochemistry of brachiopods: oxygen and carbon isotopic records of Paleozoic oceans. Geochimica et Cosmochimica Acta 50, 1679-1696.

Vennemann, T., Hegner, E., Cliff, G. and Benz, G. 2001. Isotopic composition of recent shark teeth as a proxy for environmental conditions. Geochimica et Cosmochimica Acta 65, 1583-1599.

Vetter, L., Kozdon, R., Mora, C.I., Eggins, S.M., Valley, J.W., Hönisch, B. and Spero, H.J. 2013. Micron-scale intrashell oxygen isotope variation in cultured planktic foraminifers. Geochimica et Cosmochimica Acta 107, 267-278.

Wadleigh, M.A. and Veizer, J. 1992. $^{18}O/^{16}O$ and $^{13}C/^{12}C$ in lower Paleozoic articulate brachiopods: Implications for the isotopic composition of seawater. Geochimica et Cosmochimica Acta 56, 431-443.

Wenzel, B., Lécuyer, C. and Joachimski, M.M. 2000. Comparing oxygen isotope records of Silurian calcite and phosphate $\delta^{18}O$ compositions of brachiopods and conodonts. Geochimica et Cosmochimica Acta 64, 1859-1872.

Wheeley, J.R., Smith, M.P. and Boomer, I. 2012. Oxygen isotope variability in conodonts: implications for reconstructing Palaeozoic palaeoclimates and palaeoceanography. Journal of the Geological Society 169, 239-250.

Yamamoto, K., Asami, R. and Iryu, Y., 2011. Brachiopod taxa and shell portions reliably recording past ocean environments: toward establishing a robust paleoceanographic proxy. Geophysical Research Letters 38. doi: 10.1029/2011GL047134.

Zaccone, G., Dabrowski, K., Hedrick, M.S., Fernandes, J.M.O. and Icardo, J.M. 2015 Phylogeny, anatomy and physiology of ancient fishes. CRC Press.

Zazzo, A., Lécuyer, C. and Mariotti, A. 2004. Experimentally-controlled carbon and oxygen isotope exchange between bioapatites and water under inorganic and microbially-mediated conditions. Geochimica et Cosmochimica Acta 68, 1-12.

Žigaitė, Ž., Joachimski, M. and Lehnert, O. 2009. Oxygen Isotope Record In Biogenic Apatite: A Tool For Chemostratigraphy And Proxy In Palaeoclimate Studies, 2009 Portland GSA Annual Meeting.

Žigaitė, Ž., Karatajūtė-Talimaa, V. and Blieck, A. 2011. Vertebrate microremains from the Lower Silurian of Siberia and Central Asia: palaeobiodiversity and palaeobiogeography. Journal of Micropalaeontology 30, 97-106.

Žigaitė, Ž. and Whitehouse, M. 2014. Stable oxygen isotopes of dental biomineral: differentiation at the intra-and inter-tissue level of modern shark teeth. GFF 136, 337-340.

Žigaitė, Ž., Fadel, A., Blom, H., Perez-Huerta, A., Jeffries, T., Märss, T., and Ahlberg, P. E. 2015. Rare earth elements (REEs) in vertebrate microremains from the upper Pridoli Ohesaare beds of Saaremaa Island, Estonia: geochemical clues to palaeoenvironment. Estonian Journal of Earth Sciences, 64, 115.

7.0 Conclusions

7.1 Microvertebrate biostratigraphy

This study presents the most comprehensive analysis of the taxonomy and temporal range of microvertebrates from middle Devonian (Givetian) to Early Carboniferous (Tournaisian) aged sediments of the Canning Basin to date. The first vertebrates from the Givetian Aged Cadjebut Formation were described and represent the earliest record of placoderms (ptyctodonts and arthrodires) and chondrichthyians in the Canning Basin (Trinajstic et al., 2014). The known temporal range of Frasnian microvertebrates were refined with age ranges established for an additional 30 Famennian and Carboniferous shark species.

The earlier work of Trinajstic and George (2009) has been developed with the upper age of the thelodont *Australolepis seddoni* extended from CZ10 to CZ11 (Roelofs et al., 2015). The recovery of thelodont scales in Famennian strata from Iran led Turner and Hairapetian (2005) to suggest that the age range of *A. seddoni* extended into the Famennian. The description of this material and further finds from South Oscar Range did not support the occurrence of *A. seddoni* within the Famennian (see Hairapetian et al., 2015). However, the discovery of a new genus and species of thelodont, ?*Arianalepis* sp. indet from the Famennian (Upper *marginifera*/*trachytera* conodont zone) of the South Oscar Range, and Iran confirms the presence of Famennian thelodonts in Australia (Hairapetian et al., 2015) and suggests that scales recovered from mineral drill core (Turner, 1997) belong to this new genus. The small quantity of scales recovered, and poor preservation of the material, makes a definite determination impossible but tentative attribution to *Arianalepis* sp. was made (Hairapetian et al., 2015). The genus *Arianalepis* is also

known from Famennian (CZ) Hodjek, Iran and provides additional data for the biostratigraphic correlation between north-western Australia and central Iran (Hairapetian et al., 2015). In addition, these occurrences mark the youngest record of thelodonts globally. Thelodonts are not known past the end Givetian in the northern hemisphere and previous to this study the youngest occurrence was restricted to the Frasnian of Gondwana (Turner and Dring, 1981; Trinajstic and George, 2009).

The recovery of additional chondrichthyan teeth from the Horse Spring section of the Frasnian aged Virgin Hills Formation (Roelofs et al., 2015) has refined ages of phoebodont species determined by Trinajstic and George (2009) and aligned their temporal ranges more closely to the standard Frasnian phoebodont zonation of Ginter and Ivanov (1996). In addition, previously undocumented variation in *Phoebodus bifurcatus* and *Phoebodus latus* was described from the recovered teeth.

Famennian aged chondrichthyan teeth identified as *Thrinacodus tranquillus*, *Deihim mansureae, Lissodus lusavorichi* and *Protacrodus serra* were recovered from the Bugle Gap Limestone and Casey Falls sections and represent the first record of these taxa from the Canning Basin (Roelofs et al., 2015). The age ranges for *Thrinacodus tranquillus* and *Deihim mansureae* teeth recovered from the Canning Basin conform to the known age ranges of these species outside of Australia. The documented age ranges of these shark species in Iran and south China indicate a middle Famennian age for the sampled site at Bugle Gap, which is consistent with the age determined by conodonts obtained from the same site. *Lissodus lusavorichi* and *Protacrodus serra* were recovered from limestone beds dated as Lower *crepida*/Upper *marginifera* Conodont Zone. This represents the oldest occurrence of these two species, previously recovered from strata no older than *expansa* CZ (Ginter et al., 2002). The contrast in age ranges between the

Canning Basin and Iran and south China could indicate a Gondwanan origin for these species or instead that further collecting is required to establish refined biostratigraphic resolution.

A general Tournaisian age has previously been attributed to the Laurel Formation based on long ranging conodonts (Ncioll and Druce, 1979). Elements attributed to *Bispathodus aculeatus plumulus* and *Clydagnathus cavusformis* were recovered in this work, however these did not further refine the age range for the Formation. An early Tournaisian age for sampled sites is, however, provided by the presence of *Thrinacodus ferox* but absence of the later form *Thrinacodus bicupsidatus*. This age is supported by the overlap of the age ranges from *Protacrodus aequalis* (*sulcata CZ*, Ivanov, 1996) and *Protacrodus* sp. 1 (*sulcata-duplicata* CZ, Habibi and Ginter, 2011). This refined age range for the Lower Laurel Formation clearly demonstrates the utility of microvertebrates in dating facies that lack diagnostic conodont faunas. Although there remains much work to be done on Late Devonian and Early Carboniferous microvertebrates in Australia, work undertaken in the 1990s (See Bliek and Turner 2000 and reference therein) indicates that refined ages can be obtained using microvertebrates. This work (Roelofs et al., 2015; Roelofs et al., 2015) illustrates that where conodonts are absent or long ranging, microvertebrates provide excellent age resolution throughout the discontinuous reefs outcrops and Carboniferous ramp deposits in the Canning Basin.

7.2 Chondrichthyan biofacies

The Famennian chondrichthyan biofacies model proposed by Ginter (2000) was applicable to the shallow water shark assemblage from the Famennian Bugle Gap limestone. Although a major reorganisation of vertebrate taxa occurred at the

end-Devonian, shark taxa with crushing dentitions appear to have continuously occupied the same shallow water niche spaces through the Late Devonian and into the Early Carboniferous. The similar niche occupation indicates shark teeth can be used, at least in part, for determining depositional facies into the Early Carboniferous.

7.3 Palaeogeographical implications

The microvertebrate fossils recovered in this work indicate the Canning Basin lay at an area of faunal overlap with West Gondwana, South China and the more easterly parts of East Gondwana. The Late Devonian saw increased cosmopolitanism in many groups including brachiopods (Copper, 1998), ammonoids (House, 1973; Playford et al., 2009), trilobites (McNamara et al., 2009), crustaceans (Rode and Lieberman 2005), conodonts (Klapper, 2007; Girard et al., 2010) and fish (Ginter and Turner 1999). The Frasnian microvertebrate fauna recovered in this work from the Canning Basin reflects this cosmopolitanism. It is particularly evident in the phoebodont species *Phoebodus latus*, *Phoebodus bifurcatus* and *Phoebodus fastigatus*, which are found throughout Laurussia and along the northern margins of Gondwana. The presence of the species *Diademodus dominicus* sp. nov. in the Canning Basin is the first known occurrence of this genera outside Laurussia and provides evidence for a more widespread distribution of pelagic sharks.

The extensive shallow marine shelf that connected the northern margins of Gondwana to the Indochina, Tarim and South China blocks is the likely migration route that resulted in the regional faunal connections noted (Roelofs et al., 2015). The presence of both Frasnian and Famennian thelodonts in Iran and north-western Australia provides evidence for the close proximity of these areas (Hairapetian et al.,

2015). This is supported by the shared presence of five Late Devonian shark species including *Phoebodus bifurcatus, Thrinacodus tranquillus, Protacrodus serra, Deihim mansureae* and *Lissodus lusavorichi*.

The close faunal relationships between the Canning Basin and the Indochina and South China regions, identified in Late Devonian conodont (Burrett et al., 1990; Girard et al., 2010) and fish (Long, 1993) assemblages, are further supported by the presence of the chondrichthyan species *Phoebodus latus, Thrinacodus tranquillus* and *Protacrodus serra, Deihim* sp. 1 and Protacrodontidae gen. et sp. indet. 1. The faunal relationships between these regions in the Early Carboniferous are less evident with only pelagic species, *Thrinacodus ferox* and *Thrinacodus bicuspidatus,* found in common between the Canning Basin and the South China region. A separation, also seen in the plant and animal faunas (Metcalfe, 1988, 1998) is likely due to the northern migration of the South China block at this time (Scotese and McKerrow, 1990; Golonka et al., 1994; Metcalfe, 1994). In contrast, shallow water chondrichthyan species from the east and west of the Canning Basin are still present in the Tournaisian. Here we see a mixture of three geographic types, including: i) cosmopolitan species such as *Thrinacodus ferox* which are found throughout Laurussia and across the north Gondwanan margin; ii) species with more western Gondwanan affinities such as *Protacrodus* sp. 1 which has so far only been documented in Iran and the Canning Basin, and: iii) shark species such as *Cladodus thomasi* which have only been documented in an area to the east of the Canning Basin.

Microvertebrate faunas can be used to support palaeogeographical reconstructions (Young, 2003). However, establishing conclusions primarily based on direct comparisons of microvertebrate assemblages are currently difficult due to

the limited number of studies on temporally equivalent sites, particularly from the Tournaisian. In addition, work needs to be compiled on microvertebrate faunas from range of facies types as the many taxa show strong biofacies controls. This will allow for reliable conclusions on faunal relationships to be established, as seen currently from global phoebodont faunas.

7.4 Microvertebrates as palaeoclimatic proxies

Bioapatite has proven to be a reliable O-isotope storage medium for reconstructing the Palaeozoic $\delta^{18}O$ record (e.g Joachimski et al., 2009). Conodonts analysed from Frasnian, Famennian and Tournaisian strata in the Canning Basin preserved $\delta^{18}O$ values comparable to temporarily equivalent pan tropical sites (Chapter 6). This indicates the Canning Basin existed as an open marine system during the Late Devonian. GIRMS analysis of microvertebrates showed a typical 2-4‰ depletion in $\delta^{18}O$ when compared to associated conodonts - an observation seen in previous works on Palaeozoic microvertebrates (Žigaitė et al., 2010, Barham et al., 2012).

The employment of SIMS enabled successful isolation of O-isotope ratios in different tissue types. Dentine tissues showed highly variable depleted $\delta^{18}O$ values when compared to values from associated conodont elements. The hypermineralised tissues present in acanthodian scales and the teeth and scales of chondrichthyan and palaeoniscoids, hosted $\delta^{18}O$ values comparable to that of conodonts. The degree of mineralisation of these tissues is inferred to have controlled the variability of $\delta^{18}O$ values recorded. Dentine is less mineralised than enamel and enameloid tissues, thus allowing for easier fluid flow and increasing the susceptibility of the incorporated phosphate to both microbial and diagenetic alteration.

The $\delta^{18}O$ values obtained from microvertebrate hard tissues demonstrate that the hypermineralised tissues of multiple microvertebrate taxa can be used as a palaeoenvironmental proxy, potentially from the Ordovician to the present day. Microvertebrate fossils possess the potential to be used as a substitute for brachiopods or bulk rock carbonates, where diagenesis has compromised the reliability of these proxies. The presence of microvertebrates in restricted and freshwater to brackish systems widens the potential of these fossils in palaeoclimatic and chemostratigraphic applications. Microvertebrate fossils can now be utilised in facies that lack reliable O-hosting mediums, and elicit a reliable and correlatable signatures.

7.5 Concluding statements

This study has contributed to an overarching study on the merits of integrating different chronostratigraphic methods in order to achieve greater correlative resolution (Linkage project LP0883812). All techniques showed good resolution in fore-reef to toe of slope facies (Playton et al., 2013; Appendix 2). However, it was over the extinction boundaries where the integrated approach proved most useful. The restricted facies associated with the shallow water reefal platform were less well constrained when only single method approaches were used. Analysis of the shallow water ramp facies that comprise the Fairfield Group showed microvertebrates have the potential to provide age constraints in facies lacking traditionally used age diagnostic fossils. In addition, the enamel present in the fossils of microvertebrate taxa show potential to be incorporated in chemostratigraphic correlation correlation throughout the majority of the Phanerozoic and across a range of facies.

7.6 References

Barham, M., Joachimski, M., Murray, J., Williams, D., 2012a. Diagenetic alteration of the structure and $\delta^{18}O$ signature of Palaeozoic fish and conodont apatite: Potential use for corrected isotope signatures in palaeoenvironmental interpretation. Chemical Geology 298, 11-19.

Burrett, C.F., Long, J. A. and Stait, B. 1990. Early-Middle Palaeozoic biogeography of Asian Terranes derived from Gondwana. Memoirs of the Geological Society of London 12, 163-174.

Copper, P. 1998. Evaluating the Frasnian-Famennian mass extinction: Comparing brachiopod faunas. Acta Palaeontologica Polonica 43, 137-154.

Ginter, M. and Ivanov, A. 1995a. Middle/Late Devonian phoebodont-based ichthyolith zonation. Geobios, Memoire Special 19, 351-355.

Ginter, M. and Turner, S. 1999. The early Famennian recovery of phoebodont sharks. Acta Geologica Polonica 49, 105-117.

Girard, C., Phuong, T.H., Savage, N. and Renaud, S. 2010. Temporal dynamics of the geographic differentiation of Late Devonian *Palmatolepis* assemblages in the Prototethys. Acta Palaeontologica Polonica 55, 675-687.

Golonka, J., Ross, M., and Scotese, C. 1994. Phanerozoic paleogeographic and paleoclimatic modelling maps. Canadian Society of Petroleum Geologists, 17:1-47.

Habibi, T. and Ginter, M. 2011. Early Carboniferous chondrichthyans from the Mobarak Formation, Central Alborz Mountains, Iran. Acta Geologica Polonica 61, 27-34.

Hairapetian, V., Roelofs, B.P., Trinajstic, K.M., and Turner, S. 2015. Famennian survivor turiniid thelodonts of North and East Gondwana. Geological Society, London, Special Publications 423, 423-433..

House, M. 1973. An analysis of Devonian goniatite distributions. Palaeontology Special Papers 12, 305-317.

Ivanov, A. 1996. The Early Carboniferous chondrichthyans of the South Urals, Russia. Geological Society, London, Special Publications 107, 417-425.

Joachimski, M., Breisig, S., Buggisch, W., Talent, J., Mawson, R., Gereke, M., Morrow, J., Day, J. and Weddige, K. 2009. Devonian climate and reef evolution: insights from oxygen isotopes in apatite. Earth and Planetary Science Letters 284, 599-609.

Klapper, G. 2007. Frasnian (Upper Devonian) conodont succession at Horse Spring and correlative sections, Canning Basin, Western Australia. Journal of Paleontology 81, 513-537.

Long, J.A. 1993. Palaeozoic vertebrate biostratigraphy of SouthEast Asia and Japan. In: Long, J.A. (ed.) Palaeozoic vertebrate biostratigraphy and biogeography, pp. 277-289. Belhaven Press, London.

McNamara, K., Feist, R. and Ebach, M. 2009. Patterns of evolution and extinction in the last harpetid trilobites during the Late Devonian (Frasnian). Palaeontology 52, 11-33.

Metcalfe, I. 1988. Origin and assembly of south-east Asian continental terranes. Geological Society, London, Special Publications 37, 101-118.

Metcalfe, I. 1994. Gondwanaland origin, dispersion, and accretion of East and Southeast Asian continental terranes. Journal of South American Earth Sciences 7, 333-347.

Metcalfe, I. 1998. Palaeozoic and Mesozoic geological evolution of the SE Asian region: multidisciplinary constraints and implications for biogeography, pp. 25-41. In Hall, R. and Holloway, J.D. (eds.), Biogeography and Geological Evolution of SE Asia. Backhuys Publishers, Amsterdam, Netherlands.

Nicoll, R.S. and Druce, E.C. 1979. Conodonts from the Fairfield Group, Canning Basin, Western Australia. Bureau of Mineral Resources Australia Bulletin 190, 1-134.

Playford, P.E, Hocking, R.M. and Cockbain, A.E. 2009. Devonian reef complexes of the Canning Basin, Western Australia. Geological Survey of Western Australia Bulletin 145.

Playton, T. E., Montgomery, P., Tohver, E., Hillbun, K., Katz, D., Haines, P., Trinajstic, K., Yan, M., Hansma, J., Pisarevsky, S., Kirschvink, J., Cawood, P., Grice, K., Tulipani, S., Ratcliffe, K., Wray, D., Caulfield-Kerney, S., Ward, P. and Playford, P.E. 2013. Development of a regional stratigraphic framework for Upper Devonian reef complexes using integrated chronostratigraphy: Lennard Shelf, Canning Basin, Western Australia. In: Keep, M. and Moss, S. J. (Eds). The Sedimentary Basins of Western Australia IV. Proceedings of the Petroleum Exploration Society of Australia Symposium, Perth, Western Australia.

Rode, A.L. and Lieberman, B.S. 2005. Integrating evolution and biogeography: A case study involving Devonian crustaceans. Journal of Paleontology 79, 267-276.

Roelofs, B., Playton, T., Barham, M., and Trinajstic, K. 2015. Upper Devonian microvertebrates from the Canning Basin, Western Australia. Acta Geologica Polonica 65, 69-101.

Trinajstic, K. and George, A.D. 2009. Microvertebrate biostratigraphy of Upper Devonian (Frasnian) carbonate rocks in the Canning and Carnarvon basins of Western Australia. Palaeontology 52, 641-659.

Trinajstic, K., Roelofs, B., Burrow, C., Long, J., and Turner, S. 2014. Devonian vertebrates from the Canning and Carnarvon Basins with an overview of Paleozoic vertebrates of Western Australia. Journal of the Royal Society of Western Australia 97, 133-151.

Turner, S. 1997. Sequence of Devonian thelodont scale assemblages in East Gondwana. In: Klapper, G., Murphy, M. A. and Talent, J. A. (Eds). Paleozoic Sequence Stratigraphy, Biostratigraphy, and Biogeography: Studies in Honor of Dr J. Granville ("Jess") Johnson. Geological Society of America, Special Papers 321, 295-315.

Turner, S. and Dring, R.S. 1981. Late Devonian thelodonts (Agnatha) from the Gneudna Formation, Carnarvon Basin, Western Australia. Alcheringa 5, 39-48.

Turner, S. and Hairapetian, V. 2005. Thelodonts from Gondwana. In: Hairapetian, V. and Ginter, M. (Eds). IGCP 491 Armenia Field Conference, Devonian Vertebrates of the Continental Margins, May 24-28. Ichthyolith Issues, Special Publication 24.

Scotese, C.R. and McKerrow, W.S. 1990. Revised World maps and introduction. In: McKerrow, W.S. and Scotese, C.R. (Eds). Palaeozoic Palaeogeography and Biogeography. Geological Society, London, Memoir 12, 1-21.

Smith, T.E., Kelman, A.P., Nicoll, R.S., Laurie, J.R. and Le Poidevin, S.R. 2013. Geoscience Australia's Basin Biozonation and Stratigraphy Chart

Series. Basin Biozonation and Stratigraphy Chart Series. Geoscience Australia, Canberra.

Young, G.C. 2003. North Gondwana mid-Palaeozoic connections with Euramerica and Asia: Devonian vertebrate evidence. In Königshof, P. and Schindler, E. (eds), Mid-Palaeozoic Bio- and Geodynamics: The North Gondwana - Laurussia interaction (Frankfurt a.M., 11-21 May 2001). Courier Forschungs-Institut Senckenberg 242,169-185.

Žigaitė, Ž., Joachimski, M.M., Lehnert, O. and Brazauskas, A. 2010. δ 18O composition of conodont apatite indicates climatic cooling during the Middle Pridoli. Palaeogeography, Palaeoclimatology, Palaeoecology 294, 242-247.

Appendix 1

Roelofs, B., Barham, M., Cliff, J., Joachimski, M., Martin, L. and Trinajstic, K. Assessing the fidelity of marine vertebrate microfossil $\delta^{18}O$ signatures and their potential for palaeo-ecological and -climatic reconstructions. Palaeogeography, Palaeoclimatology, Palaeoecology.

Palaeogeography, Palaeoclimatology, Palaeoecology xxx (2016) xxx–xxx

Contents lists available at ScienceDirect

Palaeogeography, Palaeoclimatology, Palaeoecology

journal homepage: www.elsevier.com/locate/palaeo

Assessing the fidelity of marine vertebrate microfossil $\delta^{18}O$ signatures and their potential for palaeo-ecological and -climatic reconstructions

Brett Roelofs [a,*], Milo Barham [a,b], John Cliff [c], Michael Joachimski [d], Laure Martin [e], Kate Trinajstic [b,f]

[a] Department of Applied Geology, Curtin University, GPO Box U1987, Perth, WA 6845, Australia
[b] The Institute for Geoscience Research (TIGeR), Department of Applied Geology, Curtin University, GPO Box U1987, Perth, Australia
[c] Environmental Molecular Science Laboratory (EMSL), Pacific Northwest National Laboratory, P.O. Box 999, Richland, WA 99352, USA
[d] GeoZentrum Nordbayern, University of Erlangen-Nuremberg, Schlossgarten 5, 91054 Erlangen, Germany
[e] Centre for Microscopy, Characterisation and Analysis (CMCA), The University of Western Australia, Perth, WA 6009, Australia
[f] Department of Environment and Agriculture, Curtin University, GPO Box U1987, Perth, WA 6845, Australia

ARTICLE INFO

Article history:
Received 3 May 2016
Received in revised form 13 October 2016
Accepted 15 October 2016
Available online xxxx

Keywords:
SIMS
GIRMS
Apatite
Temperature
Histology
Oxygen-isotopes

ABSTRACT

Conodont biogenic apatite has become a preferred analytical target for oxygen isotope studies investigating ocean temperature and palaeoclimate changes in the Palaeozoic. Despite the growing application in geochemically-based palaeoenvironmental reconstructions, the paucity or absence of conodont fossils in certain facies necessitates greater flexibility in selection of robust oxygen-bearing compounds for analysis. Vertebrate microfossils (teeth, dermal denticles, spines) offer a potential substitute for conodonts from the middle Palaeozoic. Vertebrate bioapatite is particularly advantageous given a fossil record extending to the present with representatives across freshwater to fully marine environments, thus widening the scope of oxygen isotope studies on bioapatite. However, significant tissue heterogeneity within vertebrates and differential susceptibility of these tissues to diagenetic alteration have been raised as potential problems affecting the reliability of the oxygen isotope ratios as palaeoclimatic proxies. Well-preserved vertebrate microfossils and co-occurring conodont fossils from the Upper Devonian and Lower Carboniferous of the Lennard Shelf, Canning Basin, Western Australia, were analysed using bulk (gas isotope ratio mass spectrometry, GIRMS) and in-situ (secondary ion mass spectrometry, SIMS) methodologies, with the latter technique allowing investigation of specific tissues within vertebrate elements. The $\delta^{18}O_{conodont}$ results may be interpreted in terms of palaeolatitudinally and environmentally sensible palaeo-salinity and -temperature and provide a baseline standard for comparison against vertebrate microfossil $\delta^{18}O$ values. Despite an absence of obvious diagenetic modification, GIRMS of vertebrate denticles yielded $\delta^{18}O$ values depleted in ^{18}O by 2–4‰ relative to co-occurring conodonts. SIMS analysis of dentine tissues exhibited significant heterogeneity, while hypermineralised tissues in both scales and teeth produced $\delta^{18}O$ values comparable with those of associated conodonts. The susceptibility of permeable phosphatic fossil tissues to microbial activity, fluid interaction and introduction of mineral precipitates post-formation is demonstrated in the dentine of vertebrate microfossils, which showed significant heterogeneity and consistent depletion in ^{18}O relative to conodonts. The hypermineralised tissues present in both teeth and scales appear resistant to many diagenetic processes and indicate potential for palaeoclimatic reconstructions and palaeoecological investigations.

1. Introduction

The Palaeozoic marine oxygen isotope record is punctuated by a series of excursions and perturbations reflecting climatic events that are often associated with significant biological reorganisations (e.g. Brand, 1989; Gruszczyński et al., 1989; Caplan and Bustin, 1999; Veizer et al., 1999; Jeppsson et al., 1999; Joachimski and Buggisch, 2002; Kaiser et al., 2006; Trotter et al., 2008; Schobben et al., 2015). Fluctuations in the oxygen isotope record have been elicited from analysis of marine organisms with the ability to precipitate mineralised tissues in isotopic equilibrium with the ambient water. The shells of Palaeozoic low-Mg calcite brachiopod taxa have been commonly used (Popp et al., 1986; Veizer et al., 1986, 1997; Brand, 1989, 2004; Carpenter et al., 1991; Hays and Grossman, 1991; Wadleigh and Veizer, 1992; Azmy et al., 1998; Mii et al., 1997, 1999; Van Geldern et al., 2006; Korte et al., 2008) due to their relative abundance, ease of sampling and the relative resistance of low-Mg calcite, compared to aragonite or high-Mg calcite, to post-mortem modification. Recent work however has shown that even low-Mg calcite is highly susceptible to diagenesis over time (Cummins et al., 2014). This issue is compounded by imperfect

* Corresponding author.
E-mail address: brett.roelofs@postgrad.curtin.edu.au (B. Roelofs).

http://dx.doi.org/10.1016/j.palaeo.2016.10.018
0031-0182/

screening methods for the identification of recrystallised calcite, which may cause resetting of oxygen isotope values (e.g. Wenzel et al., 2000). In addition, O-isotope heterogeneity has been identified in a number of brachiopod shells, indicating fractionation is occurring during the formation of these hard tissues (e.g. Auclair et al., 2003; Yamamoto et al., 2011; Rollion-Bard et al., 2016). The typically sessile ecology of brachiopods also means that each analysis must be independently considered in the context of the specific temperature and chemistry of the water depth it inhabited. Consequently, this limits the comparison of oxygen isotope signatures to brachiopod taxa occupying similar ecological niches (Popp et al., 1986; James et al., 1997).

Bioapatite offers a more physically and chemically resistant oxygen-bearing alternative to brachiopod calcite due to a greater mineral hardness and stability of the P–O bond in PO_4^{3-} (e.g., Grimes et al., 2003; Joachimski et al., 2004). The mineralised feeding elements of conodonts (Lindström et al., 1974; Dzik, 1991; Goudemand et al., 2011) comprise a relatively homogenous chemical composition ($Ca_5Na_{0.13}(PO_4)_{3.01}(CO_3)_{0.16}F_{0.73}(H2O)_{0.85}$, Pietzner et al., 1968) and have become increasingly used in oxygen isotope studies. Despite a non-ubiquitous internal structure among all taxa (Donoghue, 1998; Trotter et al., 2007), the mineralised element crowns typically comprise a translucent finely crystallised hyaline tissue and an inner albid tissue (Lindström, 1964; Pietzner et al., 1968; Barnes et al., 1973; Donoghue, 1998; Trotter et al., 2007; Jones et al., 2012). Analysis of their hypermineralised tissues indicates conodont elements offer greater uniformity in $\delta^{18}O$ values in comparison to those obtained from brachiopod calcite (e.g. Wallace and Elrick, 2014). Consistent oxygen isotope signatures have been observed between conodont genera belonging to different biofacies in the Late Devonian (Joachimski et al., 2009) and Carboniferous (Joachimski and Lambert, 2015), supporting a shared near sea-surface marine habitat and free swimming lifestyle, as suggested from their biology (e.g. Gabbott et al., 1995). This observation may be dependent on location, time period and genera analysed, as recent work on Ordovician (Quinton and MacLeod, 2014), Permian (Joachimski et al., 2012) and Triassic (Trotter et al., 2015) conodonts has shown discernible differences in $\delta^{18}O$ values between some genera. Despite some taxon-specific discrepancies in $\delta^{18}O$, correlatable oxygen isotope ratios have proven useful in wider geographical comparisons (e.g. Joachimski et al., 2009).

The biostratigraphic utility and widespread distribution and abundance of conodont elements in many marine deposits has facilitated the development of a temporally resolved isotope record spanning many significant faunal reorganisations associated with climatic perturbations from the Ordovician (Trotter et al., 2008) to the Triassic (Joachimski et al., 2009; Rigo et al., 2012; Sun et al., 2012; Trotter et al., 2015). However, conodont fossils are not ubiquitous in all facies, limiting their potential as a sea surface temperature proxy in many regions. Even where present, a paucity of conodont elements can preclude preferred single genera sample analysis and fine resolution sampling due to minimum sample mass requirements in standard analytical methodologies. As a consequence of these limitations, other common, diagenetically resistant oxygen-bearing compounds must be identified to expand accurate palaeoenvironmental interpretations across different temporal intervals and depositional settings.

We studied a range of vertebrate microfossil elements using GIRMS to determine the stability of biogenic phosphate over geological timescales, as well as the degree to which ecology and diagenesis influence oxygen isotope ratios in different vertebrate microfossil remains. Secondary ion mass spectrometry (SIMS) analysis was applied to test whether all vertebrate microfossil tissues are equally prone or resistant to alteration of their O-isotopic ratios. In order to establish the validity of vertebrate microfossil $\delta^{18}O$ signatures and their potential use as palaeoclimatic indicators, the oxygen isotope ratios of vertebrate microfossils were compared with those of co-occurring conodonts. Both GIRMS and SIMS analyses were undertaken on Frasnian (Upper Devonian) conodont samples as well as multiple Famennian (Upper Devonian) and Tournaisian (Lower Carboniferous) conodont and vertebrate remains to i) document any potential discrepancies between the two methods and; to ii) identify potential causes of disruption of primary oxygen isotope signatures in different vertebrate tissues.

2. Background

2.1. Vertebrate microfossil histology

Marine vertebrate microfossils (typically <5 mm in size) most commonly comprise teeth, scales and fin spines. The hard tissues of vertebrates are highly heterogeneous, consisting of three broad types; bone, dentine and enamel. These tissues are differentiated by the levels of mineralisation and organic matter content. Bone comprises a 50–70% mineralised component with 20–40% organic matter and 5–10% water (Clarke, 2008). Dentine is approximately 70% mineralised with 20–24% protein and 6–10% water, whereas enamel is highly mineralized (96%) with only 1% protein and approximately 3% water, which is present on or between the hydroxyapatite crystals (Stack, 1955; Pasteris et al., 2008; Goldberg et al., 2011; Hand and Frank, 2014). The O-hosting sites within biogenic apatite also differ significantly between vertebrate hard tissues (Pasteris et al., 2008). Bone and dentine comprise 6 and 5 wt% CO_3^{2-} respectively, with only ~3.5 wt% present in enamel (LeGeros and LeGeros, 1984; Cerling and Sharp, 1996). This low CO_3^{2-} concentration compared to dentine and bone, in addition to a high degree of mineralisation (>80 wt%, Li et al., 2013), makes the hypermineralised tissues (enamel, enameloid, ganoine and acrodin) present in vertebrate teeth and scales more resistant to physical and chemical alteration. Detailed information on tooth and scale histology of analysed taxa is provided in the Supplementary material (A1-VH).

2.2. Application of vertebrate tissues in Palaeozoic oxygen isotope studies

Oxygen isotopes of vertebrate bioapatite tissues have been previously used to determine palaeoenvironmental conditions in the Palaeozoic (Kolodny and Luz, 1991; Barham et al., 2012a; Fischer et al., 2013) and Mesozoic (Kolodny and Raab, 1988; Kolodny and Luz, 1991; Lécuyer et al., 1993; Pucéat et al., 2003; Billon-Bruyat et al., 2005; Fischer et al., 2012). Applying gas isotope ratio mass spectrometry (GIRMS) to Palaeozoic vertebrate fossils, however, has produced inconsistent results when whole fossils are used. Analysis of Upper Devonian actinopterygian teeth (Joachimski and Buggisch, 2002) initially suggested that original oxygen isotope ratios were preserved in the tooth apatite. Other works however, have revealed that Palaeozoic vertebrate teeth and dermal denticles are typically depleted in ^{18}O (relative to conodont elements) between 2.4 and 2.9‰ (Barham et al., 2012a; Žigaite et al., 2010). This has led to the suggestion that vertebrate microfossil elements are susceptible to diagenetic affects and thus may not preserve original isotopic signatures (Barham et al., 2012a). However, given that secondary alteration may be tissue-specific or screened and subsequently avoided, the potential still exists for the geochemistry of these fossils to serve as a palaeoclimatic archive.

3. Materials and methods

3.1. Sample collection, processing and imaging

Upper Devonian vertebrate microfossils are common in the distal slope facies of the Virgin Hills Formation (late Frasnian - middle Famennian; Fig. 1; Playford et al., 2009; Trinajstic and George, 2009; Trinajstic et al., 2014; Roelofs et al., 2015) and in the conodont-poor facies of the Fairfield Group (Upper Devonian-Lower Carboniferous) (Roelofs et al., 2016; Thomas, 1957, 1959). Twenty kilogram samples were collected from single beds at Horse Spring (18°11′41″ S, 126°01′69″ E) (sample prefix VHS), Oscar Hill (18°04′07″ S, 125°26′41″ E) (sample prefixes OH, Si) and Laurel Downs (18°01′37″ S, 125°18′43″

Please cite this article as: Roelofs, B., et al., Assessing the fidelity of marine vertebrate microfossil δ18O signatures and their potential for palaeoecological and -climat..., Palaeogeogr. Palaeoclimatol. Palaeoecol. (2016), http://dx.doi.org/10.1016/j.palaeo.2016.10.018

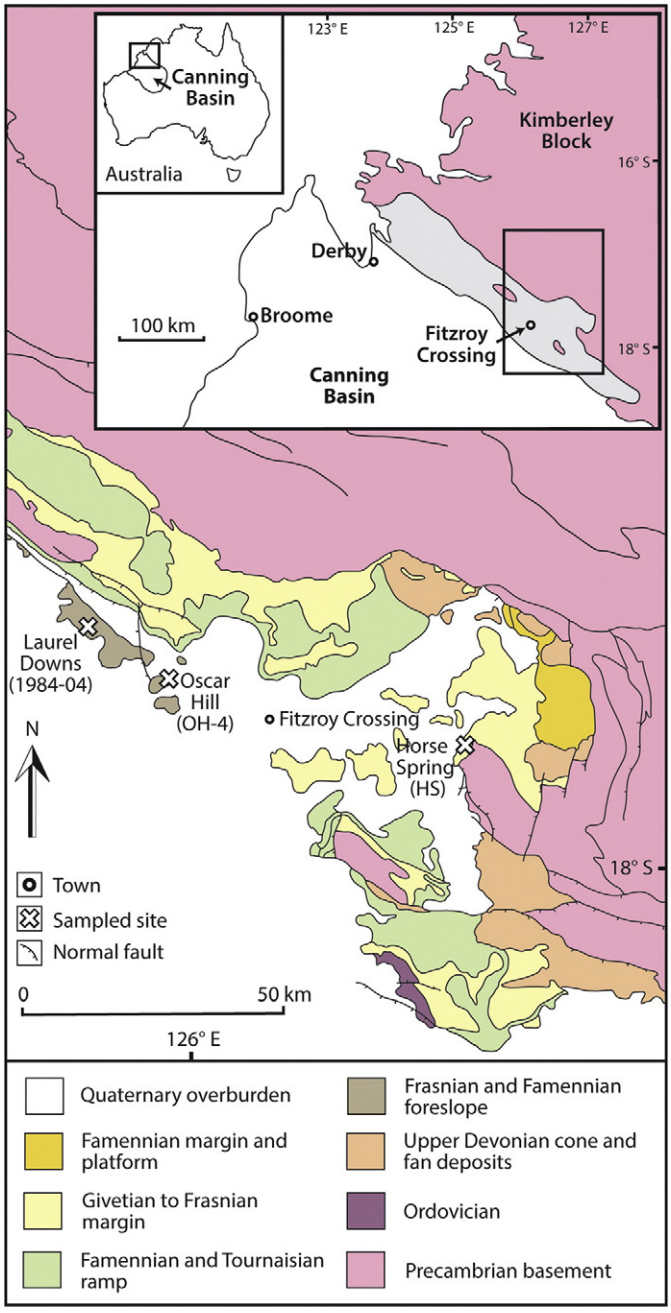

Fig. 1. Regional geology map and sampled sites from the Lennard Shelf, Canning Basin, Western Australia.
(Modified from Playford et al., 2009.)

E) (sample prefixes 1984, CCA, MT and MTM) (Fig. 1) and processed using a buffered 10% acetic acid solution (following the methodology of Jeppsson et al., 1999). The rock samples were disaggregated as whole rocks with rinsing occurring every 24–48 h, depending on the degree of disaggregation. This process was repeated, with fresh 10% buffered acetic acid, until the rocks had been sufficiently broken down to allow for the removal of isolated fossils. Residues were rinsed and sieved (0.125 mm sieve) to further separate microfossils before picking the >0.125 mm fraction under a Nikon stereomicroscope. Detailed examination of microfossils was performed using a Hitachi TM-3030 desktop Scanning Electron Microscope (SEM) at Curtin University with accelerating voltages ranging from 5 to 15 kV and variable pressures. Eight larger holocephalan teeth (>10 mm mesio-distally) were recovered directly from the disaggregated rock residues. A single tooth (MTM1-H9) was exposed from the rock sample along its labial face and extracted prior to processing. Additional imaging of analysed specimens was performed using a Leica stereomicroscope camera at the Western Australian Museum.

Horse Spring samples yielded 200 conodont elements corresponding to Conodont Zone (CZ) 11 (Frasnian; Klapper, 1988). Conodont yields from Oscar Hill samples taken for this study yielded mainly undiagnostic elements with a single long ranging Famennian conodont *Spathognathodus aciedentatus* recovered. Previous sampling by Nicoll and Druce (1979) indicated a latest Famennian age (*praesulcata* Conodont Zone) for outcrop at Oscar Hill. Tournaisian rock samples (Table 2) were collected from a bioclastic limestone bed of the Laurel Formation (sample number 1984-04), exposed approximately 35 km northwest of the town of Fitzroy Crossing (Fig. 1). A Tournaisian age is supported by the presence of the conodont taxa *Clydagnathus cavusformis* and *Bispathodus aculeatus*, and is consistent with previous age determinations (Druce and Radke, 1979; Nicoll and Druce, 1979). A refinement of early Tournaisian for the sampled area is indicated by the overlap of shark species *Thrinacodus ferox*, *Protacrodus aequalis* and *Protacrodus* sp. 1 (Roelofs et al., 2016).

3.2. Analytical methodology

The GIRMS method has conventionally been used to accurately determine the $\delta^{18}O$ values of pooled apatite fossils through the analysis of chemically purified Ag_3PO_4. To obtain ~1 mg of fossil material required for replicate analyses, samples comprising multiple vertebrate microfossil elements, or single elements comprising multiple tissue types, are often required. The incorporation of different fossil tissues within analyses reduces data confidence as tissue geochemistry is differently affected by biological processes including organism physiology (e.g. Thorrold et al., 1997), post-mortem microbial activity (Blake et al., 1997, 1998; Zazzo et al., 2004) as well as physico-chemical influences such as diagenesis (e.g. Iacumin et al., 1996).

The use of laser ablation techniques on biogenic phosphate has demonstrated the potential to quantify variation in $\delta^{18}O$ from in-situ tissues (Cerling and Sharp, 1996). Such in-situ techniques minimise potential contamination and alteration of samples during preparation and reduce the required sample size (Brady, 2004). Trotter et al. (2008) later established the use of secondary ion mass spectrometry (SIMS) on biogenic phosphate to elicit reliable $\delta^{18}O$ values from both fossil and modern tissue. The success of this work has been replicated with a particular focus on conodonts, in reconstructing Palaeozoic palaeoclimates and palaeoceanographies (Rigo et al., 2012; Wheeley et al., 2012; Trotter et al., 2015; Chen et al., 2016). Whether this technique can be applied to Palaeozoic vertebrates, and the preservation of $\delta^{18}O$ in highly heterogeneous fossil tissues, have not been thoroughly explored. Application of this technique to modern shark teeth (Trotter et al., 2008; Žigaitė and Whitehouse, 2014) has shown preservation of original oxygen isotope signatures in hypermineralised tissues as well as heterogeneity and depletion of ^{18}O within the more permeable dentine (Žigaitė and Whitehouse, 2014).

Following the approach of Trotter et al. (2008), aliquots of a single large fragment of Durango apatite crystal were used as an oxygen isotope standard for comparison between GIRMS and SIMS methods and published data. It should be noted that recent work by Sun et al. (2016) has highlighted a 4.4‰ inter-crystal $\delta^{18}O$ variation between Durango apatite crystals as well as intra-crystal variation that ranged from 0.7–1.8‰. To minimise the potential effects of crystal heterogeneity, ion probe spots were concentrated on small areas within small fragments of a single crystal. Additionally, as this work focuses on intra-fossil variation as well as comparing fossils on the same mount, potential variation between crystal fragments does not significantly alter the conclusions of this work.

Please cite this article as: Roelofs, B., et al., Assessing the fidelity of marine vertebrate microfossil δ18O signatures and their potential for palaeoecological and -climat..., Palaeogeogr. Palaeoclimatol. Palaeoecol. (2016), http://dx.doi.org/10.1016/j.palaeo.2016.10.018

3.2.1. GIRMS oxygen isotope analyses

Stable oxygen isotope ratios were determined on conodont and vertebrate microfossil material at the Stable Isotope Laboratory of the University of Erlangen-Nürnberg, Germany, following a modified version of the procedure developed by O'Neil et al. (1994) and described in Joachimski et al. (2009). Conodont, vertebrate microfossil and Durango apatite samples (0.7–2.0 mg) were chemically converted to trisilverphosphate (Ag_3PO_4) and the oxygen isotope ratios of ~0.2 mg sample aliquots were analysed as CO produced in a high temperature conversion elemental analyser (TC–EA) attached on-line to a ThermoFisher Delta V Plus mass spectrometer. Oxygen isotope compositions are reported in δ notation in ‰ relative to Vienna Standard Mean Ocean Water (VSMOW) (Table 1). The analyses were calibrated by performing a two-point calibration (Paul et al., 2007) using NBS 120c (+21.7‰) and a commercial Ag3PO4 (+9.9‰). All standards were calibrated to TU1 (+21.11‰) and TU2 (+5.45‰; Vennemann et al., 2002). A laboratory standard, as well as NBS 120c were used as control standards and processed together with the samples. Replicate analyses of the international standard NBS 120c and internal laboratory standards were performed between every four unknowns, as well as at the start and end of each measuring day to monitor accuracy and reproducibility. Reproducibility was typically ±0.2‰ (1σ). NBS 120c was measured as +21.7 ± 0.1‰ (1σ, n = 12) VSMOW (within uncertainty reported by LaPorte et al., 2009). Most samples were measured in triplicate, with limited Ag_3PO_4 from samples OH4-C and 1984-C only allowing duplicate and single analyses, respectively.

3.2.2. SIMS oxygen isotope analyses

Conodont and vertebrate microfossils, with fragments of a Durango apatite crystal were mounted on double sided tape attached to standard glass plates. Large holocephalan teeth were cut labio-lingually using a Dremel rotary tool and ground flat with 1200 grit sandpaper prior to mounting on the tape along the smooth surface. Struers EpoFix epoxy resin was used to form standard one-inch round mounts and then polished to expose the desired tissues using successively finer polishing cloths to a 1 μm finish. The mounts were then carefully cleaned with detergent, distilled water and isopropanol in an ultrasonic bath and coated with gold (30 nm in thickness) prior to SIMS analyses.

Oxygen isotope ratios were determined using a Cameca IMS 1280 multi-collector ion microprobe located at the Centre for Microscopy, Characterisation and Analysis (CMCA), University of Western Australia (UWA) in March and November 2014. Analyses were performed with a ca. 2.5 nA Cs^+ beam with a total impact energy of 20 keV rastered on a ca. 20 × 20 μm area on the sample surface. Instrument parameters included a magnification of 130× between the sample and field aperture (FA), 400 μm contrast aperture (CA), 4000 μm FA, 110 μm entrance slit, 400 μm exit slits, and a 40 eV band pass for the energy slit with a 5 eV gap toward the high energy side. Secondary O^- ions were accelerated to 10 keV and analysed with a mass resolving power of approximately 2200 using dual Faraday Cup detectors. A normal-incidence electron gun was used to provide charge compensation and NMR regulation was employed for magnetic field control.

Ten seconds of pre-sputtering was followed by automatic centering of the secondary beam in the FA and CA. Each analysis consisted of 20 four-second cycles, which gave an average internal precision of ±0.2‰ (1σ). Analytical sessions were monitored for drift and precision using a bracketing standard (Durango apatite; +9.9 ± 0.3‰, (1σ, n = 9); characterised via GIRMS of three samples analysed in triplicate from the same crystal) for every six sample analyses. Instrumental mass fractionation (IMF) was corrected using Durango apatite following the procedure described in Kita et al. (2009). The spot-to-spot reproducibility (external precision) was typically ±0.3–0.4‰ (1σ) on Durango apatite during all of the analytical sessions, except two sessions at ±0.2‰ (sample HT2) and ±0.5‰ (sample MVM2). Uncertainty on each spot was calculated by propagating the errors on instrumental mass fractionation determination and internal error on each sample data point. The resulting uncertainty was typically between ±0.3 and ±0.6‰ (1σ). Raw $^{18}O/^{16}O$ ratios and corrected $\delta^{18}O$ (reported relative to VSMOW) are presented in Table 2.

4. Results

4.1. Fossil preservation

Visual inspection (both macro- and microscopic) confirmed conodont elements were well-preserved, showing no evidence of coarsening crystallites, pitting, overgrowths or other visible signs of diagenetic

Table 1
Late Famennian and early Tournaisian vertebrate microfossils and standards analysed using gas isotope ratio mass spectrometry (GIRMS).

Location	Sample no.	Formation (Fm.)	Age	Sample	Taxa	Sample size (mg)	n[a]	$\delta^{18}O$ (‰)	1σ
Horse Spring	VHS-312	Virgin Hills Fm.	Fr[b]	*Ancyrodella*	Conodont	0.88	3	19.0	0.2
Oscar Hill	OH-4 A	Gumhole Fm.	Fn[c]	Palatal teeth	Palaeoniscoid	0.99	3	17.0	0.1
Oscar Hill	OH-4 B	Gumhole Fm.	Fn[c]	Scale	Protacrodont	2.04	3	17.1	0.2
Oscar Hill	OH-4C	Gumhole Fm.	Fn[c]	Scale	Ctenacanthid	0.60	2	16.0	0.6
Oscar Hill	OH-4 D	Gumhole Fm.	Fn[c]	Tooth cusp	*Helodus*	0.89	3	17.2	0.3
Oscar Hill	OH4-SS1	Gumhole Fm.	Fn[c]	Spine	Shark	–	3	16.3	0.1
Laurel Downs	1984-04 A	Laurel Fm.	Tn[d]	Scale	Ctenacanthid	1.25	3	16.9	0.1
Laurel Downs	1984-04 B	Laurel Fm.	Tn[d]	Palatal teeth	Palaeoniscoid	0.82	3	18.0	0.2
Laurel Downs	1984-04 C	Laurel Fm.	Tn[d]	Radial bone	Palaeoniscoid	0.70	1	15.9	0.1
Laurel Downs	1984-04 D	Laurel Fm.	Tn[d]	Teeth	Palaeoniscoid	0.85	3	15.7	0.5
Laurel Downs	1984-04 E	Laurel Fm.	Tn[d]	Scale	Palaeoniscoid	1.51	3	17.3	0.6
Laurel Downs	1984-04 F	Laurel Fm.	Tn[d]	Tooth cusp	Holocephalan	1.63	3	17.3	0.2
Laurel Downs	1984-04 M	Laurel Fm.	Tn[d]	Tooth cusp	Holocephalan	0.87	3	17.7	0.1
Laurel Downs	1984-04 G	Laurel Fm.	Tn[d]	Scales	Acanthodian	0.77	3	17	0.4
Laurel Downs	1984-04 H	Laurel Fm.	Tn[d]	Palatal teeth	Palaeoniscoid	1.42	3	18.1	0.4
Laurel Downs	1984-04 J	Laurel Fm.	Tn[d]	Scale	Lungfish	1.44	3	16.5	0.2
Laurel Downs	1984-04 K	Laurel Fm.	Tn[d]	Scale	Protacrodont	1.13	3	16.1	0.3
Laurel Downs	1984-04 L	Laurel Fm.	Tn[d]	Scale	Protacrodont	0.96	3	17.3	0.5
Laurel Downs	MTM1-H1	Laurel Fm.	Tn[d]	Tooth cusp	Holocephalan	–	3	19.1	0.1
Laurel Downs	MTM1-H4	Laurel Fm.	Tn[d]	Tooth cusp	Holocephalan	–	3	16	0.2
Laurel Downs	MTM1-H5	Laurel Fm.	Tn[d]	Tooth cusp	Holocephalan	–	3	18.8	0.2
Laurel Downs	MTM1-H8	Laurel Fm.	Tn[d]	Tooth cusp	Holocephalan	–	3	18.8	0.1
Laurel Downs	MTM1-H9	Laurel Fm.	Tn[d]	Tooth cusp	Holocephalan	–	3	17.4	0.3
Laurel Downs	MT4-LPS	Laurel Fm.	Tn[d]	Scale	Lungfish	–	3	15.1	0.0

[a] Number of replicate analysis.
[b] Frasnian.
[c] Famennian.
[d] Tournaisian.

Please cite this article as: Roelofs, B., et al., Assessing the fidelity of marine vertebrate microfossil δ18O signatures and their potential for palaeoecological and -climat..., Palaeogeogr. Palaeoclimatol. Palaeoecol. (2016), http://dx.doi.org/10.1016/j.palaeo.2016.10.018

Table 2
$\delta^{18}O$ values of late Famennian to early Tournaisian microfossils analysed using SIMS.

Location	Sample no.	Formation (Fm.)	Age	Sample	Taxa	Tissue	n[a]	$\delta^{18}O$ (‰)	1σ
Horse Spring	VHS-312a	Virgin Hills Fm.	Fr[b]	P-element	*Palmatolepis*	Hyaline	4	19.1	0.3
Horse Spring	VHS-312b	Virgin Hills Fm.	Fr[b]	P-element	*Ancyrodella*	Hyaline	4	19.2	0.3
Oscar Hill	OH4-CS2	Gumhole Fm.	Fn[c]	S-element	Conodont	Hyaline	5	19.9	0.5
Oscar Hill	Si-OH4i[d]	Gumhole Fm.	Fn[c]	S-element	Conodont	Hyaline	2	20.1	1
Oscar Hill	Si-OH4ii[d]	Gumhole Fm.	Fn[c]	S-element	Conodont	Hyaline	2	18.8	0
Oscar Hill	OH4-SS1	Gumhole Fm.	Fn[c]	Shark spine	Unknown	Dentine	4	16.5	0.4
Oscar Hill	OH4-SS1	Gumhole Fm.	Fn[c]	Shark Spine	Unknown	Dentine	3	18.5	0.3
Oscar Hill	OH4-Pri	Gumhole Fm.	Fn[c]	Scale	Protacrodont	Unknown	2	17.9	0.1
Oscar Hill	OH4-Prii	Gumhole Fm.	Fn[c]	Scale	Protacrodont	Unknown	2	12.8	1
Laurel Downs	CCA1	Laurel Fm.	Tn[e]	P-element	*Clydagnathus*	Hyaline	5	20.9	0.9
Laurel Downs	CCA2	Laurel Fm.	Tn[e]	P-element	*Clydagnathus*	Hyaline	4	19.9	0.4
Laurel Downs	1984-04 Ac	Laurel Fm.	Tn[e]	Scale	Acanthodian	Unknown	2	20.6	1.6
Laurel Downs	1984-04 Ac	Laurel Fm.	Tn[e]	Scale	Acanthodian	Dentine	1	16.7	n/a
Laurel Downs	1984-04 Pr	Laurel Fm.	Tn[e]	Scale	Protacrodont	Unknown	3	20.1	0.3
Laurel Downs	1984-04 Ct	Laurel Fm.	Tn[e]	Scale	Ctenacanthid	Unknown	2	20.6	2.1
Laurel Downs	1984-04 Pcd	Laurel Fm.	Tn[e]	Scale	Palaeoniscoid	Unknown	2	19.5	1.3
Laurel Downs	MT4-LPSi[d]	Laurel Fm.	Tn[e]	Scale	Lungfish	Unknown	3	8.8	1.9
Laurel Downs	MT4-LPSi[d]	Laurel Fm.	Tn[e]	Scale	Lungfish	Unknown	5	14.9	1.3
Laurel Downs	MT4 Ptp	Laurel Fm.	Tn[e]	Palatal teeth	Palaeoniscoid	Cusp	4	15.7	0.5
Laurel Downs	MT4 Ptp	Laurel Fm.	Tn[e]	Palatal teeth	Palaeoniscoid	Dentine	4	14.9	1.1
Laurel Downs	Mt-4 PN	Laurel Fm.	Tn[e]	Tooth	Palaeoniscoid	Acrodin	4	20.7	0.5
Laurel Downs	Mt-4 PN	Laurel Fm.	Tn[e]	Tooth	Palaeoniscoid	Dentine	3	15.9	0.9
Laurel Downs	1984-04 AG1	Laurel Fm.	Tn[e]	Tooth	*Ageleodus* sp.	Dentine	3	17.2	0.1
Laurel Downs	1984-04 AG1	Laurel Fm.	Tn[e]	Tooth	*Ageleodus* sp.	Dentine	5	13.1	1.1
Laurel Downs	1984-04 AG1	Laurel Fm.	Tn[e]	Tooth	*Ageleodus* sp.	Dentine	2	10.1	2.5
Laurel Downs	1984-04 Dh1	Laurel Fm.	Tn[e]	Tooth	Protacrodont	Enameloid	3	17.9	0.4
Laurel Downs	1984-04 Dh1	Laurel Fm.	Tn[e]	Tooth	Protacrodont	Dentine	3	16.2	0.2
Laurel Downs	1984-04 Dh1	Laurel Fm.	Tn[e]	Tooth	Protacrodont	Dentine	3	13.8	0.5
Laurel Downs	1984-04 Dh2	Laurel Fm.	Tn[e]	Tooth	Protacrodont	Enameloid	4	19.2	0.2
Laurel Downs	1984-04 Dh2	Laurel Fm.	Tn[e]	Tooth	Protacrodont	Dentine	4	16.4	0.7
Laurel Downs	1984-04 Dh3	Laurel Fm.	Tn[e]	Tooth	Protacrodont	Enameloid	3	18.9	0.3
Laurel Downs	1984-04 Sti[d]	Laurel Fm.	Tn[e]	Tooth	Cladodont	Dentine	4	7.5	2.1
Laurel Downs	1984-04 Sti[d]	Laurel Fm.	Tn[e]	Tooth	Cladodont	Dentine	4	11.5	0.8
Laurel Downs	1984-04 Stii[d]	Laurel Fm.	Tn[e]	Tooth	Cladodont	Dentine	4	16.1	2.7
Laurel Downs	MTM1-H1	Laurel Fm.	Tn[e]	Tooth	Holocephalan	Surface en[e]	5	18.1	0.5
Laurel Downs	MTM1-H1	Laurel Fm.	Tn[e]	Tooth	Holocephalan	Surface en[e]	5	9.2	0.9
Laurel Downs	MTM1-H1	Laurel Fm.	Tn[e]	Tooth	Holocephalan	Dentine	5	19.5	0.2
Laurel Downs	MTM1-H1	Laurel Fm.	Tn[e]	Tooth	Holocephalan	Dentine	5	15.6	0.8
Laurel Downs	MTM1-H1	Laurel Fm.	Tn[e]	Tooth	Holocephalan	Dentine	5	17.6	0.1
Laurel Downs	MTM1-H4	Laurel Fm.	Tn[e]	Tooth	Holocephalan	Dentine	4	18.7	0.1
Laurel Downs	MTM1-H4	Laurel Fm.	Tn[e]	Tooth	Holocephalan	Dentine	4	19.2	0.4
Laurel Downs	MTM1-H5	Laurel Fm.	Tn[e]	Tooth	Holocephalan	Dentine	4	17.3	0.2
Laurel Downs	MTM1-H5	Laurel Fm.	Tn[e]	Tooth	Holocephalan	Dentine	4	17.3	0.3
Laurel Downs	MTM1-H9	Laurel Fm.	Tn[e]	Tooth	Holocephalan	Surface en[f]	3	5.9	2.2
Laurel Downs	MTM1-H9	Laurel Fm.	Tn[e]	Tooth	Holocephalan	Pore en[f]	3	21.4	0.3
Laurel Downs	MTM1-H9	Laurel Fm.	Tn[e]	Tooth	Holocephalan	Surface en[f]	3	17.8	0.4
Laurel Downs	MTM1-H9	Laurel Fm.	Tn[e]	Tooth	Holocephalan	Pore en[f]	2	21.8	0.1
Laurel Downs	MTM1-H9	Laurel Fm.	Tn[e]	Tooth	Holocephalan	Pore en[f]	1	21.4	n/a
Laurel Downs	MTM1-H9	Laurel Fm.	Tn[e]	Tooth	Holocephalan	Surface en[f]	3	19.5	0.7
Laurel Downs	MTM1-H9	Laurel Fm.	Tn[e]	Tooth	Holocephalan	Dentine	3	17.2	0.4

[a] Number of replicate analysis.
[b] Frasnian.
[c] Famennian.
[d] i and ii notation indicate different individual fossils.
[e] Tournaisian.
[f] Enameloid.

modification (Fig. 2; Nöth, 1998). Vertebrate microfossil elements are similarly apparently well-preserved with smooth lustrous surfaces present on the cusps of teeth and dermal denticle crowns. In cross section, the dentine of all teeth was light grey to white in colour with the exception of sample MTM1-H9, which showed a dark grey discolouration around one margin that correlates to the previously exposed labial surface of the tooth. Reddish coloured staining is present within the basal tissue in sample MTM1-H1, along with calcite cement in some of the pore canals that extend from the cusp surface to the basal tissue.

4.2. GIRMS $\delta^{18}O$ analysis of vertebrate microfossil elements

The $\delta^{18}O$ values of Famennian vertebrate microfossils ranged from +16.2–17.1‰ (VSMOW) (Table 1) with a mean of +16.7‰. The $\delta^{18}O$ values obtained from the Tournaisian vertebrate microfossil samples are more variable than Famennian values, ranging from +15.7 to 19.1‰. The largest disparity in $\delta^{18}O$ was measured in the outer cusp tissue of Tournaisian holocephalan teeth (+16.0 to 19.1‰, mean of +17.8‰; Fig. 3). Similar $\delta^{18}O$ values were obtained from ctenacanthid (+16.0‰) and protacrodont (+17.1‰) scales from the Famennian. Inter-taxa variation of <1.2‰ was found for Tournaisian acanthodian (+17.0‰), lungfish (+16.5‰), ctenacanthiform (+16.9‰), protacrodont (+16.1 and +17.2‰) and palaeoniscoid scales (+19.0‰) (Table 1). Significant intra-specific disparity in $\delta^{18}O$ values within Tournaisian vertebrate scales was seen between protacrodont scales recording values of +16.1 and +17.2‰. The lowest $\delta^{18}O$ values were recorded in Tournaisian palaeoniscoids, with values of +15.7 (radial bone) and +15.9‰ (tooth) (Fig. 3). However, $\delta^{18}O$ values of associated palatal teeth were consistently higher at +18.0‰ (sample 1984-B) and +18.1‰ (sample 1984-H).

Please cite this article as: Roelofs, B., et al., Assessing the fidelity of marine vertebrate microfossil δ18O signatures and their potential for palaeoecological and -climat..., Palaeogeogr. Palaeoclimatol. Palaeoecol. (2016), http://dx.doi.org/10.1016/j.palaeo.2016.10.018

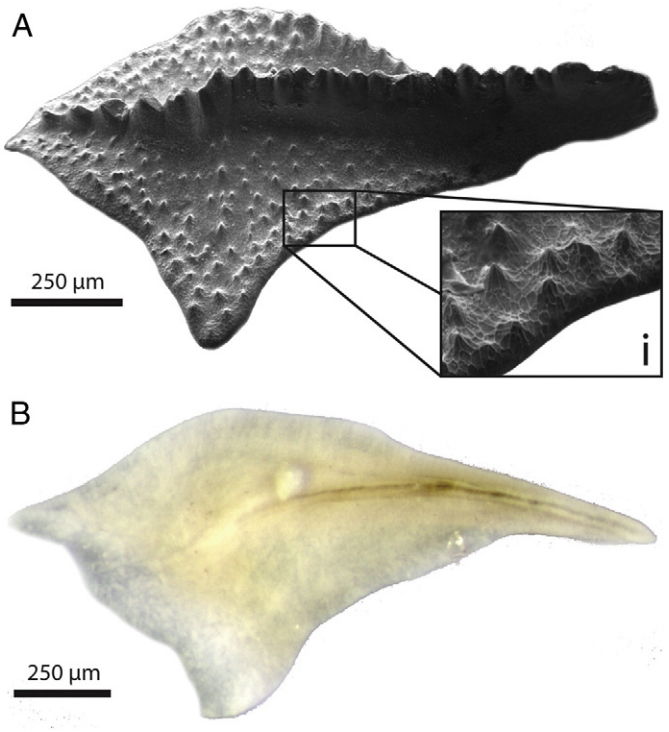

Fig. 2. Frasnian *Palmatolepis* P-elements. (A) Back-scattered electron microscope image in aboral view with ×4 magnified inset (i) highlighting the well-preserved ornamentation. (B) Stereo microscope image of a polished *Palmatolepis* sp. element showing the well-preserved internal microstructures and low Colour Alteration Index (CAI).

4.3. SIMS $\delta^{18}O$ analyses

In-situ oxygen isotope analyses were performed on three late Famennian and two early Tournaisian conodont elements (Table 2). Conodont $\delta^{18}O$ values from averaged spot analyses on three late Famennian S-elements range from +18.7 to 20.8‰ (Table 2), with an average value of +19.6 ± 0.5‰. Two to five individual spots were analysed on the blades of the S-elements with a deviation between spots on each element ranging from 0 to +1.0‰ (Table 2). Two P_1 elements (sensu Purnell et al., 2000) of the early Tournaisian conodont *Clydagnathus cavusformis* produced average $\delta^{18}O$ values of +19.9‰ (±0.4‰, n = 4) and +20.9‰ (±0.9‰, n = 5).

Clusters of three to five spots (within an area of <1 mm^2), were focused on enameloid, dentine and basal tissues of four holocephalan teeth (Fig. 4). Occasionally, one or more analytical spots missed the tissue targeted and average values were determined from remaining spot analyses. Average $\delta^{18}O$ values of spots (n = 5) targeting enameloid tissues in tooth MTM1-H1 produced values for spot clusters of +9.2 ± 0.9 and +18.0 ± 0.2‰ (Fig. 5A). The same enameloid tissue in sample MTM1-H9 was analysed, with individual clusters comprising two to three spots from four areas of the tooth (Fig. 5B) producing average $\delta^{18}O$ values between +21.4 ± 0.7 and +21.8 ± 0.1‰. Dentine was analysed in all four holocephalan teeth with an average $\delta^{18}O$ value of +17.9 ± 1.4‰ (1σ, n = 35). No consistent differences in $\delta^{18}O$ are present between upper dentine, close to the occlusal surface of the tooth, and lower dentine tissues, located toward the basal body (Fig. 5). The enamel of three protacrodont teeth was tested using clusters of three to four spots and exhibited average $\delta^{18}O$ values of +17.9 ± 0.4‰ (n = 3), +18.9 ± 0.2‰ (n = 3) and +19.2 ± 0.3‰ (n = 3) (Figs. 4, 6b). The dentine tissues in one tooth (1984-Dh1) showed a progressive depletion in ^{18}O from near the cusp apex (+16.2 ± 0.2‰) to less mineralised dentine in the basal tissues (+13.8 ± 0.5‰) (Fig. 4). A similar decrease in $\delta^{18}O$ is seen over 10 individual spots in an *Ageleodus* shark tooth (AG1, Fig. 6C), which presented a general trend in $\delta^{18}O$ from +17.3‰ in the cusp dentine, to +8.3‰ in the basal tissue. Three sets of analyses were performed on the dentine tissue of three cladodont cusps, which showed average $\delta^{18}O$ values between +7.5 ± 2.1 (n = 4) and +11.5 ± 2.7 (n = 4) ‰ (Table 2).

Two sets of $\delta^{18}O$ values were recorded from different areas on a Famennian shark spine, a series of three spots near the margin of the spine (average + 16.5 ± 0.3‰, n = 4) and three spots located centrally (+18.5 ± 0.4‰, n = 3). An average $\delta^{18}O$ value of +20.3‰ was recorded for scale crown surface tissues across different taxa from the Tournaisian samples. A difference of up to 2.1‰ was observed between spots on individual tissues. Dentine tissues from a Famennian protacrodont scale (+12.8 ± 1.0‰, n = 2), Tournaisian lungfish (+8.8 ± 1.9‰, n = 3 and +14.9 ± 1.3‰, n = 5) and an acanthodian scale (+16.7 ± 1.3‰) recorded $\delta^{18}O$ values consistently lower than the tissues close to the crown surfaces of the scales.

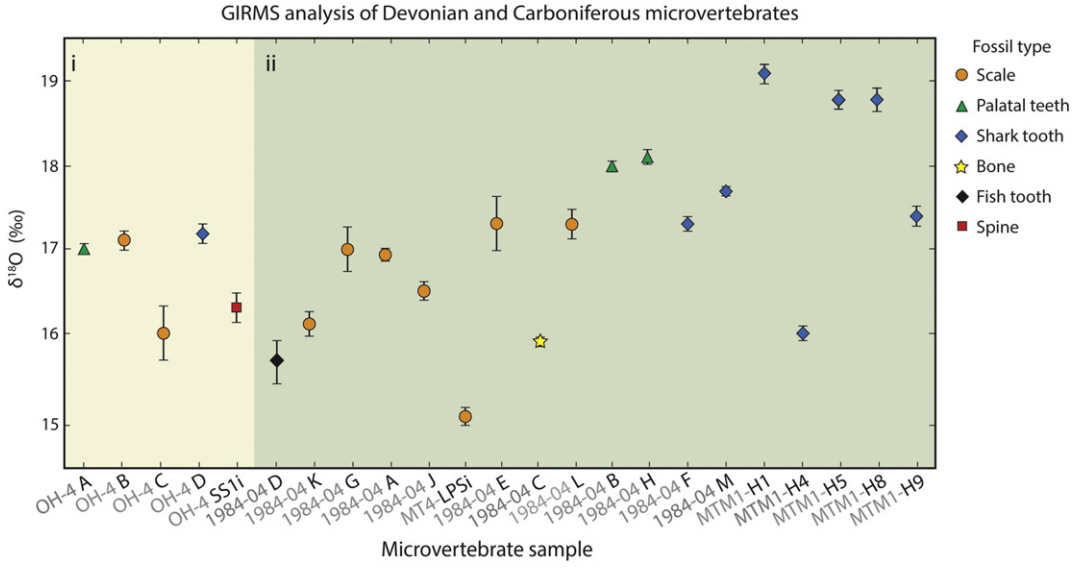

Fig. 3. Gas isotope ratio mass spectrometry (GIRMS) analyses of vertebrate microfossil elements from the late Famennian (i) and early Tournaisian (ii). Data points give average value of replicate analyses, vertical bars represent 1 std.dev. Coeval conodont values obtained from SIMS (late Famennian = +19.6 ± 0.5‰ and; early Tournaisian = +20.3 ± 0.8‰) were generally higher than vertebrate microfossil values analysed by GIRMS.

Please cite this article as: Roelofs, B., et al., Assessing the fidelity of marine vertebrate microfossil δ18O signatures and their potential for palaeoecological and -climat..., Palaeogeogr. Palaeoclimatol. Palaeoecol. (2016), http://dx.doi.org/10.1016/j.palaeo.2016.10.018

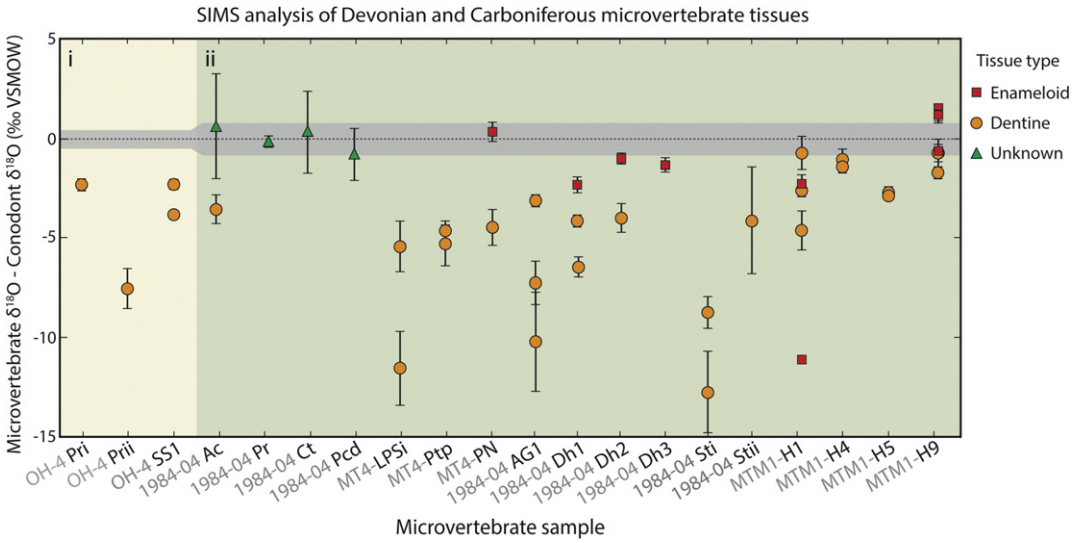

Fig. 4. Secondary ion mass spectrometry (SIMS) $\delta^{18}O$ analyses of vertebrate microfossil elements from the late Famennian (i) and early Tournaisian (ii). Data points are the averages of spot clusters with 1 std.dev. given by the vertical error bars. Average vertebrate microfossil $\delta^{18}O$ values are plotted as difference relative to the $\delta^{18}O$ of co-occurring conodonts to focus on the tissue-specific differences regardless of geological age. Conodont $\delta^{18}O$ values were obtained from secondary ion mass spectrometry (SIMS) ($\delta^{18}O_{conodont}$ values for the late Famennian = +19.6 ± 0.5‰ and; early Tournaisian = +20.3 ± 0.8‰). Grey area represents 1 std.dev. of average co-occurring $\delta^{18}O_{conodont}$ obtained by SIMS.

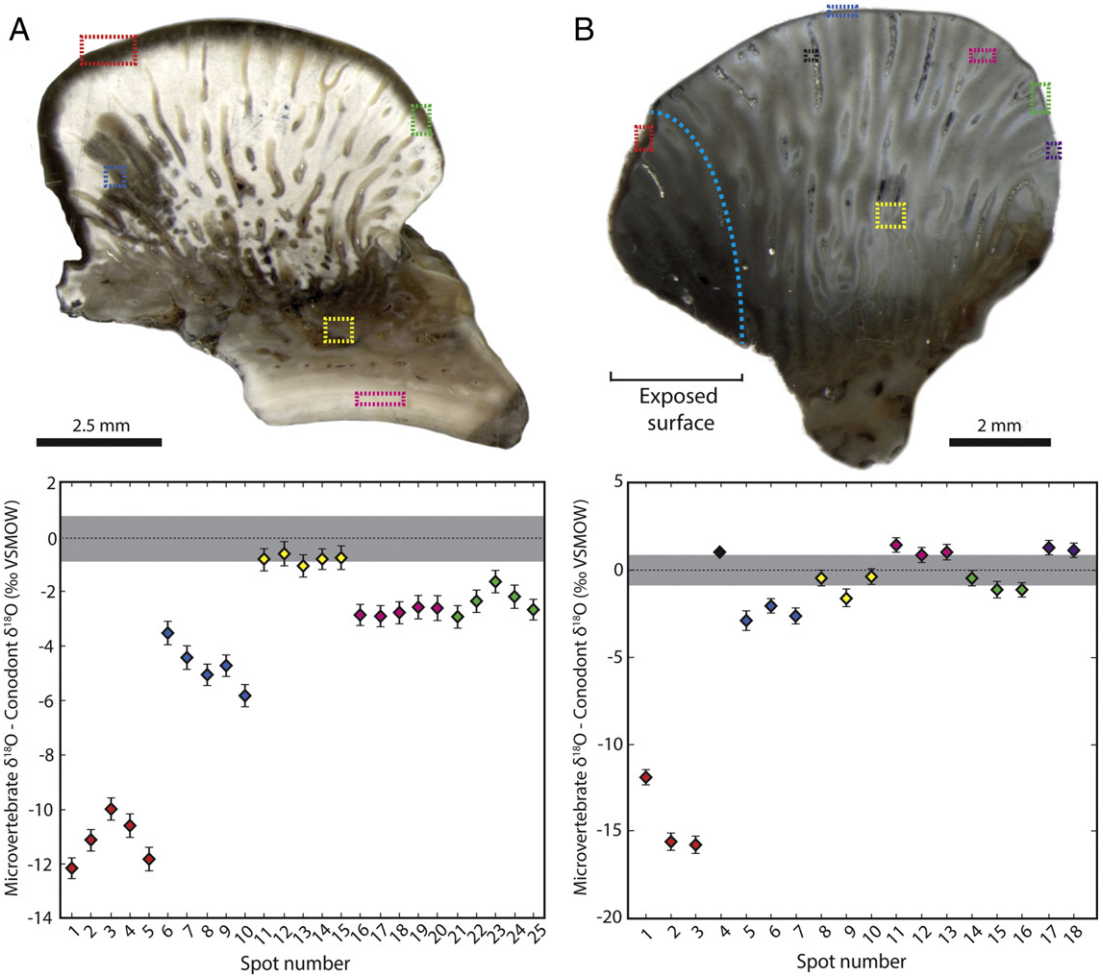

Fig. 5. $\delta^{18}O$ of tissue types from two early Tournaisian holocephalan teeth compared to average $\delta^{18}O$ of coeval conodonts (+20.3 ± 0.8‰). (A) Tooth (MTM1-H1) showing analysis of enameloid and dentine tissues; (A) analysis of a tooth (MTM1-H9) showing variation in $\delta^{18}O$ values associated with exposure of the labial surface (indicated by dashed line). Coloured boxes correspond to spot clusters depicted in the graphs A, B. Grey area represents 1 std.dev. (±0.8‰) of the average $\delta^{18}O$ of associated conodonts analysed by SIMS. For (B) spot numbers 1–3, 5–7 and 14–16 represent surface enameloid with pore enamel represented by spot numbers 4, 11–13 and 17–18. (For interpretation of the references to colour in this figure legend, the reader is referred to the web version of this article.)

Please cite this article as: Roelofs, B., et al., Assessing the fidelity of marine vertebrate microfossil δ18O signatures and their potential for palaeo-ecological and -climat..., Palaeogeogr. Palaeoclimatol. Palaeoecol. (2016), http://dx.doi.org/10.1016/j.palaeo.2016.10.018

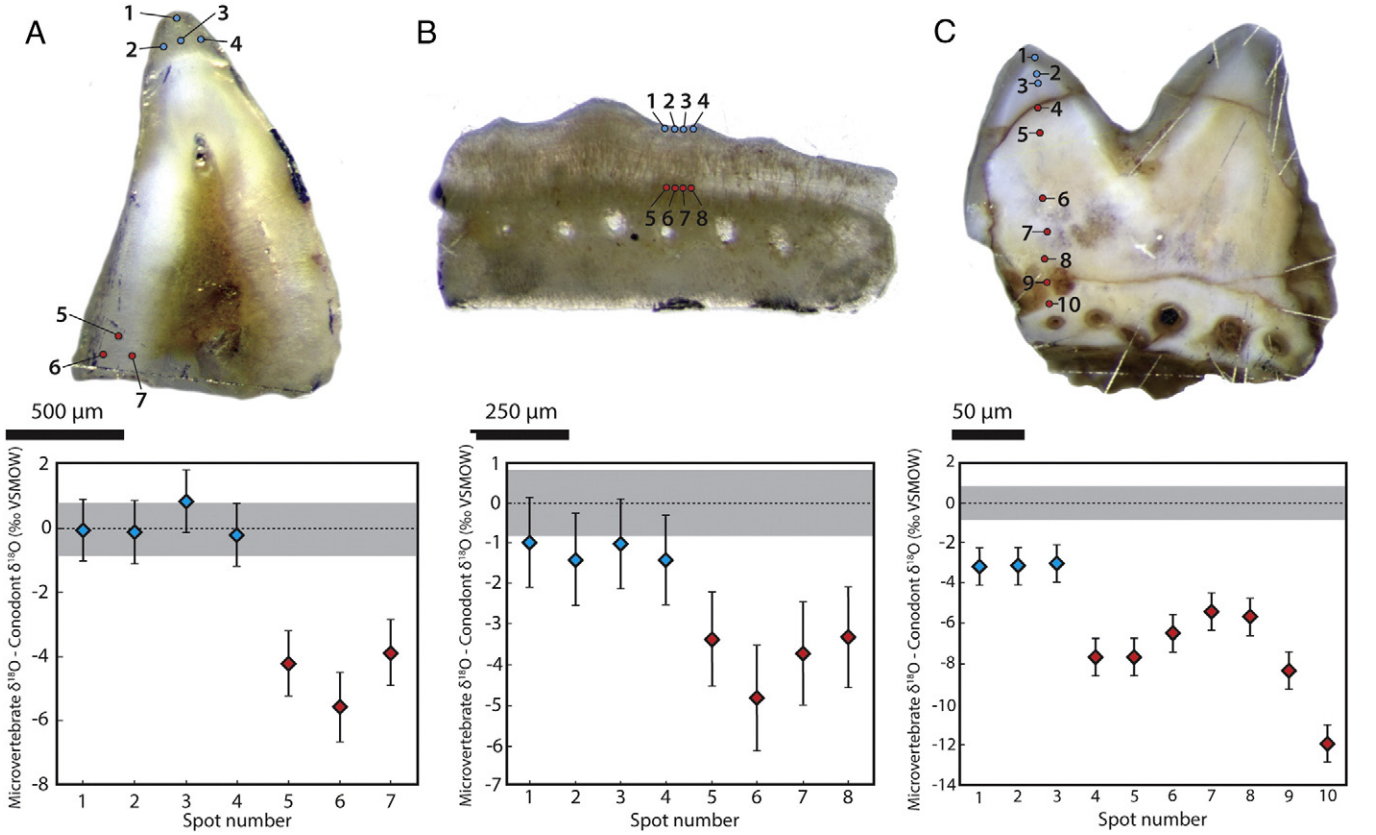

Fig. 6. Systematic $\delta^{18}O$ variation in early Tournaisian vertebrate microfossil tissues analysed via SIMS. Location of ion-probe spots indicated on stereo-microscope images of polished analytical surface. (A) Palaeoniscoid fish tooth (MT-4 PN) with acrodin cap and dentine tissue analysed; (B) analysis of enameloid and dentine tissues from Protacrodont tooth (1984-04 Dh2), referred to as *Dalmehodus* cf. *turnerae* (Roelofs et al., 2016); (c) tooth of the chondrichthyan *Ageleodus* (1984-04 AG1) showing a transect of spot analyses from the cusp apex to the base. All values plotted relative to a co-occurring conodont $\delta^{18}O$ value of $+20.3 \pm 0.8‰$. Grey areas in graphs represent 1 std.dev. ($\pm 0.8‰$) of $\delta^{18}O$ analyses of co-occurring conodonts.

5. Discussion

5.1. Comparison of GIRMS and SIMS $\delta^{18}O$ analyses

Traditional GIRMS targets the PO_4^{3-} group and eliminates analysis of any less stable oxygen compounds (carbonate, organics, water) (Firsching, 1961; Wright and Hoering, 1989; Crowson et al., 1991; O'Neil et al., 1994). The use of whole vertebrate microfossils, in order to obtain minimum sample masses (~0.3–1 mg) required for this method, can be problematic. Potential differences in the O-isotopic signal of fossilised phosphate tissues may be masked when vertebrate bioapatite is homogenised. The highly permeable and porous nature of fossil dentine, which is the bulk component of fossil teeth and dermal denticles, is highly susceptible to physical and chemical alteration (Kohn and Cerling, 2002; Koch, 2007). This susceptibility results, in part, from significant porosity and permeability increasing potential isotopic exchange between bioapatite and circulating fluids associated with diagenesis, as well as the potential for microbe mediated phosphate precipitation and alteration (Kolodny et al., 1983; Kastner et al., 1990; Blake et al., 1997, 1998; Zazzo et al., 2003).

The use of SIMS, as an alternative method for obtaining targeted $\delta^{18}O$ data from fossil bioapatite, is advantageous where fossil yields are below the mass required by GIRMS methods and when samples comprise different tissues (Wenzel et al., 2000; Trotter et al., 2008, 2015). However, SIMS indiscriminately analyses any oxygen-bearing compounds, including PO_4^{3-}, CO_3^{2-} and OH^- present within bioapatite (Passey and Cerling, 2006; Aubert et al., 2012). The presence of the CO_3^{2-} anion in bioapatite (either primary or as a secondary cement) can be particularly problematic as it is more susceptible to diagenetic alteration than PO_4^{3-}, with the C–O bond comparably weaker than the P–O bond (e.g. Iacumin et al., 1996).

Recent work by Wheeley et al. (2012) suggested $\delta^{18}O_{conodont}$ values obtained from SIMS were comparable with those of GIRMS for Silurian conodonts. However, it must be noted, offsets of ~1‰ between SIMS and GIRMS methods were observed in some Silurian conodont genera (Wheeley et al., 2012). Subsequent work by Trotter et al. (2015) showed an average offset of $0.6 \pm 0.2‰$ between the two methodologies, similar to earlier work of 0.7‰ (Trotter et al., 2008). Published data are currently considered insufficient to fully assess the presence and/or reasons for any discrepancies; however, it appears small but measurable offsets exist. Here fragments from a single crystal of Durango apatite were utilised to calibrate SIMS analyses. GIRMS analysis gave an average $\delta^{18}O$ value of $+9.9‰$ ($\pm 0.3‰$, 1σ) from triplicate analysis of three individual fragments of the same crystal, within error of the published value of $+9.8‰$ reported by Rigo et al. (2012). GIRMS analysis of the conodont genera *Ancyrodella* ($+19.0 \pm 0.2‰$) indicated a $< 0.2‰$ difference when compared to the $\delta^{18}O$ values obtained from SIMS of both *Ancyrodella* ($+19.2‰ \pm 0.3‰$) and *Palmatolepis* ($+19.1‰$) P_1 conodont elements from the same sample. The $\delta^{18}O_{conodont}$ values resolved from the two methods indicate valid comparisons can be made between SIMS and GIRMS analyses within error.

5.2. Canning Basin $\delta^{18}O_{conodont}$ values in a global context

The presence of open marine conditions in the Canning Basin, in the Late Devonian and Early Carboniferous, is important if $\delta^{18}O_{conodont}$ values are to be used as a globally representative baseline to assess the validity and palaeoenvironmental relevance of $\delta^{18}O$ values from

vertebrate microfossils. The significant faunal cosmopolitanism found in ammonoid (Becker and House, 2009), conodont (Nicoll and Druce, 1979; Klapper, 2007) and vertebrate microfossil taxa (Turner, 1982; Trinajstic and George, 2009; Hairapetian et al., 2015; Roelofs et al., 2015, 2016; Trinajstic et al., 2014) in the Late Devonian and Early Carboniferous suggests that pathways existed for significant faunal exchange. Furthermore, the recovery, from the Lennard Shelf, of globally correlative carbon isotope signatures associated with the Kellwasser Event (Stephens and Sumner, 2003; Playton et al., 2013; George et al., 2014; Hillbun et al., 2015), and presence of a significant regression (Talent et al., 1993) and negative $\delta^{13}C$ excursion (Andrew et al., 1994) related to the Hangenberg Event, are all suggestive of a local marine system coupled to global oceanic conditions. Despite these indicators of an open marine system, the $\delta^{18}O_{conodont}$ values from Frasnian Conodont Zone 11 (*jamieae* CZ) in the Canning Basin (+19.1–19.5‰) are approximately 1–1.5‰ higher than the $\delta^{18}O_{conodont}$ values (normalised to NBS 120c = +21.7‰) from latitudinally equivalent sites reported in Joachimski et al. (2004, 2009). The difference between the Canning Basin CZ 11 values and other sites may be due to local variations in temperature and salinity and demonstrate the importance of natural global variations in water composition, particularly when constructing composite isotope curves. In contrast to the Frasnian sample, a paucity of conodont elements from the Famennian and Tournaisian makes it difficult for well constrained ages and, therefore, direct comparison of Canning Basin $\delta^{18}O_{conodont}$ with coeval global values. The Oscar Hill locality, from which the Famennian samples were taken, suggested deposition occurred during the latest Famennian based on conodont elements (*praesulcata* CZ, Nicoll and Druce, 1979). An average $\delta^{18}O_{conodont}$ value of +19.6‰ is comparable to values from other latitudinally similar sites from the *praesulcata* CZ from the Cantabrian Mountains, Spain (~ + 19.4‰) and Montagne Noire, France (~ + 17.6–19.5‰) (Buggisch et al., 2008; values were corrected by −0.7‰ to account for a difference in the reported $\delta^{18}O$ of standard NBS 120c). An early Tournaisian age for the Carboniferous sample was inferred from conodont and vertebrate microfossil remains. The average $\delta^{18}O$ value for *C. cavusformis* P_1-elements tested was +20.4 ± 0.9‰. This is similar to the $\delta^{18}O_{conodonts}$ from the *sulcata* CZ interval (~ + 19.7–20.5‰, values were corrected by −0.7‰ to account for a difference in $\delta^{18}O$ of standard NBS 120c) in the Cantabrian Mountains, Spain (Buggisch et al., 2008). The results indicate that conodonts from the Frasnian to the Tournaisian in the Canning Basin are preserving isotopic signatures similar to conodonts from other pan tropical sites.

5.3. $\delta^{18}O$ variation in vertebrate microfossil tissues

The enameloid and dentine of four holocephalan teeth, all attributed to the same species, showed significant differences in $\delta^{18}O$ values as a result of histology, and therefore, mineral composition and susceptibility to diagenesis. The dense enameloid tissue present in holocephalan teeth is similar in hardness to that of enamel (Ishiyama et al., 1984) and comprises the outer layer of the crown as well as pore linings penetrating the crown (Fig. 5). The $\delta^{18}O$ values obtained (via SIMS) adjacent to pore canals produced more consistent results (mean value of +21.5 ± 0.2‰ for pore enameloid) than the outer mineralised layer of the crown, where $\delta^{18}O$ averages of spot clusters varied between +5.9 ± 2.2 and +19.5 ± 0.2‰. The enameloid tissue found along the outer surface of tooth MTM1-H1 (Fig. 5A) shows slight (spot no. 21–25) to considerably depletion (spot no. 1–5) of ^{18}O compared to co-occurring conodont $\delta^{18}O$ values. As this is not seen on the non-exposed side of the tooth MTM1-H9 from the same sample, it may represent alteration of the outer tissues prior to burial. There is also the potential for these values to be analytical artefacts due to topography induced through the differential polishing of the tooth and resin, or may result from diagenetic alteration, as the more discoloured areas in the tooth commonly show lower $\delta^{18}O$ values (Fig. 5B). Recent work has indicated that apparently well-preserved (i.e. lustrous) hypermineralised fossil tissues (e.g. Žigaitė et al., 2015) may not necessarily be indicative of pristine geochemistry. The presence of variable 'staining' in the teeth may reflect diagenetic mineralisation or alteration and may explain the significantly lower $\delta^{18}O$ values in peripheral hypermineralised tissues.

In general, the pore enameloid (Fig. 5B spot no. 4, 11–13, 17–18) of the holocephalan teeth analysed appears to more reliably preserve the original oxygen isotope ratios in comparison to the outer enameloid tissues (Fig. 5B spot no. 1–3, 5–7, 14–16), which are more readily exposed to post-mortem (or post-shedding), as well as burial, processes. The dentine tissue analysed from four holocephalan (Table 2) did not show any consistency in $\delta^{18}O$ values between individual teeth (Table 2). In addition the most significant degree of $\delta^{18}O$ variation came from a single tooth (MTM1-H1). Here three areas within the tooth (MTM1-H1) were analysed. The first cluster of spots (Fig. 5a spot no. 6–10; +15.8 ± 0.8‰) located in the cusp dentine; the second spot cluster (Fig. 5a spot no. 11–15; +19.5 ± 0.2‰) present in an area of osteodentine; and a third spot cluster in the basal tissue (Fig. 5a spot no. 16–20; +17.6 ± 0.1‰). Of these, the spot cluster at the basal area of HTM-H1 produced an average $\delta^{18}O$ value (+19.5 ± 0.2‰ n = 5) comparable to average $\delta^{18}O_{conodont}$ from the same sample +20.3 ± 0.8‰. The high $\delta^{18}O$ value may indicate that parts of the basal tissue, even though primarily consisting of permeable dentine, may be capable of preserving the original isotopic signatures under appropriate conditions.

The general structure of acrodin present in the tooth tip of many palaeonisciform fish is similar to the woven structure of enamel in elasmobranchs (Ripa et al., 1972; Ørvig, 1978; Reif, 1985; Sasagawa et al., 2012) and thereby prospective in terms of resistance to diagenetic modification or disruption of isotopic signatures. The $\delta^{18}O$ values obtained from four spot analyses of the acrodin tip of a tooth (Mt-4 PN) support this histological robustness with a $\delta^{18}O$ value (+20.7 ± 0.2‰ n = 4) and a standard deviation (1σ = ±0.5‰) comparable with associated conodonts (Fig. 6A, Table 2). The $\delta^{18}O$ value for the palaeoniscoid tooth dentine is depleted in ^{18}O (+15.9 ± 0.9‰) and similar to values from dentine in associated vertebrate microfossil taxa.

SIMS analyses were conducted on a range of scales belonging to acanthodians, chondrichthyan and palaeoniscoids. Scales attributed to each of these groups hosted $\delta^{18}O$ values within 1‰ of coeval conodont values (Fig. 4), which indicate that some scale tissues are preserving primary isotopic signatures. However, identifying the tissues that host these signatures is difficult as the spot size from the SIMS beam is larger than some of the targeted tissues. This causes a degree of ambiguity in the $\delta^{18}O$ results due to the unquantifiable influence of surrounding tissues. The presence of ganoine, a tissue homologous with enamel (Qu et al., 2013), in some palaeoniscoid fish may explain the relatively high average $\delta^{18}O$ value of +19.5 ± 1.3‰. Reconciling the average $\delta^{18}O$ value of +20.9 ± 1.6‰ for the acanthodian scale (1984–04 Ac, Fig. 4) analysed is difficult, as scales of this taxa typically lack hypermineralised tissues and instead comprise an acellular bone base and a dentine layer covering the crown (Sire et al., 2009). Hypermineralised tissues such as ganoine have been reported in Palaeozoic acanthodians (e.g. Richter and Smith, 1995), which highlights the need for individual scales to be analysed rather than relying on the generalised histology of particular taxa. Overall, the results obtained from scales indicate that multiple taxa have the potential to be used to elicit apparently original isotopic data and interpret ancient environmental conditions.

5.4. Comparison of GIRMS and SIMS $\delta^{18}O$ analyses of vertebrate microfossils

As dentine tissues constitute the bulk of the vertebrate microfossils tested here, it is expected that results from GIRMS would be comparable to SIMS analyses of dentine from the same sample if the greater part of the signal detected by SIMS was from phosphate. This hypothesis is not fully supported by co-analysed fossils here (Fig. 7). Only two of the six analysed fossils produced average dentine $\delta^{18}O$ SIMS values within

Please cite this article as: Roelofs, B., et al., Assessing the fidelity of marine vertebrate microfossil δ18O signatures and their potential for palaeoecological and -climat..., Palaeogeogr. Palaeoclimatol. Palaeoecol. (2016), http://dx.doi.org/10.1016/j.palaeo.2016.10.018

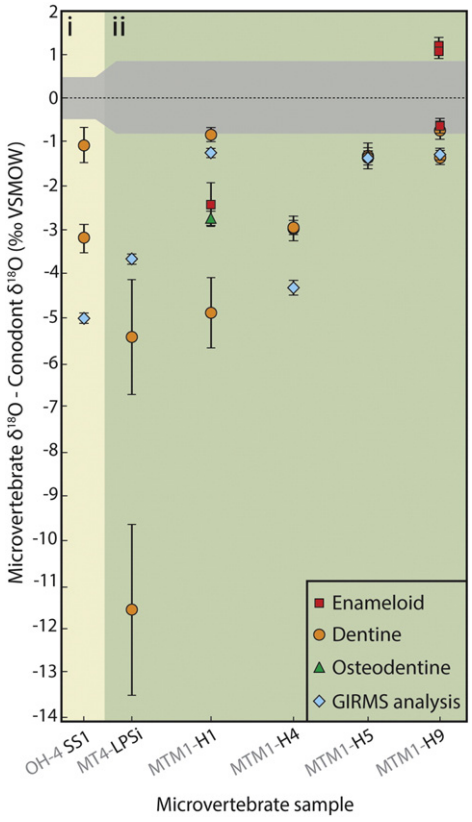

Fig. 7. Comparison of GIRMS and tissue specific targeting via SIMS analysis on individual fossil elements from the (i) Famennian (average conodont $\delta^{18}O$ value of $+19.6 \pm 0.5‰$ from three elements) and (ii) Tournaisian (average conodont $\delta^{18}O$ value of $+20.3 \pm 0.8‰$ from two elements). Grey area in the graph represents 1 std.dev. of $\delta^{18}O$ analyses of co-occurring conodonts.

<1‰ of the GIRMS values. This is likely due to an insufficient number of spots, which were unable to encompass the full range of O-isotope variation within a single fossil. SIMS analysis of the lungfish scale (MT4-LPSi, Fig. 7) highlights the significant variation even within a small cluster of spots ($\pm 1.9‰$ n = 3, $\pm 1.3‰$ n = 5). The potential for the alteration of PO_4^{3-} (since GIRMS analyses are lower than coeval conodonts inhabiting the same water mass, see Section 5.5) and contributions from other altered O-bearing compounds suggests SIMS and GIRMS may not be comparable for heterogeneous tissues. Specific analysis of hypermineralised tissues using both GIRMS and SIMS is required to determine if the variation in hypermineralised tissue is low enough to produce comparable results between the methods.

5.5. Diagenetic influences

Whole vertebrate microfossils analysed using GIRMS are commonly depleted in ^{18}O when compared to coeval conodont elements (Žigaitė et al., 2010; Barham et al., 2012a, b; Fischer et al., 2013). Since it has been demonstrated that modern fish precipitate bioapatite in isotopic equilibrium with ambient water (Kolodny et al., 1983; Vennemann et al., 2001; Pucéat et al., 2010), and the palaeoecology of many of the taxa are thought to overlap with those of coeval conodonts, the lower $\delta^{18}O$ values are interpreted to have occurred as a consequence of diagenetic changes in the less mineralised tissues. The 2.4 and 2.5‰ average offsets found for Famennian and Tournaisian specimens examined herein (Fig. 3), respectively, are close to those reported between Silurian conodonts and fish scales (2.5‰; Žigaitė et al., 2010). The low colour alteration index (CAI) of the Silurian conodonts (<1.5; Žigaitė et al., 2010) indicate thermally immature sediments, similar to what is found in the Canning Basin, and may explain the similarity of the discrepancy in $\delta^{18}O$ values. Moreover, Barham et al. (2012a) reported a more significant depletion in ^{18}O from Mississippian, Viséan ichthyoliths from Ireland that were associated with conodonts with CAI of >5, and indicated that the lower $\delta^{18}O$ values were influenced, but not necessarily controlled, by increasing diagenesis and thermal alteration. It is difficult to extrapolate the results of thermal alteration from conodonts to vertebrate microfossils given the significant taxonomic differences between these groups. However, significant degrees of homology have been identified between the hypermineralised tissues of vertebrates and conodont hyaline tissue (Donoghue, 1998; Donoghue et al., 2000; Nemliher and Kallaste, 2012). Therefore, it is not unreasonable to expect the preserved phosphate in both conodont and vertebrate hard tissues would be affected in a similar fashion to thermal maturation processes. Given the similar magnitude of conodont-vertebrate microfossil $\delta^{18}O$ offset in thermally mature (CAI ~5.5 in Barham et al., 2012a reported $\delta^{18}O$ offset of 2.9‰) and immature regions (CAI <1.5; offset of 2.5‰ from Žigaitė et al., 2010; 2.4 and 2.5‰ offsets found herein), it can be assumed that there is no linear correlation between thermal maturation and depletion of $\delta^{18}O$ in vertebrate microfossil tissues.

The lower $\delta^{18}O$ values of vertebrate microfossils may be influenced by the susceptibility of their fossil tissues to chemical processes (Ayliffe et al., 1994; Wang and Cerling, 1994; Koch et al., 1997; Kohn et al., 1999; Sharp et al., 2000; Kohn and Cerling, 2002; France and Owsley, 2015). Given the composition and porosity/permeability of their dentine tissues, recrystallisation of existing minerals (Kolodny and Luz, 1991; Kolodny et al., 1996) as well as precipitation of secondary O-bearing minerals (Martill, 1988; Blake et al., 1997; Kohn et al., 1999; Trueman et al., 2003), both with theoretically different O-isotope compositions, are more significant considerations for vertebrate microfossils during early diagenesis (Koch et al., 1997; Sharp et al., 2000; Zazzo et al., 2004). The extent to which these aforementioned causes of alteration affect O-isotope ratios will be largely determined by original structure and composition of the analysed tissues (e.g. Kohn and Cerling, 2002). Oxygen in apatite is present in the PO_4^{3-}, CO_3^{2-} and OH^- groups (Driessens and Verbeek, 1990). The phosphate component provides the most stable O-bond with no isotopic exchange observed in low temperature inorganic systems (Kolodny et al., 1983; Shemesh et al., 1988). The oxygen in carbonate however is susceptible to diagenetically induced fractionation (Luz et al., 1984; Nelson et al., 1986; Kolodny and Luz, 1991; Barrick and Showers, 1994, 1995; Wang and Cerling, 1994; Fricke et al., 1998; Kohn et al., 1999). Occurring at around 2–6 wt% in bone and dentine (LeGeros and LeGeros, 1984; Driessens and Verbeek, 1990), diagenetic affects on incorporated CO_3^{2-} may influence the final $\delta^{18}O$ values measured by SIMS. The effects of OH^- fractionation and substitution by other compounds such as CO_3^{2-} (Kohn et al., 1999) however, will not likely cause significant variation in the final $\delta^{18}O$ values as the wt% in dentine and bone is low (<1.6 wt%, Cerling and Sharp, 1996).

SIMS $\delta^{18}O$ analysis of modern shark teeth (Žigaitė and Whitehouse, 2014) identified average $\delta^{18}O$ variation of 1.2‰ within the dentine tissue. Mean variation between the parallel bundled enameloid (+21.2–23.1‰) and dentine tissue (+20.6–21.8‰) was also recorded. Žigaitė and Whitehouse (2014) noted the use of H_2O_2 in the pre-treatment cleaning process may have contributed to variation in the $\delta^{18}O$ values. However, it was concluded that organic matter, which is typically ^{18}O depleted, was the likely cause of this variation. The fossil shark and holocephali teeth tested here also showed significant discrepancies between tissues, as well as depletion in ^{18}O (Figs. 4, 5b, 6). However, such variation in the fossil specimens analysed here, cannot be attributed to original organic material as this would have degraded to the point where it would be undetectable, although decay products could have influenced the isotope ratios. Interestingly, analysis of teeth taken from freshly caught sharks (Vennemann et al., 2001) recorded comparable values between the dentine and enamel tissues using GIRMS. The isolation of PO_4^{3-} eliminates the influence of ^{18}O depleted organic matter, which may have resulted in $\delta^{18}O$ variation between the dentine and

Please cite this article as: Roelofs, B., et al., Assessing the fidelity of marine vertebrate microfossil δ18O signatures and their potential for palaeoecological and -climat..., Palaeogeogr. Palaeoclimatol. Palaeoecol. (2016), http://dx.doi.org/10.1016/j.palaeo.2016.10.018

enamel. Work by Zazzo et al. (2003), has demonstrated fractionation of phosphate within bone can occur within a few days post-mortem under oxic conditions, with the presence of microbial enzyme activity significantly increasing the rate of oxygen isotope exchange. In contrast, enamel was found to be significantly resistant to changes in the original oxygen isotope ratios (Zazzo et al., 2003). The susceptibility for isotopic alteration under microbially-mediated conditions for tissues with originally higher organic matter content, could explain the lower oxygen isotope values of the dentine of the shed teeth analysed by Žigaitė and Whitehouse (2014). Microbial "catalysts" have been previously used to explain the alteration of PO_4^{3-} $\delta^{18}O$ in bioapatite (Kolodny et al., 1983; Kastner et al., 1990). The Upper Devonian and Lower Carboniferous vertebrate microfossil elements analysed here were obtained from limestones formed in well oxygenated shallow water marine settings (Druce and Radke, 1979). Given the lack of thermal maturity or any evidence for fluid alteration of the sequences studied, microbially-induced alteration within incompletely mineralised tissues in vertebrate microfossils ex-vivo and/or during early diagenesis (eogenesis) must be considered a plausible mechanism for lower $\delta^{18}O$-values.

Evidence for recent weathering processes affecting $\delta^{18}O$-values is present in one of the holocephalan teeth (MTM1-H9, Fig. 5B), which had a portion of the occluso-labial face of the crown protruding from a rock. It is difficult to constrain the length of time the tooth was exposed, however it is likely that it was affected by a range of weathering processes including frequent scrub fires and interaction with meteoric fluids. The effect of exposure was evident with the outer enameloid layer of the tooth producing values progressively depleted in ^{18}O toward the exposed surface. The low $\delta^{18}O$ values between +5.2–5.9‰ (Fig. 5B spot no. 1–3) at the exposed face correspond to significant degradation of the enameloid and dentine. However, the affected area was small and the dentine within the tooth (+19.5 ± 0.7‰) was found to be comparable to the outer enameloid surface on the non-exposed face (+21.4‰, Fig. 6b). This suggests relative localisation of alteration and overall robustness of the tissue to short-term abiotic processes.

5.6. Palaeoecological influences

Understanding the biology of ancient sharks and fish as well as the environments they inhabited is important to contextualise variation present in tissues, particularly hypermineralised tissues, where primary isotope values are thought to be original. Glaciation, resulting in the preferential locking of ^{16}O in terrestrial ice-sheets, was present during the late Famennian and early Tournaisian (Kaiser et al., 2008). Evidence suggests these glacial conditions were not as extensive as the modern climate state (Isaacson et al., 2008), hence a $\delta^{18}O_{seawater}$ offset of −0.5‰ (VSMOW) is inferred to account for greater ^{16}O concentrations in the oceans than in the present-day. Assuming these glacial conditions and subsequent offset to $\delta^{18}O_{seawater}$, average $\delta^{18}O$ values (+17.8, +18.9 and +19.2‰) from protacrodont tooth enamel (uncorrected for diagenetic alteration due to their hypermineralised condition) indicate palaeotemperatures of between 34 and 42 °C (calculated using the equation of Lécuyer et al., 2013). Such sea-surface temperatures are considerably higher than those calculated from coeval conodont (25 and 29 °C using the equation of Lécuyer et al., 2013).

Enrichment of ^{16}O as a result of bioapatite precipitation from a water mass influenced by meteoric fluids in both the Protacrodont (Fig. 5b) teeth cannot be easily dismissed. However, this would imply migratory habits for the taxa, as the fauna and facies of the Laurel Formation indicate an exclusively marine setting (Druce and Radke, 1979). Similar to the habits of extant shark species such as *Carcharhinus leucas* (bull shark) (Thorson, 1971) and *Glyphis gangeticus* (Ganges shark) (Compagno, 1997), Palaeozoic shark taxa are known to have inhabited freshwater environments on both a permanent (e.g. Xenacanths, Ginter et al., 2010; members of the *Ageleodus* genus, Downs and Daeschler, 2001) and temporary basis (e.g. *Lissodus*, Fischer et al., 2013). Strontium isotope analysis has been previously employed on chondrichthyan taxa (Scharer et al., 2012; Fischer et al., 2013, 2014; Raoult et al., 2016) in order to quantify the salinity variable. It may be necessary to include this form of analysis in order to isolate the palaeotemperature signal of vertebrate microfossil O-isotope data when incorporating fossil taxa known to inhabit different environments.

Significant ecological differences within fully marine extant shark genera are reflected in the O-isotope ratios of the mineralised tissues (Vennemann et al., 2001). The potential migration of ancient sharks across latitudes or water depths must also be taken into account when interpreting O-isotope data from nektonic fossil taxa. Significant migratory behaviour is observed in extant taxa such as *Odontaspis ferox* (Fergusson et al., 2008), which has been found at depths of 850 m as well as very shallow coastal waters. In addition, members of the species *Carcharodon carcharias* (great white shark) have been frequently observed migrating long distances, in some cases over 20,000 km in less than a year (Bonfil et al., 2005). Migratory issues of extinct species may be compounded in groups such as the Ctenicanthiforms where tooth development is slower than that observed in modern sharks (Williams, 2001; Botella et al., 2009). Analysis of species with fast tooth replacement rates may mitigate some migratory factors as teeth are more likely to preserve local conditions. Tooth formation can be as quick as 9–12 days within some extant selachians (Moss, 1967); however, determining similar tooth replacement in Palaeozoic species is currently difficult to ascertain.

6. Conclusions

The hypermineralised bioapatite present in vertebrate teeth and scales provides a proxy capable of reconstructing marine oxygen isotope records from the middle Palaeozoic to the modern day. The densely crystalline tissues that form enamel, enameloid and acrodin show the greatest potential of preserving original oxygen isotope signatures. Results presented herein from a broad range of taxa (scales of acanthodians as well as the scales and teeth of chondrichthyans and actinopterygians) indicate eliciting palaeoenvironmental data from other vertebrate groups is likely.

The utilisation of SIMS, which permits tissue specific analysis, suggests dentine tissue is more susceptible to alteration due to a higher porosity and permeability inherited from an originally high organic component. The low CAI of conodont fossils analysed here suggests thermal maturation is not the dominant factor in the lower $\delta^{18}O$ values obtained from vertebrate microfossils. Instead, this work suggests ex-vivo microbial activity may be a more likely factor in the alteration of the original oxygen isotope ratios.

Going forward, it is clear that a range of Palaeozoic vertebrate groups offer an alternative tool for reconstructing palaeoenvironmental conditions (water mass palaeotemperature and palaeohydrological condition). In addition, the presence of potentially original isotopic signatures provides a basis for applications in chemostratigraphy where conodonts are rare or absent. SIMS analysis of targeted hypermineralised vertebrate microfossil tissues can resolve original O-isotope values, and therefore can be used in a similar fashion to, and correlated with, $\delta^{18}O_{conodont}$. However, minimising potential $\delta^{18}O$ variation as a consequence of species dependant factors such as migratory habits remains critical. Ideally analyses should include multiple species and comparisons to co-occurring or coeval conodonts from other areas.

Acknowledgments

Thanks to Daniele Lutz from the GeoZentrum Nordbayern, University of Erlangen-Nürnberg, Germany for aiding in the preparation of the fossil material for analysis. BR would like to thank the anonymous reviewers of his dissertation for their helpful comments. In addition, a thank you to the editor Thomas Algeo and the anonymous reviewers for their invaluable comments regarding the manuscript. The authors acknowledge the use of equipment, scientific and technical assistance

Please cite this article as: Roelofs, B., et al., Assessing the fidelity of marine vertebrate microfossil δ18O signatures and their potential for palaeoecological and -climat..., Palaeogeogr. Palaeoclimatol. Palaeoecol. (2016), http://dx.doi.org/10.1016/j.palaeo.2016.10.018

of the Curtin University Electron Microscope Facility, which has been partially funded by the University, State and Commonwealth Governments. In addition the authors would also like to acknowledge the facilities, and the scientific and technical assistance of the Australian Microscopy & Microanalysis Research Facility at the Centre for Microscopy, Characterisation & Analysis, The University of Western Australia, a facility funded by the University, State and Commonwealth Governments. The authors are also indebted to Catherine Boisvert, Alison Edmunds and the Melbourne Aquarium for providing access to water samples and naturally shed shark teeth, collected during routine cleaning. Further appreciation goes to Bradley McDonald for access to Durango apatite. We would also like to thank the owners of Brooking Springs and Laurel Downs stations for allowing access to outcrops. BR recognises the receipt of an Australian Postgraduate Award as well as a Curtin Completion Scholarship. This research was funded under Australian Research Council grant DP 110101127 with supporting partners including MRIWA, WA ERA, CSIRO, Chevron Australia Business Unit, Chevron Energy Technology Company, National Science Foundation and the Geological Survey of Western Australia.

Appendix A. Supplementary material

Supplementary data to this article can be found online at http://dx.doi.org/10.1016/j.palaeo.2016.10.018.

References

Andrew, A., Hamilton, P., Mawson, R., Talent, J., Whitford, D., 1994. Isotopic correlation tools in the mid-Palaeozoic and their relation to extinction events. Aust. Petrol. Explor. Assoc. J. 34, 268.

Aubert, M., Williams, I.S., Boljkovac, K., Moffat, I., 2012. In situ oxygen isotope micro-analysis of faunal material and human teeth using a SHRIMP II: a new tool for palaeoecology and archaeology. J. Archaeol. Sci. 39, 3184–3194.

Auclair, A., Joachimski, M.M., Lécuyer, C., 2003. Deciphering kinetic, metabolic and environmental controls on stable isotope fractionations between seawater and the shell of *Terebratalia transversa* (Brachiopoda). Chem. Geol. 202, 59–78.

Ayliffe, L.K., Chivas, A., Leakey, M.G., 1994. The retention of primary oxygen isotope compositions of fossil elephant skeletal phopshate. Geochim. Cosmochim. Acta 58, 5291–5298.

Azmy, K., Veizer, J., Bassett, M.G., Copper, P., 1998. Oxygen and carbon isotopic composition of Silurian brachiopods: implications for coeval seawater and glaciations. Geol. Soc. Am. Bull. 110, 1499–1512.

Barham, M., Joachimski, M., Murray, J., Williams, D., 2012a. Diagenetic alteration of the structure and $\delta^{18}O$ signature of Palaeozoic fish and conodont apatite: potential use for corrected isotope signatures in palaeoenvironmental interpretation. Chem. Geol. 298, 11–19.

Barham, M., Murray, J., Joachimski, M., Williams, D., 2012b. The onset of the Permo-Carboniferous glaciation: reconciling global stratigraphic evidence with biogenic apatite $\delta^{18}O$ records in the late Visean. J. Geol. Soc. 169, 119–122.

Barnes, C.R., Sass, D.B., Monroe, E.A., 1973. Ultra structure of some Ordovician conodonts. In: Rhodes, F.H.T. (Ed.), Conodont Paleozoology. Geological Society of America Special Paper 141, pp. 1–30.

Barrick, R.E., Showers, W.J., 1994. Thermophysiology of *Tyrannosaurus rex*: evidence from oxygen isotopes. Science 265, 222–224.

Barrick, R.E., Showers, W.J., 1995. Oxygen isotope variability in juvenile dinosaurs (*Hypacrosaurus*): evidence for thermoregulation. Paleobiology 21, 552–560.

Becker, R., House, M., 2009. Devonian ammonoid biostratigraphy of the Canning Basin. Geol. Surv. W. Aust. Bull. 145, 415–439.

Billon-Bruyat, J.P., Lécuyer, C., Martineau, F., Mazin, J.M., 2005. Oxygen isotope compositions of Late Jurassic vertebrate remains from lithographic limestones of western Europe: implications for the ecology of fish, turtles, and crocodilians. Palaeogeogr. Palaeoclimatol. Palaeoecol. 216, 359–375.

Blake, R.E., O'neil, J.R., Garcia, G.A., 1997. Oxygen isotope systematics of biologically mediated reactions of phosphate: I. Microbial degradation of organophosphorus compounds. Geochim. Cosmochim. Acta 61, 4411–4422.

Blake, R.E., O'Neil, J.R., Garcia, G.A., 1998. Effects of microbial activity on the $\delta^{18}O$ of dissolved inorganic phosphate and textural features of synthetic apatites. Am. Mineral. 83, 1516–1531.

Bonfil, R., Meÿer, M., Scholl, M.C., Johnson, R., O'Brien, S., Oosthuizen, H., Swanson, S., Kotze, D., Paterson, M., 2005. Transoceanic migration, spatial dynamics, and population linkages of white sharks. Science 310, 100–103.

Botella, H., Valenzuela-Ríos, J.I., Martínez-Pérez, C., 2009. Tooth replacement rates in early chondrichthyans: a qualitative approach. Lethaia 42, 365–376.

Brady, A., 2004. Laser ablation as a valuable tool in the stable isotope analysis of archaeological material. Totem 12, 27–32.

Brand, U., 1989. Biogeochemistry of Late Paleozoic North American brachiopods and secular variation of seawater composition. Biogeochemistry 7, 159–193.

Brand, U., 2004. Carbon, oxygen and strontium isotopes in Paleozoic carbonate components: an evaluation of original seawater-chemistry proxies. Chem. Geol. 204, 23–44.

Buggisch, W., Joachimski, M.M., Sevastopulo, G., Morrow, J.R., 2008. Mississippian $\delta^{13}C$ carb and conodont apatite $\delta^{18}O$ records—their relation to the Late Palaeozoic glaciation. Palaeogeogr. Palaeoclimatol. Palaeoecol. 268, 273–292.

Caplan, M.L., Bustin, R.M., 1999. Devonian - Carboniferous Hangenberg mass extinction event, widespread organic-rich mudrock and anoxia: causes and consequences. Palaeogeogr. Palaeoclimatol. Palaeoecol. 148, 187–207.

Carpenter, S.J., Lohmann, K.C., Holden, P., Walter, L.M., Huston, T.J., Halliday, A.N., 1991. $\delta^{18}O$ values, $^{87}Sr/^{86}Sr$ and Sr/Mg ratios of Late Devonian abiotic marine calcite: implications for the composition of ancient seawater. Geochim. Cosmochim. Acta 55, 1991–2010.

Cerling, T.E., Sharp, Z.D., 1996. Stable carbon and oxygen isotope analysis of fossil tooth enamel using laser ablation. Palaeogeogr. Palaeoclimatol. Palaeoecol. 126, 173–186.

Chen, B., Joachimski, M.M., Wang, X.D., Shen, S., Qi, Y., Qie, W., 2016. Ice volume and paleoclimate history of the Late Paleozoic ice age from conodont apatite oxygen isotopes from Naqing (Guizhou, China). Palaeogeogr. Palaeoclimatol. Palaeoecol. 448, 151–161.

Clarke, B., 2008. Normal bone anatomy and physiology. Clin. J. Am. Soc. Nephrol. (Supp 3), S131–S139.

Compagno, L.J., 1997. Threatened fishes of the world: *Glyphis gangeticus* (Müller & Henle, 1839) (Carcharhinidae). Environ. Biol. Fish 49, 400.

Crowson, R.A., Showers, W.J., Wright, E.K., Hoering, T.C., 1991. Preparation of phosphate samples for oxygen isotope analysis. Anal. Chem. 63, 2397–2400.

Cummins, R.C., Finnegan, S., Fike, D.A., Eiler, J.M., Fischer, W.W., 2014. Carbonate clumped isotope constraints on Silurian ocean temperature and seawater $\delta^{18}O$. Geochim. Cosmochim. Acta 140, 241–258.

Donoghue, P.C.J., 1998. Growth and patterning in the conodont skeleton. Philos. Trans. R. Soc. Lond. 353, 633–666.

Donoghue, P.C.J., Forey, P.L., Aldridge, R.J., 2000. Conodont affinity and chordate phylogeny. Biol. Rev. 75, 191–251.

Downs, J.P., Daeschler, E.B., 2001. Variation within a large sample of *Ageleodus pectinatus* teeth (Chondrichthyes) from the Late Devonian of Pennsylvania, USA. J. Vertebr. Paleontol. 21, 811–814.

Driessens, F.C.M., Verbeek, R.M.H., 1990. Biominerals. CRC Press, Boca Raton, Florida, USA.

Druce, E.C., Radke, B.M., 1979. The geology of the Fairfield Group, Canning Basin, Western Australia. Bureau of Mineral Resources, Australia, Bulletin 200, 1–62.

Dzik, J., 1991. Evolution of the oral apparatuses in the conodont chordates. Acta Palaeontol. Pol. 36, 265–323.

Fergusson, I.K., Graham, K.J., Compagno, L.J., 2008. Distribution, abundance and biology of the smalltooth sandtiger shark *Odontaspis ferox* (Risso, 1810) (Lamniformes: dontaspididae). Environ. Biol. Fish 81, 207–228.

Firsching, F.H., 1961. Precipitation of silver phosphate from homogeneous solution. Anal. Chem. 33, 873–874.

Fischer, J., Voight, S., Franz, M., Schneider, J.W., Joachimski, M.M., Tichomirowa, M., Götze, J., Furrer, H., 2012. Palaeoenvironments of the late Triassic Rhaetian Sea: implications from oxygen and strontium isotopes of hybodont shark teeth. Palaeogeogr. Palaeoclimatol. Palaeoecol. 353, 60–72.

Fischer, J., Schneider, J.W., Voigt, S., Joachimski, M.M., Tichomirowa, M., Tütken, T., Götze, J., Berner, U., 2013. Oxygen and strontium isotopes from fossil shark teeth: environmental and ecological implications for Late Palaeozoic European basins. Chem. Geol. 342, 44–62.

Fischer, J., Schneider, J.W., Hodnett, J.P.M., Elliott, D.K., Johnson, G.D., Voigt, S., Götze, J., 2014. Stable and radiogenic isotope analyses on shark teeth from the Early to the Middle Permian (Sakmarian–Roadian) of the southwestern USA. Hist. Biol. 26, 710–727.

France, C.A.M., Owsley, D.W., 2015. Stable carbon and oxygen isotope spacing between bone and tooth collagen and hydroxyapatite in human archaeological remains. Int. J. Osteoarchaeol. 25, 299–312.

Fricke, H.C., Clyde, W.C., O'Neil, J.R., Gingerich, P.D., 1998. Evidence for rapid climate change in North America during the latest Paleocene thermal maximum: oxygen isotope compositions of biogenic phosphate from the Bighorn Basin (Wyoming). Earth Planet. Sci. Lett. 160, 193–208.

Gabbott, S.E., Aledridge, R.J., Theron, J.N., 1995. A giant conodont with preserved muscle tissue from the upper Ordovician of South Africa. Nature 374, 800–803.

George, A.D., Chow, N., Trinajstic, K.M., 2014. Oxic facies and the Late Devonian mass extinction, Canning Basin, Australia. Geology 42, 327–330.

Ginter, M., Hampe, O., Duffin, C.J., 2010. Paleozoic Elasmobranchii: Teeth. Pfeil.

Goldberg, M., Kulkarni, A.B., Young, M., Boskey, A., 2011. Dentin: structure, composition and mineralization: the role of dentin ECM in dentin formation and mineralization. Front. Biosci. (Elite Ed.) 3, 711–735.

Goudemand, N., Orchard, M.J., Urdy, S., Bucher, H., Tafforeau, P., 2011. Synchrotron-aided reconstruction of the conodont feeding apparatus and implications for the mouth of the first vertebrates. Proc. Natl. Acad. Sci. 108, 8720–8724.

Grimes, S.T., Mattey, D.P., Hooker, J.J., Collinson, M.E., 2003. Paleogene paleoclimate reconstruction using oxygen isotopes from land and freshwater organisms: the use of multiple paleoproxies. Geochim. Cosmochim. Acta 67, 4033–4047.

Gruszczyński, M., Hałas, S., Hoffman, A., Małkowski, K., 1989. A brachiopod calcite record of the oceanic carbon and oxygen isotope shifts at the Permian/Triassic transition. Nature 337, 64–68.

Hairapetian, V., Roelofs, B.P., Trinajstic, K.M., Turner, S., 2015. Famennian survivor turiniid thelodonts of north and east Gondwana. Geol. Soc. Lond., Spec. Publ. 423.

Hand, A.R., Frank, M.E., 2014. Fundamentals of Oral Histology and Physiology. John Wiley & Sons.

Hays, P.D., Grossman, E.L., 1991. Oxygen isotopes in meteoric calcite cements as indicators of continental paleoclimate. Geology 19, 441–444.

Please cite this article as: Roelofs, B., et al., Assessing the fidelity of marine vertebrate microfossil δ18O signatures and their potential for palaeoecological and -climat..., Palaeogeogr. Palaeoclimatol. Palaeoecol. (2016), http://dx.doi.org/10.1016/j.palaeo.2016.10.018

Hillbun, K., Playton, T.E., Tohver, E., Ratcliffe, K., Trinajstic, K., Roelofs, B., Caulfield-Kerney, S., Wray, D., Haines, P., Hocking, R., 2015. Upper Kellwasser carbon isotope excursion pre-dates the F-F boundary in the Upper Devonian Lennard Shelf carbonate system, Canning Basin, Western Australia. Palaeogeogr. Palaeoclimatol. Palaeoecol. 438, 180–190.

Iacumin, P., Bocherens, H., Mariotti, A., Longinelli, A., 1996. Oxygen isotope analyses of co-existing carbonate and phosphate in biogenic apatite: a way to monitor diagenetic alteration of bone phosphate? Earth Planet. Sci. Lett. 142, 1–6.

Ishiyama, M., Sasagawa, I., Akai, J., 1984. The inorganic contentof pleromin in tooth plates of the living holocephalan, *Chimaera phantasma*, consists of a crystalline calcium phosphate known as $BCa^3(PO_4)^2$(Whitlockite). Arch. Histol. Cytol. 47, 89–94.

James, N.P., Bone, Y., Kyser, T.K., 1997. Brachiopod $\delta^{18}O$ values do reflect ambient oceanography: Lacepede Shelf, southern Australia. Geology 25, 551–554.

Jeppsson, L., Anehus, R., Fredholm, D., 1999. The optimal acetate buffered acetic acid technique for extracting phosphatic fossils. J. Paleontol. 73, 964–972.

Joachimski, M.M., Buggisch, W., 2002. Conodont apatite $\delta^{18}O$ signatures indicate climatic cooling as a trigger of the Late Devonian mass extinction. Geology 30, 711–714.

Joachimski, M.M., Lambert, L.L., 2015. Salinity contrast in the US midcontinent sea during Pennsylvanian glacio-eustatic highstands: evidence from conodont apatite $\delta^{18}O$. Palaeogeogr. Palaeoclimatol. Palaeoecol. 433, 71–80.

Joachimski, M.M., Van Geldern, R., Breisig, S., Buggisch, W., Day, J., 2004. Oxygen isotope evolution of biogenic calcite and apatite during the Middle and Late Devonian. Int. J. Earth Sci. 93, 542–553.

Joachimski, M., Breisig, S., Buggisch, W., Talent, J., Mawson, R., Gereke, M., Morrow, J., Day, J., Weddige, K., 2009. Devonian climate and reef evolution: insights from oxygen isotopes in apatite. Earth Planet. Sci. Lett. 284, 599–609.

Joachimski, M.M., Lai, X., Shen, S., Jiang, H., Luo, G., Chen, B., Sun, Y., 2012. Climate warming in the latest Permian and the Permian–Triassic mass extinction. Geology 40, 195–198.

Jones, D., Evans, A.R., Siu, K.K., Rayfield, E.J., Donoghue, P.C., 2012. The sharpest tools in the box? Quantitative analysis of conodont element functional morphology. Proc. R. Soc. Lond. B Biol. Sci. 279, 2849–2854.

Kaiser, S.I., Steuber, T., Becker, R.T., Joachimski, M.M., 2006. Geochemical evidence for major environmental change at the Devonian - Carboniferous boundary in the Carnic Alps and the Rhenish Massif. Palaeogeogr. Palaeoclimatol. Palaeoecol. 240, 146–160.

Kaiser, S.I., Steuber, T., Becker, R.T., 2008. Environmental change during the Late Famennian and Early Tournaisian (Late Devonian - Early Carboniferous): implications from stable isotopes and conodont biofacies in southern Europe. Geol. J. 43, 241–260.

Kastner, M., Garrison, R.E., Kolodny, Y., Reimers, C.E., Shemesh, A., 1990. Coupled changes of oxygen isotopes in PO_4^{3-} and CO_3^{2-} in apatite, with emphasis on the Monterey Formation, California. Phosphate Deposits of the World. 3, pp. 312–324.

Kita, N.T., Ushikubo, T., Fu, B., Valley, J.W., 2009. High precision SIMS oxygen isotope analysis and the effect of sample topography. Chem. Geol. 264, 43–57.

Klapper, G., 1988. The Montagne Noire Frasnian (Upper Devonian) conodont succession. J. Paleontol. 81, 513–537.

Klapper, G., 2007. Frasnian (Upper Devonian) conodont succession at Horse Spring and correlative sections, Canning Basin, Western Australia. J. Paleontol. 81, 513–527.

Koch, P.L., 2007. Isotopic study of the biology of modern and fossil vertebrates. Stable Isotopes in Ecology and Environmental Science. 2, pp. 99–154.

Koch, P.L., Tuross, N., Fogel, M.L., 1997. The effects of sample treatment and diagenesis on the isotopic integrity of carbonate in biogenic hydroxylapatite. J. Archaeol. Sci. 24, 417–429.

Kohn, M.J., Cerling, T.E., 2002. Stable isotope compositions of biological apatite. Rev. Mineral. Geochem. 48, 455–488.

Kohn, M.J., Schoeninger, M.J., Barker, W.W., 1999. Altered states: effects of diagenesis on fossil tooth chemistry. Geochim. Cosmochim. Acta 63, 2737–2747.

Kolodny, Y., Luz, B., 1991. Oxygen isotopes in phosphates of fossil fish — Devonian to recent. In: Taylor, H.P., O'Neil, J.R., Kaplan, I.R. (Eds.), Stable Isotope Geochemistry: A Tribute to Samuel Epstein. The Geochemical Society Special Publication 3, pp. 105–119.

Kolodny, Y., Raab, M., 1988. Oxygen isotopes in phosphatic fish remains from Israel: paleothermometry of tropical Cretaceous and Tertiary shelf waters. Palaeogeogr. Palaeoclimatol. Palaeoecol. 64, 59–67.

Kolodny, Y., Luz, B., Navon, O., 1983. Oxygen isotope variations in phosphate of biogenic apatites, I. Fish bone apatite—rechecking the rules of the game. Earth Planet. Sci. Lett. 64, 398–404.

Kolodny, Y., Luz, B., Sander, M., Clemens, W.A., 1996. Dinosaur bones: fossils or pseudomorphs? The pitfalls of physiology reconstruction from apatitic fossils. Palaeogeogr. Palaeoclimatol. Palaeoecol. 126, 161–171.

Korte, C., Jones, P.J., Brand, U., Mertmann, D., Veizer, J., 2008. Oxygen isotope values from high-latitudes: clues for Permian sea-surface temperature gradients and Late Palaeozoic deglaciation. Palaeogeogr. Palaeoclimatol. Palaeoecol. 269, 1–16.

LaPorte, D., Holmden, C., Patterson, W., Prokopiuk, T., Eglington, B., 2009. Oxygen isotope analysis of phosphate: improved precision using TC/EA CF-IRMS. J. Mass Spectrom. 44, 879–890.

Lécuyer, C., Grandjean, P., O'Neil, J.R., Cappetta, H., Martineau, F., 1993. Thermal excursions in the ocean at the Cretaceous–Tertiary boundary (northern Morocco): $\delta^{18}O$ record of phosphatic fish debris. Palaeogeogr. Palaeoclimatol. Palaeoecol. 105, 235–243.

Lécuyer, C., Amiot, R., Touzeau, A., Trotter, J., 2013. Calibration of the phosphate $\delta^{18}O$ thermometer with carbonate - water oxygen isotope fractionation equations. Chem. Geol. 347, 217–226.

LeGeros, R.Z., LeGeros, J.P., 1984. Phosphate minerals in human tissue. In: Nriagu, J.O., Moore, P.B. (Eds.), Phosphate Minerals. Springer-Verlag, New York, pp. 351–395.

Li, J., Yang, J., Li, J., Chen, L., Liang, K., Wu, W., Chen, X., Li, J., 2013. Bioinspired intrafibrillar mineralization of human dentine by PAMAM dendrimer. Biomaterials 34, 6738–6747.

Lindström, M., 1964. Conodonts. Elsevier Publishing Company, Amsterdam.

Lindström, M., Racheboeuf, P., Henry, J., 1974. Ordovician conodonts from the Postolonnec Formation (Crozon Peninsula, Massif Armoricain) and their stratigraphic significance. Geol. Palaeontol. 8, 15–28.

Luz, B., Kolodny, Y., Kovach, J., 1984. Oxygen isotope variations in phosphate of biogenic apatites, III. Conodonts. Earth Planet. Sci. Lett. 69, 255–262.

Martill, D.M., 1988. Preservation of fish in the Cretaceous Santana Formation of Brazil. Palaeontology 31, 1–18.

Mii, H., Grossman, E.L., Yancey, T.E., 1997. Stable carbon and oxygen isotope shifts in Permian seas of west Spitsbergen-global change or diagenetic artifact? Geology 25, 227–230.

Mii, H., Grossman, E.L., Yancey, T.E., 1999. Carboniferous isotope stratigraphies of North America: implications for Carboniferous paleoceanography and Mississippian glaciation. Geol. Soc. Am. Bull. 111, 960–973.

Moss, S.A., 1967. Tooth replacement in the Lemon Shark, *Negaprion brevirostis*. In: Gilbert, P.W., Mathewson, R.F, Rall, D.P. (Eds.), Sharks, Skates and Rays. Johns Hopkins University Press, Baltimore, pp. 319–330.

Nelson, B.K., DeNiro, M.J., Schoeninger, M.J., De Paolo, D.J., Hare, P.E., 1986. Effects of diagenesis on strontium, carbon, nitrogen and oxygen concentration and isotopic composition of bone. Geochim. Cosmochim. Acta 50, 1941–1949.

Nemliher, J., Kallaste, T., 2012. Conodont bioapatite resembles vertebrate enamel by XRD properties. Est. J. Earth Sci. 61, 191–192.

Nicoll, R.S., Druce, E.C., 1979. Conodonts From the Fairfield Group, Canning Basin, Western Australia. Australian Government Publishing Service.

Nöth, S., 1998. Conodont color (CAI) versus microcrystalline and textural changes in Upper Triassic conodonts from northwest Germany. Facies 38, 165–173.

O'Neil, J.R., Roe, L.J., Reinhard, E., Blake, R., 1994. A rapid and precise method of oxygen isotope analysis of biogenic phosphate. Isr. J. Earth Sci. 43, 203–212.

Ørvig, T., 1978. Microstructure and growth of the dermal skeleton in fossil actinopterygian fishes: *Boreosomus*, *Plegmolepis* and *Gyrolepis*. Zool. Scr. 7, 125–144.

Passey, B.H., Cerling, T.E., 2006. In situ stable isotope analysis ($\delta^{13}C$, $\delta^{18}O$) of very small teeth using laser ablation GC/IRMS. Chem. Geol. 235, 238–249.

Pasteris, J.D., Wopenka, B., Valsami-Jones, E., 2008. Bone and tooth mineralization: why apatite? Elements 4, 97–104.

Paul, D., Skrzypek, G., Fórizs, I., 2007. Normalization of measured stable isotopic compositions to isotope reference scales – a review. Rapid Commun. Mass Spectrom. 21, 3006–3014.

Pietzner, H., Vahl, J., Werner, H., Ziegler, W., 1968. Zur chemischen zusammensetzung und mikromorphologie der conodonten. Palaeontogr. Abt. A 128, 115–152.

Playford, P.E., Hocking, R.M., Cockbain, A.E., 2009. Devonian reef complexes of the Canning Basin, WA. Bull. Geol. Surv. W. Aust. 145, 1–444.

Playton, T., Montgomery, P., Tohver, E., Hillbun, K., Katz, D., Haines, P., Trinajstic, K., Yan, M., Hansma, J., Pisarevsky, S., 2013. Development of a regional stratigraphic framework for Upper Devonian reef complexes using integrated chronostratigraphy: Lennard Shelf, Canning Basin, Western Australia, the Sedimentary Basins of Western Australia IV. Proceedings of the Petroleum Exploration Society of Australia Symposium, Perth, Western Australia.

Popp, B.N., Anderson, T.F., Sandberg, P.A., 1986. Brachiopods as indicators of original isotopic compositions in some Paleozoic limestones. Geol. Soc. Am. Bull. 97, 1262–1269.

Pucéat, E., Lécuyer, C., Sheppard, S.M., Dromart, G., Reboulet, S., Grandjean, P., 2003. Thermal evolution of Cretaceous Tethyan marine waters inferred from oxygen isotope composition of fish tooth enamels. Paleoceanography 18, 1–13.

Pucéat, E., Joachimski, M.M., Bouilloux, A., Monna, F., Bonin, A., Motreuil, S., Morinière, P., Hénard, S., Mourin, J., Dera, G., 2010. Revised phosphate - water fractionation equation reassessing paleotemperatures derived from biogenic apatite. Earth Planet. Sci. Lett. 298, 135–142.

Purnell, M.A., Donoghue, P.C., Aldridge, R.J., 2000. Orientation and anatomical notation in conodonts. J. Inf. 74, 113–122.

Qu, Q., Zhu, M., Wang, W., 2013. Scales and dermal skeletal histology of an early bony fish *Psarolepis romeri* and their bearing on the evolution of rhombic scales and hard tissues. PLoS One 8 (doi: e61485).

Quinton, P.C., MacLeod, K.G., 2014. Oxygen isotopes from conodont apatite of the midcontinent, US: implications for Late Ordovician climate evolution. Palaeogeogr. Palaeoclimatol. Palaeoecol. 404, 57–66.

Raoult, V., Peddemors, V.M., Zahra, D., Howell, N., Howard, D.L., de Jonge, M.D., Williamson, J.E., 2016. Strontium mineralization of shark vertebrae. Sci. Rep. 6.

Reif, W.E., 1985. Squamation and ecology of sharks. Cour. Forschungsinst. Senck. 78, 12–55.

Richter, M., Smith, M., 1995. A microstructural study of the ganoine tissue of selected lower vertebrates. Zool. J. Linnean Soc. 114, 173–212.

Rigo, M., Trotter, J.A., Preto, N., Williams, I.S., 2012. Oxygen isotopic evidence for Late Triassic monsoonal upwelling in the northwestern Tethys. Geology 40, 515–518.

Ripa, L., Gwinnett, A., Guzman, C., Legler, D., 1972. Microstructural and microradiographic qualities of lemon shark enameloid. Arch. Oral Biol. 17, 118–165.

Roelofs, B., Playton, T., Barham, M., Trinajstic, K., 2015. Upper Devonian microvertebrates from the Canning Basin, Western Australia. Acta Geol. Pol. 65, 69–101.

Roelofs, B., Barham, M., Mory, A., Trinajstic, K., 2016. Late Devonian and Early Carboniferous chondrichthyans from the Fairfield Group, Canning Basin, Western Australia. Palaeontol. Electron. 19, 1–28.

Rollion-Bard, C., Saulnier, S., Vigier, N., Schumacher, A., Chaussidon, M., Lécuyer, C., 2016. Variability in magnesium, carbon and oxygen isotope compositions of brachiopod shells: implications for paleoceanographic studies. Chem. Geol. 423, 49–60.

Sasagawa, I., Yokosuka, H., Ishiyama, M., Mikami, M., Shimokawa, H., Uchida, T., 2012. Fine structural and immunohistochemical detection of collar enamel in the teeth of *Polypterus senegalus*, an actinopterygian fish. Cell Tissue Res. 347, 369–381.

Please cite this article as: Roelofs, B., et al., Assessing the fidelity of marine vertebrate microfossil δ18O signatures and their potential for palaeoecological and -climat..., Palaeogeogr. Palaeoclimatol. Palaeoecol. (2016), http://dx.doi.org/10.1016/j.palaeo.2016.10.018

Scharer, R.M., Patterson III, W.F., Carlson, J.K., Poulakis, G.R., 2012. Age and growth of endangered smalltooth sawfish (*Pristis pectinata*) verified with LA-ICP-MS analysis of vertebrae. PLoS One 7, e47850.

Schobben, M., Stebbins, A., Ghaderi, A., Strauss, H., Korn, D., Korte, C., 2015. Flourishing ocean drives the end-Permian marine mass extinction. Proc. Natl. Acad. Sci. 112, 10298–10303.

Sharp, Z.D., Atudorei, V., Furrer, H., 2000. The effect of diagenesis on oxygen isotope ratios of biogenic phosphates. Am. J. Sci. 300, 222–237.

Shemesh, A., Kolodny, Y., Luz, B., 1988. Isotope geochemistry of oxygen and carbon in phosphate and carbonate of phosphorite francolite. Geochim. Cosmochim. Acta 52, 2565–2572.

Stack, M.V., 1955. The chemical nature of the organic matrix of bone, dentin, and enamel. Ann. N. Y. Acad. Sci. 60, 585–595.

Stephens, N.P., Sumner, D.Y., 2003. Famennian microbial reef facies, Napier and Oscar Ranges, Canning Basin, western Australia. Sedimentology 50, 1283–1302.

Sun, Y., Joachimski, M.M., Wignall, P.B., Yan, C., Chen, Y., Jiang, H., Wang, L., Lai, X., 2012. Lethally hot temperatures during the Early Triassic greenhouse. Science 338, 366–370.

Sun, Y., Wiedenbeck, M., Joachimski, M.M., Beier, C., Kemner, F., Weinzierl, C., 2016. Chemical and oxygen isotope composition of gem-quality apatites: implications for oxygen isotope reference materials for secondary ion mass spectrometry (SIMS). Chem. Geol. 440, 164–178.

Talent, J.A., Mawson, R., Andrew, A.S., Hamilton, P.J., Whitford, D.J., 1993. Middle Palaeozoic extinction events: faunal and isotopic data. Palaeogeogr. Palaeoclimatol. Palaeoecol. 104, 139–152.

Thomas, G., 1957. Lower Carboniferous deposits in the Fitzroy Basin, Western Australia. Aust. J. Sci. 19, 160–161.

Thomas, G., 1959. The Lower Carboniferous Laurel Formation of the Fitzroy Basin. Bureau of Mineral Resources Australia Report. 38, pp. 21–36.

Thorrold, S.R., Campana, S.E., Jones, C.M., Swart, P.K., 1997. Factors determining $\delta^{13}C$ and $\delta^{18}O$ fractionation in aragonitic otoliths of marine fish. Geochim. Cosmochim. Acta 61, 2909–2919.

Thorson, T.B., 1971. Movement of bull sharks, *Carcharhinus leucas*, between Caribbean Sea and Lake Nicaragua demonstrated by tagging. Copeia 336–338.

Trinajstic, K., George, A.D., 2009. Microvertebrate biostratigraphy of Upper Devonian (Frasnian) carbonate rocks in Canning and Carnarvon Basins of Western Australia. Palaeontology 52, 641–659.

Trinajstic, K., Roelofs, B., Burrow, C., Long, J., Turner, S., 2014. Devonian vertebrates from the Canning and Carnarvon basins with an overview of Paleozoic vertebrates of Western Australia. J. R. Soc. West. Aust. 97, 133–151.

Trotter, J.A., Fitzgerald, J.D., Kokkonen, H., Barnes, C.R., 2007. New insights into the ultrastructure, permeability, and integrity of conodont apatite determined by transmission electron microscopy. Lethaia 40, 97–110.

Trotter, J.A., Williams, I.S., Barnes, C.R., Lécuyer, C., Nicoll, R.S., 2008. Did cooling oceans trigger Ordovician biodiversification? Evidence from conodont thermometry. Science 321, 550–554.

Trotter, J.A., Williams, I.S., Nicora, A., Mazza, M., Rigo, M., 2015. Long-term cycles of Triassic climate change: a new $\delta^{18}O$ record from conodont apatite. Earth Planet. Sci. Lett. 415, 165–174.

Trueman, C., Benton, M.J., Palmer, M., 2003. Geochemical taphonomy of shallow marine vertebrate assemblages. Palaeogeogr. Palaeoclimatol. Palaeoecol. 197, 151–169.

Turner, S., 1982. Middle Palaeozoic elasmobranch remains from Australia. J. Vertebr. Paleontol. 2, 117–131.

Van Geldern, R., Joachimski, M., Day, J., Jansen, U., Alvarez, F., Yolkin, E., Ma, X.P., 2006. Carbon, oxygen and strontium isotope records of Devonian brachiopod shell calcite. Palaeogeogr. Palaeoclimatol. Palaeoecol. 240, 47–67.

Veizer, J., Fritz, P., Jones, B., 1986. Geochemistry of brachiopods: oxygen and carbon isotopic records of Paleozoic oceans. Geochim. Cosmochim. Acta 50, 1679–1696.

Veizer, J., Bruckschen, P., Pawellek, F., Diener, A., Podlaha, O.G., Jasper, T., Korte, C., Carden, G.A.F., Strauss, H., Azmy, K., Ala, D., 1997. Oxygen isotope evolution of Phanerozoic seawater. Paleogeogr. Paleoclimatol. Paleoecol. 132, 159–172.

Veizer, J., Ala, D., Azmy, K., Bruckschen, P., Buhl, D., Bruhn, F., Carden, G.A., Diener, A., Ebneth, S., Godderis, Y., 1999. $^{87}Sr/^{86}Sr$, $\delta^{13}C$ and $\delta^{18}O$ evolution of Phanerozoic seawater. Chem. Geol. 161, 59–88.

Vennemann, T., Hegner, E., Cliff, G., Benz, G., 2001. Isotopic composition of recent shark teeth as a proxy for environmental conditions. Geochim. Cosmochim. Acta 65, 1583–1599.

Vennemann, T.W., Fricke, H.C., Blake, R.E., O'Neil, J.R., Colman, A., 2002. Oxygen isotope analysis of phosphates: a comparison of techniques for analysis of Ag_3PO_4. Chem. Geol. 185, 321–336.

Wadleigh, M.A., Veizer, J., 1992. $^{18}O/^{16}O$ and $^{13}C/^{12}C$ in lower Paleozoic articulate brachiopods: implications for the isotopic composition of seawater. Geochim. Cosmochim. Acta 56, 431–443.

Wallace, Z.A., Elrick, M., 2014. Early Mississippian orbital-scale glacio-eustasy detected from high-resolution oxygen isotopes of marine apatite (conodonts). J. Sediment. Res. 84, 816–824.

Wang, Y., Cerling, T.E., 1994. A model of fossil tooth and bone diagenesis—implications for paleodiet reconstruction from stable isotopes. Palaeogeogr. Palaeoclimatol. Palaeoecol. 107, 281–289.

Wenzel, B., Lécuyer, C., Joachimski, M.M., 2000. Comparing oxygen isotope records of Silurian calcite and phosphate $\delta^{18}O$ compositions of brachiopods and conodonts. Geochim. Cosmochim. Acta 64, 1859–1872.

Wheeley, J.R., Smith, M.P., Boomer, I., 2012. Oxygen isotope variability in conodonts: implications for reconstructing Palaeozoic palaeoclimates and palaeoceanography. J. Geol. Soc. 169, 239–250.

Williams, M.E., 2001. Tooth retention in cladodont sharks: with a comparison between primitive grasping and swallowing, and modern cutting and gouging feeding mechanisms. J. Vertebr. Paleontol. 21, 214–226.

Wright, E.K., Hoering, T.C., 1989. Separation and purification of phosphates for oxygen isotope analysis. Annual Report of the Director, Geophysical Laboratory, Carnegie Institute. 2150, pp. 137–141.

Yamamoto, K., Asami, R., Iryu, Y., 2011. Brachiopod taxa and shell portions reliably recording past ocean environments: toward establishing a robust paleoceanographic proxy. Geophys. Res. Lett. 38. http://dx.doi.org/10.1029/2011GL047134.

Zazzo, A., Lécuyer, C., Mariotti, A., 2004. Experimentally-controlled carbon and oxygen isotope exchange between bioapatites and water under inorganic and microbially-mediated conditions. Geochim. Cosmochim. Acta 68, 1–12.

Žigaitė, Ž., Whitehouse, M., 2014. Stable oxygen isotopes of dental biomineral: differentiation at the intra-and inter-tissue level of modern shark teeth. GFF 136, 337–340.

Žigaite, Ž, Joachimski, M.M., Lehnert, O., Brazauskas, A., 2010. d18O composition of conodont apatite indicates climatic cooling during the Middle Pridoli. Palaeogeogr. Palaeoclimatol. Palaeoecol. 294, 242–247.

Žigaitė, Ž., Fadel, A., Blom, H., Perez-Huerta, A., Jeffries, T., Märss, T., Ahlberg, P.E., 2015. Rare earth elements (REEs) in vertebrate microremains from the upper Pridoli Ohesaare beds of Saaremaa Island, Estonia: geochemical clues to palaeoenvironment. Est. J. Earth Sci. 64, 115–120.

Please cite this article as: Roelofs, B., et al., Assessing the fidelity of marine vertebrate microfossil δ18O signatures and their potential for palaeoecological and -climat..., Palaeogeogr. Palaeoclimatol. Palaeoecol. (2016), http://dx.doi.org/10.1016/j.palaeo.2016.10.018

Appendix 2

Hansma, J., Tohver E., Yan, M., Trinajstic, K., **Roelofs, B**., Peek, S., Slotznick, S.P., Kirschvink, J., Playton, P. Haines, P. and Hocking, R. 2014. Late Devonian carbonate magnetostratigraphy from the Oscar and Horse Spring Ranges, Lennard Shelf, Canning Basin, Western Australia. Earth and Planetary Science Letters 409, 232-242.

Earth and Planetary Science Letters 409 (2015) 232–242

Contents lists available at ScienceDirect

Earth and Planetary Science Letters

www.elsevier.com/locate/epsl

Late Devonian carbonate magnetostratigraphy from the Oscar and Horse Spring Ranges, Lennard Shelf, Canning Basin, Western Australia

Jeroen Hansma [a,*], Eric Tohver [a], Maodu Yan [b], Kate Trinajstic [c], Brett Roelofs [c], Sarah Peek [d], Sarah P. Slotznick [d], Joseph Kirschvink [d], Ted Playton [e], Peter Haines [f], Roger Hocking [f]

[a] School of Earth and Environment, The University of Western Australia, 35 Stirling Highway, Crawley, Perth, Western Australia 6009, Australia
[b] Key Laboratory of Continental Collision and Plateau Uplift, Institute of Tibetan Plateau Research, CAS Center for Excellence in Tibetan Plateau Earth Sciences, Building 3, Courtyard 16, Lin Cui Road, Chaoyang District, Beijing 100101, China
[c] Department of Chemistry, Curtin University, GPO Box U1987, Perth, Western Australia 6845, Australia
[d] Division of Geological and Planetary Sciences, California Institute of Technology, MC 170-25 1200 E. California Blvd., Pasadena, CA 91125, USA
[e] Chevron Energy Technology Company, Carbonate Stratigraphy Research & Development, 1500 Louisiana St., Rm 27134, Houston, TX 77002, USA
[f] Geological Survey of Western Australia, Mineral House, 100 Plain Street, East Perth, Western Australia, 6004, Australia

ARTICLE INFO

Article history:
Received 27 November 2012
Received in revised form 27 October 2014
Accepted 31 October 2014
Available online 20 November 2014
Editor: C. Sotin

Keywords:
Devonian
magnetostratigraphy
biostratigraphy
Canning Basin
Lennard Shelf

ABSTRACT

The Late Devonian was a time of major evolutionary change encompassing the fifth largest mass extinction, the Frasnian–Famennian event. In order to establish a chronological framework for global correlation before, during, and following the Frasnian–Famennian mass extinction, we carried out a coupled magnetostratigraphic and biostratigraphic study of two stratigraphic sections in the Upper Devonian carbonate reef complexes of the Lennard Shelf, in the Canning Basin, Western Australia. Magnetostratigraphy from these rocks provides the first high-resolution definition of the Late Devonian magnetic polarity timescale. A 581-m-reference section and an 82-m overlapping section through the marginal slope facies (Napier Formation) of the Oscar Range as well as a 117-m section at Horse Spring (Virgin Hills Formation) were sampled at decimeter to meter scale for magnetostratigraphy. Conodont biostratigraphy was used to correlate both sections, and link magnetostratigraphic polarity zones to a globally established biostratigraphy. A stable, Characteristic Remanent Magnetization (ChRM) with dual polarities (NE, shallowly upward and SW, shallowly downward) is recovered from ~60% of all samples, with magnetite inferred to be the chief magnetic carrier from thermal demagnetization characteristics. These directions define a geomagnetic pole at 49.5°S/285.8°E and $\alpha_{95} = 2.4$ ($n = 501$), placing the Canning Basin at 9.9°S during the Late Devonian, consistent with carbonate reef development at this time. A conservative interpretation of the magnetostratigraphy shows the recovery of multiple reversals from both sections, not including possible cryptochrons and short duration magnetozones. Field tests for primary remanence include positive reversal tests and matching magnetozones from an overlapping section in the Oscar Range. A strong correlation was found between magnetic polarity stratigraphies of the Oscar Range and Horse Spring sections, and we correlate 12 magnetostratigraphic packages. The relative stratigraphic thicknesses of the isochronous sediments from these two sections indicate that carbonate accumulation was ~4.5× faster in the middle slope deposits at Oscar Range than in the more distal, lower slope Horse Spring deposits for the middle Frasnian through Famennian. The magnetic field during the Late Devonian underwent a relatively high reversal frequency with good potential for regional and global correlation, and should prove useful in deciphering a high-resolution chronostratigraphy across the Lennard Shelf to enable higher confidence examination of reef development across a major biotic crisis.

* Corresponding author.
E-mail address: jeroen.hansma@geo.uio.no (J. Hansma).

http://dx.doi.org/10.1016/j.epsl.2014.10.054
0012-821X/

1. Introduction

In the most recent major compilation of the Geological Time Scale by Gradstein et al. (2012) the magnetic stratigraphy of Late Devonian time is largely unknown, and is regarded as a 'mixed' polarity interval. This is based on dual polarity magnetizations reported for the carbonate reef complexes of the Canning Basin, Western Australia (Hurley and Van der Voo, 1987, 1990; Chen et al., 1995). The sampling scheme for these studies was site based, intended to establish primary paleomagnetic poles for Late Devonian paleogeography, so the history of geomagnetic reversals from these rocks remains unexplored. It is the purpose of this work to examine in greater detail the pattern of geomagnetic reversals during the Frasnian and Famennian, and test correlation between different sections within the Lennard Shelf using biostratigraphy coupled with magnetostratigraphy. In contrast to Late Devonian magnetostratigraphy, the biostratigraphy is well constrained within the basin and fore reef complexes, with refined conodont and ammonoid zonations that relate well to the global Late Devonian zonations (Klapper, 1989, 1997, 2007). Microvertebrate (Trinajstic and George, 2009), palynomorph (Playford, 1976, 2009) and coral (Brownlaw, 2000) biostratigraphic frameworks are also developed for this time. The well-constrained stratigraphic ranges for Devonian conodont taxa within the Canning Basin make them extremely useful for correlation and provide a suitable control for testing the utility of the magnetozones in this study.

Chronostratigraphy during the Late Devonian is of particular significance as this time period includes the Frasnian–Famennian boundary. The mass extinction that occurred at this time is among the 'big 5' mass extinctions in the geological record (Raup and Sepkoski, 1982). Isotope geochronology is one way to assess rock ages during this time but this is dependent on the occurrence of suitable minerals (e.g., zircon from volcanic ashbeds) and active volcanism. Biostratigraphic techniques are also limited by the presence of suitable index fossils and are inadequate when fossils are provincial, facies-dependent, or the sample size is limited (such as from core). Magnetostratigraphy provides another approach to establishing a robust and accurate chronostratigraphic framework for the Late Devonian, and when coupled with biostratigraphy can be used to correlate time during the Late Devonian.

1.1. Geology

In the Late Devonian, Australia formed the northeastern portion of Gondwana and occupied low, southerly latitudes (Hurley and Van der Voo, 1987). A carbonate reef complex developed on the Lennard Shelf of the Canning Basin, located on the (present-day) SW margin of the Paleoproterozoic Kimberley basement block (Fig. 1). The rugose coastline of the Kimberley block led to differential development of reefal carbonate platforms with variable depositional and oceanographic settings. For example, the Oscar Range locality represents an isolated platform that formed on an island of Precambrian metasedimentary basement, detached from the main shoreline. Here, Frasnian carbonate facies abut the metamorphic basement and Frasnian–Famennian marginal-slope facies extend around the edges of the platform. Conversely, the Horse Spring locality represents a relatively sheltered mini-basin within a large embayment along a broad land-attached shelf (Hurley and Lohmann, 1989; Playford et al., 2009).

The Devonian record of reef growth throughout the Canning Basin demonstrates a pattern of backstepping throughout most of the Frasnian, as a result of rising relative sea level. During this time, dominant reef builders were stromatoporoids, corals, and microbes (Playford et al., 2009). Starting in the Late Frasnian through Famennian, a period of stable sea level is recorded by reef progradation (Hurley and Lohmann, 1989; Playford et al., 2009).

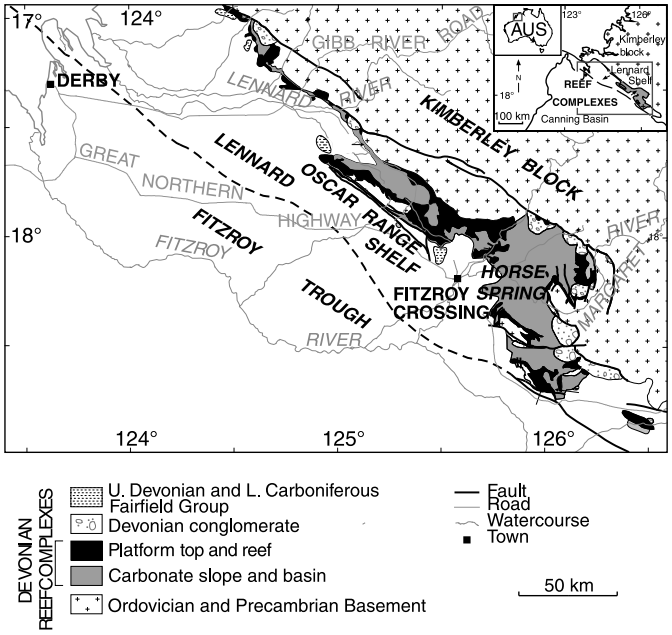

Fig. 1. Simplified geological map of the Lennard Shelf, showing sample sites. (Playford and Hocking, 2009; Playford et al., 2009.)

The extinction of stromatoporoids and corals precedes a period of microbe-dominated reef growth until the cessation of growth by the late Famennian (Playford et al., 2009), when the carbonate system transformed into an open marine, mud-rich shelf reflected in the Carboniferous Fairfield Group. Some localized deposits of Mississippi Valley Type Pb–Zn deposits formed during the Carboniferous (Brannon et al., 1996; Christensen et al., 1996; Symons and Arne, 2003, 2005), reflecting the passage of chemically active fluids at this time (Playford and Wallace, 2001). Later, during the Permo-Carboniferous glaciation, Devonian–Carboniferous carbonates were regionally planed by ice sheets, resulting in significant removal of the Fairfield Group and a regional unconformity with underlying Devonian reefal limestones and overlying Permian Grant Group glacial sandstones and diamictites (Playford et al., 2009).

The study was conducted in two areas with continuous exposures of stratigraphy. Both Horse Spring and Oscar Range have very well-exposed Frasnian to Famennian slope successions. These areas are ideal for magnetostratigraphic sampling because they do not contain significant unconformities. The deep-water environment of the Horse Spring section was also submerged continuously throughout the transgressive–regressive oscillations of the late Devonian, and deposition there was likely to be continuous.

The 20–30° dipping, middle slope facies of the Oscar Range transect (Napier Formation) are dominated by platform-top-derived grainstones and reefal margin-derived bioclastic float-rudstones to megabreccia blocks. Grainstones exhibit a range of compositions reflecting material shedding from shallow environments, from non-skeletal-dominated (commonly peloids, coated grains, and ooids) to skeletal-rich (commonly brachiopods, crinoids and *Renalcis* fragments), and are often normally graded. Bioclastic floatstones–rudstones are common in the Frasnian succession and are enriched in fragmented stromatoporoid and coral debris, reflecting mechanical reworking of skeletal communities at the margin and subsequent downslope transport. Megabreccia deposits with meter-scale boulders and multi-meter isolated blocks of microbial boundstone occur along discrete horizons or as thick complexes on the slope, and are generated through brittle gravitational failure of an early-lithified, encrusted margin and uppermost slope (Playton, 2008). Local microbially encrusted patches and *in situ* mat-like to domal stromatolitic boundstones are volumetrically minor but represent

periods of lesser slope accumulation rates, as described by George (1999) for this and other localities.

Deposits of the Horse Spring section (Virgin Hills Formation) dip at 10–20° and are indicative of a more-distal, lower slope setting when compared to those of the Oscar Range section. Similar grainstones and debris deposits (megabreccias and blocks) are present in lesser proportions, and bioclastic float-rudstones are rare. Mixed siliciclastic-carbonate silt and silty peloid-skeletal wackestone to packstone beds comprise a substantial percentage of the deposits, likely reflecting greater transport distance, a greater contribution of suspended material background deposition, and slower depositional rates than at Oscar Range. More abundant intraclastic breccias are also observed, where previously deposited silty to grainy beds higher on the slope were reworked as clasts and deposited in this setting.

Horizontal sediment in geopetal structures, for instance stromotactis in cavities of sponge fossils, indicates that formation dips reflect primary depositional dips. These have been previously documented at other localities (Playford et al., 2009), and were observed within the studied sections.

2. Methodology

Middle Frasnian through Famennian marginal slope stratigraphic successions of the Oscar Range are very well exposed, and the Horse Spring transect is the type section for conodont biostratigraphy across the Lennard Shelf (Klapper, 2007). For these reasons we chose these sections for outcrop sampling. Palaeomagnetic samples were collected using a handheld, gasoline Pomeroy drill. One-inch diameter, ten-centimeter long core samples were collected at 0.5–1 m intervals through 581 m of marginal slope stratigraphy at Oscar Range until the contact with the overlying Fairfield Group was encountered (754 samples). The base of the Oscar Range section is located at 17°54′52.98″S, 125°17′58.98″E and top of section is 17°55′26.18″S, 125°17′21.98″E. Sampling at Horse Spring was done at decimetre to sub-meter intervals over a 117 m thick section (295 samples). The Horse Spring section is located between 18°11′43.91″S, 126°1′54.88″E and 18°11′40.06″S, 126°1′59.66″E. An overlapping 82 m section in the Oscar Range was sampled to demonstrate internal consistency of magnetization (82 samples). The parallel section at the Oscar Range site overlaps with the highest (and youngest) part of the primary stratigraphic section, and two beds were walked out as stratigraphic tie points between the sections. Lateral migration of the sample section by compass projection, and targeting of matrix sediment within breccias avoided sampling of rotated reef blocks. Large hand samples were taken at regular spacing and around critical stratigraphic intervals in conjunction with core sampling to provide conodont- and fish-based biostratigraphic control to constrain the magnetostratigraphy. Biostratigraphic samples were sent to Macquarie University, Sydney, for acid digestion, and the resulting residues separated into light and heavy fractions using heavy liquid separation (polytungstenate). The heavy and light fractions were picked for conodont elements and microvertebrates. The 15-fold conodont zonation (Girard et al., 2006), modified from the original 13-fold zonation of the Montagne Noire succession (Klapper, 1989) and subsequently replicated in the Canning Basin (Klapper, 1997, 2007), is used as it presents higher resolution than the standard 9-fold zonation of Ziegler and Sandberg (1990) for the areas studied. For the Famennian the standard zonations (Ziegler and Sandberg, 1990) are utilized.

Paleomagnetic cores were cut into 10 cm^3 specimens and Oscar Range samples were thermally demagnetized using a Magnetic Measurements thermal oven and measured on a 2G cryogenic magnetometer at the University of Western Australia. Samples from Horse Spring were measured on a 2G cryogenic magnetometer at California Institute of Technology, and were treated by low temperature cycling, followed by mixed alternating field and thermal demagnetization using the Rock and Paleomagnetic Instrument Development (RAPID) system protocol (Kirschvink et al., 2008). Magnetic directions were determined by principal component analysis (Kirschvink, 1980) or by using the arc method of McFadden and McElhinny (1988) with the aid of PalaeoMag software (Jones, 2002).

Magnetic stratigraphies were defined by plotting directions as an angle from the mean virtual geomagnetic pole (VGP) of the entire dataset, with the mean VGP normalized to 0° for normal polarity samples and 180° for reversed polarity samples. Where the characteristic remanent direction from a single sample crosses the magnetic equator, defined as 90° along a great circle from the mean direction, we infer that a reversal of magnetic polarity is recorded. Two or more stratigraphically adjacent samples of the same polarity define a magnetozone, whereas zones indicated by only one sample are interpreted as ambiguous.

3. Results

3.1. Directional analysis

Natural remanent magnetic intensity for samples with stable magnetic directions varied from 10^{-4} to 10^{-6} A/m. A number of samples had NRM intensities of 10^{-7} A/m or lower but hosted no stable magnetization. 291 samples from Oscar Range and 148 from Horse Spring show a low temperature component below 200 °C blocking temperature (Fig. 2A and 2B). This is interpreted to be due to goethite present within samples and the direction of magnetization is close to the time-averaged, present-day field. We infer that this direction represents a viscous magnetic overprint of the samples acquired during the Brunhes normal field.

Above 200 °C, thermal demagnetization reveals a characteristic component trending towards the origin. The path toward the origin is of variable stability, with highly linear (low maximum angular deviation, MAD), and more erratic (high MAD) traces. Many samples became unstable after heating above 475 °C, with only a small number remaining stable above this temperature. This is likely due to a dominance of magnetite as a remanence-hosting phase, combined with the weak intensity of magnetism in both Devonian times and carbonate rocks.

From the Oscar Range collection, 654 samples yield a high temperature magnetization, with 361 primary directions passing statistical treatment described below (Fig. 2C and 2E). A total of 235 high temperature directions were recovered from Horse Spring, 140 of which are considered primary (Fig. 2D and 2F). This dual polarity component is similar to the expected Devonian directions for the Canning Basin and Gondwana APWP (Chen et al., 1995; Hurley and Van der Voo, 1987; McElhinny et al., 2003; Torsvik et al., 2008) and is considered to be primary. Fig. 3 shows eight examples of samples with characteristic reversed and normal field directions preserved. The remainder of the high temperature magnetic components (roughly two-thirds of the samples) are typically better defined by line fits with MAD values $<15°$, and can be divided into two populations, high inclination results with an N–S direction (mostly negative, northerly) that correspond to probable Permo-Carboniferous overprinting, and randomly oriented directions of uncertain origin and significance.

For both sections characteristic remanent directions were transformed into single specimen lower hemisphere VGP space (black and grey points in Fig. 2E and 2F). Although scatter is present, VGPs are concentrated in the southwestern quadrant, and are most concentrated around the expected direction for Canning Basin based upon Gondwana's APWP for Late Devonian times (Torsvik et al., 2008). While it is expected that over periods of

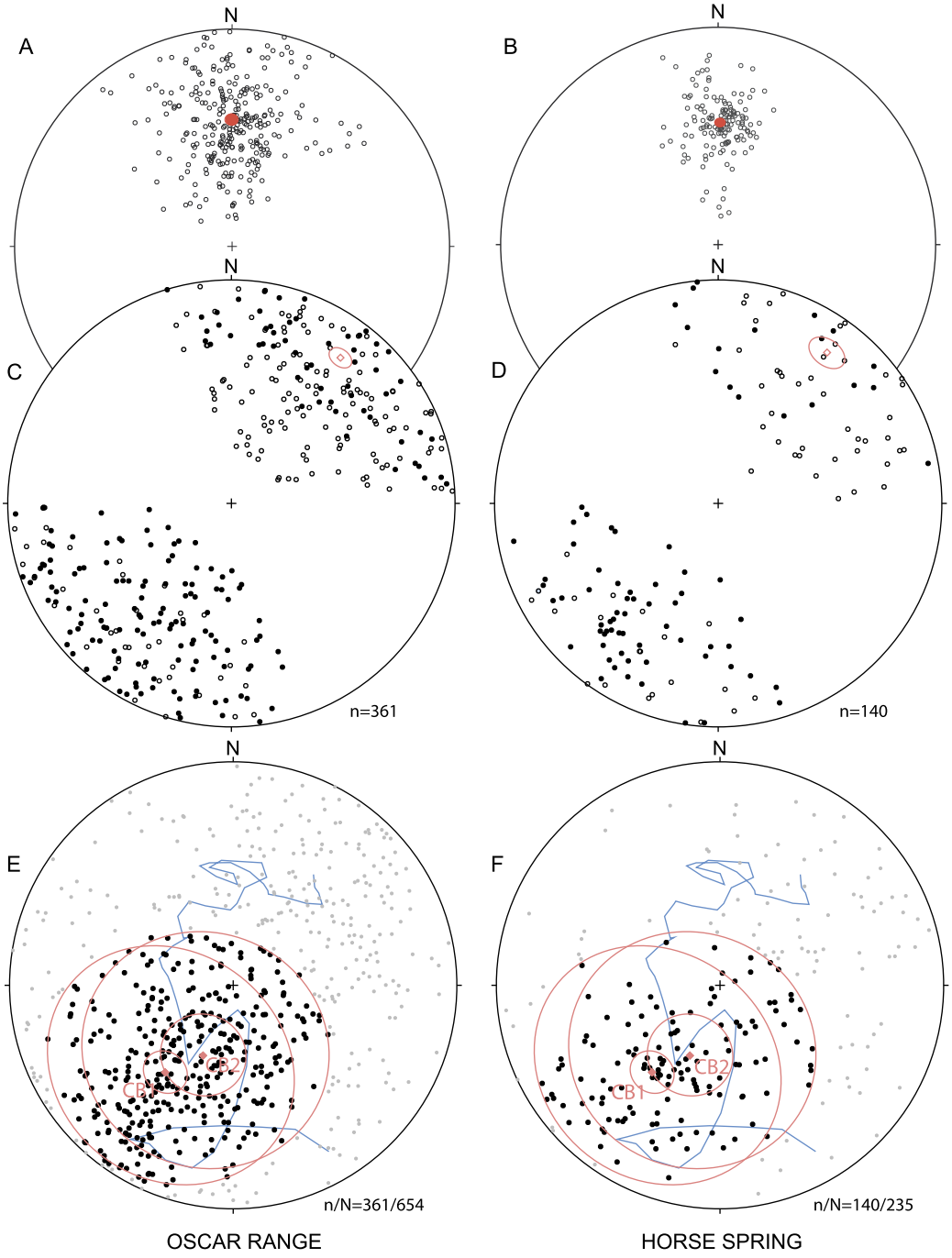

Fig. 2. Equal area stereonets of (A) low temperature overprinting components corresponding to present day field directions from Oscar Range. The red dot shows the 95% Fisher mean (Declination = 359.8, Inclination = −41.2, $k = 14.0$, $\alpha_{95} = 2.29$, $n = 291$), (B) low temperature overprinting components from Horse Spring. The red dot shows the 95% Fisher mean (Declination = 0.9, Inclination = −43.2, $k = 35.0$, $\alpha_{95} = 1.99$, $n = 148$). Devonian directions from (C) Oscar Range and (D) Horse Spring. Grey Diamonds in (C) and (D) show Fisher mean directions encircled by their 95% confidence cones. (E) Oscar Range and (F) Horse Spring characterizing directions plotted as lower hemisphere VGPs along with CB1 (Hurley and Van der Voo, 1987), CB2 (Chen et al., 1995) poles and Gondwana's APWP (blue) rotated to Australian co-ordinates (Torsvik et al., 2008). Small red ellipses indicate the α_{95} for each pole, and large red ellipses show the limit of the 45° VGP cut off. Black points indicate accepted directions and grey points indicate excluded directions. (For interpretation of the references to color in this figure legend, the reader is referred to the web version of this article.)

paleomagnetic secular variation (PSV) VGP scatter is Fisherian (Deenen et al., 2012) both datasets show a clearly elongate VGP distribution. The non-Fisherian elongation of VGPs is interpreted as the expression of APW of Australia during ~20 Ma accumulation of the reef section in the Late Devonian, superposed by PSV and directional scatter due to other effects (lightning etc.). Both earlier Canning Basin poles (CB1 and CB2) plot amongst the most concentrated region of VGPs, and we applied a 45° VGP cut off excluding directions that lie outside small circles centred upon either Canning Basin poles (black points in Fig. 2E and 2F) in order to avoid interpretation based upon suspect directions.

The Devonian directions from the Oscar Range and Horse Spring (Fig. 2C and 2D) encapsulate the mean of the other population within their 95% confidence ellipses. Magnetism from both sections pass C quality reversals tests, supporting an interpretation of a possibly primary depositional remanence (McFadden and McElhinny, 1990). Directions from the Oscar Range have a 1.48° difference between means for normal and reversed populations, and 19.22°

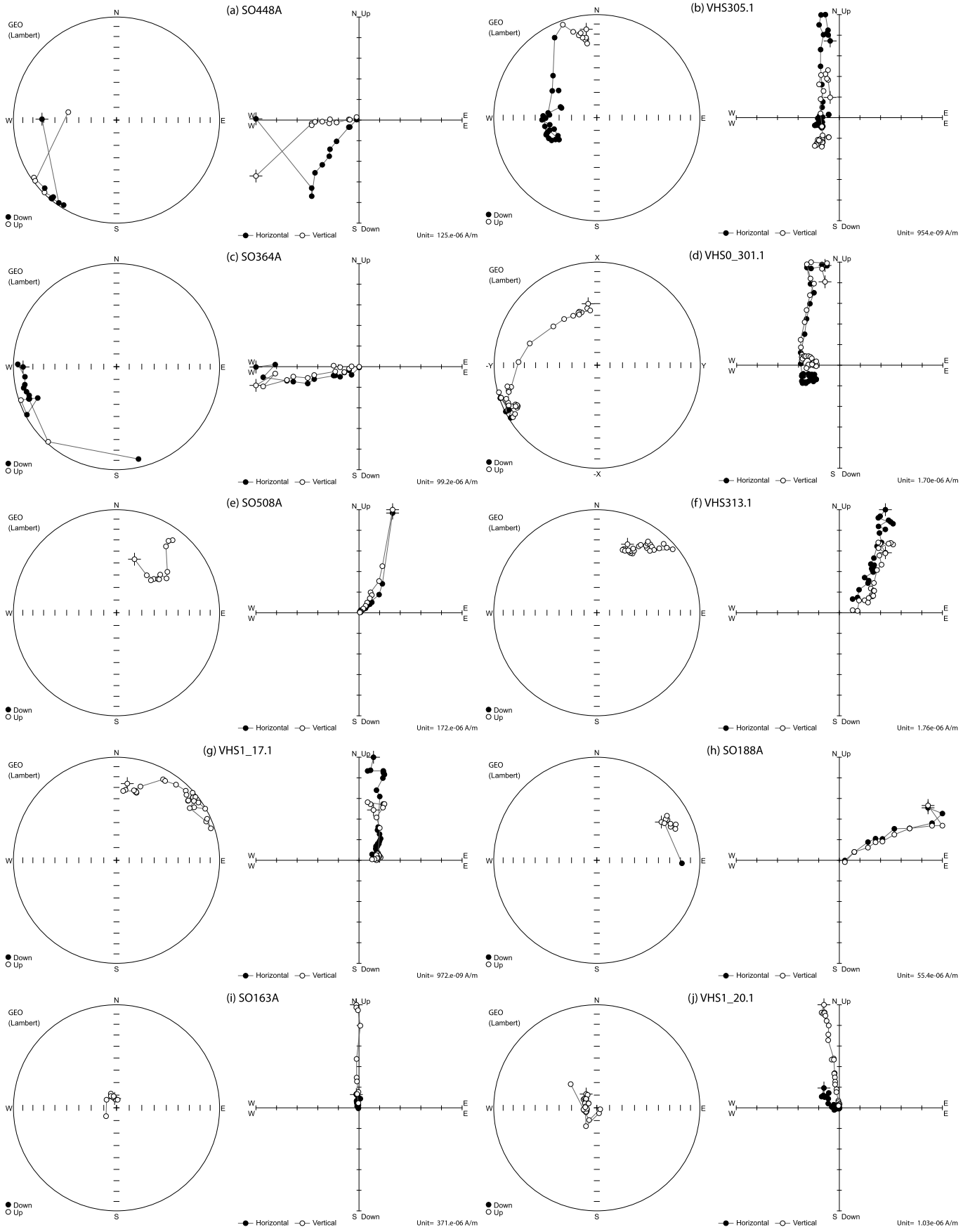

Fig. 3. Orthographic, and equal area plots of demagnetization data for (a)–(d) Late Devonian reversed directions, (e)–(h) Late Devonian normal directions, and anomalous directions (i)–(j). Filled points (lower hemisphere/declination) hollow points (upper hemisphere/inclination).

Table 1
Distribution of conodont species at Oscar Range, Napier Formation.

Stage	Frasnian												Famennian											
Zone	5-10	6-10	10	13	13b								Upper *Pa. triangularis* – Mid *Pa. crepida*				Upper *Pa. triangularis* – Upper *Pa. crepida*	Upper *Pa. crepida* – *Rhomboidea*	*Rhomboidea* - Lower *Pa. marginifera*	Upper *Pa. crepida* – Lower *Pa. marginifera*	*Marginifera*			Upper *Pa. marginifera* - *Pa. trachytera*
Sample number (m)	38.8	109.9	112.8	177.8	192.8	198.8	204.2	213.5	218.8	222.3	223.8	228.7	233.2	238.8	243.9	293.8	283.8	345	393.8	443.5	491.5	541.5	566.5	600
An. buckeyensis					X																			
An. gigas		X	X																					
I. alternatus															X									
Pa .punctata	X																							
Pa. plana			X																					
Pa. proversa			X																					
Pa. kireevae			X																					
Pa. bogartensis				X			X																	
Pa. rhenana					X																			
Pa. beckeri					X																			
Pa. boogaardi						X	X	X																
Pa. klugi					X																			
Pa. junianensis					X																			
Pa. niccolli					X			X		X														
Pa. winchelli					X			X	X	X	X													
Pa .linguiformis					X				X	X	X	X												
Pa. tenuipunctata													X											
Pa. glabra sp.													X	X										
Pa. triangularis													X	X	X									
Pa. subperlobata															X	X	X							
Pa. minuta minuta													X	X	X	X	X	X	X		X			X
Po. brevilamina															X									
Pa. glabra glabra																			X					
Pa. glabra pectinata																			X	X		X		
Pa. confluens																			X					
Sc. Velifera																					X			
Icriodus																						X		
Polygnathus sp.																						X	X	
Pa. graciis gracilis																								X

critical angle (95% confidence level). Horse Spring populations have a 1.8° difference between means and a 19.74° critical angle (95% confidence level). Using all Devonian directions defines a geomagnetic pole at 49.5°S/285.8°E with $\alpha_{95} = 2.4$ ($n = 501$). This result places the Canning Basin at 9.9°S during the Late Devonian, consistent with carbonate reef development at this time.

3.2. Biostratigraphy

3.2.1. Oscar Range (Table 1)

The lower part of the section is characterized by long ranging conodont taxa (zones 5–10). Finer resolution is achieved in the upper part of the section with conodont zone (CZ) 10 constrained at 112.8 m. In addition the jawless fish *Australolepis seddoni* with a known age range of CZ 6–10 (Trinajstic and George, 2009; Turner, 1997) occurs in this sample, further confirming this range. Both CZ 13 and 13b are identified at 177.8 m and 192.8 m respectively and appear to be particularly robust (up to 228.7 m). However, CZ 13c cannot be determined and it is the upper limit of this zonation that defines the Frasnian extinction event in the Canning Basin (Klapper, 2009). The first Famennian zone identified is at 233.2 m and is determined by the co-occurrence of *Pa. triangularis*, *Pa. superlobata* and *Pa. minuta minuta*. This indicates that Frasnian–Famennian boundary lies above the 228.7 m interval and below the 233.2 m interval of the section. The boundary is arbitrarily placed at the centrepoint between the youngest Frasnian sampling locality and oldest Famennian samples. It is of note that the stage boundary region also contains a reversal in the conservative interpretative magnetostratigraphies. A conodont assemblage (sample number 600) was collected from above the reefal section and is dated as CZ Lower *Pa. marginifera* and is determined to be part of the Fairfield Group. This sample indicates that the reefs became extinct before the end of the Famennian.

3.2.2. Horse Spring (Table 2)

The biostratigraphy of the Horse Spring section is well documented and the position of the Frasnian–Famennian boundary is consistently placed at above 35.75 m and below 35.95 m (Klapper, 2007; Playford et al., 2009; Trinajstic and George, 2009). From our sampling the boundary lies between 34.6 m and 36.65 m. The lower 2 m of the section comprises CZ 4–10, however, the condensed nature of the section meant that the first paleomagnetic hole was drilled at 1.6 m within CZ 10. Samples obtained from 2.2–6.8 m fall with CZ 11. There is then a sharp decline in conodont taxa, both in numbers and diversity through CZ 12 and then a rapid recovery and speciation through CZ 13a, which is then fol-

Table 2
Distribution of conodont species at Horse Spring, Virgin Hills Formation.

Stage	Frasnian												Famennian							
Zone	10	11	12		13a	13b				13b-c		13c	*triangularis*	*Upper triangularis*	*Upper triangularis - crepida*	*crepida - rhomboidea*			*crepida - marginifera*	
Level (m)	1.6-1.9	2.2-6.8	11.35-11.65	13	19.85-20	23.2	25.75	26.7	28-28.05	30.9	31.35	34.6	36.65	39.2	48	58.2	69.2	79.9	91	101.8
An. buckeyensis		X		X			X													
An. curvata	X				X	X														
An. gigas	X	X																		
An. idoes							X	X												
I. alternatus													X							
Pa. hassi	X	X	X																	
Pa. mulleri			X																	
Pa. feisti		X																		
Pa. kiriveeae		X					X													
Pa. bogartensis				X	X	X					X	X								
Pa. boogaardi						X	X													
Pa. winchelli					X	X	X													
Pa. klugi						X	X													
Pa. rhenana						X														
Pa. beckeri							X													
Pa. juntianensis			X				X		X											
Pa .linguiformis							X	X												
Pa. niccolli							X													
Pa .punctata	X						X													
Pa. triangularis												X	X							
Pa. perlobata															X	X	X			
Pa. subperlobata														X						
Pa. minuta minuta															X	X	X	X	X	X
Pa. delicatula platys														X						
Pa.quadrantinodosalobata																X	X			
Pa. regularis															X					
Pa. glabra pectinata																	X	X	X	X
Pa. glabra elongata																				X
Pa. gracilus gracilis																				X
Po. decorosa					X															
Po. brevilamina												X	X	X						
Ph. bifurcatus		X																		
Ph. fastigatus		X																		
Ph. Latus		X																		
Icriodus		X																		
Diademodus sp.		X																		
Pheobodus sp.		X																		
A. Seddoni		X																		
Ancryodella sp.										X										

lowed by another decrease in both diversity and numbers through CZ 13b–c. The first Famennian sample is identified at 36.65 m and dated as early to middle *Pa. triangularis* based on the presence of *Pa. triangularis* and *Polygnathus brevilamina*. The Famennian section extends into the *Pa. crepida* zone, with the uppermost samples containing long ranging taxa indicating a possible minimum age of lower *Pa. marginifera*. However, Klapper (2009) obtained finer resolution with his data indicating the section is no younger then *Pa. crepida*. Table 2 describes the conodont biostratigraphy from the Upper Frasnian to Mid-Famennian of the Horse Spring section.

3.3. Late Devonian magnetostratigraphy

There are multiple magnetic reversals recorded in the Late Devonian rocks within both sections. Fig. 4 depicts the magnetostratigraphy from the Oscar Range and Fig. 5 from Horse Spring. The magnetic declination and inclination data from stratigraphically ordered samples are plotted as angles from the virtual geomagnetic pole (VGP) calculated from the mean direction. Numerous geomagnetic reversals are observed in the remainder of the section, although some magnetozones are recorded by single samples. Many of these single-sample "chrons" are adjacent to one another, indicating a period of rapid polarity changes that extend over tens of metres. Because these zones are excessively short, it is possible that they do not record the time-averaged geomagnetic fields, or represent magnetic excursions (Coe and Glen, 2004), or even the delayed acquisition of magnetization (van Hoof and Langereis, 1991). As such, we regard the polarity assignments of these intervals as uncertain. These single sample cryptozones are shown as ambiguous intervals of mixed polarity (grey in the column of Fig. 4 and Fig. 5), and reversed or normal magnetozones are defined only where two or more samples with the same polarity exist. Some uncertainty in the interpreted polarity reflects poor recovery of a robust paleomagnetic remanence, such as the base of the Oscar Range section or the middle Famennian portion (50–70 m) at Horse Spring, which are regarded as "undefined" or mixed polarity, respectively. Once zones defined by single samples are combined as "mixed polarity zones" a total of 44 unambiguous polarity zones remain in the Oscar Range section and 21 at Horse Spring.

At the Oscar Ranges site, a test of the strata-bound magnetic reversal pattern was carried out by sampling of a parallel section ~200 m from the main section. The matching pattern of geomagnetic reversals is shown in Fig. 4, with thin red lines indicating the interpreted correlation in magnetozones. Both sections preserve a matching pattern of magnetic polarities marked by a reversal at

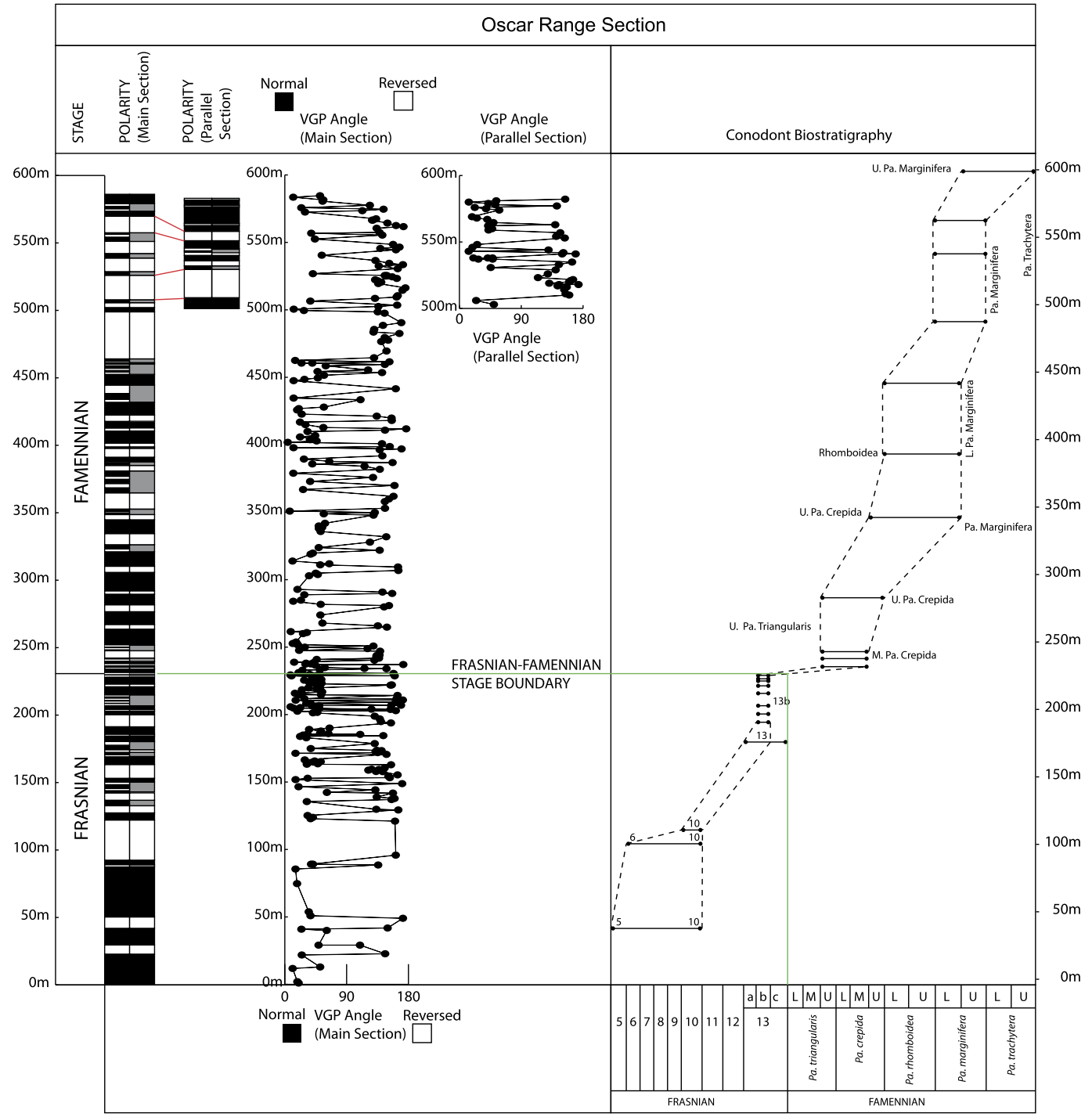

Fig. 4. Magnetostratigraphy of the Oscar Range section. Age constraints from conodont stratigraphy are plotted against magnetostratigraphic polarity columns for the main and parallel sections. The left hand polarity columns show all normal and reversed chrons, while the right hand columns have chrons defined by a single sample as ambiguous grey regions. Correlations between the two sections are displayed with red lines. Graphs of VGP angle are also shown. Dashed lines show the possible age range for a given stratigraphic interval. The green line marks the Frasnian–Famennian boundary. (For interpretation of the references to color in this figure legend, the reader is referred to the web version of this article.)

507.5 m in the main section and the base of the short, parallel section. The following normal polarity has been correlated to a single normal polarity determination in the main section. Following this there are two well-defined reversed and normal polarity magnetozones that correlate between both sections. Matching normal and reversed polarity sequences for both the overlapping and parallel sections provide strong evidence for a primary depositional remanence, as well as demonstrate internal consistency within the main section.

Fig. 6 shows the correlation of the pattern of magnetozones between Horse Spring and Oscar Range, based on 11 prominent chronostratigraphic tie-points defined by the tops and bottoms of the longest duration magnetozones. The strength of these correlations can be evaluated by comparing thicknesses between correlated surfaces (Fig. 7). While sedimentation rate will be increasingly variable as the interval of observation decreases, over longer durations it approaches a bulk sedimentation rate. Our assumption is that the 10s of meters thick packages defined by these

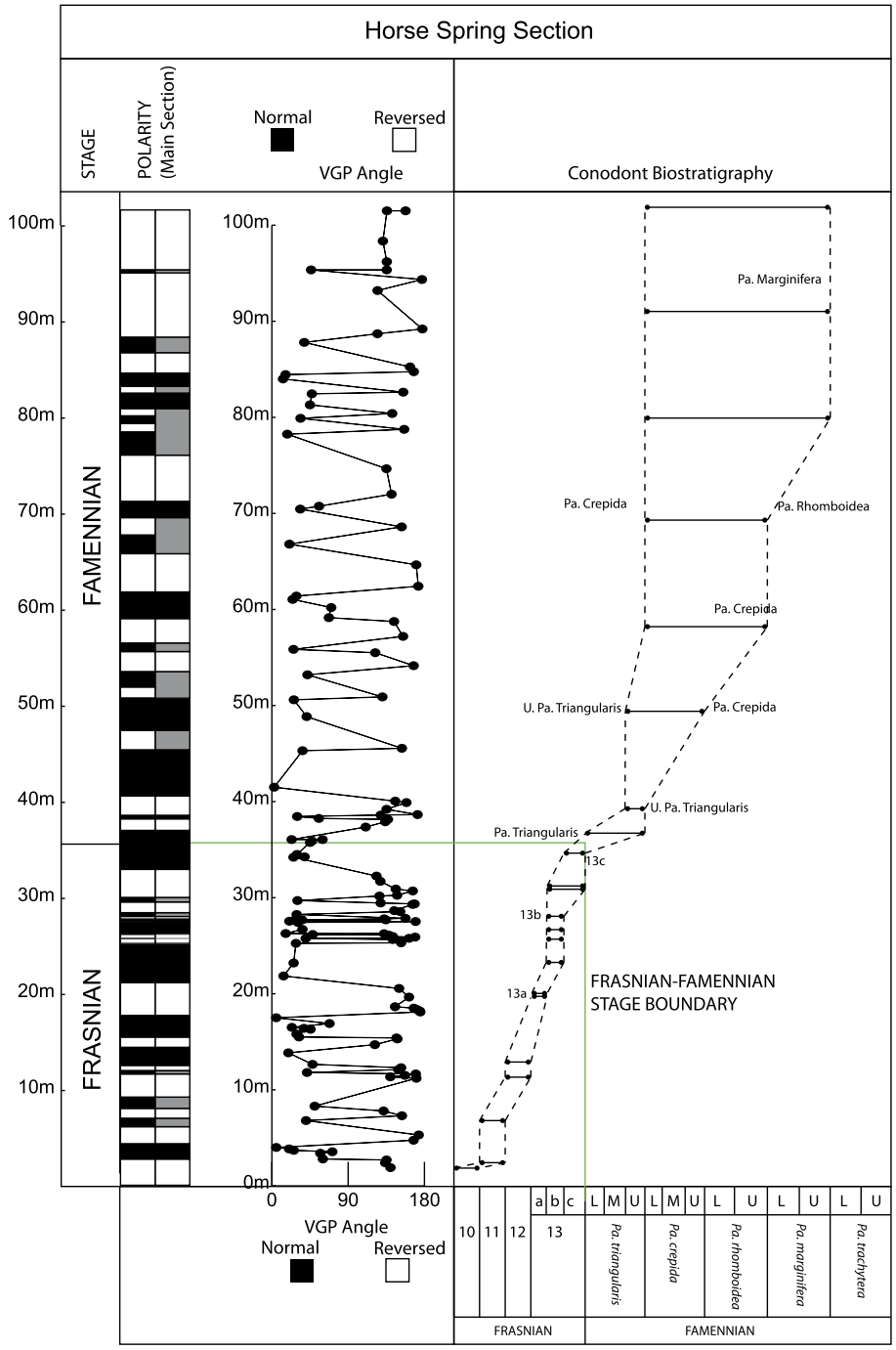

Fig. 5. Magnetostratigraphy of the Horse Spring section: age constraints from conodont stratigraphy are plotted against the magnetostratigraphic polarity column, and graph of VGP angle. The left hand polarity column shows all normal and reversed chrons, while right hand column has chrons defined by a single sample as ambiguous grey regions. Dashed lines show the possible age range for a given stratigraphic interval. The green line marks the Frasnian–Famennian boundary. (For interpretation of the references to color in this figure legend, the reader is referred to the web version of this article.)

surfaces average out short duration changes in sedimentation rate. The correlations contain enough stratigraphy between picks to average out higher frequency changes that may be occurring within. A strong linear correlation of magnetozone packages is apparent between the Oscar Range and Horse Spring sections. Taking the total thickness of the accumulated sediments during the relevant, correlated interval allows us to calculate that bulk rates of deposition in packstone-dominated slopes at Oscar Range was ~4.5 times faster than the dominantly wackestone–siltstone deposition at Horse Spring.

4. Discussion and conclusions

The results of this study indicate that geomagnetic reversals during the Late Devonian are common, as suggested by previous workers using much shorter sampling intervals (Hurley and Van der Voo, 1990). The geological timescale of Gradstein et al. (2012) indicates that the Late Devonian spans ~23.75 Myr (million years). As such the reversal rate for 44 polarity intervals from the Oscar Range is similar to the Paleogene reversal frequency of 2–5 reversals/Myr (Pal and Roberts, 1988). If single

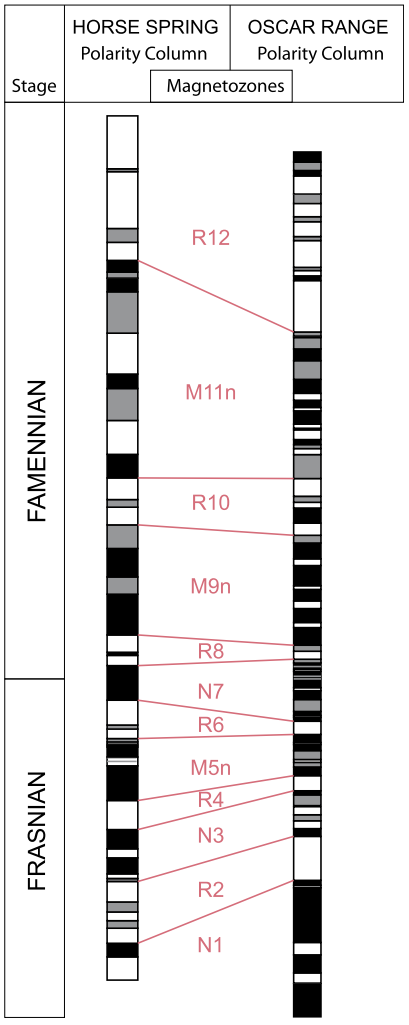

Fig. 6. Correlation of magnetozones between Horse Spring and Oscar Range. Labeled is the broad structure N = dominantly normal zone, R = dominantly reversed zone, M = mixed zone (lowercase suffix indicates normal/reversed bias within the interval). Numbering scheme starts at the base and increases upwards.

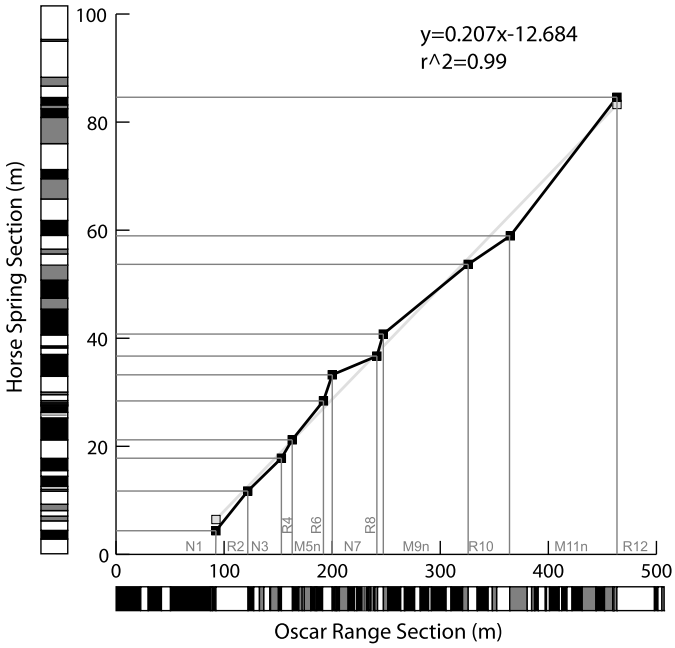

Fig. 7. Correlation diagram between Oscar Range and Horse Spring. Black points correspond to boundaries of magnetostratigraphic packages in Fig. 6. The grey line shows the linear model fit. Axes show stratigraphic level in meters.

sample chrons are included this rate increases. It is possible that the single sample chrons could also be the result of delayed onset of magnetization (van Hoof and Langereis, 1991). Although these cryptochrons present problems for correlation, the broad structure of magnetic reversals during the Late Devonian was reproducible, and shows strong correlation.

A magnetic reversal was observed near the Frasnian–Famennian stage boundary at both localities. It may prove to be a useful reversal on which the Frasnian–Famennian boundary can be determined in rocks lacking index fossils. Furthermore, magnetostratigraphy coupled with biostratigraphy appears to have the potential to increase intra-stage level correlation during the Late Devonian. For instance, the Upper Triangularis–Mid Crepida conodont constraint for 250–300 m in the Oscar Range section contains a number of reversals, which may prove useful for sub-stage correlation.

This correlation has allowed the comparison of depositional rate in a more proximal slope environment (Oscar Range) to a distal slope (Horse Spring) and shown that the proximal slope is accumulating at a rate ~4.5× faster, as reflected by debris- and grain-dominated deposits. Slope accumulation rate is related to proximity to the reefal margin and platform-top, from where the majority of sediment is derived, as well as oceanographic setting, which affects the productivity of these carbonate source factories. The Oscar Range locality is interpreted to be in a relatively proximal slope setting, as evidenced by steep depositional dips (up to 30°), and as such, is dominated by mud-poor deposits with higher depositional rates (debris and grainstone) that were capable of freezing along steep gradients with minimal downslope transport distances. In contrast, Horse Spring slope strata have lower depositional dips (typically less than 20°), indicating a more distal setting, with accordingly greater proportions of silty deposits that accumulated at lower rates via dilute turbidite or suspension processes. Furthermore, the transect at the Oscar Range is located along the open ocean-facing side of an isolated carbonate platform, where fine-grained terrigenous input is at a minimum, normal marine circulation is prevalent, and wave or current energy is unhampered – an ideal scenario for maximum carbonate productivity. The Horse Spring locality, on the other hand, is located on the inward margin of a large-scale (50 km across) embayment along the hinterland-attached Lennard Shelf, where fine-grained terrigenous material is available, minibasin restriction is more likely, and open-ocean swells and bottom currents are more inhibited – factors that can easily dampen carbonate productivity. Thus, the variations in position along the slope profile and paleogeographic setting from the Oscar Range to Horse Spring localities are interpreted as key controls on overall changes in sediment accumulation rates, as demonstrated by the integrated magnetostratigraphic- and biostratigraphic-based correlations presented here.

4.1. Conclusions

This study presents the first comprehensive magnetic stratigraphy for the Late Devonian covering the Middle Frasnian through to Late Famennian. Sampling of Middle Frasnian to Famennian slope environments of the Lennard Shelf reefal platform complexes has shown frequent geomagnetic field reversals. Multiple polarity zones were recovered from both the Oscar and Horse Spring Ranges. Correlations between the two sections were constrained with conodont biostratigraphy. The Frasnian–Famennian boundary was found to fall between 228.7–233.2 m along the Oscar Range section and between 34.6–36.65 m at Horse Spring. Integration

of biostratigraphy and magnetostratigraphy allowed for a more confident correlation framework. Magnetic directions correspond to those expected for the Canning Basin during the Late Devonian, with a paleopole of 49.5°S/285.8°E and $\alpha_{95} = 2.4$ ($n = 501$). This yields a paleolatitude of 9.9°S consistent with carbonate reef development during the Late Devonian. C-class reversal tests for both sections, and matching magnetozones from the overlapping stratigraphic section provide strong evidence for primary magnetization and internal consistency of magnetozones in the Oscar Range, while correlation of Horse Spring to Oscar Range results demonstrates robustness. Enhanced chronostratigraphic correlation capability of Late Devonian strata can be achieved using this integrated approach of magnetostratigraphy, coupled with biostratigraphy. A reference framework is presented here. The establishment of such frameworks allows for unprecedented examination of depositional systems, stratigraphic evolution, and global phenomena such as the Frasnian–Famennian biotic crisis.

Acknowledgements

A special thanks goes first to the Aboriginal tribes of the Bunaba and Gooniyandi (Kuniandi) people who allowed us to work in the lands that hold their rich spiritual history. We would like to thank the Australian Research Council (Grant LP0883812) without whose support this work would have not been possible. Thanks go to Chevron, for offering resources and collaborators for this research. We are grateful to the Geological Survey of Western Australia for use of their vehicles and logistical support. Special thanks go to Colin and Maria Morgan of Wundargoodie Aboriginal Safaris for field and logistical support. Thanks also go to Ray Addenbrooke, Trevor Holland, Kelly Hillbun, Peter Ward, Tom Tobin, Sergei Pisarevsky, Svenja Tulipani, and Luca Lanci for assistance in the field and fruitful discussions. Thanks go to the two reviewers, Cor Langereis and an anonymous reviewer whose input helped significantly improve this manuscript.

Appendix A. Supplementary material

Supplementary material related to this article can be found online at http://dx.doi.org/10.1016/j.epsl.2014.10.054.

References

Brannon, J.C., Cole, S.C., Podosek, F.A., Ragan, V.M., Coveney, R.M.J., Wallace, M.V., Bradley, A.J., 1996. Th–Pb and U–Pb dating of ore-stage calcite and Paleozoic fluid flow. Science 271, 491–493.

Brownlaw, R.L.S., 2000. Rugose Coral Biostratigraphy and Cyclostratigraphy of the Middle and Upper Devonian Carbonate Complexes, Canning Basin, Western Australia. University of Queensland, Queensland.

Chen, Z., Li, Z.X., Powell, C.M., 1995. Paleomagnetism of the Upper Devonian reef complexes, Canning Basin, Western Australia. Tectonics 14, 154–167.

Christensen, J.N., Halliday, A.N., Kesler, S.E., 1996. Rb–Sr dating of sphalerite and the ages of Mississippi-Valley type Pb–Zn deposits. In: Sangster, D.F. (Ed.), Carbonate-Hosted Lead–Zinc Deposits. Society of Economic Geologists, pp. 527–535.

Coe, R.S., Glen, J.M.G., 2004. The complexity of reversals. In: Channell, J.E.T., Kent, D.V., Lowrie, W., Meert, J.G. (Eds.), Timescales of the Internal Geomagnetic Field. American Geophysical Union, Washington D.C., pp. 221–232.

Deenen, M.J.L., Langereis, C.G., van Hinsbergen, D.J.J., Biggin, A.J., 2012. Geomagnetic secular variation and the statistics of palaeomagnetic directions. Geophys. J. Int. 186, 509–520.

George, A.D., 1999. Deep-water stromatolites, Canning Basin, northwestern Australia. Palaios 1999, 493–505.

Girard, C., Klapper, G., Feist, R., 2006. Subdivision of the terminal Frasnian linguiformis conodont Zone, revision of the correlative interval of Montagne Noire Zone 13, and discussion of stratigraphically significant associated trilobites. In: Over, D.J., Morrow, J.R., Wignall, P.B. (Eds.), Understanding Late Devonian and Permian–Triassic Biotic and Climatic Events: Towards an integrated Approach. Elsevier, Amsterdam, pp. 181–198.

Gradstein, F.M., Ogg, J.G., Schmidz, M.D., Ogg, G.M., 2012. The Geologic Time Scale. Elsevier, The Netherlands.

Hurley, N.F., Lohmann, K.C., 1989. Diagenesis of Devonian reefal carbonates in the Oscar Range, Canning Basin, Western Australia. J. Sediment. Petrol. 59, 127–146.

Hurley, N.F., Van der Voo, R., 1987. Paleomagnetism of Upper Devonian reefal limestones, Canning basin, Western Australia. Geol. Soc. Am. Bull. 98, 138–146.

Hurley, N.F., Van der Voo, R., 1990. Magnetostratigraphy, Late Devonian iridium anomaly, and impact hypotheses. Geology (Boulder) 18, 291–294.

Jones, C.H., 2002. User-driven integrated software lives: "PaleoMag" paleomagnetics analysis on the Macintosh. Comput. Geosci. 28, 1145–1151.

Kirschvink, J.L., 1980. The least-squares line and plane analysis of palaeomagnetic data. Geophys. J. R. Astron. Soc. 62, 699–718.

Kirschvink, J.L., Kopp, R.E., Raub, T.D., Baumgartner, C.T., Holt, J.W., 2008. Rapid, precise, and high-sensitivity acquisition of paleomagnetic and rock-magnetic data: development of a low-noise automatic sample changing system for superconducting rock magnetometers. Geochem. Geophys. Geosyst. 9, 1–18.

Klapper, G., 1989. The Montagne Noire Frasnian (Upper Devonian) conodont succession. In: McMillan, N.J., Embry, A.F., Glass, D.J. (Eds.), Devonian of the World. In: Memoir. Canadian Society of Petroleum Geologists, Calgary, pp. 449–459.

Klapper, G., 1997. Graphic correlation of Frasnian (Upper Devonian) sequences in Montagne Noire. France, and western Canada. In: Klapper, G., Murphy, M.A., Talent, J.A. (Eds.), Paleozoic Sequence Stratigraphy, Biostratigraphy, and Biogeography: Studies in Honor of J. Granville ("Jess") Johnson. Geological Society of America, pp. 13–129.

Klapper, G., 2007. Frasnian (Upper Devonian) conodont succession at Horse Spring and correlative sections, Canning Basin, Western Australia. J. Paleontol. 81, 513–537.

Klapper, G., 2009. Upper Devonian Conodonts in the Canning Basin. In: Playford, P.E., Hocking, R.M., Cockbain, A.E. (Eds.), Devonian Reef Complexes of the Canning Basin, Western Australia. Geological Survey of Western Australia.

McFadden, P.L., McElhinny, M.W., 1990. Classification of the reversal test in paleomagnetism. Geophys. J. Int. 103, 725–729.

McElhinny, M.W., Powell, C.M., Pisarevsky, S.A., 2003. Paleozoic terranes of eastern Australia and the drift history of Gondwana. Tectonophysics 362, 41–65.

McFadden, P.L., McElhinny, M.W., 1988. The combined analysis of remagnetization circles and direct observations in palaeomagnetism. Earth Planet. Sci. Lett. 87, 161–172.

Pal, P.C., Roberts, P.H., 1988. Long-term polarity stability and strength of the geomagnetic dipole. Nature 331, 702–705.

Playford, G.E., 1976. Plant microfossils from the Upper Devonian and Lower Carboniferous of the Canning Basin, Western Australia. Palaeontographica B 158, 1–71.

Playford, G.E., 2009. Review of Devonian palynology, Canning Basin. In: Playford, P.E., Hocking, R.M., Cockbain, A.E. (Eds.), Devonian Reef Complexes of the Canning Basin. Geological Survey of Western Australia, Perth, pp. 441–444.

Playford, P.E., Hocking, R.M., 2009. Plate 8, Lennard Shelf. In: Playford, P.E., Hocking, R.M., Cockbain, A.E. (Eds.), Devonian Reef Complexes of the Canning Basin. Geological Survey of Western Australia.

Playford, P.E., Hocking, R.M., Cockbain, A.E., 2009. Devonian Reef Complexes of the Canning Basin, Western Australia. Geological Survey of Western Australia, Perth.

Playford, P.E., Wallace, M.V., 2001. Exhalative mineralization in Devonian reef complexes of the Canning Basin, Western Australia. Econ. Geol. 96, 1595–1610.

Playton, T.E., 2008. Characterization, Variations, and Controls of Reef-Rimmed Carbonate Foreslopes. University of Texas, Austin.

Raup, D.M., Sepkoski, J.J., 1982. Mass extinctions in the marine fossil record. Science 215, 1501–1503.

Symons, N.P., Arne, D.C., 2003. Paleomagnetic dating of mineralization in the Kapok MVT deposit, Lennard Shelf, Western Australia. J. Geochem. Explor. 78–79, 267–272.

Symons, N.P., Arne, D.C., 2005. Paleomagnetic constraints on Zn–Pb ore genesis of the Pillara Mine, Lennard Shelf, Western Australia. Miner. Depos. 39, 944–959.

Torsvik, T.H., Van der Voo, R., Preeden, U., Niocaill, C.M., Steinberger, B., Doubrovine, P., van Hinsbergen, D.J.J., Domeier, M., Gaina, C., Tohver, E., Meert, J.G., McCausland, P.J.A., Cocks, L.R.M., 2008. Phanerozoic polar wander, palaeogeography and dynamics. Earth-Sci. Rev. 114, 325–368.

Trinajstic, K., George, A.D., 2009. Microvertebrate biostratigraphy of Upper Devonian (Frasnian) carbonate rocks in the Canning and Carnarvon Basins of Western Australia. Palaeontology 52, 641–659.

Turner, S., 1997. Sequence of Devonian thelodont scale assemblages in East Gondwana. Spec. Pap. Geol. Soc. Am. 321, 295–315.

van Hoof, A.A.M., Langereis, C.G., 1991. Reversal records in marine marls and delayed acquisition of remanent magnetization. Nature 351, 223–225.

Ziegler, A.M., Sandberg, C.A., 1990. The Late Devonian standard conodont zonation. CFS, Cour. Forsch. inst. Senckenb. 121, 1–115.

Appendix 3

Hillbun, K., Katz, D., Playton, T., Trinajstic, K., Tohver, E., Ratcliff, K., Caulfield-Kerney, S., Wray, D., Haines, P., Hocking, R., Roelofs, B., Montgomery, P. and Ward. P. 2015. Upper Kellwasser excursion pre-dates the F-F boundary in the Upper Devonian Lennard Shelf carbonate system, Canning Basin, Western Australia. Palaeogeography, Palaeoclimatology, Palaeoecology 438, 180-190.

Upper Kellwasser carbon isotope excursion predates the F–F boundary in the Upper Devonian Lennard Shelf carbonate system, Canning Basin, Western Australia

ARTICLE *in* PALAEOGEOGRAPHY PALAEOCLIMATOLOGY PALAEOECOLOGY · AUGUST 2015

Impact Factor: 2.34 · DOI: 10.1016/j.palaeo.2015.07.035

13 AUTHORS, INCLUDING:

Eric Tohver

University of Western Australia

108 PUBLICATIONS **956** CITATIONS

SEE PROFILE

Kate Trinajstic

Curtin University

53 PUBLICATIONS **390** CITATIONS

SEE PROFILE

Peter W. Haines

Geological Survey of Western Australia

105 PUBLICATIONS **688** CITATIONS

SEE PROFILE

Paul Montgomery

Chevron

20 PUBLICATIONS **303** CITATIONS

SEE PROFILE

Palaeogeography, Palaeoclimatology, Palaeoecology 438 (2015) 180–190

Contents lists available at ScienceDirect

Palaeogeography, Palaeoclimatology, Palaeoecology

journal homepage: www.elsevier.com/locate/palaeo

Upper Kellwasser carbon isotope excursion pre-dates the F–F boundary in the Upper Devonian Lennard Shelf carbonate system, Canning Basin, Western Australia

Kelly Hillbun [a,*], Ted E. Playton [b], Eric Tohver [c], Ken Ratcliffe [d], Kate Trinajstic [e], Brett Roelofs [e], Samuel Caulfield-Kerney [f], David Wray [f], Peter Haines [g], Roger Hocking [g], David Katz [h], Paul Montgomery [i], Peter Ward [a]

[a] University of Washington, ESS Dept. Box 351310, 4000 15th Avenue N.E., Seattle, WA, 98195, USA
[b] Chevron Energy Technology Company, Houston, TX, USA
[c] University of Western Australia, Perth, WA, Australia
[d] Chemostrat Ltd., Welshpool Powys, UK
[e] Curtin University, Perth, WA, Australia
[f] University of Greenwich, London, UK
[g] Geological Survey of Western Australia, East Perth, WA, Australia
[h] Whiting Petroleum Corporation, Denver, CO, USA
[i] Chevron Energy Technology Company, Aberdeen, UK

ARTICLE INFO

Article history:
Received 13 April 2015
Received in revised form 21 July 2015
Accepted 22 July 2015
Available online 31 July 2015

Keywords:
Kellwasser
Upper Devonian
F–F boundary
Carbon isotopes
Lennard Shelf carbonate system
Canning Basin

ABSTRACT

Here we report four high-resolution carbon isotope records in addition to trace element data for the Frasnian–Famennian (F–F) boundary interval in the Lennard Shelf carbonate system of the Canning Basin, Western Australia. This region lacks the characteristic black shale horizons associated with the global Late Devonian Kellwasser extinction events, yet still exhibits a trend in carbon isotope character similar to what has been reported from elsewhere in the world (two positive $\delta^{13}C$ excursions with ~3–4‰ amplitudes). Enrichments in select trace element ratios suggest that both excursions are related to periods of oxygen deprivation and perhaps increased biological productivity. Given the continuous and stratigraphically expanded nature of Lennard Shelf sections, together with high-density sampling constrained by both conodont biostratigraphy and magnetostratigraphy, we observe that the Upper Kellwasser isotope excursion (maximum $\delta^{13}C$ values) and associated trace element enrichments occur distinctly lower than the F–F boundary level. These results have implications for the paleoenvironmental conditions leading up to the Late Devonian Mass Extinction in terms of ocean chemistry and circulation patterns. This data set allows for a rare, detailed look at the temporal relationship between the Kellwasser events and the F–F boundary and constrains the pattern of carbon isotope perturbations at the intra-zonal scale.

1. Introduction

The Late Devonian Mass Extinction (LDME) is recognized as one the five greatest biotic crises of the Phanerozoic (Sepkoski, 1986). Decades of research on numerous European localities has led to the understanding that there are actually two separate extinction pulses known as the Upper and Lower Kellwasser events in the *linguiformis* (or Montagne Noire Zones 13b and 13c of Klapper, 1989) and *rhenana* (Montagne Noire Zones 12 and 13a) conodont zones, respectively, of the late Frasnian. These horizons are characterized by significant faunal turnover, positive carbon isotope excursions (average amplitude of about +3‰), and the deposition of black shales and bituminous limestones (e.g. McGhee, 1996), and are thought to reflect widespread anoxic conditions (Feist, 1985; Buggisch, 1991; Wendt and Belka, 1991; Hallam and Wignall, 1999) during pulses of sea level transgression (Johnson et al., 1985; Sandberg et al., 1988, 2002; Buggisch, 1991).

However, the timing of the carbon isotope excursion associated with the Upper Kellwasser deposits and extinctions in Europe (herein referred to as the Upper Kellwasser excursion) is not well constrained and the cause(s) poorly understood. The majority of Late Devonian geochemical studies document Upper Kellwasser excursion maxima at or slightly higher than the F–F boundary (e.g. Joachimski et al., 2002; Xu et al., 2003; Buggisch and Joachimski, 2006; George et al., 2014). As a result, they inadvertently lump the succession of related geo- and

* Corresponding author. Tel.: +1 650 274 9832.
E-mail address: khillbun@uw.edu (K. Hillbun).

http://dx.doi.org/10.1016/j.palaeo.2015.07.035
0031-0182/

bio-events together and give the illusion that the Upper Kellwasser excursion and F–F boundary are time-equivalent. This can be particularly problematic when attempting to make chronostratigraphic correlations or to determine causal mechanisms.

Exacerbating these problems are the conflicting isotope records that have been reported for this time period, with some workers noting either the absence of isotopic excursions (Geldsetzer et al., 1987), or the occurrence of negative excursions (Goodfellow et al., 1988; Wang et al., 1991), or the absence of organic-rich deposits (e.g. Joachimski and Buggisch, 1993; Bond et al., 2004). These discrepancies have generated debate over the role of global anoxia as a potential kill mechanism. Paleo-redox data for this time interval are also contradictory: whereas the trace element analyses from most studies have given credence to oceanic anoxia (e.g. Riquier et al., 2006), others infer oxic conditions (e.g. George et al., 2014). Furthermore, in many localities around the world, F–F boundary sections are highly condensed (e.g. Joachimski et al., 2002), or incomplete due to unconformities and depositional hiatuses related to the sharp marine regression in the uppermost Frasnian (Johnson et al., 1985; Sandberg et al., 1988; Geldsetzer et al., 1993; Muchez et al., 1996; Stephens and Sumner, 2003), and/or limited in terms of sampling density or biostratigraphic control at the intra-biozonal scale (e.g. Bratton et al., 1999; Stephens and Sumner, 2003; van Geldern et al., 2006).

This contribution reports new data from the northern margin of Gondwana in order to constrain the timing of the Upper Kellwasser excursion and to better understand the causal mechanism(s) relating to the Kellwasser events. Here we present four detailed carbon isotope profiles, constrained at the intra-zonal level by high-resolution conodont biostratigraphy and magnetostratigraphy. We obtained our data from measured outcrop sections through organic-poor facies in variable slope environments of the Lennard Shelf mixed carbonate-siliciclastic system, Canning Basin, Western Australia (Fig. 1). In this region, middle-slope breccia-grainstone and upper-slope boundstone settings appear to be stratigraphically expanded relative to many other global localities. In Europe, for example, Conodont Zone 13 (Fig. 2) is generally <2 m thick (Buggisch and Joachimski, 2006), whereas in this study, the same interval of time is represented by >20 m of stratigraphy. As such, our sections provide a continuous, more expanded view of upper Frasnian to lower Famennian strata and allow for a more detailed examination of the Upper Kellwasser excursion as it relates to the timing of the F–F boundary. The stable isotope data, with some accompanying trace element analyses, also provide insight into changes in the global carbon pool and redox conditions of the ocean during this time.

2. Area descriptions, methods & materials studied

During the Middle Devonian, subsidence and rifting of the Canning Basin (e.g. Veevers and Wells, 1961; Kennard et al., 1994) led to the prolific growth of carbonate reefs along the shallow terraces of the Lennard Shelf. Today, over 350 km of Middle to Late Devonian carbonates are exposed in the northern part of the basin and have been subjected to decades of stratigraphic, paleontological, and geochemical research (Guppy et al., 1958b; Playford and Lowry, 1966; Druce, 1976; Playford, 1980; Becker and House, 1997; George et al., 1997; Stephens and Sumner, 2003; Nothdurft et al., 2004; Playford et al., 2009; and others). During the interval of time most relevant to this study, namely, the Late Frasnian and Early Famennian, the reefal platform and slope system exhibited progradational growth morphology and experienced episodic collapse events that transported large amounts of material down-slope (Playford, 1980; Sandberg et al., 2002; Playton, 2008; Playford et al., 2009). An abrupt fall in sea level coincident with the F–F boundary resulted in the sub-aerial exposure and erosion of platform-top facies while sedimentation continued uninterrupted on

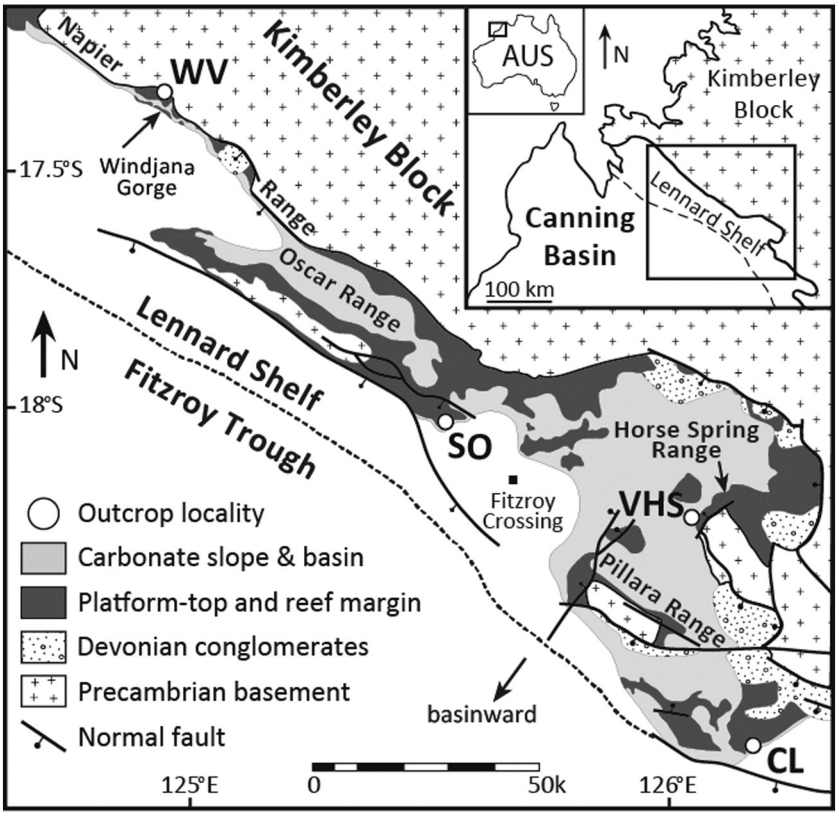

Fig. 1. Map of field area (modified after Playford et. al., 2009). Samples for this study were collected from four outcrops along the Lennard Shelf in Western Australia; Casey Falls (CL), Virgin Hills Formation at Horse Spring Range (VHS), South Oscar Range (SO), and the Windjana Gorge area (WV). Insets show the location of the Lennard Shelf carbonate system in relation to the Canning Basin and Australia.

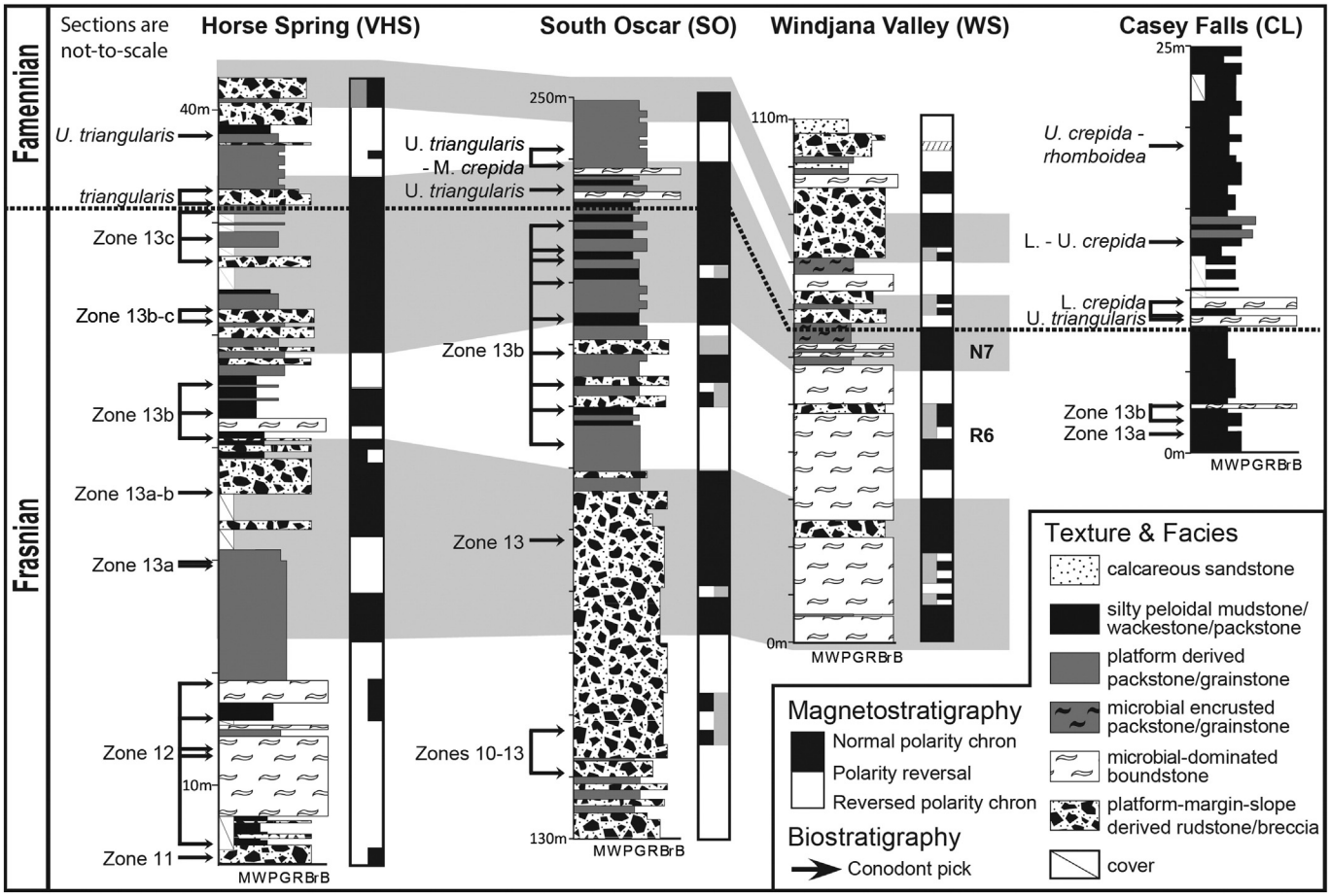

Fig. 2. Measured sections showing bio- and magnetostratigraphic control used for correlation and to constrain the position of the F–F boundary. Paleomagnetic reversal records (partials) are from Hansma et al. (2015) and E. Tohver (personal communication). Grey shading shows correlation of normal (and mixed-normal) polarity chrons. M = mudstone, W = wackestone, P = packstone, G = grainstone, R = rudstone, Br = breccia, B = bound/bafflestone.

the slope and in the basin. As such, deeper water settings were preferentially targeted in this study because of their potential for stratigraphic completeness.

Four stratigraphic sections from sites spanning 200 km across the Lennard Shelf outcrop belt were investigated in detail for facies and stratigraphy, and sampled for carbon isotope and trace element geochemistry, biostratigraphy, and magnetostratigraphy (Fig. 1). Samples include plugs (2.5 cm diameter, 10 cm length) and hand specimens, and were collected at a spacing of 16–95 cm (1 sample/59 cm on average) from three relatively thick (ca. 50–250 m) middle- and upper-slope sections (Table 1) in the southeastern part of the Oscar Range (SO; 17°54.983′S, 125°17.9′E), from the Virgin Hills formation in the Horse Spring Range (VHS; 18°12.133′S, 126°01.483′E), and north of Windjana Gorge (WV; 17°23.767′S, 124°56.767′E) in the Napier Range.

For comparison purposes, samples from one relatively condensed transect through silt-dominated lower-slope deposits at Casey Falls in the Lawford Range (CL; 18°43.983′S, 126°5.119′E) were also obtained. Specimens for geochemical and isotopic analysis were typically taken from >5 cm below the modern surface (i.e., deepest portion of plug sample). Sampling of breccias excluded blocks and allochems, instead targeting the matrix and marine cements, to ensure that geochemical analyses were representative of the time of deposition and that paleomagnetic analyses were conducted on presumably unrotated material.

Integrated magnetostratigraphy and conodont biostratigraphy provided the primary temporal constraints for the geochemical analyses. The paleomagnetic reversal records were derived from previously published data sets analyzed at the University of Western Australia; data for VHS and SO were reported by Hansma et al. (2015), and WV

Table 1
Depositional characteristics and isotopic data associated with Kellwasser equivalent excursions 1 and 2. Amplitude and maximum $\delta^{13}C$ values are reported relative to VPDB. Data for excursion 1 at WV and CL are not available because neither section extended into the age-appropriate strata. See Fig. 1 for non-abbreviated locality names.

Section	Paleogeographic setting	Depositional environment	Excursion 1 (L.KW equivalent)			Excursion 2 (U.KW equivalent)		
			Associated facies	Amp.	Max.	Associated facies	Amp.	Max.
SO	Isolated, open marine	Middle–upper slope	Skeletal-rich megabreccia	+3.4‰	+4.4‰	Platform-derived packstone/grainstone, breccia	+2.5‰	+3.9‰
VHS	Land attached, broad embayment	Middle slope	Skeletal-peloidal packstone/grainstone, microbial-dominated boundstone	+3.5‰	+4.7‰	Platform-derived grainstone, megabreccia, wackestone	+3.2‰	+4.6‰
WV	Land attached	Upper slope	Not available			Massively bedded microbial boundstone, megabreccia	+2.5‰	+3.4‰
CL	Land attached, reef spine	Lower slope	Not available			Silt-dominated wackestone/packstone	+2.8‰	+3.5‰

was evaluated by E. Tohver (personal communication). Paleomagnetic data for CL were not incorporated into this study—due to the relatively condensed nature of this section, magnetostratigraphic correlations were ambiguous. Samples obtained for conodont analysis were collected from all sections but were only age diagnostic for the SO, VHS, and CL sections (Hansma et al., 2015; Roelofs et al., 2015). For additional constraint, an independent conodont study (Klapper, 2007) conducted at the VHS site was incorporated into our work.

For carbon isotopes, 350 samples were analyzed at the Stable Isotope Research Facility at the University of Washington; 82 are presented from the SO section, 169 from VHS, 66 from WV, and 33 from CL. Hillbun et al. (in revision) evaluated all samples for diagenetic alteration and showed that bulk-rock analyses record primary marine $\delta^{13}C$ values useful for regional and global correlations. Samples that were previously identified as potentially dolomitized, recrystallized, or otherwise altered were not included in this study. Following the bulk-rock methodology of Stephens and Sumner (2003), and the quality control workflow of Hillbun et al. (in revision), sample cores were polished and then drilled using a hand-held Woodtek drill with a diamond coated bit. All sample powders were reacted with phosphoric acid at 70 °C in an automated Kiel device with the resulting CO_2 gas analyzed by a ThermoFinnigan MAT253 mass spectrometer. The analytical precision of $\delta^{13}C_{carb}$ and $\delta^{18}O$ analyses based on sample replicates and laboratory standards is ≤± 0.1 ‰. Data were corrected using laboratory standards and are reported here in standard delta notation relative to VPDB.

Trace element analyses for the SO section were carried out by Chemostrat, Inc. Each sample was ground to a powder in a ball mill, and following Li-metaborate fusion, was analyzed using inductively coupled plasma optical emission spectrometry and mass spectrometry (ICP-OES MS). The methods of fusion and analysis are those described in Jarvis and Jarvis (1995). These analytical methods result in data for both major- and trace elements, reported as oxide percent by weight and parts per million by weight (ppm), respectively. Precision for the major element data was generally better than 2% and ca. 3% for the high-abundance trace element data derived by ICP-OES. The remaining trace elements determined from the ICP-MS were generally less precise, with analytical error of ca. 5%. Analytical error is ± 1% for major and ± 3–7 ppm for trace elements depending on abundance. Expanded uncertainty values (95% confidence) that incorporate all likely errors within a statistical framework derived from 11 batches of 5 certified reference materials (CRMs), each prepared in duplicate, are typically 5–7% (relative) for major elements, and 7–12 % (relative) for trace elements.

3. Results

3.1. Bio- and magnetostratigraphic constraints on the F–F boundary

To determine the location of the F–F boundary, the widely used standard conodont zonations of the Frasnian (Montagne Noire succession, Klapper, 1989; Girard et al., 2005) and Famennian (Ziegler and Sandberg, 1990) are applicable to our sections in the Lennard Shelf (Fig. 2). As defined at the boundary-stratotype section in Montagne Noire, France (House et al., 2000), the lower boundary of the *triangularis* Zone, and base of the Famennian Stage, is marked by the lowest occurrence of Palmatolepis *subperlobata*. In our VHS section, the interval between the lower *triangularis* Zone and the uppermost part of Frasnian Zone 13 (i.e. the margin of error around the stratigraphic position of the F–F) is only 20 cm; in the SO section it is less than 4.3 m, and in CL it is no more than 5.7 m. At VHS and SO, the F–F boundary is arbitrarily placed at the stratigraphic midpoint between the latest known Frasnian (35.75 m and 228.7 m, respectively) and earliest known Famennian (35.95 m and 233 m, respectively) strata (Fig. 2). At CL, the boundary is less biostratigraphically constrained but is currently placed just below the lowest observed occurrence of P. *subperlobata,* at the base of the first microbial boundstone (at 7.5 m).

Magnetostratigraphic correlation of WV with previously examined records from VHS and SO (Hansma et al., 2015) revealed seven major magnetozones for the interval of time studied (Fig. 2; Frasnian conodont Zone 11 to Famennian *crepida* Zone). Four periods of mixed, dominantly reversed polarity and three periods of normal polarity have been recognized, and the F–F boundary has been identified within the N7 normal chron. In the WV section, where biostratigraphic control is lacking, the boundary is constrained within the N7 chron, an interval that is ~10 m thick; the F–F boundary is arbitrarily placed at the center point of this chron (Fig. 2).

3.2. Carbon isotope stratigraphy

High-resolution carbon isotope stratigraphy reveals two major positive excursions stratigraphically lower than the F–F boundary. The timing and amplitude of these perturbations are comparable between sections, despite differences in facies, depositional environments, and paleogeographic settings (Table 1). Furthermore, petrographic analysis of selected samples reveals excellent preservation of original fabrics, relatively minor amounts of calcite recrystallization, and the absence of dolomitization, suggesting that the isotopic composition of the original seawater is represented (Hillbun et al., in revision).

Excursion 1 (Fig. 3) is stratigraphically lower than excursion 2 and is observed in only two sections. In SO, an increase in $\delta^{13}C$ values from + 1‰ to + 4.4‰ (max value) is measured from megabreccia deposits and constrained within conodont Zones 10 and 13. In the VHS section, isotope values recorded in thick grainstone beds increase from + 1.2‰ to + 4.7‰ (max value) within Zones 12 and 13a. While excursion 1 exhibits similar amplitudes and maximum values in both sections, the interval of elevated values in SO is noticeably expanded stratigraphically down-section relative to VHS. Based on conodont biostratigraphy, excursion 1 can be correlated with the deposition of the Lower Kellwasser Horizon in Europe (e.g. Buggisch and Joachimski, 2006), and we interpret it to be time-equivalent to the Lower Kellwasser excursion reported from localities around the world (Joachimski et al., 2002; Xu et al., 2003; Stephens and Sumner, 2003; George et al., 2014; and others).

Excursion 2 is documented in all four localities (Fig. 3). In both SO and VHS, $\delta^{13}C$ values increase from + 1.4 ‰ and + 1.3 ‰ (baseline values) to + 3.9 ‰ and + 4.6 ‰ (max. values), respectively, within conodont Zone 13b. Isotopic data from WV show a positive shift (~ + 0.9‰ baseline values to + 3.4‰ max values) occurring wholly within the R8 chron, which is constrained within conodont Zone 13b, and possibly 13a, based on magnetostratigraphic correlation. Although resolution of conodont biostratigraphic control is less precise in the condensed CL section, the data are similar; $\delta^{13}C$ values from silt-dominated, lower slope facies begin to increase in Zone 13b (and possibly the very uppermost part of Zone 13a) from + 0.7 ‰ (baseline values), and reach maximum values (+ 3.5 ‰) just below the first appearance of *Pa. subperlobata*.

In all sections, increasing $\delta^{13}C$ values associated with excursion 2 can be roughly correlated with the onset of deposition of the Upper Kellwasser horizon in Europe during Zone 13b (Fig. 3). However, maximum isotope values associated with the Lennard Shelf excursion begin to decline towards more baseline values during the upper Frasnian, before the F–F boundary and the cessation of Upper Kellwasser shale deposits in Europe. In VHS, SO, and WV in particular, the F–F is clearly not associated with a positive shift in $\delta^{13}C$ values. The transition from the uppermost Frasnian into the *triangularis* Zone of the lower Famennian is marked by slightly elevated $\delta^{13}C$ values relative to Frasnian baseline values of + 1 to + 1.5 ‰. This slow recovery trend, albeit typically observed only in the *triangularis* Zone, is characteristic of European isotope records (e.g. Buggisch and Joachimski, 2006). Given the temporal constraints provided by the bio- and magnetostratigraphy data, we interpret excursion 2 as the Upper Kellwasser excursion, but it pre-dates conventional timing. Rather

than maximum $\delta^{13}C$ values being coincident with or closely adjacent to the F–F boundary, they occur distinctly lower, in upper Frasnian strata.

3.3. Trace elements as tests for anoxia and productivity

Based on the work of previous studies (e.g. Adams and Weaver, 1958; Jones and Manning, 1994; Algeo and Maynard, 2004; Rimmer, 2004), trace element ratios of U/Th and V/Cr are used to evaluate the state of marine oxygen levels. Because uranium and vanadium are commonly concentrated in sediments deposited under reducing conditions (Shaw et al., 1990; Emerson and Huested, 1991), comparing them with non-redox sensitive elements that are typically found in the detrital fraction (Th and Cr) can provide insight into changes in paleo-oxygenation. Typical range estimates for oxic, dysoxic, and anoxic water conditions have been suggested for U/Th and V/Cr ratios (Jones and Manning, 1994) and are employed here for reference. Given these threshold values, both paleo-redox proxies indicate low-oxygen levels (Fig. 4) which correspond to the $\delta^{13}C$ excursions associated with both Kellwasser events noted in this study (Fig. 3). For the Upper Kellwasser in particular, it appears that V/Cr values remain elevated for a longer period of time relative to U/Th.

Elemental ratios of Cu/Al and Ni/Al are reported for their use as reliable indicators of changes in paleo-bioproductivity (e.g. Piper and Perkins, 2004; Riquier et al., 2006; Perkins et al., 2008), particularly in the absence of preserved organic-rich material. While a variety of trace elements behave as micronutrients in oxic marine environments and are deposited in association with the organic carbon flux from surface primary productivity, both nickel and copper may be retained within their host sediments even if the organics are partially or completely re-mineralized after deposition (Tribovillard et al., 2006). In our study, the measured ratios of Cu/Al and Ni/Al exhibit less obvious trends than the ratios of U/Th and V/Cr; there is considerable scatter associated with the Lower Kellwasser interval in both proxies, but the elevated values are correlative with the isotopic excursion. For the Upper Kellwasser, relative enrichments in Ni/Al and Cu/Al are observed near and above maximum $\delta^{13}C$ values, respectively.

4. Discussion

4.1. Discrepancy in timing

The interval of time surrounding the Frasnian–Famennian (F–F) boundary is generally marked by two positive carbon isotope excursions (~3‰ average amplitude) in the marine carbonate record that correspond to the well-studied, organic-rich Kellwasser horizons and associated extinction events first described from sections in Central Europe and Morocco (McGhee et al., 1986; Buggisch, 1991; Joachimski and Buggisch, 1993; Joachimski et al., 1994, 2002). Despite the lack of

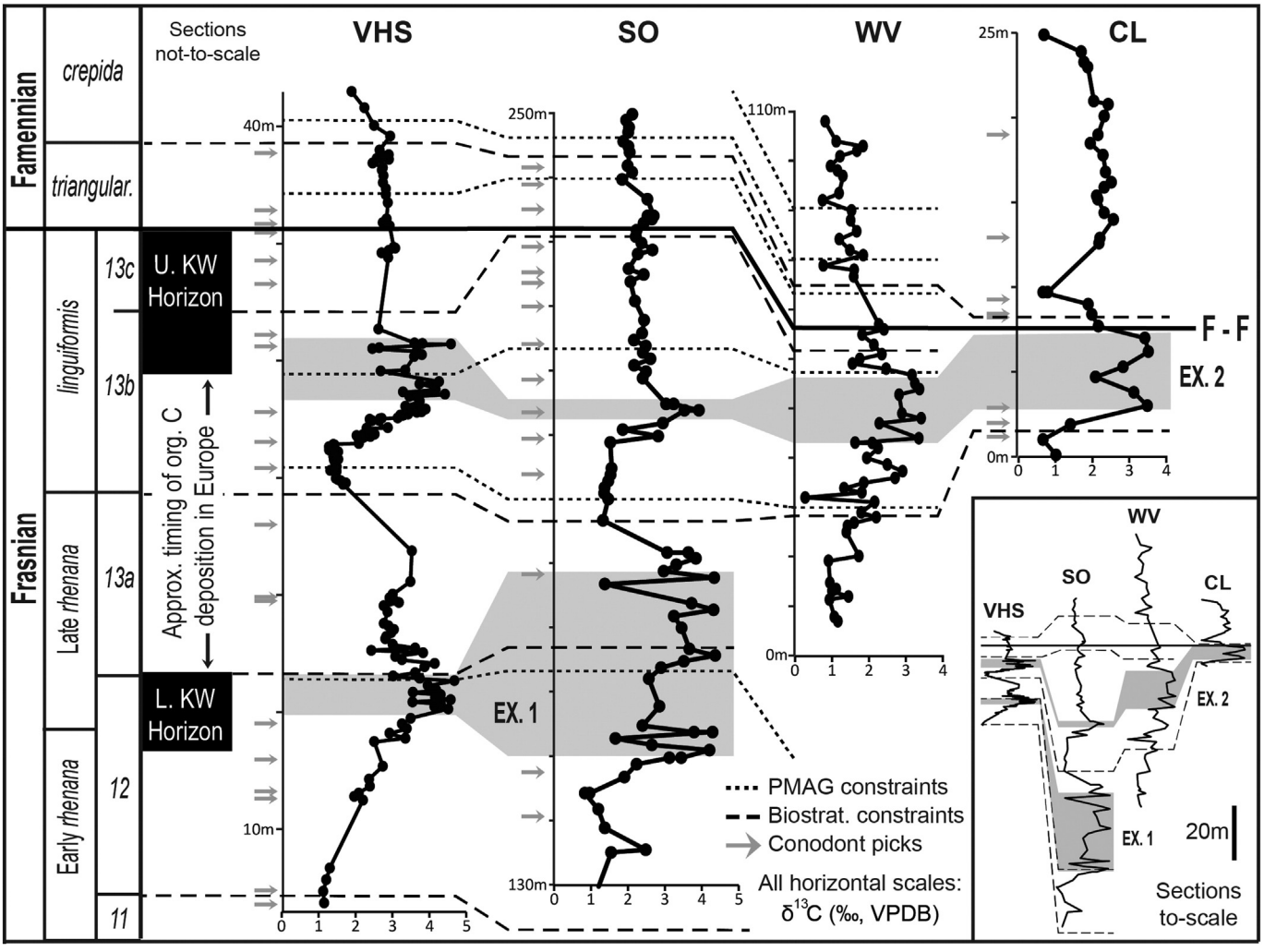

Fig. 3. Comparison of isotopic profiles across the F–F boundary in the Lennard Shelf carbonate system. Grey highlighting of maximum $\delta^{13}C$ values shows the stratigraphic positions of excursions (Ex.) 1 and 2 relative to the standard (Ziegler and Sandberg, 1990) and Montagne Noire (Klapper, 1989) conodont zonations. Position of the F–F boundary is constrained by bio- and magnetostratigraphic data (see Fig. 2 for magnetostratigraphic correlation). Inset shows isotopic profiles to-scale; dashed lines show biostratigraphic correlations and the solid line = the Frasnian–Famennian (F–F) boundary.

similarly aged organic-rich deposits in the Lennard Shelf system, we report a European-like trend in carbon isotope values from four different measured sections. While the absence of black shales and bituminous limestones from this time interval in Western Australia has created some doubt over the global nature of the two Kellwasser events, our geochemical results are consistent with the hypothesis that the Kellwasser events are indeed world-wide phenomena, and the trace element data support a period of at least dysoxia (if not anoxia) associated with the events. Our evidence for a $\delta^{13}C$ excursion associated with the Lower Kellwasser event within Zones 12 and 13a is consistent across datasets in this study and corroborates the record from other sections in Australia (Stephens and Sumner, 2003; George et al., 2014) and Europe (e.g. Buggisch and Joachimski, 2006). However, our chronostratigraphically constrained record of the Upper Kellwasser excursion, particularly the timing of maximum $\delta^{13}C$ values, suggests that the geochemical event is distinct from and pre-dates the F–F boundary, in contrast with other workers' findings (Fig. 5).

There are four possible ways to reconcile our data with the global data set. First, the data may reflect local phenomena or paleoenvironmental conditions unique to the Lennard Shelf and thus have no global implications. Second, a discrepancy in timing could be due either to a diachronous appearance of upper Frasnian conodont faunas or to differences in biostratigraphic resolution, possibly related to variable sampling densities. Third, these Lennard Shelf sections may represent a rarely preserved, expanded interval of the F–F transition that is not present elsewhere possibly because of highly condensed facies assemblages or unrecognized depositional hiatuses. Lastly, differences in paleogeography and ocean circulation between different study areas may account for the variation in the timing of isotopic excursions, reflecting differences in riverine input or restricted circulation in intracratonic basins, for example.

The first hypothesis, that of highly localized $\delta^{13}C$ patterns, is at odds with the broad and replicable patterns in $\delta^{13}C$ values recognized from the Lennard Shelf, in this study and others (Joachimski et al., 2002; Stephens and Sumner, 2003; George et al., 2014), which are similar in shape and amplitude to the well-studied excursions associated with the Kellwassers and equivalent horizons documented throughout Europe (e.g. Buggisch and Joachimski, 2006), North Africa (Joachimski et al., 2002), North America (e.g. Wang et al., 1996), and China (Xu et al., 2003). The refined timing of the Upper Kellwasser excursion is consistent between multiple sections of our study, regardless of differing slope facies and paleogeographic settings. Sections in Kowala, Poland, and Bou Ounebdou, Morocco (Joachimski et al., 2002) also reported similar findings of elevated $\delta^{13}C$ values below the F–F boundary. However, these authors argued that the expected stratigraphic continuations of the excursions were muted by recrystallization during the anaerobic oxidation of organic matter. The lack of correlative organic-rich sediments in our Lennard Shelf sections precludes this as a possible explanation for our results.

In addition to studies in the Canning Basin, the occurrence of positive excursions without accompanying anoxic sediments has been documented at the Wolayer Glatcher site in Austria (Joachimski and Buggisch, 1993) and in Nevada, USA (Joachimski et al., 2002). These authors' assessment that the anomalies in $\delta^{13}C$ reflect global changes in the total dissolved marine carbon reservoir, as opposed to local anoxia, is corroborated by our findings from Western Australia. A similar argument has been made for the isotopic data associated with the oceanic anoxic events in the Cretaceous Period; that is, the deposition of black shales and sub-oxic conditions were regional but their effects on the marine $\delta^{13}C$ record were global (e.g. Tsikos et al., 2004; Wagreich, 2009). We therefore conclude that the Lennard Shelf isotope record is a viable marine proxy that documents the extensive burial of organic carbon in other sedimentary basins around the world (North America, Europe, China, and North Africa).

The second hypothesis invoking the diachronous appearance of conodonts is considered unlikely. Extensive work in the Canning Basin has established that the Lennard Shelf conodont succession is comparable and time-equivalent to the standard conodont zonations used globally for the upper Frasnian and lower Famennian with no discrepancies between first and last appearance data of key species (Glenister and Klapper, 1966; Druce, 1976; Klapper, 1989, 2007; Ziegler and Sandberg, 1990; Klapper et al., 1993). Bioturbation was also ruled out as a possible explanation for the observed discrepancy because the isotope excursion believed to represent the Upper Kellwasser event was found to occur as much as 20 m or more below the F–F boundary (SO), a depth too great to reasonably account for any biological displacement of material.

In terms of sampling density and resolution, our study has very good constraints around the F–F boundary, and where we lack conodont control, magnetostratigraphy aids our correlations. However, isotopic studies commonly differ, sometimes significantly, in their biostratigraphic resolution. In the Canning Basin, for example, conodont samples were collected at a density of >1 sample per meter from the VHS section in the Horse Spring Range (this study; Klapper, 2007), allowing for the distinction of individual Montagne Noire conodont zones, including each subdivision of Zone 13 (a, b, and c). In contrast, zonal resolution

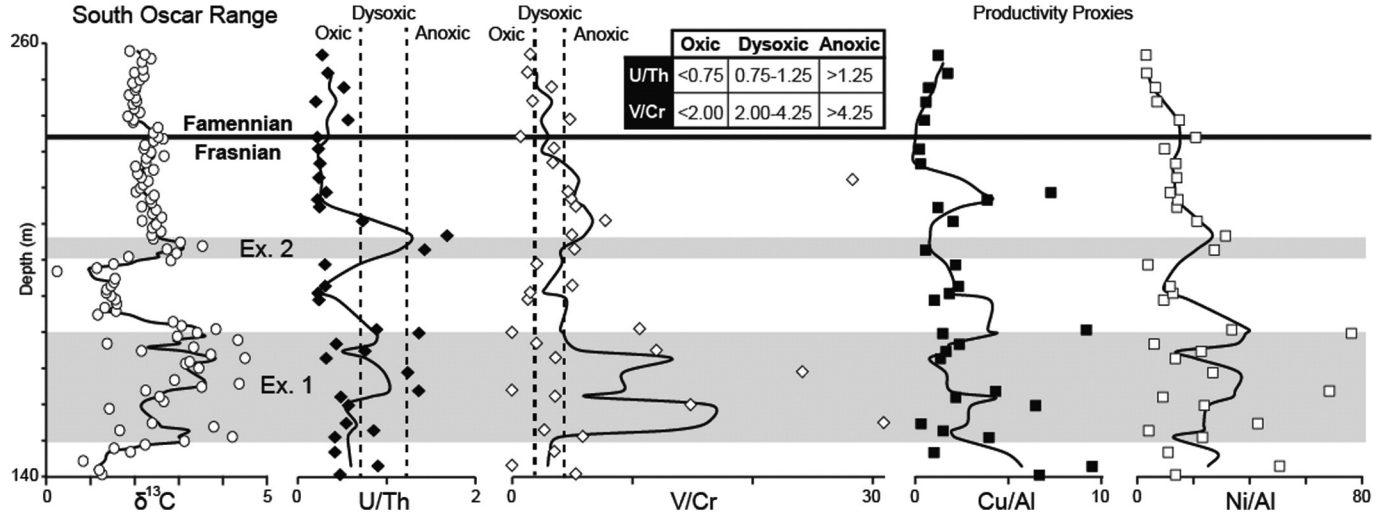

Fig. 4. Chemostratigraphic profiles of elemental ratios used as qualitative proxies for paleo-redox conditions and bioproductivity. Shaded areas represent the stratigraphic position of maximum carbon isotope values associated with the Lower and Upper Kellwasser excursions (Ex. 1 and 2, respectively; Ex. = excursion). Trace element ratio thresholds for oxic, dysoxic, and anoxic water conditions from Jones and Manning (1994).

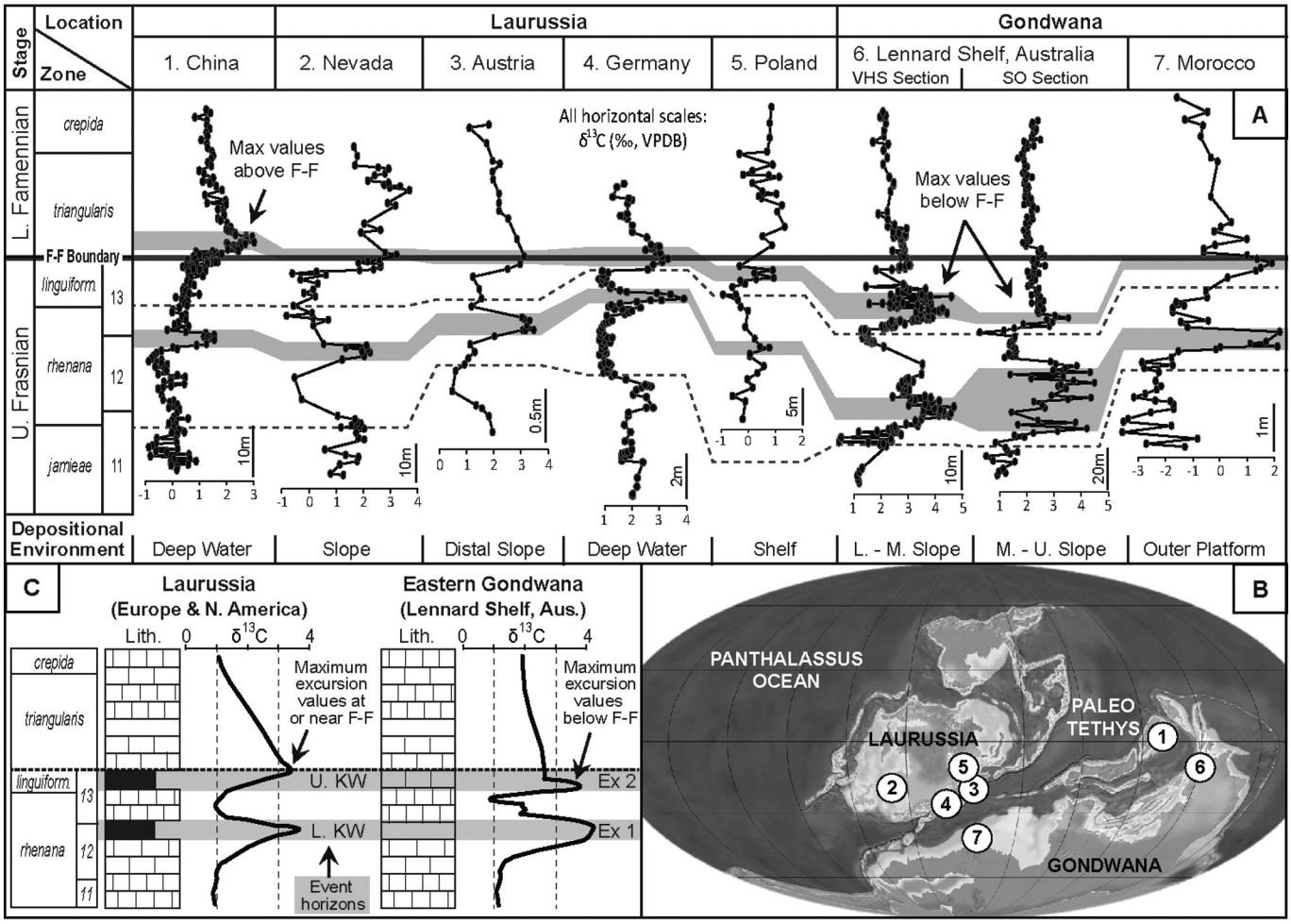

Fig. 5. A. Comparison of $\delta^{13}C$ maxima for the Upper and Lower Kellwasser geochemical events from Guilin, China (Xu et al., 2003); Devils Gate, Nevada (Joachimski et al., 2002); Wolayer Glacier, Austria (Buggisch and Joachimski, 2006); Benner Quarry, Germany (Joachimski and Buggisch, 1993); Kowala, Poland (Joachimski et al., 2002); the Lennard Shelf, Western Australia (this study); and Bou Ounebdou, Morocco (Joachimski et al., 2002). The depositional environment for each section has been indicated and biostratigraphic constraints drawn in accordance with the original data. B. Paleo reconstruction of the Late Devonian (Blakey, 2008) showing locations of the various $\delta^{13}C$ records. C. Generalized lithologic and isotopic trends across the F–F boundary for sections in Laurussia and Eastern Gondwana (modified from Joachimski and Buggisch, 1993).

for the isotopic record at Dingo Gap (George et al., 1997, cited in Stephens and Sumner, 2003) was not achieved; the low sample-density average (1 sample each ca. 5 m) created an apparent compression of the isotopic excursions (Fig. 6). This problem of low resolution is exacerbated by the tendency for authors to cite prior work in place of providing the actual biostratigraphic data (e.g. Wang et al., 1996; Joachimski et al., 2002; Stephens and Sumner, 2003; Xu et al., 2003), rendering chronostratigraphic comparisons at the zonal level difficult to assess.

This problem of uneven sampling density is especially true for the Lennard Shelf where isotopic profiles for the Late Frasnian and Early Famennian appear to differ slightly from one another in the timing of their excursions (Fig. 6). For example, a recent study of a basinal core near our VHS section reported a large positive excursion, interpreted to represent the Upper Kellwasser, as occurring entirely above the F–F boundary in the *triangularis* Zone (George et al., 2014). The authors also documented another two $\delta^{13}C$ anomalies just below the boundary, constrained by a limited number of samples, two samples over 20 m spanning Frasnian conodont Zones 6–13 and three samples from conodont Zone 13. The constraints for these two lower excursions suggest a correlation with our reported excursions, and thus represent the Lower and Upper Kellwasser events, respectively. None of our studied sections record the Famennian excursion reported by George et al. (2014).

The other prominent C-isotope study of the F–F interval in the Canning Basin (Stephens and Sumner, 2003) also showed two positive isotope excursions at Dingo Gap; one occurring below the boundary and the other straddling it (Fig. 6). George et al. (2014) interpreted the broad upper excursion, which had two distinct peaks, as representing both Kellwasser events. However, the conodont resolution for Dingo Gap is not sufficiently detailed to determine with any certainty the zones in which the excursions actually occur. At this time, it remains unclear if differences in biostratigraphic resolution within the Canning Basin, and potentially elsewhere, can account for the observed discrepancy in timing.

The third and fourth scenarios presented are the most plausible as they are most consistent with- and easily explained by our results. In three of our measured sections the isotopic expression of the Upper Kellwasser was observed in continuous succession in grainstone, breccia, and massive boundstone from middle- and upper-slope settings where depositional dips were relatively steep (up to 30°) and sedimentation rates presumably greater (Playton, 2008; Hansma et al., 2015). A combination of expanded stratigraphy and high-density sampling demonstrates that the timing of maximum values associated with the Upper Kellwasser excursion is different than previously documented (Figs. 2 and 3). Our results from the distal-slope sediments (CL section) differ from the other three in that the section is highly condensed (conodont

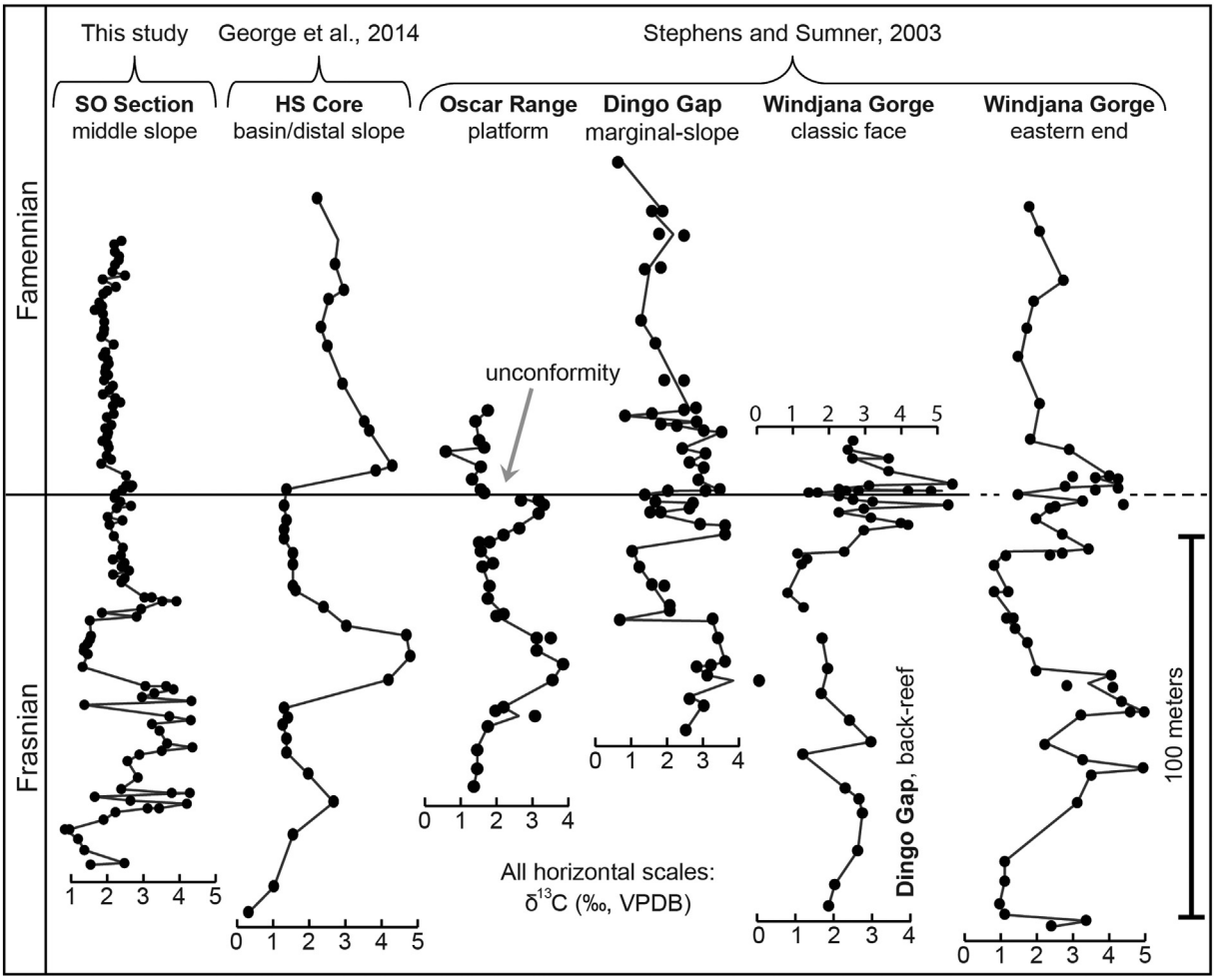

Fig. 6. Comparison of carbon isotope profiles and relative timing of $\delta^{13}C$ excursions (maximum values), from various studies in the Lennard Shelf carbonate system (Stephens and Sumner, 2003; George et al., 2014; this study).

Zone 13b to *crepida* Zone is <10 m thick) and exhibits maximum $\delta^{13}C$ values at or near the F–F boundary, typifying the problems created by condensed sections. We attribute these differences primarily to low sedimentation rates. While the presence of an end-Frasnian depositional hiatus or unconformity may also render isotopic records incomplete, there is no definitive evidence for this in our section. In the case of the South Oscar Range section studied by Stephens and Sumner (2003), a positive $\delta^{13}C$ excursion with maximum values below the F–F boundary was observed in platform-top settings, but its potential extent remains unknown due to a documented unconformity. In any case, the isotopic pattern observed at CL is more comparable to those reported from sections in Europe and Morocco (Fig. 5), possibly because the isotopic data associated with the Upper Kellwasser event in these regions are commonly derived from similarly condensed facies or incomplete sections.

In contrast to results from most geochemical studies during the Late Devonian, the low oxygen conditions recorded by the trace element data at SO do not appear to persist up to the F–F boundary; like the $\delta^{13}C$ data, they occur entirely within Frasnian conodont Zone 13b (Fig. 4). This finding is comparable to findings from the Great Basin in North America where anoxic conditions also pre-dated the F–F (Bratton et al., 1999). Evidence from the fossil record suggests that the most severe pulse of the Late Devonian mass extinction likewise occurred before the boundary (McGhee, 1996); many groups became extinct before the end of the Frasnian (brachiopods, Dutro, 1981) at the base of the Upper Kellwasser horizon including trilobites (e.g. Feist, 1991), goniatites (Becker and House, 1994), ostracods (Casier, 1987; Olempska, 2002), and rugose corals (Ma and Bai, 2002). In the Canning Basin, there also was a dramatic loss of conodont biodiversity at the end of conodont Zone 13b (Klapper, 2009) and a regional extinction of all ammonoid genera at the onset of 13c (Becker and House, 2009). Assuming that the global carbon pool indicates a return to less stressful conditions after the Upper Kellwasser and associated extinction events, but prior to the F–F boundary, the geological record from settings with more restricted water circulation would have experienced a lag in the recovery of $\delta^{13}C$ values to baseline values. Effectively, this lag would persist until early Famennian times due to the sequestration of some localities from the global marine carbon reservoir. On a basin scale, however, the lag in isotopic values would be contemporaneous and thus $\delta^{13}C$ trends would remain useful, at least as a regional correlation tool.

The paleogeography of the Late Devonian (Fig. 5) indicates varying potential for isolation of some regions from the marine carbon reservoir. For example, almost all European, North American, and North African sections were located in shallow, epicontinental settings at this time. Ongoing convergence between Laurussia and Gondwana forced the closing of the Rheic Ocean and constricted the southwestern part of the Paleotethys seaway (Keppie and Ramos, 1999; Stampfli et al., 2002; Torsvik et al., 2012). Shallow water settings in the affected regions became increasingly susceptible to the effects of the end-Frasnian regression and also experienced an increased influx of continentally derived material from weathering and erosion associated with active orogenies (e.g. Dalziel et al., 1994). Logically, carbonate sedimentation and reef development in these regions would have

been heavily influenced by local sources of dissolved inorganic carbon (DIC) and the development of low oxygen conditions in such relatively restricted settings. Comparatively, the Canning Basin had fewer external controls; the Lennard Shelf carbonate system experienced open circulation with sea water during the Late Devonian (Carpenter et al., 1991), and there were no active mountain building events in Western Australia during that time span (Plumb, 1979; Forman and Wales, 1981). Consequently, it's unlikely that our observed discrepancy in timing of the Upper Kellwasser was a product of regional scale variations in the DIC pool. Moreover, carbonate deposition, as it pertains to reef growth, may have been more prolific in the Canning Basin because periods of more stressful paleoenvironmental conditions were likely shorter lived.

4.2. Possible excursion mechanisms

The black shales and bituminous limestones characteristic of the Kellwasser horizons in Europe are commonly interpreted to have been deposited under reducing oceanic conditions during intervals of substantial carbon burial (Wilde and Berry, 1984; Joachimski and Buggisch, 1993; Becker and House, 1994; Wignall, 1994; Algeo et al., 1995). The geochemical results from this Lennard Shelf study are consistent with such a scenario. The pattern of trace elements in the SO section does not support persistent or pervasive anoxia, but the U/Th and V/Cr patterns do indicate stressed, reducing oceanic conditions concurrent with both excursions. The record of low oxygen conditions is clearer for the Upper Kellwasser interval with the more diffuse pattern from the Lower Kellwasser suggesting more intermittent periods of oxygen restriction. While middle-slope settings may reflect water oxygenation by deep currents, the megabreccia-dominated slope facies from which the Lower Kellwasser was analyzed likely indicate reefal collapse and re-deposition of platform-derived material, which may reflect more oxic conditions, within an overall anoxic environment (lower) on the slope.

Reduced oxygen levels in the SO section may be related to the prevalence of bottom-water anoxia in the deepest parts of the global ocean (e.g. Goodfellow et al., 1989). Decades of research have shown that the Frasnian stage is coincident with a globally warm climate, the proliferation of land plants, and eustatic sea level rise punctuated by transgressive-regressive cycles—conditions that are favorable to episodic ocean stratification and the formation of anoxia in deep-water settings (Brass et al., 1982; Johnson et al., 1985; Wilde and Berry, 1986; Tyson and Pearson, 1991; Algeo et al., 1995; Hallam and Wignall, 1999; Averbuch et al., 2005). Short-term transgressive pulses have been shown to correlate with the two Kellwasser excursions in both Europe (Johnson et al., 1996; Buggisch and Joachimski, 2006) and the Canning Basin (Stephens and Sumner, 2003). These transgressive episodes would result in a landward migration of oxygen-depleted waters from bathyal settings into shallower environments such as the Lennard Shelf System.

These findings that support anoxia contradict the conclusions of George et al. (2014), who described the positive excursions in the Lennard Shelf as occurring in "oxic facies." These authors hypothesized that the $\delta^{13}C$ anomalies could be attributed to an increase in biological productivity due to enhanced nutrient influxes from continental weathering during times of lowered relative sea level. While our geochemical results support a relative increase in marine productivity during the Upper Kellwasser interval, and perhaps to a lesser extent for the Lower Kellwasser, it seems unlikely that (regional) enhanced land-derived nutrient loading was the driving factor. Relatively distal sections, such as those on the lower slope and in the basin (i.e., section VHS of this study; George et al., 2014), are not typically affected by terrestrial influx; productivity blooms are commonly restricted to near-shore environments where the influence of continentally derived material is greatest (Riquier et al., 2006). The lack of active orogenies in Western Australia at this time further decreases the likelihood of extensive nutrient transport. A more probable explanation for the observed trace element pattern, at least for the Upper Kellwasser, is that localized phosphorous renewal under deep-water anoxic conditions led to eutrophication (Ingall and Jahnke, 1997), resulting in the expansion of oxygen-deprived water into shallower depositional settings. This hypothesis was similarly suggested for the Upper Kellwasser in the Harz Mountains of Germany by Riquier et al. (2006).

In the event that terrestrially sourced productivity was the primary driver of paleoenvironmental change and isotopic excursions recorded in the Lennard Shelf System, we would expect to see some vestige of the organic byproducts, particularly in sections (SO, WV) that have high sedimentation rates conducive to the preservation of organic matter (e.g. Muller and Suess, 1979; Sageman and Lyons, 2003) and which represent relatively proximal settings compared to the basinal core studied by George et al. (2014). However, no such organic-rich material was detected. The wholesale decomposition of organic material is unlikely, given that all isotopic profiles documented from the Lennard Shelf display no evidence of a ^{12}C influx from organic carbon remineralization (this study; Joachimski et al., 2002; Stephens and Sumner, 2003; George et al., 2014).

5. Conclusion

This work presents an integrated view from the northern margin of Gondwana, constraining the pattern of carbon isotope perturbations across the Frasnian–Famennian transition at the intra-zonal scale. The Lennard Shelf isotope record has been interpreted as a viable marine proxy that reflects global oceanic conditions and the burial of organic carbon in sedimentary basins elsewhere. Minor differences in the chemostratigraphic profiles notwithstanding, studies of the Canning Basin indicate depleted $\delta^{13}C$ values at or below the F–F boundary (Fig. 6). We propose that the relative depletion reflects a sudden decline in primary productivity at the end of the Frasnian, much like negative excursions observed at other mass extinction boundaries (e.g. Zachos et al., 1989; Holser, 1997; Galli et al., 2005; Stanley, 2010).

Despite the absence of lithological evidence for the well-known Kellwasser events, two positive $\delta^{13}C$ excursions have been identified from four Lennard shelf outcrops that are comparable in amplitude to Late Devonian sections around the world. Well-constrained biostratigraphy and magnetostratigraphy in the three stratigraphically expanded sections helped to constrain the Upper Kellwasser carbon isotope excursion (maximum values) to MN Zone 13b and thus differentiate it in time from the F–F boundary. These results suggest that major environmental and biotic stressors on the global marine carbon pool leading up to a mass extinction may have diminished before the F–F boundary itself. As a result, isotopic records with prolonged excursions into the Famennian may be experiencing a lag effect due to isolation of the DIC pool in more restricted, shallow-marine basins. These results demonstrate that isotopic data alone are insufficient to determine the position of a major mass extinction boundary in geological time. However, integrated data sets, such as the one presented in this study, demonstrate that $\delta^{13}C$ excursions, at least within a basin, can be used as chronostratigraphic markers and thus have utility for correlation.

Geochemical data for the Upper Kellwasser interval are most consistent with the interpretation that a globally warm climate and eustatic highs during the Late Devonian led to the formation of bottom-water anoxia in deep ocean basins that periodically spread into shallower settings on the Lennard Shelf via transgressive pulses and/or the development of eutrophic conditions due to phosphorous regeneration. These conditions are arguably widespread, but the Lennard Shelf is unique in that it records the global signal (geochemically) without accompanying lithological evidence (i.e. black shales). A similar scenario for the Lower Kellwasser is postulated although the role of eutrophication remains to be determined; as such, further trace element analyses are needed.

Acknowledgments

We are grateful to the Australian Research Council (grant LP0883812), MERIWA (grant M396), WAERA, CSIRO, Arc Energy, Chevron, NAI, and the ESS Department at the University of Washington; without their generous support, this work would not have been possible. A special thanks to Ray Addenbrooke, Kliti Grice, Jerone Hansma, Mitch Harris, Trevor Holland, Joe Kirschvink, Sergei Pisarevsky, Shane Schoepfer, and Tom Tobin for their assistance in the field and/or input during discussions. Additional thanks to the Geological Survey of Western Australia and Wundargoodie Aboriginal Safaris for their logistical support during field work. We would also like to acknowledge the UW IsoLab for their help with the many isotope analyses.

References

Adams, J.A.S., Weaver, C.E., 1958. Thorium-to-uranium ratios as indicators of sedimentary processes: example of concept of geochemical facies. AAPG Bull. 42, 387–430.
Algeo, T.J., Maynard, J.B., 2004. Trace-element behavior and redox facies in core shales of Upper Pennsylvanian Kansas-type cyclothems. Chem. Geol. 206, 289–318.
Algeo, T.J., Berner, R.A., Maynard, J.B., Scheckler, S.E., 1995. Late Devonian oceanic anoxic events and biotic crises: "rooted" in the evolution of vascular land plants? GSA Today 5 (45), 64–66.
Averbuch, O., Tribovillard, N., Devleeschouwer, X., Riquier, L., Mistiaen, B., van Vliet-Lanoe, B., 2005. Orogenic-induced continental weathering and organic carbon burial as major causes for climatic cooling at the Frasnian-Famennian boundary (ca 376 Ma BP). Terra Nova 17, 25–34.
Becker, R.T., House, M.R., 1994. Kellwasser events and goniatite successions in the Devonian of the Montagne Noire with comments on possible causations. Cour. Forsch.-Inst. Senckenberg 169, 45–77.
Becker, R.T., House, M.R., 1997. Sea level changes in the Upper Devonian of the Canning Basin, Western Australia. Cour. Forsch.-Inst. Senckenberg 199, 129–146.
Becker, R.T., House, M.R., 2009. Devonian ammonoid biostratigraphy of the Canning Basin. Devonian Reef Complexes of the Canning Basin, Western Australia. Geological Survey of Western Australia Bulletin, pp. 415–431.
Blakey, R., 2008. Gondwana paleogeography from assembly to breakup—a 500 my odyssey. Geol. Soc. Am. Spec. Pap. 441, 1–28.
Bond, D., Wignall, P.B., Racki, G., 2004. Extent and duration of marine anoxia during the Frasnian–Famennian (Late Devonian) mass extinction in Poland, Germany, Austria and France. Geol. Mag. 141, 173–193.
Brass, G.W., Southam, J.R., Peterson, W.H., 1982. Warm saline bottom water in the ancient ocean. Nature 296, 620–623.
Bratton, J.F., Berry, W.B.N., Morrow, J.R., 1999. Anoxia pre-dates Frasnian–Famennian boundary mass extinction horizon in the Great Basin, USA. Palaeogeogr. Palaeoclimatol. Palaeoecol. 154, 275–292.
Buggisch, W., 1991. The global Frasnian-Famennian»Kellwasser Event«. Geol. Rundsch. 80, 49–72.
Buggisch, W., Joachimski, M., 2006. Carbon isotope stratigraphy of the Devonian of Central and Southern Europe. Palaeogeogr. Palaeoclimatol. Palaeoecol. 240, 68–88.
Carpenter, S.J., Lohmann, K.C., Holden, P., Walter, L.M., Huston, T.J., Halliday, A.N., 1991. δ18O values, and Sr/Mg ratios of Late Devonian abiotic marine calcite: implications for the composition of ancient seawater. Geochim. Cosmochim. Acta 55.
Casier, J.G., 1987. Etude biostratigraphique et pal´eo´ecologique des ostracodes du r´ecif de marbre rouge du Hautmont `a Vodel´ee (partie sup´erieure du Frasnien, Bassin de Dinant, Belgique). Rev. Pal´eobiol. 6, 193–204.
Dalziel, I.W.D., Dalla Salda, L.H., Gahagan, L.M., 1994. Paleozoic Laurentia-Gondwana interaction and the origin of the Appalachian-Andean mountain system. Geol. Soc. Am. Bull. 106, 243–252.
Druce, E.C., 1976. Conodont biostratigraphy of the Upper Devonian reef complexes of the Canning Basin, Western Australia. Bull. Bur. Mineral Resour. Geol. Geophys. 158 (303 pp.).
Emerson, S.R., Huested, S.S., 1991. Ocean anoxia and the concentrations of molybdenum and vanadium in seawater. Mar. Chem. 34, 177–196.
Feist, R., 1985. Devonian stratigraphy of the Southeastern Montagne Noire (France). Cour. Forsch.-Inst. Senckenberg 75, 331–352.
Feist, R., 1991. The Late Devonian trilobite crisis. Hist. Biol. 5, 197–214.
Forman, D.J., Wales, D.W., 1981. Geological evolution of the Canning Basin, Western Australia. Bur. Miner. Resour. Aust. Bull. 210, 91.
Galli, M.T., Jadoul, F., Bernasconi, S.M., Weissert, H., 2005. Anomalies in global carbon cycling and extinction at the Triassic/Jurassic boundary: evidence from a marine C-isotope record. Palaeogeogr. Palaeoclimatol. Palaeoecol. 216, 203–214.
Geldsetzer, H.H.J., Goodfellow, W.D., McLaren, D.J., Orchard, M.J., 1987. Sulfur-isotope anomaly associated with the Frasnian-Famennian extinction, Medicine Lake, Alberta, Canada. Geology 15, 393–396.
Geldsetzer, H.H.J., Goodfellow, W.D., McLaren, D.J., 1993. The Frasnian-Famennian extinction event in a stable cratonic shelf setting: Trout River, Northwest Territories, Canada. Palaeogeogr. Palaeoclimatol. Palaeoecol. 104, 81–95.
George, A.D., Playford, P.E., Powell, C.M., Tornatora, P.M., 1997. Lithofacies and sequence development on an Upper Devonian mixed carbonate-siliciclastic fore-reef slope, Canning Basin, Western Australia. Sedimentology 44, 843–867.
George, A.D., Chow, N., Trinajstic, K.M., 2014. Oxic facies and the Late Devonian mass extinction, Canning Basin, Australia. Geology 42, 327–330.
Girard, C., Klapper, G., Feist, R., 2005. Subdivision of the terminal Frasnian linguiformis conodont Zone, revision of the correlative interval of Montagne Noire Zone 13, and discussion of stratigraphically significant associated trilobites. In: Over, J.D., Morrow, J.R., Wignall, P.B. (Eds.), Understanding Late Devonian and Permian-Triassic Biotic and Climatic Events: Towards an Integrated ApproachDevelopments in Palaeontology and Stratigraphy. Elsevier, pp. 181–198.
Glenister, B.F., Klapper, G., 1966. Upper Devonian conodonts from the Canning Basin, Western Australia. J. Paleontol. 40, 777–842.
Goodfellow, W.D., Geldsetzer, H.H.J., McLaren, D.J., Orchard, M.J., Klapper, G., 1988. The Frasnian–Famennian extinction: current results and possible causes. pp. 9–21.
Goodfellow, W.D., Geldsetzer, H.H.J., McLaren, D.J., Orchard, M.J., Klapper, G., 1989. Geochemical and isotopic anomalies associated with the Frasnian–Famennian extinction. Hist. Biol. 2, 51–72.
Guppy, D.J., Lindner, A.W., Rattigan, J.H., Casey, J.N., 1958. The geology of the Fitzroy Basin, Western Australia. Aust. Bur. Miner. Resour. Bull. 36, 116.
Hallam, A., Wignall, P.B., 1999. Mass extinctions and sea-level changes. Earth Sci. Rev. 48, 217–250.
Hansma, J., Tohver, E., Yan, M., Trinajstic, K., Roelofs, B., Peek, S., Slotznick, S., Kirschvink, J., Playton, T.E., Haines, P., Hocking, R.M., 2015. Late Devonian carbonate magnetostratigraphy from the Oscar and Horse Spring Ranges, Lennard Shelf, Canning Basin, Western Australia. Earth Planet. Sci. Lett. 409, 232–242.
Hillbun, K., Katz, D., Playton, T.E., Trinajstic, K., Machel, H.G., Haines, P., Hocking, R.M., Roelfs, B., Montgomery, P., Ward, P., 2015. Global and local controls on carbon isotope fractionation in Upper Devonian carbonates from the Lennard Shelf, Western Australia: a streamlined approach for generating primary marine secular curves for regional correlation. AAPG Bull (in revision).
Holser, W., 1997. Geochemical events documented in inorganic carbon isotopes. Palaeogeogr. Palaeoclimatol. Palaeoecol. 132, 173–182.
House, M.R., Becker, R.T., Feist, R., Flajs, G., Girard, C., Klapper, G., 2000. The Frasnian/Famennian boundary GSSP at Coumiac, southern France. Cour. Forsch.-Inst. Senckenberg 225, 59–75.
Ingall, E., Jahnke, R., 1997. Influence of water-column anoxia on the elemental fractionation of carbon and phosphorus during diagenesis. Mar. Geol. 139, 219–229.
Jarvis, I., Jarvis, K.E., 1995. Plasma spectrometry in earth sciences: techniques, applications and future trends. Chem. Geol. 95, 1–33.
Joachimski, M.M., Buggisch, W., 1993. Anoxic events in the late Frasnian—causes of the Frasnian–Famennian faunal crisis? Geology 21, 675–678.
Joachimski, M., Buggisch, W., Anders, T., 1994. Mikrofazies, Conodontenstratigraphie und Isotopengeochemie des Frasne/Famenne-Grenzprofils Wolayer Gletscher (Karnische Alpen). Jb. Geol. B.-A. 50, 183–195.
Joachimski, M.M., Pancost, R.D., Freeman, K.H., Ostertag-Henning, C., Buggisch, W., 2002. Carbon isotope geochemistry of the Frasnian–Famennian transition. Palaeogeogr. Palaeoclimatol. Palaeoecol. 181, 91–109.
Johnson, J.G., Klapper, G., Sandberg, C.A., 1985. Devonian eustatic fluctuations in Euramerica. Geol. Soc. Am. Bull. 96, 567–587.
Johnson, J.G., Klapper, G., Elrick, M., 1996. Devonian transgressive-regressive cycles and biostratigraphy, Northern Antelope Range, Nevada: establishment of reference horizons for global cycles. Palaios 11, 3–14.
Jones, B., Manning, D.A.C., 1994. Comparison of geochemical indices used for the interpretation of paleoredox conditions in ancient mudstone. Chem. Geol. 111, 111–129.
Kennard, J.M., Jackson, M.J., Romine, K.K., Shaw, R.D., Southgate, P.N., 1994. Depositional sequences and associated petroleum systems of the Canning Basin, WA. In: Purcell, P.G., Purcell, R.R. (Eds.), The Sedimentary Basins of Western Australia. Proceedings of Petroleum Exploration Society of Australia Symposium, Perth, WA, pp. 657–676.
Keppie, J.D., Ramos, V.A., 1999. Odyssey of terranes in the Iapetus and Rheic oceans during the Paleozoic. In: Ramos, V.A., Keppie, J.D. (Eds.), Laurentia-Gondwana Connections before Pangea. Geological Society of America Special Papers, pp. 267–276 Geological Society of America, Boulder, Colorado.
Klapper, G., 1989. The Montagne Noire Frasnian (Upper Devonian) conodont succession. Devonian World 3, 449–468.
Klapper, G., 2007. Frasnian (Upper Devonian) conodont succession at Horse Spring and correlative sections, Canning Basin, Western Australia. J. Paleontol. 81, 513–537.
Klapper, G., 2009. Upper Devonian conodonts in the Canning Basin. Devonian Reef Complexes of the Canning Basin, Western Australia. Geological Survey of Western Australia Bulletin, pp. 405–414.
Klapper, G., Feist, R., Becker, R.T., House, M.R., 1993. Definition of the Frasnian/Famennian Stage boundary. Episodes 16, 433–441.
Ma, X.P., Bai, S.L., 2002. Biological, depositional, microspherule, and geochemical records of the Frasnian/Famennian boundary beds, South China. Palaeogeogr. Palaeoclimatol. Palaeoecol. 181, 325–346.
McGhee, G.R., 1996. The Late Devonian mass extinction: the Frasnian/Famennian crisis. Columbia University Press, New York.
McGhee, G.R., Orth, C.J., Quintana, L.R., Gilmore, J.S., Olsen, E.J., 1986. Late Devonian "Kellwasser Event" mass-extinction horizon in Germany: no geochemical evidence for a large-body impact. Geology 14, 776–779.
Muchez, P., Boulvain, F., Dreesen, R., Hou, H.F., 1996. Sequence stratigraphy of the Frasnian–Famennian transitional strata: a comparison between South China and southern Belgium. Palaeogeogr. Palaeoclimatol. Palaeoecol. 123.
Muller, P.J., Suess, E., 1979. Producivity, sedimentation rate, and sedimentary organic matter in the oceans - I. Organic carbon preservation. Deep-Sea Res. 26, 1347–1362.
Nothdurft, L.D., Webb, G.E., Kamber, B.S., 2004. Rare earth element geochemistry of Late Devonian reefal carbonates, Canning Basin, Western Australia: confirmation of a seawater REE proxy in ancient limestones. Geochim. Cosmochim. Acta 68, 263–283.

Olempska, E., 2002. The Late Devonian Upper Kellwasser Event and entomozoacean ostracods in the Holy Cross Mountains, Poland. Acta Palaeontol. Pol. 47, 247–266.
Perkins, R.B., Piper, D.Z., Mason, C.E., 2008. Trace-element budgets in the Ohio/Sunbury shales of Kentucky: constraints on ocean circulation and primary productivity in the Devonian-Mississippian Appalachian Basin. Palaeogeogr. Palaeoclimatol. Palaeoecol. 265, 14–29.
Piper, D.Z., Perkins, R.B., 2004. A modem vs. Permian black shale—the hydrography, primary productivity, and water-column chemistry of deposition. Chem. Geol. 206, 177–197.
Playford, P.E., 1980. Devonian "great barrier reef" of Canning Basin, Western Australia. AAPG Bull. 64, 814–840.
Playford, P.E., Lowry, D.C., 1966. Devonian reef complexes of the Canning Basin, Western Australia. Bull. Geol. Surv. W. Aust. 118, 150.
Playford, P.E., Hocking, R.M., Cockbain, A.E., 2009. Devonian Reef complexes of the Canning Basin, Western Australia. Bull. Geol. Surv. W. Aust. 145.
Playton T. E. (2008) Characterization, variations, and controls of reef-rimmed carbonate foreslopes. Unpublished, The University of Texas at Austin.
Plumb, K.A., 1979. The tectonic evolution of Australia. Earth-Sci. Rev. 14, 205–249.
Rimmer, S.M., 2004. Geochemical paleoredox indicators in Devonian–Mississippian black shales, Central Appalachian Basin (USA). Chem. Geol. 206, 373–391.
Riquier, L., Tribovillard, N., Averbuch, O., Devleeschouwer, X., Riboulleau, A., 2006. The Late Frasnian Kellwasser horizons of the Harz Mountains (Germany): two oxygen-deficient periods resulting from different mechanisms. Chem. Geol. 233, 137–155.
Roelofs, B., Playton, T., Barham, M., Trinajstic, K., 2015. Upper Devonian microvertebrates from the Canning Basin, Western Australia. Acta Palaeontol. Pol. 65.
Sageman, B.B., Lyons, T.W., 2003. Geochemistry of fine-grained sediments and sedimentary rocks. Treatise Geochem. 7, 115–158.
Sandberg, C.A., Poole, F.G., Johnson, J.G., 1988. Upper Devonian of Western United States. pp. 183–220.
Sandberg, C.A., Morrow, J.R., Ziegler, W., 2002. Late Devonian sea-level changes, catastrophic events, and mass extinctions. Spec. Pap. Geol. Soc. Am. 473–488.
Sepkoski, J.J., 1986. Global bioevents and the question of periodicity. In: Walliser, O. (Ed.), Global bio-events. Springer-Verlag, Berlin, pp. 47–61.
Shaw, T.J., Geiskes, J.M., Jahnke, R., 1990. Early diagenesis in differing depositional environments: the response of transition metals in pore water. Geochim. Cosmochim. Acta 54, 1233–1246.
Stampfli, G.M., von Raumer, J.F., Borel, G.D., 2002. Paleozoic evolution of pre-Variscan terranes: from Gondwana to the Variscan collision. In: Martinez Catalan, J.R., Hatcher Jr., R.D., Arenas, R., Diaz Garcia, F. (Eds.), Variscan-Appalachian dynamics: The building of the late Paleozoic basement. Geological Society of America Special Papers Geological Society of America, Boulder, Colorado.
Stanley, S.M., 2010. Relation of Phanerozoic stable isotope excursions to climate, bacterial metabolism, and major extinctions. PNAS 107, 19185–19189.
Stephens, N.P., Sumner, D.Y., 2003. Late Devonian carbon isotope stratigraphy and sea level fluctuations, Canning Basin, Western Australia. Palaeogeogr. Palaeoclimatol. Palaeoecol. 191, 203–219.
Torsvik, T.H., Van Der Voo, R., Preeden, U., Mac, Niocaill C., Steinberger, B., Doubrovine, P.V., van Hinsbergen, D.J.J., Domeier, M., Gaina, C., Tohver, E., Meert, J.G., McCausland, P.J.A., Cocks, L.R.M., 2012. Phanerozoic polar wander, paleogeography and dynamics. Earth Sci. Rev. 114, 325–368.
Tribovillard, N., Algeo, T.J., Lyons, T.W., Riboulleau, A., 2006. Trace metals as paleoredox and paleoproductivity proxies: An update. Chem. Geol. 232, 12–32.
Tsikos, H., Jenkyns, H.C., Walsworth-Bell, B., Petrizzo, M.R., Forster, A., Kolonic, S., Erba, E., Premoli-Silva, E., Baas, M., Wagner, T., Sinninghe-Damste, J.S., 2004. Carbon-isotope stratigraphy recorded by the Cenomanian-Turonian Oceanic Anoxic Event: correlation and implications based on three key localities. J. Geol. Soc. Lond. 161, 711–719.
Tyson, R.V., Pearson, T.H., 1991. Modern and ancient continental shelf anoxia: an overview. Geol. Soc. Lond. 58, 1–24.
Van Geldern, R., Joachimski, M.M., Day, J., Jansen, U., Alvarez, F., Yolkin, E.A., Ma, X.P., 2006. Carbon, oxygen and strontium isotope records of Devonian brachiopod shell calcite. Palaeogeogr. Palaeoclimatol. Palaeoecol. 240, 47–67.
Veevers, J.J., Wells, A.T., 1961. The geology of the Canning Basin, Western Australia. Bureau of Mineral Resources, Geology and Geophysics.
Wagreich, M., 2009. Coniacian-Santonian oceanic red beds and their link to Oceanic Anoxic Event 3. In: Hu, X., Wang, C., Scott, R.W., Wagreich, M., Jansa, L. (Eds.), Cretaceous Oceanic Red Beds: Stratigraphy, Composition, Origins, and Paleoceanographic and Paleoclimatic Significance. SEPM Special Publication, pp. 235–242.
Wang, K., Orth, C.J., Attrep, M., Chatterton, B.D.E., Hou, H., Geldsetzer, H.H.J., 1991. Geochemical evidence for a catastrophic biotic event at the Frasnian/Famennian boundary in south China. Geology 19, 776–779.
Wang, K., Geldsetzer, H.H.J., Goodfellow, W.D., Krouse, H.R., 1996. Carbon and sulfur isotope anomalies across the Frasnian–Famennian extinction boundary, Alberta, Canada. Geology 24, 187–191.
Wendt, J., Belka, Z., 1991. Age and depositional environment of Upper Devonian (early Frasnian to early Famennian) black shales and limestones (Kellwasser Facies) in the eastern Anti-Atlas, Morocco. Facies 25, 51–90.
Wignall, P.B., 1994. Black shales. Oxford University Press, New York.
Wilde, P., Berry, W.B.N., 1984. Destabilization of the oceanic density structure and its significance to marine "Extinction" events. Palaeogeogr. Palaeoclimatol. Palaeoecol. 48, 143–162.
Wilde, P., Berry, W., 1986. The role of oceanographic factors in the generation of global bio-events. In: Walliser, O. (Ed.), Global Bio-EventsLecture Notes in Earth Sciences. Springer, Berlin/Heidelberg, pp. 75–91.
Xu, B., Gu, Z., Liu, Q., Wang, C., Li, Z., 2003. Carbon isotopic record from Upper Devonian carbonates at Dongcun in Guilin, southern China, supporting the world-wide pattern of carbon isotope excursions during Frasnian–Famennian transition. Chin. Sci. Bull. 48, 1259.
Zachos, J.C., Arthur, M.A., Dean, W.E., 1989. Geochemical evidence for suppression of pelagic marine productivity at the Cretaceous/Tertiary boundary. Nature 337, 61–64.
Ziegler, W., Sandberg, C.A., 1990. The Late Devonian standard conodont zonation. Cour. Forsch.-Inst. Senckenberg 121, 115.

Appendix 4

Playton, T.E., Tohver, E., Hillbun, K.,Hocking, R.M., Haines, P.W., Trinajstic, K., **Roelofs, B.,** Katz, D.A., Kirschvink, J., Grice, K., Montgomery, P., Hansma, J., Yan, M., Pisarevsky, S., Tulipani, S., Ratcliffe, R., Caulfield-Kerney, S. and Wray, D. 2016. Integrated Stratigraphic Correlation of Upper Devonian Platform-to-Basin Carbonate Sequences, Lennard Shelf, Canning Basin, Western Australia: Advances in Carbonate Margin-to-Slope Sequence Stratigraphy and Stacking Patterns. Society for Sedimentary Geology.

Integrated Stratigraphic Correlation of Upper Devonian Platform-to-Basin Carbonate Sequences, Lennard Shelf, Canning Basin, Western Australia: Advances in Carbonate Margin-to-Slope Sequence Stratigraphy and Stacking Patterns

Ted E. Playton[1], Eric Tohver[2], Kelly Hillbun[3], Roger M. Hocking[4], Peter W. Haines[4], Kate Trinajstic[5], Brett Roelofs[5], David A. Katz[6], Joseph Kirschvink[7], Kliti Grice[5], Paul Montgomery[8], Jeroen Hansma[2], Maodu Yan[9], Sergei Pisarevsky[2], Svenja Tulipani[5], Ken Ratcliffe[10], Samuel Caulfield-Kerney[11], David Wray[11]

[1]Tengizchevroil, Atyrau, Kazakhstan (research conducted while at Chevron Energy Technology Company, Houston, Texas, USA); [2]University of Western Australia, Perth, Western Australia; [3]Univeristy of Washington, Seattle, Washington; [4]Geological Survey of Western Australia, Perth, Western Australia; [5]Curtin University, Perth, Western Australia; [6]Whiting Petroleum, Denver, CO, USA; [7]California Institute of Technology, Pasadena, CA, USA; [8]Chevron Energy Technology Company, Houston, Texas, USA; [9]Institute for Tibetan Plateau Research, Beijing, China; [10]Chemostrat Ltd., Welshpool, UK; [11]University of Greenwich, Kent, UK

Abstract: High-resolution, time-significant correlations are integral to meaningful stratigraphic frameworks in depositional systems, but may be difficult to achieve using traditional sequence stratigraphic or biostratigraphic approaches alone, particularly in geologically complex settings. In steep, reefal carbonate margin-to-slope systems, such correlations are essential to unravel shelf-to-basin transitions, characterize strike variability, and develop predictive sequence stratigraphic models – concepts which are currently poorly understood in these heterogeneous settings. The Canning Basin Chronostratigraphy Project (CBCP) integrates multiple independent datasets (including biostratigraphy, magnetostratigraphy, stable isotope chemostratigraphy, and sequence

stratigraphy) extracted from Upper Devonian (Frasnian and Famennian) reefal platform exposures along the Lennard Shelf, Canning Basin, Western Australia. These were used to generate a well-constrained stratigraphic framework and shelf-to-basin composite reconstruction of the carbonate system.

The resultant integrated framework allows for unprecedented analysis of carbonate margin-to-slope heterogeneity, depositional architecture, and sequence stratigraphy along the Lennard Shelf. Systems tract architecture, facies partitioning, and stacking patterns of margin to lower-slope environments were assessed for six composite-scale sequences that form part of a transgressive-to-regressive supersequence and span the Frasnian-Famennian (F-F) biotic crisis. Variations are apparent in margin styles, foreslope facies proportions, dominant resedimentation processes, downslope contributing sediment factories, and vertical rock successions, related to hierarchical accommodation signals and ecological changes associated with F-F boundary. We present these results in the form of carbonate margin-to-basin sequence stratigraphic models and associations that link seismic-scale architecture to fine-scale facies heterogeneity. These models provide a predictive foundation for characterization of steep-sided flanks of reefal carbonate platform systems that is useful for both industry and academia. This study emphasizes the utility of an integrated stratigraphic approach and the insights gained from better-constrained facies and stratal architecture analysis; insights that were not achievable with traditional sequence stratigraphic or biostratigraphic techniques alone.

INTRODUCTION

Carbonate Slope Sequence Stratigraphy

Vertical stacking patterns used for sequence stratigraphic interpretation in carbonate platform-top settings have been well-established and used for decades (e.g., Goldhammer et al. 1990, Kerans and Nance 1991, Goldhammer et al. 1993, Kerans and Fitchen 1995, Read 1995, Kerans and Tinker 1997, Tinker 1998, Lehrmann and Goldhammer 1999). Trends in high-frequency cycle thickness, facies proportions, facies offset, diagnostic indicator facies, and exposure indices can be used to interpret sequences and systems tracts from one-dimensional successions of rock (Kerans and Tinker 1997). These patterns have been calibrated to two-dimensional sequence and systems tract architecture (e.g., Kerans 1995, Tinker 1998, Osleger and Tinker 1999, Kerans and Kempter 2002). Furthermore, it has been recognized that cycle types vary along the platform-top depositional profile (e.g., Kerans 1995, Kerans and Fitchen 1995) and high-frequency facies proportions can be partitioned by systems tract (Kerans 2002).

The best-constrained carbonate margin and slope sequence stratigraphic concepts are derived from the Modern and Recent, where depositional patterns and architectures can be linked rigorously to well-accepted proxies for eustatic sea level changes (e.g., Grammer and Ginsburg 1992, Droxler and Schlager 1985). Seminal concepts such as "highstand shedding" (Droxler and Schlager 1995) have been developed from these datasets. However, Modern and Recent datasets come with temporal and climatic limitations (e.g., tracking single high-frequency cycles or sequences within peak icehouse conditions, respectively) that may not be applicable throughout the entire rock record. Outcrop studies, encompassing more of the rock record and diverse climatic settings with different relative sea level behavior (e.g., Brown and Loucks 1993, Eberli et al. 1993, Fitchen et al. 1995, Janson et al. 2007), are also instructive. Yet, often these datasets lack the high-resolution constraints and physical linkages from slope to margin and/or platform-top settings required to reduce uncertainties in the sequence stratigraphic interpretation. Playton et al. (2010) provides a framework to describe carbonate margins and slopes in terms of their deposit types, margin styles, spatial architecture, and end-members, but does not discuss sequence stratigraphic relationships in detail.

In general, the architecture of sequences and systems tracts, and their internal facies stacking patterns and trends in proportions, are poorly understood for carbonate margin-to-basin settings and transitions. Playton and Kerans (2015 a, b) provide a detailed description of such relationships with Devonian examples from the Lennard Shelf and discuss the impact of long-term accommodation, ecological, and climatic controls on margin-to-slope sequence development. However, as is the case with other outcrop datasets, many stratigraphic relationships and reconstructions are inferred due to lack of continuous outcrop and/or low-resolution biostratigraphic data. The sequence stratigraphic models and concepts presented here build on those of Playton and Kerans (2015 a, b) and document additional constraint in the stratigraphic framework

developed through the Canning Basin Chronostratigraphy Project (CBCP).

Canning Basin Chronostratigraphy Project

Subsurface datasets do not typically provide the constraints necessary to correlate and characterize carbonate margin-slope-basin reservoir facies with certainty or at an adequate scale. Seismic data and biostratigraphic control are seldom at a desirable resolution, and rock data available through core has predictive limitations because sequence stratigraphic rules and stacking patterns are not sufficiently developed for reef, slope, and basinal settings. There is a need for improved characterization and predictive capabilities in these settings, with significant carbonate reservoirs or plays, such as 1) Tengiz and Karachaganak Fields, Kazakhstan (e.g., Collins et al. 2006, 2013, Katz et al. 2010) involving margin-to-middle-slope productive facies, 2) Poza Rica Field, Mexico and numerous examples in the Midland Basin, west Texas (e.g., Montgomery 1996, Janson et al. 2011, Clayton and Kerans 2013) that are conventional basin floor reservoirs, and 3) the "Wolfberry" play in the Midland Basin, west Texas (e.g., Bellian et al. 2012) which is an unconventional lower-slope to basin reservoir trend. The objective of the Canning Basin Chronostratigraphy Project (CBCP) is to generate a well-constrained chronostratigraphic framework through integration of multiple independent data types, with a focus on carbonate shelf-to-basin correlation and sequence architecture (Playton et al. 2013). Here, we use 'chronostratigraphic' to mean the identification and correlation of time-significant surfaces and time-equivalent intervals as constrained by multiple corroborating datasets. Correlations and frameworks are presented herein against stratigraphic thickness tied to well-established conodont biozones - not absolute time, as significant uncertainty remains in radiometric age dates at the high-frequency scale (i.e., biozone scale; e.g., Kaufmann 2006)

The well-preserved Middle to Upper Devonian (Givetian, Frasnian, and Famennian) carbonate outcrops of the Lennard Shelf, northeastern Canning Basin, Western Australia (Figure 1), were chosen to carry out this study. This exposure belt is optimal due to 1) minimal structural and diagenetic overprinting since deposition, 2) well-exposed platform-top, reef, slope, and basinal depositional settings, and 3) a well-established pre-existing geological foundation to leverage. This underpinning of previous work consists of more than five decades of research, comprehensively summarized by Playford et al. (this volume) and Playford et al. (2009), which provides a framework for basin development, structural setting, evolution of the reefal carbonate platforms, facies models, and numerous other characteristics of the depositional system along the Lennard Shelf. Another key advantage for the CBCP is a robust biostratigraphic framework from conodonts (e.g., Klapper 2007) cephalopods (e.g., Becker et al. 1993, Becker and House 1997), and other various vertebrates (e.g., Trinajstic and George 2009). Examples of other important work on the margins and slopes of the Lennard Shelf include Playford (1980, 1984), Kerans (1985), George et al. (1997), Ward (1999), Copp (2000), and Playton

(2008). However, these are still limited in terms of slope sequence stratigraphic understanding and margin to slope architecture due to the inability to correlate between localities or from coeval platform-top successions. Playton and Kerans (2015 a, b) contributed significantly to characterization of margin and slope settings along the Lennard Shelf within the supersequence framework and ecological context surrounding the Frasnian-Famennian (F-F) biotic crisis; however, their findings are limited to the coarse biostratigraphic resolution and lack of continuous outcrop common to all previous studies. This discontinuous nature of the Lennard Shelf outcrops and inability to walk out stratigraphic relationships introduces the need for using other independent constraints to link physically disconnected localities. In this sense, the correlation workflows established in this study are analogous and applicable to subsurface settings with interwell uncertainty.

Data for this study was collected 1) over 30+ Myr (Gradstein et al. 2012) of reefal platform development from the Givetian to Famennian to generate a regional stratigraphic framework for the system, 2) in platform-top, reef, slope, and basinal environments for correlation of depositional profiles, and 3) across different paleogeographic settings to demonstrate the viability of regional correlation. Hand samples and one-inch plugs were collected and tied to detailed sedimentological logs from outcrops, and shallow Winkie cores (tripod-mounted, small-scale coring system from the surface) and deep subsurface cores were also incorporated. The samples and cores were analyzed for magnetostratigraphy (polarity reversals and magnetic susceptibility), stable isotope chemostratigraphy (inorganic carbon and oxygen), elemental chemostratigraphy, conodont-fish biostratigraphy, biomarker and compound-specific geochemistry, and natural gamma ray profiles (Playton et al. 2013). This paper focuses on the integration of magnetostratigraphic, isotopic, biostratigraphic, and sequence stratigraphic constraints, as they proved most useful for regional correlation. Other integrated stratigraphic studies on carbonate systems have been carried out successfully (e.g., Montgomery et al. 2011, Davies et al. 2013), but do not rely as heavily on the specific integration of magnetostratigraphy, carbon isotope chemostratigraphy, biostratigraphy, and sequence stratigraphic concepts.

Geologic Setting and Scope

In the Middle Devonian, rifting generated deep troughs and structural highs in the eastern Canning Basin, now preserved in present-day northern Western Australia (Begg 1987; Drummond et al. 1991). The northwest-southeast trending Fitzroy Trough developed along the northeastern margin of the Canning Basin and was fringed to the north by shallow marine settings of the Lennard Shelf, which were preferred sites for land-attached and isolated carbonate platform development. The uplifted Precambrian hinterland of the Kimberley Block confined the Lennard Shelf to the northeast and supplied fine to coarse siliciclastics to the system throughout carbonate development (e.g., Playford 1980).

The reefal carbonate system along the Lennard Shelf represents a supersequence (Figure 2) spanning more than 25 Myr of time

(2nd-order of Sarg et al. 1999; after Playford et al. 2009, Playton and Kerans 2015 a, b; absolute age after Gradstein et al. 2012). Margins backstepped with intervening pulses of aggradation from the Givetian to Middle Frasnian, representing long-term high accommodation conditions of the supersequence TST. Just prior to the Middle-Upper Frasnian boundary, margins shifted from long-term aggradation and backstepping to progradation, representing the supersequence MFS. Finally, margins overall prograded from Late Frasnian to Middle Famennian time, representing long-term lower accommodation conditions of the supersequence HST.

Within the supersequence framework, a subordinate sequence architecture exists and is subdivided into five Givetian-Middle Frasnian backstepping and aggrading sequences (supersequence TST) and two prograding Upper Frasnian sequences (supersequence early HST; Figure 2) (after Playford et al. 2009, Playton and Kerans 2015 a, b). Famennian sequences that constitute the remainder of the supersequence HST are undefined; however, high-frequency sequences have been interpreted in middle-slope settings (Playton and Kerans 2015 b). The seven defined Givetian and Frasnian sequences are likely 3rd-order in duration (*sensu* Goldhammer et al. 1991), but due to inexact absolute age control, we will refer to them here as composite sequences with the recognition that they are components of supersequence systems tracts. We aim to use this existing supersequence and composite sequence framework for the Givetian and Frasnian and define the Famennian sequences that constitute the remainder of the supersequence HST, with the ultimate goal of establishing a hierarchical template to analyze carbonate shelf-to-basin facies arrangements and architecture.

Reefal assemblages in the Givetian and Frasnian consisted of stromatoporoids and corals with variable microbial components, and platform-top settings included skeletal-peloidal pack-grainstones, bioclastic rudstones, stromatoporoid boundstone biostromes, and muddier, peloidal subtidal and intertidal facies (Playford et al. 2009). In the Famennian, reefal margins had shifted entirely into microbial assemblages (Playford 1980), and platform tops became more oolitic (Frost 2007). Encrusted upper slope environments developed in the Late Frasnian and persisted throughout the Famennian, and detrital foreslope facies can be classified into debris-dominated, grain-dominated, and mud-dominated deposits (Playton 2010, Playton and Kerans 2015b).

Given the above-mentioned dramatic change in carbonate factories, another important factor in assessing margin-to-slope sequence development is the Frasnian-Famennian (F-F) interval. The F-F event is touted as the fifth largest Phanerozoic biotic crises, and had a substantial impact on reef-building biota in particular (for background, see Playford 1980, Raup and Sepkoski 1982, Playford et al. 2009, and Playton and Kerans 2015 b). Characterizing the composite sequences just prior to (Upper Frasnian Sequence 7; Figure 2) and immediately following (currently undefined) the F-F boundary, will help determine the impact of leadup and recovery phases surrounding this major extinction.

The carbonate system exposed along the Lennard Shelf provides an excellent opportunity to study carbonate margin and slope development within a combination of hierarchical accommodation and ecological controls, and the CBCP is designed to better analyze this through the addition of shelf-to-basin correlation constraints. Within the refined stratigraphic framework, we focus on margin-to-basin sequence architecture, margin styles, slope stacking patterns, and margin-to-slope facies heterogeneity. These margin-to-basin characteristics are described in terms of large-scale patterns, such as debris-, grain-, and mud-dominated slopes, and escarpment versus accretionary margins (after Playton et al. 2010). Given this dataset and objectives, we present herein:

1) a Lennard Shelf regional correlation framework and stratigraphic reference chart for the Late Devonian based on an integrated approach;

2) a well-constrained shelf-to-basin reconstruction of the Lennard Shelf, highlighting margin and slope development and sequence stratigraphic expression; and

3) an examination of carbonate slope sequences, systems tracts, and stacking patterns, with the aim of generating conceptual models and predictive relationships.

DATASET AND METHODOLOGY

Stratigraphic Transects and Sampling

The CBCP field data collection goal was to achieve detailed measuring and high-density sample coverage for shelf-to-basin carbonate environments (inner and outer platform-top, reef, slope, and basin) across the Middle-Late Devonian stages (Givetian, Frasnian, Famennian) exposed along the Lennard Shelf. Key outcrop transects (measured sections) with an appropriate degree of stratigraphic overlap were chosen to fulfill these coverage requirements, and shallow Winkie cores or subsurface cores were incorporated to fill in gaps in outcrop measured section availability (Figure 3). Samples collected were tied to detailed stratigraphic logs, including oriented outcrop plugs and hand samples (required for paleomagnetics), unoriented hand samples, and large slabs to document complex depositional fabrics. Shallow Winkie drilling provided oriented cores up to 40 meters from the surface, while subsurface cores made available up to 700 meters of unoriented stratigraphy. In total, nearly 6800 samples were collected and 4000 meters of stratigraphy were measured and described from 17 measured sections and cores along a 200 kilometer transect with 10-100 kilometer spacing (Table 1). Across the dataset, the average vertical sample spacing was 59 cm, with a range from 16 cm to 95 cm, and depositional environment and sedimentation rate was accounted for during collection to avoid data resolution biases; settings with interpreted low sedimentation rates (i.e., distal slope or basinal environments) were sampled at higher frequencies than those with high sedimentation rates (i.e., middle-slope grain-dominated or debris-dominated environments). Additionally, the matrix within debris deposits was targeted for collection while allochthonous blocks of resedimented, previously-lithified material were avoided, to minimize measurement

ambiguity in detrital slope facies. To ensure the desired sample coverage, key platform-top, margin, slope, and basin outcrop localities around the Lennard Shelf exposure belt were prioritized based on extent, exposure, preservation, and accessibility (Figure 4). Detailed facies schemes were developed to describe the dominant rock types, settings and processes along Givetian, Frasnian, and Famennian depositional profiles (Table 2; Figure 5). Appendices 1-14 contain the detailed sedimentary log, conodont control, stable carbon isotopic profile, paleomagnetic reversals, and interpreted sequence stratigraphy for each measured section and core, and provide summaries of location (Figure 1), paleogeography, age, facies assemblages, depositional environment(s), vertical succession, and lithology. Section names and mnemonics are informal terms as used in the field for ready reference to data transects.

Correlation Constraints

The refined regional stratigraphic framework presented here builds on the work of Playford et al. (2009) and Playton and Kerans (2015 a, b), and uses conodont biostratigraphy, paleomagnetic reversals, and stable carbon isotopes as the principal correlation constraints. These data all have global significance and their primary signals were well-preserved in enough instances to use with confidence. Elemental suites, magnetic susceptibility, outcrop gamma ray, biomarkers, and compound specific isotopes were less useful for regional stratigraphy due to commonly intermixed siliciclastics and uncommon organic-rich rocks, and thus not discussed here. Absolute dating via U-Pb geochronology was attempted on samples with little visible alteration and were selected from both platform-top sections (WNA and WNB; Appendices 2-3) and the purest carbonate section (SO; Appendix 6); however, results were erroneous or lacked the necessary precision, again due to the intermixing of siliciclastics inherent to the Lennard Shelf. The following sections summarize the key correlation constraints, including previous studies, CBCP contributions (Table 3), general methodology, and limitations.

Conodont Biostratigraphy

Middle-Late Devonian biozones, largely defined from conodonts and cephalopods, are well established globally from work in Europe, the Lennard Shelf, and other localities (Klapper 1989, Ziegler and Sandberg 1990, Becker et al. 1993, Klapper 1997, Girard et al. 2005, Klapper 2007, Trianjstic and George 2009). This enormous collection of past work around the world provides a high-quality foundation for the other datasets collected, such as paleomagnetic reversals and stable carbon isotopes. Although leveraging from previous work was critical, the CBCP rigorously collected additional conodonts (and less so fish) at each locality, tying into, infilling, and/or extending datasets from published accounts, or generating new biostratigraphic profiles in undocumented localities (Roelofs et al. 2015). Despite the robustness of conodont biostratigraphy, a fundamental limitation is the virtual absence of age-diagnostic species in shallower reefal margin or platform-top settings; the short-ranging

organisms useful for constraint preferred deeper slope and basinal settings. In addition to this restriction, certain paleogeographic settings appear to favor conodont abundance over others, as slope localities with associated narrow shelves and abundant siliciclastic influx are known for low yields of useable conodont remains. Thus, three measured sections served as the "reference conodont profiles" for the CBCP dataset (SO, VHS, and CL sections; Appendices 6-8), which were closely tied to the global references and provided biostratigraphic context to other constraints that could be cross-correlated to transects with lesser biostratigraphic control.

The two most significant global extinction events in the dataset, the Givetian-Frasnian (G-F) and Frasnian-Famennian (F-F) extinctions, were key biostratigraphic markers. The G-F faunal turnover is substantial in terms of biodiversity like the F-F, but is less understood and documented. The F-F boundary in the CBCP dataset is constrained to an interval less than 5.5 meters thick in the SO, VHS, and CL measured sections (Appendices 6-8), and has previously been resolved with centimeter-precision solely from conodonts (Klapper 2007). The G-F boundary, of lesser importance to this study than the F-F, has virtually no biostratigraphic control, but is picked in the lower few meters of the MR1 Winkie core (Appendix 11) based on a distinctive biomarker character (Tulipani et al. 2015), and in the PGH measured section (Appendix 9) based on very poorly-constrained vertical successions in coral morphology and assemblage.

Paleomagnetic Polarity Reversals

A somewhat unique strength of paleomagnetic polarity in terms of chronostratigraphic utility is that it is a truly global phenomenon that is independent of environment and setting. For much of the Phanerozoic geologic timescale, paleomagnetic polarity reversals are well-defined and can be used as a global reference; however, the Middle to Late Devonian global reversal record has to date been poorly defined (Gradstein et al. 2012). Thus, for the purposes of the CBCP, there was no available reference to reproduce, and consequently the Middle-Late Devonian paleomagnetic polarity record had to be generated via this dataset in order to achieve project success (Hansma et al. 2015). To accomplish this, chrons or chron packages (intervals of constant or distinctive mixed polarity) were identified that could be correlated across the dataset within tightly-constrained conodont control, with the limitation that biostratigraphic constraint was partial, confined to slope and basin transects. However, many of the key transects of the CBCP are in slope and basin positions, and these were sufficient to establish a composite reversal stratigraphy across the dataset. The episodic nature of resedimentation in these settings did not introduce significant uncertainty or noise in the correlations, as indicated by excellent repeatability around the dataset within conodont control. Hansma et al. (2015) describes in detail the intensive process carried out to ensure extraction of primary paleomagnetic signals.

Twenty-seven Givetian to Middle Famennian chrons or chron packages were established (modified after Hansma et al. 2015) that are tied to the conodont zones,

adding a significant amount of granularity to the Devonian global paleomagnetic record, and providing numerous additional correlation pinning points across the Lennard Shelf (Figure 6). Mixed polarity zones were encountered - meaning reversal rate was frequent but with a dominant interval polarity - and their bounds were correlated with confidence. However, their internal complexity was not always well-reproduced across the dataset.

Stable Carbon Isotopes

Unlike the Middle to Upper Devonian paleomagnetic global reference record prior to the CBCP, well-accepted and constrained secular stable inorganic carbon isotope curves have been assembled from datasets across the world (e.g., Joachimski et al. 2002; Bing et al. 2003; Buggisch and Joachimski 2006) and are available for correlation purposes. These reference curves exhibit well-expressed isotopic excursions that are closely tied to conodont biozones, occurrences of anoxic facies, and biotic events; this combination makes Devonian carbon isotopes excellent candidates for chronostratigraphic constraints. CBCP sampling relied heavily on slope and basin transects with the most conodont control to resolve these Middle-Upper Devonian carbon excursions. Carbon isotope signatures were well-reproduced across the dataset, despite the potential for discontinuous foreslope deposition.

In order to extract global isotopic excursions from the Lennard Shelf rocks, primary signals representing the Devonian ocean inorganic carbon pool must be collected, as overprints like meteoric or burial diagenesis and siliciclastic contamination can compromise the native marine signal. Thus, a rigorous quality control process was developed that handles extremely large datasets (thousands of samples) whilst effectively filtering out diagenetically-altered samples (see Hillbun et al. in review for details). This procedure results in high-confidence interpretations of isotopic profiles believed to represent the primary marine inorganic carbon character of the Devonian oceans. A limitation encountered was in platform-top settings, where pervasive meteoric diagenesis and siliciclastic contamination effectively polluted any remnant of the Devonian oceanic isotopic expression, thereby rendering stable carbon isotopes ineffective for chronostratigraphy (Hillbun et al. in review). Stable inorganic oxygen isotopes were incorporated into the quality control workflow as an indicator of certain styles of diagenesis.

Eleven stable inorganic carbon isotope excursions were identified and nine were correlated, within conodont control, across the dataset in the slope and basinal transects, providing an excellent suite of independent correlation constraints (Figure 6) (after Hillbun 2015, Hillbun et al. 2015, in review). Four of the excursions are documented global events from previous studies (falsiovalis, Lower and Upper Kellwasser, and Enkeberg events, after Buggisch and Joachimski 2006), two of which were identified in only one transect and therefore not reproducible across the dataset. The remaining seven were correlatable around the CBCP dataset but not defined consistently in other studies, either elsewhere around the world or along the Lennard Shelf.

Lennard Shelf Regional Stratigraphy and Reconstruction

To construct a regional framework, we honored multiple independent signals embedded in the rock record in conjunction with sequence stratigraphic concepts to interpret and correlate time-significant surfaces across the Lenard Shelf. The end-product, a predictive sequence stratigraphic framework, abides by all constraints, but is ultimately governed by the sedimentology of the rocks and the observed stratigraphic relationships. Due to the nature of the Lennard Shelf outcrop belt (Figure 1), transect localities are physically disconnected over great distances (i.e., walkout ties were impossible across major localities) and correlation solutions are non-unique – a challenge also inherent in subsurface datasets. However, the agreement of multiple independent data types greatly reduces the range of possibilities and uncertainty in making correlation decisions.

Degree of Confidence and Limitations

As in every dataset, the CBCP dataset has gaps, limitations, and uncertainties where assumptions and less-constrained interpretations are required. In particular, the CBCP dataset works with globally-recognized events and intervals that impart a high degree of confidence, but also utilizes lower-confidence regional signals and assumed global signals that were not previously defined (Table 4). The globally-defined conodont biozones and Lower and Upper Kellwasser isotope excursions are the highest confidence anchors of the regional framework (Table 3). However, regional isotope excursions (those that correlate across the Lennard Shelf but are not recognized globally) and the polarity reversal record also serves as an important set of pinning points for correlation; although not global, their repeatability across the dataset lends credibility for use as chronostratigraphic constraints. The CBCP polarity reversal record is a special case in that a global reference for this time period was previously undefined, and this larger study establishes it for the first time (Hansma et al. 2015). Accordingly, the transects of the CBCP had a range of utility (Table 4), some with very little control (e.g., PGH, UD2, HD14; Appendices 9, 13, and 14) but still proved useful in the final reconstruction, and some that serve as cornerstones (reference transects) for the framework to which the other transects are tied (WNA, WNB, SO, VHS, CL, MR1; Appendices 2, 3, 6, 7, 8, and 11).

Three key interlinked limitations, some of which are unique to the CBCP, presented challenges with respect to shelf-to-basin correlation, related to: 1) extraction of conodont data for biostratigraphy; 2) preservation of primary carbon isotope signals; and 3) stacking pattern criteria for sequence stratigraphic interpretation. Platform-top settings were practically devoid of any useful conodont or isotopic information for correlation. Despite these limitations, the platform-top transects exhibited clean reversal records and importantly contain stacking pattern information that was valuable for sequence

stratigraphic interpretation. One dimensional stacking pattern analysis, utilizing criteria such as facies proportions, facies offset, cycle thickness, indicator facies, and exposure indicators (*sensu* Kerans and Tinker 1997), was performed in platform-top transects to identify systems tracts, sequence boundaries, and maximum flooding surfaces. Presence and thickness of stromatoporoid bioherms and laminated or fenestral tidal flats proved to be a critical indicator facies for stacking pattern analysis, and the proportion of open marine versus restricted rock types was a key parameter to define cycles and systems tracts. The proportions of shallow marine siliciclastics were less useful, however, due to their highly localized nature, inconsistency relative to carbonate shallowing or deepening trends, and seemingly sporadic influx across the narrow carbonate shelf. Unlike these tools available for platform-top sequence interpretation, the CBCP slope transects, consisting of resedimented material and microbially-encrusted deposits, exhibit successions that are poorly understood with respect to sequence stratigraphy; the advantage of the slope transects are the pristinely-preserved carbon isotope records and abundant biostratigraphic control. Integrating the CBCP dataset therefore required consolidation of multiple signals, each with differing degrees of confidence and utility, based upon the section type and/or setting being interpreted. Differences in information preservation and quality amongst the variable environments are common for any dataset, and underscore the power of integrating multiple constraints to develop a regional framework.

Platform-to-Slope Correlation and Slope Sequence Stratigraphy

Considering the above, the following limitations posed a challenge when correlating platform sections to slope sections: 1) without biostratigraphic control in the platform-top, it was unclear how to correlate reversals into the slope, and 2) picking sequence stratigraphic surfaces and systems tracts in the slope was difficult as slope stacking patterns are not well-established. To overcome this, beds were physically traced from the platform-top sections (WNA and WNB sections; Appendices 2-3) into a key nearby outcrop exposure, the Classic Face in Windjana Gorge (Figure 7). The Classic Face is a world-class locality for observing carbonate platform-to-slope transitions across the long-term shift from margin aggradation to progradation (see Playford et al. 2009, Playton and Kerans 2015 a). There are key geometries in the Classic Face that allow confident placement into the supersequence architecture (Figure 2), as well as some surrounding biostratigraphic pinning points. This linkage to the sequence succession defined at the Classic Face allowed for extrapolation of coarse age information to the otherwise temporally-unconstrained platform-top transects. These coarse constraints were sufficient to correlate reversals from platform-top to slope sections, thereby linking more robust age control into the shallower settings and extending sequence stratigraphic interpretations into the slope. In slope intervals with no platform-top equivalents within the dataset, the F-F boundary, identified by conodonts, was also a key marker to hinge sequence stratigraphic interpretations from, as it is a significant

sequence boundary (Playford et al. 2009). Additionally, the Kellwasser events are interpreted to be coincident with MFSs in multiple studies (e.g., Buggisch and Joachimski 2006).

The application of platform-constrained sequence stratigraphic interpretations, and other pinning points, to the slope allowed for examination of slope stacking patterns, systems tracts, and sequence development. In doing so, an empirical relationship was extracted that links carbon isotopic trends to slope sequence stratigraphy (Hillbun et al. this volume). A commonly observed pattern was carbon isotope values trending positive during Frasnian sequence TSTs, and negative during HSTs. MFSs tended to be associated with carbon isotope value maxima and SBs with carbon isotope value minima. The model to explain this linkage between the oceanic carbon pool and sequence stratigraphy along the Lennard Shelf is discussed in Hillbun et al. (this volume) and entails changes in circulation patterns during TST versus HST settings (after Katz et al. 2007). This relationship was independently observed enough times that a proxy was developed for a slope sequence stratigraphic interpretation method that utilizes carbon isotope trends when stratigraphic overlap to platform-top equivalents was not possible. This provides another valuable tool for generating the sequence stratigraphic framework and extrapolating platform-top defined sequences to multiple slope sections across the dataset.

Development of the Lennard Shelf Framework and Reconstruction

Employing the above methods, an integrated stratigraphy was generated that links all time-significant markers and intervals with a conforming sequence stratigraphic framework for the Middle-Late Devonian of the Lennard Shelf (Figure 8). The workflow used to incorporate components and arrive at a final stratigraphic framework is as follows:

1) define the underpinning biostratigraphic constraints in slope and basin transects;
2) within biostratigraphic control, identify and correlate global isotope excursions in slope and basin transects;
3) within biostratigraphic and global isotopic control, correlate through-going polarity reversal packages across slope and basin transects;
4) utilize sparse age information extrapolated from nearby key outcrops (Classic Face, Windjana Gorge; Figure 7) and correlate platform-top reversals to slope and basin reversals;
5) within biostratigraphic, isotopic, and established polarity reversal control, identify and correlate regional isotope excursions in slope and basin transects; and
6) interpret a conforming sequence stratigraphic framework based on sedimentology that honors all established constraints, considers the various degrees of confidence around the dataset, and utilizes the proxies developed that link isotopic expression in the slope with systems tracts.

This process involved integration and iteration at each step to find the best correlation solution where all constraints agreed within the flexibility of the

components and dataset. Conodont picks and the two global carbon isotope excursions of the dataset (Lower and Upper Kellwasser events) were firm markers with virtually no flexibility during iteration; however, the exact placement of paleomagnetic chron boundaries could vary (up to tens of meters in some cases) between sample points and depending on the interpreted limits of mixed polarity packages. Similarly, regional isotope excursions in stratigraphically-expanded sections within a single conodont biozone occasionally had more than one correlation possibility. In terms of sequence stratigraphy, platform-top sections were fixed benchmarks for the slope where there was stratigraphic overlap, but isotopic expression provided constraint for sequence definition away from platform control. These combinations of relatively precise and broad controls gave flexibility in iteration to a final set of constraints and sequence stratigraphy, where all pinning points were honored and in agreement (with none violated). There were no cases where constraints overrode others of equal confidence to establish correlation, and the rocks themselves were used for sequence interpretation only within the boundaries of the surrounding controls (i.e., conceptual sequence models did not govern the interpretation of the constraints). This agreement across multiple independent data types built confidence that the chronostratigraphic signals were uncompromised and the sequence stratigraphic framework is valid.

Once completed, the finalized suite of correlations and pinning points allowed the construction of an improved Middle-Late Devonian stratigraphic chart that highlights the qualitative age relationships between conodont biozones, polarity reversals, carbon isotope events, and carbonate sequence development (Figure 6). Twenty-seven paleomagnetic chrons were defined, about two thirds of which are considered medium-high confidence and correlatable across the dataset, with the remainder likely valid but not defendable due to lack of stratigraphic overlap. Eleven carbon isotope events were defined, with two linked to the global reference and considered as high-confidence, seven considered as medium-high confidence with repeatability around the dataset but not linked to the global reference, and two of lower-confidence due to lack of stratigraphic overlap but linked to the global reference. Twelve composite sequences (likely 3rd-order; *sensu* Goldhammer et al. 1991) and their systems tracts were identified; two in the Givetian, seven in the Frasnian (after Playton 2008, Playford et al. 2009, Playton and Kerans 2015 a, b), and three in the Famennian. Well-constrained sequence stratigraphic interpretations in Middle Frasnian to Middle Famennian upper, middle, and lower slope, and basinal settings were achieved for the first time. The Givetian sequences were largely defined by one-dimensional, platform-top stacking pattern analysis and not tied to any pre-existing framework, whereas Frasnian Sequences 1-3 were poorly sampled in this study and based largely on Playford et al. (2009). Frasnian Sequences 4-7 were refined after Playford et al. (2009) and Playton and Kerans (2015a), and very well constrained in this study. The Middle-Upper Frasnian boundary was here placed within the composite HST of Sequence 5, slightly different than previous studies

which defined it at the top of Sequence 5 (Playford et al. 2009, Playton and Kerans 2015 a). Famennian Sequences 1-3 are well-constrained and defined here for the first time. Sequences could not be distinguished for a portion of the Middle Famennian due to facies homogeneity from pervasive calcimicrobial encrustation and lack of stratigraphic overlap across the dataset ("MFa" in Figure 6, "Sequences" column). In general, the stratigraphic framework defined here is considered high confidence for Middle Frasnian to Middle Famennian time. Givetian, Early Frasnian, and Middle Famennian (MFa) intervals were well-sampled and contributed robust data profiles, but either lacked sufficient stratigraphic overlap with other transects for repeatability or had insufficient biostratigraphic control to be considered higher confidence.

In addition to regional correlations and stratigraphic relationships, this linkage of physically disconnected localities allows for the development of new representations of the Lennard Shelf Devonian carbonate system. The significantly increased correlation control provides an opportunity to reconstruct the carbonate system with greater accuracy than before, both in terms of scale and the actual geometrical relationships of the shelf-to-basin stratigraphic system and sequence architecture (Figures 9 and 10). Although the dataset, as a whole, trends mostly along the strike of the Devonian carbonate system (Figure 1), a fairly uniform sampling of the different depositional environments allows for reconstruction of a collapsed, dip-oriented composite regional cross section. In addition to the integrated stratigraphic constraints, reconstruction of the stratal architecture entailed 1) honoring the actual transect surface topography and depositional dip data collected along transects (corrected for tilt through geopetal measurement), 2) the use of previous work to follow the large-scale backstepping to prograding evolution (Playford et al. 2009), and 3) estimates of platform thicknesses, backstepping distances, underlying topography, and spatial transect placement. Once the stratal framework was constructed true to scale and with no vertical exaggeration, rock data along transects were control points for interpreting the shelf-to-basin facies distributions.

These results advance our understanding and ability to characterize the carbonate system along the Lennard Shelf in several respects (Table 5), including: 1) high-resolution correlation of disconnected localities over approximately 200 kilometers (previously not possible), spanning the Windjana Gorge, South Oscar Range, Horse Spring, and Casey Falls areas; 2) upper-middle-lower-slope and basin correlation for the Middle Frasnian to Middle Famennian and platform to basin correlation across the supersequence MFS; 3) scaled shelf to basin composite reconstruction of the system tied to numerous transects and honoring all depositional information; 4) refinement of the Frasnian composite sequences and their relationship with the conodont zones; 5) definition of three Lower to Middle Famennian composite sequences and their systems tracts; and 6) definition of the expression of sequences and systems tracts within slope strata. A detailed comparison between the results of this study and the interpretations of Playton and Kerans (2015 a, b) are presented later (see Discussion),

focusing on aggradational escarpments during supersequence TSTs, periods of sustained collapse around supersequence MFSs, pre- and post-F-F-extinction impacts on slope deposition, and hierarchical trends observed in slope deposits.

In addition to the above, recognition of a conspicuous Middle Famennian interval (MFa; Figures 6 and 9, Table 5) warrants extra discussion and requires further work. This progradational interval appears to represent a Famennian carbonate system that evolved into one dominated by platform-top grain shedding with simultaneous, extensive microbial encrustation down to water depths not observed in any other outcrop or subsurface datasets (>> 500 meters downslope; see Playton et al. 2010, Playton and Kerans 2015 b for discussion of deep boundstone margin analogs). We are unable to further delineate the MFa internally due to lack of stratigraphic overlap (CL Section contains the only record; Appendix 8) and a grain-dominated boundstone-encrusted grainstone succession that obscures facies stacking analysis. However, Hillbun et al. (this volume) subdivides the MFa interval into four composite sequences (Famennian sequences 4-7; see their Figures 2 and 6) based solely on isotopic expression observed in the CL measured section (Appendix 8) and the proxy developed for systems tract interpretation in slope settings. Despite the many remaining questions on this peculiar interval, the MFa marks the final phase of reefal platform development along the Lennard Shelf prior to transition into a more cold-water-assemblage, distally-steepened ramp of the Late Famennian-Tournaisian (Fairfield Group; Playford et al. 2009).

MARGIN-TO-BASIN SEQUENCE STRATIGRAPHIC MODELS

The resultant reconstructed shelf-to-basin sequence architecture and facies mosaic depiction of the Lennard Shelf highlights slope types and margin styles across the Middle-Late Devonian supersequence and Frasnian-Famennian extinction interval. It also allows a spectrum of analysis and comparisons not previously possible. The following sections will describe in detail the development of six composite sequences, the Frasnian 4-7 and Famennian 1-2 sequences, as they evolved from supersequence TST, MFS, and HST accommodation conditions, and as they progressed through the lead-up and recovery periods associated with the F-F extinction (Figures 9 and 10).

Lower-Middle Frasnian Composite Sequence 4

Lower-Middle Frasnian Sequence 4 was deposited in the supersequence TST when margins and sequences backstepped relative to one another with intervening pulses of aggradation (Figure 10). The TST of Sequence 4 exhibits the development of a growth escarpment (after Playton et al. 2010), where vertical margin aggradation eventually outpaced its coeval foreslope deposits resulting in onlapping slope stratal geometries (Figure 11A). The overall setting was stable as the margin stacked vertically upon solid underlying foundations. Consequently, foreslopes were grain-dominated from platform-top shedding, with little debris generated from collapse. However, there was a point when the vertical escarpment margin

constructed enough relief and slope profiles became significantly underfilled such that the profile became highly susceptible to collapse triggers. During this time in the Late TST, the margin tended to fail at various points along strike, generating reentrant paleogeography and debris deposits that came to rest on the slope and periodically in the basin (Figure 11B). At the MFS, the margin backstepped and reinitiated landward of the previous margin and began to construct relief (Figure 11C). Foreslope systems were poorly developed at this time and composed of a grain-dominated veneer that draped the former slope profile and infilled around debris topography. In the HST, margins were accretionary, weakly prograded, and maintained stability due to the solid substrate of the relict platform-top; thus, foreslopes were grain-dominated from platform-top shedding and contained little debris from margin collapse (Figure 11D). Variations in this sequence model entail greater backstepping distances where weakly prograding HSTs did not advance to the former margin, producing a net backstepped sequence (see Playton and Kerans 2015 a).

The most distinctive stacking pattern is best expressed in the middle slope and is symmetrical, with a concentration of debris just beneath the MFS that is bracketed below and above by grain-dominated deposits (Figures 12 and 13A). This particular pattern is dependent on the position, in both a dip and strike sense, of the debris accumulation as they were strike discontinuous and could occur kilometers into the basin or freeze in steeper middle-slope settings. Thus, in some cases the entire middle-slope sequence may consist only of stacked grain-dominated deposits. The margin also exhibits an obvious stacking pattern with slope deposits overlying platform-top facies, highlighting backstepping at the MFS. A shallowing upward succession, often comprised of sediment gravity flows overlain by *in situ* margin deposits, is common above the previously transgressed platform-top facies. The silt-dominated basinal setting does not display a clear stacking pattern, but slight increases in grain content are observed immediately beneath the MFS and in the Late HST, possibly reflecting very distal equivalents of debris deposition and maximum progradational extent, respectively.

Middle-Upper Frasnian Composite Sequence 5

Middle-Upper Frasnian Sequence 5 is where the supersequence MFS is defined; the point where margins began to shift from long-term backstepping and aggradation to progradation (Figure 10). In the Early TST of Sequence 5, aggradational escarpments were again developed through vertical aggradation of the margin and the inability of foreslope deposits to fill the slope profile to the level of the coeval margin; this underfilling was amplified due to the inherited relief from underlying backstepped topography (Figure 14A). This style of vertical margin growth was initially stable, and grain-dominated slopes developed accordingly. By Late TST time, the margin had constructed considerable relief, the slope profile was substantially underfilled, and margins were consequently more likely to collapse (Figure 14B). Hence, margins underwent sustained mass wasting and evolved into an erosional escarpment

with associated debris-dominated slopes that onlapped lower down in the profile. In the HST of Sequence 5, margins, already unstable, were unable to prograde over dramatically underfilled profiles with insufficient substrate. This resulted in sustained instability and mass wasting, debris-dominated slope development, and the continuation of an erosional escarpment margin configuration (Figures 13C and 14C).

Most of the slope consists of thick, amalgamated successions of debris with unclear stacking organization (Figure 15). At the margin, scarps of truncated platform strata with onlapping debris are observed (Figure 13C). The lower slope records the grain-dominated toesets that are equivalent to updip debris. A more silt-dominated interval (silt-sized carbonate and quartz grains) brackets the MFS, producing a symmetrical stacking pattern; the lack of grainy material around the MFS may indicate backfilling of the slope in an updip position at that time. The basinal setting is again not highly diagnostic, but shows a vague upward decrease in silt content starting within the TST; this timing may be coeval with the onset of escarpment mass wasting and is reflected in the basin with a slight increase in grain export.

Upper Frasnian Composite Sequence 6

Upper Frasnian Sequence 6 is in the Early HST of the supersequence, when margins were unable to prograde, despite lower-accommodation conditions, due to inherited underfilled profiles with inadequate substrates to support progradation (Figure 10). The TST of Sequence 6 inherited the highly unstable profile from Sequence 5, prompting continued mass wasting during aggradation and an erosional escarpment configuration with associated debris-dominated foreslopes (Figure 16A). In the Early HST, margins were able to prograde to a point, but subsequently failed; this occurred in pulses and episodically as the system neared the final stages of slope regrading and equilibration (Figure 16B). These represent the last phases of downslope debris shedding and completion of slope profile infilling such that an angle-of-repose substrate was established for progradation. Once the debris substrate was fully developed by the Late HST, the margin was able to prograde and evolved into an accretionary margin with shelf-to-slope interfingering relationships (Figure 16C). During this final stage of Sequence 6, slopes were grain-dominated reflecting the margin had reached stability (Figure 13B, D).

Sequence 6 stacking patterns for middle- and upper-slope settings exhibit an upward transition from debris-dominated to grain-dominated deposits, reflecting the shift from mass wasting to stable progradation (Figures 13B, D and 17). Boundstone tongues are also observed in upper-slope successions during the early pulses of progradation in the Early HST. Lower-slope and basinal settings both display upward increases in platform-top derived material, again reflecting updip debris backfilling processes that transition into offbank shedding during progradation. In lower-slope settings during the TST, microbial boundstone bioherms occur locally, creating positive topography within a more silt-dominated seascape; thus, lower-slope TST stacking patterns can vary laterally from purely boundstone to silty strata.

Upper Frasnian Composite Sequence 7

Upper Frasnian Sequence 7 is in the Early HST of the supersequence, when margins were stably prograding; however, this sequence was also the prelude to the F-F boundary when changing ecological variables were beginning to affect sediment factories that contribute to slope and basin deposition (Figure 10). The TST of Sequence 7 exhibits an aggradational margin with a significantly expanded upper-slope microbial boundstone setting where encrustation became dominant up to 200 meters downslope from the platform edge, based on reconstructed water depth (Figures 13D and 18A). A unique upper-middle-slope style also developed, comprised of a mixed siliciclastic-carbonate silt-dominated terrain with numerous gullies that served as conduits for bypassing material. The middle slope is accordingly grain-dominated as it was the recipient of the bypassed material, although these grain-dominated deposits are conspicuously micro-peloidal with intermixed silt (versus more typical skeletal-peloidal-coated grain assemblages; Figure 13B). In general, the TST slopes were rather poorly developed, with representative grain and debris contributors evidently subdued in productivity and/or downslope shedding. The HST of Sequence 7 exhibits fairly strong margin progradation and maintains the deep microbial boundstone upper-slope factory (Figure 18B). The slopes were mixed debris- and grain-dominated, indicating more typical platform-top and margin shedding processes had resumed after the TST.

The stacking patterns of Sequence 7 (Figure 19) are symmetrical in the lower and middle slope, in that debris deposits are concentrated in the Early HST, possibly indicating greater margin instability at the onset of composite-scale progradation. The TSTs of middle- and lower-slope settings will vary in character (thus the stacking pattern will vary) depending on the exact profile position of the silt-dominated gullied slope setting or downdip grain-dominated apron. The Late HSTs of middle- and lower-slope settings tend to both exhibit upward successions from grain- to mud-dominated deposits, possibly reflecting the gradual decline of platform-top carbonate factory production as the F-F event was approached. Upper-slope stacking is unclear as it consists dominantly of boundstone related to the development of a well-established encrusted upper-slope setting. Basinal patterns exhibit an upward increase in grain content relative to silt, probably again reflecting an increase in offbank shedding throughout the sequence.

Lower Famennian Composite Sequence 1

The first composite sequence in the Famennian was progradational as forced by the supersequence HST setting, and represented the recovery period after the F-F extinction (Figure 10). The TST of Famennian Sequence 1 has a peculiar architecture with a middle slope thicker than its equivalent upper slope (Figure 20A). The upper slope reconstructs to be a thin, yet still deep on the slope, veneer of microbial boundstone. The middle slope was dominated by an anomalously thick stack of oolitic-coated grain grainstone, and the lower slope

was grain-dominated but with an unusual proportion of debris deposits. We interpret these characteristics together to indicate that the TST of Sequence 1 was a time of subdued margin growth, with slope bypass of material from dominantly platform-top ooid factories. The HST of Sequence 1 was progradational with a deep boundstone margin, foreslopes that contained substantially more debris deposits than in the TST, and an overall basinward-fining pattern from debris-rich to grain-dominated to mud-dominated assemblages (Figure 20B).

The upper slope of Sequence 1 displays rather undiagnostic stacking patterns with interbedded debris and boundstone (Figure 21), but the middle slope exhibits a clear asymmetrical pattern with a thick grain-dominated TST and thinner, more debris-rich HST. Lower-slope stacking is also asymmetrical but in the opposite sense, with greater debris proportions in the TST and an upward transition from grain- to mud-dominated deposits in the HST. Basinal stacking displays increased skeletal content in the HST, possibly reflecting recovery of some faunal groups subsequent to the extinction.

Lower-Middle Famennian Composite Sequence 2

Famennian Sequence 2 was strongly progradational as it was in the heart of the supersequence HST, and deposited long after the F-F biotic crisis, when carbonate factories presumably were functioning at full capacity (Figure 10). The TST margin of Sequence 2 is interpreted to have an aggradational component, but also reconstructs to have been weakly progradational, reflecting the longer-term forcing of the supersequence HST (Figure 22A). The sustained deep microbial boundstone factory also contributed to progradation during the TST. TST foreslopes, however, were overall grain-dominated, suggesting a net stability of the margin, some progradation notwithstanding. The HST of Sequence 2 exhibited strong progradation of the deep microbial margin and upper slope, which resulted in episodic instability, collapse, and consequent debris tongue deposition on the slope. The foreslopes generated, thus, were mixtures of grain-dominated and debris deposits and gradually decreased basinward in the coarser particle fractions (Figure 22B).

The stacking patterns for Sequence 2 (Figure 23) show a uniform succession down the slope, consisting of more debris-rich HSTs yielding asymmetrical, coarsening upward vertical stacks, and reflecting the changing progradational trajectories from TST to HST. Basinal stacking is less clear than that of the slope, although rare debris is present in the HST (Figure 13E).

DISCUSSION

Carbonate Margin and Slope Sequence Stratigraphic Concepts

The complex shelf-to-basin depositional and architectural evolution recorded along the Lennard Shelf, and now described with substantially higher resolution and confidence than before, can be distilled into a succinct set of predictive concepts and associations that are broadly applicable to reefal carbonate margin and slope systems. Terms and classifications used to describe the trends

below are after Playton et al. (2010). These predictive associations are particularly useful for characterization of steep-sided carbonate subsurface reservoirs with seismic-scale, supersequence backstepping-to-prograding architectures. Seismic volumes can typically resolve supersequence-scale systems tracts and long-term TST versus HST geometries, but the Lennard Shelf models illustrate the sub-seismic margin and slope facies associations, proportions, architectures, and their temporal arrangements, that are generally well beyond the interpretive limits of most subsurface datasets.

Margins and Slopes during Supersequence TSTs

Supersequence TSTs represent long-term high accommodation conditions, thus reefal margins have the tendency to backstep and aggrade. Margins often construct relief from relatively flat underlying substrates and over time outpace their own equivalent foreslope accumulations through vertical aggradation, producing an escarpment configuration with onlapping slope strata beneath coeval reefal environments; these are termed growth escarpments. A threshold of maximum escarpment development is reached when the slope profile is underfilled to the point where the margin becomes susceptible to failure, collapses, and generates debris deposits on the slope and in the basin. This occurs in the Late TST of the composite sequence, just prior to backstepping at the MFS (Figure 11). Up to and after this point, margins throughout the composite sequence are stable, from either building upward instead of outward, and/or through the presence of a flat underlying substrate. Thus, middle- and lower-slope stacking patterns will contain a symmetrical record, with debris deposits concentrated just beneath the composite sequence MFS, and grain-dominated deposits bracketing the debris below and above (Figures 12 and 13A). This style of organization can be predicted at a subordinate sequence scale within a supersequence TST. Age-equivalent reefal margins of the Alberta Basin in Western Canada (e.g., Workum and Hedinger 1989, Whalen et al. 2000) can be classified as growth escarpments; yet, it is difficult to compare middle-slope stacking patterns meaningfully due to different sequence stratigraphic criteria for interpretation of backstepping surfaces, degrees of basin fill from external input, backstepping distances, and margin declivities. However, Whalen et al. (2000) mapped tongues of debris in slope settings bracketed below and above by grain- to mud-dominated deposits for their backstepping Sequence 3, similar to the overall vertical succession described here.

Margins and Slopes during Supersequence MFSs

Around the supersequence MFS, at the long-term transition from margin aggradation and backstepping to progradation, slope profiles are significantly underfilled and margins are highly unstable. This results in sustained collapse, the formation of erosional escarpments, and the generation of debris-dominated slopes. Only after prolonged mass wasting of the margin produced enough debris to infill the slope profile and emplace a substrate for progradation, could the margin successfully advance basinward and evolve an

accretionary, interfingering configuration. Thus, around the supersequence MFS, debris-dominated slopes are likely over one or two subordinate (i.e., third-order) sequences and margins will predictably evolve from erosional escarpments to accretionary configurations (Figures 14 and 16). Internal stacking patterns on the slope will be somewhat indistinct, precluding subdivision into subordinate sequences. This is due to anomalously thick, amalgamated successions of debris, but thin grain-dominated intervals likely mark the onset and terminus of the slope readjustment and infilling period (i.e., the base of Frasnian Sequence 5 and cap of Frasnian Sequence 6; Figures 15 and 17). This pattern of collapse and debris-dominated slope development around supersequence MFSs is observed in multiple other outcrop and subsurface datasets, including the highly comparable, age-equivalent western Canadian system and Late Paleozoic isolated carbonate platforms of the Pricaspian Basin in western Kazakhstan (see Discussion and References in Playton and Kerans 2015 a).

Margins and Slopes during Supersequence HSTs

During the supersequence HST, the overall setting is accommodation limited and margins are consequently progradational. This repeated tendency for margins to strongly build outward at sub-horizontal trajectories results in frequent local and episodic failure. These local points of oversteepening quickly heal, re-accrete, and eventually fail again. This process is repeated continuously at numerous points along strike at any given time during progradation, resulting in debris tongue deposition on the slope. Within a composite-scale sequence, the HSTs are more strongly progradational compared to the TSTs; hence, HST margins fail more often and produce greater proportions of debris on the slope than TST margins (Figure 22). It follows that the composite sequence middle-lower-slope stacking patterns will reflect this with greater debris proportions in the HSTs, producing a coarsening upward, asymmetrical succession (Figure 23). Moreover, supersequence debris accumulations will have a similar overall organization, with greater debris proportions in the prograding HST sequences compared to that of the TST backstepping sequences. These patterns of TST versus HST debris proportions, both at supersequence and subordinate sequence scales, are not widely documented in other datasets, but were briefly overviewed in Playton et al. (2010) and discussed further and Playton and Kerans (2015 b).

Margins and Slopes during Global Biotic Crises

Global biological and ecological stress intervals will have particular characteristics and nuances throughout geological history. However, concerning carbonates in a broad sense, periods of biotic stress are reflected in changing of entire carbonate factories and adverse effects on certain components. As a consequence, elevated microbial activity is common during these times, indicating rapid opportunistic filling of niches held by organisms in decline. Moreover, margins may abruptly shift from shallow euphotic configurations to deeper oligophotic styles. In terms of slope development, anomalous

styles or highly partitioned stratigraphic packaging may result from pauses or transformations of the typical sources of downslope sediment (Figures 18 and 20).

In terms of stacking patterns or predictive trends (Figures 19 and 21), three likely phenomena should be considered based on observations from the Lennard Shelf dataset (see Playton and Kerans 2015 b for further discussion): 1) abrupt starved slope intervals indicating a temporary hiatus in production and downslope shedding from the usual carbonate factories (e.g., the silt-dominated gullied slope system in the TST of Frasnian Sequence 7); 2) signs of elevated microbial activity in any setting (e.g., downslope expansion of upper-slope microbial boundstone starting in Frasnian Sequence 7; Figure 13D); and 3) the dominance of a single sediment source contributing to slope deposits, often indicating the first carbonate factory to recover post-extinction while others remain in stress (e.g., ooid-dominated slopes in the TST of Famennian Sequence 1). While these factors can certainly impact margin-to-slope architecture, the influence of accommodation drivers will persist, and likely dominate geometric development during biotic crises. Thus, the key indicators of extinction intervals on carbonate slopes are typically rather rapid or uncharacteristic compositional variations that depart from more commonly observed stacking patterns. George and Chow (2002) and Playford et al. (2009) looked at multiple measured sections around the F-F boundary in middle- to lower-slope settings along the Lennard Shelf and repeatedly observed evidence for reduced carbonate factory production and resultant starved slope conditions at the extinction surface. These findings indicate that a distinctive signature of paused carbonate factories is likely to mark the actual boundary on the slope, and may be equivalent to an unconformity or disconformity on the platform top. Our dataset additionally proposes recognizable characteristics that define the extinction interval – the onset of biotic stress and recovery to a healthy, productive carbonate system.

Comparison with Playton and Kerans (2015 a, b)

Growth Escarpments

Growth escarpments represent a margin and slope evolution that is controlled by high accommodation conditions during long-term TSTs. Playton et al. (2010) first proposed the concept of growth escarpments, dominantly based on Lennard Shelf data, and Playton and Kerans (2015 a; their Figures 3 and 5-9) describe their architectures, compositions, and controls in detail. This study largely corroborates these previous findings in terms of the systems tract interpretations, timing of reefal margin failure, and nature of the weakly prograding HSTs. The PGH measured section and the HD14 core (Figure 1, Table 1, and Appendices 9 and 14) exhibit 1) upward-deepening outer platform to reef-flat facies successions, with 2) overlying margin-to-slope deposits that indicate progradation through upward-shallowing facies successions and/or an outcrop expression of basinward margin advance. This stacking respectively indicates TST conditions with aggrading margins followed by MFS backstepping and subsequent weak HST progradation, which agrees with the

sequence stratigraphic interpretation of Playton and Kerans (2015 a, b). The middle-slope equivalent to this type of succession can be observed in the SO measured section (Sequence 4, but relevant for older backstepping sequences; Figure 12) with 1) grain-dominated slopes during the TST reflecting stable aggradational margins; 2) slope debris deposits just prior to backstepping in the Late TST indicating a sensitivity to failure triggers during peak escarpment growth and collapse; and 3) overlying grain-dominated deposits recording the weak progradation of a stable margin with a solid underlying foundation. Playton and Kerans (2015 a; their Figure 7D) observed a margin reentrant, generated from large-scale failure, equivalent to the latest stages of escarpment growth immediately before an interpreted backstepping event. This supports the Late TST collapse that we also propose here, and represents a mechanism and timing for margin failure not discussed in Playton et al. (2010).

Timing of Collapse around the Supersequence MFS

Both Playton and Kerans (2015 a; their Figures 10 and 12-13) and this study soundly document the dominant margin failure process and consequent debris-dominated slope development at the supersequence MFS, as slope profiles adjust during the change from aggradation to progradation (Figures 14-17). Playton and Kerans (2015 a) suggest that most debris shedding is concentrated during the HSTs of the composite sequences that bracket the turnaround, and that TSTs represent phases of stability characterized by either grain shedding or microbial encrustation of collapsed margins. However, this study finds that once slope adjustment has commenced, debris shedding continues without interruption, regardless of systems tract, until the profile has sufficiently infilled to support progradation. Specifically, we observe margin failure throughout all of Sequences 5 and 6 with the exception of the Earliest TST of Sequence 5 and Latest HST of Sequence 6 (Figures 15 and 17). While the mapping of Playton and Kerans (2015 a) is not affected by these findings, it should be recognized that much of the slope debris during this period also originates from the TST margins of Sequences 5 and 6. This indicates that placement of the supersequence MFS, and subordinate sequence MFSs during this phase, should be within the thick successions of debris on the slope, rather than at the bases. Furthermore, the microbially-encrusted collapse scarp discussed in Playton and Kerans (2015 a) may not be as sequence stratigraphically significant as proposed. Instead, these encrustations may simply be locally preserved accumulations reflecting the alternating collapse and re-healing process that occurs throughout all systems tracts. The base of the microbially-encrusted veneer present at the Classic Face in Windjana Gorge (Playton and Kerans 2015 a, after Playford et al. 2009) defines the base of Sequence 6 in that particular margin location; however, further downslope the microbial accumulation may not coincide with the sequence boundary. More substantially, these observations point to a failure mechanism that results in repeated, high-frequency collapses along a vertical scarp during periods of sustained

aggradation - a mechanism not discussed in Playton et al. (2010).

Recovery Period after the F-F Boundary

The characterization in this study of the sequence leading up to the F-F boundary (Frasnian Sequence 7; Figures 18 and 19) conforms to the descriptions of Playton and Kerans (2015 b). These and our current observations effectively capture margin and slope development just prior to the significant event (i.e., silt-dominated TST settings and downslope microbial boundstone expansion). Herein, Famennian Sequence 1 is the sequence immediately after the F-F boundary, representing the post-extinction recovery period (Figures 20 and 21), and is analogous in terms of timing to the "Lowermost Famennian" of Playton and Kerans (2015 b). However, the two depositional models vary somewhat in terms of the importance placed on certain processes and resulting facies proportions (see Figure 3C in Playton and Kerans 2015 b). In this study, the middle- and lower-slope transects for Famennian Sequence 1 represent an open-ocean facing setting on the seaward side of an outboard structure, and within a large (> 50 kilometers across) embayment in the Lennard Shelf, respectively (Figure 1, SO and VHS sections, respectively). These sections indicate copious bypass of oolitic grain-dominated material and some debris immediately following the F-F boundary, suggesting ooid shoals were among the first carbonate factories to recover and prosper. The upper-slope control transect (WV section, Figure 1) for this study is located at the entrance of an elongate margin reentrant that, although within a paleogeographic embayment, likely had a direct connection with the open ocean. This section exhibits a debris-rich setting with intercalations of microbial boundstone, indicating the typical interfingering at the upper-middle-slope transition. This constrains the water depth of the encrusted upper-slope environment down to approximately 200 meters, comparable to that of the preceding sequence, Frasnian Sequence 7 (Figure 18). The model for the upper- and middle-slope settings of the Lowermost Famennian of Playton and Kerans (2015 b) was largely derived from exposures in Windjana Gorge proper, in a highly complex reentrant-promontory configuration with a depocenter somewhat sheltered from the open ocean (see their Figure 5). They describe the microbial boundstone factory expanding downslope beyond the relict depth of the previous Frasnian Sequence 7 and encroaching into apparently middle-slope environments. Moreover, a distinctive characteristic of the Lowermost Famennian is the paucity of platform-derived material in the middle slope, including oolitic grain-dominated deposits.

These disparities in platform-derived contribution and the degree of downslope microbial encrustation post-dating the F-F boundary observed in the two datasets can be attributed to variability associated with different paleogeographic settings. The extraordinary amount of oolitic accumulation recorded in the middle slopes at the SO section is likely related to its position on the seaward edge of a somewhat isolated carbonate island. A similar pattern holds for the VHS section due to its location within a well-circulated mega-embayment. The upper

slope microbial boundstone factory was already fully developed in Frasnian Sequence 7 and was in equilibrium with the other slope contributors, thus does not appear to expand further in this study. Conversely, the complex paleogeographic setting of Windjana Gorge is here interpreted to have had an impact on the recovery of platform-top factories, ooid shoals included, explaining the Lowermost Famennian observations of Playton and Kerans (2015 b). The delayed establishment of shallow water factories coincided with an elevation in microbial encrustation and resultant downslope expansion, suggestive of the opportunistic behavior of microbial communities. Furthermore, the likely poorer-marine circulation at Windjana Gorge may have itself been more favorable for microbial activity. The overall themes of the post-F-F recovery period still hold across both datasets (i.e., struggling and/or dominant single factories, extensive microbial activity), but the contrasts discussed here underscore the potential variability generated due to paleogeography and other controls on oceanographic processes, even during global phenomena.

Hierarchical Trends in Middle-Slope Debris Proportions

In this study, we observe a hierarchical pattern in middle-slope debris proportions with greater abundances in supersequence and composite sequence HSTs when compared to their counterpart TSTs (Figures 9, 10, 22, and 23). This again is attributed to a greater propensity for margin instability and local collapse from the outward extending trajectories inherent to progradational phases, and this association appears to hold true at different temporal scales. Playton and Kerans (2015 b) interpret the Famennian middle slopes in terms of high-frequency sequences, with debris-dominated LSTs, silt-dominated TSTs, and grain-dominated HSTs (their Figures 9, 13, and 22C). Their model for LST collapse entails slight downstepping of the microbial margin and upper slope during platform-top emergence, resulting in a strong offlapping geometry and extreme localized instability. Data from this study suggest this configuration and consequential process of failure is more common in composite-scale HSTs. It also indicates that a lower-frequency signal can be extracted from the detailed mapping of Playton and Kerans (2015 b), through documentation of debris deposit proportions within their high-frequency sequence stacking. Moreover, these observations imply that a hierarchical sequence stratigraphic expression exists in carbonate slope deposits similar to the numerous well-documented datasets in carbonate platform-top settings (e.g., Goldhammer et al. 1990, Kerans and Fitchen 1995, Tinker 1998); in these cases the expression is best developed in middle-slope settings where the suite of diagnostic facies are present, debris deposits being a critical indicator facies. As observed here, composite-sequence-scale accommodation conditions are linked to the development, and thus likelihood for collapse, of upper-slope-centered, microbial boundstone margin wedges during high-frequency LSTs. Perhaps these LST accumulations are poorly developed during composite-scale TSTs due to lesser degrees of exposure and downstepping.

Margin Failure Timing and Mechanisms

Numerous studies have commented on the timing and triggering mechanisms for brittle failure of early-lithified, reefal carbonate margins (e.g., Cook et al. 1972, Cook and Mullins 1983), and a range of intrinsic and extrinsic controls have been proposed. Playton et al. (2010) provide classifications for collapse scale and frequency, and generalize that margin failure is more likely during long-term progradation versus aggradation and backstepping, and highly concentrated around long-term transitions from aggradation to progradation (supersequence-scale MFSs). Playton and Kerans (2015 a, b) corroborate these statements with Lennard Shelf data, and additionally interpret collapse to occur during the high-frequency LSTs within lower-frequency progradational successions. Our dataset allows further investigation of the timing and mechanisms for reefal margin collapse using the added constraints of a hierarchical, slope sequence stratigraphic framework.

Collapse during the TST

This study and Playton and Kerans (2015 a) observed that escarpment margins within the overall backstepping supersequence TST become unstable and fail just prior to backstepping events when escarpment walls developed the greatest relief. On the composite-sequence-scale, the timing of these failures is in the Late TST, immediately before backstepping at the MFS and coeval with vertical margin and platform-top aggradation (Figure 11). This study and Playton and Kerans (2015 a) also documented a period of sustained failure bracketing the supersequence MFS as margins and slope profiles adjusted across the aggradation-to-progradation turnaround and over the span of two composite sequences (Frasnian Sequences 5 and 6). Playton and Kerans (2015 a) interpreted that collapse occurred only in the composite-scale HSTs of Sequences 5 and 6, owing to margin outbuilding over unstable or inadequate substrates. However, this study proposes failure also in the TSTs of Sequences 5 and 6, during vertical aggradation of the margin and platform top (Figures 15 and 17).

Thus, this study recognizes multiple instances of composite-sequence-scale TST failure of vertically-aggrading escarpment margins, a timing that is not discussed in Playton et al. (2010). In fact, their study (ibid.) considered aggradational trajectories unlikely to favor collapse. A highly-constrained sequence stratigraphic platform-to-slope correlation allows examination of the mechanism behind the observed TST failure (Figure 24). Platform-top TST stacking patterns that are equivalent to debris deposits on the slope display higher-frequency cycle sets within overall aggradational successions. The cycle sets consist of deepening upward cycles passing into shallowing upward cycles, thus represent small-scale backstepping to prograding alternations. As the escarpment margins approached great relief and declivity through aggradation, they became highly susceptible to collapse. We interpret high-frequency progradational pulses at the margin, recorded within the cycle set stacking on the platform, as the cause of TST collapse.

Small outbuilding events at the escarpment edge are adequate to initiate medium- to large-scale failure along an already highly unstable margin profile. This configuration appears to develop distinctly in the Late TSTs of composite sequences within supersequence TSTs, and persists across entire composite-scale TSTs across the supersequence MFS.

Collapse during the HST

Instability and failure are common during times of long-term progradation due to overall outbuilding margin trajectories over poorly developed or non-existent substrates. This was proposed as one of the more likely mechanisms by Playton et al. (2010) and discussed at length in Playton and Kerans (2015 b). Playton and Kerans (2015 b) interpret debris deposits within the supersequence HST to represent the LSTs of internal high-frequency sequences. These deposits coincided with margin- and upper-slope-centered wedges of microbial boundstone that developed while the platform top was largely exposed. These wedges accrete sub-horizontally in a basinward direction and become highly prone to local collapse along strike. High-frequency silt-dominated TST deposits and grain-dominated HST deposits follow and bury the LST debris to construct a clinothem, the fundamental building block of a progradational slope system.

This study was able to establish a composite-sequence-scale stratigraphy within the Famennian, providing an internal framework for the supersequence HST and enabling investigation of the distribution of high-frequency debris deposits within the sequence hierarchy. We find that debris deposits are more concentrated in composite sequence HSTs than in TSTs (Figure 23). This suggests that either the development of high-frequency LST margin wedges, or their collapse potential, varies depending on position within the lower-frequency setting. It is conceivable that wedge trajectories were likely closer to horizontal (or even downstepping) during composite HSTs versus TSTs, thus more prone to failure. It is also possible that the balance of the rate of margin outbuilding relative to the accumulation rate of detrital sediment along the slope profile changed whether within a composite HST or TST, in turn influencing collapse through the availability of underlying substrate. Further work is required to fully understand this process, but it is important to recognize the hierarchical organization we observe in margin failure patterns within the longer-term progradational succession, and that failure in these settings is induced via mechanisms that force an already outbuilding margin at the angle of repose to periodically accrete beyond the angle of yield.

Middle-Slope Stacking Patterns

Stacking pattern analysis for carbonate platform-top settings has been widely applied for decades and allows for two-dimensional predictions away from one-dimensional successions of facies (e.g., Goldhammer et al. 1990, Kerans and Nance 1991, Goldhammer et al. 1993, Kerans and Fitchen 1995, Read 1995, Kerans and Tinker 1997, Lehrmann and Goldhammer 1999). Making possible this methodology is the sensitive response of shallow water carbonate production and

accumulation to accommodation changes, and the assumption that stratigraphic record left behind is largely complete. Kerans and Tinker (1997) provide an excellent workflow and set of criteria to interpret sequences and systems tracts from one-dimensional stacks of carbonate shallow water deposits, including the usage of facies proportions, cycle thickness, indicator facies, facies offset, and exposure indices to interpret the accommodation history and migration of facies belts over time in a particular system.

In carbonate slope environments, however: 1) the assumptions that sediments are sensitive to and will likely infill accommodation does not apply, 2) exposure indicators are non-existent in most positions along high-relief slope profiles, 3) thickness patterns of sediment packages are generally meaningless given the degree of strike variability commonly observed, and 4) facies offset is often undiagnostic as highly varying deposit types are frequently juxtaposed vertically (as well as laterally). These reasons have led to the underdevelopment of carbonate slope stacking pattern criteria; however, our dataset provides sufficient control to establish generalized rules at the composite and supersequence scales. We find that the proportions of debris-, grain-dominated-, and mud-dominated deposits are useful for interpreting carbonate slope vertical successions. Middle-, and less so, lower-slope settings provide the best information as adequate representations of the key deposit types are generally present. The three families of deposit types (debris, grain-dominated, and mud-dominated; see Playton et al. 2010) are all meaningful in terms of source carbonate factory and process, though we find debris deposits to be the most effective as an indicator facies as they tend to occur at distinctive positions within the hierarchy of sequences and form the basis for the vertical patterns we observe in slope strata. We here propose three fundamental middle-slope stacking patterns, organized by position within the supersequence and relevant for steep reefal margin systems (Figure 25).

Composite Sequence Succession within the Supersequence TST

These successions are symmetrical with debris deposit cores and bracketed above and below with grain-dominated deposits (Figure 25A). The proportions of grain-dominated deposits are at least twice that of the debris; however, this ratio can vary along strike. Thicknesses are generally less than one hundred meters as these slope accumulations are onlapping wedges (versus laterally extensive prograding clinothem systems). These successions represent growth escarpment evolution and composite sequence development within the supersequence TST, where margins a) aggrade stably in the Early TST, producing grain-dominated slopes, b) surpass a threshold of instability in the Late TST resulting in collapse and slope debris deposition, c) backstep at the MFS, and d) weakly prograde in the HST while maintaining stability, thus feeding grain-dominated slopes.

Succession across the Supersequence MFS

These symmetrical successions consist of thick and amalgamated stacks of debris

deposits with significantly thinner grain-dominated bases and caps, and are conspicuously debris-rich intervals within extensive slope successions (Figure 25B). The overall proportions heavily favor debris deposits, with thicknesses potentially well over one hundred meters. These successions indicate the period of prolonged and sustained margin mass wasting as the slope profile readjusts and is gradually infilled with debris. This characteristically occurs at the transition from long-term aggradation and backstepping to progradation around the supersequence MFS. Placement of the supersequence MFS is likely in the lower half of the debris succession, as the majority of failure and slope infilling occurs in the supersequence Early HST, when the system is unable to prograde. The grain-dominated base of the succession reflects the final stages before the margin shifts to an erosional escarpment, and similarly, the grain-dominated cap marks the development of accretionary margins after regrading of the slope profile to the angle of repose. We observe here that this overall succession occurs over the span of two composite sequences (Frasnian Sequences 5 and 6), but definition of the composite-scale systems tracts and bounding surfaces is difficult due to the amalgamated nature of the debris succession.

Composite Sequence Succession within the Supersequence HST

These slope successions show an upward increase in debris deposits, producing a coarsening upward, asymmetrical profile (Figure 25C). Debris-poor (< 10%) lower portions represent composite-scale TSTs and are generally grain-dominated. Debris-rich (25-50%) upper portions represent composite-scale HSTs and show alternations between grain-dominated- and debris deposits with variable preservation of mud-dominated deposits. Overall stratigraphic thicknesses can be greater than one hundred meters as these are transects of prograding clinothems. These successions are found within supersequence HSTs, during overall progradational settings, where high-frequency collapse events are more likely to occur in composite HSTs versus TSTs. The Lennard Shelf dataset (after Playton and Kerans 2015 b) suggests that high-frequency margin failure occurs at accommodation minima, thus debris deposits have sequence stratigraphic significance and can be used to further delineate the internal architecture of composite HSTs. As the debris deposits are less prevalent in composite TSTs, internal high-frequency sequence architecture is likely obscured and more difficult to define.

Signals of Ecological Stress

In addition to accommodation controls, carbonate systems also strongly respond to changes in environmental conditions, resulting in perturbations in productivity and the active source factories that contribute to middle-slope deposits. The ability to examine sediment successions that pre- and postdate the F-F boundary allows for general facies trends and relationships to be developed. These are not stacking patterns per se, rather signals or diagnostic features that may indicate temporal proximity to a major biotic crisis (Figure 26). In the Lennard Shelf case, the pre-extinction lead-up period entailed an increase in biotic stresses that were reflected

in the slope through changes in sediment type (Figure 26A). Fairly abrupt starved slope intervals, dominated by muddy background deposits with little margin or platform-top contribution, indicate a temporary pause in the previously flourishing factories that normally dominated slope deposition. These intervals may correspond to anoxic events that are manifested through transgressions, and thus can have sequence stratigraphic significance (i.e., Frasnian Sequence 7 TST, Figures 18 and 19; also see Playton and Kerans 2015 b). Increased occurrences of microbial boundstone, such as downslope expansion of the encrusted upper-slope environment, can represent elevated microbial activity related to the opportunistic response to other struggling biota. Immediately prior to the extinction boundary itself, successions showing an upward decrease in the proportions of margin- and platform-top-derived sediment can reflect the decline of species and productivity. The exact vertical ordering and combinations of these indicators of biotic stress are variable and will depend on the dynamics of each system, but still provide a set of criteria to predict the preceding response in carbonate slope deposits to an extinction boundary.

Following the F-F extinction boundary, we observed two styles of sedimentation in middle-slope settings before margin and platform-top factories recovered and slope deposits returned to the typical, expected successions (Figure 26B, C). In one example, an anomalously thick stack of oolitic grain-dominated deposits overwhelmed the slope (Figure 26B), reflecting the early rebound of the ooid shoal factory while the remaining factories were not yet re-established in the extinction aftermath. Other areas exhibited pervasive microbial encrustation of the middle slope, with debris- and grain-dominated deposits interspersed and suspended in a labyrinth of boundstone (Figure 26C). The boundstone patterns suggest a near-continuous growth and accumulation, conceptually similar to "background sedimentation", and seemingly not partitioned in time and space with episodic debris and grain shedding events. In general, these trends describe a period of post-extinction recovery, where the majority of the former carbonate factories require time to re-equilibrate and re-establish, and opens a window of opportunity for niche-filling microbial communities and/or more resilient factories to produce and deposit prolifically in light of the reduced competition. In our dataset, this stage seems to be about the duration of a composite-scale systems tract and happens to coincide with the Famennian Sequence 1 TST, but the sequence stratigraphic significance and linkage is not well understood.

Caution with Middle-Slope Stacking Patterns

Caution should be taken when applying or interpreting the aforementioned criteria for slope sequence stratigraphy. The nature of carbonate slopes associated with steep, reefal margins is inherently highly heterogeneous laterally and vertically, and, since debris deposits are a key indicator facies, their presence is not always sufficient for optimal sequence interpretation. Strike variability needs to be appreciated and supporting data, such as carbon isotope profiles, can significantly aid and corroborate systems tract

definition (see Hillbun et al. this volume). This assumes that debris deposits are generated via intrinsic collapse processes related to margin trajectory. However, extrinsic triggering mechanisms (e.g., seismicity and tsunamis) are well-documented and need to be considered to avoid erroneous interpretations. Furthermore, the Lennard Shelf system is one that constructed great relief over a long period of geologic time, developed near-vertical escarpments, and contained a substantial microbial component concentrated in the margins for most of its evolution; other carbonate systems will undoubtedly have their own particularities that may or may not correspond directly to the patterns discussed here.

CONCLUSIONS

Carbonate slopes are exceptional repositories of sediment and recorders of carbonate system evolution. The Canning Basin Chronostratigraphy Project generated a high-resolution, shelf-to-basin sequence stratigraphic framework across the Lennard Shelf that allows for unique examination of carbonate margin and slope development within highly-constrained accommodation and ecological contexts. We achieved this through integration of multiple independent datasets extracted from the rock record to generate a high-confidence suite of constraints for sequence stratigraphic interpretation in variable settings. We here propose carbonate margin-to-basin sequence stratigraphic conceptual models and facies successions for composite-scale sequences throughout supersequence TST, MFS, and HST evolution, and across a global biotic crisis. We find that deposit proportions, facies associations, vertical stratigraphic patterns, margin architecture, and shelf-to-basin geometry vary with respect to position within the supersequence and in lead up or recovery periods around an extinction interval. The concepts herein provide relationships to link seismic-scale architecture with fine-scale heterogeneity, and predictive tools to better characterize these highly complex systems. These findings are useful for subsurface industry applications and also lay a foundation for further academic research.

ACKNOWLEDGEMENTS

We especially thank the Aboriginal tribes of the Bunaba and Gooniyandi (Kuniandi) people who allowed us to conduct this research on their sacred lands. Thanks to Paul Montgomery and Peter Cawood for the integrated chronostratigraphic vision, and to Phil Playford for introduction to the outcrop belt. Special thanks to reviewers John Weissenberger, Ken Potma, William Morgan, Brian Pratt, and Charles Kerans for feedback and guidance that greatly improved the quality of the manuscript. Funding was supplied by the Australian Research Council Linkage Program (Grant LP0883812), ARC-QEII Grant Program, ARC-DORA-3 Grant Program, MERIWA, WAERA, CSIRO, Buru, Chevron Australian Business Unit, Chevron Energy Technology Company, the University of Greenwich, and Chemostrat, Ltd. Field support and safety was provided by Wundargoodie Aboriginal Safaris (Colin and Maria Morgan and family and crew), the Geological Survey of Western Australia,

Chevron Australian Business Unit, and Steve Meyer, Sean O'Connell, and Bill Robinson of Chevron. Thanks to Windjana Gorge National Park, Napier Downs, the Mimbi Community, Mount Pierre Station, Fossil Downs Station, Brooking Downs Station, the Pillara Mine, and the Cadjebut Mine for field area access and resources. Thanks to R. Addenbrooke, H. Allen, A. Duffy, G. Beacher, M. Diamond, T. Holland, J. Hsieh, L. Lanci, K. Liebe, E. Maslen, L. McEvoy, S. Shoepfer, U. Singh, M. Thorp, T. Tobin, A. Vonk, F. Wellmann, and K. Williford for field assistance. Thanks to E. Davies, M. Ducea, J. Klemm, F. Pardini, T. Raub, G. Rotberg, J. Sano, S. Slotznick, P. Ward, and M. Wright for logistical and/or analytical contributions. R.M. Hocking and P.W. Haines publish with the permission of the Executive Director of the Geological Survey of Western Australia.

References

Becker, R.T. and House, M.R., 1997, Sea level changes in the Upper Devonian of the CanningBasin, Western Australia: Courier Forschungsinstitut Senckenberg, v. 199, p. 129-146.

Becker, R.T., House, M.R., and Kirchgasser, W.T., 1993, Devonian goniatite biostratigraphy and timing of facies movements in the Frasnian of the Canning Basin, Western Australia, in, Hailwood, E.A., and Kidd, R.B., eds., High Resolution Stratigraphy: Geological Society of London Special Publication 70, p. 293-321.

Begg, J., 1987, Structuring and controls on Devonian reef development on the northwest Barbwire and adjacent terraces, Canning Basin: Australian Petroleum Exploration Association Journal, v. 27, p. 137-151.

Bellian, J.A., Playton, T.E., Kenter, J.A.M., Harris, P.M., and Kerans, C., 2012, The reciprocal nature of carbonate and siliciclastic-dominated slope channel deposits (abs.): American Association of Petroleum Geologists Annual Convention and Exhibition, April 22-25, Long Beach, California.

Bing, X., Zhaoyan, G., Qiang, L., Chengyuan, W., Zhenliang, L., 2003, Carbon isotopic record from Upper Devonian carbonates at Dongcun in Guilin, southern China, supporting the world-wide pattern of carbon isotope excursions during Frasnian-Famennian transition: Chinese Science Bulletin, v. 48, p. 1259-1264.

Brown, A.A., and Loucks, R.G., 1993, Influence of sediment type and depositional processes on stratal patterns in the Permian Basin-margin Lamar Limestone, McKittrick Canyon, Texas, in Loucks, R.G. and Sarg, J.F., eds., Carbonate Sequence Stratigraphy, American Association of Petroleum Geologists Memoir, no. 57, p. 133- 156.

Buggisch, W., and Joachimski, M.M., 2006, Carbon isotope stratigraphy of the Devonian of Central and Southern Europe: Palaeogeography, Palaeoclimatology, and Palaeoecology, v. 240, p. 68-88.

Clayton, J.L., and Kerans, C., 2013, Reservoir compartmentalization of a depp-water ooid fan, Happy Field, Permian Basin: in Verwer, K., Playton, T.E., and Harris, P.M., eds., Deposits, architecture, and controls of carbonate margin, slope, and basinal settings, Society for Sedimentary Geology Special Publication no. 105, p. 359-383.

Collins, J.F., Narr, W., Harris, P.M., Playton, T.E., Jenkins, S., Tankersley, and Kenter, J.A.M., 2013, Lithofacies, depositional environments, burial diagenesis, and dynamic field behavior in a Carboniferous slope reservoir, Tengiz Field (Republic of Kazakhstan), and comparison with outcrop analogs: in Verwer, K., Playton, T.E., and Harris, P.M., eds., Deposits, architecture, and controls of carbonate margin, slope, and basinal settings, Society for Sedimentary Geology Special Publication no. 105, p. 50-83.

Collins, J.F., Kenter, J.A.M., Harris, P.M., Kuanysheva, G., Fischer, D.J., and Steffen, K.L., 2006, Facies and reservoir quality variations in the Late Visean to Bashkirian outer platform, rim, and flank of the Tengiz Buildup, Pricaspian Basin, Kazakhstan: in Harris, P.M. and Weber, L.J., eds., Giant hydrocarbon reservoirs of the world: From rocks to reservoir characterization and modeling, American Association of Petroleum Geologists Memoir 88, p. 55-95.

Cook, H.E., McDaniel, P.N., Mountjoy, E.W., and Pray, L.C., 1972, Allochthonous carbonate debris flows at Devonian bank ('reef') margins, Alberta, Canada: Bulletin of Canadian Petroleum Geology, v. 20, no. 3, p. 439-497.

Cook, H.E. and Mullins, H.T., 1983, Basin margin environment, *in* Scholle, P.A., Bebout, D.G., and Moore, C.H., eds., Carbonate depositional environments: American Association of Petroleum Geologists Memoir 33, p. 539-618.

Copp, I.A., 2000, Subsurface facies analysis of Devonian reef complexes, Lennard Shelf, Canning Basin, Western Australia: Geological Survey of Western Australia Report 58, 127p.

Davies, E.J., Ratcliffe, K.T., Montgomery, P., Pomar, L., Ellwood, B.B., and Wray, D.S., 2013, Magnetic susceptibility (χ) stratigraphy and chemostratigraphy applied to an isolated carbonate platform reef complex; Llucmajor Platform, Mallorca, in Verwer, K., Playton, T.E., and Harris, P.M., eds., Deposits, Architecture, and Controls of Carbonate Margin, Slope and Basinal Settings, Society for Sedimentary Geology Special Publication 105, p. 142-156.

Droxler, A.W. and Schlager, W., 1985, Glacial versus interglacial sedimentation rates and turbidite frequency in the Bahamas: Geology, v. 13, p. 799-802.

Drummond, B.J., Sexton, M.J., Barton, T.J., and Shaw, R.D., 1991, The nature of faulting along the margins of the Fitzroy Trough, Canning Basin, and implications for the tectonic development of the trough: Exploration Geophysics, v.22, p. 111-115.

Eberli, G.P., Bernoulli, D., Sanders, D., and Vecsei, A., 1993, From aggradation to progradation; the Maiella Platform, Abruzzi, Italy, in Simo, J.A.T., Scott, R.W., and Masse, J.P., eds., Cretaceous carbonate platforms: American Association of Petroleum Geologists Memoir, no. 56, p. 213-232.

Fitchen, W.M., Starcher, M.A., Buffler, R.T., and Wilde, G.L., 1995, Sequence stratigraphic framework and facies models of early Permian carbonate platform margins, Sierra Diablo, West Texas, in Garber, R.A., and Lindsay, R.F., eds., Wolfcampian-Leonardian shelf margin facies of the Sierra Diablo – Seismic scale models for subsurface exploration, West Texas Geological Society

Annual Field Trip Guidebook, no. 95-97, p. 23-66.

Frost, III, E.L., 2007, Facies heterogeneity, platform architecture and fracture patterns of the Devonian reef complexes, Canning Basin, Western Australia: unpublished PhD dissertation, University of Texas at Austin, Austin, Texas, 156 p.

Frost, III, E.L. and Kerans, C., 2010, Controls on syndepositional fracture patterns, Devonian reef complexes, Canning Basin, Western Australia: Journal of Structural Geology, v. 32, p. 1231-1249.

George, A.D., Playford, P.E., Powell, C.McA., and Tornatora, P.M., 1997, Lithofacies and sequence development on an Upper Devonian mixed carbonate-siliciclastic fore-reef slope, Canning Basin, Western Australia: Sedimentology, v. 44, p. 843-867.

George, A.D. and Chow, N., 2002, The depositional record of the Frasnian/Famennian boundary interval in a forereef succession, Canning Basin, Western Australia, *in* Racki, G., and House, M.R., eds., Late Devonian biotic crisis; Ecological, depositional, and geochemical records: Palaeogeography, Palaeoclimatology, Palaeoecology, v. 181, p. 347-374.

Girard, C., Klapper, G., and Feist, R., 2005, Subdivision of the Terminal Frasnian Linguiformis Conodont Zone, Revision of the Correlative Interval of Montagne Noire Zone 13, and Discussion of Stratigraphically Significant Associated Trilobites, in, Over, J.D., Morrow, J.R., and Wignall, P.B., eds., Understanding Late Devonian and Permian-Triassic Biotic and Climatic Events: Towards an Integrated Approach: Elsevier Developments in Palaeontology and Stratigraphy, v. 20, p. 181-198.

Goldhammer, R.K., Dunn, P.A., and Hardie, L.A., 1990, Depositional cycles, composite sea level changes, cycle stacking patterns, and the hierarchy of stratigraphic forcing: examples from platform carbonates of the Alpine Triassic: Geological Society of America Bulletin, v. 102, p. 535-562.

Goldhammer, R.K., Oswald, E.J., and Dunn, P.A., 1991, The hierarchy of stratigraphic forcing: an example from middle Pennsylvanian shelf carbonates of the Paradox Basin, *in* Franseen, E., and Watney, L., eds., Sedimentary modeling: Computer simulation of depositional sequences, Kansas Geological Survey Bulletin, p. 361-413.

Goldhammer, R.K., P.J. Lehmann, and P.A. Dunn, 1993, The origin of high-frequency platform carbonate cycles and third-order sequences (Lower Ordovician El Paso Group, west Texas): constraints from outcrop data and stratigraphic modeling: Journal of Sedimentary Petrology, v. 63, p. 318-359.

Gradstein, F.M., Ogg, J.G., Schmitz, M., and Ogg, G., 2012, The Geologic Time Scale 2012: Elsevier, 1176 p.

Grammer, G.M. and Ginsburg, R.N., 1992, Highstand versus lowstand deposition on carbonate platform margins: Insight from Quaternary foreslopes in the Bahamas: Marine Geology, v. 103, p. 125-136.

Hansma, J., Tohver, E., Yan, M., Trinajstic, K., Roelofs, B., Peek, S., Slotznick, S.P., Kirschvink, J., Playton, T.E., Haines, P.W., Hocking, R.M., 2015, Late Devonian carbonate magnetostratigraphy from the Oscar and Horse Spring Ranges, Lennard Shelf, Canning Basin, Western

Australia: Earth and Planetary Science Letters, v. 409, p. 232-242.

Hillbun, K., 2015, Re-evaluating the Late Devonian mass extinction: A new perspective from the Canning Basin, Western Australia: unpublished PhD dissertation, University of Washington, Seattle, Washington, 278 p.

Hillbun, K., Playton, T.E., Tohver, E., Ratcliffe, K., Trinajstic, K., Roelofs, B., Caulfield-Kerney, S., Wray, D., Haines, P.W., Hocking, R.M., Katz, D.A., Montgomery, P., and Ward, P., 2015, Upper Kellwasser carbon isotope excursion pre-dates the F-F boundary in the Upper Devonian Lennard Shelf carbonate system, Canning Basin, Western Australia: Palaeogeography, Palaeoclimatology, and Palaeoecology, v. 438, p. 180-190.

Hillbun, K., Katz, D.A., Playton, T.E., Trinajstic, K., Machel, H., Bourgeois, J., Haines, P.W., Hocking, R.M., Roelofs, B., and Ward, P., in review, Global and local controls on carbon isotope fractionation in Upper Devonian carbonates from the Lennard Shelf, Western Australia: A revised approach for generating primary marine secular curves for regional correlation: American Association of Petroleum Geologists Bulletin.

Hillbun, K., Playton, T.E., Katz, D.A., Tohver, E., Trinajstic, K., Haines, P.W., Hocking, R.M., Roelofs, B., Montgomery, P., this volume, Correlation and sequence stratigraphic interpretation of Upper Devonian carbonate slope facies using carbon isotope chemostratigraphy, Lennard Shelf, Canning Basin, Western Australia, in, Playton, T.E., Kerans, C., Weissenberger, J., and Montgomery, P., eds., New Advances in Devonian Carbonates: Outcrop Analogs, Reservoirs, and Chronostratigraphy: SEPM Special Publication *in press*.

Janson, X., Kerans, C., Bellian, J.A., and Fitchen, W., 2007, Three-dimensional geological and synthetic seismic model of Early Permian redeposited basinal carbonate deposits, Victorio Canyon, west Texas: American Association of Petroleum Geologists Bulletin, v. 91, p. 1405-1436.

Janson, X., Kerans, C., Loucks, R., Marhx, M.A., Reyes, C., and Murguia, F., 2011, Seismic architecture of a Lower Cretaceous platform-to-slope system, Santa Agueda and Poza Rica Fields, Mexico: American Association of Petroleum Geologists Bulletin, v. 95, no. 1, p. 105-146.

Joachimski, M.M., Pancost, R.D., Freeman, K. H., Ostertag-Henning, C., and Buggisch, W., 2002, Carbon isotope geochemistry of the Frasnian–Famennian transition: Palaeogeography, Palaeoclimatology, Palaeoecology, v. 181, p. 91–109.

Katz, D., Buoniconti, M., Montañez, I., Swart, P., Eberli, G., and Smith, L., 2007, Timing and local perturbations to the carbon pool in the Lower Mississippian Madison Limestone, Montana and Wyoming: Palaeogeography, Palaeoclimatology, Palaeoecology, v. 256, p. 231–53.

Katz, D.A., Playton, T.E., Bellian, J.A., Harris, P.M., Harrison, C., and Maharaja, A., 2010, Slope heterogeneity and production results in a steep-sided Upper Paleozoic isolated carbonate platform reservoir, Karachaganak Field, Kazakhstan: Society of Petroleum Engineers Caspian Carbonates Technology Conference Paper, Atyrau, Kazakhstan, no. 139960, p. 1-7.

Kaufmann, B., 2006, Calibrating the Devonian Time Scale: A synthesis of U-Pb ID-TIMS ages and conodont stratigraphy: Earth Science Reviews, v. 76, p. 175-190.

Kerans, C., 1985, Petrology of Devonian and Carboniferous carbonates of the Canning and Bonaparte Basins: Western Australian Mining and Petroleum Research Institute Report, v. 12, 203 p.

Kerans, C. and H.S. Nance, 1991, High frequency cyclicity and regional depositional patterns of the Grayburg Formation, Guadalupe Mountains, New Mexico: Society of Sedimentary Geology Permian Basin Section Publication 91-32, p. 53-69.

Kerans, C., 1995, Use of one- and two-dimensional cycle analysis in establishing high frequency sequence frameworks, in Read, J.F., Kerans, C., and Weber, L.J., eds., Milankovitch sea level changes, cycles and reservoirs on carbonate platforms in greenhouse and ice-house worlds: Society of Sedimentary Geology Short Course Notes, no. 35, p. 103-123.

Kerans, C. and W.M. Fitchen, 1995, Sequence hierarchy and facies architecture of a carbonate-ramp system: San Andres Formation of Algerita Escarpment and western Guadalupe Mountains, West Texas and New Mexico: Bureau of Economic Geology Report of Investigations, no. 235, 86 p.

Kerans, C., and Tinker, S.W., eds., 1997, Sequence stratigraphy and characterization of carbonate reservoirs, Society for Sedimentary Geology Short Course Notes, no. 40, 140 p.

Kerans, C., 2002, Styles of rudist buildup development along the northern margin of the Maverick Basin, Pecos River Canyon, southwest Texas: Transactions Gulf Coast Association of Geological Societies, v. 52, p. 501-516.

Kerans, C., and Kempter, K., 2002, Hierarchical stratigraphic analysis of a carbonate platform, Permian of the Guadalupe Mountains: American Association of Petroleum Geologists Datapages Discovery Series, no. 5, CD-ROM.

Klapper, G., 1989, The Montagne Noire Frasnian (Upper Devonian) Conodont Succession: Devonian of the World 3, p. 449-468.

Klapper, G., 1997, Graphic correlation of Frasnian (Upper Devonian) sequences in Montagne Noire, France, and western Canada, in, Klapper, G., Murphy, M.A., Talent, J.A., eds., Paleozoic sequence stratigraphy, biostratigraphy, and biogeography: Studies in Honor of J. Granville ("Jess") Johnson: Geological Society of America, p. 113-129.

Klapper, G., 2007, Frasnian (Upper Devonian) conodont succession at Horse Spring and correlative sections, Canning Basin, Western Australia: Journal of Paleontology, v. 81, p. 513-537.

Lehrmann, D.J., and Goldhammer, R.K., 1999, Secular variation in parasequence and facies stacking patterns of platform carbonates: A guide to application of stacking-pattern analysis in strata of diverse ages and settings, *in* Harris, P.M., Saller, A.H., and Simo, J.A., eds., Advances in carbonate sequence stratigraphy: Application to reservoirs, outcrops, and models, Society for Sedimentary Geology Special Publication no. 63, p. 187-226.

Montgomery, P., Ratcliffe, K.T., and Wray, D., 2011, Application of whole rock

inorganic geochemistry to stratigraphic understanding of mixed carbonate evaporite reservoirs, an example from the First Eocene of the Wafra Field, PZ (abs.): American Association of Petroleum Geologists Annual Convention and Exhibition, April 10-13, Houston, Texas.

Montgomery, S.L., 1996. Permian 'Wolfcamp' limestone reservoirs, Powell Ranch Field, eastern Midland Basin. American Association of Petroleum Geologists Bulletin, 80, 1349-1365.

Osleger, D.A., and Tinker, S.W., 1999, Three-dimensional architecture of Upper Permian high-frequency sequences, Yates-Capitan shelf margin, Permian Basin, USA, *in* Harris, P.M., Saller, A.H., and Simo, J.A., eds., Advances in carbonate sequence stratigraphy: Application to reservoirs, outcrops, and models: Society for Sedimentary Geology Special Publication, v. 63, p. 169-185.

Playford, P.E., 1980, Devonian 'great barrier reef' of the Canning Basin, Western Australia: American Association of Petroleum Geologists Bulletin, v. 64, p. 814-840.

Playford, P.E., 1984, Platform-margin and marginal-slope relationships in Devonian reef complexes of the Canning Basin, in, Purcell, P.G., ed., Canning Basin Symposium Proceedings, Perth: Geological Society of Australia and Petroleum Exploration Society of Australia, p. 189-214.

Playford, P.E., Hocking, R.M., and Cockbain, A. E., 2009, Devonian reef complexes of the Canning Basin, Western Australia: Geological Survey of Western Australia, Bulletin 145, 444p.

Playford, P.E., Hocking, R.M., and Cockbain, A.E., this volume, Devonian reef complexes of the Canning Basin, Western Australia: A historical review, in, Playton, T.E., Kerans, C., Weissenberger, J., and Montgomery, P., eds., New Advances in Devonian Carbonates: Outcrop Analogs, Reservoirs, and Chronostratigraphy: SEPM Special Publication *in press*

Playton, T.E., 2008, Characterization, variations, and controls of reef-rimmed carbonate foreslopes: unpublished Ph.D. dissertation, The University of Texas at Austin, Austin, Texas, 283 p.

Playton, T.E., Janson, X., and Kerans, C., 2010, Carbonate slopes (Chapter 18), in James, N.P. and Dalrymple, R.W., eds., Facies Models 4, GEOtext 6, Geological Association of Canada, St. Johns, NL, Canada, p. 449-476.

Playton, T.E., Hocking, R.M., Montgomery, P., Tohver, E., Hillbun, K., Katz, D.A., Haines, P.W., Trinajstic, K., Yan, M., Hansma, J., Pisarevsky, S., Kirschvink, J., Cawood, P., Grice, K., Tulipani, S., Ratcliffe, K., Wray, D., Caulfield-Kerney, S., Ward, P., and Playford P.E., 2013, Development of a regional stratigraphic framework for Upper Devonian reef complexes using integrated chronostratigraphy: Lennard Shelf, Canning Basin, Western Australia, in Keep, M., and Moss, S.J., eds., Sedimentary Basins of Western Australia IV: Proceedings of the Petroleum Exploration Society of Australia Symposium, August 18-21, Perth, Western Australia, 14 p.

Playton, T.E., and Kerans, C., 2015a, Late Devonian carbonate margins and foreslopes of the Lennard Shelf, Canning Basin, Western Australia, Part A: Development during backstepping and the aggradation-to-progradation transition:

Journal of Sedimentary Research, v. 85, p. 1334-1361.

Playton, T.E., and Kerans, C., 2015b, Late Devonian carbonate margins and foreslopes of the Lennard Shelf, Canning Basin, Western Australia, Part B: Development during progradation and across the Frasnian-Famennian biotic crisis: Journal of Sedimentary Research, v. 85, p. 1362-1392.

Raup, D.M., and Sepkoski, J.J., 1982, Mass extinctions in the marine fossil record: Science, v.215, p. 1501–1503.

Read, J.F., 1995, Overview of carbonate platform sequences, cycle stratigraphy and reservoirs in greenhouse and icehouse worlds, *in* Read, J.F., Kerans, C., and Weber, L.J., eds., Milankovitch sea-level changes, cycles, and reservoirs on carbonate platforms in greenhouse and icehouse worlds, Society of Economic Paleontologists and Mineralogists Short Course Notes, v. 35, p. 1-106.

Roelofs, B., Playton, T.E., Barham, M., and Trinajstic, K., 2015, Upper Devonian microvertebrates from the Canning Basin, Western Australia: Acta Geologica Polonica, v. 65, p. 69-101.

Sarg, J.F., Markello, J.R., and Weber, L. J., 1999, The second-order cycle, carbonate-platform growth, and reservoir, source, and trap prediction, in, Harris, P.M., Saller, A.H., and Simo, J.A., eds., Advances in carbonate sequence stratigraphy; Application to reservoirs, outcrops and models: Society for Sedimentary Geology Special Publication 63, p. 11-34.

Stephens, N.P., and Sumner, D.Y., 2003, Late Devonian carbon isotope stratigraphy and sea level fluctuations, Canning Basin, Western Australia: Palaeogeography, Palaeoclimatology, Palaeoecology, v. 191, p. 203-219.

Tinker, S.W., 1998, Shelf-to-basin facies distribution and sequence stratigraphy of a steep-rimmed carbonate margin: Capitan depositional system, McKittrick Canyon, New Mexico and Texas: Journal of Sedimentary Research, v. 68, p. 1146-1174.

Trinajstic, K., and George, A.D., 2009, Microvertebrate biostratigraphy of Upper Devonian (Frasnian) carbonate rocks in the Canning and Carnarvon Basins of Western Australia: Palaeontology, v. 52, p. 641-659.

Tulipani, S., Grice, K., Greenwood, P.F., Haines, P.W., Sauer, P.E., Schimmelmann, A., Summons, R.E., Foster, C.B., Bottcher, M.E., Playton, T.E., Schwark, L., 2015, Changes of palaeoenvironmental conditions recorded in Late Devonian reef systems from the Canning Basin, Western Australia: A biomarker and stable isotope approach: Gondwana Research, v. 409, p. 61-68.

Ward, W.B., 1999, Tectonic control on backstepping sequences revealed by mapping of Frasnian backstepped platforms, Devonian reef complexes, Napier Range, Canning Basin, Western Australia, in, Harris, P.M., Saller, A.H., and Simo, J.A., eds., Society for Sedimentary Geology Special Publication 63, p. 47-74.

Whalen, M.T., Eberli, G.P., van Buchem, F.S.P., and Mountjoy, E.W., 2000, Facies models and architecture of Upper Devonian carbonate platforms (Miette and Ancient Wall), Rocky Mountains, Alberta, Canada, in, Homewood, P.W. and Eberli, G.P., eds., Genetic stratigraphy on the exploration and production scales; Case studies from the Upper Devonian of Alberta

and the Pennsylvanian of the Paradox Basin: Bulletin des Centres de Recherches Exploration-Production Elf-Aquitaine Memoire, v. 24, p. 139-175.

Workum, R. H., and Hedinger, A. S., 1989, Burnt Timber and Scalp Creek margins, Frasnian Fairholme reef complex, Alberta, in, Geldsetzer, Helmut H. J., James, Noel P., and Tebbutt, Gordon E., eds., Reefs*;* Canada and adjacent areas: Memoir – Canadian Society of Petroleum Geologists, December 1988, v. 13, p. 552-556.

Ziegler, W., and Sandberg, C.A., 1990, The Late Devonian Standard Conodont Zonation: Courier Forschungsinstitut Senckenberg, v. 121, p. 1-115.

Figure Captions

Figure 1: Simplified outcrop exposure and location maps of part of the Lennard Shelf, Canning Basin, Western Australia (modified after Playford et al. 2009, Frost and Kerans 2010). Red labels indicate data collection localities of the CBCP. WNA-B = Windjana North A-B measured sections. WS = Windjana Slope measured section. WV = Windjana Valley measured section. SO = South Oscars measured section. PRQ = Pillara Road Quarry measured section. VHS = Horse Spring measured section. HD14 = Horse Spring subsurface core. UD2 = Horseshoe Range subsurface core. NHW = Henwood West measured section. PGH = Guppy Hills measured section. WK1 = Wade Knoll Winkie core. CL = Casey Falls measured section. MR1 = McWhae Ridge Winkie core.

Figure 2: Idealized composite cross section and sequence architecture of the Middle-Upper Devonian carbonate system of the Lennard Shelf (modified after Playton and Kerans 2015 a, b). Thin black form lines denote internal stratal architecture. Individual Famennian high-frequency sequences are not shown. HST = highstand systems tract. TST = transgressive systems tract. MFS = maximum flooding surface.

Figure 3: Diagram showing CBCP sampling coverage in terms of age (y-axis), depositional environment (x-axis), and sample transect type (colors). F-F boundary = Frasnian-Famennian extinction boundary. U, M, and L indicate Upper, Middle, and Lower subdivisions of Stages, respectively, and are arbitrarily spaced. Single sections or cores can record multiple environments over time, as indicated by connecting dashed lines. WNA, WNB, WS, and WV sections, and CL-MR1 transects, respectively, were physically linked through walkouts – the all other stratigraphic correlations were achieved through agreement of multiple data profiles. Refer to Figure 1 for distances between localities along the Lennard Shelf.

Figure 4: Examples of CBCP outcrop localities (after Playton et al. 2013). (a) Frasnian inner platform cycles of the Windjana North B Section (WNB). (b) Frasnian reef-flat cycles of the Windjana North A Section (WNA). (c) Frasnian middle- to upper-slope strata of the Windjana Slope Section (WS). (d) Frasnian middle-slope strata of the South Oscars Section (SO). (e)

Famennian upper-slope strata of the Casey Falls Section (CL). Yellow circles indicate people for scale. See Figure 1 for locations along the Lennard Shelf.

Figure 5: Outcrop photo examples of facies documented for the CBCP. a) Crinkly laminated fenestral peloidal wackestone, Givetian inner platform top, Guppy Hills Section (GHB). b) Moldic *Amphipora* stromatoporoid rudstone, Frasnian outer platform top, Windjana North A Section (WNA). c) Horizontally-accreting *Actinostroma* stromatoporoid framestone, Frasnian reef core, Henwood West Section (NHW). Basinward is to the left. d) Steeply-dipping stromatactoid microbial boundstone, Famennian upper slope, Casey Falls Section (CL). e) Megabreccia with meter-scale boulders and quartz-rich matrix, Famennian middle slope, Windjana Valley Section (WV). f) Mottled silty peloidal wackestone, Famennian toe of slope, Casey Falls Section (CL). See Figure 1 for locations along the Lennard Shelf.

Figure 6: Middle-Upper Devonian (Givetian, Frasnian, and Famennian) chronostratigraphic chart developed from the CBCP, showing geologic sub-divisions, conodont biozones, paleomagnetic polarity chrons, stable carbon excursions, and sequence stratigraphic framework. Absolute ages from Gradstein et al. (2012). In Low Confidence Lower Frasnian, conodont zones relative to sequences adapted from Playford et al. (2009). Light grey sub-columns (left) in "Paleomagnetic Chron" indicate mixed polarity zones with dominant interval polarity on right. Global carbon isotope excursions identified in red (after Buggisch and Joachimski 2006). FSV = falsiovalis excursion. LKW = Lower Kellwasser excursion. UKW = Upper Kellwasser excursion. ENK = Enkeberg excursion.

Figure 7: Walkout correlation between the Classic Face in Windjana Gorge and the WNB measured section (interpretation and age context for Classic Face after Playford et al. 2009, Playton and Kerans 2015 a). Coarse stratigraphic context extrapolated from Classic Face to WNB was sufficient to calibrate Middle vs. Upper Frasnian intervals and correlate reversals into conodont-constrained slope sections. See Figure 2 and Appendix 1 for sequence architecture and measured section legend, respectively. See Figure 6 for reversal chart. Seq = sequence. SB = sequence boundary. MFS = maximum flooding surface. TST = transgressive

systems tract. HST = highstand systems tract. F-F = Frasnian-Famennian. W = wackestone. P = packstone. G = grainstone. B = boundstone.

Figure 8: Regional cross section and integrated chronostratigraphy of key shelf-to-basin (right-to-left) stratigraphic sections across CBCP dataset with master correlations, and finalized sequence stratigraphic interpretation. Sections are not datumed due to non-horizontal timeline profiles, and not at the same vertical scale due to large thickness differences. Inset in lower right shows measured sections (dark blue) at same scale, corrected for post-depositional tilt, and reconstructed in space along Lennard Shelf depositional profiles (dashed), with no vertical exaggeration. See Figure 1 and Appendix 1 for section locations and facies legend, respectively. Dark grey and white bands are normal and reversed polarity chrons, respectively, and light grey bands are mixed polarity chrons. Green striped bands are positive carbon isotope excursion correlation zones, and orange striped bands are negative excursion correlation zones.

Figure 9: Regional shelf-to-basin composite reconstruction of the Middle-Upper Devonian of the Lennard Shelf, showing facies distributions and architectures within sequence stratigraphic framework (red and blue surfaces and triangles) and conodont zones (see also Figure 6). Bold black lines are measured sections true to actual transect surface topography. Cores shown as vertical wells. No vertical exaggeration. Stratal reconstruction honors extensive depositional dip data collected along transects, and includes correction for post-depositional tilt. Asterisks indicate less-constrained transects. Facies honor measured section and core descriptions. Backstepping events of Playford et al. (2009) in blue text.

Figure 10: Hierarchical supersequence and composite sequence framework for the Middle-Upper Devonian of the Lennard Shelf. Bold black lines are measured sections true to actual surface topography and corrected for tilt. Asterisks denote less-constrained transects chronostratigraphically. G-F = Givetian-Frasnian boundary. F-F = Frasnian-Famennian boundary. Middle-Upper Frasnian boundary occurs within HST of Sequence 5 (Fr5). a) Supersequence architecture of the Lennard Shelf. Blue shading defines the supersequence TST, red shading defines the supersequence HST, and the supersequence MFS is the boundary between blue and red fills in the uppermost Middle Frasnian. b) Composite sequence

architecture of the Lennard Shelf. Red and blue triangles denote systems tracts, and red and blue lines denote sequence boundaries and maximum flooding surfaces, respectively. Grey shading indicates undefined Middle Famennian strata (MFa interval).

Figure 11: Lower-Middle Frasnian Composite Sequence 4 margin-to-slope development within the supersequence TST when margins were undergoing long-term backstepping. Red lines are sequence boundaries and blue line is maximum flooding surface. In upper right inset, placement within supersequence architecture shown in orange, and blue and green lines are supersequence MFS and F-F boundary, respectively. dom'd = dominated. a) TST setting: margins evolved into escarpments through aggradation and had associated grain-dominated foreslopes. Margins became increasingly sensitive to collapse triggers. b) Late TST setting: margins failed, producing reentrants and debris in slope or basinal settings. c) MFS-Early HST setting: margins backstepped at the MFS, reinitiated, and began to construct relief. The former slope profile was draped with bypassed sediment. d) HST setting: margins weakly prograded and had associated grain-dominated foreslopes.

Figure 12: Lower-Middle Frasnian Composite Sequence 4 stacking patterns for margin, middle-slope, and basinal environments. Color legend pertains to measured sections. See Figure 11 for supersequence context and model color scheme. See Appendices for measured sections. Margin succession is from the PGH measured section and used as a proxy for Sequence 4. Middle-slope succession is from the SO measured section. Basin succession is from the MR1 Winkie core. dom'd = dominated. bndstn = boundstone. rudstn = rudstone. gnstn = grainstone. pkstn = packstone. wkstn = wackestone.

Figure 13: Outcrop photographs of systems tracts and significant sequence stratigraphic surfaces recorded in margin, slope, and basinal strata. rudstn = rudstone. gnstn = grainstone. pkstn = packstone. wkstn = wackestone. A) Frasnian Composite Sequence 4 (Fr4) TST to HST succession recorded in middle slope setting, along SO transect (Appendix 6). Symmetrical pattern of megabreccia interval bracketed by grain-dominated deposits is observed, representing Early TST grain shedding during aggradation, Late TST margin collapse, backstepping at the MFS, and HST grain shedding. B) Upper portion of Frasnian Composite

Sequence 6 (Fr6) and lower portion of Frasnian Composite Sequence 7 (Fr7) recorded in middle slope setting, along SO transect (Appendix 6). Fr6 shows transition from debris-dominated to grain-dominated slopes reflecting slope readjustment subsequent to the supersequence MFS. Abrupt change in grain composition is observed in Fr7, likely related to pre-extinction effects. Fr7 MFS coincides with the Upper Kellwasser isotopic event (UKW). C) Supersequence MFS in margin position with megabreccia deposits abutting fractured in situ reefal facies, along WS transect (Appendix 4). Supersequence MFS coincides with Frasnian Composite Sequence 5 (Fr5) MFS. Fr5 HST megabreccia deposits are younger than collapse events that formed the erosional scarp during the TST of Fr5. D) Upper portion of Frasnian Composite Sequence 6 (Fr6) and lower portion of Frasnian Composite Sequence 7 (Fr7) recorded in upper-to-middle slope setting, along WS transect (Appendix 4). Debris-dominated to grain-dominated slope deposition can be observed in the Fr6 HST. The TST of Fr7 is marked by an abrupt downslope expansion of the microbial boundstone factory, interpreted to be related to pre-extinction effects. E) Famennian Composite Sequence 2 (Fa2) TST to HST succession recorded in toe-of-slope setting, along CL transect (Appendix 8). Stratigraphic thickness shown is approximately 40 meters. Interbedded silt and silty wackestone-packstone dominate the overall succession, with conspicuous debris horizons and boundstone lenses present in the HST.

Figure 14: Middle-Upper Frasnian Composite Sequence 5 margin-to-slope development bracketing the supersequence MFS when margins underwent the long-term transition from backstepping and aggradation to progradation. Red lines are sequence boundaries and blue line is maximum flooding surface. In upper right inset, placement within supersequence architecture shown in red, and blue and green lines are supersequence MFS and F-F boundary, respectively. dom'd = dominated. a) Early TST setting: escarpment margins developed from aggradation with associated grain-dominated foreslopes. b) Late TST setting: margins continued to aggrade, built relief, and developed severe instability resulting in sustained mass wasting and the formation of an erosional escarpment with associated debris-dominated foreslopes. c) HST setting: margins were unable to prograde over underfilled escarpment profile and consequently failed, maintaining debris-dominated foreslopes and an erosional escarpment configuration.

Figure 15: Middle-Upper Frasnian Composite Sequence 5 stacking patterns for upper-slope, middle-slope, lower-slope, and basinal environments. Color legend pertains to measured sections. See Figure 13 for supersequence context and model color scheme. See Appendices for measured sections. Upper-slope succession is from the WS measured section. Middle-slope succession is from the SO measured section. Lower-slope succession is from the VHS measured section. Basin succession is from the MR1 Winkie core. dom'd = dominated. bndstn = boundstone. rudstn = rudstone. gnstn = grainstone. pkstn = packstone. wkstn = wackestone.

Figure 16: Upper Frasnian Composite Sequence 6 margin-to-slope development within the supersequence Early HST when margins were unable to prograde over relict escarpment profiles. Red lines are sequence boundaries and blue line is maximum flooding surface. In upper right inset, placement within supersequence architecture shown in beige, and blue and green lines are supersequence MFS and F-F boundary, respectively. dom'd = dominated. a) TST setting: margin aggradation on inherited escarpment profile resulted in continued instability and mass wasting with associated debris-dominated foreslopes. b) Early HST setting: pulses of progradation resulted in margin failure, emplacing the final volumes of debris substrate required for progradation. c) Late HST setting: With available debris substrate, margins transitioned into accretionary configurations and prograded with associated grain-dominated foreslopes.

Figure 17: Upper Frasnian Composite Sequence 6 stacking patterns for upper-slope, middle-slope, lower-slope, and basinal environments. Color legend pertains to measured sections. See Figure 15 for supersequence context and model color scheme. See Appendices for measured sections. Upper-slope succession is from the WS measured section. Middle-slope succession is from the SO measured section. Lower-slope succession is from the VHS measured section. Basin succession is from the MR1 Winkie core. bndstn = boundstone. rudstn = rudstone. gnstn = grainstone. pkstn = packstone. wkstn = wackestone.

Figure 18: Upper Frasnian Composite Sequence 7 margin-to-slope development within the supersequence prograding HST just prior to the F-F boundary. Red lines are sequence boundaries and blue line is maximum flooding surface. In upper right inset, placement within

supersequence architecture shown in purple, and blue and green lines are supersequence MFS and F-F boundary, respectively. dom'd = dominated. a) TST setting: margins aggraded and the encrusted upper-slope environment expanded significantly downslope. Upper-middle-slope environments were silt-dominated with coarser gully fills and equivalent to downdip, bypassed grain-dominated settings. Distal slope settings were overall poorly developed. b) HST setting: margins were progradational with deep boundstone environments and basinward-fining (debris-to-grain-dominated) foreslopes.

Figure 19: Upper Frasnian Composite Sequence 7 stacking patterns for upper-slope, middle-slope, lower-slope, and basinal environments. Color legend pertains to measured sections. See Figure 17 for supersequence context and model color scheme. See Appendices for measured sections. Upper-slope succession is from the WV measured section. Upper-middle-slope inset succession from CF4 measured section in Playton and Kerans (2015 b, their Figure 8). Middle-slope succession is from the SO measured section. Lower-slope succession is from the VHS measured section. Basin succession is from the CL measured section. dom'd = dominated. bndstn = boundstone. rudstn = rudstone. gnstn = grainstone. pkstn = packstone. wkstn = wackestone.

Figure 20: Lower Famennian Composite Sequence 1 margin-to-slope development within the supersequence prograding HST just subsequent to the F-F boundary. Red line is sequence boundary, blue line is maximum flooding surface, and green line is F-F boundary (also a sequence boundary). In upper right inset, placement within supersequence architecture shown in light blue, and blue and green lines are supersequence MFS and F-F boundary, respectively. dom'd = dominated. a) TST setting: margins were weakly progradational with a thin upper-slope boundstone veneer. Middle slopes exhibited anomalously thick stacks of oolitic grainstone (red) and debris in lower-slope settings, suggesting bypass. b) HST setting: margins were strongly progradational with deep microbial boundstone and basinward-fining (debris-to-grain-dominated) foreslopes.

Figure 21: Lower Famennian Composite Sequence 1 stacking patterns for upper-slope, middle-slope, lower-slope, and basinal environments. Lower green line is F-F boundary (also a

sequence boundary). Color legend pertains to measured sections. See Figure 19 for supersequence context and model color scheme. See Appendices for measured sections. Upper-slope succession is from the WV measured section. Middle-slope succession is from the SO measured section. Lower-slope succession is from the VHS measured section. Basin succession is from the CL measured section. dom'd = dominated. bndstn = boundstone. rudstn = rudstone. gnstn = grainstone. pkstn = packstone. wkstn = wackestone.

Figure 22: Lower-Middle Famennian Composite Sequence 2 margin-to-slope development within the supersequence HST when margins were strongly progradational. Red lines are sequence boundaries and blue line is maximum flooding surface. In upper right inset, placement within supersequence architecture shown in blue, and blue and green lines are supersequence MFS and F-F boundary, respectively. dom'd = dominated. a) TST setting: margins were weakly progradational and with deep boundstone upper slopes and grain-dominated foreslopes. b) HST setting: margins were strongly progradational with deep boundstone upper slopes and mixed debris- and grain-dominated foreslopes.

Figure 23: Lower-Middle Famennian Composite Sequence 2 stacking patterns for upper-slope, middle-slope, lower-slope, and basinal environments. Color legend pertains to measured sections. See Figure 21 for supersequence context and model color scheme. See Appendices for measured sections. Upper-slope succession is from the WV measured section. Middle-slope succession is from the SO measured section. Lower-slope succession is from the VHS measured section. Basin succession is from the CL measured section. bndstn = boundstone. rudstn = rudstone. gnstn = grainstone. pkstn = packstone. wkstn = wackestone.

Figure 24: SO and WNB measured sections with platform-top to middle-slope correlations and highlighting progradational pulses at cycle-set scale (dark green arrows along WNB) during overall aggradational succession. Progradational pulses in composite sequence TSTs are here interpreted as the mechanism for margin failure during platform and margin aggradation, resulting in stacked debris deposits on the slope during the TST. Facies and correlation control (including conodont picks, paleomagnetic polarity reversals, and carbon isotopes) shown with composite sequence and cycle set interpretations (red-blue and yellow-green triangles,

respectively). See Appendix 1 for detailed legend. See Figures 8 and 9 for chronostratigraphic information. See Appendices 3 and 6 for detailed measured section data.

Figure 25: Idealized vertical facies successions in a middle-slope setting showing composite sequence stacking patterns at various points within a supersequence. dom'd = dominated. a) Composite sequence stacking within a supersequence TST. Starved slope drape recording margin backstepping at the MFS may be poorly preserved. b) Stacking across long-term transition from aggradation to progradation at the supersequence MFS. Composite sequences are amalgamated during erosional escarpment phase, thus exact placement of systems tracts shown are somewhat arbitrary. Supersequence MFS is positioned low within the debris succession as the majority of slope infilling occurs in the supersequence Early HST. c) Composite sequence stacking within a supersequence HST. Occurrences of debris represent high-frequency LSTs (see Playton and Kerans 2015 b).

Figure 26: Idealized vertical facies successions in a middle-slope setting showing precursor and aftermath indications of an extinction interval. Successions are schematic to capture the breadth of observations, thus exact vertical relationships and combinations can vary. dom'd = dominated. bndstn = boundstone. a) Facies and relationships indicating the onset of biotic stress and lead up period prior to an extinction boundary. b) Succession indicating the early rebound of a single carbonate factory subsequent to an extinction boundary, while other factories recover later. c) Succession indicating ubiquitous microbial encrustation subsequent to an extinction boundary, suggesting "continuous" microbial growth and episodic deposition of other sediment types.

Table 1: Table of CBCP dataset by section or core, including data type, location (see Figure 1), age, depositional environment, stratigraphic thickness, and samples collected. Parallel sections are closely-spaced, overlap sections to ensure data repeatability.

Table 2: Table of facies scheme used for the CBCP. EOD = environment of deposition. See Appendix 1 for color scheme used in measured sections.

Table 3: Table outlining foundational work and CBCP studies pertaining to the primary constraints used for regional correlation.

Table 4: Tables showing confidence levels for CBCP measured sections and cores (a) and markers or intervals used for chronostratigraphy (b). Green = highest confidence. Yellow = medium-high confidence. Red = low confidence. See Table 1 for measured section abbreviations. “Regional constraints” are those correlated across the CBCP dataset but not linked to global references. LKW = Lower Kellwasser. UKW = Upper Kellwasser. FSV = falsiovalis. ENK = Enkeberg.

Table 5: Table showing CBCP advances in Lennard Shelf understanding and characterization by theme, with comparison to previous work.

Appendix 1: Legend for measured sections, core descriptions and correlations, including schemes for CBCP universal facies, conodont picks, description textural profiles, paleomagnetic polarity reversals, stable carbon isotopes, surfaces-markers, and sequence stratigraphy.

Appendix 2: Windjana North A (WNA) measured section with correlation constraints. See Appendix 1 for legend and Figure 1 for location along the Lennard Shelf. WNA is located in the Napier Ranges just northwest of Windjana Gorge (17°23'35.49"S, 124°57'14.43"E to 17°23'50.92"S, 124°56'58.08"E). Paleogeographically, the Windjana Gorge area reflects a very narrow point along the Lennard Shelf (less than 5 kilometers shelf width in places) that is rich in siliciclastics, and part of a linear margin tens of kilometers long, but with complex, finer-scale (kilometer or less) reentrant-promontory configurations superimposed along strike. WNA is Middle-Upper Frasnian in age, based on physical walk-outs to key control outcrops (i.e., the Classic Face in Windjana Gorge; Playford et al. 2009, Playton and Kerans 2015 a). WNA facies consist of 1) cyclic skeletal-peloid grainstones-packstones, bioclastic rudstones-floatstones, peloidal packstones-wackestones-mudstones, and siliciclastics, representing inner platform-top settings; and 2) cyclic skeletal-peloid grainstones-packstones, bioclastic rudstones-floatstones, and *in situ*, bedded stromatoporoid framestones, indicative of outer

platform-top to reef-flat settings. WNA facies transition upward from inner platform-top assemblages to outer platform-top to reef-flat assemblages. Inner platform-top carbonates are commonly dolomitic, whereas outer platform to reef-flat carbonates are dominantly limestone, with variable degrees of intermixed siliciclastics in both. Physical walk-outs between WNA, WNB, and WS measured sections were achieved.

Appendix 3: Windjana North B (WNB) measured section with correlation constraints. See Appendix 1 for legend and Figure 1 for location along the Lennard Shelf. WNB is located about 900 meters along strike of WNA (17°23'54.31"S, 124°57'22.90"E to 17°24'16.81"S, 124°57'11.05"E) with a similar paleogeographic setting, age, and age control. Facies exposed at WNB consist of 1) cycles of skeletal-peloid grainstones-packstones, bioclastic rudstones-floatstones, peloidal packstones-wackestones-mudstones, and siliciclastics, representing inner platform-top settings; and 2) fingers of skeletal-peloid grainstones-packstones, bioclastic rudstones-floatstones, and *in situ*, bedded stromatoporoid framestones, indicative of the transition into outer platform-top and reef-flat settings. Stratigraphically upward, WNB facies remain dominantly inner platform-top assemblages, with intervals of increased proportions of outer platform-top to reef-flat assemblages. Inner platform-top facies are commonly dolomitic, and outer platform to reef-flat intercalations are generally mixed limestone-dolomite, with variable degrees of intermixed siliciclastics in both. A physical walk-out between WNA and WNB measured sections was achieved, as well as a walk-out from WNB into Windjana Gorge.

Appendix 4: Windjana Slope (WS) measured section with correlation constraints. See Appendix 1 for legend and Figure 1 for location along the Lennard Shelf. WS is located in the Napier Ranges just northwest of Windjana Gorge (17°23'15.14"S, 124°57'3.00"E to 17°23'37.47"S, 124°56'45.88"E), and is paleogeographically similar to WNA in terms of the broader margin setting. WS is Middle to Upper Frasnian in age, based on physical walk-outs to key control outcrops (i.e., the Classic Face in Windjana Gorge), some recoverable biostratigraphic control, and correlations to key control sections. Facies exposed at WS consist of 1) intervals of stromatoporoid framestones with intercalations of skeletal-peloid grainstones-packstones and bioclastic rudstones-floatstones, representing reef core to reef-flat settings; 2) intervals of margin-derived breccia-blocks, platform-derived grainstone-packstone of variable

composition, graded siliciclastics, and tongues of *in situ* microbial boundstone, indicative of middle-slope settings and the middle-upper-slope transition; and 3) intervals of bedded microbial boundstone representing upper-slope environments. Depositional dips in slope strata, corroborated by geopetals, range from 20-30^{o} after tilt correction. Stratigraphically upward, WS facies abruptly shift from *in situ* reefal margin settings to allochthonous middle-slope settings across an irregular truncation surface, interpreted as a margin reentrant collapse feature. The succession above the truncation surface shows alternations of carbonate grain-dominated-, siliciclastic-dominated-, and carbonate debris-dominated middle-slope assemblages. The uppermost portion of WS consists of upper-slope *in situ* boundstones. Partial or patchy dolomite, apparently non-facies selective but sometimes fabric selective, is common in the lower half of WS, while the upper half of the section is dominantly limestone with variable degrees of intermixed siliciclastics throughout. Physical walk-outs between WS, WNA, and WV measured sections were achieved.

Appendix 5: Windjana Valley (WV) measured section with correlation constraints. See Appendix 1 for legend and Figure 1 for location along the Lennard Shelf. WV is located in the Napier Ranges just northwest of Windjana Gorge (17°23'44.53"S, 124°56'49.61"E to 17°24'5.44"S, 124°56'21.24"E; slightly further than the WS transect) and shares a similar paleogeographic setting as WS. WV is Upper Frasnian to Middle Famennian in age, based on recovered biostratigraphic control as well as correlations to key control sections. Facies exposed at WV consist of intervals of 1) graded, platform-derived grainstone-packstone, 2) margin-derived breccia-blocks, and 3) *in situ* microbial boundstone-encrusted grainstone, indicative of alternations between middle-slope allochthonous- and upper-slope autochthonous environments. Depositional dips, corroborated by geopetals, range from 25-40^{o} after tilt correction. Stratigraphically upward, there are multiple alternations of middle- and upper-slope deposits. WV strata are dominantly limestone throughout, with variable degrees of intermixed siliciclastics.

Appendix 6: South Oscars (SO) measured section with correlation constraints. See Appendix 1 for legend and Figure 1 for location along the Lennard Shelf. SO is located in the southern Oscar Range (17°54'53.14"S, 125°17'59.13"E to 17°55'25.94"S, 125°17'22.05"E) and has a

nearby parallel section for validation (SOB section; 17°55'16.58"S, 125°17'20.95"E to 17°55'22.02"S, 125°17'16.95"E). Paleogeographically, the Oscar Range was a topographic and structural high composed of basement rocks, outboard of the Lennard Shelf proper. It served as a nucleation point for carbonates to form a partially detached, carbonate-fringed island – the SO section is on the seaward side of the structure and is sheltered from siliciclastic input, thus representing the purest carbonate setting across the CBCP dataset. The SO section extends from Lower Frasnian to Middle Famennian in age, based on robust biostratigraphic control. Facies exposed at SO consist of 1) graded, platform-derived grainstone-packstone, 2) margin- and platform-derived bioclastic rudstone-floatstone, 3) margin-derived breccia-blocks, 4) a curious silty, wispy-laminated micropeloidal packstone-grainstone facies, and 5) interbeds of *in situ* microbial boundstone-encrusted grainstone, all indicative of dominantly middle-slope environments with encroachments of the upper-middle-slope transition. Depositional dips, corroborated by geopetals, range from 20-30^{o} after tilt correction. Stratigraphically upward, facies grade from those deposited in dominantly allochthonous middle-slope environments to a mixed detrital-*in situ* assemblage of the upper-middle-slope transition. Middle-slope assemblages and deposit proportions (i.e., grain- vs. debris-dominated) vary throughout the stratigraphy. SO strata are dominantly limestone throughout, with very little dolomite and no macroscopically-observed siliciclastics.

Appendix 7: Horse Spring (VHS-Virgin Hills South) measured section with correlation constraints. See Appendix 1 for legend and Figure 1 for location along the Lennard Shelf. VHS is located in the Horse Spring Range (18°11'45.97"S, 126° 1'55.99"E to 18°11'38.63"S, 126° 1'49.59"E). Paleogeographically, the Horse Spring Range tracks a segment along a large (> 50 kilometers across) embayment within the Lennard Shelf, thus local dip directions are west-northwesterly (as opposed to regional southwest dips toward the Fitzroy Trough). VHS is Lower Frasnian to Middle Famennian in age, based on robust biostratigraphic control. Facies exposed at VHS consist of 1) graded, platform-derived grainstone-packstone, 2) mottled to wispy silty skeletal-peloidal packstones-wackestones-mudstones, 3) lesser margin-derived breccia-blocks and intraclastic-bioclastic rudstones-floatstones, and 4) rare *in situ* microbial boundstone, all indicative of lower-slope environments. Depositional dips, corroborated by geopetals, range from 10-15^{o} after tilt correction. Vertically, facies are quite interbedded with

no striking patterns, however intervals are observed with greater proportions of margin-derived debris. VHS strata are dominantly limestone throughout, with very little dolomite and no macroscopically-observed siliciclastics except for silt-sized fractions intermixed into muddier deposits.

Appendix 8: Casey Falls (CL) measured section with correlation constraints. See Appendix 1 for legend and Figure 1 for location along the Lennard Shelf. CL is located in the southern Lawford Range (18°44'0.03"S, 126° 5'8.96"E to 18°44'9.39"S, 126° 5'41.23"E) and has a parallel section for validation (CLB section; 18°44'3.93"S, 126° 5'34.88"E to 18°44'7.31"S, 126° 5'40.43"E). Paleogeographically, the Lawford Range and greater Bugle Gap area display exhumed Lower Frasnian paleo-reef topography with extremely complex spine and pinnacle configurations generated from backstepping – the CL section records subsequent progradation and downlap over this relict topography with local dip directions to the south-southeast contrasting with regional southwesterly dips. CL is Upper Frasnian to Middle Famennian in age, based on robust biostratigraphic control. Facies exposed at CL consist of 1) silty skeletal-peloid packstone-wackestone-mudstone with minor microbial boundstone interbeds and platform-derived grainstones, representing a lower-slope to basinal environment; and 2) steeply-dipping, bedded microbial boundstone and encrusted grainstone, indicative of upper-slope settings. Margin-derived breccias and blocks are rare to absent throughout the succession. Depositional dips, corroborated by geopetals and after tilt correction, range from 10-20^{o} in siltier deposits (although believed to be enhanced by differential compaction over underlying margins) and 25-40^{o} in boundstone deposits. Stratigraphically upward, facies grade and interfinger gradually from silt-dominated lower-slope-basinal deposits to upper-slope boundstones, resulting in an odd succession with seemingly no intermediate middle-slope setting of debris, grainstone, and rudstone (see Playton and Kerans 2015 b). CL strata are dominantly limestone throughout, with no dolomite or macroscopically-observed siliciclastics except for silt-sized fractions intermixed into muddier deposits. A key marker bed (shrub-like *Frutexites* microbialite; Playford et al. 2009) that is unique and distinctive in the area is observed in the basal portion of the CL section and marks the top of the MR1 Winkie core, providing a tie point between the two transects.

Appendix 9: Guppy Hills (PGH-Pillara Guppy Hills) measured section with correlation constraints. See Appendix 1 for legend and Figure 1 for location along the Lennard Shelf. PGH extends across the western end of Guppy Hills, south of the Hull Range (18°17'52.90"S, 126° 9'0.76"E to 18°17'28.23"S, 126° 9'19.85"E) and has a parallel section for validation (GHB section; 18°18'0.30"S, 126° 9'15.56"E to 18°17'55.31"S, 126° 9'18.16"E). Paleogeographically, the Hull Range and Guppy Hills areas show complex paleo-topography along the Lennard Shelf due to basement-cored structures that produced elongate and irregular reentrant-promontory configurations – thus slope portions of the PGH section dip northerly in contrast to the regional southwest dips into the Fitzroy Trough. Siliciclastic sources were abundant and close by. PGH is interpreted to be Givetian to Lower Frasnian in age based on coarse coral successions, but is very poorly constrained biostratigraphically (e.g., George et al. 2009b interprets it to be all Lower Frasnian based on Hull Range extrapolations). Facies exposed at PGH consist of 1) cycles of skeletal-peloid grainstones-packstones, bioclastic rudstones-floatstones, peloidal packstones-wackestones-mudstones, and siliciclastics, representing inner platform-top settings; 2) cyclic skeletal-peloid grainstones-packstones, bioclastic rudstones-floatstones, and *in situ*, bedded stromatoporoid framestones, indicative of outer platform-top to reef-flat settings; and 3) dipping, bedded stromatactoid microbial boundstone, diagnostic of encrusted slope environments. Depositional dips in slope strata, corroborated by geopetals, range from 10-15^{o} after tilt correction. Stratigraphically upward, facies grade from inner platform-top to outer platform-top to reef-flat settings, followed by an abrupt transition into slope deposits across an interpreted backstep surface. At the backstep surface, a few meters of graded grain-dominated deposits are present, interpreted to be sediment gravity flows equivalent to a landward margin. Inner platform-top carbonate facies are commonly dolomitic, and outer platform to reef-flat and slope boundstone carbonate facies are dominantly limestone, with variable degrees of intermixed fine siliciclastics.

Appendix 10: Henwood West (NHW-North Henwood West) measured section with correlation constraints. See Appendix 1 for legend and Figure 1 for location along the Lennard Shelf. NHW is located south of the Horseshoe Range (18°14'6.29"S, 126°10'15.94"E to 18°13'57.99"S, 126°10'20.81"E). Paleogeographically, the Henwood West area is in the same setting as that described for Guppy Hills (PGH), but the NHW section is interpreted to be

Upper Frasnian to Lower Famennian in age based on reef assemblage observations. The F-F boundary is well-exposed with clear Famennian reef flat facies overlying Frasnian reef front facies, but the NHW section is not a critical transect for the CBCP. Facies exposed at NHW consist of 1) boundstones ranging from stromatoporoid framestones to microbial boundstones, representing reef-core settings; and 2) cyclic grainstone-packstone ranging in composition from non-skeletal to skeletal, oncolitic rudstone-floatstone, *in situ* Lithiotid (razor clam) floatstone, conglomeratic to fine-grained siliciclastics, and a few occurrences of columnar stromatolitic microbial boundstone, all indicative of outer platform-top and platform-crest to reef-flat environments. In reef-core intervals, encrusting stromatoporoids display horizontally-accreting fabrics reflecting growth upon sub-vertical surfaces. Stratigraphically upward, facies grade from reef-core (with decreasing stromatoporoids upward) to reef-flat to outer-platform and platform-crest settings, signifying progradation. Reef-core facies are dominantly limestone with some patchy intermixed siliciclastics, and the shallower settings are chiefly a mixed limestone-siliciclastic lithology.

Appendix 11: McWhae Ridge (MR1) Winkie core with correlation constraints. See Appendix 1 for legend and Figure 1 for location along the Lennard Shelf. MR1 was drilled on the flank of McWhae Ridge in the Lawford Range (18°43'59.61"S, 126° 4'46.02"E). Paleogeographically, the McWhae Ridge area is in the same overall setting as that described for Casey Falls (CL), however McWhae Ridge itself is a Lower Frasnian drowned reef spine and the MR1 core samples younger, sidelapping strata along its flank. MR1 is Upper Givetian to Lower Famennian in age based on moderately well-constrained biostratigraphy. Facies of MR1 consist of silty skeletal-peloid mudstone-wackestone with minor packstone and rare intraclastic rudstone, representative of toe of slope or basinal environments. Depositional dips are 10-15^{o} but are probably steepened by compaction against underlying paleo-topography. There are no readily identifiable vertical patterns or changes in setting throughout the core, and the dominant lithology is limestone with exception to scattered occurrences of intermixed siliciclastic silt. A key marker bed (shrub-like *Frutexites* microbialite; Playford et al. 2009) that is unique and distinctive in the area marks the top of MR1 and can be observed in the basal portion of the CL section, providing a tie point between the two transects.

Appendix 12: Wade Knoll (WK1) Winkie core with correlation constraints. See Appendix 1 for legend and Figure 1 for location along the Lennard Shelf. WK1 was drilled in Paddy's Valley between the Emmanuel and Laidlaw Ranges (18°39'25.04"S, 126° 0'5.19"E). Paleogeographically, Paddy's Valley is in the same overall setting as that described for Casey Falls (CL), however is in the center of an intra-platform mini-basin between two elongate reefal platforms. WK1 has no biostratigraphic control but spuds on a Lower Frasnian marker bed – it is unknown what age the core base is and is not a critical transect in the CBCP dataset. Facies of WK1 consist of silty skeletal-peloid mudstone-wackestone-packstone with rare intraclastic rudstone, representative of toe of slope or basinal environments. Depositional dips are 3^{o} or less after tilt correction. There are no readily identifiable vertical patterns or changes in setting throughout the core, and the dominant lithology is limestone.

Appendix 13: Horseshoe Range (UD2) subsurface core with correlation constraints. See Appendix 1 for legend and Figure 1 for location along the Lennard Shelf. UD2 was drilled in the Horseshoe Range (approximately 18°13'19.80"S, 126°11'53.94"E). Paleogeographically, the Horseshoe Range is in the same overall setting as that described for Guppy Hills (PGH), however is on the inboard side of complex basement-cored topography (i.e., is directly attached to the hinterland) and reflects a fairly narrow (~5 kilometers) shelf with a prevalent siliciclastic source. UD2 has no biostratigraphic control but can be placed within the stratigraphic framework with moderate confidence due to its isotopic profile and extensive facies record – this interpretation defines UD2 as Middle Frasnian to Middle Famennian in age. The facies in UD2 include all slope assemblages described previously (silt-dominated, grain-dominated, siliciclastic-dominated, debris-dominated, boundstone-dominated), reefal margin microbial boundstones, and outer platform-top and platform-crest assemblages similar to those described for NHW but with the addition of teepee pisolite and muddier shoreline facies, and absence of fine- to conglomeratic siliciclastics. The vertical succession throughout all of UD2 is a classic upward prograding or shallowing sequence of facies, grading from middle slope to upper slope to reef core to reef flat to platform top. The platform-top succession itself displays trends in facies proportions and cycle-bed thickness. The dominant lithology throughout UD2 is mixed limestone-siliciclastic; however dolomitic zones with variable degrees of intermixed siliciclastics are present, probably related to Mississippi Valley Type mineralization.

Appendix 14: Horse Spring (HD14) subsurface core with correlation constraints. See Appendix 1 for legend and Figure 1 for location along the Lennard Shelf. HD14 was drilled in the Horse Spring Range (approximately 18°13'51.40"S, 126° 3'20.10"E). The paleogeographic setting is as for the VHS section. HD14 has no biostratigraphic control, but our best estimate is Upper Givetian to Lower Frasnian age. Facies and the vertical succession of HD14 are similar to those described for PGH, but with a greater proportion of inner platform-top assemblages. A pronounced backstep with encrusted slope overlying outer platform is also observed at HD14, but we interpret this to be a younger backstepping event than that at PGH. The dominant lithology throughout HD14 is dolomite with scattered intermixing of siliciclastics, with exception to the uppermost interval above the backstep surface, which is dominantly limestone.

Figure 4-combined

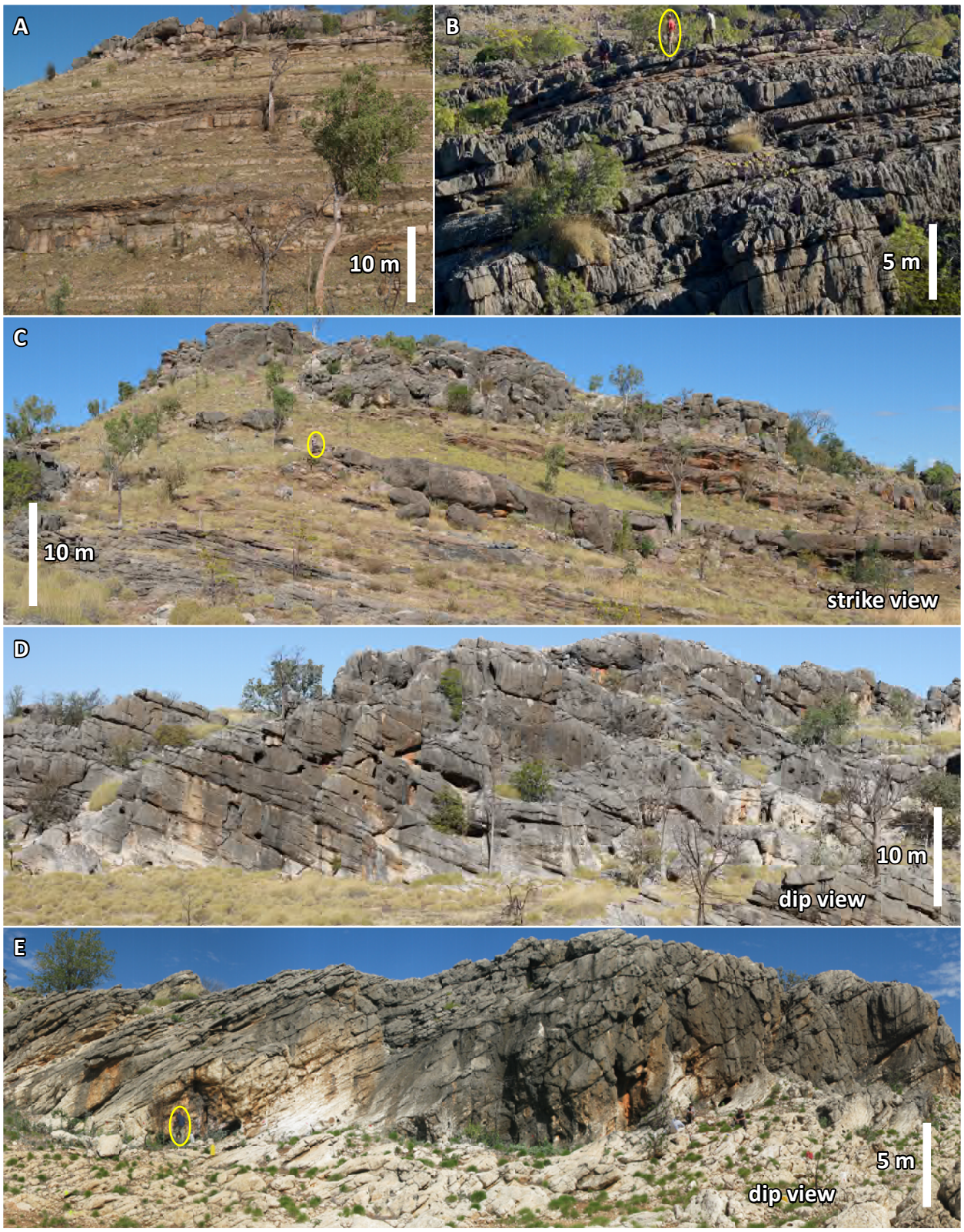

Figure 5-combined

Figure 6

Period	Epoch	Stage	Sub-stage	Conodont Zone	Paleomagnetic Chron	Carbon Isotope Excursion	Sequences	Supersequences	Confi-dence
Devonian	Upper	Famennian	Middle	Upper *marginifera*	undefined	**Fa11p (ENK)**	MFa	M-U Dev HST	low
					Fa-MR19				
					Fa-N18				
					Fa-MN17				
					Fa-R16	Fa10n	Fa3 SB		high
							Fa3 HST		
						Fa9p	Fa3 MFS		
							Fa3 TST		
				rhomboidea-marginifera		Fa8n	Fa2 SB		
							Fa2 HST		
			Lower		Fa-MN15	Fa7p	Fa2 MFS		
							Fa2 TST		
				Upper *crepida-rhomboidea*		Fa6n	Fa1 SB		
							Fa1 HST		
					Fa-R14	Fa5p	Fa1 MFS		
					Fa-MN13		Fa1 TST		
				Upper *triangularis-crepida*	Fa-R12				
					Fa-N11				
					Fa-R10				
				triangularis	FF-MN9		Fr7 SB (F-F)		
		F-F 374.5 Mybp							
		Frasnian	Upper	13b-c			Fr7 HST		
				13b	Fr-MR8	**Fr4p (UKW)**	Fr7 MFS		
							Fr7 TST		
							Fr6 SB		
				13a-b			Fr6 HST		
				12-13a	Fr-MN7	**Fr3p (LKW)**	Fr6 MFS		
							Fr6 TST		
				12	Fr-MR6		Fr5 SB		
				11			Fr5 HST		
			Middle	10	Fr-N5				
				9-12	Fr-R4	Fr2p	Fr5 MFS	M-U Dev MFS	
					Fr-N3		Fr5 TST	M-U Dev TST	
					Fr-R2				
					Fr-MN1				
				7			Fr4 HST		low
			Lower	6 6-8	Fr-MR1'		Fr4 TST		
				4-6			Fr3 HST		
					Fr-MN2'		Fr3 TST		
				2-3			Fr2 HST		
					Fr-MR3'		Fr2 TST		
				1			Fr1 HST		
					Fr-N4'	**Fr1p (FSV)**	Fr1 MFS		
							Fr1 TST		
		G-F 385.3 Mybp			Fr-MR5'		G2 SB (G-F)		
	Middle	Givetian		unknown			G2 HST		
					G-MN6'				
							G2 TST		
					G-R7'		G1 HST		
							G1 TST		
					G-MN8'				

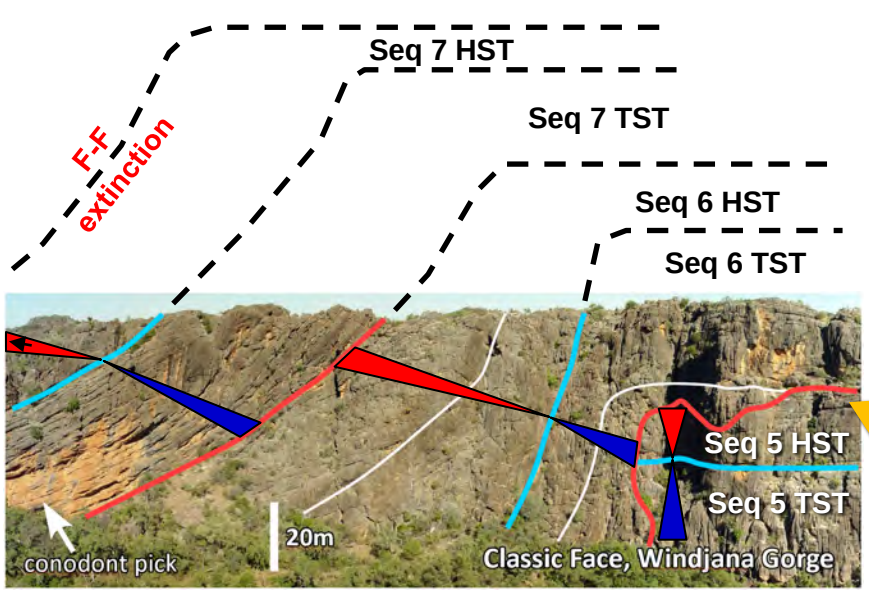
Seq 7 HST
Seq 7 TST
Seq 6 HST
Seq 6 TST
F-F extinction
Seq 5 HST
Seq 5 TST
20m
conodont pick
Classic Face, Windjana Gorge

walkout

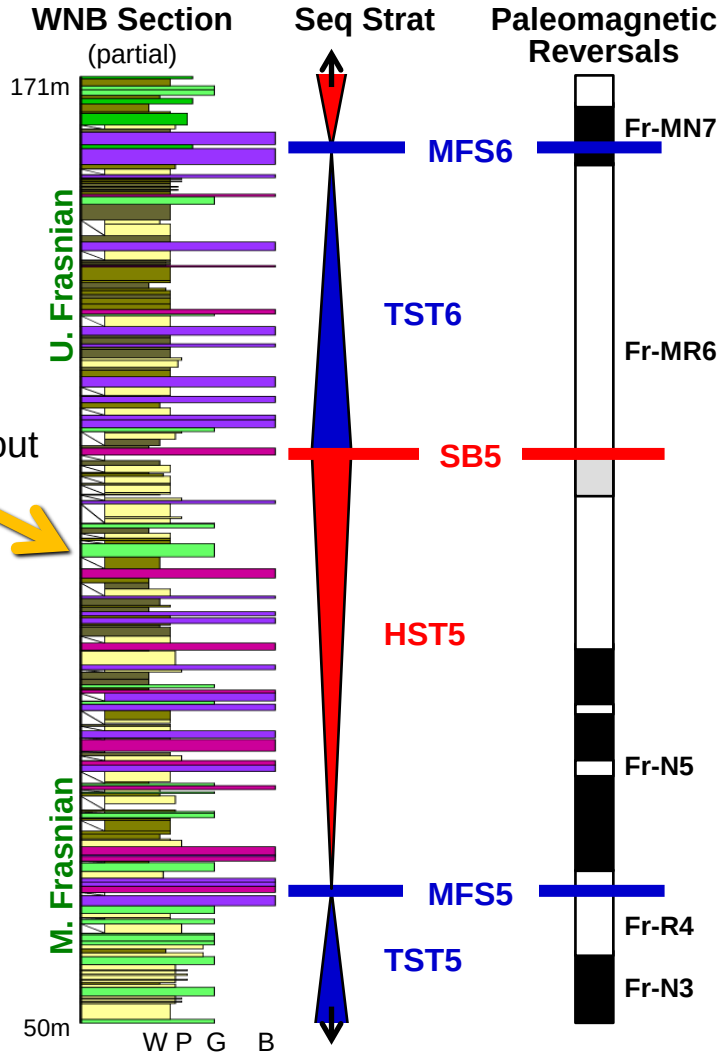
WNB Section
(partial)
Seq Strat
Paleomagnetic Reversals
171m
50m
U. Frasnian
M. Frasnian
W P G B
MFS6
TST6
SB5
HST5
MFS5
TST5
Fr-MN7
Fr-MR6
Fr-N5
Fr-R4
Fr-N3

Figure 8-combined (meant to be 44x110" fold-out)

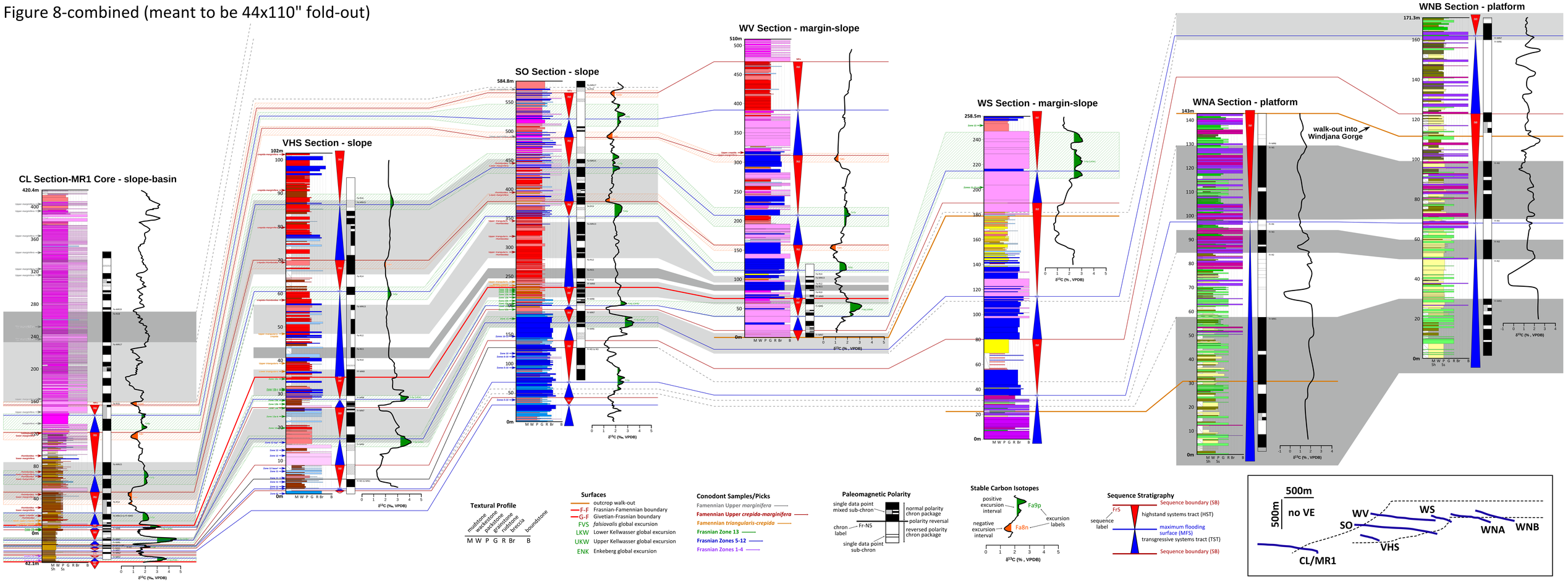

Figure 9-combined (meant to be 11x17)

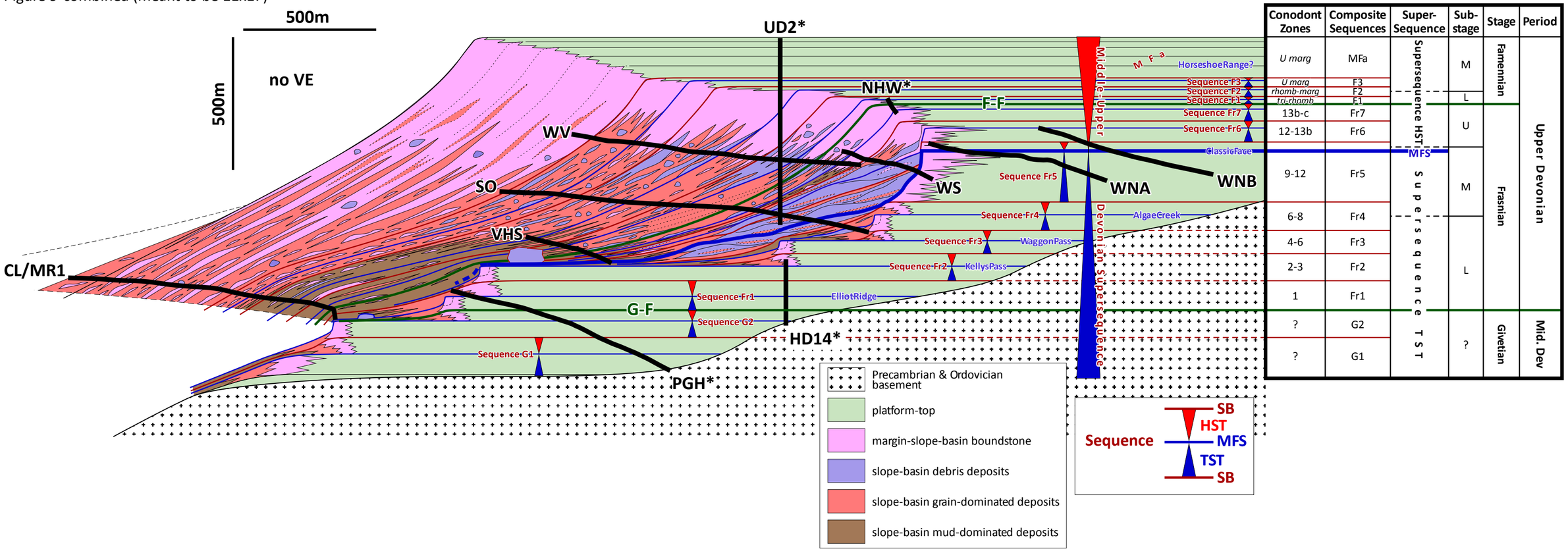

Conodont Zones	Composite Sequences	Super-Sequence	Sub-stage	Stage	Period
U marg	MFa	Supersequence HST	M	Famennian	Upper Devonian
U marg	F3				
rhomb-marg	F2		L		
tri-rhomb	F1				
13b-c	Fr7		U		
12-13b	Fr6				
		MFS			
9-12	Fr5		M	Frasnian	
6-8	Fr4	Supersequence TST			
4-6	Fr3				
2-3	Fr2		L		
1	Fr1				
?	G2		?	Givetian	Mid. Dev
?	G1				

Figure 10-combined

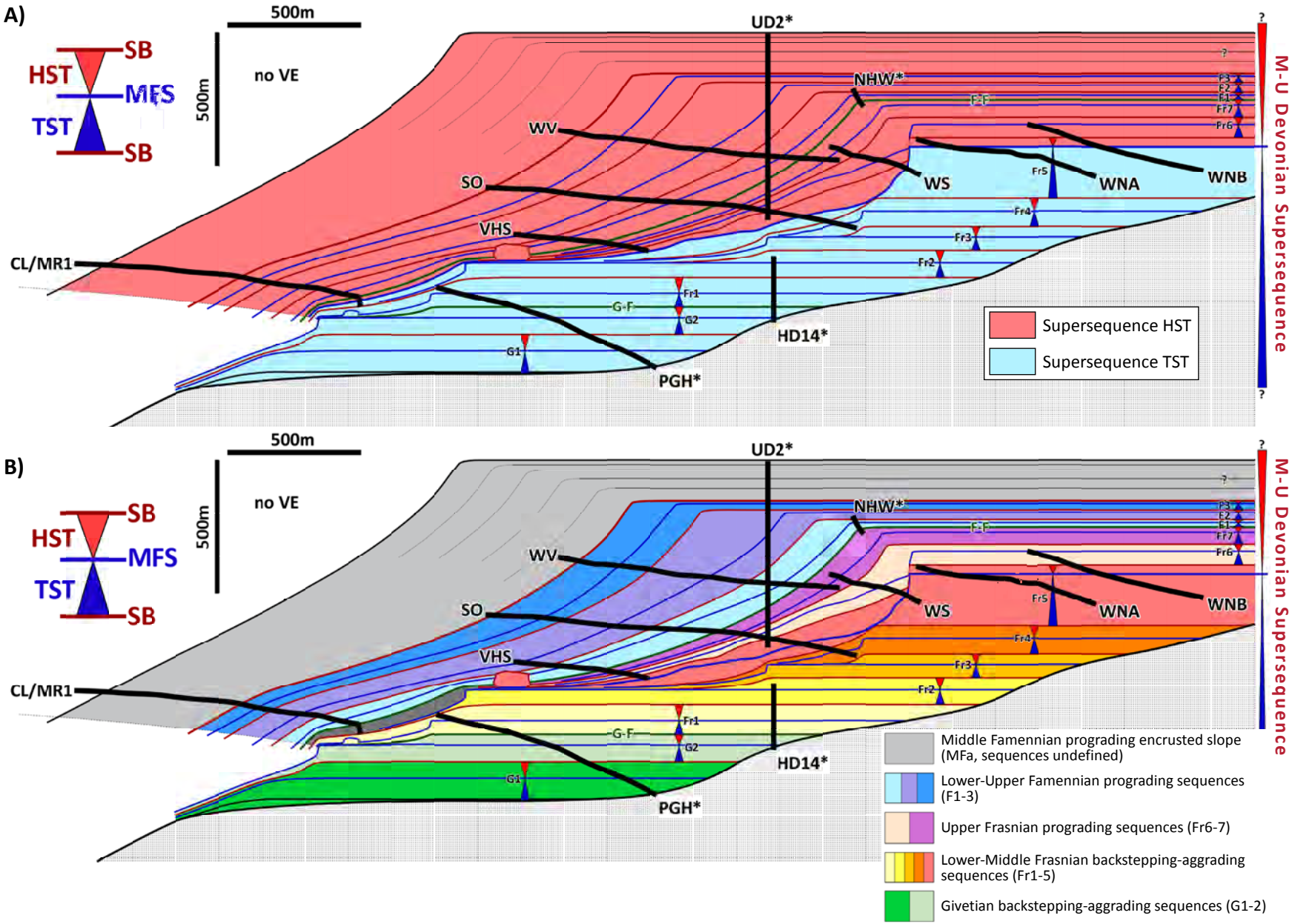

Figure 11-combined

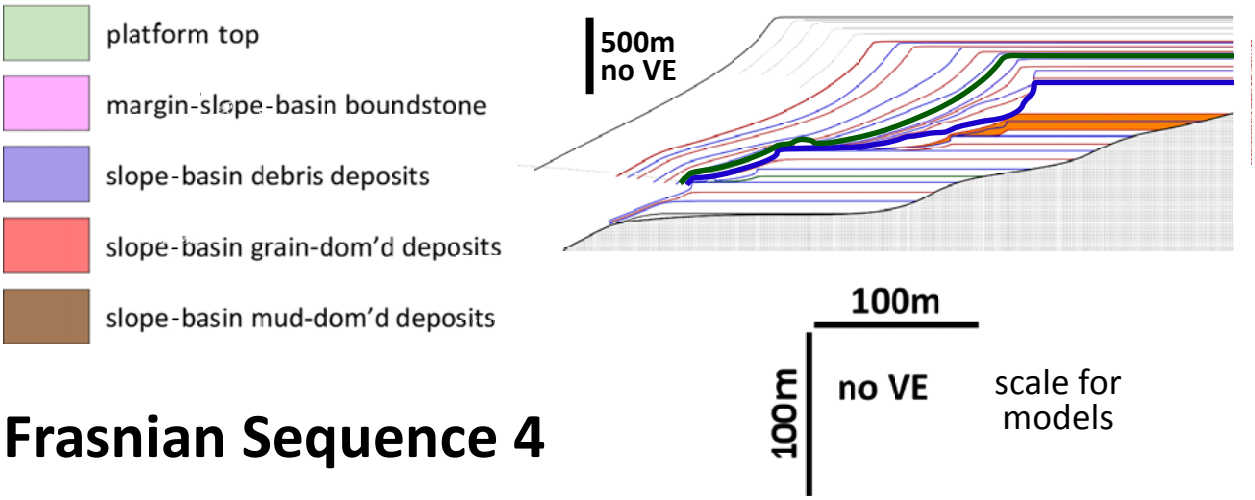

Frasnian Sequence 4

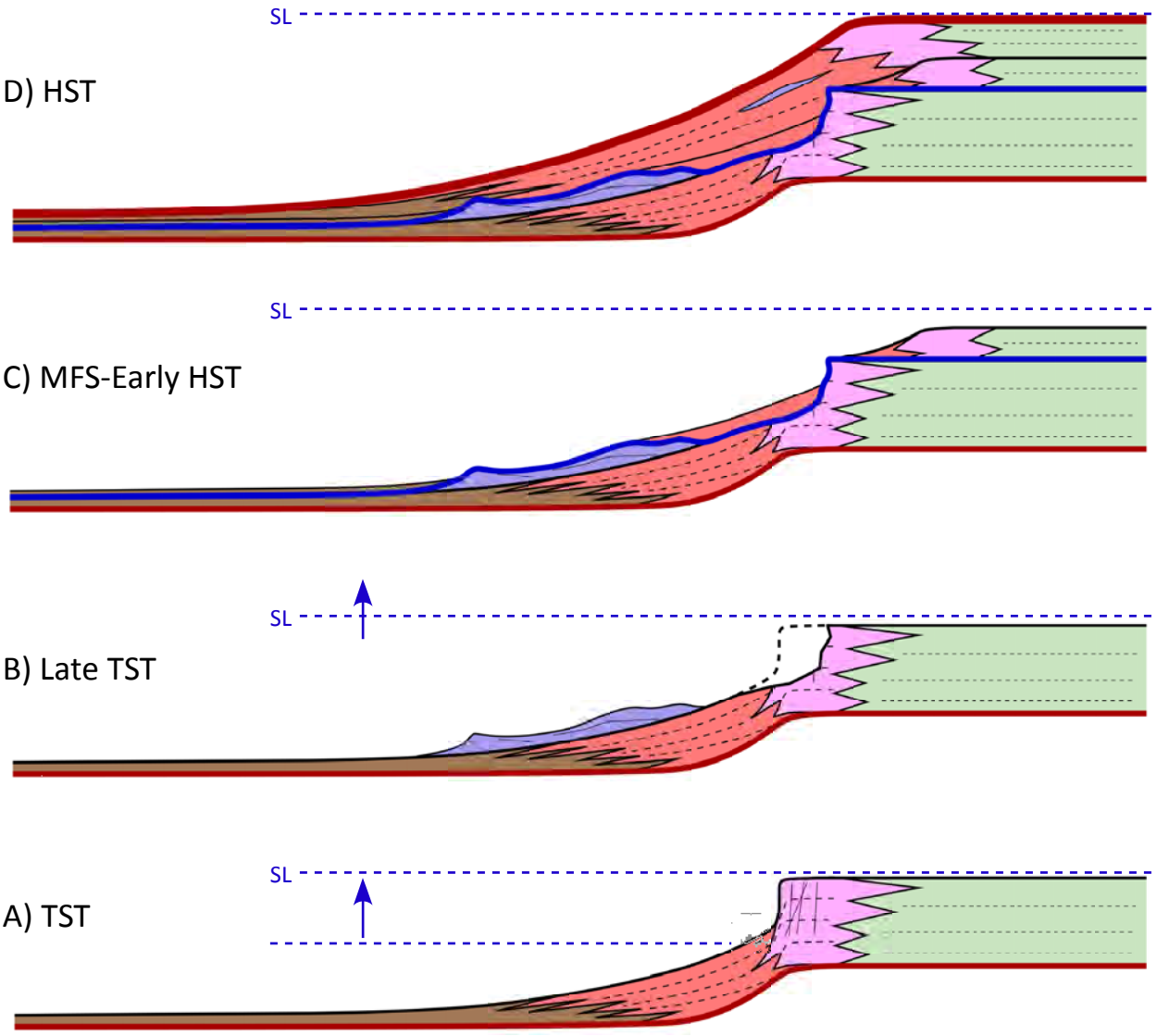

Figure 12-combined

Frasnian Sequence 4

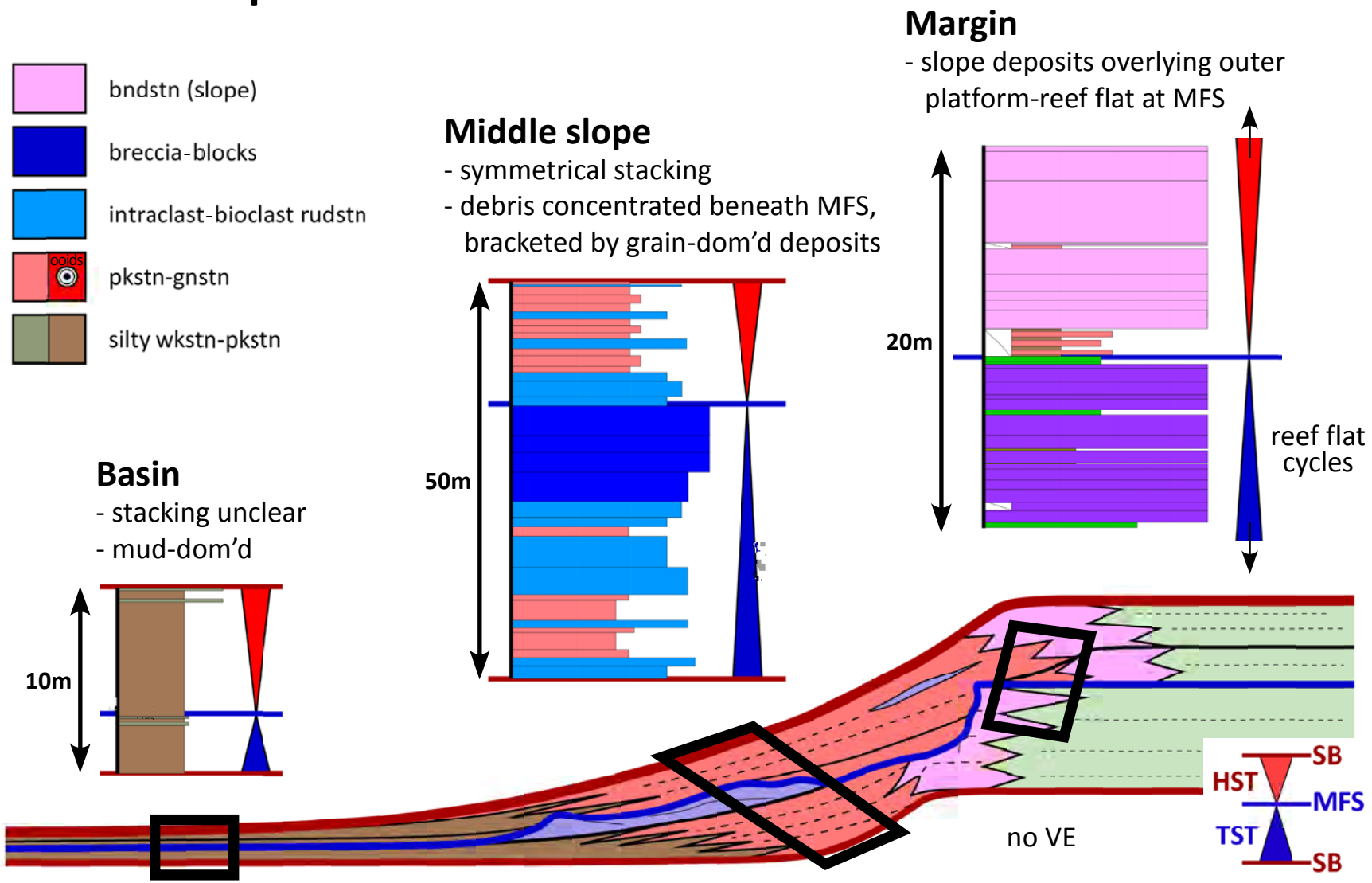

Fig 13-combined

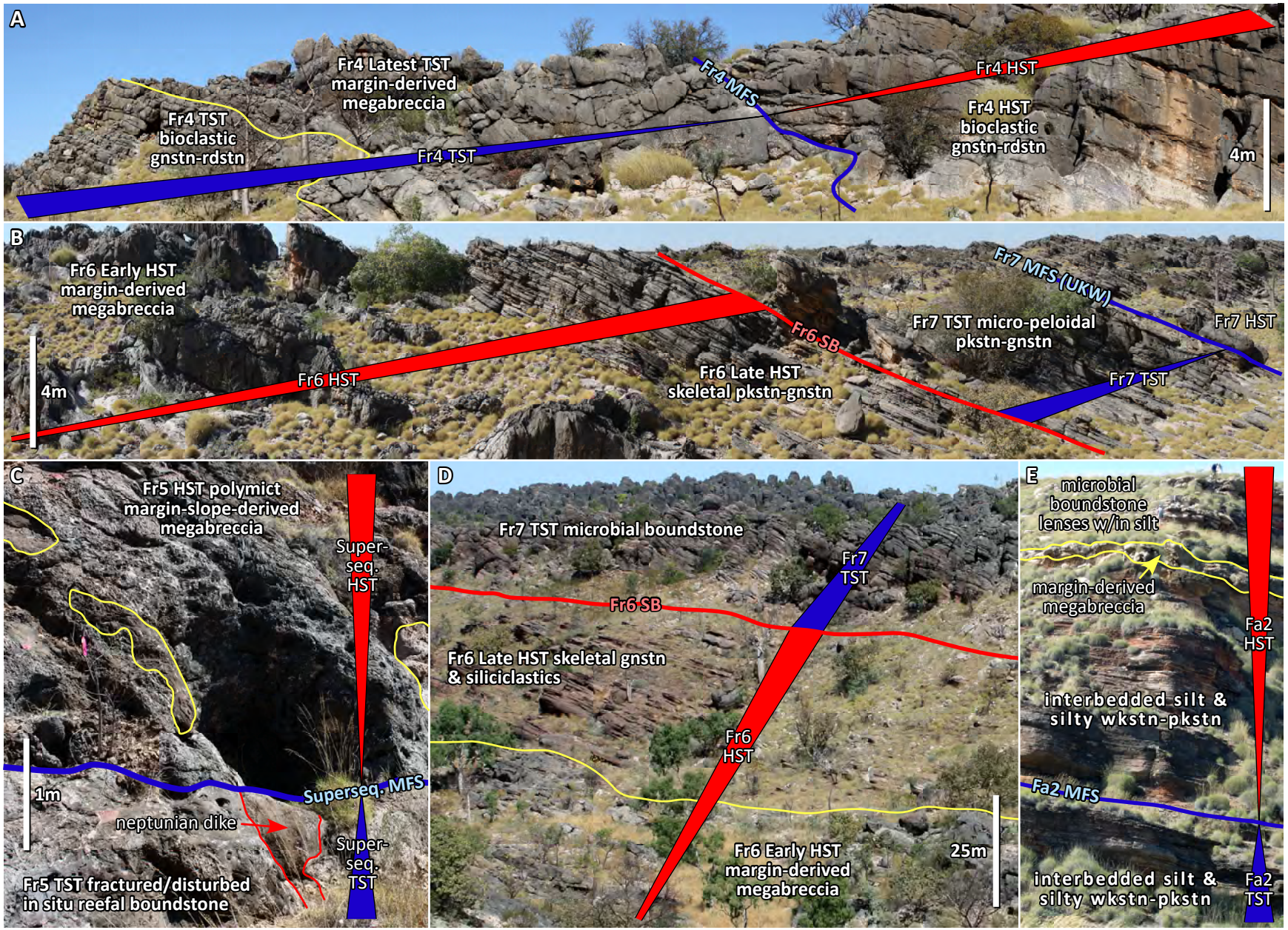

Section/Core Name	Type	Location	Age	Depositional Environment	Thickness (m)	Samples Collected
Windjana North A (WNA)	outcrop measured section	north of Windjana Gorge	M-U Fras	platform-top-reef flat	143	314
Windjana North B (WNB)	outcrop measured section	north of Windjana Gorge	M-U Fras	platform-top-reef flat	171.3	368
Windjana Slope (WS)	outcrop measured section	north of Windjana Gorge	M-U Fras	reef to middle-upper slope	258.5	369
Windjana Valley (WV)	outcrop measured section	north of Windjana Gorge	U Fras-M Fam	middle-upper slope	510	535
South Oscars (SO)*	outcrop measured section	southern Oscar Range	L Fras-M Fam	middle-upper slope	666.6	905
Horse Spring (VHS)	outcrop measured section	west of Horseshoe Range	L Fras-M Fam	lower-middle slope	102	312
Casey Falls (CL)*	outcrop measured section	Mimbi area	U Fras-M Fam	lower-upper slope	520.2	833
Guppy Hills (PGH)*	outcrop measured section	south of Horseshoe Range	Giv-L Fras	platform-top-reef flat-slope	496.1	797
Henwood West (NHW)	outcrop measured section	near Horseshoe Range	U Fras-L Fam	reef to platform-top	66.6	120
Pillara Quarry (PRQ)	quarry-cut measured section	Pillara Mine	Giv	reef flat-upper slope	14	89
McWhae Ridge (MR1)	shallow Winkie core	Mimbi area	Giv-L Fam	lower slope-basin	42.2	155
Wade Knoll (WK1)	shallow Winkie core	north of Mimbi area	Giv?-L Fras	lower slope-basin	37.95	73
UD2	subsurface core	Horseshoe Range	M Fras-M Fam	middle slope to platform-top	703	1358
HD14 (Horse Spring)	subsurface core	west of Horseshoe Range	Giv-L Fras	platform-top-reef flat-slope	250.6	546
*includes parallel sections				**Totals:**	**3982.05**	**6774**

Table 1

Figure 14-combined

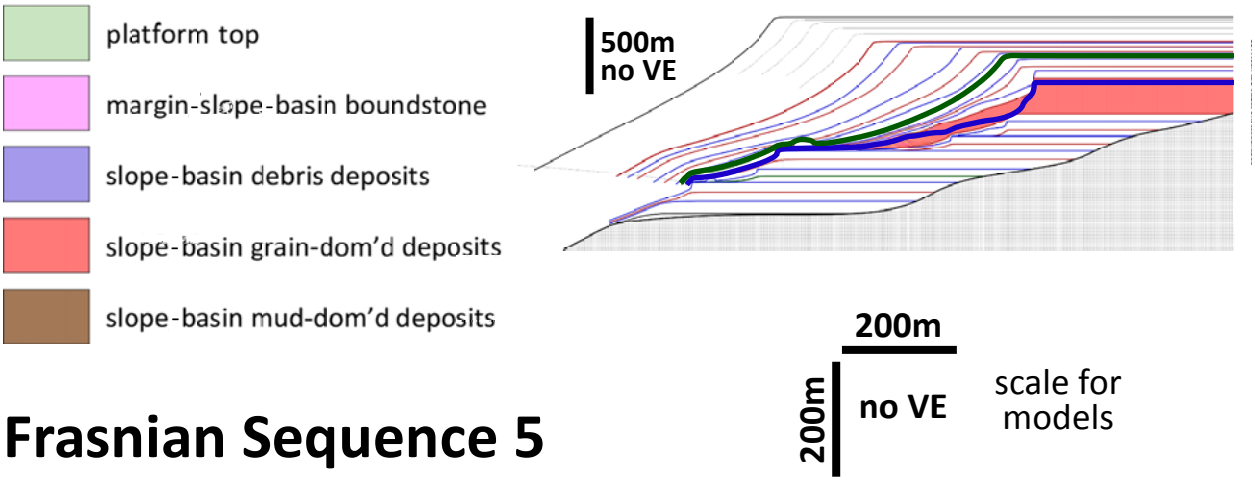

Frasnian Sequence 5

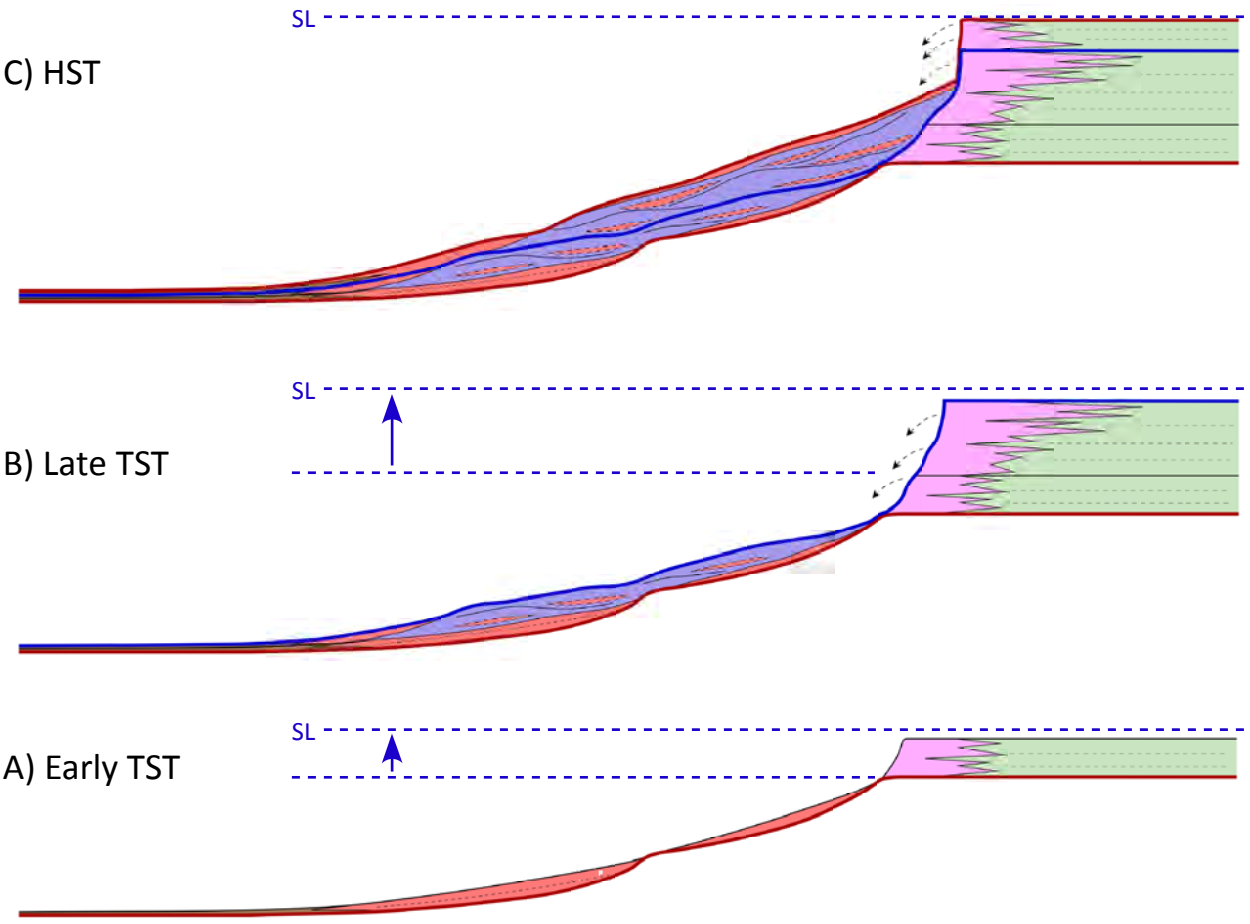

Figure 15-combined

Frasnian Sequence 5

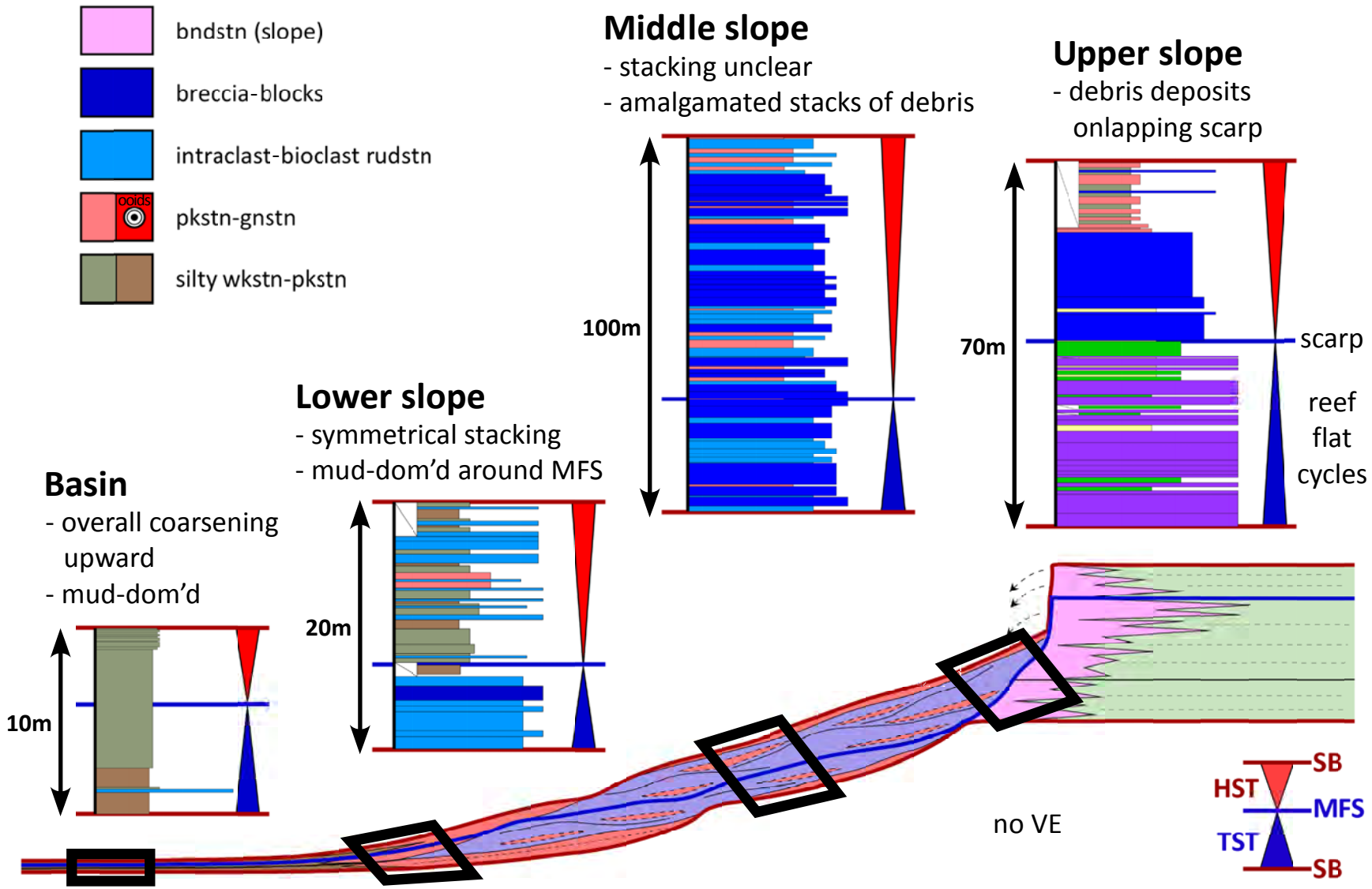

Figure 16-combined

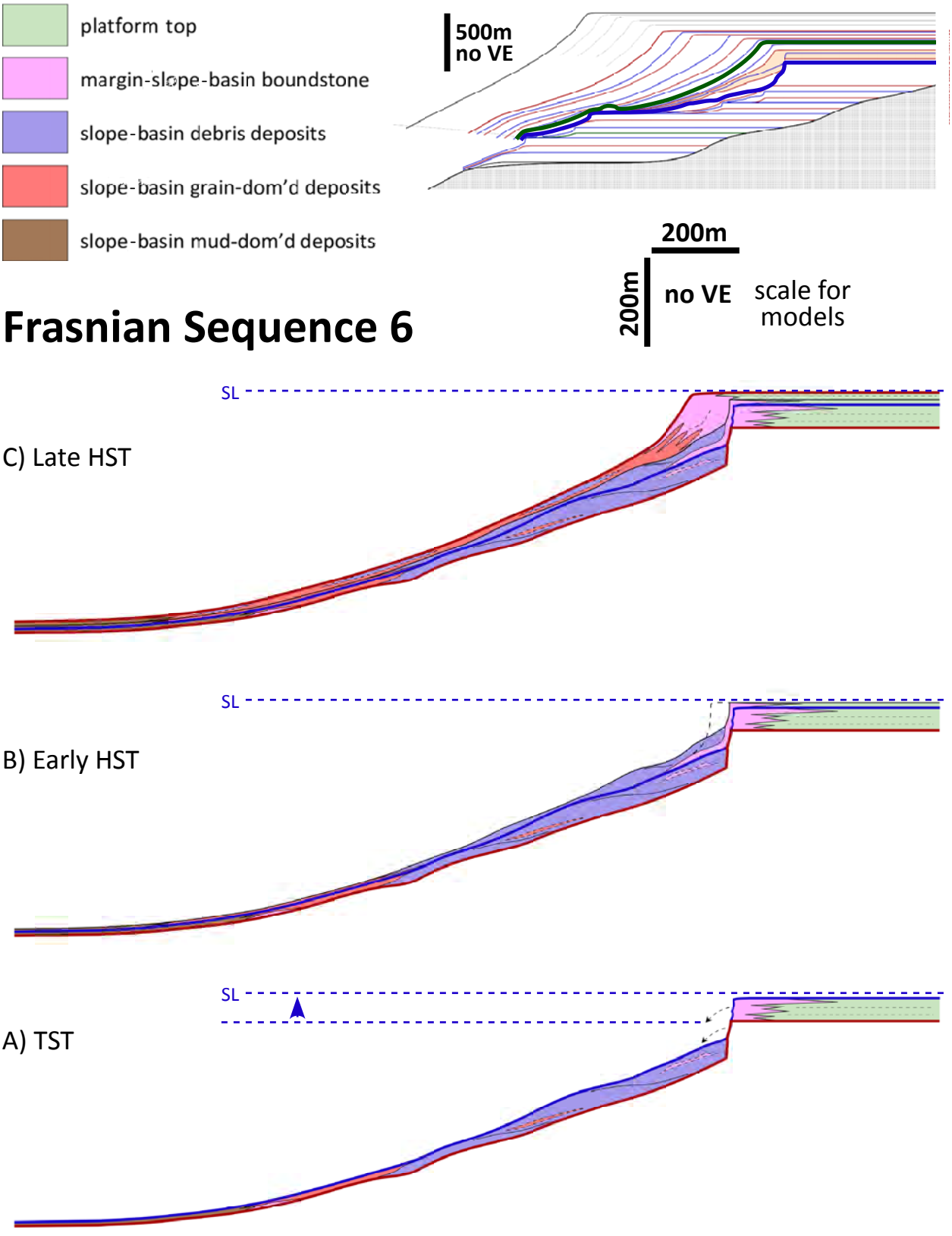

Figure 17-combined

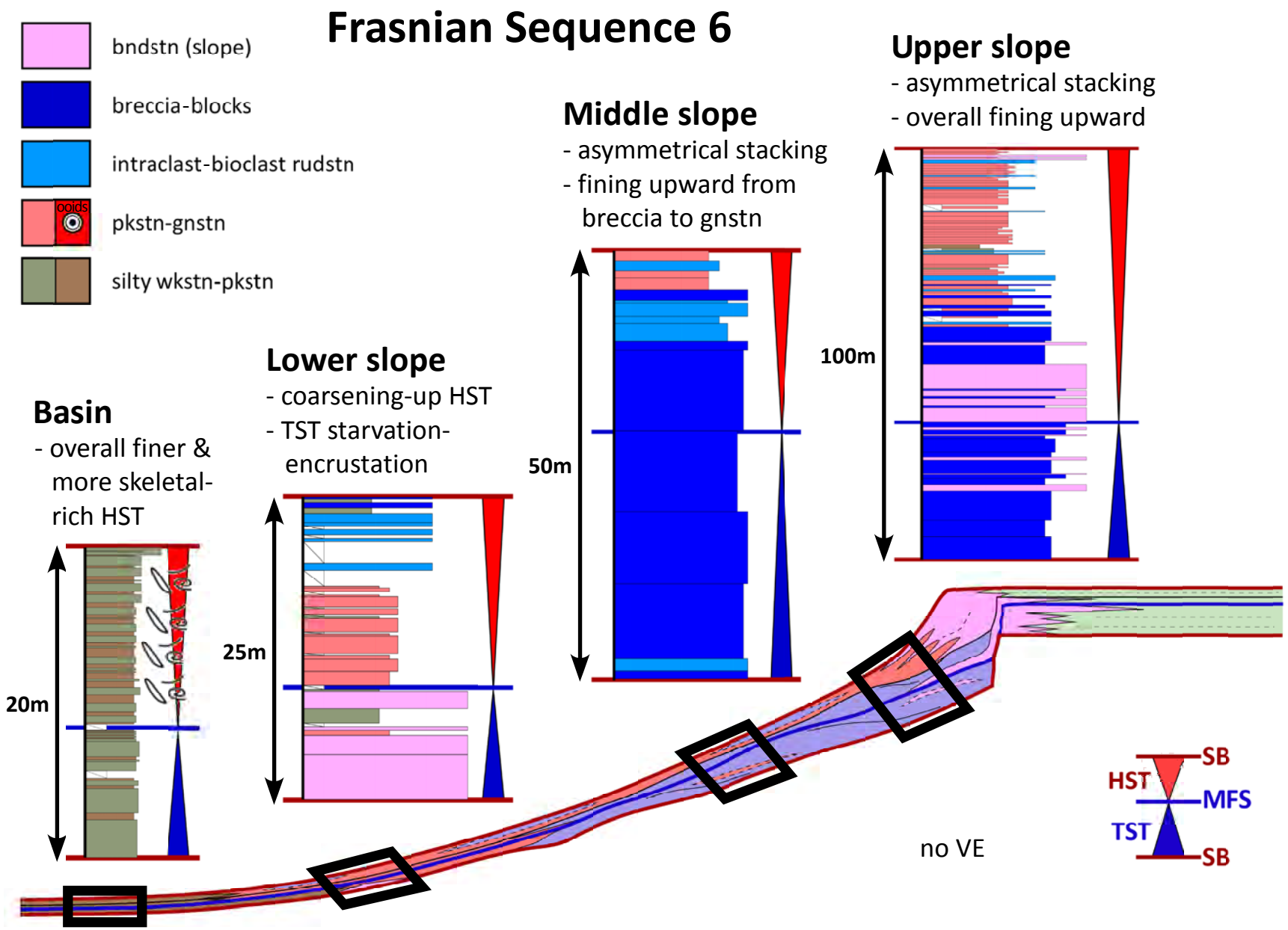

Figure 18-combined

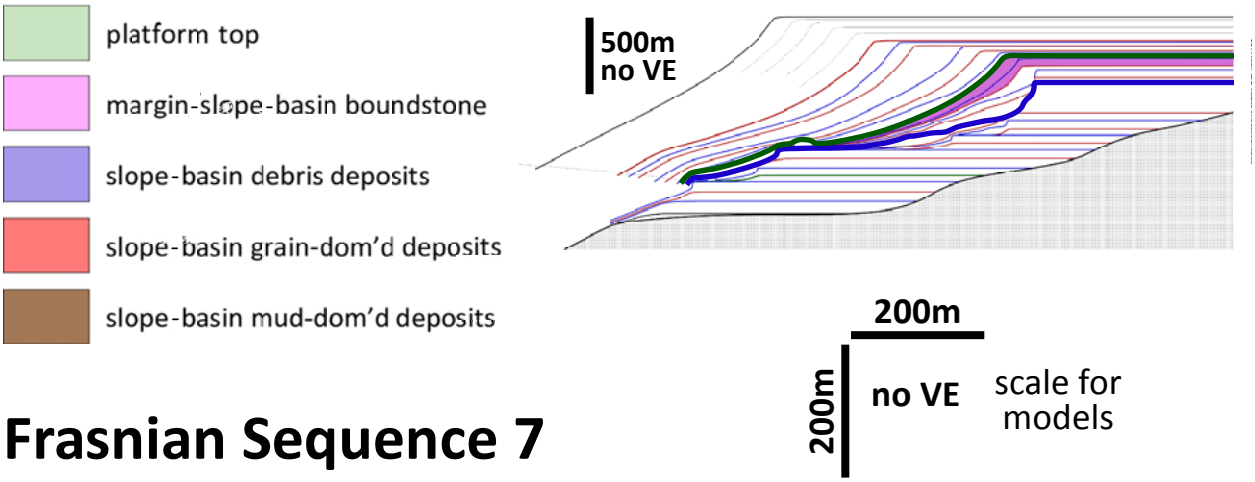

Frasnian Sequence 7

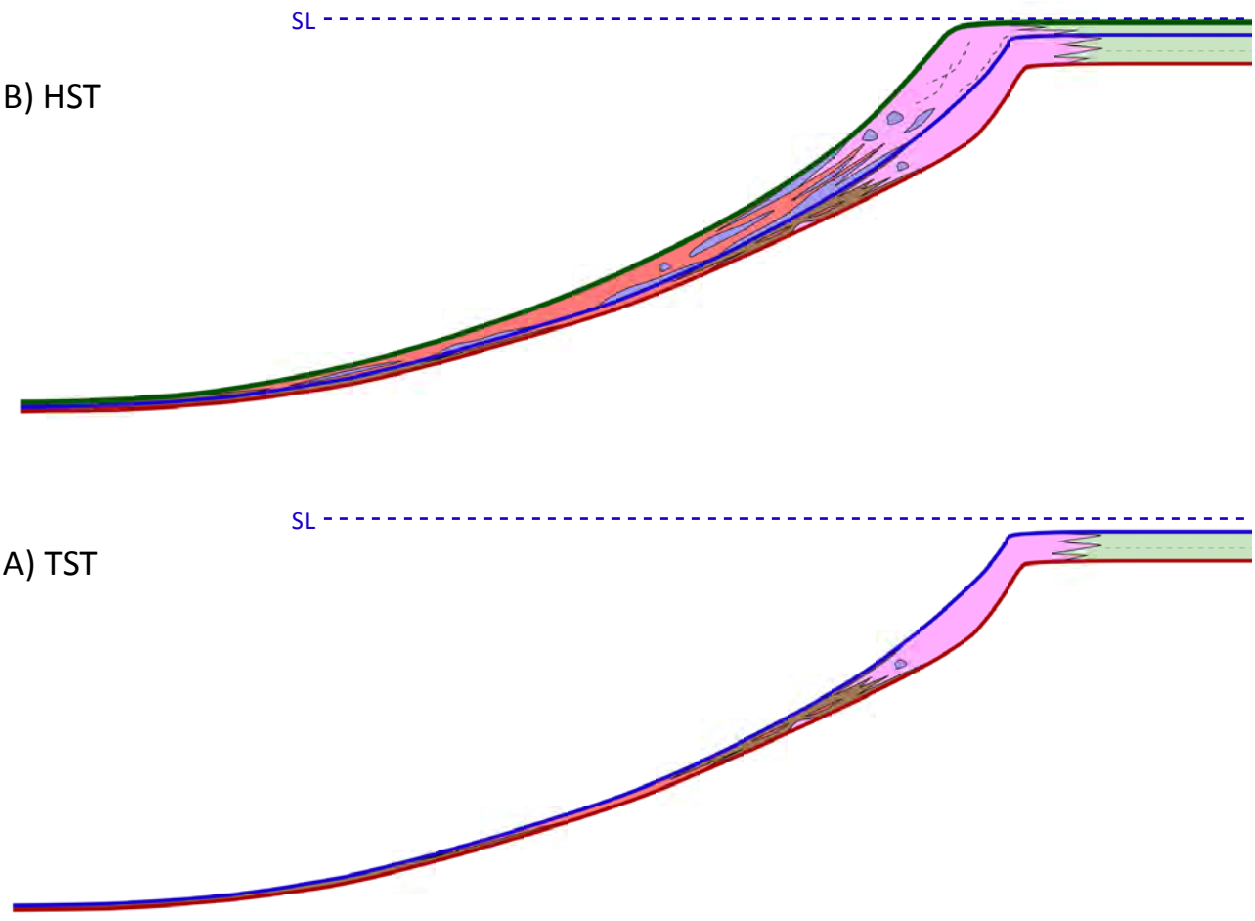

Figure 19-combined

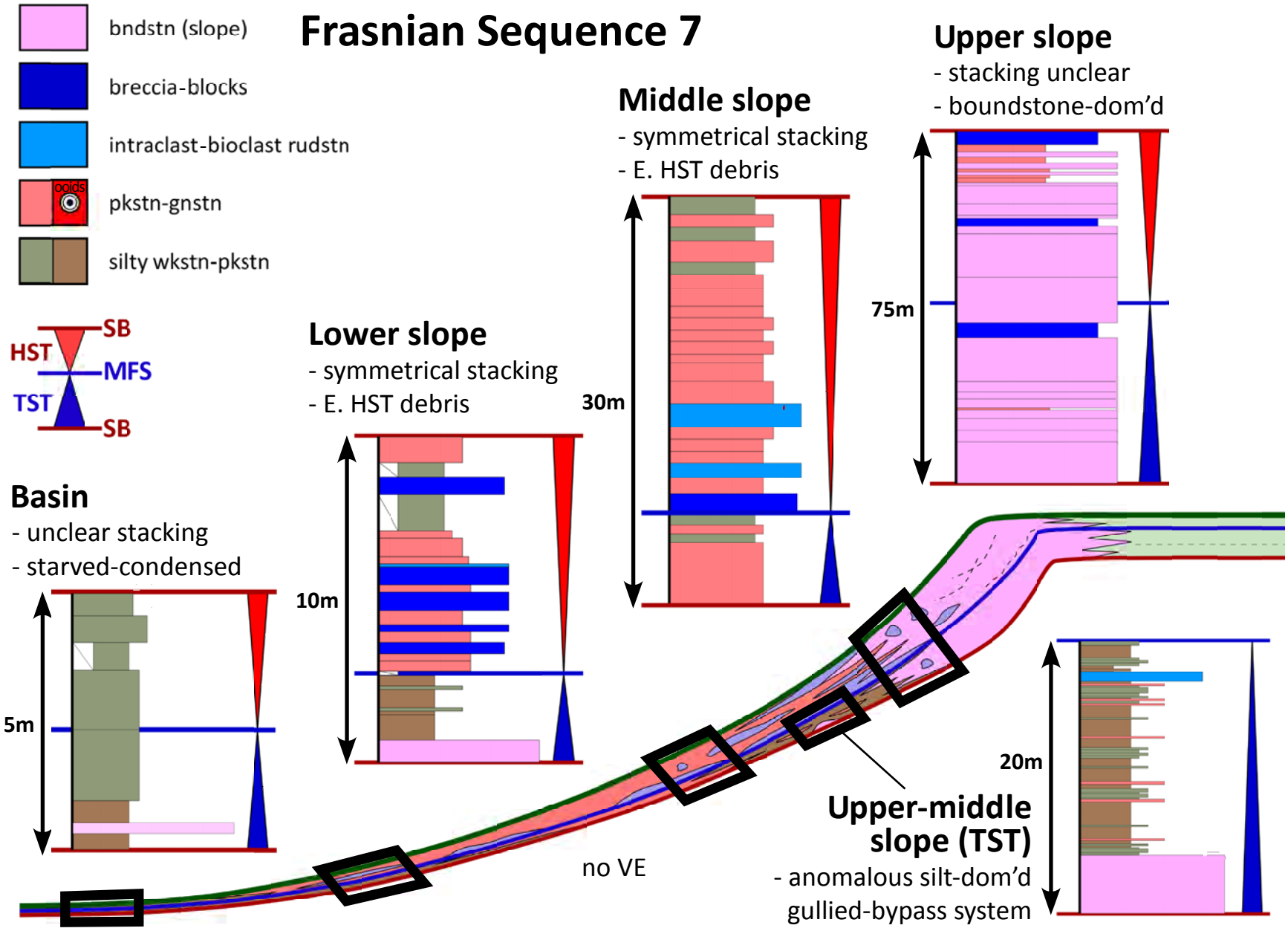

Figure 20-combined

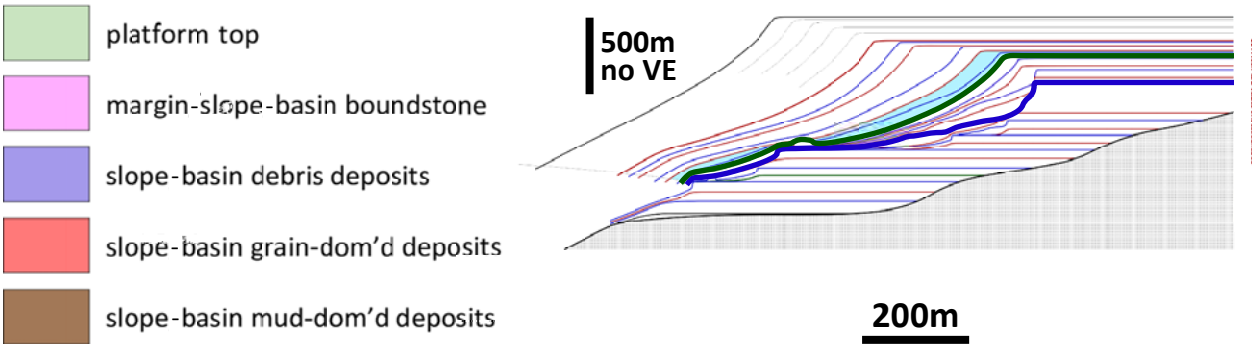

Famennian Sequence 1

200m
200m
no VE
scale for models

B) HST

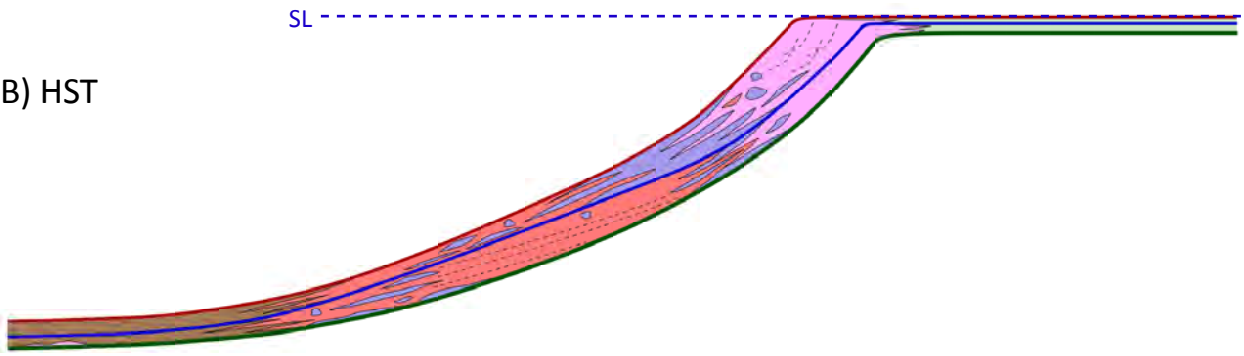

A) TST

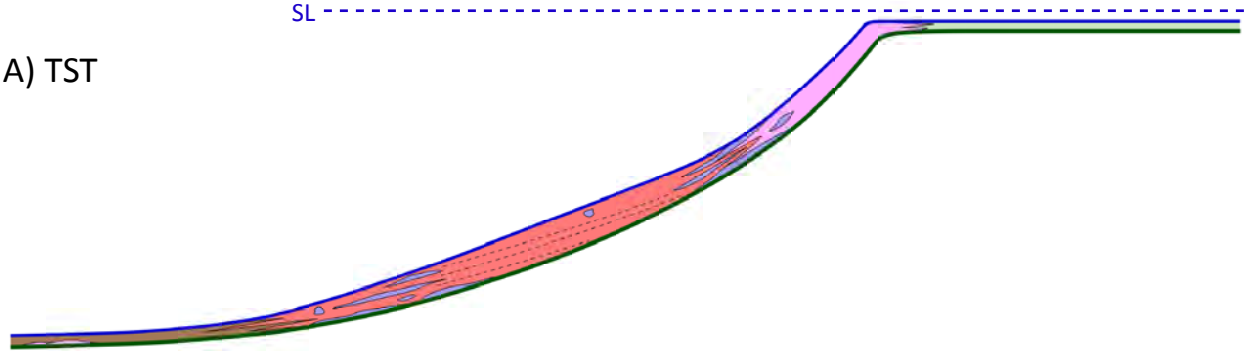

Figure 21-combined

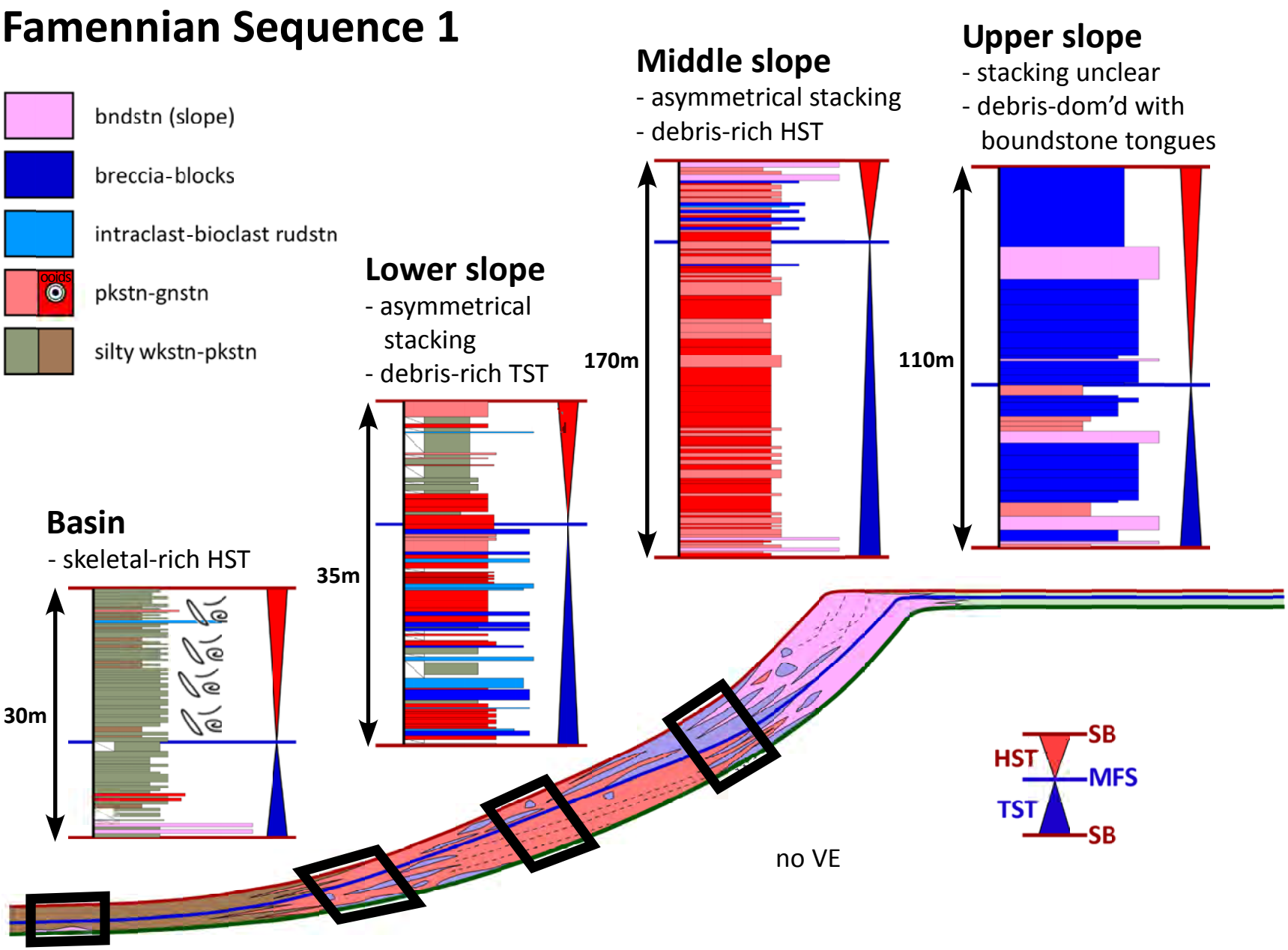

Figure 22-combined

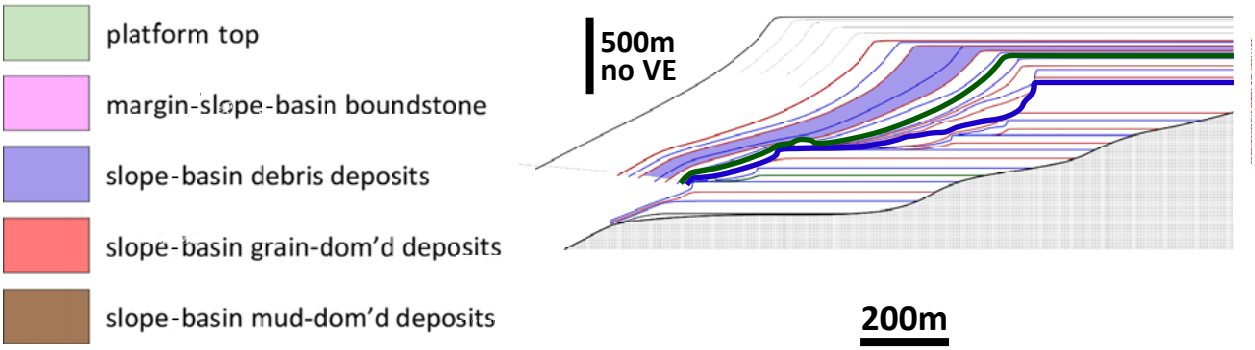

Famennian Sequence 2

B) HST

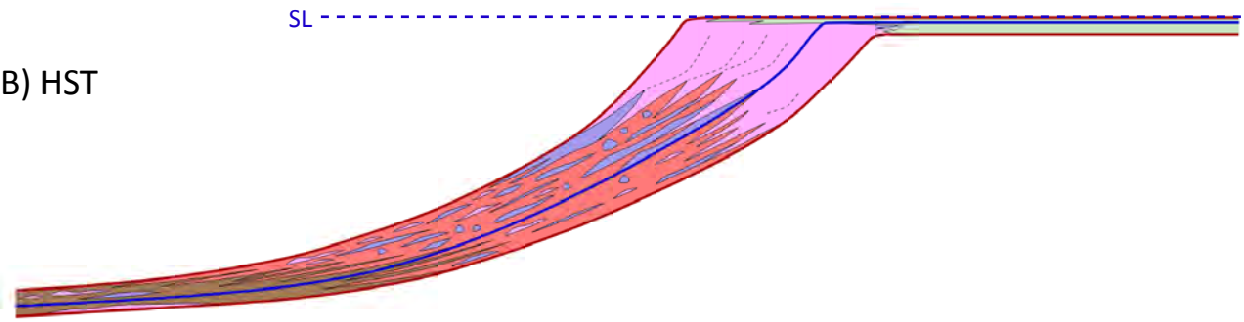

A) TST

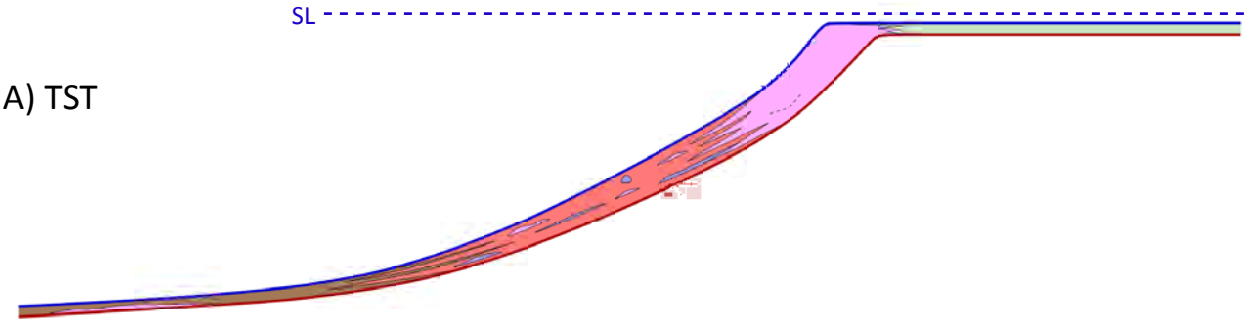

Figure 23-combined

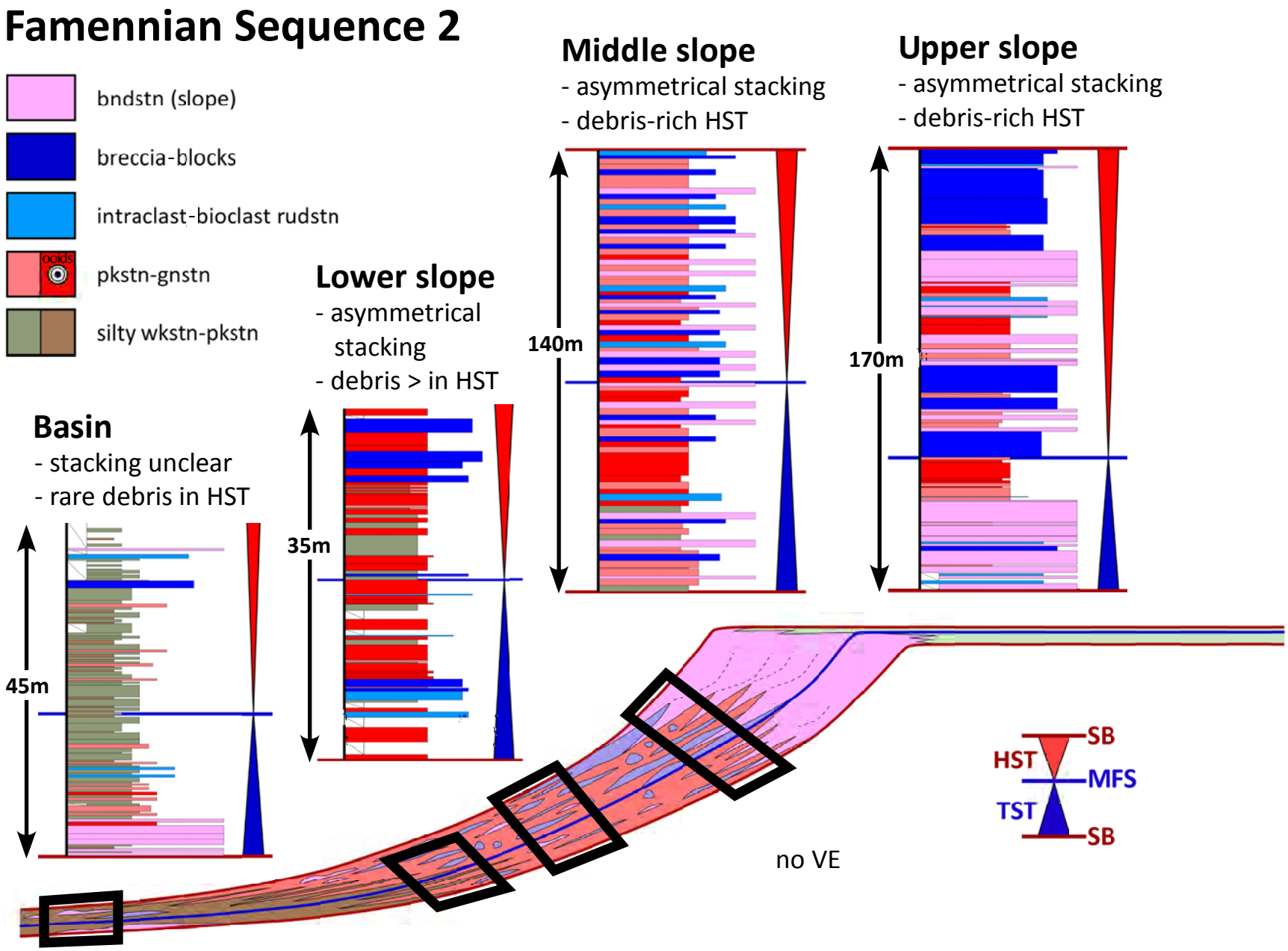

Major EOD	Rock Description	Setting
Shelf-Shoreline	rugose coral-encrusting stromatoporoid boundstone-floatstone w/ organic-rich matrix	*in situ* Givetian transgressive shelf
	organic-rich argillaceous mudstone-wackestone +/- open marine skeletals	Givetian transgressive shelf
	skeletal-lithiotid boundstone-floatstone	+/- *in situ* Famennian outer platform top
	peloid-skeletal oncolitic floatstone-rudstone	outer platform top (common in Famennian)
	skeletal-peloid packstone-grainstone	outer platform top
	bioclastic floatstone-rudstone	outer platform top
	non-skeletal-dominated packstone-grainstone	platform-top crest (common in Famennian)
	teepee-pisolite complex	Famennian platform-top crest
	burrowed peloidal wackestone-packstone; +/- skeletals	inner platform top
	fenestral peloidal mudstone-wackestone; +/- stromatolitic laminations	inner platform top
	massive-laminated siliciclastic siltstone	siliciclastic-dominated shallow marine shelf
	massive-stratified siliciclastic sandstone	siliciclastic-dominated shallow marine shelf
	siliciclastic conglomerate	siliciclastic-dominated shoreline-fluvial plain
In Situ Margin-Slope	stromatolitic-stromatactoid microbial boundstone	*in situ* slope bioherms-biostromes
	stromatactoid skeletal-microbial boundstone	*in situ* encrusted upper slope-deeper margin
	encrusted-microbially stabilized skeletal-peloid-coated grain packstone-grainstone	encrusted upper slope-deeper margin
	fenestral-massive *Renalcis* -dominated microbial boundstone	*in situ* Famennian reef
	fenestral-stromatactoid microbial-*Renalcis* -*Actinostroma* boundstone	*in situ* Frasnian reef
	well-bedded stromatolitic-stromatactoid microbial boundstone	*in situ* Famennian reef flat
	well-bedded *Stachyodes* -*Actinostroma* boundstone; variable encrustation	*in situ* Givetian-Frasnian reef flat
	Amphipora -*Stachyodes* boundstone-floatstone	+/- *in situ* Givetian-Frasnian reef flat-outer platform top
Transported Slope-Basin	reefal margin-slope-derived megabreccia-allochthonous block(s)	resedimented slope
	platform-margin-slope-derived bioclastic rudstone-breccia	resedimented slope (rare in basin)
	slope-derived intraclastic rudstone-breccia	resedimented slope (rare in basin)
	platform-derived skeletal-peloid packstone-grainstone	resedimented slope (rare in basin)
	platform-derived non-skeletal-dominated packstone-grainstone	resedimented slope (rare in basin)
	fine-medium calcareous sandstone	resedimented slope
	platform-margin-slope-derived silty skeletal-peloid wackestone-packstone	resedimented slope-basin
	margin-slope-derived silty peloidal wackestone-packstone +/- wisps-laminations	resedimented slope-basin
	margin-slope-derived silty (micro)peloidal mudstone-wackestone +/- wisps-laminations	resedimented slope-basin
Other	crystalline rock	basement

Table 2

Figure 24-combined

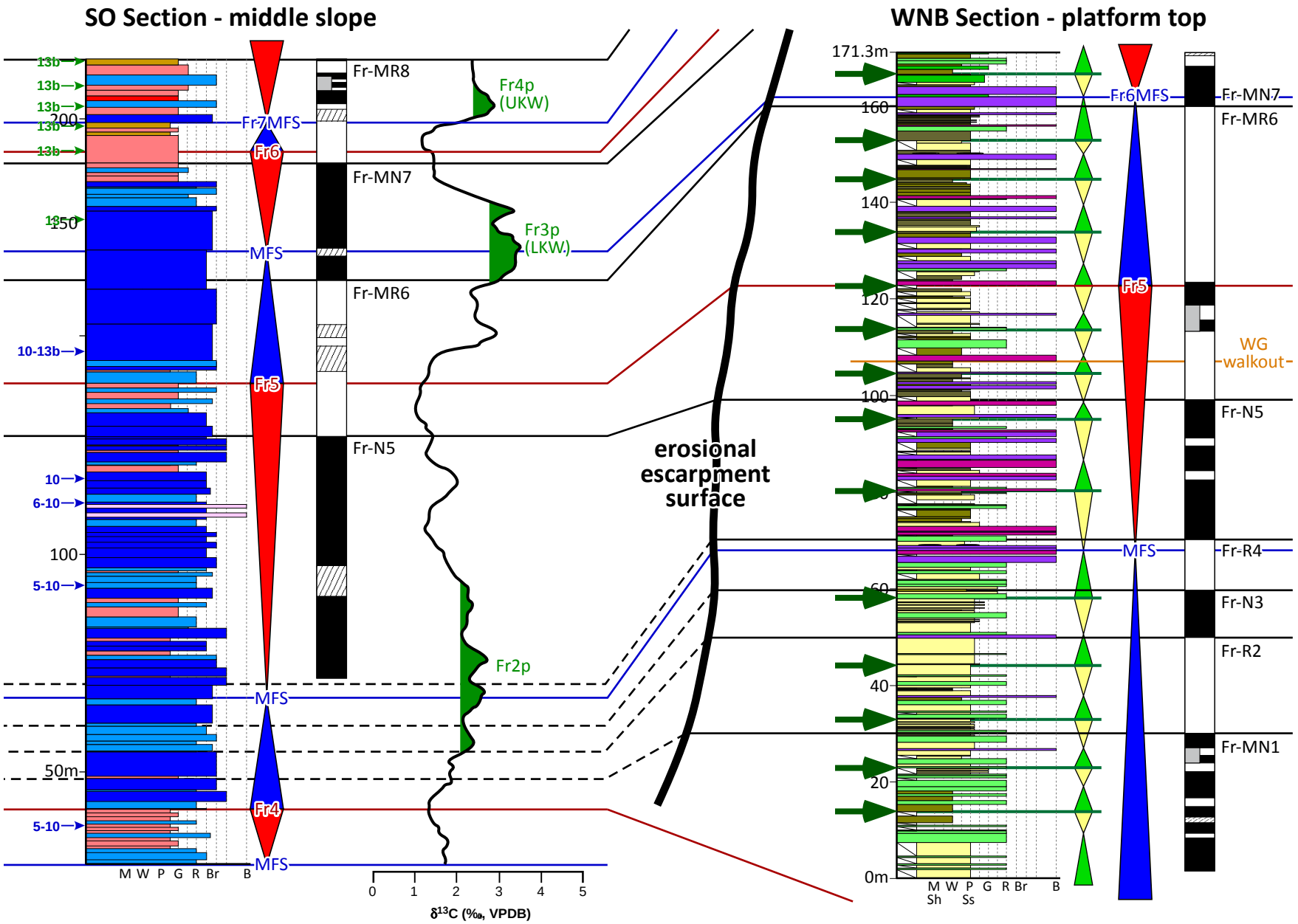

Figure 25-combined

Middle Slope Stacking Patterns - accommodation signals

A) composite sequence within supersequence TST

- symmetrical, debris-cored & bracketed w/ grain-dom'd deposits
- approx. 67% grain-dom'd deposits, 33% debris deposits

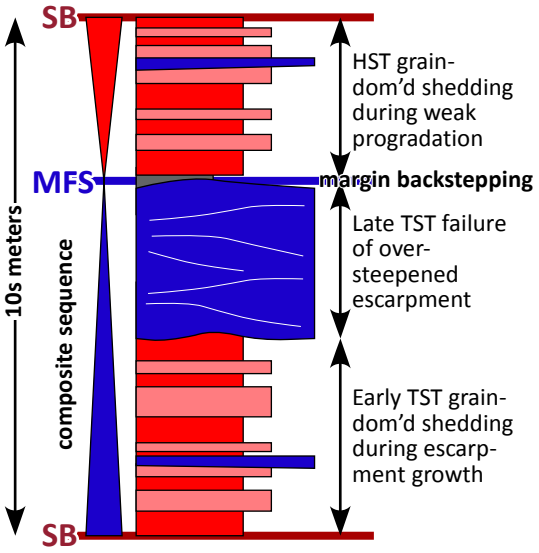

B) across supersequence MFS

- symmetrical, debris-dom'd w/ grain-dom'd cap & base
- approx. 80% debris deposits, 20% grain-dom'd deposits

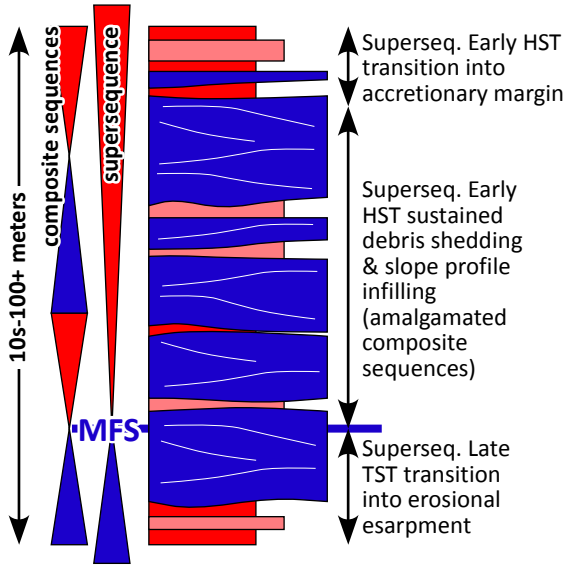

C) composite sequence within supersequence HST

- asymmetrical, upward increase in debris deposits
- < 10% debris deposits in TST, 25-50% debris deposits in HST

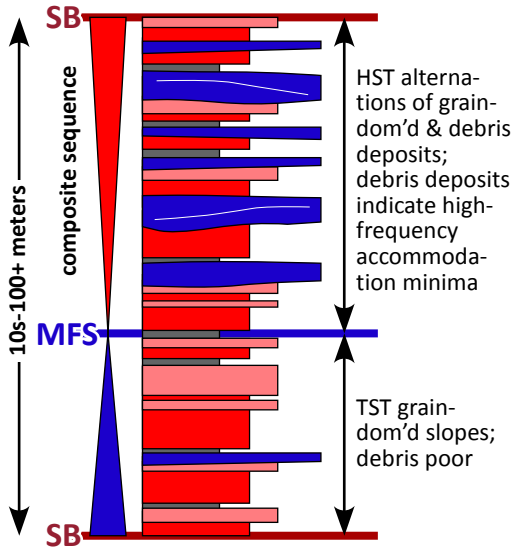

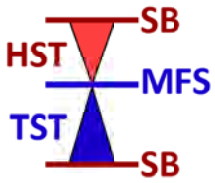

debris deposits

grain-dom'd deposits

mud-dom'd deposits

Figure 26-combined

Middle Slope Stacking Patterns - ecological signals

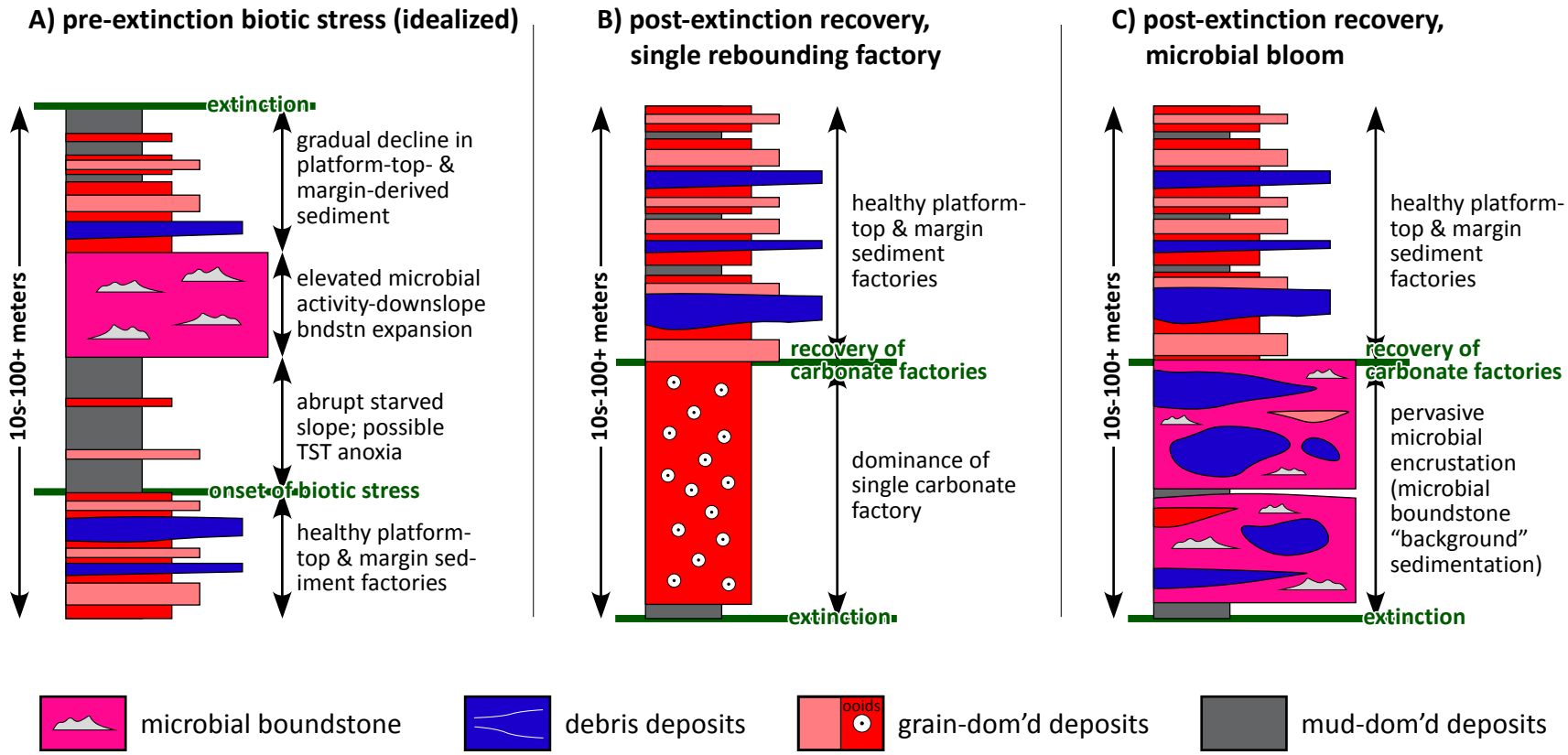

Table 3

Constraint	**Previous Work**	**This Study**
Sequence stratigraphy	Playford et al. (2009); Playton and Kerans (2015 a, b)	this paper
Conodont, cephalopod, & fish biostratigraphy	Klapper (1989); Ziegler and Sandberg (1990); Becker et al. (1993); Klapper (1997); Becker and House (1997); Girard et al. (2005); Klapper (2007); Trinajstic and George (2009)	Roelofs et al. (2015)
Magnetostratigraphy	none pertaining to regional correlation	Hansma et al. (2015)
Stable carbon isotope chemostratigraphy	Joachimski et al. (2002); Bing et al. (2003); Stephens and Sumner (2003); Buggisch and Joachimski (2006)	Hillbun (2015); Hillbun et al. (2015); Hillbun et al. (in review); Hillbun et al. (this volume)

a) Sections	
WNA	some independent global to regional constraints
WNB	some independent global to regional constraints
WS	some independent global to regional constraints
WV	some independent global to regional constraints
SO	numerous independent global to regional constraints
VHS	numerous independent global to regional constraints
CL	numerous independent global to regional constraints
PGH	few-none independent global to regional constraints
NHW	few-none independent global to regional constraints
MR1	numerous independent global to regional constraints
WK1	few-none independent global to regional constraints
UD2	few-none independent global to regional constraints
HD14	few-none independent global to regional constraints

b) Markers and Intervals	
all magnetic polarity reversals	correlatable across dataset; not linked to global reference
all biostratigraphic picks	correlatable across dataset; linked to global reference
LKW & UKW carbon excursions	correlatable across dataset; linked to global reference
FSV & ENK carbon excursions	isolated occurrences; linked to global reference
all other carbon excursions	correlatable across dataset; not linked to global reference
elemental trends	not correlatable across dataset; no global reference
magnetic susceptibility trends	not correlatable across dataset; no global reference
outcrop gamma ray trends	not correlatable across dataset; no global reference
biomarker trends	not correlatable across dataset; no global reference

Table 4

Table 5

Theme	Previous Work		This Study
Correlations across Lennard Shelf	F-F identified in many localities (Playford et al. 2009); detailed biostratigraphic profiles collected at many localities but not consistently tied to sedimentary logs or sequence stratigraphy (e.g., Becker et al. 1993, Klapper 2007, Trinajstic and George 2009)		numerous correlation tie points and high-confidence sequence stratigraphic interpretation that connects strata across Windjana Gorge, South Oscar Range, Horse Spring, and Casey Falls areas, particularly for extended slope and basin sections
Shelf-to-basin correlation	not previously attempted		platform-slope-basin correlation across supersequence MFS interval; upper-middle-lower-slope to basin correlation for Middle Frasnian to Middle Famennian
Lennard Shelf Composite Reconstruction	schematic reconstruction, no scale, not constrained to data, over-representation of basin fill (Playford et al. 2009); reconstruction but constrained only to two data transects (Playton and Kerans 2015 a, b)	scaled	scaled reconstruction, constrained by 8 overlapping, strongly correlated transects that span upper-slope to basin environments (platform top included in some intervals), all depositional information honored
Frasnian sequences*	Sequence 1 - Zone 1 (Playford et al. 2009)**	not defined	Sequence Fr1 & systems tracts - Zone 1 (after Playford et al. 2009)
	Sequence 2 - Zones 2-3 (Playford et al. 2009)	Phase 2 - Zones 2-3 (George et al. 2009)	Sequence Fr2 & systems tracts - Zones 2-3 (after Playford et al. 2009)
	Sequence 3 - Zones 4-6 (Playford et al. 2009)	Phases 3-4 - Zones 4-6 (George et al. 2009)	Sequence Fr3 & systems tracts - Zones 4-6 (after Playford et al. 2009)
	Sequence 4 - Zones 6-8 (Playford et al. 2009)	Phases 5-6 - Zones 6-8 (George et al. 2009): short-lived regression	Sequence Fr4 & systems tracts - Zones 6-8 (after Playford et al. 2009)
	Sequence 5 - Zones 9-10 (Playford et al. 2009): supersequence MFS, Middle Frasnian	Phase 7 - Zones 9-11 (George et al. 2009)	Sequence Fr5 & systems tracts - Zones 9-12: supersequence MFS, Middle-Upper Frasnian boundary in Sequence 5 HST
	Sequence 6 - Zones 11-13 (Playford et al. 2009)	Phase 8 - Zones 12-13 (George et al. 2009)	Sequence Fr6 & systems tracts - Zones 12-13b
			Sequence Fr7 & systems tracts - Zones 13b-c
Lower-Middle Famennian sequences	1 sequence, no systems tract subdivision (Playford et al. (2009)		3 sequences (Fa1-3) with systems tracts
Middle Famennian (MFa) interval	1 sequence, no systems tract subdivision (Playford et al. (2009)		sequences not defined; likely multiple sequences but further work required
Slope & basin sequence stratigraphy	not previously attempted		slope composite sequence and systems tracts interpretations & models for Middle Frasnian to Middle Famennian

*Sequence boundaries of Playford et al. (2009) and George et al. (2009) are defined at backstepping events, which are MFSs here (see Playton and Kerans 2015a); thus, disparities on conodont ranges by sequence are expected.

**Sequence 1 of Playford et al. (2009) includes the Givetian; Givetian sequences of this study are poorly constrained, thus comparison not discussed here

Figure 1-combined

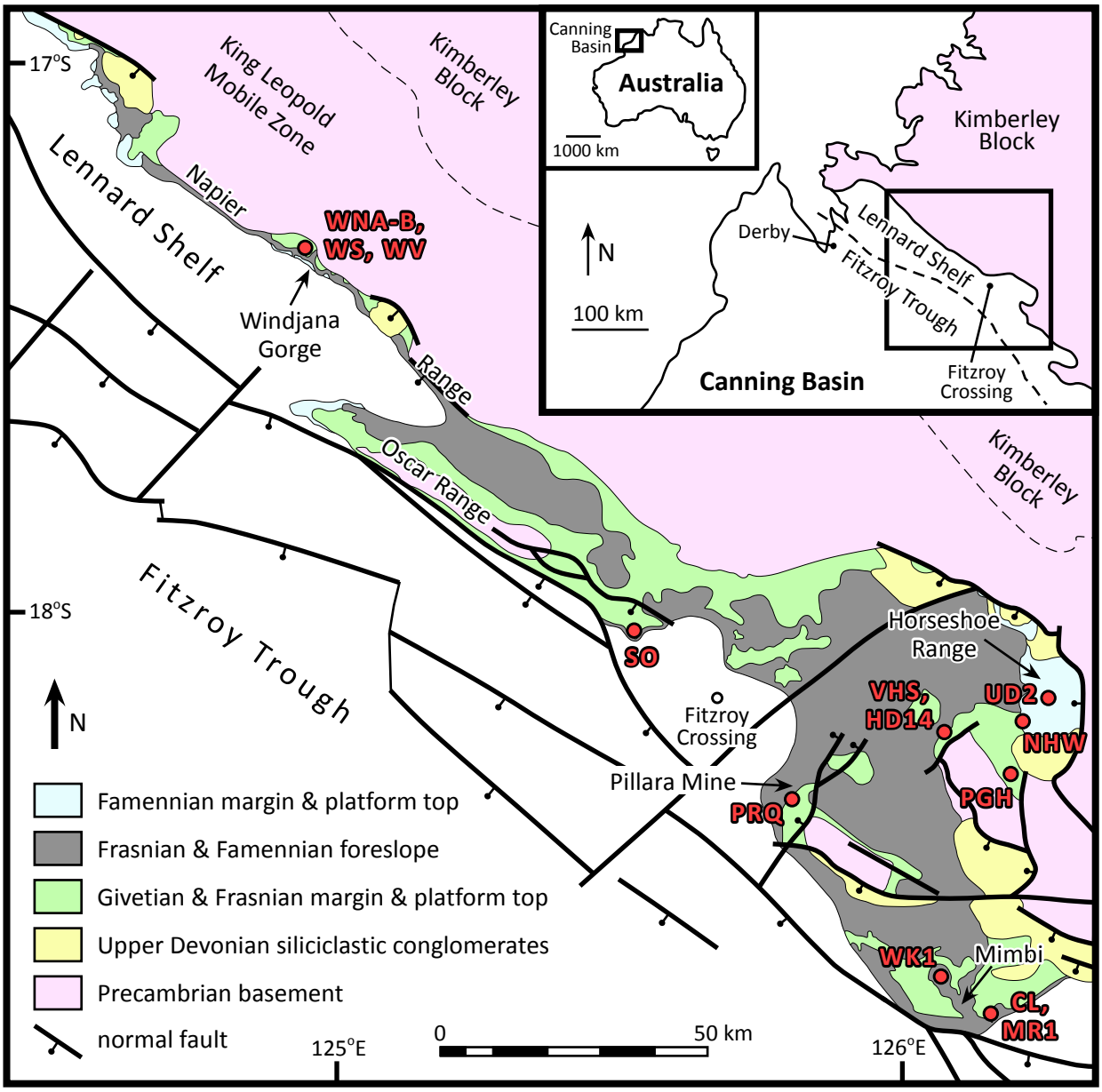

Figure 2-combined

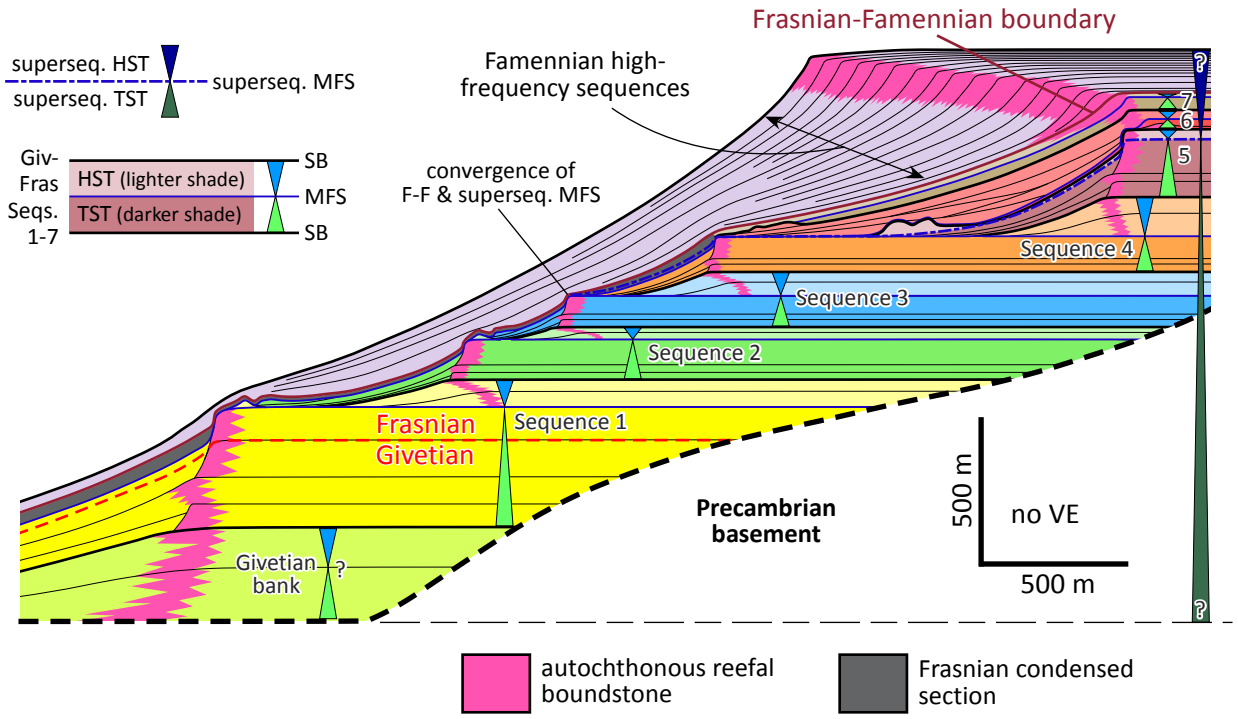

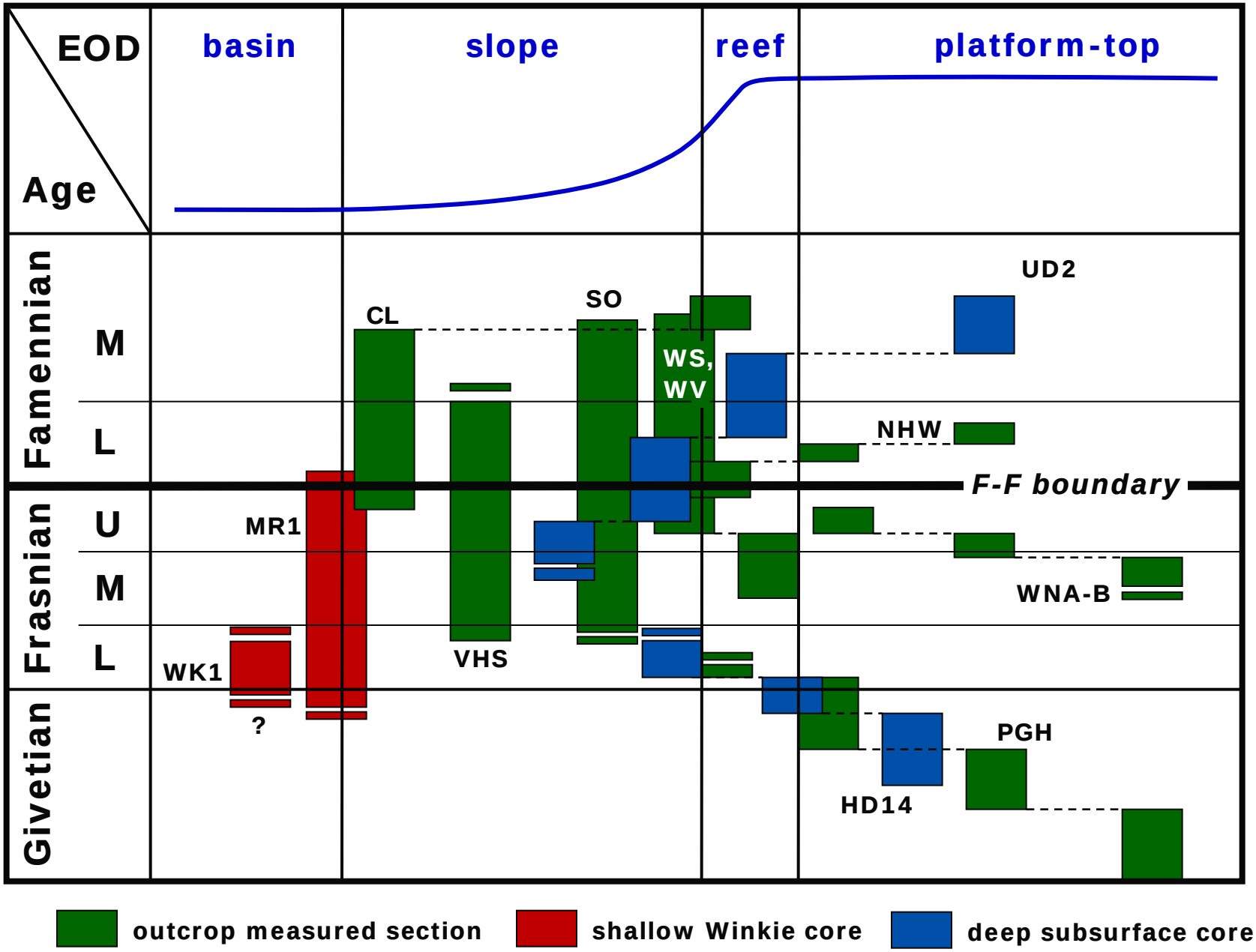

Figure 3-combined

Appendix 5

Statements of Contribution for the papers that formed Chapters 2, 3, 4 and 5 in this thesis.

TO WHOM IT MAY CONCERN

I, Brett Peter Ashworth Roelofs, contributed 20% to the publication entitled:

Trinajstic, K., **Roelofs, B.**, Burrow, C., Long, J., and Turner, S. 2014. Devonian vertebrates from the Canning and Carnarvon Basins with an overview of Paleozoic vertebrates of Western Australia. *Journal of the Royal Society of Western Australia,* 97:133-151.

Signasture of Candidate  *Date*: 15/01/2016

I as Co-Author, endorse that this level of contribution by the candidate indicated above is appropriate.

Kate Trinajstic *Signature*:  *Date*: 15/01/2016

Carole Burrow *Signature*  *Date*: 18/01/2016

John Long *Signature*  *Date*: 18/01/2016

Sue Turner *Signature* 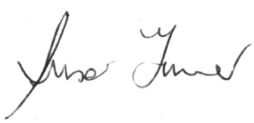 *Date*: 18/01/2016

TO WHOM IT MAY CONCERN

I, Brett Peter Ashworth Roelofs, contributed 80% to the publication entitled:

Roelofs, B. and Playton, T. and Barham, M. and Trinajstic, K. 2015. Upper Devonian microvertebrates from the Canning Basin, Western Australia, *Acta Geologica Polonica*, 65:69-100.

Signasture of Candidate  *Date*: 15/01/2016

I as Co-Author, endorse that this level of contribution by the candidate indicated above is appropriate.

Ted Playton *Signature*:  *Date*: 19/01/2016

Milo Barham *Signature* 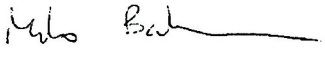 *Date*: 18/01/2016

Kate Trinajstic *Signature*  *Date*: 15/01/2016

TO WHOM IT MAY CONCERN

I, Brett Peter Ashworth Roelofs, contributed 90% to the Australian section, which comprised 50% of the publication entitled:

Hairapetian, V., **Roelofs, B.P.A.**, Trinajstic, K.M., and Turner, S. 2015. Famennian survivor turiniid thelodonts of North and East Gondwana. *Geological Society, London, Special Publications*, SP423.

Signasture of Candidate  *Date*: 15/01/2016

I as Co-Author, endorse that this level of contribution by the candidate indicated above is appropriate.

Vachik Hairapetian *Signature*:  *Date*: 18/01/2016

Kate Trinajstic *Signature*  *Date*: 15/01/2016

Sue Turner *Signatuer* 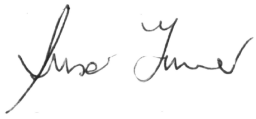 *Date*: 18/01/2016

TO WHOM IT MAY CONCERN

I, Brett Peter Ashworth Roelofs, contributed 80% to the publication entitled:

Roelofs, B., Barham, M., Mory, A. and Trinajstic, K. 2016. Late Devonian and Early Carboniferous chondrichthyans from the Fairfield Group, Canning Basin, Western Australia. *Palaeontologia Electronica*, 191:28.

Signasture of Candidate *Date:* 15/01/2016

I as Co-Author, endorse that this level of contribution by the candidate indicated above is appropriate.

Milo Barham *Signature*: *Date*: 18/01/2016

Arthur Mory *Signature* *Date*: 19/01/2016

Kate Trinajstic *Signature* K.Trinajstic *Date*: 15/01/2016

Appendix 6

The following documents relate to copyright of materials included in this thesis.

PERMISSION TO USE COPYRIGHT MATERIAL AS SPECIFIED BELOW:

Trinajstic K, Roelofs B, Burrow C, Long J & Turner S. 2014. Devonian vertebrates from the Canning and Carnarvon Basins with an overview of Paleozoic vertebrates of Western Australia. Journal of the Royal Society of Western Australia 97, 133-151.

I hereby give permission for Brett Roelofs to include the abovementioned material in his higher degree thesis for Curtin University, and to communicate this material via the espace@Curtin institutional repository. This permission is granted on a non-exclusive basis and for an indefinite period.

I confirm that The Royal Society of Western Australia is the copyright owner of the specified material.

Name: P H Armstrong

Position: Editor-in-Chief

Date: 13 Jan 2016

Signed: P H Armstrong

Title:	Upper Devonian microvertebrates from the Canning Basin, Western Australia
Author:	Brett Roelofs, Ted Playton, Milo Barham, et al.
Publication:	Acta Geologica Polonica
Publisher:	De Gruyter
Date:	Mar 27, 2015

Creative Commons

The request you have made is considered to be non-commercial/educational. As the article you have requested has been distributed under a Creative Commons Attribution-NonCommercial-NoDerivative Works Unported License (CC BY-NC-ND), you may reuse this material for non-commercial/educational purposes without obtaining additional permission from the De Gruyter, providing that the author and the original source of publication are fully acknowledged.

For full terms and conditions of the Creative Commons license, please see the attached link http://creativecommons.org/licenses/.

Permissions

Open Access Articles

Articles that have the Open Access padlock logo can be used freely without permission. However, if you re-use figures or other parts of the article you must acknowledge the author and the source of the material. If your article uses more than 25% of an Open Access article or if more than 25% of your article comes from an Open Access article it could constitute duplicate publication and be in contravention of normal publishing ethics.

Articles with the 'Free' logo are not the same as Open Access and are subject to the conditions below.

Other Articles

All articles published in Geological Society books and journals that do not have the Open Access padlock logo, including ones that are free to access online, are subject to the conditions below. Information on using other GSL material including the Geoscientist magazine is at the foot of this page.

Use of PDFs

Authors: Information on the use of PDFs and other versions of your paper can be found here.

Information on the use of PDFs by others can be found in the Lyell Collection pages.

Obtaining a PDF of an article

Non-subscribers should use the Pay-Per-View facility to purchase access to the PDF. Once you have access, you will be able to download and save a copy (for your personal use only).

Corresponding authors of papers will have received an email with instructions on how to download the PDF. Contributing authors requiring access should contact the corresponding author. We do not provide free access to articles directly to other individuals.

If you are at an institution in a developing country, you might be entitled to free access to the Lyell Collection through the International Network for the Availability of Scientific Publications. Please see INASP for more information.

Re-publishing material from Geological Society of London copyright

Using material from GSL publications

Extensive quotation (more than c. 100 words) and reproduction of previously published illustrations (even if re-drawn) require permission from the rights holder (GSL in this case). In the UK, material remains in copyright until 70

years after the death of the author.

Material that can be used without permission

Authors may re-use their own material without permission subject to the exceptions listed below. They may include the whole article in a PhD or other thesis provided that it will not be published, and that the original source is fully acknowledged in the standard form. If the thesis is to be included in the institution's electronic repository or other online host, authors must use their own finally accepted version, not the typeset PDF (unless it is Gold Open Access). Authors may not re-publish their whole article, or a substantial part of it, without permission. Such permission will be granted only in exceptional circumstances.

Anyone may use up to three items (text extracts of 100 words or less, figures or tables) from GSL published material without permission or charge provided that a proper acknowledgement of source is used with the item. There are no free items if written permission is required from us (e.g. a letter of authorisation or completion of a form) - please use the application form below.

The abstracts of articles can be reproduced without permission or fees provided that a full reference and a link to the article abstract page are included.

Please check that GSL is the original publisher and that the material has not been taken from another source. For a figure that has been modified or re-drawn in a GSL publication the rights are still held by the original copyright holder. In those cases, you must contact the original rights holder.

GSL is not usually the rights holder for cover photographs, and permission must be sought from the owner/photographer.

If your article forms part of a multi-author book, the publisher must ensure that the total number of items from GSL publications does not exceed three (this does not apply to journal issues).

Supplementary material

Most supplementary material items on the Geological Society figshare portal at https://geolsoc.figshare.com/ are licensed under the CC-BY license. They are openly available, but an appropriate credit including the authors, title, source link, license link and an indication of any changes made, must be given to the original item in all cases. For example:

- Perdiou, A., Thibault, N., Anderskouv, K., van Buchem, F., Buijs, G. J. A., Bjerrum, C. J. 2015. Orbital calibration of the late Campanian carbon isotope event in the North Sea. figshare, https://doi.org/10.6084/m9.figshare.c.2134362 used under a Creative Commons Attribution Licence 4.0

Please visit http://creativecommons.org/licenses/by/4.0/ and https://wiki.creativecommons.org/wiki/Best_practices_for_attribution for more information and guidance.

Datasets on the Geological Society figshare portal at https://geolsoc.figshare.com/ are licensed under the CC0 license. Others can copy, modify, distribute and perform the work, even for commercial purposes, all without asking permission. The moral responsibility to cite the source remains, as is common in scientific research, although CC0 does not legally require attribution.

Re-using material in another GSL publication

You may use material from GSL publications in another GSL publication without permission from GSL subject to the exceptions listed below. However, if there are more than three items from an individual article, you must seek the author's consent directly. If he/she does not respond within four weeks, you can assume that consent is given.

Uses where permission is required

For more than three items, please use Rightslink to obtain permission; there will be a charge of $25 per item (NB: GSL Fellows are entitled to a discount and should use the form below).

If there are more than three items from an individual article, you must also seek the author's consent. If he/she does not respond within four weeks, you can assume consent. You should contact the author at the address on the original article, or use Google Scholar or other search engine to trace them. Authors are responsible for ensuring that their mail gets forwarded when they move. For papers published before 1980, a more pragmatic approach can be taken with author consent. If you want GSL to check the authors' contact details there may be a charge for the service and there is no guarantee that we have the correct address.

For Fellows of the Geological Society and those unable to use Rightslink, requests must be made using the form below.

Current fees for republishing GSL material;

- Processing fee per request: £10 for email requests and replies; £20 when written permission is required (e.g. a letter of authorisation or completion of a form).
- Item fee for each figure, table or extract: £15 per item (there are no free items if written permission is needed)
- 50% discount for GSL Fellows
- VAT at the standard rate of 20%

Applications

Please use Rightslink or download and complete the request form: pdf (Adobe Reader required) or Word.

Exceptions

The Geological Society of London has a strong policy against duplicate publication and does not allow republication of whole articles, or substantial parts of them, unless there are very exceptional circumstances.

You may not use more than 25% of any GSL published article in a single publication and no publication should contain more than 25% in total from GSL publications. This does not prevent the inclusion of whole articles in course packs and the like (which do not constitute republication).

You may not post a typeset PDF of a GSL article on any website, repository or server (see Lyell Collection terms and conditions for more information).

For enquiries please contact sales@geolsoc.org.uk

Using material from other journals published by GSL

Permission requests for Scottish Journal of Geology (SJG), Proceedings of the Yorkshire Geological Society (PYGS) and Journal of Micropalaeontology (JM) should be addressed to the editor of the journal.

The co-published journals Petroleum Geoscience and Geochemistry: Exploration, Environment, Analysis are handled in the same way as other GSL publications.

Geology Today is published for GSL and GA by Wiley. Please see their website for permission details.

Photocopying and digital copying

You may make limited hard copies of an article for your own research or educational purposes (not including course packs) if you have access rights to the material. You do not need to request permission to do this.

For more extensive copying or digital reproduction, you need to obtain a licence from the Copyright Licensing Agency, the Copyright Clearance Center or from your local reproduction rights agency.

Lecture and presentations

You may include material from Society copyright in a visual presentation if you have access rights to the material and provided that you will not circulate digital or hard copies of your presentation. You do not need to request permission to do this. If you wish to circulate copies of your presentation to students or others, please obtain 'course-pack' permission from the Copyright Licensing Agency: www.cla.co.uk or the Copyright Clearance Center: www.copyright.com or from your local reproduction rights agency.

Using other GSL material

Permission to reprint material from the Society's unpublished archives/art collection should be made to the Society's Archivist.
Permission to use material from the Society's website should be made to Webteam.
Permission to use material from the *Geoscientist* magazine should be made to Ted Nield.

Government of **Western Australia**
Department of **Mines and Petroleum**

Non-exclusive licence of copyright

Re: Paper no. PE 583

Author : Arthur J Mory

Address: Petroleum Division, 100 Plain Street, East Perth, Western Australia 6004

Title: **Late Devonian and Early Carboniferous chondrichthyans from the Fairfield Group, Canning Basin, Western Australia**

Dear Sir/Madam

NON-EXCLUSIVE LICENCE OF COPYRIGHT

I authorize Palaeontologia Electronica/Society of Vertebrate Paleontology to publish the manuscript listed above, throughout the world in any form and in any language (including without limitation on optical disk, transmission over the Internet and other communication networks, and in any electronic form).

This is a non-exclusive copyright licence. Palaeontologia Electronica/Society of Vertebrate Paleontology is not licensed to transfer this copyright to any other party.

Yours sincerely

DJ Flint

for Rick Rogerson
DIRECTOR
1-12-2015

Please complete this section, then copy this page and return it to Geological Survey of Western Australia by fax (+618) 9222 3444 or by post, to, Mineral House, 100 Plain Street (cnr Adelaide Tce), East Perth, Western Australia 6004.

I accept this non-exclusive licence to publish the above mentioned paper in Palaeontologia Electronica and agree to protect the copyright of this publication in accordance with the *Copyright Act* 1968.

Signed .....

Society of Vertebrate Paleontology

Date .....

Creative Commons Legal Code

Attribution 4.0 International

Official translations of this license are available in other languages.

Creative Commons Corporation ("Creative Commons") is not a law firm and does not provide legal services or legal advice. Distribution of Creative Commons public licenses does not create a lawyer-client or other relationship. Creative Commons makes its licenses and related information available on an "as-is" basis. Creative Commons gives no warranties regarding its licenses, any material licensed under their terms and conditions, or any related information. Creative Commons disclaims all liability for damages resulting from their use to the fullest extent possible.

Using Creative Commons Public Licenses

Creative Commons public licenses provide a standard set of terms and conditions that creators and other rights holders may use to share original works of authorship and other material subject to copyright and certain other rights specified in the public license below. The following considerations are for informational purposes only, are not exhaustive, and do not form part of our licenses.

> ***Considerations for licensors:*** *Our public licenses are intended for use by those authorized to give the public permission to use material in ways otherwise restricted by copyright and certain other rights. Our licenses are irrevocable. Licensors should read and understand the terms and conditions of the license they choose before applying it. Licensors should also secure all rights necessary before applying our licenses so that the public can reuse the material as expected. Licensors should clearly mark any material not subject to the license. This includes other CC-licensed material, or material used under an exception or limitation to copyright.* *More considerations for licensors.*

> ***Considerations for the public:*** *By using one of our public licenses, a licensor grants the public permission to use the licensed material under specified terms and conditions. If the licensor's permission is not necessary for any reason–for example, because of any applicable exception or limitation to copyright–then that use is not regulated by the license. Our licenses grant only permissions under copyright and certain other rights that a licensor has authority to grant. Use of the licensed material may still be restricted for other reasons, including because others have copyright or other rights in the material. A licensor may make special requests, such as asking that all changes be marked or described. Although not required by our licenses, you are encouraged to respect those requests where reasonable.* *More considerations for the public.*

Creative Commons Attribution 4.0 International Public License

By exercising the Licensed Rights (defined below), You accept and agree to be bound by the terms and conditions of this Creative Commons Attribution 4.0 International Public License ("Public License"). To the extent this Public License may be interpreted as a contract, You are granted the Licensed Rights in consideration of Your acceptance of these terms and conditions, and the Licensor grants You such rights in consideration of benefits the Licensor receives from making the Licensed Material available under these terms and conditions.

Section 1 – Definitions.

a. **Adapted Material** means material subject to Copyright and Similar Rights that is derived from or based upon the Licensed Material and in which the Licensed Material is translated, altered, arranged, transformed, or otherwise modified in a manner requiring permission under the Copyright and Similar Rights held by the Licensor. For purposes of this Public License, where the Licensed Material is a musical work, performance, or sound recording, Adapted Material is always produced where the Licensed Material is synched in timed relation with a moving image.
b. **Adapter's License** means the license You apply to Your Copyright and Similar Rights in Your contributions to Adapted Material in accordance with the terms and conditions of this Public License.
c. **Copyright and Similar Rights** means copyright and/or similar rights closely related to copyright including, without limitation, performance, broadcast, sound recording, and Sui Generis Database Rights, without regard to how the rights are labeled or categorized. For purposes of this Public License, the rights specified in Section 2(b)(1)-(2) are not Copyright and Similar Rights.
d. **Effective Technological Measures** means those measures that, in the absence of proper authority, may not be circumvented under laws fulfilling obligations under Article 11 of the WIPO Copyright Treaty adopted on December 20, 1996, and/or similar international agreements.
e. **Exceptions and Limitations** means fair use, fair dealing, and/or any other exception or limitation to Copyright and Similar Rights that applies to Your use of the Licensed Material.
f. **Licensed Material** means the artistic or literary work, database, or other material to which the Licensor applied this Public License.
g. **Licensed Rights** means the rights granted to You subject to the terms and conditions of this Public License, which are limited to all Copyright and Similar Rights that apply to Your use of the Licensed Material and that the Licensor has authority to license.
h. **Licensor** means the individual(s) or entity(ies) granting rights under this Public License.
i. **Share** means to provide material to the public by any means or process that requires permission under the Licensed Rights, such as reproduction, public display, public performance, distribution, dissemination, communication, or importation, and to make material available to the public including in ways that members of the public may access the material from a place and at a time individually chosen by them.
j. **Sui Generis Database Rights** means rights other than copyright resulting from Directive 96/9/EC of the European Parliament and of the Council of 11 March 1996 on the legal protection of databases, as amended and/or succeeded, as well as other essentially equivalent rights anywhere in the world.
k. **You** means the individual or entity exercising the Licensed Rights under this Public License. **Your** has a corresponding meaning.

Section 2 – Scope.

a. **License grant.**
    1. Subject to the terms and conditions of this Public License, the Licensor hereby grants You a worldwide, royalty-free, non-sublicensable, non-exclusive, irrevocable license to exercise the Licensed Rights in the Licensed Material to:
        A. reproduce and Share the Licensed Material, in whole or in part; and
        B. produce, reproduce, and Share Adapted Material.
    2. Exceptions and Limitations. For the avoidance of doubt, where Exceptions and Limitations apply to Your use, this Public License does not apply, and You do not need to comply with its terms and conditions.
    3. Term. The term of this Public License is specified in Section 6(a).
    4. Media and formats; technical modifications allowed. The Licensor authorizes You to exercise the Licensed Rights in all media and formats whether now known or hereafter created, and to make technical modifications necessary to do so. The Licensor waives and/or agrees not to assert any right or authority to forbid You from making technical modifications necessary to exercise the Licensed Rights, including technical modifications necessary to circumvent Effective Technological Measures. For purposes of this Public License, simply making modifications authorized by this Section 2(a)(4) never produces Adapted Material.
    5. Downstream recipients.
        A. Offer from the Licensor – Licensed Material. Every recipient of the Licensed Material automatically receives an offer from the Licensor to exercise the Licensed Rights under the terms and conditions of this Public License.
        B. No downstream restrictions. You may not offer or impose any additional or different terms or conditions on, or apply any Effective Technological Measures to, the Licensed Material if doing so restricts exercise of the Licensed Rights by any recipient of the Licensed Material.

6. No endorsement. Nothing in this Public License constitutes or may be construed as permission to assert or imply that You are, or that Your use of the Licensed Material is, connected with, or sponsored, endorsed, or granted official status by, the Licensor or others designated to receive attribution as provided in Section 3(a)(1)(A)(i).

b. **Other rights.**

1. Moral rights, such as the right of integrity, are not licensed under this Public License, nor are publicity, privacy, and/or other similar personality rights; however, to the extent possible, the Licensor waives and/or agrees not to assert any such rights held by the Licensor to the limited extent necessary to allow You to exercise the Licensed Rights, but not otherwise.
2. Patent and trademark rights are not licensed under this Public License.
3. To the extent possible, the Licensor waives any right to collect royalties from You for the exercise of the Licensed Rights, whether directly or through a collecting society under any voluntary or waivable statutory or compulsory licensing scheme. In all other cases the Licensor expressly reserves any right to collect such royalties.

Section 3 – License Conditions.

Your exercise of the Licensed Rights is expressly made subject to the following conditions.

a. **Attribution.**

1. If You Share the Licensed Material (including in modified form), You must:

   A. retain the following if it is supplied by the Licensor with the Licensed Material:
      i. identification of the creator(s) of the Licensed Material and any others designated to receive attribution, in any reasonable manner requested by the Licensor (including by pseudonym if designated);
      ii. a copyright notice;
      iii. a notice that refers to this Public License;
      iv. a notice that refers to the disclaimer of warranties;
      v. a URI or hyperlink to the Licensed Material to the extent reasonably practicable;
   B. indicate if You modified the Licensed Material and retain an indication of any previous modifications; and
   C. indicate the Licensed Material is licensed under this Public License, and include the text of, or the URI or hyperlink to, this Public License.
2. You may satisfy the conditions in Section 3(a)(1) in any reasonable manner based on the medium, means, and context in which You Share the Licensed Material. For example, it may be reasonable to satisfy the conditions by providing a URI or hyperlink to a resource that includes the required information.
3. If requested by the Licensor, You must remove any of the information required by Section 3(a)(1)(A) to the extent reasonably practicable.
4. If You Share Adapted Material You produce, the Adapter's License You apply must not prevent recipients of the Adapted Material from complying with this Public License.

Section 4 – Sui Generis Database Rights.

Where the Licensed Rights include Sui Generis Database Rights that apply to Your use of the Licensed Material:

a. for the avoidance of doubt, Section 2(a)(1) grants You the right to extract, reuse, reproduce, and Share all or a substantial portion of the contents of the database;
b. if You include all or a substantial portion of the database contents in a database in which You have Sui Generis Database Rights, then the database in which You have Sui Generis Database Rights (but not its individual contents) is Adapted Material; and
c. You must comply with the conditions in Section 3(a) if You Share all or a substantial portion of the contents of the database.

For the avoidance of doubt, this Section 4 supplements and does not replace Your obligations under this Public License where the Licensed Rights include other Copyright and Similar Rights.

Section 5 – Disclaimer of Warranties and Limitation of Liability.

a. **Unless otherwise separately undertaken by the Licensor, to the extent possible, the Licensor offers the Licensed Material as-is and as-available, and makes no representations or warranties of any kind concerning the Licensed Material, whether express, implied, statutory, or other. This includes, without limitation, warranties of title, merchantability, fitness for a particular purpose, non-infringement, absence of latent or other defects, accuracy, or the presence or absence of errors, whether or not known or discoverable. Where disclaimers of warranties are not allowed in full or in part, this disclaimer may not apply to You.**
b. **To the extent possible, in no event will the Licensor be liable to You on any legal theory (including, without limitation, negligence) or otherwise for any direct, special, indirect, incidental, consequential, punitive, exemplary, or other losses, costs, expenses, or damages arising out of this Public License or use of the Licensed Material, even if the Licensor has been advised of the possibility of such losses, costs, expenses, or damages. Where a limitation of liability is not allowed in full or in part, this limitation may not apply to You.**

c. The disclaimer of warranties and limitation of liability provided above shall be interpreted in a manner that, to the extent possible, most closely approximates an absolute disclaimer and waiver of all liability.

Section 6 – Term and Termination.

a. This Public License applies for the term of the Copyright and Similar Rights licensed here. However, if You fail to comply with this Public License, then Your rights under this Public License terminate automatically.

b. Where Your right to use the Licensed Material has terminated under Section 6(a), it reinstates:

    1. automatically as of the date the violation is cured, provided it is cured within 30 days of Your discovery of the violation; or
    2. upon express reinstatement by the Licensor.

    For the avoidance of doubt, this Section 6(b) does not affect any right the Licensor may have to seek remedies for Your violations of this Public License.
c. For the avoidance of doubt, the Licensor may also offer the Licensed Material under separate terms or conditions or stop distributing the Licensed Material at any time; however, doing so will not terminate this Public License.
d. Sections 1, 5, 6, 7, and 8 survive termination of this Public License.

Section 7 – Other Terms and Conditions.

a. The Licensor shall not be bound by any additional or different terms or conditions communicated by You unless expressly agreed.
b. Any arrangements, understandings, or agreements regarding the Licensed Material not stated herein are separate from and independent of the terms and conditions of this Public License.

Section 8 – Interpretation.

a. For the avoidance of doubt, this Public License does not, and shall not be interpreted to, reduce, limit, restrict, or impose conditions on any use of the Licensed Material that could lawfully be made without permission under this Public License.
b. To the extent possible, if any provision of this Public License is deemed unenforceable, it shall be automatically reformed to the minimum extent necessary to make it enforceable. If the provision cannot be reformed, it shall be severed from this Public License without affecting the enforceability of the remaining terms and conditions.
c. No term or condition of this Public License will be waived and no failure to comply consented to unless expressly agreed to by the Licensor.
d. Nothing in this Public License constitutes or may be interpreted as a limitation upon, or waiver of, any privileges and immunities that apply to the Licensor or You, including from the legal processes of any jurisdiction or authority.

Creative Commons is not a party to its public licenses. Notwithstanding, Creative Commons may elect to apply one of its public licenses to material it publishes and in those instances will be considered the "Licensor." The text of the Creative Commons public licenses is dedicated to the public domain under the CC0 Public Domain Dedication. Except for the limited purpose of indicating that material is shared

under a Creative Commons public license or as otherwise permitted by the Creative Commons policies published at creativecommons.org/policies, Creative Commons does not authorize the use of the trademark "Creative Commons" or any other trademark or logo of Creative Commons without its prior written consent including, without limitation, in connection with any unauthorized modifications to any of its public licenses or any other arrangements, understandings, or agreements concerning use of licensed material. For the avoidance of doubt, this paragraph does not form part of the public licenses.

Creative Commons may be contacted at creativecommons.org.

Additional languages available: Bahasa Indonesia, Nederlands, norsk, suomeksi, te reo Māori, українська, 日本語. Please read the FAQ for more information about official translations.

AUTHOR AND USER RIGHTS

INTRODUCTION

Elsevier requests transfers of copyright, or in some cases exclusive rights, from its journal authors in order to ensure that we have the rights necessary for the proper administration of electronic rights and online dissemination of journal articles, authors and their employers retain (or are granted/transferred back) significant scholarly rights in their work. We take seriously our responsibility as the steward of the online record to ensure the integrity of scholarly works and the sustainability of journal business models, and we actively monitor and pursue unauthorized and unsubscribed uses and re-distribution (for subscription models).

In addition to authors' scholarly rights, anyone who is affiliated with an institution with a journal subscription can use articles from subscribed content under the terms of their institution's license, while there are a number of other ways in which anyone (whether or not an author or subscriber) can make use of content published by Elsevier, which is free at the point of use or accessed under license.

Author Rights

As a journal author, you have rights for a large range of uses of your article, including use by your employing institute or company. These rights can be exercised without the need to obtain specific permission.

How authors can use their own journal articles

Authors publishing in Elsevier journals have wide rights to use their works for teaching and scholarly purposes without needing to seek permission.

Table of Author's Rights

	Preprint version (with a few exceptions- see below *)	Accepted Author Manuscript	Published Journal Articles
Use for classroom teaching by author or author's institution and presentation at a meeting or conference and distributing copies to attendees	Yes	Yes	Yes
Use for internal training by author's company	Yes	Yes	Yes
Distribution to colleagues for their research use	Yes	Yes	Yes
Use in a subsequent compilation of the author's works	Yes	Yes	Yes
Inclusion in a thesis or dissertation	Yes	Yes	Yes
Reuse of portions or extracts from the article in other works	Yes	Yes with full acknowledgement of final article	Yes with full acknowledgement of final article
Preparation of derivative works (other than for commercial purposes)	Yes	Yes with full acknowledgement of final article	Yes with full acknowledgement of final article
Preprint servers	Yes	Yes with the specific written permission of Elsevier	No
Voluntary posting on open web sites operated by author or author's institution for scholarly purposes	Yes (author may later add an appropriate bibliographic citation, indicating subsequent publication by Elsevier and journal title)	Yes, with appropriate bibliographic citation and a link to the article once published	Only with the specific written permission of Elsevier
Mandated deposit or deposit in or posting to subject-oriented or centralized repositories	Yes under specific agreement between Elsevier and the repository	Yes under specific agreement between Elsevier and the repository**	Yes under specific agreement between Elsevier and the repository
Use or posting for commercial gain or to substitute for services provided directly by journal	Only with the specific written permission of Elsevier	Only with the specific written permission of Elsevier	Only with the specific written permission of Elsevier

** Voluntary posting of Accepted Author Manuscripts in the arXiv subject repository is permitted.

Examples of use or posting for commercial gain:

- Posting by companies of employee-authored works for use by customers of those companies (e.g. pharmaceutical companies and physician prescribers)

- Commercial exploitation such as directly associating advertising with posting or charging fees for document delivery or access

***Which journals have different pre-print policies?**

If an electronic pre-print of an article is placed on a public server prior to its submission to an Elsevier journal, this is not generally viewed by Elsevier as 'prior publication' and will not disqualify the article from further consideration by Elsevier, nor will Elsevier require the removal of that pre-print version.

However Cell Press and The Lancet have different pre-print policies and will not consider for publication articles that have already been posted publicly. This is a rule agreed upon by The International Committee of Medical Journal Editors. Information on Cell Press policy on pre-prints is available, as is *The Lancet* pre-print policy. There are a number of other journals published by Elsevier (principally journals published on behalf of third party owners) that also have their own pre-print policies which will be set out in the Guide for Authors for the relevant journal.

Does Elsevier request a transfer of copyright?

Elsevier requests a transfer of copyright for articles published under subscription-based business models but we generally use different licensing approaches for other publishing models where we offer authors a variety of Creative Commons licenses for some of our author-pays journals and are piloting a range of options. More information on Creative Commons licenses can be found at: http://creativecommons.org/licenses

For subscription-based publishing, we ask for a transfer of copyright for a number of reasons, mainly because:

(i) By having the ability to exercise all rights under copyright, Elsevier is able to quickly launch new products and services, and to make agreements with other platforms and services to enrich published content and to make it more accessible and usable. Authors may be based in a number of different countries, which will have their own copyright regimes. Copyright assignments give more legal certainty, particularly in relation to future rights in new technologies.

(ii) Elsevier uses copyright to protect the integrity of the journal articles in cases of plagiarism, copyright infringement and other third party infringements. The journal subscription business model depends on a substantial body of subscribing customers providing financial support to a particular journal, and "free-riding" infringements diminish this model.

(iii) An assignment of rights under copyright means that we can more easily show that we own the rights and do not have to seek the participation of the author or obtain power of attorney from the author in order to bring an enforcement action.

Remember, even though we ask for a transfer of copyright, our journal authors retain (or are granted back) significant scholarly rights.

For a more detailed discussion, see STM Position Paper on the benefits of copyright assignments at http://www.stm-assoc.org/2007_10_01_Copyright_Assignment_Benefits.pdf

Where can I find more information on Elsevier's posting and copyright policies?

Please visit our Article Posting Policies information page.

You can also download here your practical guide to Elsevier's copyright policy.

Does Elsevier claim rights in an author's supporting data?

Elsevier supports the general principle that raw research data should be made freely available to all researchers and encourages the public posting of the raw data outputs of research. (Note that this is distinct from charts, tables, etc. which may be included within an article and in which rights would be transferred or licensed to Elsevier as part of the article, in the same way as text, illustrations or photographs.)

Elsevier therefore does not claim rights in the raw datasets that may be submitted with an article and the author can make these datasets freely available from other (web) locations.

If supported by the author and journal editor, and when a dataset is hosted in a repository that ensures data integrity and supports long-term preservation and inward linking, Elsevier can further support the discoverability of that dataset by connecting it with the published journal article on ScienceDirect through linking from an article or entity or through article interoperability. For examples of how this could work in practice, see: http://www.stm-assoc.org/2011_12_02_Innovations_Aalbersberg_Connecting_to_data_sets.pdf

For more information on industry positions on this issue supported by Elsevier, see:

Joint Statement from STM and DataCite on the Linkability and Citability of Research Data, June 2012: http://datacite.org/node/65

Declaration on STM Publishing, November 2007:
http://www.stm-assoc.org/2007_11_01_Brussels_Declaration.pdf

STM/ALPSP Statement, June 2006:
http://www.alpsp.org/Ebusiness/AboutALPSP/ALPSPStatements/Statementdetails.aspx?ID=55

How can I obtain permission to use my article for other purposes?

Our Subscription User Rights, Access Rights and Licensed Rights pages describe additional usages that can be made of Elsevier-owned material. To secure permission to use material from other Elsevier books, journals, databases or other products, to use your own material for purposes other than those outlined above, or if another author wishes to use all or part of your article as a resource, select:

OBTAINING PERMISSION TO USE ELSEVIER MATERIAL

Can I post my published journal article on open websites?

A published journal article is the definitive final record of published research that appears in the journal and embodies all value-adding publisher activities, including copy editing, formatting and, if relevant, pagination, along with the stewardship of the scholarly record.

You can use your branded and formatted published article for all of the personal and institutional purposes described above. However, in order to safeguard the correct scientific record, Elsevier does not permit the posting of published journal articles (either the pdf file provided by Elsevier or HTML files) on any open websites.

As part of its contribution to the stewardship of the scientific literature, Elsevier works with third parties (e.g. national libraries) to preserve its journal articles for posterity and in perpetuity, and invests to drive their usage. Elsevier strictly enforces an absolute guideline on the location of its published journal articles: each branded and formatted published journal article will reside only on a completely controlled site because this is the only way that we as the publisher can guarantee that each published journal article is permanent, authentic and unaltered as part of the 'minutes of science'.

Since Elsevier adds significant value to the final published journal article, we need to take these steps to ensure that this value is maintained, both for Elsevier and for our authors. However, we view preprints and accepted author manuscripts as less formal versions of the article and we therefore take a more liberal approach towards these, as described in more detail on our Author Posting Policies.

Am I allowed to post my published journal article to websites to fulfil drug regulation authority approval of therapeutic agents?

The posting of the published article to websites to fulfil drug regulation authority approval of therapeutic agents is not permitted. However, Elsevier permits the inclusion of an article title and abstract to fulfil drug regulation authority requirements, provided this is accompanied by a link to the published journal article on Elsevier's website. There are also reprint and license arrangements available to facilitate medical requirements.

Does Elsevier assist its authors to comply with the manuscript archiving requirements of funding bodies?

Elsevier has established agreements and developed policies to allow authors who publish in Elsevier journals to comply with the manuscript archiving requirements of a variety of funding bodies, including the US-based National Institutes of Health. For more information on existing arrangements, or if you are an institution or funding body and would like to discuss putting in place a new agreement with Elsevier, please see http://www.elsevier.com/wps/find/authorsview.authors/fundingbodyagreements

When Elsevier changes its author usage policies, are those changes also retroactive?
Yes, when Elsevier changes its policies to enable greater academic use of journal materials (such as the changes several years ago in our web-posting policies) or to clarify the rights retained by journal authors, Elsevier is prepared to extend those author rights retroactively with respect to articles published in journal issues produced prior to the policy change.

How do I obtain a journal publishing agreement?
You will receive a form automatically by post or e-mail once your article is received by Elsevier's Editorial-Production Department. View a generic example of the agreement. Some journals will use another variation of this form.

Can you provide me with a PDF file of my article?
Many Elsevier journals are now offering authors e-offprints – free electronic versions of their published articles. E-offprints are watermarked PDF versions, and are usually delivered within 24 hours, much quicker than print

Permitted Use Under Standard License

		Academic License	Government License	Corporate License
1	Access, search, browse and view for individual use	x	x	x
2	Print individual articles & chapters for individual use	x	x	x
3	Download individual articles & chapters for individual use	x	x	x
4	Incorporate links on Subscriber's intranet	x	x	x
5	Incorporate links on Subscriber's internet websites	x	x	x
6	Incorporate links into electronic coursepacks for text based content	x	x	
7	Inter Library Loan permitted	x	x	
8	Scholarly Sharing	x	x	
9	Submit electronically to gov't/regulatory agency			x
10	Submit via paper to gov't/regulatory agency			x
11	Provide print or electronic copies of graphical images for grant applications	x	x	
12	Provide print or electronic copies of individual items for grant applications	x	x	
13	Make Electronic Copies for personal use	x	x	x
14	Allow "Walk-in" Library Patrons	x	x	
15	Coursepacks: use of downloaded excerpts from subscribed and non-subscribed titles	x	x	
16	Coursepacks: use of printed excerpts from subscribed and non-subscribed titles	x	x	
17	Coursepacks: use of downloaded and printed excerpts from subscribed or non-subscribed titles	x	x	

Professional use of articles [1-3 above]

Current SciVerse ScienceDirect subscription agreements allow authorized users to access, search, browse and view subscribed content, including journal articles, and to print or download a limited number of articles, abstracts and records.

In general, Elsevier does not allow copying, printing or downloading entire issues of journals or otherwise substantially or systematically reproducing or retaining Elsevier-published articles.

Local database retention of Elsevier-published articles is only permitted if an institution or corporation has made an explicit agreement with Elsevier to acquire retention rights or if the institution or corporation has a digital rights license with a local reproduction rights organization (RRO). For more information on your local RRO and what they can offer, visit the International Federation of Reproduction Rights Organisations' website at www.iffro.org

Links to articles [4 and 5 above]

Any institute with a current ScienceDirect subscription may provide links on the institute's intranet, home page, library website or online catalog to subscribed Elsevier journals or articles. The ScienceDirect info site offers shortcut URLs to help information professionals put in place deep links to subscribed Elsevier journals or articles. For more information, see www.info.sciverse.com/sd/shortcutlinks

Coursepacks and eReserves [6 and 15-17 above]

Any academic or government institute with a current ScienceDirect subscription agreement can incorporate links to subscribed content, including full-text articles, into electronic coursepacks or eReserve lists for use in connection with courses offered for academic credit by the subscribing institute.

For any similar use for a non-accredited course or one offered by a corporation, an institute or corporation must obtain prior written permission from Elsevier and a fee may be required. Anyone interested in such permission should contact the Elsevier Global Rights department at permissions@elsevier.com

Interlibrary loan [7 above]

The interlibrary loan (ILL) policy for electronic journals is included in each institution's ScienceDirect subscription agreement. In short, this allows and provides for the use of electronic journal articles as a source for fulfillment of ILL requests, with some restrictions.

Elsevier grants subscribing institutes the right to use articles from subscribed ScienceDirect content as source material for ILLs subject to the following conditions:

- Each ILL request must come from an academic or other noncommercial, noncorporate research library located in the same country as the subscriber
- Each requested article must be printed by the subscriber (not applicable to US customers) and mailed, faxed or transmitted by Ariel (or a similar ILL system) to the requesting library

If a corporate or commercial entity is seeking a ScienceDirect article, instead of requesting ILL, that entity may use ScienceDirect's Pay per View service on a guest basis. For details, see www.info.sciverse.com/sd/ppv. Please also refer to http://myelsevier.com

Scholarly sharing of articles [8 above]

Current ScienceDirect subscription agreements permit authorized users to transmit excerpts of subscribed content, such as an article, by e-mail or in print, to known research colleagues for the purpose of scholarly study or research. Recipients of such scholarly sharing do not themselves have to be affiliated with an institute with a ScienceDirect subscription agreement.

Live reference

If they are both affiliated with the same institute, then a librarian can take a user electronically to any Elsevier article to which that institute has subscribed access. The librarian can also e-mail an Elsevier article, included in the library's subscription, to the user.

If, however, someone is not affiliated with the same institute as the librarian, then that user is not an authorized user at the librarian's institution. The librarian therefore cannot link the user directly to Elsevier articles or e-mail the Elsevier articles to the user. The librarian can, however, explain to the user how to request Elsevier articles through ILL or acquire them through ScienceDirect's Pay per View service.

Use by library guests [14 above]

Any institute with a current ScienceDirect subscription may allow members of the general public to use terminals physically located at that institute's library to access, search, browse, view and print articles in subscribed Elsevier journals. Some libraries impose their own usage restrictions on such 'walk-in users'. Commercial entities that wish to make copies for commercial purposes should obtain prior authorization from Elsevier or a local reproduction rights organization.

Access Rights

This section provides information on access to Elsevier content that is free at the point of use.

Sponsored articles and open access journals

Elsevier offers authors a variety of Creative Commons licences for its author-pays journals and is piloting a range of options. More information on Creative Commons licences can be found at: http://creativecommons.org/licenses

However, there may be some individual journals (including those owned by third parties on whose behalf the journal is published by Elsevier) for which Elsevier provides a bespoke user licence.

Open archives

This involves making journal articles from a subscription journal freely available on ScienceDirect after a journal specific embargo period. This can be done in two ways:

1. Journal Level

Here a specific journal makes articles within the journal freely available after a specific time period following publication. Elsevier has a number of journals that offer free access after a limited embargo period.

To see a list of Elsevier open archive journals, please follow this link.

2. Institutional Level

Here selected articles associated with a particular institution are made freely available after a specific time period following publication. Elsevier is running two pilots to understand the uptake and use of this delayed access model. We do not make all articles from that institution available and these pilots have been set up using a list of journals from which articles may be selected for inclusion in the pilot.

Under both models, once the embargo period has passed, the content is available for personal, non-commercial use on the basis of the standard terms and conditions of use for www.sciencedirect.com.

Procedia and third party journals hosted by Elsevier
Elsevier hosts on ScienceDirect certain content that is free at the point of use- principally Procedia and a number of third party journals for which the peer review and publication process is managed by that third party.

This content is available for personal, non-commercial use on the basis of the standard terms and conditions of use for www.sciencedirect.com.

Free walk-in access via public libraries
Any public library or institute with a current ScienceDirect subscription may allow members of the general public to use terminals physically located at that institute's library to access, search, browse, view and print articles in subscribed Elsevier journals. Some libraries impose their own usage restrictions on such 'walk-in users'.

Licensed Rights

Purchase of individual articles
Anyone may use Pay per View on ScienceDirect and purchase individual full-text journal articles. This service allows users to purchase direct access to articles. HTML and PDF access is instant and available for 24 hours on ScienceDirect; in addition, purchased articles can be downloaded and stored locally for future use. Articles from a number of Elsevier's journals are also available as part of DeepDyve (www.deepdyve.com) , the largest online rental service for professional and scholarly research articles. use

Reprints of articles
For customers who wish to purchase individual or commercial reprints of an article published by Elsevier, permission can be obtained from Elsevier.

Short quotes and reproduction of material from articles
Anyone may in written work quote from an article published by Elsevier, as long as the quote comprises only a short excerpt such as one or two sentences. An appropriate citation, including the journal title, must be provided.

If the intended use is for scholarly content, noncommercial research or educational purposes, an institution or academic may, without seeking permission from Elsevier, use:

- a single text extract of fewer than 100 words or a series of extracts totaling no more than 300 words
- a maximum of 2 figures from a journal article or a total of 5 from a journal volume

These guidelines reflect Elsevier's endorsement of the International Association of Scientific, Technical & Medical Publishers' 2008 guidelines for quotation and other academic uses of excerpts from journal articles. For more information on these guidelines, see www.stm-assoc.org/document-library/ (see Guidelines for Quotations from Journal Articles).

If the intended use or the material needed differs from the categories described above, Elsevier's prior written permission must be obtained.

Photocopies of articles
National copyright laws generally permit photocopying of an article for personal use.

Elsevier requires permission and a fee for all other photocopying, including multiple or systematic copying, copying for advertising or promotional purposes, copying for resale and copying for all forms of document delivery. Special rates are available for educational institutions (which do not have a subscription with Elsevier) wishing to make photocopies for nonprofit classroom use. (Authors will have the right to use their own material in the classroom as set out in the Author Rights section.)

How to obtain permission from Elsevier
Anyone may request permission via Rightslink, the Copyright Clearance Center's service available at the top of the HTML version of every journal article on ScienceDirect. Alternatively, e-mail requests to permissions@elsevier.com or (for individual or commercial reprints) to reprints@elsevier.com For more information, see:

OBTAINING PERMISSION TO USE ELSEVIER MATERIAL

ELSEVIER LICENSE
TERMS AND CONDITIONS

Feb 09, 2016

This is a License Agreement between Brett Roelofs ("You") and Elsevier ("Elsevier") provided by Copyright Clearance Center ("CCC"). The license consists of your order details, the terms and conditions provided by Elsevier, and the payment terms and conditions.

All payments must be made in full to CCC. For payment instructions, please see information listed at the bottom of this form.

Supplier	Elsevier Limited The Boulevard,Langford Lane Kidlington,Oxford,OX5 1GB,UK
Registered Company Number	1982084
Customer name	Brett Roelofs
Customer address	App. Geology Curtin Uni. GPO Box U1987 Perth, Western Australia 6845
License number	3786800037978
License date	Jan 12, 2016
Licensed content publisher	Elsevier
Licensed content publication	Earth and Planetary Science Letters
Licensed content title	Late Devonian carbonate magnetostratigraphy from the Oscar and Horse Spring Ranges, Lennard Shelf, Canning Basin, Western Australia
Licensed content author	Jeroen Hansma,Eric Tohver,Maodu Yan,Kate Trinajstic,Brett Roelofs,Sarah Peek,Sarah P. Slotznick,Joseph Kirschvink,Ted Playton,Peter Haines,Roger Hocking
Licensed content date	1 January 2015
Licensed content volume number	409
Licensed content issue number	n/a
Number of pages	11
Start Page	232
End Page	242
Type of Use	reuse in a thesis/dissertation
Portion	full article
Format	both print and electronic
Are you the author of this Elsevier article?	Yes
Will you be translating?	No
Title of your thesis/dissertation	Utilisation of microvertebrates in biostratigraphy and chemostratigraphy
Expected completion date	Feb 2016
Estimated size (number of	300

ELSEVIER LICENSE
TERMS AND CONDITIONS

Feb 09, 2016

This is a License Agreement between Brett Roelofs ("You") and Elsevier ("Elsevier") provided by Copyright Clearance Center ("CCC"). The license consists of your order details, the terms and conditions provided by Elsevier, and the payment terms and conditions.

All payments must be made in full to CCC. For payment instructions, please see information listed at the bottom of this form.

Supplier	Elsevier Limited The Boulevard,Langford Lane Kidlington,Oxford,OX5 1GB,UK
Registered Company Number	1982084
Customer name	Brett Roelofs
Customer address	App. Geology Curtin Uni. GPO Box U1987 Perth, Western Australia 6845
License number	3786800037978
License date	Jan 12, 2016
Licensed content publisher	Elsevier
Licensed content publication	Earth and Planetary Science Letters
Licensed content title	Late Devonian carbonate magnetostratigraphy from the Oscar and Horse Spring Ranges, Lennard Shelf, Canning Basin, Western Australia
Licensed content author	Jeroen Hansma,Eric Tohver,Maodu Yan,Kate Trinajstic,Brett Roelofs,Sarah Peek,Sarah P. Slotznick,Joseph Kirschvink,Ted Playton,Peter Haines,Roger Hocking
Licensed content date	1 January 2015
Licensed content volume number	409
Licensed content issue number	n/a
Number of pages	11
Start Page	232
End Page	242
Type of Use	reuse in a thesis/dissertation
Portion	full article
Format	both print and electronic
Are you the author of this Elsevier article?	Yes
Will you be translating?	No
Title of your thesis/dissertation	Utilisation of microvertebrates in biostratigraphy and chemostratigraphy
Expected completion date	Feb 2016
Estimated size (number of	300

pages)	
Elsevier VAT number	GB 494 6272 12
Permissions price	0.00 AUD
VAT/Local Sales Tax	0.00 AUD / 0.00 GBP
Total	0.00 AUD

Terms and Conditions

INTRODUCTION

1. The publisher for this copyrighted material is Elsevier. By clicking "accept" in connection with completing this licensing transaction, you agree that the following terms and conditions apply to this transaction (along with the Billing and Payment terms and conditions established by Copyright Clearance Center, Inc. ("CCC"), at the time that you opened your Rightslink account and that are available at any time at http://myaccount.copyright.com).

GENERAL TERMS

2. Elsevier hereby grants you permission to reproduce the aforementioned material subject to the terms and conditions indicated.
3. Acknowledgement: If any part of the material to be used (for example, figures) has appeared in our publication with credit or acknowledgement to another source, permission must also be sought from that source. If such permission is not obtained then that material may not be included in your publication/copies. Suitable acknowledgement to the source must be made, either as a footnote or in a reference list at the end of your publication, as follows:
"Reprinted from Publication title, Vol /edition number, Author(s), Title of article / title of chapter, Pages No., Copyright (Year), with permission from Elsevier [OR APPLICABLE SOCIETY COPYRIGHT OWNER]." Also Lancet special credit - "Reprinted from The Lancet, Vol. number, Author(s), Title of article, Pages No., Copyright (Year), with permission from Elsevier."
4. Reproduction of this material is confined to the purpose and/or media for which permission is hereby given.
5. Altering/Modifying Material: Not Permitted. However figures and illustrations may be altered/adapted minimally to serve your work. Any other abbreviations, additions, deletions and/or any other alterations shall be made only with prior written authorization of Elsevier Ltd. (Please contact Elsevier at permissions@elsevier.com)
6. If the permission fee for the requested use of our material is waived in this instance, please be advised that your future requests for Elsevier materials may attract a fee.
7. Reservation of Rights: Publisher reserves all rights not specifically granted in the combination of (i) the license details provided by you and accepted in the course of this licensing transaction, (ii) these terms and conditions and (iii) CCC's Billing and Payment terms and conditions.
8. License Contingent Upon Payment: While you may exercise the rights licensed immediately upon issuance of the license at the end of the licensing process for the transaction, provided that you have disclosed complete and accurate details of your proposed use, no license is finally effective unless and until full payment is received from you (either by publisher or by CCC) as provided in CCC's Billing and Payment terms and conditions. If full payment is not received on a timely basis, then any license preliminarily granted shall be deemed automatically revoked and shall be void as if never granted. Further, in the event that you breach any of these terms and conditions or any of CCC's Billing and Payment terms and conditions, the license is automatically revoked and shall be void as if never granted. Use of materials as described in a revoked license, as well as any use of the materials beyond the scope of an unrevoked license, may constitute copyright infringement and publisher reserves the right to take any and all action to protect its copyright in the materials.

9. Warranties: Publisher makes no representations or warranties with respect to the licensed material.
10. Indemnity: You hereby indemnify and agree to hold harmless publisher and CCC, and their respective officers, directors, employees and agents, from and against any and all claims arising out of your use of the licensed material other than as specifically authorized pursuant to this license.
11. No Transfer of License: This license is personal to you and may not be sublicensed, assigned, or transferred by you to any other person without publisher's written permission.
12. No Amendment Except in Writing: This license may not be amended except in a writing signed by both parties (or, in the case of publisher, by CCC on publisher's behalf).
13. Objection to Contrary Terms: Publisher hereby objects to any terms contained in any purchase order, acknowledgment, check endorsement or other writing prepared by you, which terms are inconsistent with these terms and conditions or CCC's Billing and Payment terms and conditions. These terms and conditions, together with CCC's Billing and Payment terms and conditions (which are incorporated herein), comprise the entire agreement between you and publisher (and CCC) concerning this licensing transaction. In the event of any conflict between your obligations established by these terms and conditions and those established by CCC's Billing and Payment terms and conditions, these terms and conditions shall control.
14. Revocation: Elsevier or Copyright Clearance Center may deny the permissions described in this License at their sole discretion, for any reason or no reason, with a full refund payable to you. Notice of such denial will be made using the contact information provided by you. Failure to receive such notice will not alter or invalidate the denial. In no event will Elsevier or Copyright Clearance Center be responsible or liable for any costs, expenses or damage incurred by you as a result of a denial of your permission request, other than a refund of the amount(s) paid by you to Elsevier and/or Copyright Clearance Center for denied permissions.

LIMITED LICENSE

The following terms and conditions apply only to specific license types:
15. **Translation**: This permission is granted for non-exclusive world **English** rights only unless your license was granted for translation rights. If you licensed translation rights you may only translate this content into the languages you requested. A professional translator must perform all translations and reproduce the content word for word preserving the integrity of the article.
16. **Posting licensed content on any Website**: The following terms and conditions apply as follows: Licensing material from an Elsevier journal: All content posted to the web site must maintain the copyright information line on the bottom of each image; A hyper-text must be included to the Homepage of the journal from which you are licensing at http://www.sciencedirect.com/science/journal/xxxxx or the Elsevier homepage for books at http://www.elsevier.com; Central Storage: This license does not include permission for a scanned version of the material to be stored in a central repository such as that provided by Heron/XanEdu.
Licensing material from an Elsevier book: A hyper-text link must be included to the Elsevier homepage at http://www.elsevier.com . All content posted to the web site must maintain the copyright information line on the bottom of each image.

Posting licensed content on Electronic reserve: In addition to the above the following clauses are applicable: The web site must be password-protected and made available only to bona fide students registered on a relevant course. This permission is granted for 1 year only. You may obtain a new license for future website posting.
17. **For journal authors:** the following clauses are applicable in addition to the above:
Preprints:
A preprint is an author's own write-up of research results and analysis, it has not been peer-reviewed, nor has it had any other value added to it by a publisher (such as formatting,

copyright, technical enhancement etc.).
Authors can share their preprints anywhere at any time. Preprints should not be added to or enhanced in any way in order to appear more like, or to substitute for, the final versions of articles however authors can update their preprints on arXiv or RePEc with their Accepted Author Manuscript (see below).
If accepted for publication, we encourage authors to link from the preprint to their formal publication via its DOI. Millions of researchers have access to the formal publications on ScienceDirect, and so links will help users to find, access, cite and use the best available version. Please note that Cell Press, The Lancet and some society-owned have different preprint policies. Information on these policies is available on the journal homepage.
Accepted Author Manuscripts: An accepted author manuscript is the manuscript of an article that has been accepted for publication and which typically includes author-incorporated changes suggested during submission, peer review and editor-author communications.
Authors can share their accepted author manuscript:

- immediately
  - via their non-commercial person homepage or blog
  - by updating a preprint in arXiv or RePEc with the accepted manuscript
  - via their research institute or institutional repository for internal institutional uses or as part of an invitation-only research collaboration work-group
  - directly by providing copies to their students or to research collaborators for their personal use
  - for private scholarly sharing as part of an invitation-only work group on commercial sites with which Elsevier has an agreement
- after the embargo period
  - via non-commercial hosting platforms such as their institutional repository
  - via commercial sites with which Elsevier has an agreement

In all cases accepted manuscripts should:

- link to the formal publication via its DOI
- bear a CC-BY-NC-ND license - this is easy to do
- if aggregated with other manuscripts, for example in a repository or other site, be shared in alignment with our hosting policy not be added to or enhanced in any way to appear more like, or to substitute for, the published journal article.

Published journal article (JPA): A published journal article (PJA) is the definitive final record of published research that appears or will appear in the journal and embodies all value-adding publishing activities including peer review co-ordination, copy-editing, formatting, (if relevant) pagination and online enrichment.
Policies for sharing publishing journal articles differ for subscription and gold open access articles:
Subscription Articles: If you are an author, please share a link to your article rather than the full-text. Millions of researchers have access to the formal publications on ScienceDirect, and so links will help your users to find, access, cite, and use the best available version.
Theses and dissertations which contain embedded PJAs as part of the formal submission can be posted publicly by the awarding institution with DOI links back to the formal publications on ScienceDirect.
If you are affiliated with a library that subscribes to ScienceDirect you have additional private sharing rights for others' research accessed under that agreement. This includes use for classroom teaching and internal training at the institution (including use in course packs and courseware programs), and inclusion of the article for grant funding purposes.
Gold Open Access Articles: May be shared according to the author-selected end-user

license and should contain a CrossMark logo, the end user license, and a DOI link to the formal publication on ScienceDirect.
Please refer to Elsevier's posting policy for further information.
18. **For book authors** the following clauses are applicable in addition to the above: Authors are permitted to place a brief summary of their work online only. You are not allowed to download and post the published electronic version of your chapter, nor may you scan the printed edition to create an electronic version. **Posting to a repository:** Authors are permitted to post a summary of their chapter only in their institution's repository.
19. **Thesis/Dissertation**: If your license is for use in a thesis/dissertation your thesis may be submitted to your institution in either print or electronic form. Should your thesis be published commercially, please reapply for permission. These requirements include permission for the Library and Archives of Canada to supply single copies, on demand, of the complete thesis and include permission for Proquest/UMI to supply single copies, on demand, of the complete thesis. Should your thesis be published commercially, please reapply for permission. Theses and dissertations which contain embedded PJAs as part of the formal submission can be posted publicly by the awarding institution with DOI links back to the formal publications on ScienceDirect.

Elsevier Open Access Terms and Conditions
You can publish open access with Elsevier in hundreds of open access journals or in nearly 2000 established subscription journals that support open access publishing. Permitted third party re-use of these open access articles is defined by the author's choice of Creative Commons user license. See our open access license policy for more information.
Terms & Conditions applicable to all Open Access articles published with Elsevier:
Any reuse of the article must not represent the author as endorsing the adaptation of the article nor should the article be modified in such a way as to damage the author's honour or reputation. If any changes have been made, such changes must be clearly indicated.
The author(s) must be appropriately credited and we ask that you include the end user license and a DOI link to the formal publication on ScienceDirect.
If any part of the material to be used (for example, figures) has appeared in our publication with credit or acknowledgement to another source it is the responsibility of the user to ensure their reuse complies with the terms and conditions determined by the rights holder.
Additional Terms & Conditions applicable to each Creative Commons user license:
CC BY: The CC-BY license allows users to copy, to create extracts, abstracts and new works from the Article, to alter and revise the Article and to make commercial use of the Article (including reuse and/or resale of the Article by commercial entities), provided the user gives appropriate credit (with a link to the formal publication through the relevant DOI), provides a link to the license, indicates if changes were made and the licensor is not represented as endorsing the use made of the work. The full details of the license are available at http://creativecommons.org/licenses/by/4.0.
CC BY NC SA: The CC BY-NC-SA license allows users to copy, to create extracts, abstracts and new works from the Article, to alter and revise the Article, provided this is not done for commercial purposes, and that the user gives appropriate credit (with a link to the formal publication through the relevant DOI), provides a link to the license, indicates if changes were made and the licensor is not represented as endorsing the use made of the work. Further, any new works must be made available on the same conditions. The full details of the license are available at http://creativecommons.org/licenses/by-nc-sa/4.0.
CC BY NC ND: The CC BY-NC-ND license allows users to copy and distribute the Article, provided this is not done for commercial purposes and further does not permit distribution of the Article if it is changed or edited in any way, and provided the user gives appropriate credit (with a link to the formal publication through the relevant DOI), provides a link to the license, and that the licensor is not represented as endorsing the use made of the work. The full details of the license are available at http://creativecommons.org/licenses/by-nc-nd/4.0.
Any commercial reuse of Open Access articles published with a CC BY NC SA or CC BY

NC ND license requires permission from Elsevier and will be subject to a fee.
Commercial reuse includes:

- Associating advertising with the full text of the Article
- Charging fees for document delivery or access
- Article aggregation
- Systematic distribution via e-mail lists or share buttons

Posting or linking by commercial companies for use by customers of those companies.

20. **Other Conditions**:

v1.8

Questions? customercare@copyright.com or +1-855-239-3415 (toll free in the US) or +1-978-646-2777.

ELSEVIER LICENSE
TERMS AND CONDITIONS

Nov 01, 2016

This Agreement between Brett Roelofs ("You") and Elsevier ("Elsevier") consists of your license details and the terms and conditions provided by Elsevier and Copyright Clearance Center.

License Number	3980500866918
License date	Nov 01, 2016
Licensed Content Publisher	Elsevier
Licensed Content Publication	Palaeogeography, Palaeoclimatology, Palaeoecology
Licensed Content Title	Upper Kellwasser carbon isotope excursion pre-dates the F–F boundary in the Upper Devonian Lennard Shelf carbonate system, Canning Basin, Western Australia
Licensed Content Author	Kelly Hillbun,Ted E. Playton,Eric Tohver,Ken Ratcliffe,Kate Trinajstic,Brett Roelofs,Samuel Caulfield-Kerney,David Wray,Peter Haines,Roger Hocking,David Katz,Paul Montgomery,Peter Ward
Licensed Content Date	15 November 2015
Licensed Content Volume Number	438
Licensed Content Issue Number	n/a
Licensed Content Pages	11
Start Page	180
End Page	190
Type of Use	reuse in a thesis/dissertation
Intended publisher of new work	other
Portion	full article
Format	both print and electronic
Are you the author of this Elsevier article?	Yes
Will you be translating?	No
Order reference number	
Title of your thesis/dissertation	Utilisation of microvertebrates in biostratigraphy and chemostratigraphy
Expected completion date	Nov 2016
Estimated size (number of pages)	500
Elsevier VAT number	GB 494 6272 12
Requestor Location	Brett Roelofs App. Geology Curtin Uni. GPO Box U1987 Perth, Western Australia 6845 Australia Attn: Brett Roelofs
Total	0.00 USD
Terms and Conditions	

INTRODUCTION

1. The publisher for this copyrighted material is Elsevier. By clicking "accept" in connection with completing this licensing transaction, you agree that the following terms and conditions apply to this transaction (along with the Billing and Payment terms and conditions established by Copyright Clearance Center, Inc. ("CCC"), at the time that you opened your Rightslink account and that are available at any time at http://myaccount.copyright.com).

GENERAL TERMS

2. Elsevier hereby grants you permission to reproduce the aforementioned material subject to the terms and conditions indicated.
3. Acknowledgement: If any part of the material to be used (for example, figures) has appeared in our publication with credit or acknowledgement to another source, permission must also be sought from that source. If such permission is not obtained then that material may not be included in your publication/copies. Suitable acknowledgement to the source must be made, either as a footnote or in a reference list at the end of your publication, as follows:
"Reprinted from Publication title, Vol /edition number, Author(s), Title of article / title of chapter, Pages No., Copyright (Year), with permission from Elsevier [OR APPLICABLE SOCIETY COPYRIGHT OWNER]." Also Lancet special credit - "Reprinted from The Lancet, Vol. number, Author(s), Title of article, Pages No., Copyright (Year), with permission from Elsevier."
4. Reproduction of this material is confined to the purpose and/or media for which permission is hereby given.
5. Altering/Modifying Material: Not Permitted. However figures and illustrations may be altered/adapted minimally to serve your work. Any other abbreviations, additions, deletions and/or any other alterations shall be made only with prior written authorization of Elsevier Ltd. (Please contact Elsevier at permissions@elsevier.com)
6. If the permission fee for the requested use of our material is waived in this instance, please be advised that your future requests for Elsevier materials may attract a fee.
7. Reservation of Rights: Publisher reserves all rights not specifically granted in the combination of (i) the license details provided by you and accepted in the course of this licensing transaction, (ii) these terms and conditions and (iii) CCC's Billing and Payment terms and conditions.
8. License Contingent Upon Payment: While you may exercise the rights licensed immediately upon issuance of the license at the end of the licensing process for the transaction, provided that you have disclosed complete and accurate details of your proposed use, no license is finally effective unless and until full payment is received from you (either by publisher or by CCC) as provided in CCC's Billing and Payment terms and conditions. If full payment is not received on a timely basis, then any license preliminarily granted shall be deemed automatically revoked and shall be void as if never granted. Further, in the event that you breach any of these terms and conditions or any of CCC's Billing and Payment terms and conditions, the license is automatically revoked and shall be void as if never granted. Use of materials as described in a revoked license, as well as any use of the materials beyond the scope of an unrevoked license, may constitute copyright infringement and publisher reserves the right to take any and all action to protect its copyright in the materials.
9. Warranties: Publisher makes no representations or warranties with respect to the licensed material.
10. Indemnity: You hereby indemnify and agree to hold harmless publisher and CCC, and their respective officers, directors, employees and agents, from and against any and all claims arising out of your use of the licensed material other than as specifically authorized pursuant to this license.
11. No Transfer of License: This license is personal to you and may not be sublicensed, assigned, or transferred by you to any other person without publisher's written permission.
12. No Amendment Except in Writing: This license may not be amended except in a writing signed by both parties (or, in the case of publisher, by CCC on publisher's behalf).
13. Objection to Contrary Terms: Publisher hereby objects to any terms contained in any purchase order, acknowledgment, check endorsement or other writing prepared by you, which terms are inconsistent with these terms and conditions or CCC's Billing and Payment

terms and conditions. These terms and conditions, together with CCC's Billing and Payment terms and conditions (which are incorporated herein), comprise the entire agreement between you and publisher (and CCC) concerning this licensing transaction. In the event of any conflict between your obligations established by these terms and conditions and those established by CCC's Billing and Payment terms and conditions, these terms and conditions shall control.

14. Revocation: Elsevier or Copyright Clearance Center may deny the permissions described in this License at their sole discretion, for any reason or no reason, with a full refund payable to you. Notice of such denial will be made using the contact information provided by you. Failure to receive such notice will not alter or invalidate the denial. In no event will Elsevier or Copyright Clearance Center be responsible or liable for any costs, expenses or damage incurred by you as a result of a denial of your permission request, other than a refund of the amount(s) paid by you to Elsevier and/or Copyright Clearance Center for denied permissions.

LIMITED LICENSE

The following terms and conditions apply only to specific license types:

15. **Translation**: This permission is granted for non-exclusive world **English** rights only unless your license was granted for translation rights. If you licensed translation rights you may only translate this content into the languages you requested. A professional translator must perform all translations and reproduce the content word for word preserving the integrity of the article.

16. **Posting licensed content on any Website**: The following terms and conditions apply as follows: Licensing material from an Elsevier journal: All content posted to the web site must maintain the copyright information line on the bottom of each image; A hyper-text must be included to the Homepage of the journal from which you are licensing at http://www.sciencedirect.com/science/journal/xxxxx or the Elsevier homepage for books at http://www.elsevier.com; Central Storage: This license does not include permission for a scanned version of the material to be stored in a central repository such as that provided by Heron/XanEdu.

Licensing material from an Elsevier book: A hyper-text link must be included to the Elsevier homepage at http://www.elsevier.com . All content posted to the web site must maintain the copyright information line on the bottom of each image.

Posting licensed content on Electronic reserve: In addition to the above the following clauses are applicable: The web site must be password-protected and made available only to bona fide students registered on a relevant course. This permission is granted for 1 year only. You may obtain a new license for future website posting.

17. **For journal authors:** the following clauses are applicable in addition to the above:

Preprints:

A preprint is an author's own write-up of research results and analysis, it has not been peer-reviewed, nor has it had any other value added to it by a publisher (such as formatting, copyright, technical enhancement etc.).

Authors can share their preprints anywhere at any time. Preprints should not be added to or enhanced in any way in order to appear more like, or to substitute for, the final versions of articles however authors can update their preprints on arXiv or RePEc with their Accepted Author Manuscript (see below).

If accepted for publication, we encourage authors to link from the preprint to their formal publication via its DOI. Millions of researchers have access to the formal publications on ScienceDirect, and so links will help users to find, access, cite and use the best available version. Please note that Cell Press, The Lancet and some society-owned have different preprint policies. Information on these policies is available on the journal homepage.

Accepted Author Manuscripts: An accepted author manuscript is the manuscript of an article that has been accepted for publication and which typically includes author-incorporated changes suggested during submission, peer review and editor-author communications.

Authors can share their accepted author manuscript:

- immediately

- via their non-commercial person homepage or blog
- by updating a preprint in arXiv or RePEc with the accepted manuscript
- via their research institute or institutional repository for internal institutional uses or as part of an invitation-only research collaboration work-group
- directly by providing copies to their students or to research collaborators for their personal use
- for private scholarly sharing as part of an invitation-only work group on commercial sites with which Elsevier has an agreement

- after the embargo period
  - via non-commercial hosting platforms such as their institutional repository
  - via commercial sites with which Elsevier has an agreement

In all cases accepted manuscripts should:

- link to the formal publication via its DOI
- bear a CC-BY-NC-ND license - this is easy to do
- if aggregated with other manuscripts, for example in a repository or other site, be shared in alignment with our hosting policy not be added to or enhanced in any way to appear more like, or to substitute for, the published journal article.

Published journal article (JPA): A published journal article (PJA) is the definitive final record of published research that appears or will appear in the journal and embodies all value-adding publishing activities including peer review co-ordination, copy-editing, formatting, (if relevant) pagination and online enrichment.
Policies for sharing publishing journal articles differ for subscription and gold open access articles:
Subscription Articles: If you are an author, please share a link to your article rather than the full-text. Millions of researchers have access to the formal publications on ScienceDirect, and so links will help your users to find, access, cite, and use the best available version.
Theses and dissertations which contain embedded PJAs as part of the formal submission can be posted publicly by the awarding institution with DOI links back to the formal publications on ScienceDirect.
If you are affiliated with a library that subscribes to ScienceDirect you have additional private sharing rights for others' research accessed under that agreement. This includes use for classroom teaching and internal training at the institution (including use in course packs and courseware programs), and inclusion of the article for grant funding purposes.
Gold Open Access Articles: May be shared according to the author-selected end-user license and should contain a CrossMark logo, the end user license, and a DOI link to the formal publication on ScienceDirect.
Please refer to Elsevier's posting policy for further information.
18. **For book authors** the following clauses are applicable in addition to the above:
Authors are permitted to place a brief summary of their work online only. You are not allowed to download and post the published electronic version of your chapter, nor may you scan the printed edition to create an electronic version. **Posting to a repository:** Authors are permitted to post a summary of their chapter only in their institution's repository.
19. **Thesis/Dissertation**: If your license is for use in a thesis/dissertation your thesis may be submitted to your institution in either print or electronic form. Should your thesis be published commercially, please reapply for permission. These requirements include permission for the Library and Archives of Canada to supply single copies, on demand, of the complete thesis and include permission for Proquest/UMI to supply single copies, on demand, of the complete thesis. Should your thesis be published commercially, please reapply for permission. Theses and dissertations which contain embedded PJAs as part of the formal submission can be posted publicly by the awarding institution with DOI links back to the formal publications on ScienceDirect.

Elsevier Open Access Terms and Conditions

You can publish open access with Elsevier in hundreds of open access journals or in nearly 2000 established subscription journals that support open access publishing. Permitted third party re-use of these open access articles is defined by the author's choice of Creative Commons user license. See our open access license policy for more information.

Terms & Conditions applicable to all Open Access articles published with Elsevier:

Any reuse of the article must not represent the author as endorsing the adaptation of the article nor should the article be modified in such a way as to damage the author's honour or reputation. If any changes have been made, such changes must be clearly indicated.

The author(s) must be appropriately credited and we ask that you include the end user license and a DOI link to the formal publication on ScienceDirect.

If any part of the material to be used (for example, figures) has appeared in our publication with credit or acknowledgement to another source it is the responsibility of the user to ensure their reuse complies with the terms and conditions determined by the rights holder.

Additional Terms & Conditions applicable to each Creative Commons user license:

CC BY: The CC-BY license allows users to copy, to create extracts, abstracts and new works from the Article, to alter and revise the Article and to make commercial use of the Article (including reuse and/or resale of the Article by commercial entities), provided the user gives appropriate credit (with a link to the formal publication through the relevant DOI), provides a link to the license, indicates if changes were made and the licensor is not represented as endorsing the use made of the work. The full details of the license are available at http://creativecommons.org/licenses/by/4.0.

CC BY NC SA: The CC BY-NC-SA license allows users to copy, to create extracts, abstracts and new works from the Article, to alter and revise the Article, provided this is not done for commercial purposes, and that the user gives appropriate credit (with a link to the formal publication through the relevant DOI), provides a link to the license, indicates if changes were made and the licensor is not represented as endorsing the use made of the work. Further, any new works must be made available on the same conditions. The full details of the license are available at http://creativecommons.org/licenses/by-nc-sa/4.0.

CC BY NC ND: The CC BY-NC-ND license allows users to copy and distribute the Article, provided this is not done for commercial purposes and further does not permit distribution of the Article if it is changed or edited in any way, and provided the user gives appropriate credit (with a link to the formal publication through the relevant DOI), provides a link to the license, and that the licensor is not represented as endorsing the use made of the work. The full details of the license are available at http://creativecommons.org/licenses/by-nc-nd/4.0.

Any commercial reuse of Open Access articles published with a CC BY NC SA or CC BY NC ND license requires permission from Elsevier and will be subject to a fee.

Commercial reuse includes:

- Associating advertising with the full text of the Article
- Charging fees for document delivery or access
- Article aggregation
- Systematic distribution via e-mail lists or share buttons

Posting or linking by commercial companies for use by customers of those companies.

20. **Other Conditions**:

v1.8

Questions? customercare@copyright.com or +1-855-239-3415 (toll free in the US) or +1-978-646-2777.

Publications

Permission to use SEPM Materials

Permissions for Using SEPM Publications

Use of PDFs

IMPORTANT: Authors may not post the final PDF or any proof version of the paper to any institutional website, or article sharing free access websites, such as or ResearchGate or Academia.edu, etc. Authors are encouraged to share e-print PDFs with those individuals that have requested copies, similar to printed reprint distribution. SEPM is continuously reviewing the online digital publishing landscape to better serve authors and users. SEPM is closely monitoring efforts to resolve these issues such as discussed at http://www.stm-assoc.org/stm-consultations/scn-consultation-2015/.

See SEPM Open Access Policy for Gold and Green OA options.

Obtaining a PDF of an article

Subscribers to online access of SEPM publications may download PDFs of any article for their own personal use and research. Subscribers may also create printed copies of the PDFs, again, only for their own personal use and research.

Non-subscribers may use the Pay-Per-View facility to purchase access to the PDF. Once you have access, you will be able to download and save a copy (for your personal use only). You may also request an e-print of an article from the author(s).

Corresponding authors of papers will have received an e-mail with instructions on how to download an e-print PDF. Contributing authors requiring access should contact the corresponding author. We do not provide free access to articles directly to other individuals.

Re-publishing material from SEPM copyright

Using material from SEPM publications

Extensive quotation (more than c. 100 words) and reproduction of previously published illustrations (even if redrawn) require permission from the copyright holder.

Material that can be used without permission

Authors may reuse their own material without permission subject to the exceptions listed below. They may include the whole article in a PhD or other thesis provided that it will not be published, and that the original source is fully acknowledged in a standard format. Authors may not republish their whole article, or a substantial part of it, without permission. Such permission will be granted depending on circumstances.

For non-commercial purposes, anyone may use up to three items (text extracts of 100 words or less, figures or tables) from SEPM published material without permission or charge provided that a proper acknowledgement of source is used with the item. If you require written permission, please contact the permissions editors listed in the section below.

The abstracts of articles can be reproduced without permission or fees provided that a full reference and a link to the article abstract page are included.

Please check that SEPM is the original copyright holder and that the material has not been taken from another source. In those cases, you must contact the original copyright holder.

If your article forms part of a multi-author book, the publisher must ensure that the total number of items from SEPM copyright does not exceed three (this does not apply to journal issues).

****Note: Use of content from Concepts in Sedimentology and Paleontology No. 9, however, is prohibited from any use of separate content. Only the whole book may be purchased and used.**

Reusing material in another SEPM publication

You may use material from SEPM copyright in another SEPM publication without permission from SEPM subject to the exceptions listed below.

Uses where permission is required

For more than three items, please contact the appropriate Permissions Editor for that publication series to obtain permission.

Exceptions

SEPM has a strong policy against duplicate publication and does not allow republication of whole articles, or substantial parts of them, unless there are very exceptional circumstances.

You may not use more than 25% of any SEPM published article in a single publication and no publication should contain more than 25% in total from SEPM Copyright. This does not prevent the inclusion of whole articles in course packs and the like (which do not constitute republication).

You may not post a typeset PDF of a SEPM article on any website, repository or server (see author exceptions).

Photocopying and digital copying

You may make limited hard copies of an article for your own research or educational purposes (not including course packs) if you have access rights to the material. You do not need to request permission to do this.

For more extensive copying or digital reproduction, you need to obtain a license from the Copyright Clearance Center: www.copyright.com or from your local reproduction rights agency.

Lecture and presentations

You may include material from Society copyright in a visual presentation if you have access rights to the material and provided that you will not circulate digital or hard copies of your presentation for commerical purposes. You do not need to request permission to do this. If you wish to circulate copies of your presentation to students or others, please obtain 'course-pack' permission from the Copyright Clearance Center: www.copyright.com or from your local reproduction rights agency.

Permission to use SEPM material
Permission, unless otherwise excepted here, to reprint material from the Society's publications should be made to the Permissions Editors for the various publications.

- Permission to use material from the Society's website should be made to Howard Harper.
- Permission to use material from The Sedimentary Record should be made to Howard Harper.
- Permission to use material from The Journal of Sedimentary Research (or Journal of Sedimentary Petrology) should be made to Melissa Lester.
- Permission to use material from PALAIOS and Journal of Paleontology (1927-1985) should be made to Kathleen Huber.
- Permission to use material from SEPM book publications should be made to Michele Tomlinson.

Authors Use

Corresponding and contributing authors have transferred copyright (and all rights under it), or have granted full publishing rights in their work, to SEPM. In assigning copyright authors are not forfeiting their rights to use their contribution elsewhere, provided it does not directly detract from or undermine the Society's legitimate benefits under the rights granted to it. Please note that authors continue to enjoy the following rights:

1. Patent and trademark rights.

2. The right to be identified as the Author.

3. The right to share with colleagues 'preprints' (i.e. "Authors Original", prior to peer review), provided that this is not done for commercial purposes, and to post preprints to publicly accessible websites.

4. In the case of journal articles, and prior to publication by the Society, the right to post a 'postprint' (i.e. "Accepted Version", in the final form accepted by SEPM for publication) to authors' personal web pages or to an institutional web site or repository maintained by the institution to which they are affiliated. Any such posted work must be accompanied by a notice: "Accepted for publication in [name of publication] as of [date]".

5. The right to use the separate content or data or figures in authors' research, and in courses that they are teaching or by others within an institution or company where the author is employed but not allow free public access to content.

6. The right to incorporate the content of the contribution in other works of which they are the author, including personal compilations and books of which they are the author.

In the case of 3 to 6 above, these rights are intended to help authors in their academic and professional work, and are subject to three conditions:

a. These rights may not be used for commercial purposes;
b. These rights should not be used in a way that involves duplicate publication that will compete with the Society's own publications; and
c. Each use must contain an acknowledgement to the journal/book as the original source of publication in the form: "[Journal/Book] [Volume/Publication Year] [URL of the item as published by SEPM Society for Sedimentary Geology] © SEPM Society for Sedimentary Geology [Year]."

- On publication within the SEPM online publications corresponding authors will receive an email and URL enabling access to free PDF e-print downloads. Accessed PDFs may be saved to the author's hard drive or other personal

electronic media and emailed or copied to colleagues or third parties (again, for legitimate purposes only). Details will be provided on publication.

- Other than the use outlined above no Society publication may be captured or downloaded electronically into any format without the Society's specific written permission.
- Permission must be sought for uses other than those defined above – please contact the appropriate Permissions Editor
- **IMPORTANT: Authors may not post the final PDF or any proof version of the paper to any institutional website, or article sharing free access websites, such as Academics.edu or ResearchGate. etc. Authors are encouraged to share e-print PDFs with those individuals that have requested copies, similar to printed reprint distribution.**
- **SEPM is continuously reviewing the online digital publishing landscape to better serve authors and users. SEPM is closely monitoring efforts to resolve these issues such as discussed at http://www.stm-assoc.org/stm-consultations/scn-consultation-2015/.**